FACTORS INFLUENCING PERFORMANCE OF A LATERALLY LOADED PILE WITHIN AN MSE WALL SYSTEM

By

Wessam Khaled Mohammed

Submitted to the graduate degree program in the Department of Civil, Environmental, and Architectural Engineering and Graduate Faculty of the University of Kansas in partial fulfillment of the requirements for the degree of Master's in Science

_____

Chair: Dr. Jie Han

_____

Dr. Robert L. Parsons

_____

Dr. Steven D. Schrock

Date Defended: 09 December 2016

The thesis committee for Wessam Khaled Mohammed certifies that
this is the approved version of the following thesis:

FACTORS INFLUENCING PERFORMANCE OF A LATERALLY LOADED PILE WITHIN AN MSE WALL SYSTEM

_____

Chair: Dr. Jie Han

_____

Dr. Robert L. Parsons

_____

Dr. Steven D. Schrock

Date Approved:

Acknowledgment

Throughout my three academic years at the University of Kansas, I have blessed with many people who supported and guided me to finish my Master's degree in civil engineering. These people not only affected my academic life but also change my social and personal life. I consider my advisor, Prof. Jie Han, one of them and also an ideal of how a professor should be. Thus, I would like to appreciate his advices and encouragement during my study and his acceptance of me as a member in the University of Kansas Geotechnical Society (KUGS). Furthermore, I would like to thank Prof. Robert L. Parsons for his guidance and advice and Prof. Steven D. Schrock for his serving as a member in my graduate committee.

My deep appreciation is forwarded to my sponsor, the Higher Committee for Education Development in Iraq (HCED), for its financial support to achieve my Master's degree. Also, I would like to give my thanks and appreciation to all members of KUGS for their help and support to complete my research. Moreover, I would like to thank the technicians of the Civil, Environmental, and Architectural Engineering Department of the University of Kansas for their help with the test box of my research. Finally, this degree would not have been achieved without the support and encouragement of my family, especially my dear wife who shared many obstacles with me during the three years of study in the United States.

Table of Contents

Abstract

Mechanically stabilized earth (MSE) walls have been wildly used in various important infrastructures, such as bridge abutments. The need for a shallow or deep foundation in an MSE wall for bridge support has been increasing. Different types of piles are used for this purpose, but the effect of their location within the MSE wall system is not fully investigated. In fact, there are no accepted design methods or procedures for piles in MSE walls. So far, limited full-scale studies have been conducted to evaluate the behavior of a laterally loaded pile within an MSE wall. In this study, the factors influencing performance of laterally loaded piles in MSE walls were investigated in the laboratory using reduced-scale models.

Eighteen model tests were conducted in this study. The influence factors investigated in this study included pile offset, wall height, reinforcement length and spacing, and geogrid-wall facing connection. Three pile offset distances were chosen: 127, 254, and 381 mm. Two wall heights of 450 and 720 mm were considered. The regular reinforcement length was equal to 315 mm for low wall tests while that was 504 m for the high wall tests. In addition, a long reinforcement length of 900 mm was considered. Moreover, two reinforcement spacing of 90 and 135 mm were used. Finally, mechanical connection and frictional connection were used in this study.

In order to investigate the effect of the pile offset, the model tests were designed in three groups. Group 1 had three tests with low walls, three different pile offsets, regular reinforcement length, small reinforcement spacing, and mechanical connection between wall facing and geogrid. Group 2 includes three categories. Category 1 of Group 2 had three tests with high walls, three different pile offsets, regular reinforcement length, large reinforcement spacing, and mechanical connection. Category 2 of Group 2 had three tests with high walls, three different pile offsets, regular reinforcement length, small reinforcement spacing, and mechanical connection. Category

3 of Group 2 had three tests with high walls, three different pile offsets, regular reinforcement length, small reinforcement spacing, and frictional connection between geogrid and wall facing. Group 3 also includes three categories. Category 1 of Group 3 had two tests with high walls, two large pile offsets, long reinforcement length, large reinforcement spacing, and mechanical connection. Category 2 of Group 3 had two tests with high walls and two large pile offsets, long reinforcement length, small reinforcement spacing, and mechanical connection. Category 3 of Group 3 had two tests with high walls, two large pile offsets, long reinforcement length, small reinforcement spacing, and frictional connection.

In addition, eighteen tests of this study were grouped into eight comparison sets to investigate the effects of wall height, reinforcement length and spacing, and geogrid-wall facing wall connection. Each set had two or three tests with different pile offsets. In addition to the change of pile offset, each set had one factor varied to investigate its effect.

The study results and comparisons show that the increase of the pile offset reduced the lateral deflections of the pile and the lateral deflections of wall facing along the vertical centerline. The increase of the wall height and the reinforcement length increased the pile capacity and reduced the lateral deflections of wall facing along the vertical centerline. The increase of the reinforcement spacing reduced the pile capacity and increased the lateral deflections of wall facing along the vertical centerline. The change of the geogrid-wall connection from fictional connection to mechanical connection increased the capacity of the pile especially for the long reinforcement tests. The pressure behind the upper part of the wall facing increased by the decrease of the pile offset while the pressure behind the lower part of the wall facing increased by the reduce of the reinforcement length. Finally, pile location within the maximum tensile zone of the geogrid layer is a critical factor that affects the geogrid strain.

Table of Figures

List of tables

Chapter 1 Introduction

Mechanically stabilized earth (MSE) walls have been widely used in the recent decades for highway and railway applications, such as bridge abutments and embankments. The cost-effectiveness, good performance, and flexibility are the main reasons for the use of this type of retaining wall instead of concrete walls. The basic principle of MSE walls is soil reinforcement. This principle was applied to construct the first MSE wall in the early 1960s by the French architect, Henri Vidal. His work has opened the door for the use of soil reinforcement in different earth structures.

In the United State, more than 8,000 walls have been built since the first reinforced retaining wall was constructed on California State Highway 39 in 1972 (Elias et al. 2001). In addition, 37 countries around the world have built more than 23,000 reinforced earth structures during the same period (Elias et al. 2001). Currently, more than half of retaining walls that are used for transportation applications are built as MSE walls in the United States (Elias et al. 2001). The MSE walls have been used in almost every state in the United States, especially in the largest road construction states, such as Georgia, Florida, Texas, Pennsylvania, New York, and California (Elias et al. 2001).

To understand the reason behind the popularity of the MSE wall, the benefits of using this type of retaining walls should be explained. The construction of the MSE wall requires less time, equipment, professional labor, space for construction operation. Therefore, it is considered as a cost-effective retaining wall. Moreover, MSE walls allow more deformation without failure, which is an important feature, especially when foundation soil is poor. MSE walls have been used for heights more than 25 meters. As a result, MSE walls have become an important option

for earth structure projects. On the other hand, the use of different soil in backfill may cause increasing in the cost because it will be changed with a high-quality fill. To maintain the function of reinforcement in soil, the reinforcement should be preserved from destructive conditions, such as corrosion of steel reinforcement, deterioration of geosynthetics, and degradation of polymer reinforcement. Furthermore, MSE walls have been increasingly used to support shallow and deep foundations, such as piles. However, there are no well-developed design method and specifications (Elias et al. 2001).

The objective of this study was to investigate the effect of different influence factors on the performance of laterally loaded piles within the MSE wall system. In this study, the factors, such as wall height, reinforcement length, reinforcement spacing, and connection type were changed at three pile offsets to find their effects on the performance of the laterally-loaded piles in the MSE wall system. After eighteen reduced-scale model tests were conducted, the test data were organized into three groups, depending on the wall height and the reinforcement length. Then, the test data were analyzed in eight sets that were classified based on the wall geometry, the reinforcement parameters, and the connection type.

The thesis has six chapters. The first chapter includes a brief introduction of this study. Chapter 2 reviews past research and studies about MSE walls, piles, their applications, and field and numerical studies of laterally-loaded piles in MSE walls. Chapter 3 presents material properties, equipment and instrumentation, test preparation, loading steps, and test designation. Chapter 4 presents the test data obtained in this study. Chapter 5 presents analysis of test data in terms of eight sets. Finally, the conclusions and recommendation are provided in Chapter 6.

Chapter 2 Literature Review

2.1. Introduction

Even though there is no design method available for a laterally loaded pile behind a mechanically stabilized earth (MSE) wall so far, design methods for the MSE wall and the laterally loaded pile in the soil are available in the literature and will be reviewed in this chapter. Moreover, this chapter will review several full-scale tests and numerical studies about laterally loaded piles behind MSE walls.

2.2. MSE wall (FHWA 2001)

MSE wall is a unique type of retaining walls that maintain its stability by using soil reinforcement. Unlike the concrete retaining wall, MSE wall is a soil retaining system that consists of different materials or parts. In general, the construction cost of MSE walls is lower than that of other types of retaining walls. MSE walls can be used for various earth structure applications, such as embankments, excavation, and bridge abutments.

2.2.1. System of MSE wall

The system of the MSE wall contains three essential parts as shown in .The first part is the backfill that mostly consists of free-draining granular soils with high friction angle to have high friction resistance with the reinforcement.

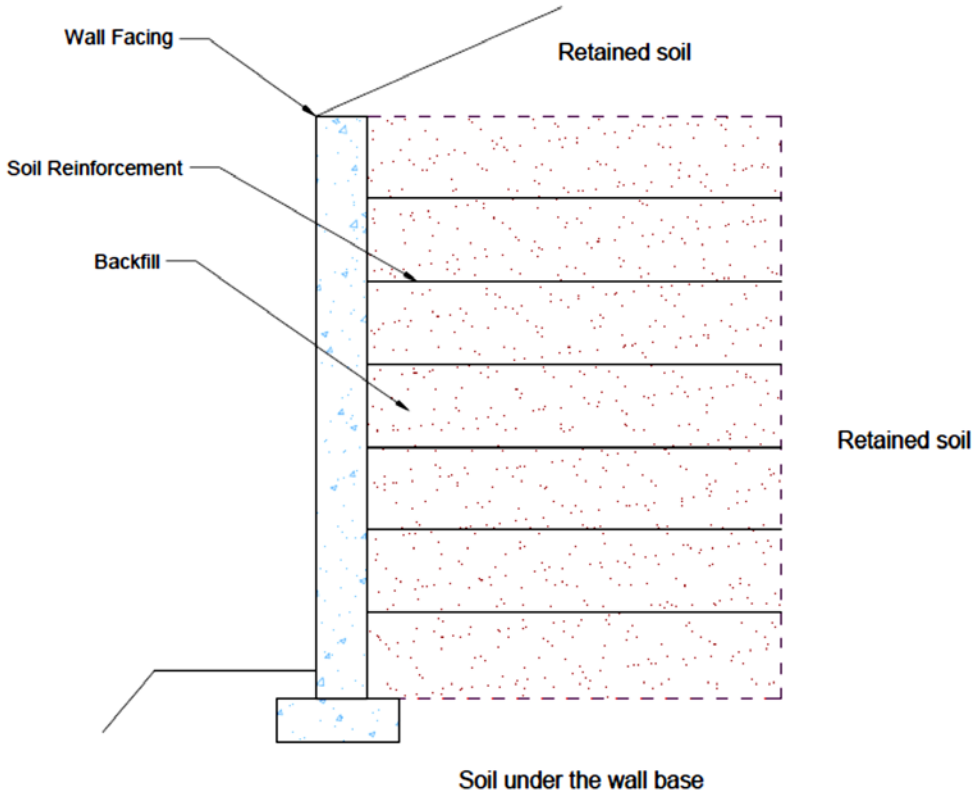

Figure 2.1 MSE wall Components.

Another part of the MSE wall is the reinforcement that is located inside the retained backfill. It is connected to the wall facing from one end and embedded in the retained soil from the other. Different types of soil reinforcements can be used in MSE wall systems, such as ribbed steel strips, steel wire meshes, and geosynthetics. These reinforcements are classified as inextensible and extensible reinforcements. The function of the reinforcement is to ensure the internal stability of the MSE wall by providing a suitable pullout or tensile resistance. The pullout resistance results from the friction on its surface (for the inextensible and extensible reinforcements) and/or the passive force at its ribs (for the inextensible reinforcements only) as shown in Figure 2.2

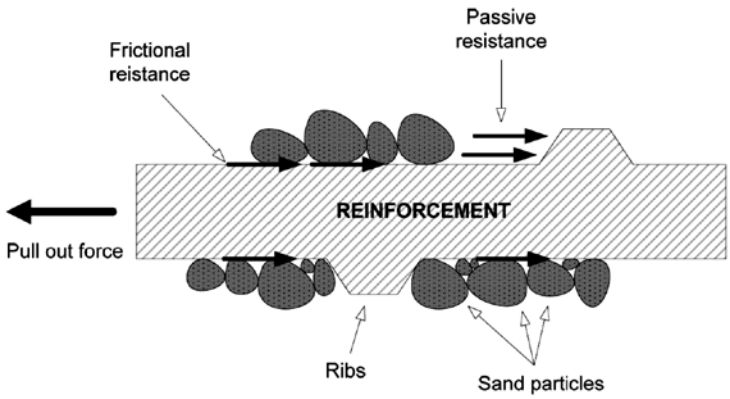

Figure 2.2 Stress transfer mechanisms in MSE wall reinforcement (FHWA 2007)

The last part of the MSE wall system is the facing. It is required to prevent the backfill from penetration out of the wall system through the reinforcement. Facing elements can be divided into different types, such as segmental precast concrete panels, dry cast modular block wall (MBW) units, welded wire grids, gabion, geosynthetic, and postconstruction facing.

2.2.2. Design of MSE wall

There are three essential design considerations for MSE walls. The first consideration is the evaluation of the internal stability of the retaining wall. This stability is affected by the capability of the reinforcement of the MSE wall to resist the friction and passive stresses that were induced within the MSE wall system. In fact, the pullout and maximum tensile forces in the reinforcement should be lower than its pullout capacity and tensile strength, respectively to ensure the internal stability.

External stability is the stability of the reinforced mass treated as a rigid body subjected to external forces. External stability is usually considered for all types of retaining walls. The possible failure modes for external stability include overturning, sliding, and bearing failure.

Finally, there is a compound failure mode, which usually passes through the MSE wall reinforced zone and retained soil behind the reinforced zone. The failure surfaces corresponding to internal, external, and compound stability are shown in Figure 2.3. The factor of safety against each failure mode should be calculated and less than that required for a project.

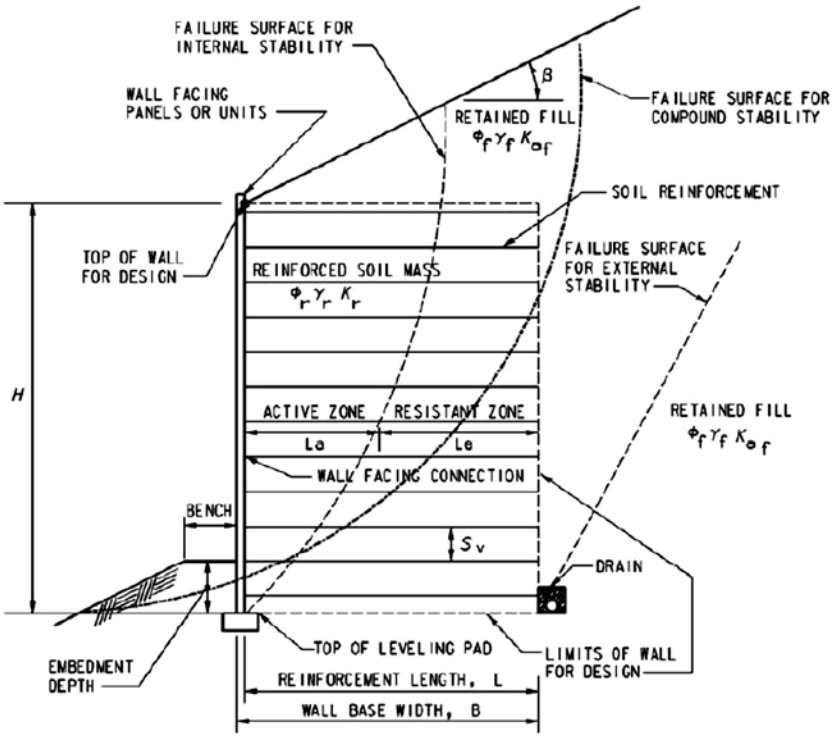

Figure 2.3 MSE wall system and failure surfaces (AASHTO 2012)

2.2.3. Construction of MSE wall

The construction of the MSE wall is simple and does not require professional equipment and labor. The construction procedure mainly depends on the facing elements to construct MSE wall with rigid facing, rigid materials should be considered such as precast panels and concrete

blocks. On the other hand, to construct MSE wall with flexible facing, flexible materials should be used such as wire mesh and geosynthetics.

2.3. Behavior of pile in cohesionless soil

In order to find the capacity of a laterally loaded pile within an MSE wall system, two-dimensional and three-dimensional behavior of a laterally loaded pile within cohesionless soil should be examined.

2.3.1. Two-dimensional behavior of pile in cohesionless soil

This behavior has been analyzed using two major procedures. The first procedure considers the subgrade reaction of the soil in its calculations, and the other procedure uses the elastic continuum theory (Poulos 1971). The methods that use the coefficient of subgrade reaction have been explained briefly herein.

Broms (1964) studied the behavior of a pile in cohesionless soil by setting a comparison between calculated results and measured data from laboratory tests. He used the coefficient of subgrade reaction in his equations and assumed that this coefficient increases linearly with the overburden depth. Broms (1964) considered the ultimate lateral resistance of the soil is three times the Rankine passive pressure. Also, he considered that the failure occurs when the lateral pressure reaches the ultimate lateral soil resistance or when the maximum moment in the pile reaches the yield capacity of the pile cross section.

Brom's objective was to determine both the lateral deflection of the pile and the ultimate resistance of the soil to lateral loading. In addition, he studied the distribution of the moment along the pile under the lateral load and provided equations for the maximum positive and negative moments. However, Brom (1964) divided piles into long and short piles with restrained and free head. Because the model piles used in this study are considered as short free-headed

piles, only this type of piles will be briefly discussed herein.

While a lateral load is applied, a short free-headed pile will deflect around a particular point near to its base. Broms (1964) called that position as the center of rotation. The maximum soil resistance is located at this center of rotation as shown in Figure 2.4. Furthermore, the part of the pile above the center of rotation is usually deflected more than the part below the center of rotation. Using the coefficient of subgrade reaction, Broms (1964) provided Equation 2.1 to determine the lateral deflection of the upper end of the pile.

$$y_0 = \frac{18\,P\,(1 + 1.33\,\frac{e}{L})}{L^2\,n_h} \qquad 2.1$$

where y_0 = lateral deflection of the pile (ft); P = lateral load (ton); e = eccentricity (ft); L = length of embedment (ft); and n_h = Terzaghi's coefficiant of subgrad reaction ($\frac{ton}{ft^3}$).

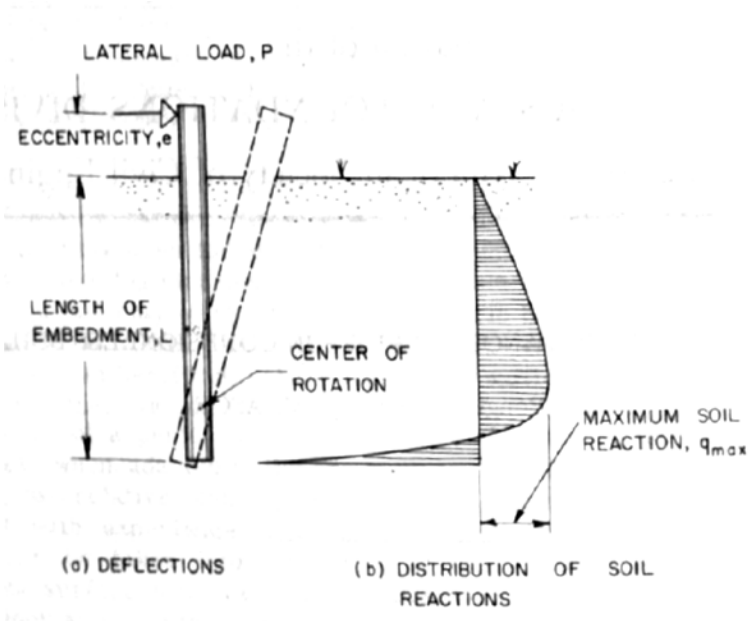

Figure 2.4 Deflection and ultimate soil resistance of a short free headed pile at failure (Broms 1964)

Broms (1964) illustrated that while the lateral loading is applied on the pile, two pressure zones will be created. These pressure zones are a passive zone in the front and an active zone in the back of the pile, and they can be calculated by using Rankine's earth pressure theory. Based on the previous studies, Broms (1964) considered the maximum lateral pressure is equal to three times the Rankine passive pressure as shown in Figure 2.5. Then, he calculated the driving and resistance moments around the center of rotation of the pile. Finally, the lateral load at failure was determined in Equation 2.2 by assuming the driving moment equal to the resistance moment at failure and the force (R) equal to zero.

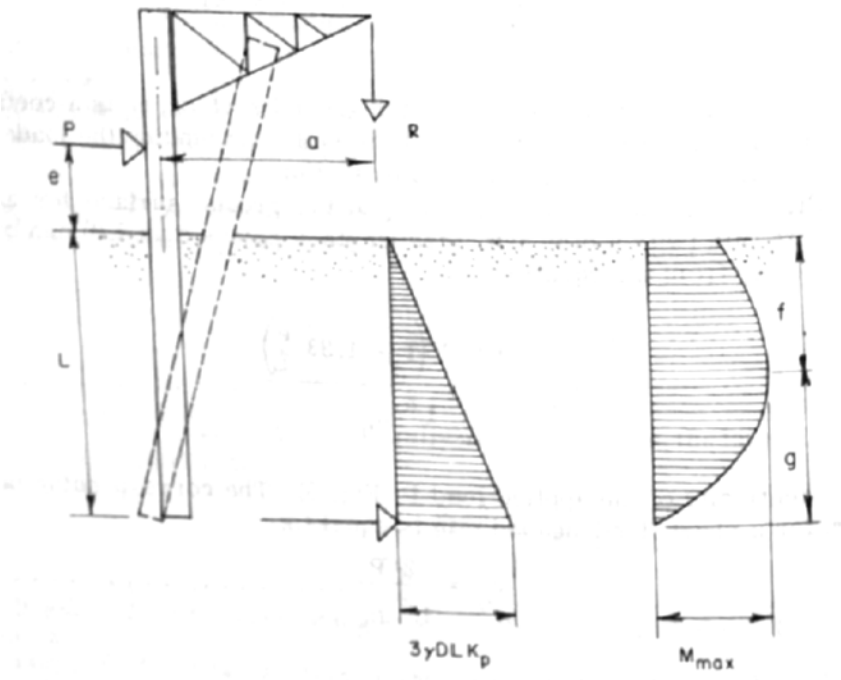

Figure 2.5 lateral pressure and moment distributions of a short free headed pile at failure (Broms 1964).

$$P = \frac{0.5\ \gamma\ D\ L^3\ K_p}{(e + L)} \qquad 2.2$$

where P = lateral load (ton); e = eccentricity (ft); D = pile diameter (ft); ϒ= soil unit weight ($\frac{lb}{ft^3}$); L = length of embedment (ft); K_P = coefficiant of passive lateral earth pressure from Rinkine's theory.

On the other hand, from the moment distribution of the short free-headed pile in Figure 2.5, the maximum positive moment is located at depth (f) from the ground surface. To find this maximum moment, the depth (f) should be determined from the lateral pressure distribution. In the case of the free-headed pile, the moment distribution mainly depends on the ultimate or yield resistance of the pile section, shear strength, and deformation features of the cohesionless soil.

Two other equations were used to obtain the ultimate resistance of the cohesionless soil to a laterally loaded pile by considering the coefficient of subgrade reaction. The first equation was presented by Hansen and Christensen (1961) while the other was provided by Fleming (1992). Hansen and Christen (1961) considered the Hansen Earth Pressure Coefficient (K_q), which depends on the friction angle of the sand, as the coefficient of the subgrade reaction as shown in Equation 2.3. On the other hand, Fleming (1992) assumed the coefficient is equal to the square of the coefficient of the passive earth pressure as shown in Equation 2.4.

$$Pu = K_q \Upsilon D Z \qquad 2.3$$

$$Pu = K_p{}^2 \Upsilon D Z \qquad 2.4$$

where Z = depth from the ground surface.

Han and Frost (2000) provide a solution for the load-deflection response of transversely isotropic piles under lateral loads by assuming a pinned boundary condition as shown in Figure

2.6. They obtained their solution based on the Timoshenko Beam Theory and considered the effect of shear deformation.

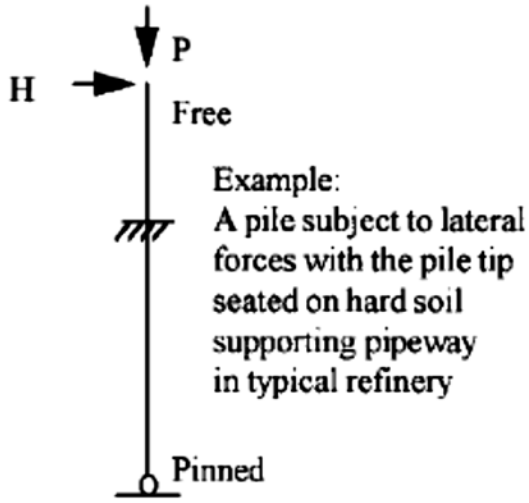

Figure 2.6 Pinned boundary condition for laterally loaded pile (Han and Frost 2000).

Even though the pile material in this study is aluminum, which is an isotropic material, the solution developed by Han and Frost (200) can be still used for analysis. The load-deflection response without considering the shear deformation effect can be expressed as Equation 2.4.

$$w = \frac{B_0 Z}{L} + \sum_{M=1}^{N} B_M \sin\frac{M\pi}{L} Z \qquad 2.4$$

where, w = Lateral dfelection; L = Length of the pile; Z = depth to the required deflection. Both matrices B_0 and B_m can be found from the matrices form in Equations 2.5 and 2.6, respectively. In order to find the matrices B_0 and B_m in these two equations, Table 2.1 should be used to assemble the matrices G_0, G_M, H_0, H_M.

$$G_0\, B_0 = H_0 \qquad 2.5$$

$$G_M\, B_M = H_M \qquad 2.6$$

Table 2.1 Deflection function and matrices G and H for pinned free head pile (Han and Frost 2000).

Boundary condition	Deflection function	$G_{gg}/G_{gm}/H_g$ $(g, m = 1, \ldots, N, g \neq m)$
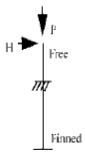	$w = \frac{B_0 z}{L} + \sum_{m=1}^{N} B_m \sin\frac{m\pi}{L} z$	$G_{00} = q^*\left(\frac{1}{12}e^4\right) - P^*$
	$\theta_b = -\frac{B_0}{L} + \sum_{m=1}^{N} \xi_m B_m \cos\frac{m\pi}{L} z$	$G_{0m} = q^*\left[-\frac{e}{m^2\pi^2}\sin m\pi e - \frac{2}{m^3\pi^3}(\cos m\pi e - 1)\right]$
		$G_{g0} = \frac{1}{2g\pi} q^*\,[-g\pi e \sin g\pi e - 2(\cos g\pi e - 1)] - \frac{1}{2} g^2\pi^2 P^*$
		$G_{gg} = \frac{1}{2}\frac{g^4\pi^2\lambda^2}{g^2\pi^2+\lambda^2} + \frac{1}{8g^2\pi^2} q^*\,[2g^2\pi^2e^2 + \cos 2g\pi e - 1] - \frac{1}{2} g^2\pi^2 P^*$
		$G_{gm} = \frac{1}{2} q^*\left[-\frac{1}{(m-g)^2\pi^2}[\cos(m-g)\pi e - 1] + \frac{1}{(m+g)^2\pi^2}[\cos(m+g)\pi e - 1]\right]$
		$H_0 = H^*L$ and $H_g = 0$

In Table 2.1, λ is the shear effect coefficient, P^* is the normalized vertical load, H^* is the normalized lateral load, q^* is the normalized soil resistance load, and e is the embedment ratio.

$$\lambda = \sqrt{\frac{G_{XZ}\, k\, A\, L^2}{E_{ZZ}\, I_{yy}}}, \qquad P^* = \frac{P\, L^2}{\pi^2\, E_{ZZ}\, I_{yy}}, \qquad H^* = \frac{H\, L^2}{\pi^2\, E_{ZZ}\, I_{yy}}, \qquad q^* = \frac{\eta\, L^2}{\pi^2\, E_{ZZ}\, I_{yy}}$$

where E_{ZZ} = longitudinal modulus; G_{XZ} = in-plane shear modulus; I_{yy} = moment of inertia about y axis; k= shear coefficient; A = cross sectional area; P= vertical load; H = horizontal load; and η = the constant of subgrade reaction.

(Han and Frost) concluded that each one of these factors has an influence effect on the load-

deflection response of the pile. When the shear effect coefficient is relatively small, the lateral deflection of the pile decreases by increasing the shear effect coefficient. On the other hand, the vertical load has a significant impact on the lateral deflection of the pile. In fact, The lateral deflection exponentially increases when the vertical load increases and reach a critical load. For the lateral load, it has a linear relationship with the lateral deflection of the pile, and this relationship is due to the assumption of a linear pile-soil system. The mode of deflection of the laterally loaded pile will be changed from rigid pile rotation to flexible pile bending by the increasing of the lateral soil resistance to a significantly large value. Logically, when the embedment length of the pile is high, the soil around the pile will provide more resistance to the lateral movement. Therefore, the deflection of the laterally loaded pile will be decreased by increasing the embedment ratio.

2.3.2. Three–dimensional behavior of pile in cohesionless soil

Reese et al. (2006) studied the three-dimensional behavior of the cohesive soil under a laterally loaded pile. They not only obtained the ultimate resistance of the soil at the ground surface but also determined the ultimate resistance at different depth of the soil. In order to achieve their goal to find the ultimate resistance, Reese et al. (2006) considered two models that correspond to the required positions of the ultimate resistance as mention early.

For the first model, they considered that the lateral load acting on the pile might develop a failure wedge inside the cohesionless soil in front of the pile as shown in Figure 2.7 Failure wedge of a laterally loaded pile in cohesionless soil: (a) planes and characteristics of the failure wedge, (b) forces acting on the wedge, and (c) forces acting on the pile (Reese et al. 2006).a. This wedge was analyzed to obtain all the forces acting on its faces in addition to the passive force F_b as shown in Figure 2.7 b. After finding the active force F_a by the Rankine theory, its

value will be subtracted from the value of F_b in order to find the total force F_{bt} as shown in Figure 2.7c . Finally, Equation 2.8 represents the ultimate soil resistance $(P_u)_{sa}$, and it can be estimated by differentiating the formula of F_{bt} respect to H.

$$(P_u)_{sa} = \gamma H \left[\frac{k_0 H \tan\phi \tan\beta}{\tan(\beta-\phi)\cos\alpha} + \frac{\tan\beta}{\tan(\beta-\phi)} (b + H \tan\beta \tan\alpha) + k_0 H \tan\beta (\tan\phi \tan\beta - \tan\alpha) - k_a b \right] \quad 2.7$$

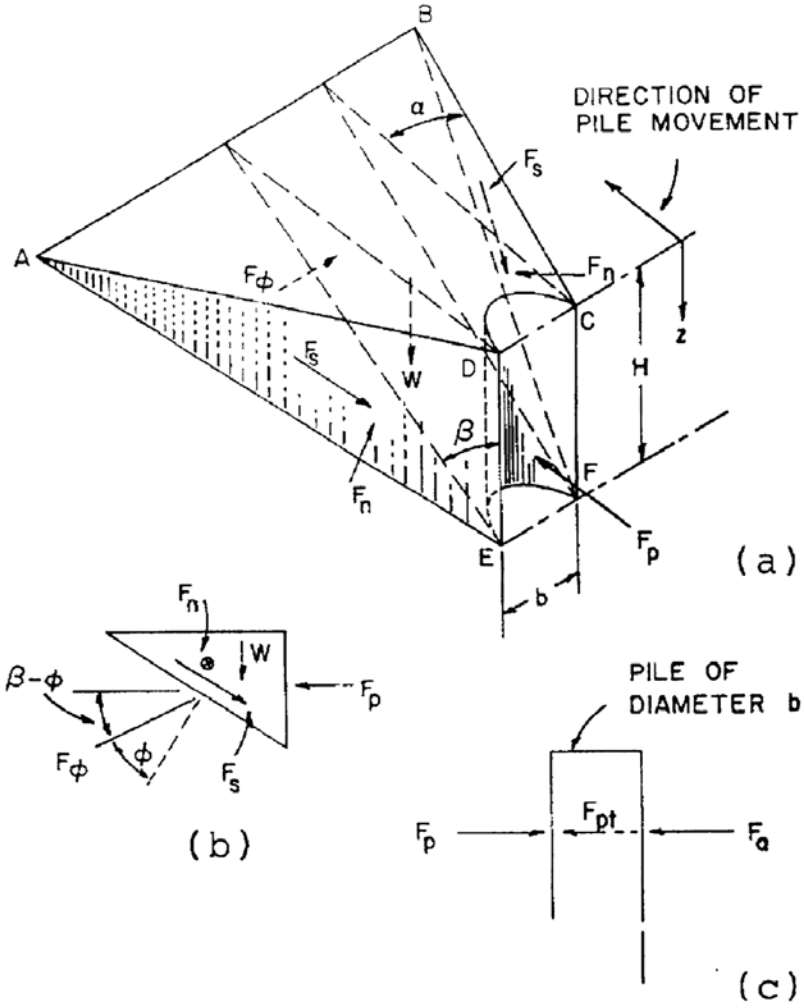

Figure 2.7 Failure wedge of a laterally loaded pile in cohesionless soil: (a) planes and characteristics of the failure wedge, (b) forces acting on the wedge, and (c) forces acting on the pile (Reese et al. 2006).

where ϕ = friction angle ; k_0 = coefficient of lateral earth pressure at rest; and k_A = minimum coefficient of active earth pressure.

The value of β is approximatively equal to (45+ϕ/2), and the value of k_A is equal to $tan^2(45 - \frac{\phi}{2})$. Furthermore, the magnitudes of α and k_0 are listed in Table 2.2 Values of α and K0 .

Table 2.2 Values of α and K_0

Parameter	Value for loos sand	Value for dense sand	Source
α	$\frac{\phi}{2}\ to\ \frac{\phi}{3}$	ϕ	(Bowman 1958)
k_0	0.6	0.4	(Sandvik and Sowers 1970)

On the other hand, to estimate the ultimate soil resistance at any point below the ground surface, a second model was considered as shown in Figure 2.8. This model required two significant assumptions based on the two-dimensional behavior. The magnitude of σ_1 is larger than the minimum active earth pressure. In addition, the states of the stress should be assumed as shown in Figure 2.8b. Equation 2.8 represents the ultimate soil resistance $(P_u)_{sb}$ according to the second model.

$$(P_u)_{sb} = k_a\ b\ \Upsilon H\ (tan^8\beta - 1) + \ k_0\ b\ \Upsilon H\ \tan\phi\ tan^4\beta \qquad 2.8$$

To obtain the ultimate soil resistance from Resse's solution, the lesser values from Equations 2.7 and 2.8 should be considered. However, Bogard and Matlock (1980) modified these two equations into more simple expressions. Each one of these new equations has factors that depend on the friction angle of the sand as shown in Equations 2.9 and 2.11.

$$(P_u)_{sa} = (C_1 Z + C_2 D)\ \Upsilon\ Z \qquad 2.9$$

$$(P_u)_{sb} = C_3 D\ \Upsilon\ Z \qquad 2.11$$

where $C_1, C_2\ and\ C_3$ = factors of Bogard and Matlock (1980).

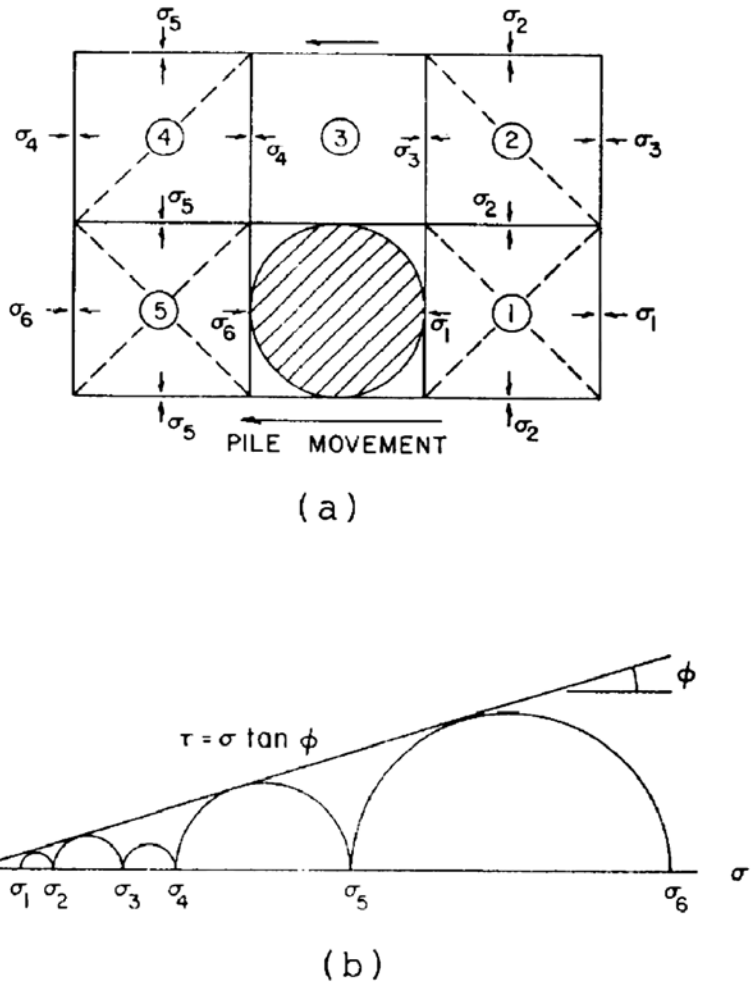

Figure 2.8 mode of soil failure at point below the ground surface: (a) pile section and surrounded stress and (b) Mohr-Coulomb diagram (Reese et al. 2006).

Another method was proposed by Briaud et al. (1983) to obtain the ultimate lateral resistance of cohesionless soils by considering F-y/Q-y mechanism as shown in Figure 2.9. In this solution, the ultimate lateral resistance (P_u) in Equation 2.12 is induced by both the frontal normal

reaction and the side friction reaction.

$$P_u = Q + F \qquad 2.11$$

where Q = net ultimate frontal normal soil resistance and F = net ultimate lateral shear drag.

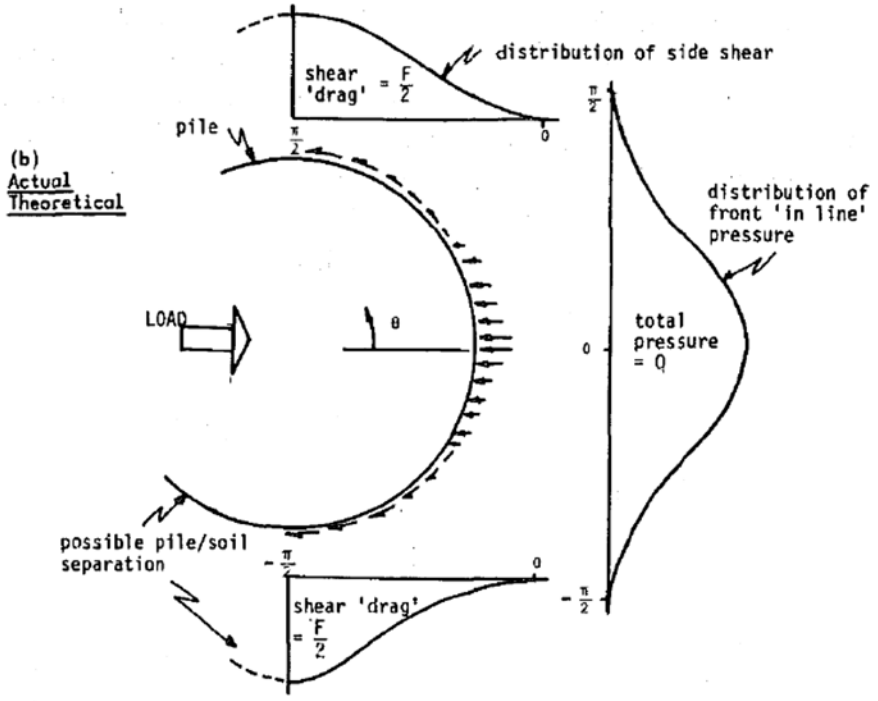

Figure 2.9 Frontal earth pressure and side friction around laterally loaded pile (Smith 1987).

The values of the net frontal normal soil resistance and net lateral shear drag can be determined from Equations 2.12 and 2.13 respectively. Special shape factors were used in these two expressions to obtain the two essential components. The first shape factor (η) is related to the nonuniform distribution of earth pressure in front of the pile while the other shape factor (ξ) is related to the nonuniform distribution of the lateral shear drag. The value of η was specified to be equal to 0.8 for a circular pile and 1.0 for a square pile. On the other hand, the value of ξ was

considered to be equal to 1.0 for a circular pile and 2.0 for a square pile (Briaud et al. 1983).

$$Q = \eta\, P_{max}\, D \qquad 2.12$$

$$F = \xi\, \tau_{max}\, D \qquad 2.13$$

In order to determine Q and F from the above eqution, P_{max} and τ_{max} should be estimated. Zhang et al. (2005) analyzed data from the published literature and proved that the equation of P_u by Fleming (1992) is the most appropriate equation for P_{max}. Moreover, they used the equation of ultimate vertical shear resistance by (API 1991) to find τ_{max}.

$$P_{max} = K_p{}^2 \Upsilon D Z \qquad 2.15$$

$$\tau_{max} = K \Upsilon Z \tan(\delta) \qquad 2.16$$

where the values of K and δ is provided by Kulhawy (1991); Kulhawy et al. (1983) and listed in Table 2.4 and 2.4 respectively.

Table 2.3 Values of K (Kulhawy 1991; Kulhawy et al. 1983)

Pile type and method of construction	K
Pile-jetted	$(0.5-0.7)K_0$
Pile-small displacement, driven	$(0.7-1.2)K_0$
Pile-large displacement, driven	$(1.0-2.0)K_0$
Drilled shaft-build using dry method with minimal sidewall disturbance and prompt concreting	$(0.9-1.0)K_0$
Drilled shaft-slurry construction with good workmanship	$(0.9-1.0)K_0$
Drilled shaft-slurry construction with poor workmanship	$(0.6-0.7)K_0$
Drilled shaft-casing method below water table	$(0.7-0.9)K_0$

Note: K_0=coefficient of lateral earth pressure at rest.

Table 2.4 Values of δ (Kulhawy 1991; Kulhawy et al. 1983)

Pile type	δ
Rough concrete	$1.0\phi'$
Smooth concrete (i.e., precast pile)	$(0.8-1.0)\phi'$
Rough steel (i.e., step-taper pile)	$(0.7-0.9)\phi'$
Smooth steel (i.e., pipe pile or *H* pile)	$(0.5-0.7)\phi'$
Wood (i.e., timber pile)	$(0.8-0.9)\phi'$
Drilled shaft built using dry method or with temporary casing and good construction techniques	$1.0\phi'$
Drilled shaft built with slurry method (higher values correspond to more careful construction methods)	$(0.8-1.0)\phi'$

(Zhang et al.) used the distribution of Prasad and Chari (1999) to calculate the ultimate lateral capacity of rigid piles for frontal and side shear resistances of cohesionless soil as shown in Figure 2.10. As a result, the total ultimate lateral capacity of rigid piles (H_u) can be determined from Equation 2.17.

$$H_u = 0.3\left(\eta\, {K_p}^2 + \xi\, K \tan(\delta)\right) Y\, a\, B\, (2.7\, a - 1.7\, L) \qquad 2.17$$

where $a = [-(0.567\mathrm{L} + 2.7e) + (5.307\, L^2 + 7.29\, e^2 + 10.54\, eL)^{0.5}\,]/2.1996$; e = eccentricity of loading; and B = D =the pile diameter.

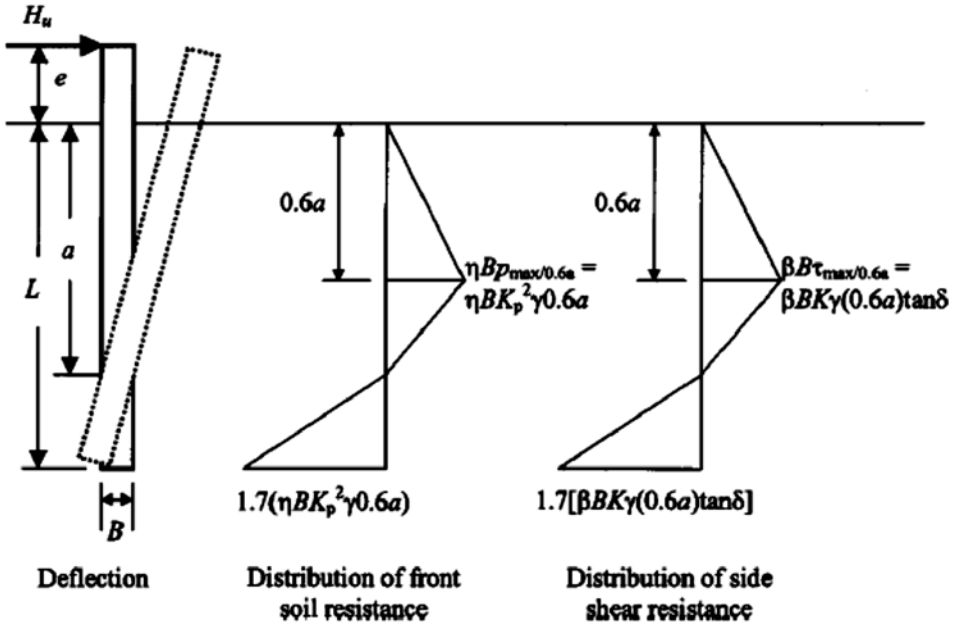

Figure 2.10 Distribution of the frontal and side shear (Zhang et al. 2005).

2.4. Pile within MSE wall system

2.4.1. Application

Even though pile construction behind an MSE wall system is not typical, it has been

increasingly used to support particular structures, such as sound walls, bill-boards, traffic signs, and bridge footings. The most important application of the piles behind the MSE wall is the mixed bridge abutment, and the piles are used to support the bridge seat as shown in Figure 2.11. Anderson and Brabant (2005) indicated that vertical and lateral loads are transmitted from the bridge seat through the piles. The vertical load is transmitted to the bed rock while the lateral load is transmitted to the fill of MSE wall. The reinforcement of the MSE wall usually resists the lateral load and prevents part of the load from reaching the wall facing. However, the use of mixed abutments in bridges has been increased in recent years in the United States because the owners and engineers are getting more experience and confidence in constructing this type of abutment.

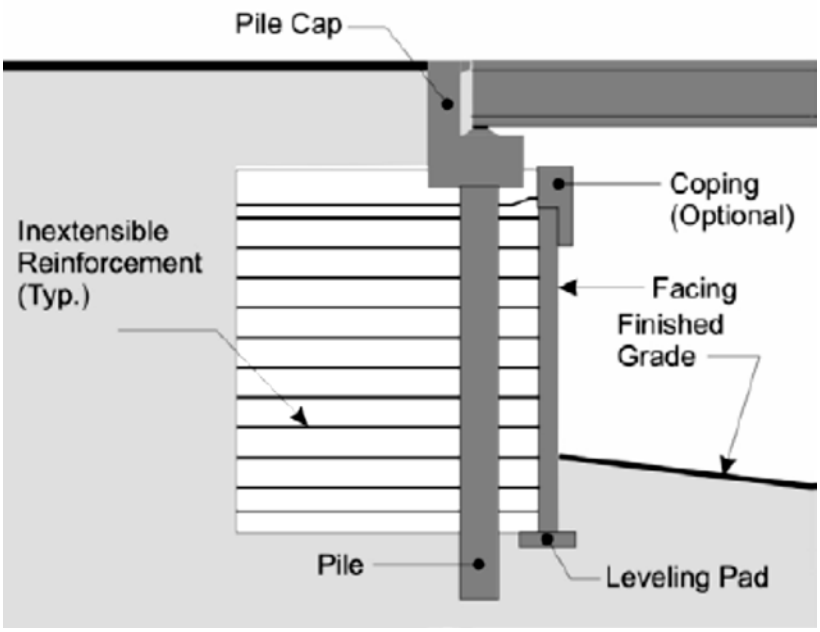

Figure 2.11 mixed abutment (Anderson and Brabant 2005)

2.4.2. Full–size model tests

There is no specified design procedure to follow in the mixed abutment. Therefore, several researchers have been motivated to conduct full-size tests to understand the behavior of the pile

and the MSE wall under lateral load.

A special technique of driving steel piles through the backfill and reinforcement of an MSE precast panel wall was investigated by (Berg et al. 2007) to identify its advantage over the regular approach. After the construction of 4.6 m high and 8.2 m long wall, four piles were driven into the backfill, and one of them was loaded to a certain pile deflection. The researchers concluded that there was no need for special equipment to drive through the reinforcement by using this technique. For facing panels, no excessive rotation, excessive lateral movement, or damage was noticed during the pile driving operation. Examination of the punched-drawn geogrid layers found no damage out of the pile location. Also, the strains of the reinforcement layers were less affected by the driving process.

The Kansas Department of Transportation constructed a six meter high MSE block wall according to the FHWA design and seven concrete piles behind this wall. Each pile had a diameter of 0.914 m behind the MSE block wall, and four of them were individually tested as shown in Figure 2.12. The other three piles were tested as group piles under the lateral load. Pierson et al. (2009) from the University of Kansas studied the capacity and deflection of these laterally loaded piles. From the measured deflection data, the researchers summarized preliminary design load values as shown in Table 2.5 at the corresponding pile deflections and Table 2.6 at the corresponding wall deflections.

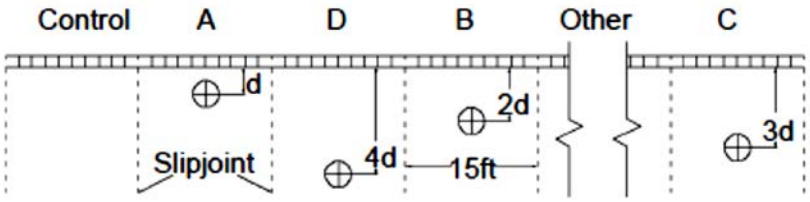

Figure 2.12 Test section (plain view) of the four indivdual piles (Pierson et al. 2009)

Lateral pile loading tests were conducted based on the pile deflections. Therefore, three loads were recorded for each deflection increment during the test. The first load was the peak load, which was recorded after reaching the required displacement. The second load was the residual load at 2.5 min after recording the peak load. The third load was the final load that was recorded before the next loading step.

Table 2.5 Load Versus pils displacement (Pierson et al.

Shaft	Distance from Facing (in.)	Displacement (in.)					
		0.5	0.75	1	2	4	Ultimate
Peak Load (kip)							
A	36	—	14	15	23	32	34
B	72	40	47	50	62	77	90
C	108	39	44	50	66	87	116
D	144	—	—	55	81	120	194
Final Load (kip)							
A	36	5.3	5.3	8	17	27	27
B	72	36	40	44	55	69	75
C	108	34	39	44	58	76	102
D	144	—	—	50	74	110	171

Table 2.6 Load Versus wall displacement(Pierson et al. 2009)

Shaft	Distance from Facing (in.)	Maximum Wall Displacement (in.)					
		0.5	0.75	1	2	4	Ultimate
Peak Load (kip)							
A	36	12	15	18	26	33	33
B	72	48	54	58	70	87	90
C	108	50	55	60	80	98	116
D	144	77	88	99	134	182	194
Final Load (kip)							
A	36	8	10	15	22	—	27
B	72	43	48	50	61	75	76
C	108	43	49	52	69	90	102
D	144	78	82	90	122	166	171

Pierson et al. (2009) concluded that an increase of the distance between the wall facing and the pile increased the lateral pile capacity and the width of the influence of the lateral load. In addition, pile group effect was noticed in the pile group test. The deflection of the wall had a slight effect on the aesthetics of the block wall.

In order to investigate the group effect of piles within an MSE wall system, Pierson et al. (2010) conducted a test on three lateral loaded piles at a distance equal to twice the diameter of a single pile by using the hydraulic system as shown in Figure 2.13. They indicated that the group effect caused a reduction in individual pile capacity. To estimate the reduction of pile capacity, two important parameters should be determined: the pile center-to-center distance (S_s) and the width of influence. The minimum pile to pile spacing to avoid side-by-side group effect ($W_{influence}$) depends on the distance between the pile and the back facing of the wall (D_w), and can be determined using Equation 2.18.

$$W_{influence} = 1.62\, D_w + 15 \qquad 2.18$$

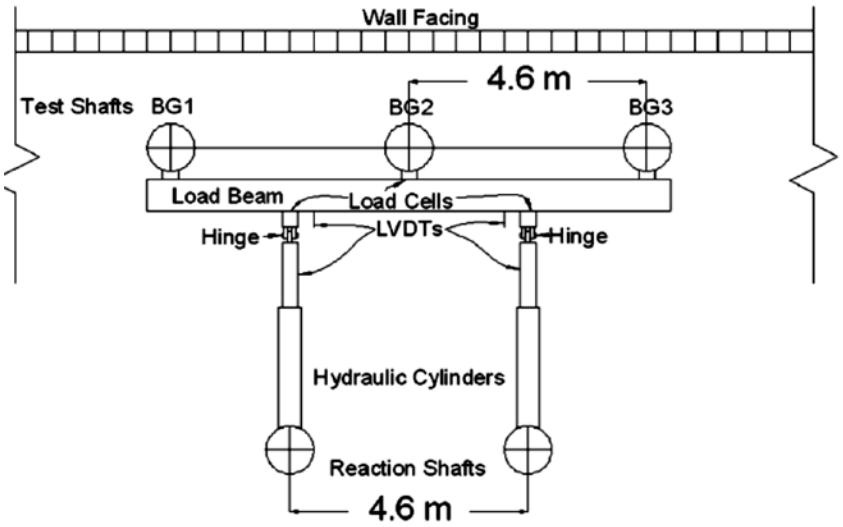

Figure 2.13 Schematic of pile group loading (Pierson et al. 2010)

The behavior of a laterally loaded pile and the width of influence are shown in Figure 2.14. This behavior is a result of the resistance of both the wall fill and the uniaxial reinforcement. This behavior can be represented with three zones: a high compression zone in front of the pile, low compression zone behind the wall facing, and two transition shear zones that extend from the two sides of the pile (Pierson et al. 2010).

After determining the width of influence, the reduction factor (η) can be found by using Equation 2.19. As a result, the reduced capacity of a pile due the group effect (P_{group}) can be estimated from Equation 2.20.

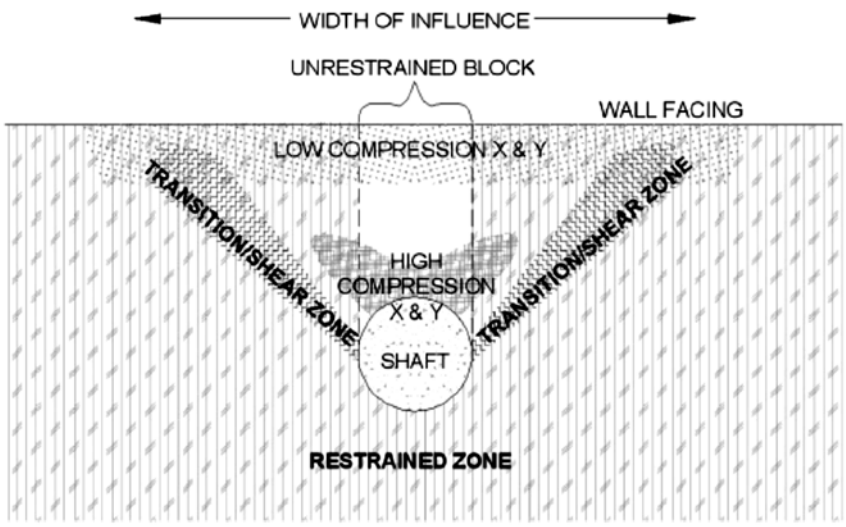

Figure 2.14 Schematic of the behavior of a latrerally loaded pile within an MSE wall (Pierson et al. 2010)

$$\eta = S_s/W_{influence} \quad (2.19)$$

$$P_{group} = \eta * P_{single} \quad (2.20)$$

In general, when the pile is laterally loaded, lateral resistance will be induced. Part of this resistance is due to the reinforcement of the MSE wall. In fact, by increasing the pullout capacity of the reinforcement, the lateral resistance to the lateral load will be increased. Rollins et al. (2011) considered the reinforcement effect on the lateral resistance by conducting a full-scale test on two piles of 0.324 m in diameter behind a 5.9 m high MSE wall. They studied the effect of the pile offset from the wall on the lateral resistance of the pile and the induced forces inside the MSE reinforcements. Thus, two pile offsets from the wall were considered in this study. The small offset was equal to 3.8 pile diameter, and the large offset was equal to 7.3 pile diameter. In order to increase the pullout capacity of the reinforcements, the length of each steel bar of the reinforcement was increased to 1.6 wall height (H) instead of the regular length of 0.7H for the

static load and 1.2H for the seismic load.

Pierson et al. (2009) found that the decrease of the pile offset from the wall reduced the lateral resistance of the pile. However, (Rollins et al.) suggested that this behavior is not applicable for all the MSE wall reinforcement lengths. In fact, for reinforcement length equal or greater than 1.6H, the effect of pile offset from the wall may be neglected as shown in Figure 2.15. This conclusion is extremely beneficial to reduce the cost of construction because the option of increasing the number of piles near to the wall or placement of piles far from the wall will not be considered.

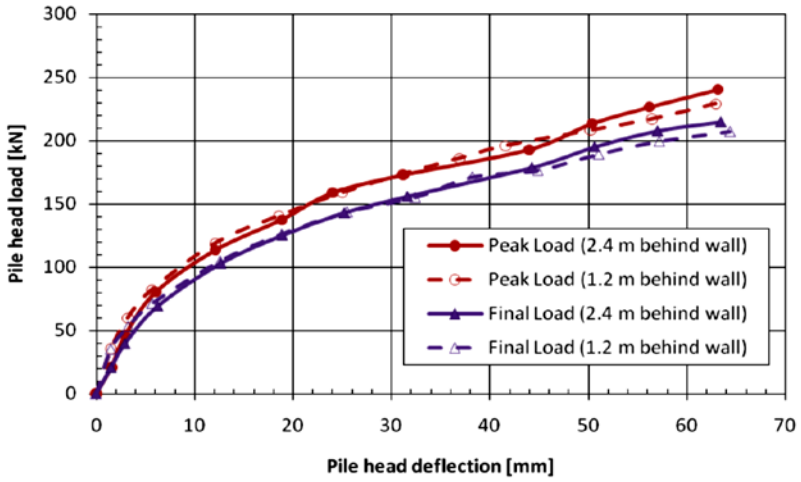

Figure 2.15 Pile head load vs head deflection at the peak and final load with different pile offset (Rollins et al. 2011)

In addition, the forces in two reinforcement layers in each test were measured and analyzed to understand their behavior. Rollins et al. (2011) concluded that the reinforcement forces at the pile offset of 3.8 pile diameter were twice higher than the reinforcement forces at the pile offset of 7.3 pile diameter. Moreover, the forces at each offset were decreased by the increase of the distance from the wall due to the friction or load transfer between the reinforcement and the

backfill soil.

Several full-scale studies used the LPILE program and the function of P-multiplier of 1 to identify the minimum pile offset required to neglect the wall effect on the pile resistance. Each one of the studies summarized below provided a plot of the P-multiplier vs. the normalized pile offset, which is the distance from the back of the wall facing to the center of the pile, to find the P-multiplier of 1 at the specified reinforcement length (L) to wall height (H) ratios.

Price (2012) investigated five piles with welded wire grid and suggested that the normalized spacing should be at least 3.8 and 5.2 pile diameter in order to obtain the P-multiplier of 1 for the L/H ratios of 1.6 and 1.1 respectively. Nelson (2013) conducted another study to investigate four piles with galvanized ribbed metal strips. He added a suggestion to the study of (Price 2012) that the minimum normalized pile offset should be equal to 4.5 to ensure the P-multiplier of 1 for the L/H ratio of 1.2. Figure 2.16 represents the results from both the Price (2012) and Nelson (2013) studies at the L/H ratios of 1.1, 1.2, and 1.6.

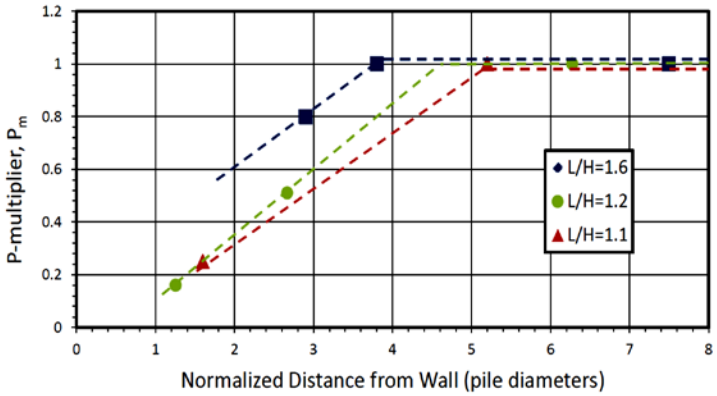

Figure 2.16 P-multiplier vs normilized distance at two L/H ratios of 1.1D and 1.6D from Price (2012) and one L/H ratio of 1.2D from (Nelson 2013)

Rollins et al. (2013) modified the results from the previous two studies by taking the equivalent height of the wall due to the surcharge. Thus, the L/H ratios were reduced and the P-

multiplier plot was modified as shown in Figure 2.17. From this plot, they indicated that the minimum pile offset to ensure P-multiplier of 1 is equal to 3.8 pile diameter without considering the effect of the L/H ratio. Moreover, Rollins et al. (2013) provided a plot between the normalized maximum induced force in the reinforcement and the normalized distance from the pile to the reinforcement for both of the grid and strip reinforcements in the Price (2012) and Nelson (2013) studies as shown in Figure 2.18 and Figure 2.19. However, the normalized induced forces in these two curves were increased by increasing the pile offset from the wall facing for both types of the reinforcement.

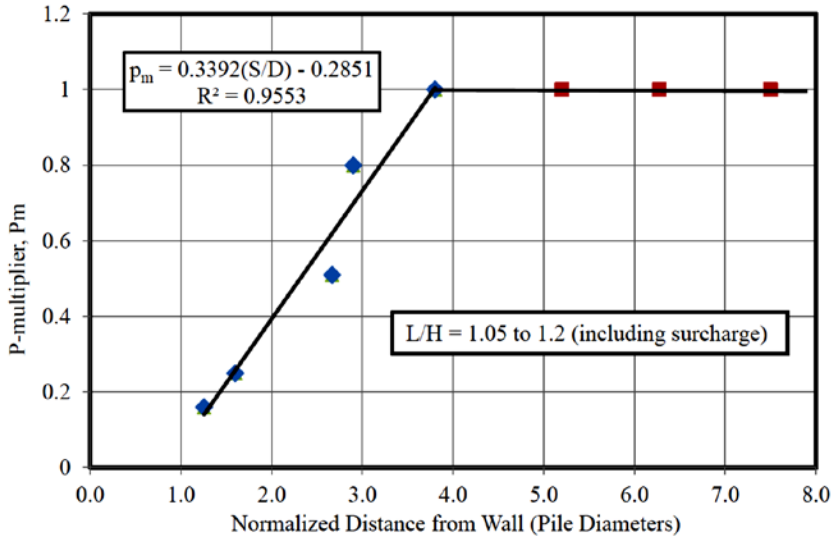

Figure 2.17 Pile head load vs head deflection at the peak and final load at different pile offset (Rollins et al. 2013)

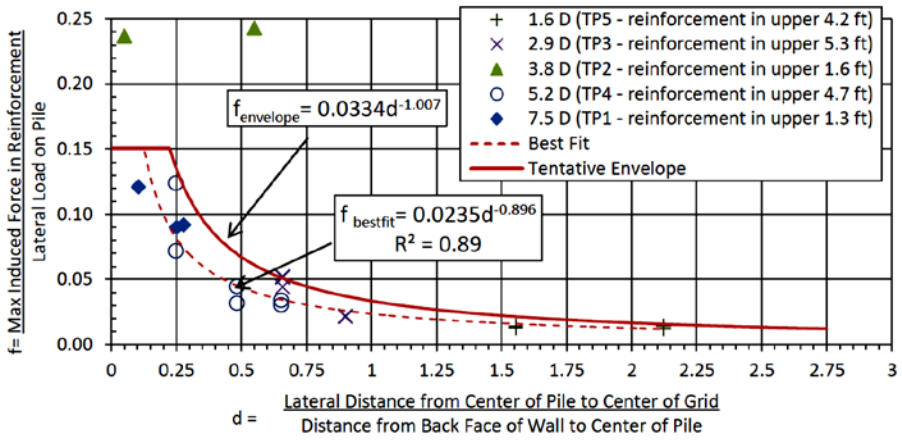

Figure 2.18 Normilized induced force vs normilized distance from pile for the grid reinforcement (Rollins et al. 2013)

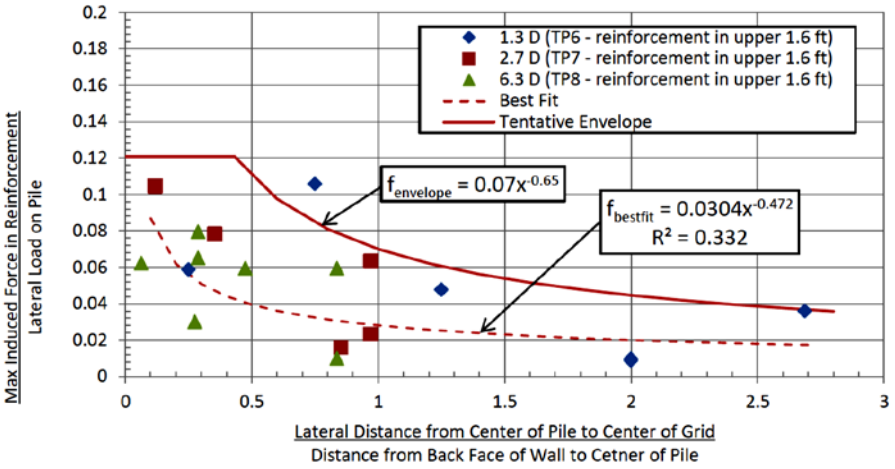

Figure 2.19 Normilized induced force vs normilized distance from pile for the strip reinforcement (Rollins et al. 2013)

Finally, Hatch (2014) performed a study on full-scale pipe piles of 304.8 mm in diameter behind an MSE wall with welded wire reinforcements. The L/H was equal to 0.9, and the pile offsets from the wall were equal to 5.3, 4.3, 3.2, 1.9 times the pile diameter. After combining the results from this study with the results from the previous studies (Nelson 2013; Price 2012), a new plot of P-multiplier was obtained. From this curve, the minimum normalized pile offset to

ensure P-multiplier of 1 was equal to 4 diameter of the pile as shown in Figure 2.20.

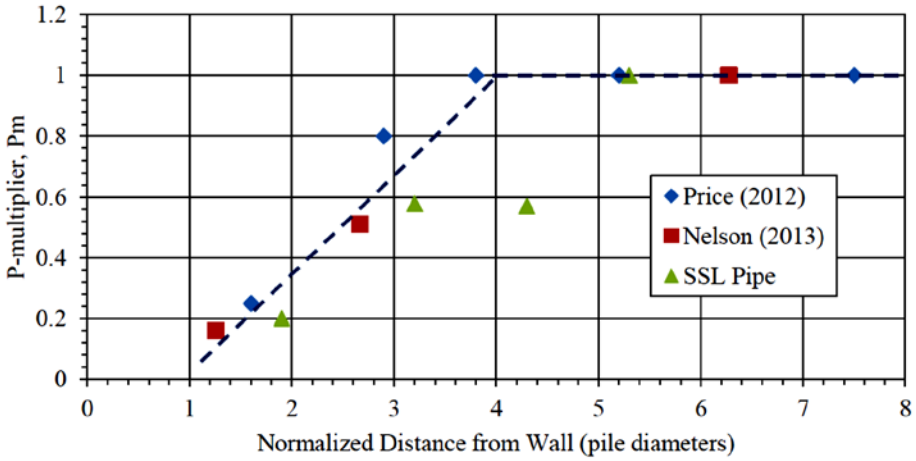

Figure 2.20 P-multiplier curve (Hatch 2014)

2.4.3. Numerical Analyses

For the case of a pile within an MSE wall system, numerical analysis can help understand the complicated interaction between the pile and the MSE wall. Huang et al. (2011) indicated that the limited horizontal extent of soil mass, the resistance from reinforcement, and the influence of MSE wall facing are the three main factors that are not considered in the routine design of laterally loaded piles and MSE walls. Huang et al. (2011) developed a three-dimensional numerical model using FLAC3D, Version 3.1 as shown in Figure 2.21.

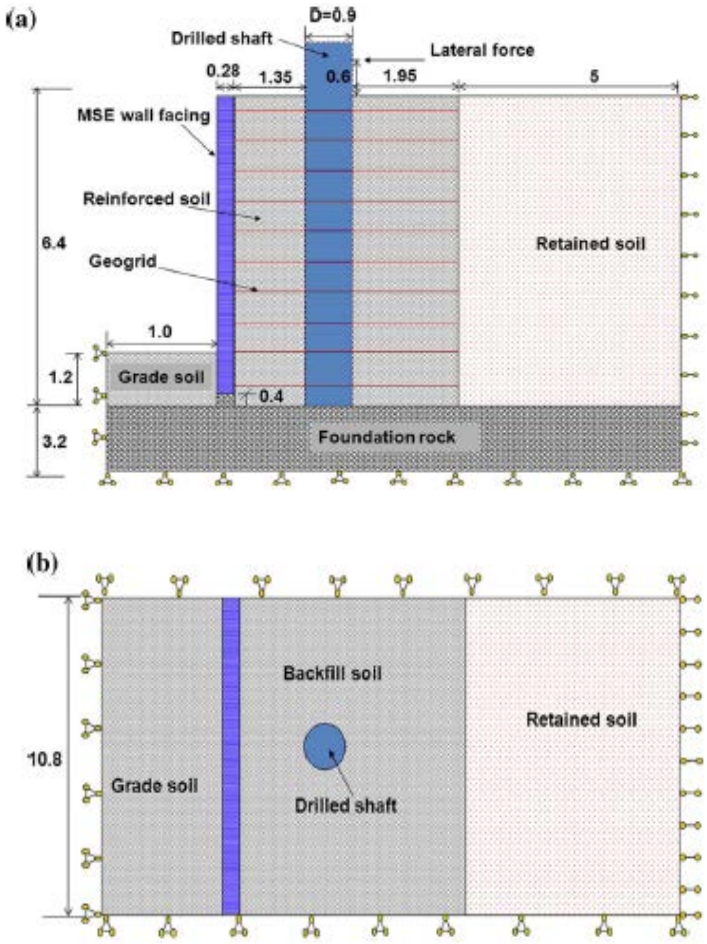

Figure 2.21 The numerical model (all unit in meter): (a) side view and (b) plain view (Huang et al. 2011)

Huang et al. (2011) selected one single pile (Pile B) in the Pierson et al. (2009) study for numerical analysis and compared the numerical results with the measured data. This pile was located at the offset of two pile diameter (1.8 m) from the MSE wall back facing as shown in Figure 2.12. Two numerical model predictions were considered to compare with the field test data. The pre-test analysis (Class-A prediction) was used to guide the design before the field test while the post-test analysis (Class-C prediction) was obtained by using the actual material properties after the field test.

A linearly elastic-perfectly plastic relationship with the Mohr-Columb model was used in the numerical simulation of the field test. After the numerical analysis of the two models was completed, a comparison was conducted between the field test data and both the post-test and the pre-test predictions. Consistent results between the numerical analysis and the field data were obtained for the pile deflection that increased linearly from the bottom of the pile to the top. This agreement supports the assumption of the elastic material for the pile in the numerical analysis (Huang et al. 2011).

Huang et al. (2011) explained the numerical results of the pile and wall deflections, the earth pressure, and the strain in the geogrid. For their post-trsts modeling, Huang et al. considered that the effect of the pile deflection on the wall facing depended on the backfill properties, the type of wall facing, and the type of soil reinforcement. The post-test analysis more closely predicted the wall deflection than the pre-test analysis, especially for the deflection at the centerline of the wall. In addition, higher earth pressures were obtained from the two numerical models as compared with the measured earth pressures from the field test. This disagreement may be due to the inaccuracy of the field test data or the modeling type of the facing of the wall. In the case of the strains of the geogrid layers, the post-test analysis provided consistent results that increased by the increase of the lateral deflection of the pile.

The pervouis numerical analysis was refind by Huang et al. (2013) to get more compatible results with the field data by considering the following four modeling aspects: (1) the confining stress-dependent modulus of the backfill material in a hyprebolic function; (2) the mobilized friction angle considered as a function of the accumlated plastic shear strain to simulate the shear strain hardening/softening behavior of the backfill; (3) modeling of individual blocks for the MSE wall facing (i.e., the blocks were considered as discrete elements with vertical and

horizontal interfaces of different properties; and (4) the compaction effect considered as the increase of the permanent lateral earth ptrssure.

Huang et al. (2013) concluded that a sterss–dependant, strain hardening/softening model was suitable to present the condition of non-linear behavior with large deformation. In addition, a non-linear increase was identified between the pile deflection and the lateral load in both the field test and refined numerical analysis as shown in Figure 2.22. The vertical deflection at the centerline of the MSE wall facing increased non-linearly from the bottom to top of the wall. The vertical deflection profile of the MSE wall facing from the numerical analysis slightly deviated at the top portion of the wall especially at high loads. This deviation is due to the weak interaction between the wall blocks at the center of the wall in the field test.

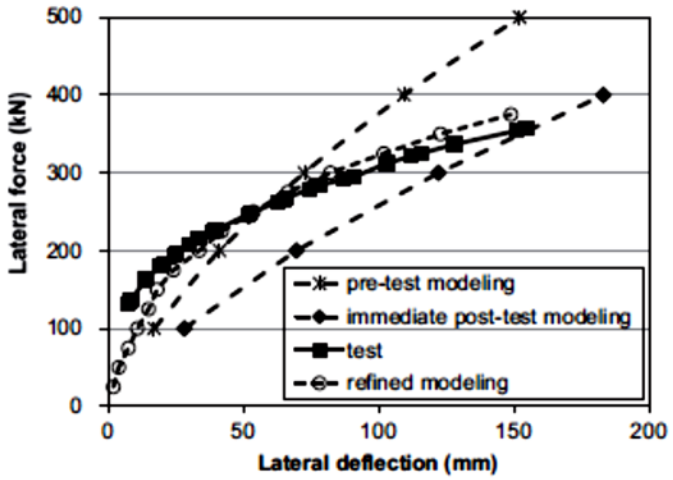

Figure 2.22 Lateral load Vs pile deflection (Huang et al. 2011)

An increase of the lateral load on the pile increased the lateral earth pressure behind the wall facing. In this case, the range of the coefficient of lateral earth pressure was between Ko (active earth pressure coefficient) to Kp (passive earth pressure coefficient) with a higher percentage of increase at the upper part of the wall elevation as shown in Figure 2.23. In addition, the strains of

the geogrid were investigated in both the field and refined numerical studies. In the numerical analysis, the geogrid was considered as a linearly elastic material due to the low measured strain level from the field test. As a result form the geogrid strain investigation, a linear relationship was noticed between the lateral deflection of the pile and the strain in the geogrid. Also, the investigation show that the maximum strain is located near the pile deflection (Huang et al. 2013).

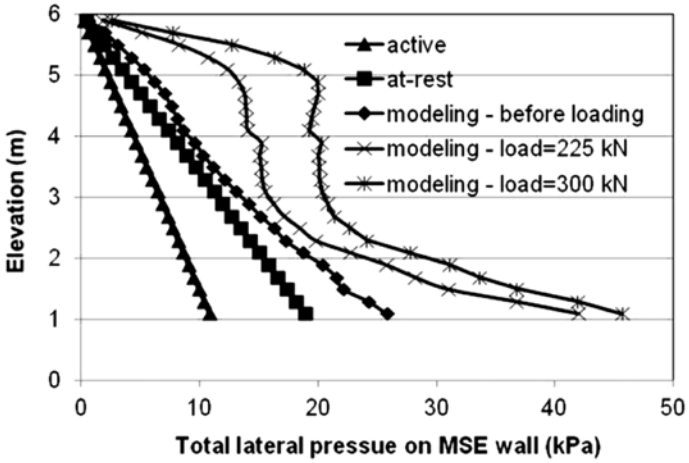

Figure 2.23 Curves of lateral earth pressure based on theoretical and numerical calculations (Huang et al. 2011)

Chapter 3 Model Tests

3.1 Introduction

This chapter includes the details of test materials, test box, instrumentation, test setup, and designation. The first section summarizes the properties of the test materials while the second section contains the details of the test box. The third section includes the instrumentation details. The fourth section presents the test setup and loading procedure. Finally, the last section presents the test groups or their designations.

3.2. Test materials

The details of test soil, wall blocks, geogrid, mechanical connectors, and pile are presented in this section.

3.2.1. Backfill soil

Kansas River sand was used in this study and its grain size distribution is shown in Figure 3.1. From this curve, the values of the mean grain size (D_{50}), the uniformity coefficient (C_U), and the coefficient of curvature (C_c) are equal to 0.55, 2.53, and 0.93, respectively. It can be classified as a poorly graded sand. Moreover, the maximum dry unit weight of the sand is equal to 18.75 $\frac{Kn}{m^3}$ while its minimum dry unit weight is equal to 16.29$\frac{Kn}{m^3}$. Triaxial tests were conducted to determine the peak friction angle of 40^o at the relative density of 70% (Xiao et al. 2015).

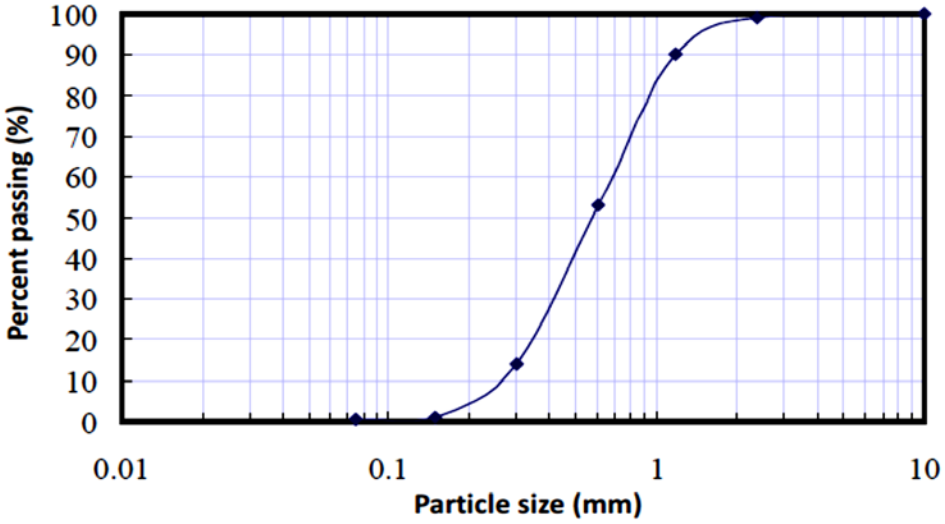

Figure 3.1 Grain size distribution of the backfill sand (Xiao et al. 2015)

3.2.2. Blocks of the wall facing

In order to model the facing of the model MSE wall, several concrete blocks were cut and prepared from larger concrete blocks as shown in Figure 3.2. The height, length, and width of each block were 45, 50, and 50mm, respectively (Xiao et al. 2015). Based on the height of these blocks, the spacing between the reinforcement layers was chosen for this study.

Figure 3.2 Facing blocks (Xiao et al. 2015)

3.2.3. Geogrid

Soil reinforcement is the important part of the MSE wall that is used to ensure its stability. In this study, the internal stability of the wall was maintained by using punched-down biaxial polypropylene geogrid with apertures. According to the manufacturer, the ultimate tensile strength was equal to 12.4 $\frac{Kn}{m}$ in the machine direction (MD) and 19 $\frac{Kn}{m}$ in the cross-machine direction (XMD). However, the most common geogrid used as reinforcement in the MSE wall is the uniaxial geogrid. Thus, two ribs for every four ribs were cut in the (MD) to simulate the uniaxial geogrid.

In order to investigate the ultimate tensile strength of the geogrid in the (XMD) before and after removing the ribs from the (MD), Xiao et al. (2015) conducted two tests with several samples according to the ASTM D6637. The first test was done without any cut in the MD, and the other test was done with a cut in the MD as shown in Figure 3.3. From Figure 3.4, Xiao et al. (2015) concluded that there was almost no effect on the ultimate tensile strength in the XMD when the number of the ribs in the MD was reduced.

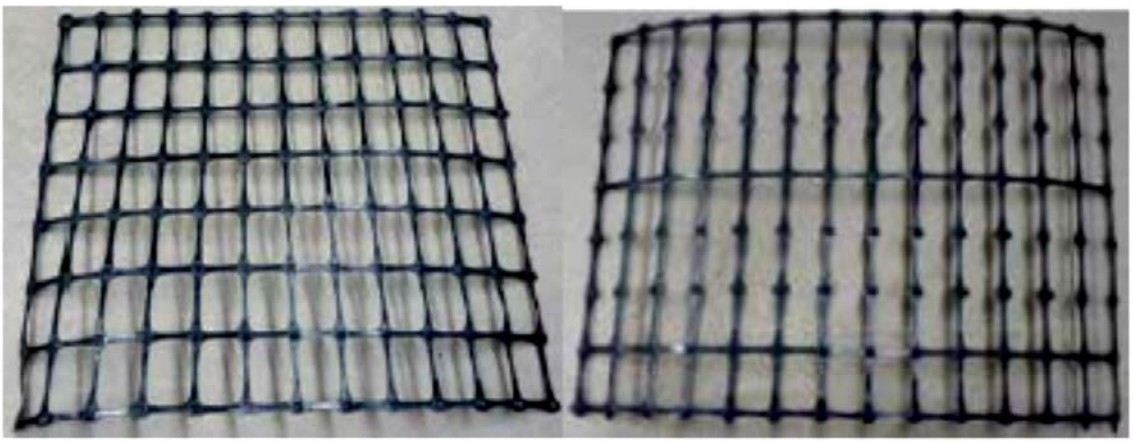

(a) (b)

Figure 3.3 Two Samples of the geogrid layer: (a) before removing the rips and (b) after removing the rips (Xiao et al. 2015)

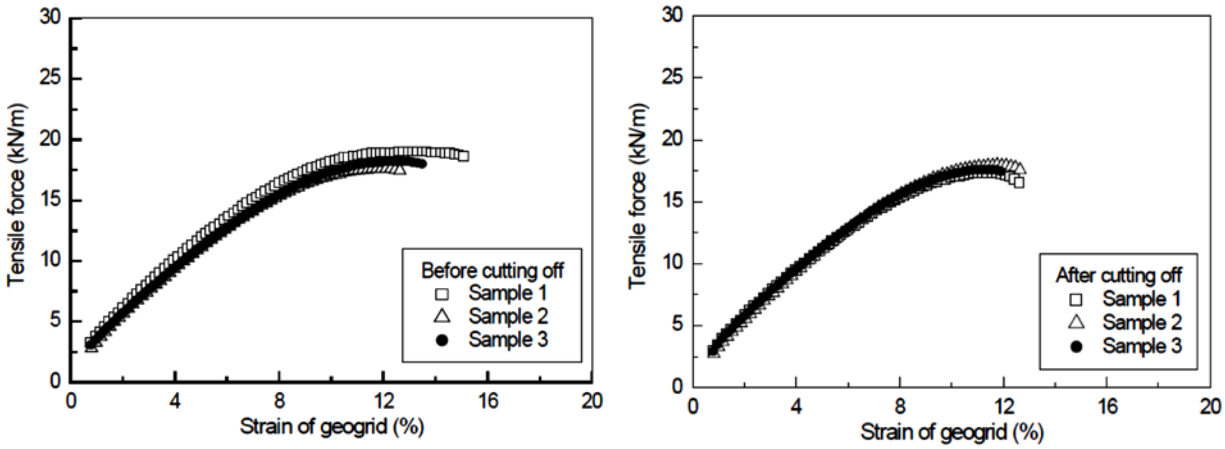

(a) (b)

Figure 3.4 Tensil strength of the geogrid in the cross-machine direction: (a) before removing the ribs and (b) after removing the ribs (Xiao et al. 2015)

Part of this study was to investigate the effect of the reinforcement length at different pile offsets on the capacity of the pile. As a result,, different lengths of the geogrid layers were used and two longitudinal strips of the geogrid were removed at the location of the pile. Three pile offsets were considered in this research: 127, 254, and 381mm. Two reinforcement lengths of 315 and 504 mm were used for the first offset. On the other hand, three reinforcement lengths of 315, 504, and 900 mm were used for the second and third offsets.

3.2.4. Mechanical connection between wall facing and soil reinforcement

A special mechanical connector was used to provide an appropriate anchorage between the wall facing and the geogrid. This connector consisted of two metal parts. The first part was a piece of aluminum angle with two holes on the sides While the other part was an aluminum bolt that went through the angle holes and fixed the geogrid as shown in Figure 3.5. The mechanical connector was used with each geogrid layer in each test except for the tests with the frictional connection. Figure 3.6 shows the wall facing without any mechanical connector. Thus, the connection between the wall blocks and the geogrid was frictional only.

Figure 3.5 Setup of the mechanical connection during the test

Figure 3.6 Setup of the frictional connection during the test

3.2.5. Test pile

In order to simulate a rigid pile seated on a hard layer, an aluminum pile of 915 mm long and 63.5 mm in outer diameter was used. This pile was connected at the base of the test box by a leveling mount. The benefit of the leveling mount was to provide a pin connection between the model pile and the hard base of the test box.

Figure 3.7 shows the pile, the leveling mount, and the pin connector. The construction of this pin connector was done by following the following steps. First, a cylindrical piece of wood with an outer diameter equal to the inner diameter of the pile was prepared. This piece of wood also had a central hole diameter equal to the diameter of the leveling mount's bolt. This bolt was inserted and fixed inside the cylindrical piece of wood, then this piece was connected to the pile using small screws. Finally, the system of the pile and the level in the mount were fixed to the base of the box using a rectangular piece of wood with a cone hole in the middle. The cone base of the leveling mount was inserted inside that cone hole of the rectangular piece of wood. Then, the sides of this piece were connected to the base of the test box using a long screw for wood.

Figure 3.7 Pile, leveling mount, and pin connector of the test

3.3. Test box

All the tests were done using a test box that had a rectangular shape as shown in Figure 3.8. The inside height, length, and width of this box were 830, 1400, and 400 mm, respectively. This box had a wooden base. In addition to three wooden sides, the front side was made of a 25-mm thick transparent plexiglass. Moreover, this box was divided into two halves for ease construction. The lower half was fixed to the base and the two wooden sides were fixed by long screws. An H-shape steel beam was attached above the lower part using a silicon glue. the steel beam was used as a base or frictional seat to the free upper part of the transparent plexiglass. The upper half was removable during the test and could be seated from the bottom on the H-beam and fixed from the side using clamps.

A special loading system was attached to the box to apply the lateral load on the pile. This system consisted of pulleys, steel cables, loading weights, a crane scale, and a loading plate. The

main purpose of the pulleys was to change the vertical load from the weights to a lateral load on the pile. The crane scale was used to record the load applied onto the pile after weights were added. To accommodate different wall heights, the loading system was modified as shown in Figure 3.9.

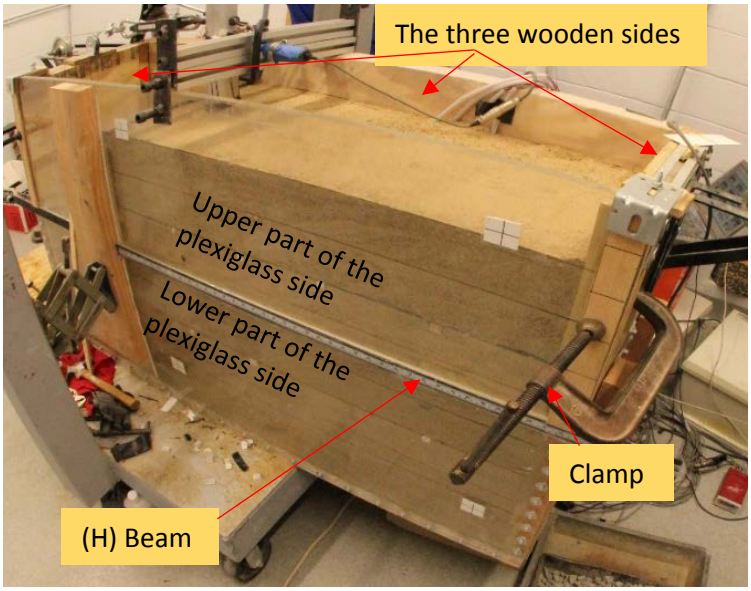

Figure 3.8 Details of the test box.

3.4. Instrumentation details

The instrumentations details of the lateral load, the pressure behind the wall, the strains in the geogrids and the pile, the deflections of the wall facing and the pile are presented below.

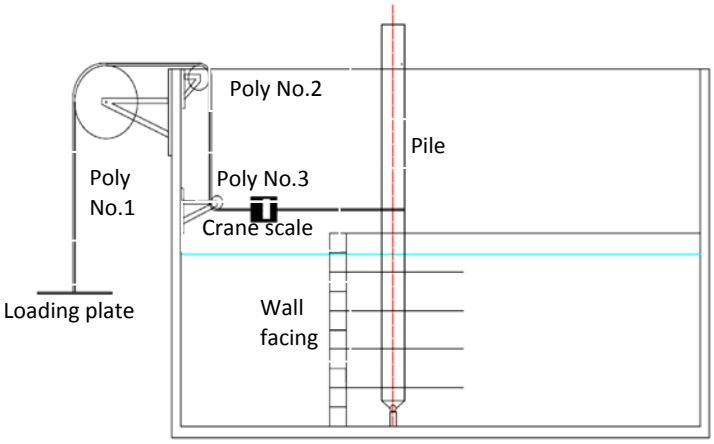

(a)

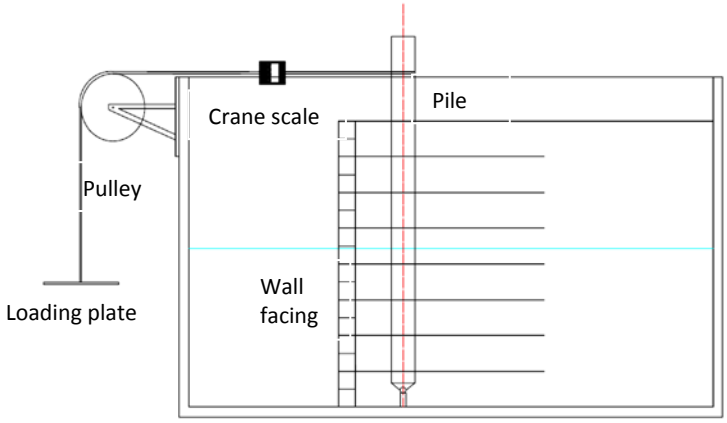

(b)

Figure 3.9 Loading system of the test box: (a) low wall, and (b) high wall.

3.4.1. Lateral load measurement

A crane scale was used as a load cell in this study to measure the lateral load on the pile as shown in Figure 3.9. The ultimate capacity of this scale was 300 kg, and its accuracy was 0.01 g. During the test, The scale was connected to the steel cable using an S hook and fixed to the pile using a U steel connector and a bolt as shown in Figure 3.10.

Figure 3.10 Load cell unit.

3.4.2. Pressure measurement

In order to measure the pressure behind the wall facing, twelve pressure cells were attached to the inner face of the wall blocks using duct tape as shown in Figure 3.11. These pressure cells were divided into several groups of three pressure cells each. These three pressure cells were organized at transverse spacing of 100 mm. The vertical spacing between the pressure cells groups depended on the wall height. For the high wall tests, four groups of pressure cells were attached to the wall facing at the distances of 202.5, 337.5, 472, and 607.5 mm from the base of the test box as shown in Figure 3.12.

Figure 3.11 Distribution of pressure cells in the transverse direction.

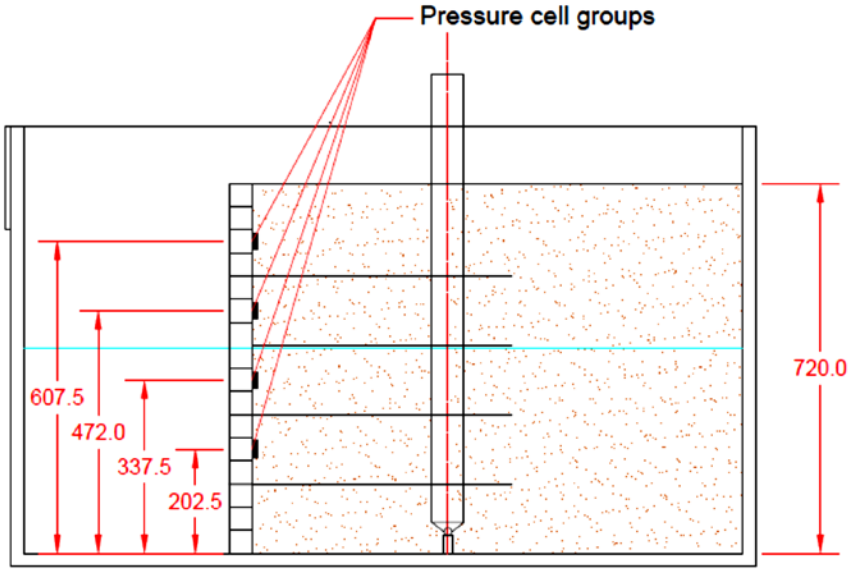

Figure 3.12 Distribution of pressure cells in the vertical direction.

Twelve pressure cells were connected with two switch boxes that had 10 channels each. Using the switch boxes, the channels were reduced from 12 (from the pressure cells) to 2 (from the switch box). Then, the data from the switch box were collected using one DC-204R Dynamic Data Acquisition System and monitored using a laptop computer. Figure 3.13 shows the two switch boxes, the data acquisition system, and the laptop computer.

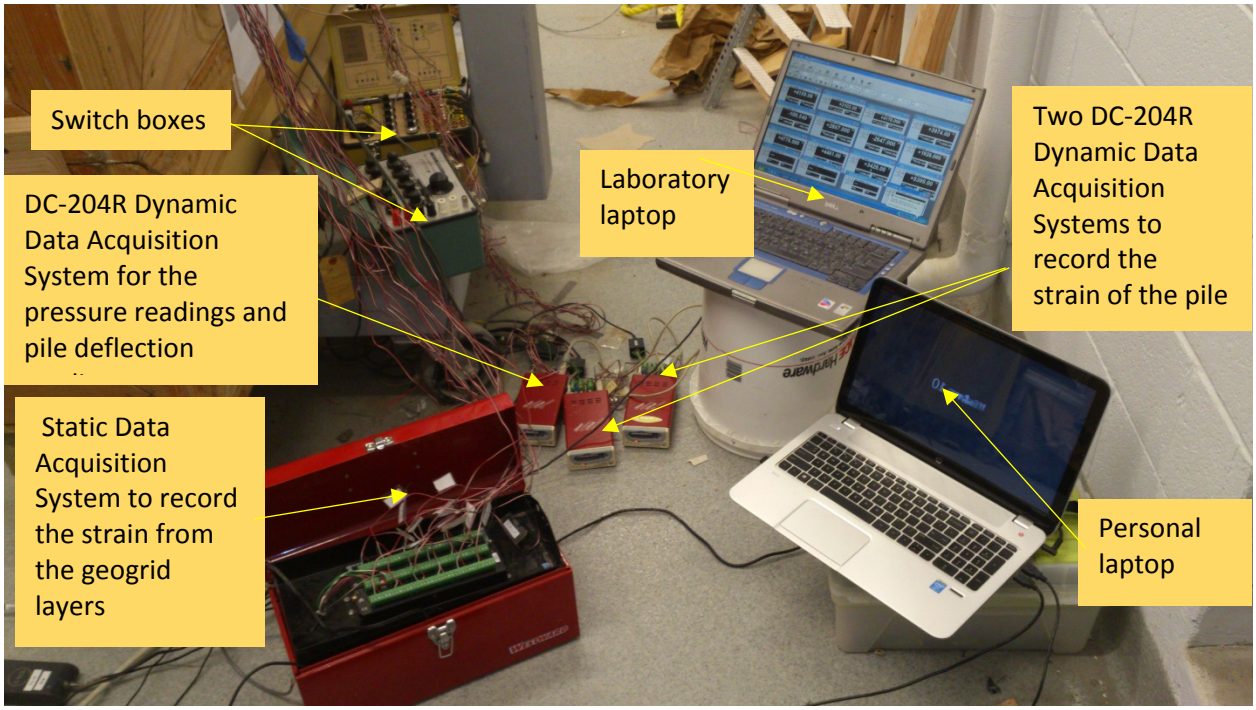

Figure 3.13 Data acquisition system.

3.4.3. Strain measurement

The strains of both the pile and the geogrid layers were obtained using strain gauges that were connected to the data acquisition system.

Strain of the pile

When the lateral load was applied on the pile, tensile and compressive stresses developed along two sides of the pile. Five pairs of strain Gauges were attached to each side of the pile using CN Cyanoacrylate adhesive as shown in Figure 3.14. All the strain Gauges had the same type of C2A-1H2 L2 S2 C1 D350LW-120 with resistance of 120±0.6% ohms. The vertical spacing between each pair was 191 mm, and the vertical distance from the lower group to the pin connection was 19 mm (Ismael 2014).

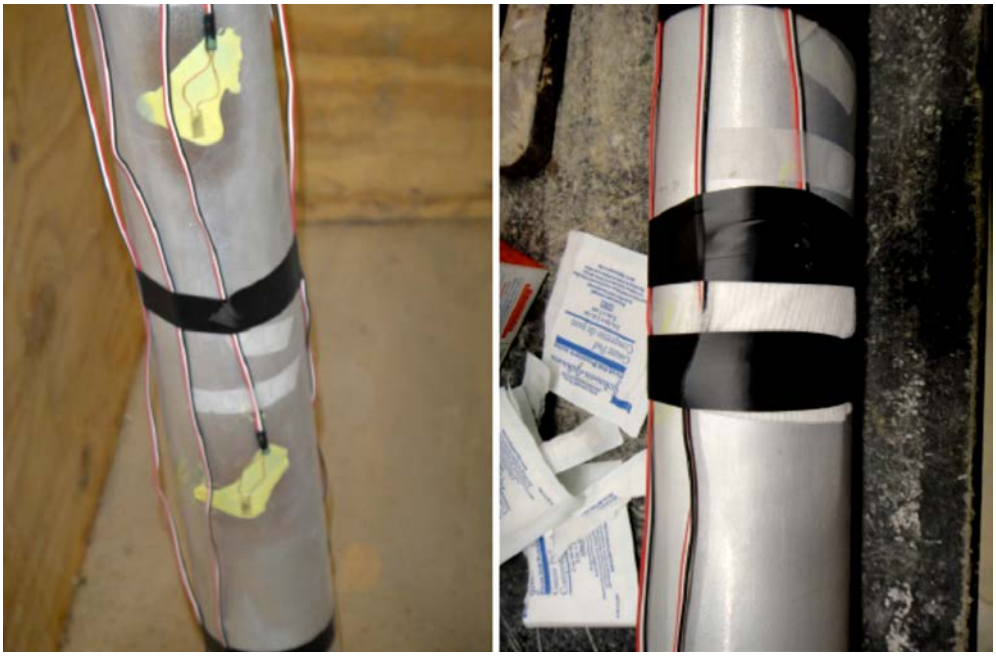

Figure 3.14 Attachment details of the strain gauges on the pile (Ismael 2014).

Figure 3.15 shows all the positions of five pairs of strain gauges along the pile. The two strain gauges in each pair were attached to each side of the pile to measure the tensile and the compressive strains. Because the location of the pin connection at the same location as strain gauge Pair 5, the readings from these strain gauges were neglected. However, to collect the data from these strain gauges, two DC-204R Dynamic Data Acquisition System were used. One of these data loggers recorded the data of the tension side, and the other recorded the data of the compressive side as shown in Figure 3.13.

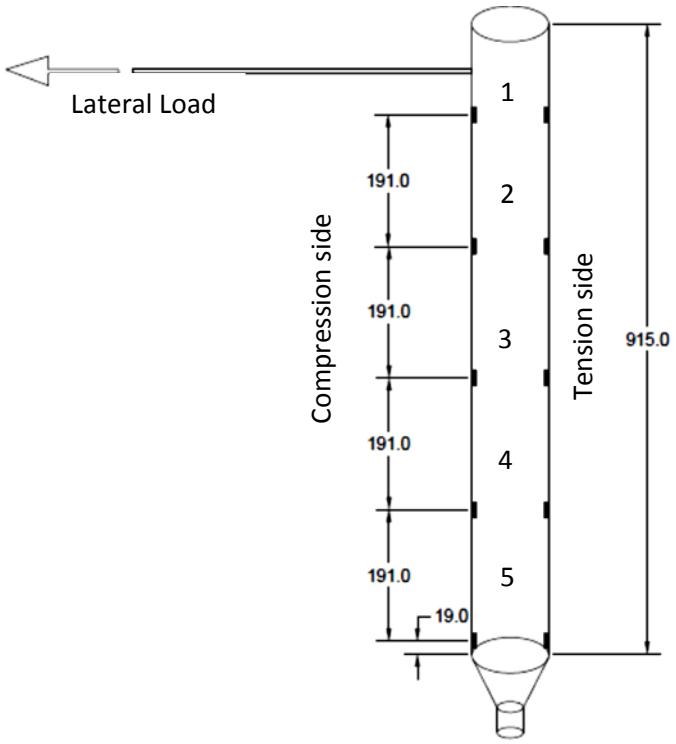

Figure 3.15 Locations of the strain gauges on the pile (all dimension in mm).

Strains of the geogrid layers

When a pile is installed in a cohesionless soil and subjected to a lateral load, two pressure zones will develop in the soil. The first zone is an active zone behind the pile, and the other zone is a passive zone in front of the pile. In this study, not only the soil responds to the lateral load from the pile but also the soil reinforcement. Several strain gauges were attached on the geogrid layers to measure their strains inside the active and passive zones of the soil. The model of these strain gauges was C2A-13-120LW-120, and they were small enough to fit on the geogrid ribs. Then, a static data acquisition system with sixteen channels was used to collect the data from these strain gauges as shown in Figure 3.13.

For each test with a high wall facing, four geogrid layers were chosen to attach the strain gauges. Totally sixteen strain gauges were used with four strain gauges on each layer. One

continuous strip next to the pile inside the geogrid was chosen to attach four strain gauges. The distance between the strain gauges depended on the length of the geogrid layer. The spacing of strain gauges was 114 mm for the short reinforcement length (i.e., 504 mm) and 230 mm for the long reinforcement length (i.e., 900 mm). Figure 3.16 shows the distribution of the strain gauges on the geogrid with the short reinforcement length at three different pile offsets. On the other hand, Figure 3.17 shows the distributions of the strain gauges on the geogrid with the long reinforcement length at two different pile offsets.

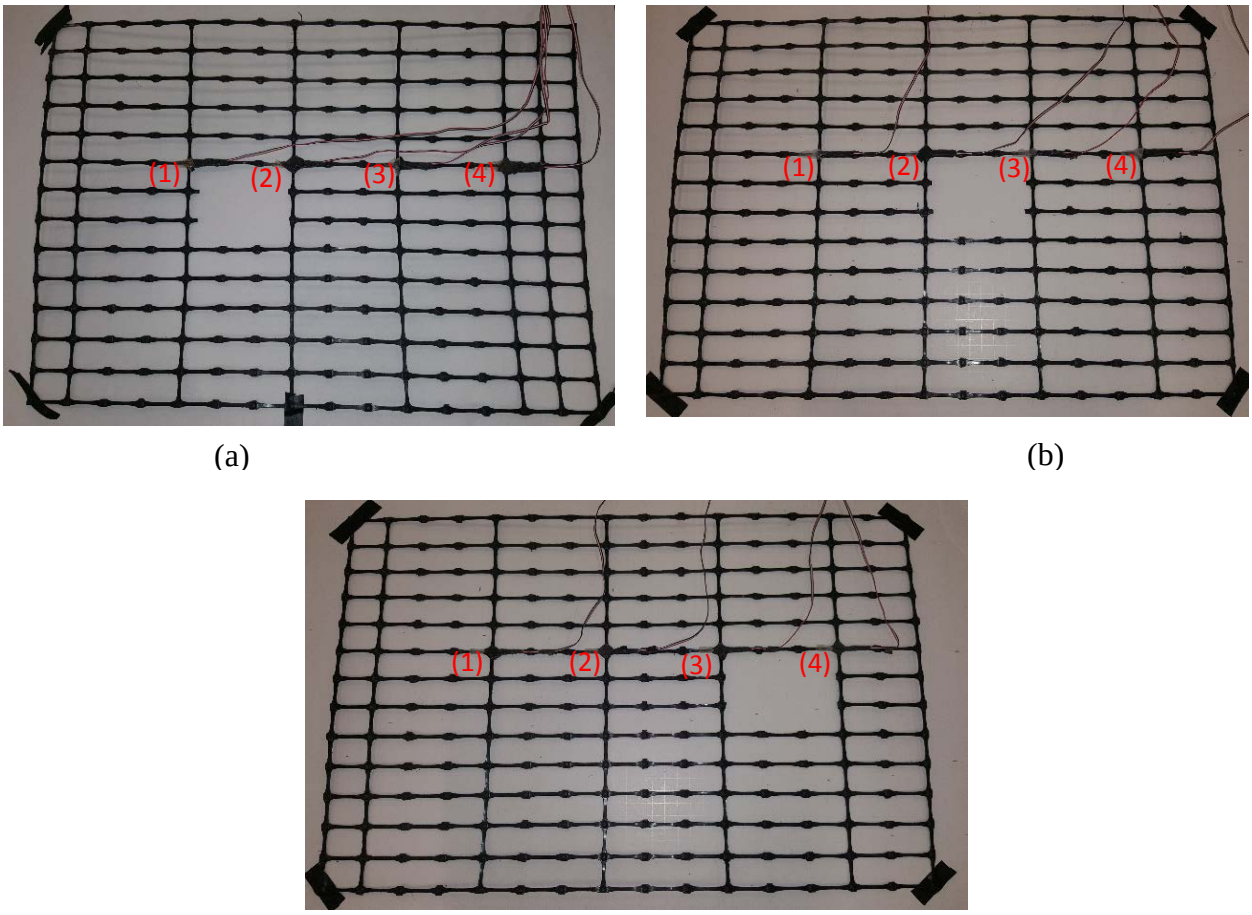

(a) (b)

(c)

Figure 3.16 Locations of strain gauges on 504-mm long geogrid layers at the pile offset of: (a) 127 mm, (b) 254 mm, and (c) 381 mm.

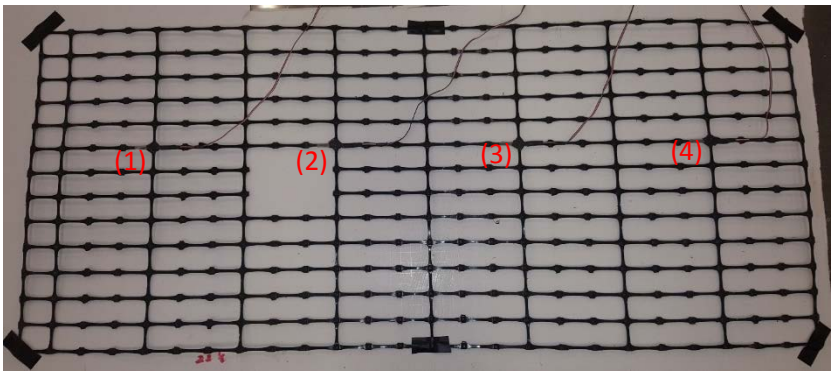

(a)

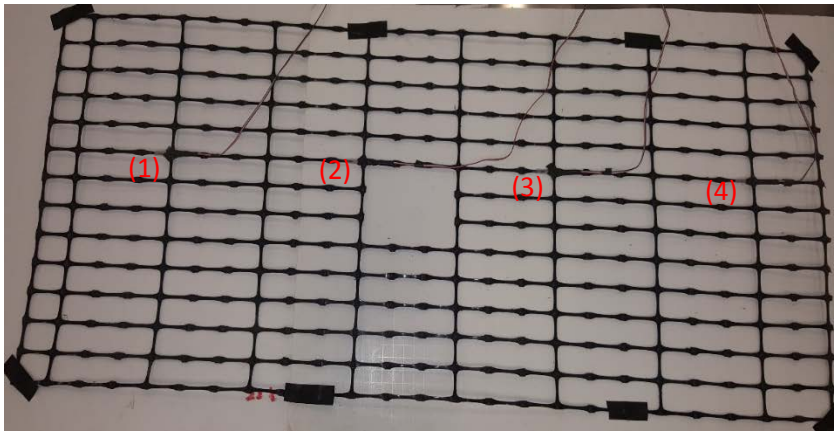

(b)

Figure 3.17 Locations of strain gauges on 900-mm long geogrid layers at the pile offset of (a) 254 mm and (b) 381mm.

For the low walls, four strain gauges were attached to only two geogrid layers at three pile offsets. In fact, two gauges in the longitudinal direction and three gauges in the transverse direction with one in common as shown in Figure 3.18 (a) & (b). For the large pile offset, the geogrid layers were similar to those shown in Figure 3.18 but without any pile hole because the offset distance was larger than the reinforcement length.

In Figure 3.18 (a) & (b), the distance between the strain gauges 1 and 2 in the longitudinal direction was 152 mm. In the other direction, the distance between strains gauges 3 and 1 was 89 mm while the distance between strain gauges 1 and 4 was 190.5 mm.

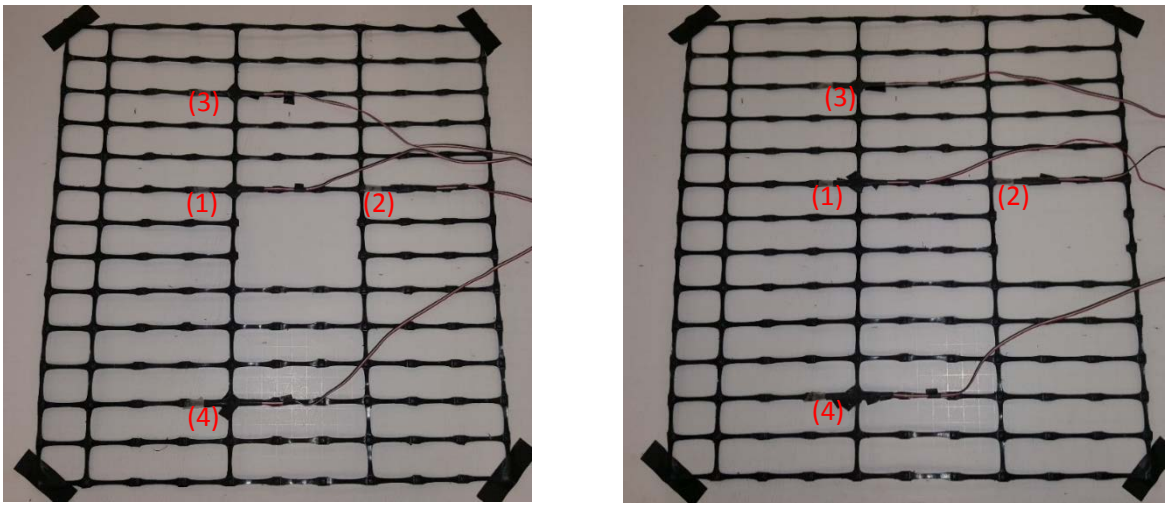

(a) (b)

Figure 3.18 Locations of strain gauges on 315-mm long geogrid layers at the pile offset of (a) 127 mm and (b) 254 mm.

The chosen geogrid layers that had the strain gauges were located in specific elevations along the wall height. Figure 3.19 shows the examples of the tests with different geogrid layouts. Each layout depends on the vertical spacing between the geogrid layers in the MSE. There is one layout for the low wall as shown in Figure 3.19 (a) while there are two layouts for the high walls. These layouts were used in the high walls with short and long reinforcement lengths as well. Figure 3.19 (b) shows the layout for the high wall with small vertical spacing of 90 mm and Figure 3.19 (c) shows the layout for the high wall with large vertical spacing of 135 mm.

All the strain gauges are organized in two gauge groups for the low wall tests and four gauge groups for the high wall. As shown in Figure 3.19, Gauges groups G1, G2, G3, and G4 included the gauges with No. 1, No. 2, No. 3, and No. 4, respectively.

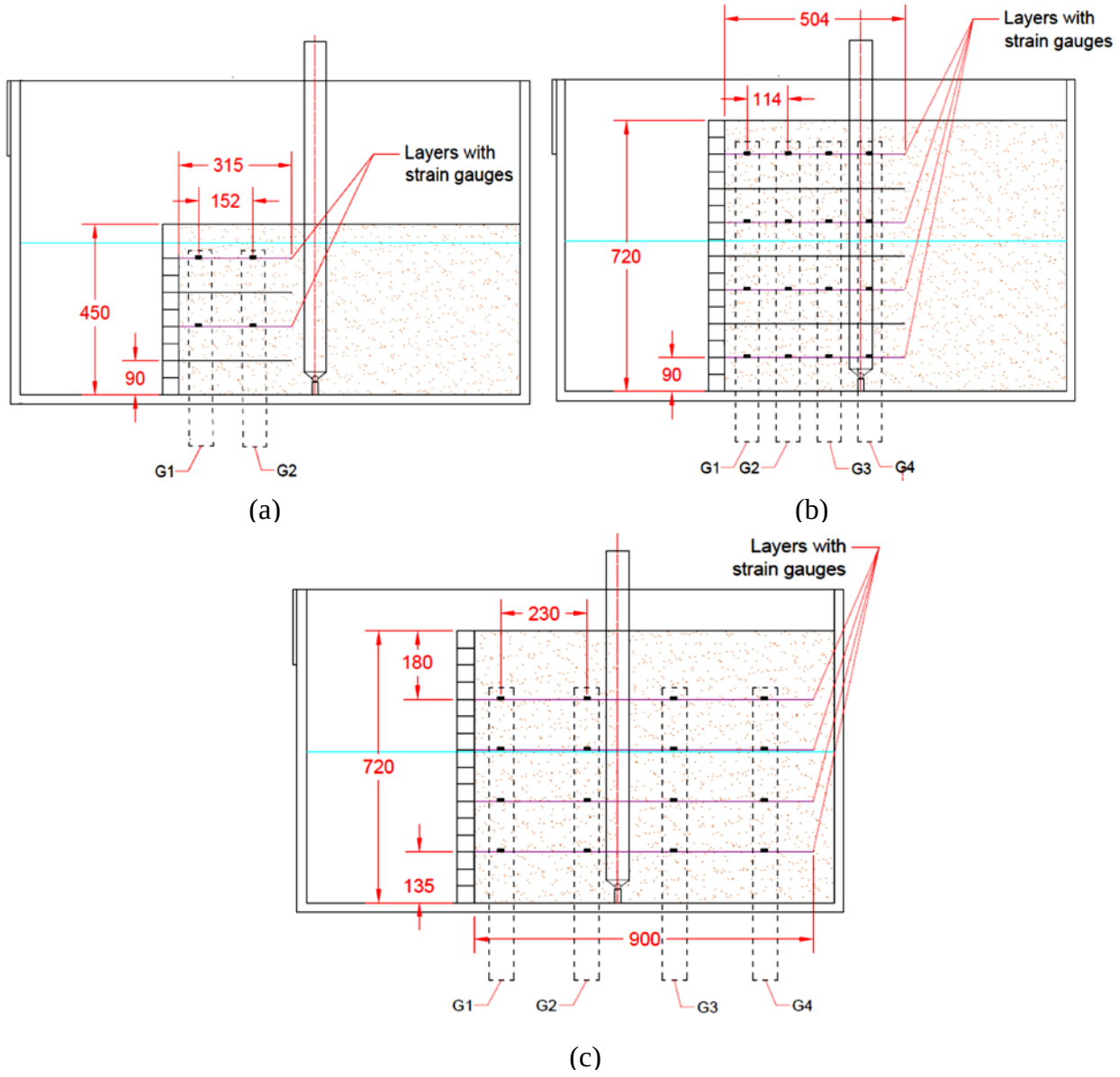

Figure 3.19 Layouts of the geogrid layers with strain gauges in (a) the low wall, (b) the high wall with small spacing, and (c) the high wall with large spacing (all dimensions in mm).

3.4.4. Deflection measurement

Two systems were used to measure the deflections in this study. The deflections of the pile were measured using displacement transducers while the deflections of the wall were measured using a camera and scale rulers.

Deflections of the pile

The deflections of the upper part of the pile were measured using a displacement transducer (type CDP-100) with a capacity equal to 100 mm and another displacement transducer with a capacity equal to 50 mm was used to measure the deflections at different heights of the pile. The location of the first transducer was approximately at the same location of the first pair of the pile strain gauges (i.e., location 1 in Figure 3.15). Figure 3.20 shows the frame for both transducers and the details of their setup during the test. The readings from both transducers were collected using two channels of one DC-204R Dynamic Data Acquisition System as shown in Figure 3.13.

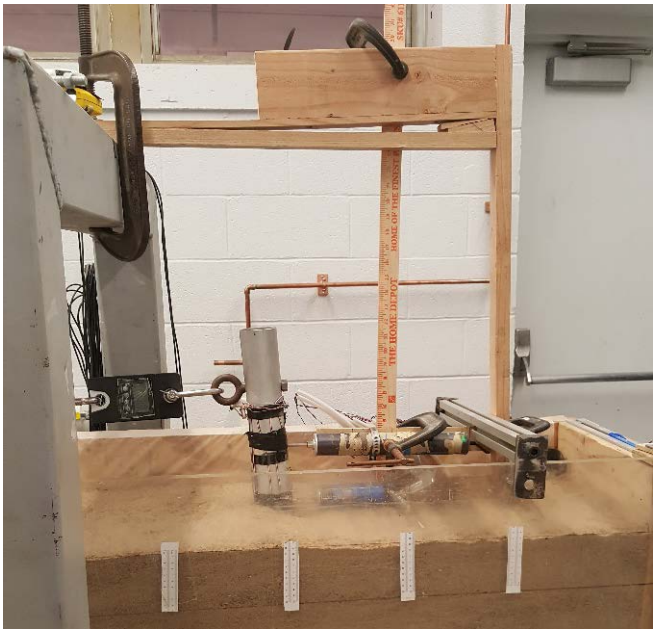

Figure 3.20 Frame and setup of two displacement transducers to record the pile deflections.

Deflections of the wall facing

To measure the surface deflections of the wall facing, a special measuring system was used as shown in Figure 3.21. This system includes three main parts. The first part was a frame that was constructed from two aluminum angle plates with punched holes and five wooden plates. The two aluminum plates were fixed together to form a channel plate and each wooden plate was connected to one hole of the channel plate and fixed by a bolt. After the frame was finished, scale papers were glued on the wooden plates.

The second part of the deflection measuring system was a group of bolts with different lengths. These bolts were attached to the surface of the facing blocks by epoxy glue. The purpose of them was to work as indicators to capture the movement of the blocks. During the test, the frame was fixed on the side of the test box and the locations of the wooden plates were adjusted beneath the indication bolts. The distance between the wooden arms was 135 mm for the high wall and 90 mm for the low height wall. The final part was the camera that captured the movement of the indicators above the scale papers. A Nikon 5500 camera with 18-55 mm VR lens was used for this purpose. This camera was put on a monopod that was fixed to the side of the test box. Figure 3.21 Figure 3.21 shows all the parts of the deflection measuring system of the wall facing.

(a)

(b)

(c)

Figure 3.21 Parts of the deflection measurement system of the wall facing: (a) the frame with the scale papers, (b) facing blocks with bolt indicators, and (c) a Nikon 5300 camera.

3.5. Test setup and loading

In general, the preparation steps were almost the same for all tests, which include:

1- The weight of sand in each layer was pre-calculated by considering the layer volume in addition to the sand at the relative density of 70%.

2- At each test or pile offset from the wall facing, the pin connection was prepared and installed with the pile as shown in Figure 3.7.

3- The geogrid layers were prepared by hanging them on the upper part of the pile through the offset holes as shown in Figure 3.22. To ensure the pile alignment in each test, it was fixed using a hollow steel bar connected to the steel frame around the test box. Also, the vertical alignment of the pile was measured by using a level.

Figure 3.22 Pile alignment

4- As shown in Figure 3.23, a plastic sheet covered the wooden side of the test box to reduce the friction between the sand and the wooden side. Moreover, indication lines were drawn on the plastic sheet and the plexiglass side of the wall to show the limits of the layer volume.

5- The wall facing was constructed putting the concrete blocks in rows to the required spacing between the geogrid layers as shown in Figure 3.14.

6- After step 5 was finished, the weighted sand was poured into the test box and compacted to the indication lines using a standard compactor. Then, the geogrid layer was placed on the compacted sand. Figure 3.11 shows the details of step 6 in addition to the attachment of the pressure cells on the inner face of the wall.

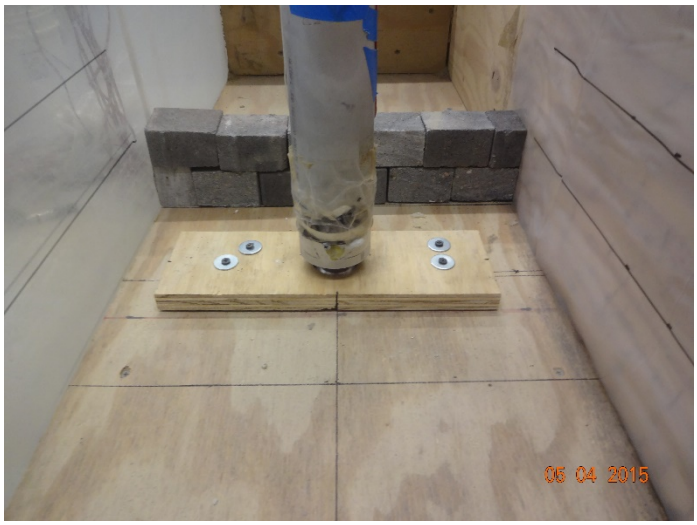

Figure 3.23 Pin connection of the pile and Plastic sheet of the wooden side.

7- Steps 5 and 7 were repeated until the total height of the wall was reached. Then, the steel bar was removed from the pile, and the loading system was connected as shown in Figure 3.10.

8- When the total height of the wall was reached, the measuring system of the wall deflection was set up as shown in Figure 3.23. The scale papers were positioned under the indicators to capture the deflections during the test by a camera.

9- The final step was to connect the strain gauges on the pile, the strain gauges on the geogrid, the pressure cells, and the displacement transducers to the data loggers. The data from these instrumentations were recorded and monitored using PC software.

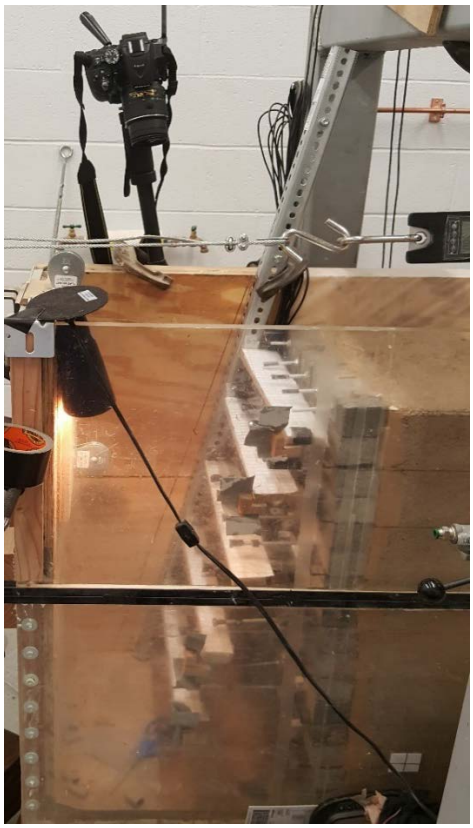

Figure 3.24 Deflection measurment system of the wall facing.

The load control procedure was used for all the tests in this study. Below are the general loading steps after the test was:

1- After the loading system to the pile was connected, the first set of ten kilogram loads were put on the loading plate. Using the pulleys, the weights were transferred to the forces acting laterally on the pile. Each load increment was held for ten minutes, then another load increment was applied.

2- Another set of five kilogram loads was used to capture the failure of the MSE wall. The holding period for each load increment in this set was 5 minutes.

3- Before each loading step, a picture of the wall facing was taken, and the readings of all pressure cells were recorded.

4- The load or the force was recorded by the crane scale after each loading step. Figure 3.25 (a) shows the loading stage after all 10 kg loads were applied while Figure 3.25 (b) shows the loading stage after the failure of the MSE wall.

5- At the end of the test, the data from each instrumentation was collected and prepared for analysis later. Then, the wall was removed in order to prepare next test.

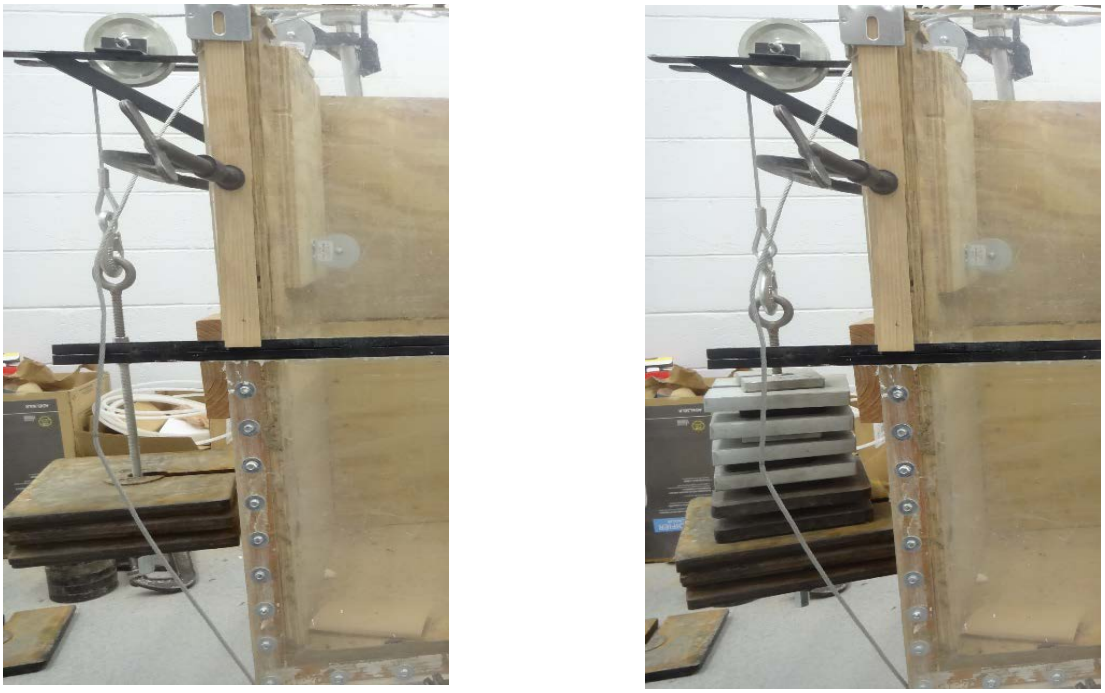

(a) (b)

Figure 3.25 Loading system during the test: (a) the frame with the scale papers, (b) the set of 10 kg load, and (c) the total load after failure.

3.6. Test Designation

Totally eighteen tests were conducted and classified into three groups. Each group had several tests at three pile offsets. The designation of each group depended on the MSE wall height and the length of the reinforcement layers. Table 3.1 shows the design parameters and the test groups.

Table 3.1 MSE wall design details and test groups.

Wall Height	Height Classification	Layer Length	Layer length Classification	Pile Offsets	Layer Spacing	Connection type	Test Group
Hb x 10 (450 mm)	Low wall	Hw x 0.7 (315 mm)	Regular reinforcement length	2d, 4d & 6d (127, 254, 381) mm	Hb x 2 (90 mm)	Mechanical	Group 1 low wall with regular reinforcement length
Hb x 16 (720 mm)	High wall	Hw x 0.7 (504 mm)	Regular reinforcement length	2d, 4d & 6d (127, 254, 381) mm	Hb x 3 (135 mm)	Mechanical	Group 2 high wall with regular reinforcement length
					Hb x 2 (90 mm)	Mechanical	
						Frictional	
		Hw x1.25 (900 mm)	Long reinforcement	4d & 6d (254, 381) mm	Hb x 3 (135 mm)	Mechanical	Group 3 high wall with long reinforcement engtth
					Hb x 2 (90 mm)	Mechanical	
						Frictional	

where Hb = the height of a single concrete block, Hw = the total height of the wall, and d = the pile diameter.

Table 3.2 shows the parameters, symbols, and values that are used in the designation of each test of the groups of this study. The designation of each test includes several symbol combinations from the parameters and the series of Table 3.2.

Table 3.2 Parameters, symbols, and values

Series	1	2	3
Wall Height H, mm	450	720	____
Layer length L, mm	315	504	900
Layer spacing S, mm	90	135	____
Pile offset D, mm	127 (2d)	254 (4d)	381 (6d)
Connection Type C	Mechanical	Frictional	____

Note : d = the diameter of the pile.

3.6.1. Group 1

This group includes three low wall tests with regular reinforcement length. In fact, the reinforcement length was equal to 0.7 times the wall height, which follows the specifications of FHWA (2007). From Table 3.1, each test in this group had different pile offsets, but had the same layer spacing and connection type. Figure 3.26 shows the three tests of Group 1. They are referred as Tests H1 L1 S1 C1 **D1**, H1 L1 S1 C1 **D2**, and H1 L1 S1 C1 **D3** at pile offsets of 127 mm, 254 mm, and 381 mm, respectively. A summary of the design details for each test is shown in Table 3.3.

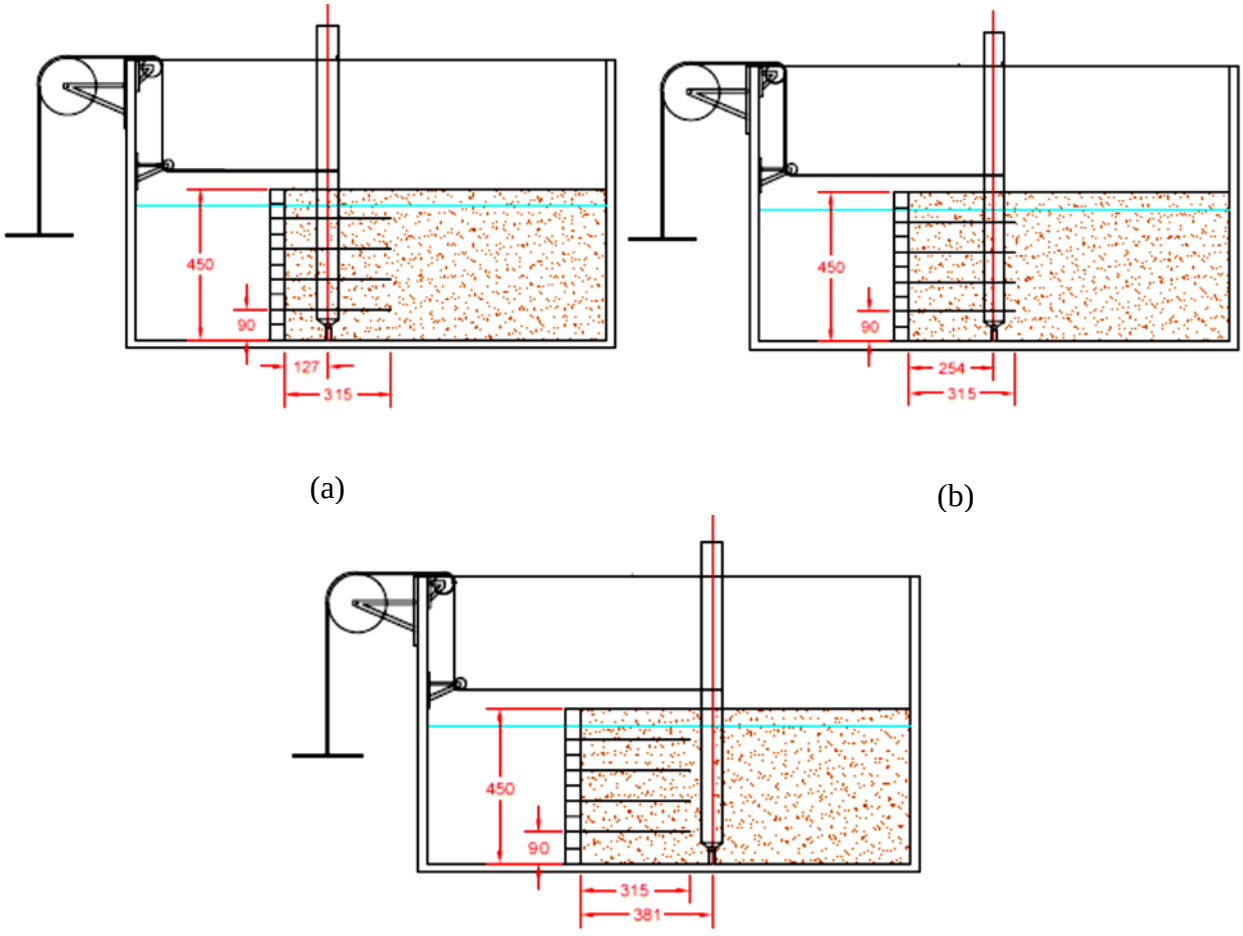

Figure 3.26 Tests details of Group 1: (a) Test H1 L1 S1 C1 D1 (b) H1 L1 S1 C1 D2 (c) H1 L1 S1 C1 D3 (all dimensions in mm).

3.6.2. Group 2

The tests in this group were classified into three categories in order to facilitate the comparisons between their results. Each category had three tests at different pile offsets. The first category had the same wall height, the same layer length, and the mechanical connection. The spacing between the reinforcement layers in this category was 135 mm for the bottom layers and 180 mm for the final upmost layer. This category included Tests H2 L2 S2 C1 **D1**, H2 L2 S2 C1 **D2**, and H2 L2 S2 C1 **D3** as shown in Figure 3.27.

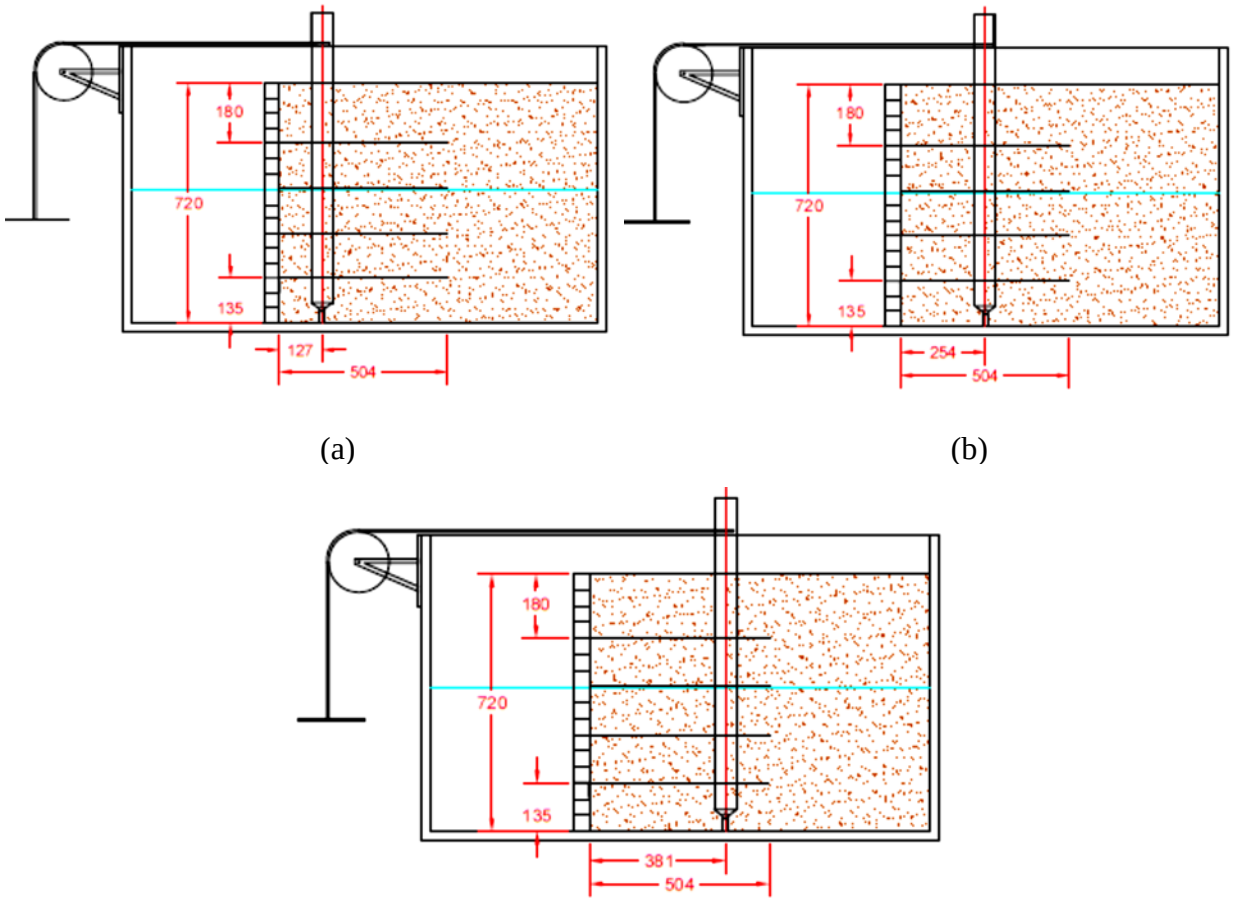

Figure 3.27 Tests details of the first category in Group 2: (a) Test H2 L2 S2 C1 D1, (b) Test H2 L2 S2 C1 D2, and (c) Test H2 L2 S2 C1 D3 (all dimensions in

The second category is shown in Figure 3.28. Their tests had the same wall height, the same layer length, the same spacing, and the mechanical connection. The spacing between the reinforcement layers was less than the previous category and equal to 90 mm. The final category had the same parameters as the second category except for the connection type. The tests in this category had fractional connection instead of mechanical connection. As shown in Figure 3.28, the second category included Tests H2 L2 S1 C1 **D1**, H2 L2 S1 C1 **D2**, and H2 L2 S1 C1 **D3** with a mechanical connection while the third category included Tests H2 L2 S1 C2 **D1**, H2 L2 S1 C2 **D2**, and H2 L2 S1 C2 **D3** with a frictional connection.

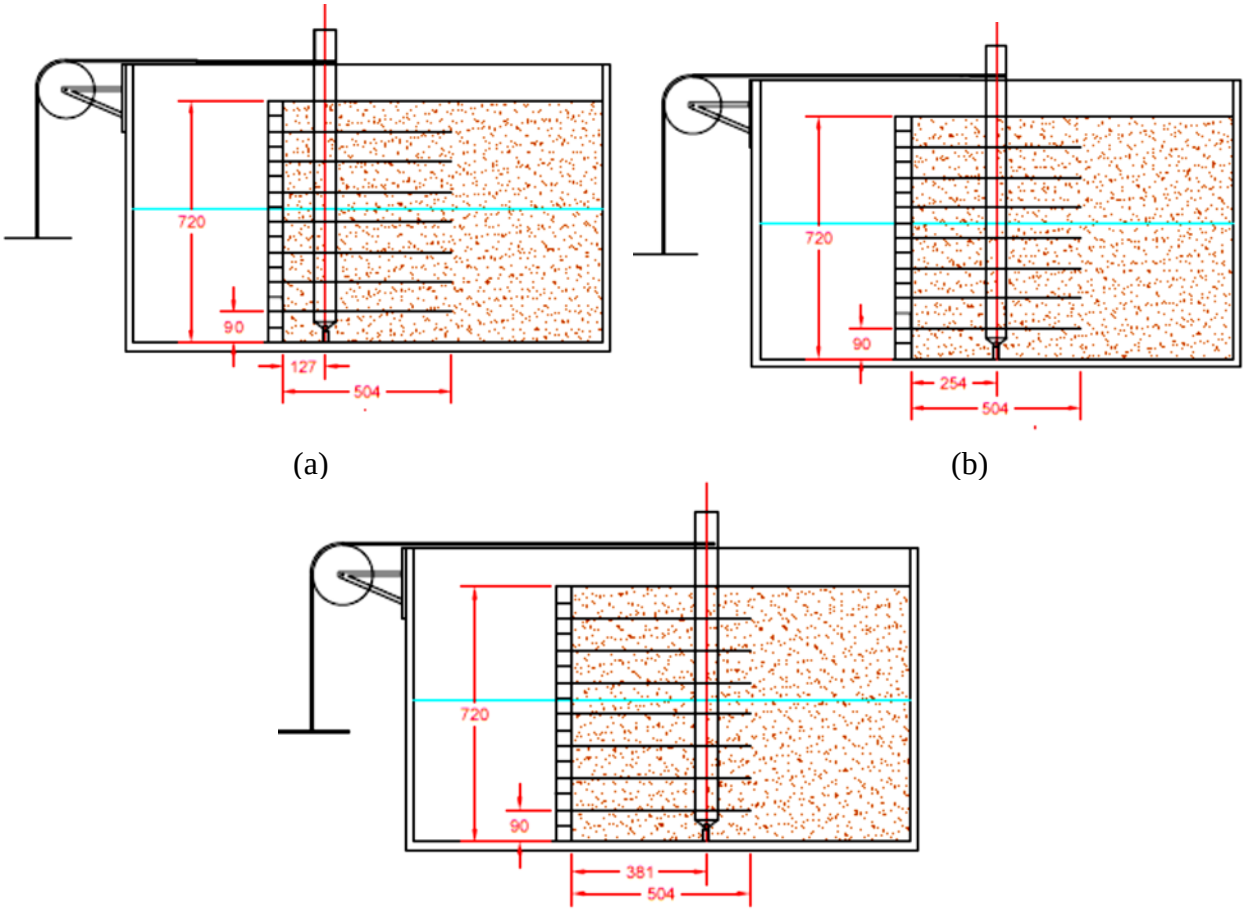

Figure 3.28 Tests details of the second and third categories in Group 2: (a) Test H2 L2 S1 C1 D1, Test H2 L2 S1 C2 D1 (b) Test H2 L2 S1 C1 D2, Test H2 L2 S1 C2 D2, and (c) Test H2 L2 S1 C1 D3, Test H2 L2 S1 C2 D3 (all dimensions in mm).

3.6.3. Group 3

This group had three categories, which are the same as Group 2, but the reinforcement length in this group was longer. In addition, each category of this group had two tests at two different pile offsets. The smallest offset was neglected because it had less effect in the case using the long reinforcement length. Figure 3.29 shows the details of the two tests in the first category. They had the same wall height, the same layer length, and the mechanical connection. As Category 1 in Group 2, the spacing between the reinforcement layers in this category was equal to 135 mm for the bottom layers and 180 mm for the final upmost layer. This category included Test H2 L3 S2 C1 **D2** and Test H2 L3 S2 C1 **D3** at pile offsets of 254 and 381 mm respectively

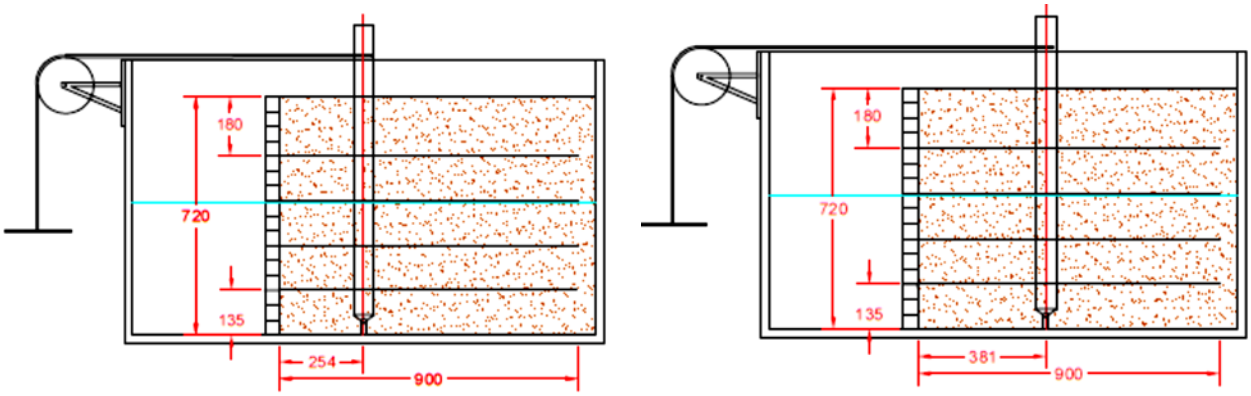

(a) (b)

Figure 3.29 Test details of the first category in Group 3: (a) Test H2 L3 S2 C1 D2 and (b) Test H2 L3 S2 C1 D3 (all dimensions in mm).

The second and the third categories had the same design details. The only difference between these two categories was the connection type. The mechanical connection was used for the second category, and the frictional connection was used for the third category. The second category included Tests H2 L3 S1 C1 **D2** and H2 L3 S1 C2 **D2** while the third category included Tests H2 L3 S1 C1 **D3** and H2 L3 S1 C2 **D3** as shown in Figure 3.30. However, Table 3.3 shows all the design values for each category in Group 3.

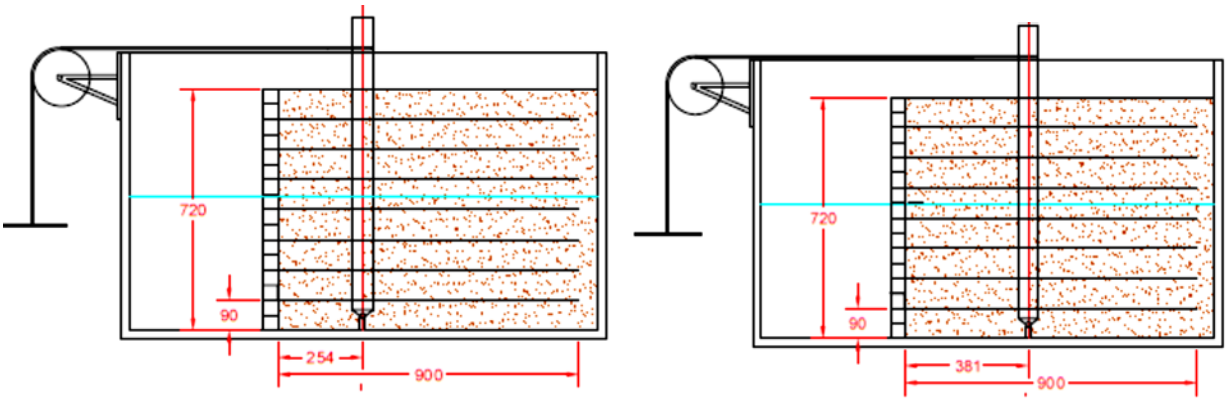

(a) (b)

Figure 3.30 Test details of the second and third categories in Group 3: (a) Test H2 L3 S1 C1 D2, Test H2 L3 S1 C2 D2 and (b) Test H2 L3 S1 C1 D3, Test H2 L3 S1 C2 D3 (all dimensions in mm).

Table 3.3 Tests clasification and detials.

Group	Category	Test Terminology	Pile offset D (mm)	Wall height H (mm)	layer length L (mm)	Layer spacing S (mm)	Connection type
1	------	H1 L1 S1 C1 D1	127	450	315	90	Mechanical
2	1	H2 L2 S2 C1 D1		720	504	135	Mechanical
	2	H2 L2 S1 C1 D1		720	504	90	Mechanical
	3	H2 L2 S1 C2 D1		720	504	90	Frictional
1	------	H1 L1 S1 C1 D2	254	450	315	90	Mechanical
2	1	H2 L2 S2 C1 D2		720	504	135	Mechanical
	2	H2 L2 S1 C1 D2		720	504	90	Mechanical
	3	H2 L2 S1 C2 D2		720	504	90	Frictional
3	1	H2 L3 S2 C1 D2		720	900	135	Mechanical
	2	H2 L3 S1 C1 D2		720	900	90	Mechanical
	3	H2 L3 S1 C2 D2		720	900	90	Frictional
1	------	H1 L1 S1 C1 D3	381	450	315	90	Mechanical
2	1	H2 L2 S2 C1 D3		720	504	135	Mechanical
	2	H2 L2 S1 C1 D3		720	504	90	Mechanical
	3	H2 L2 S1 C2 D3		720	504	90	Frictional
3	1	H2 L3 S2 C1 D3		720	900	135	Mechanical
	2	H2 L3 S1 C1 D3		720	900	90	Mechanical
	3	H2 L3 S1 C2 D3		720	900	90	Frictional

Chapter 4 Test Data

4.1 Introduction

This chapter reports major test data obtained from 18 model tests. The test data in each section or sub-section of this chapter is presented in the following order: (1) the deflections of the wall facing, (2) the strains, stresses, and moments of piles, (3) the deflections of the pile, (4) the strains of the geogrid layers, and (5) the pressures behind the wall facing. The deflections of the wall facing were obtained from the images taken by the camera, which showed the changes of the positions of the indicators above the scale papers. However, the movements of the uppermost row of the indicators were ignored the because of their limited boundary effect.

The measured strains of the pile were averaged for each loading step to find the stresses and moments on both sides of the pile. The following stress-strain relationship was used to calculate the stress along the pile:

$$E = \frac{\sigma}{\varepsilon}$$

where E = elastic modulus of aluminum, i.e., $E = 69\ X\ 10^{6}\ \frac{Kn}{m^2}$.

On the other hand, the stress-moment relationship was used to calculate the moment (M) of the pile: Its value is found by considering (I) and (C).

$$M = \frac{\sigma . I}{C}$$

where I = the moment of inertia of the hollow cylindrical pile (i.e, $1.874\ X\ 10^{-7}\ m^4$) and C = the pile outer radius (i.e., 0.032 m).

The deflection (y) along the pile was obtained by double integrating the right side of the following relationship:

$$\frac{d^2y}{dx^2} = \frac{M}{EI}$$

The integration produced two constants, which were determined by considering specific boundary conditions. In this study, the first boundary condition was at the location of the pin connection between the pile and the base of the test box. The distance from the tip of the pile to the pin connection was equal to the total length of the pile, and the moment at that location was equal to zero. In addition, the displacement of the pile at the pin connection was equal to zero. The other boundary condition corresponded to the displacement transducer and the strain gauges above the wall top surface. The distance between the tip of the pile to the second boundary condition location was measured during each test. the moment was calculated from the strains of the strain gauges and the deflections from the displacement transducer was recorded.

In addition, the strains in each geogrid layer measured by strain gauges were averaged by taking the average of all readings after applying the load to the next loading step. The earth pressures at specific heights behind the wall facing were measured by earth pressure cells. All these data are presented in this chapter.

4.2. Low walls with regular reinforcement length

For these walls, piles were placed at three different offset distances in Tests H1 L1 S1 C1 **D1**, H1 L1 S1 C1 **D2**, and H1 L1 S1 C1 **D3**. All the data from Tests H1 L1 S1 C1 **D1**, H1 L1 S1 C1 **D2**, and H1 L1 S1 C1 **D3** are presented in this section with the exception of the pressure data because several earth pressure cells failed to measure the pressures behind the wall facing.

4.2.1. Deflection of wall facing

The deflections of the wall facing along the vertical centerline in Tests H1 L1 S1 C1 **D1**, H1 L1 S1 C1 **D2**, and H1 L1 S1 C1 **D3**. are shown in Figures 4.1, 4.2, and 4.3, respectively.

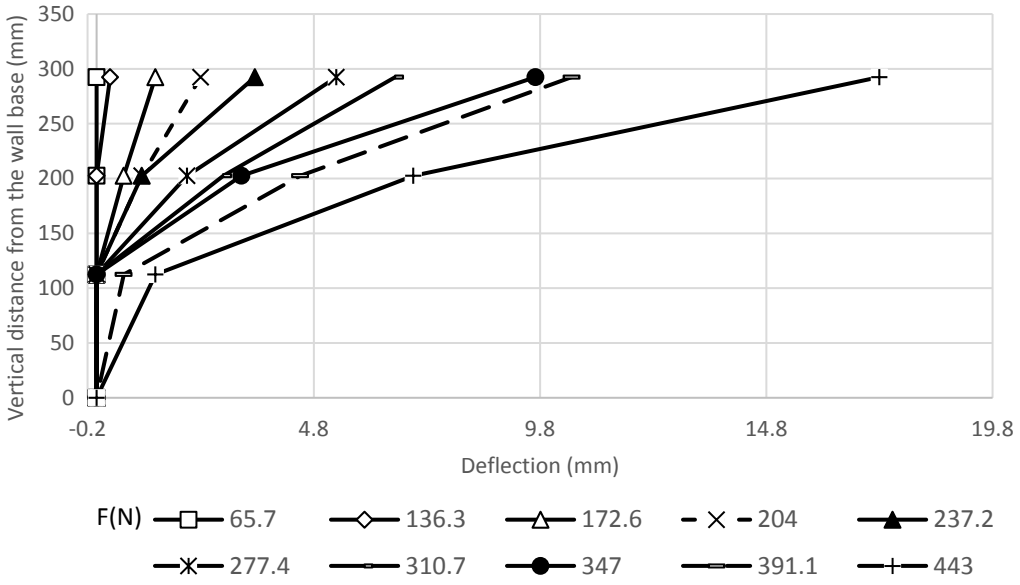

Figure 4.1 Wall facing deflections along the vertical centerline in Test H1 L1 S1 C1 D1 (pile offset = 127 mm).

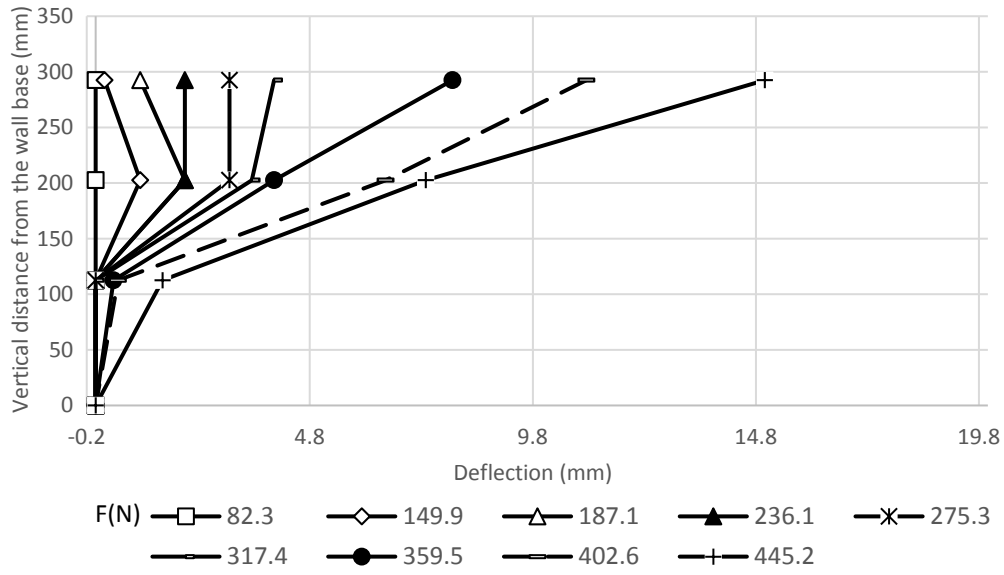

Figure 4.2 Wall facing deflections along the vertical centerline in Test H1 L1 S1 C1 D2 (pile offset = 254 mm).

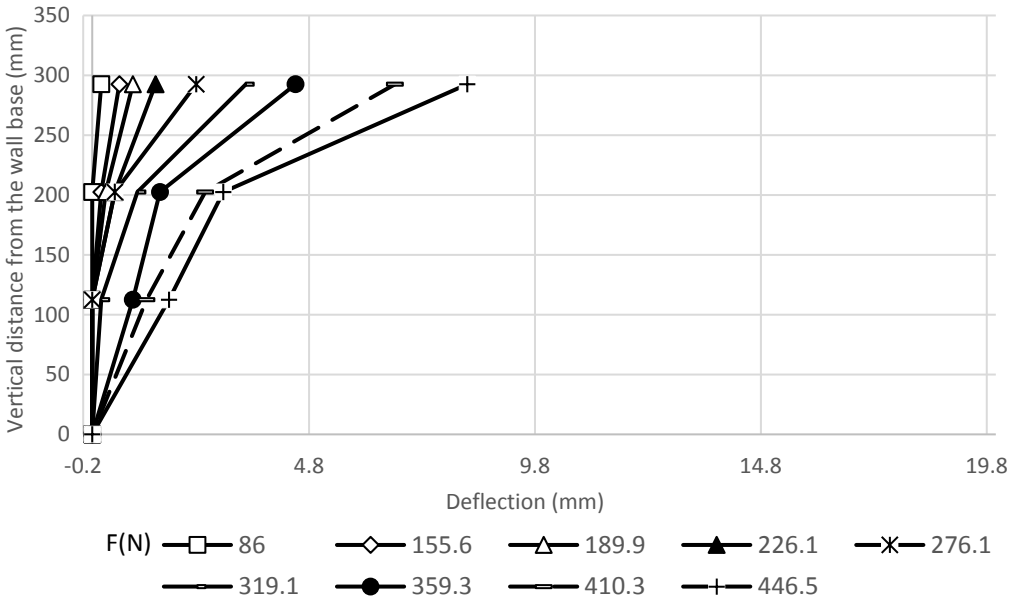

Figure 4.3 Wall facing deflections along the vertical centerline in Test H1 L1 S1 C1 D3 (pile offset = 381 mm).

The deflections of the wall facing decreased by an increase of the pile offset as shown in Figures 4.1, 4.2, and 4.3. In 1-1, Tests 2-1, and Test 3-1, the transverse deflection profiles at the maximum deflection point, which was at 65.5% of the wall height, are shown in Figures 4.4, 4.5, and 4.6.

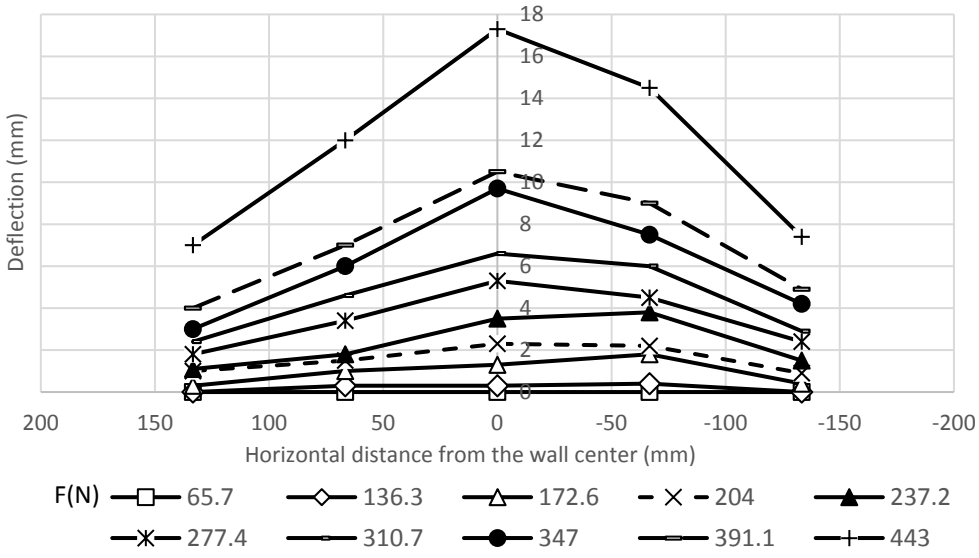

Figure 4.4 Transverse deflection profile at 292.5 mm from the wall base in Test H1 L1 S1 C1 D1 (pile offset = 127 mm).

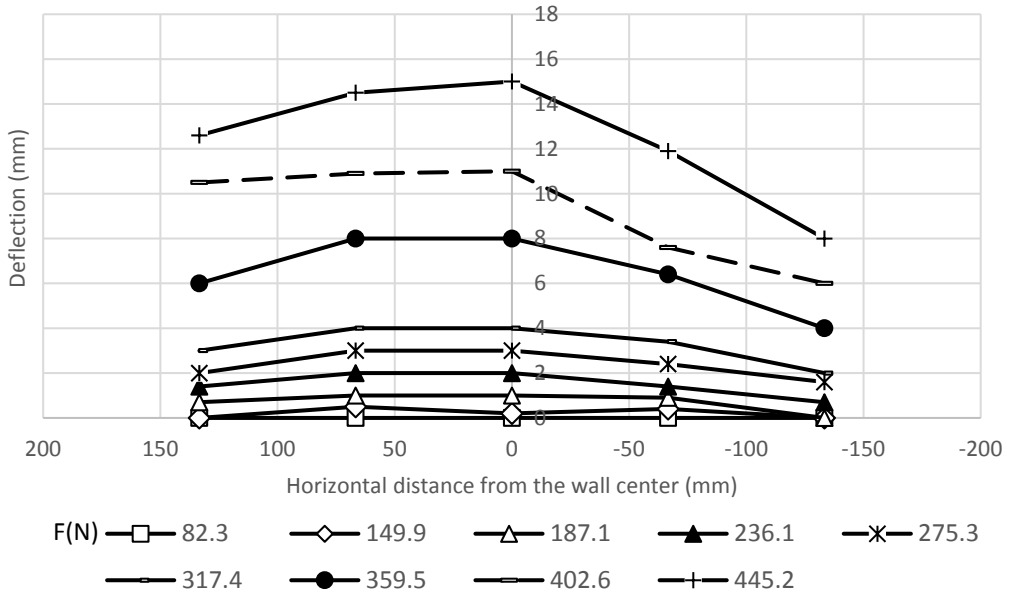

Figure 4.5 Transverse deflection profile at 292.5 mm from the wall base in Test H1 L1 S1 C1 D2 (pile offset = 254 mm).

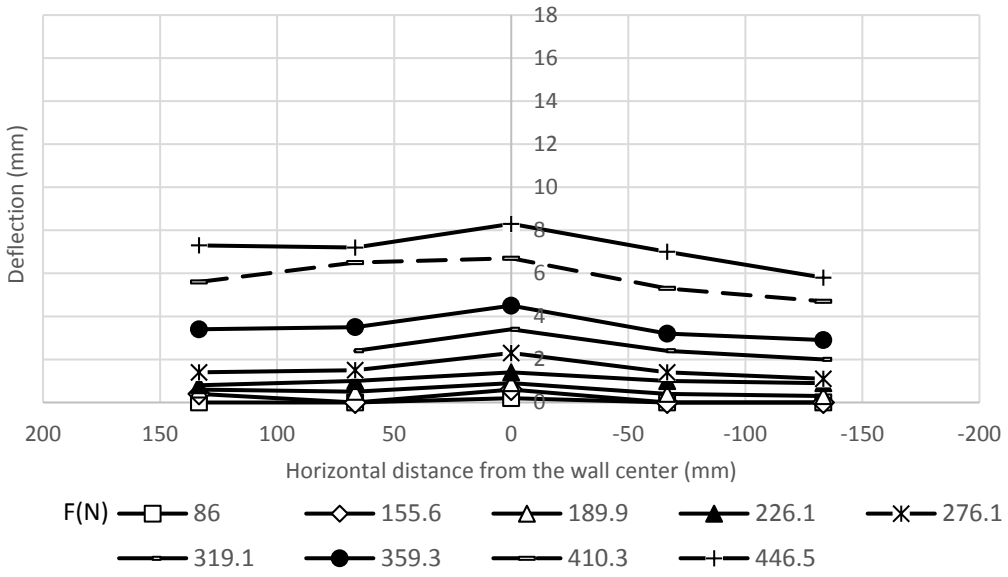

Figure 4.6 Transverse deflection profile at 292.5 mm from the wall base in Test H1 L1 S1 C1 D3 (pile offset = 381 mm).

Figures 4.4, 4.5, 4.6 show that the maximum deflection occurred in the middle of the wall. Also, the deflection distributions were more uniform by an increase of the pile offset. Other figures of the transverse deflection profiles at 202.5 mm and 112.5 mm from the wall base are shown in Section A.2.1 of Appendix A.

4.2.2. Strain, stress, and moment of pile

The measured strains along the compressive side of the pile in Tests H1 L1 S1 C1 **D1**, H1 L1 S1 C1 **D2**, and H1 L1 S1 C1 **D3** are presented in Figures 4.7, 4.8, and 4.9, respectively.

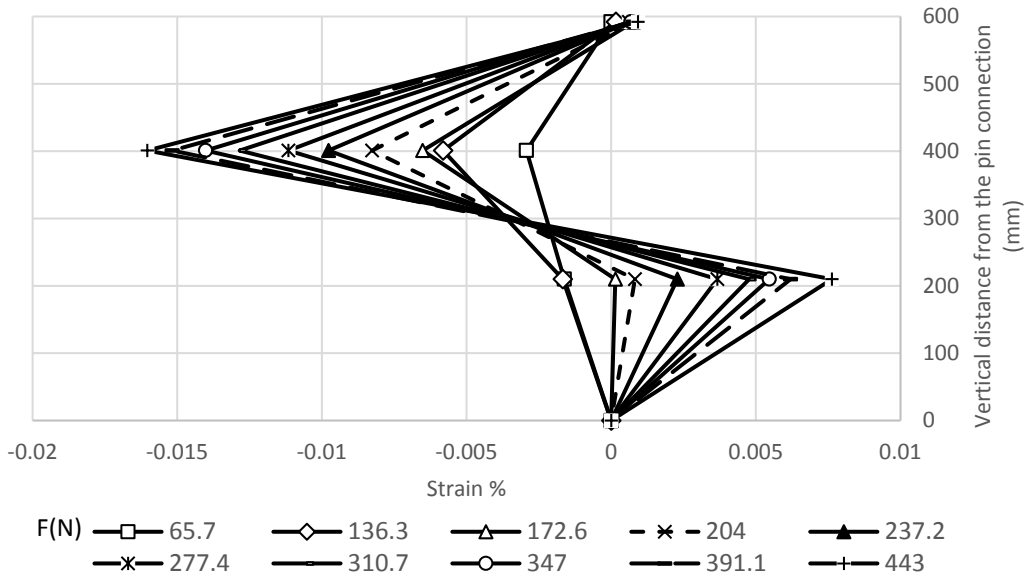

Figure 4.7 Strains along the compressive side of the pile in Test H1 L1 S1 C1 D1 (pile offset = 127 mm).

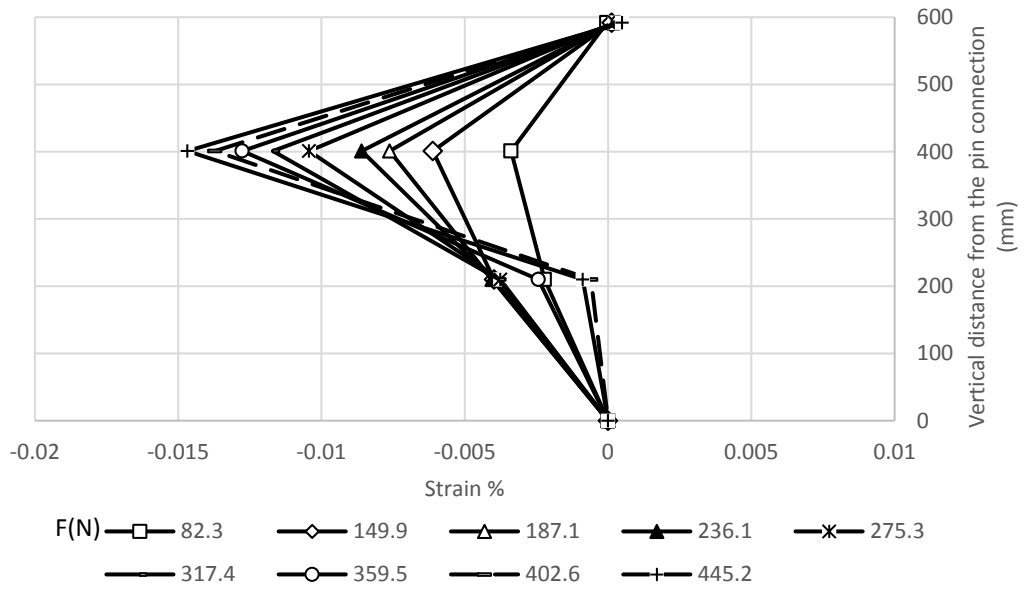

Figure 4.8 Strains along the compressive side of the pile in Test H1 L1 S1 C1 D2. (pile offset = 254 mm).

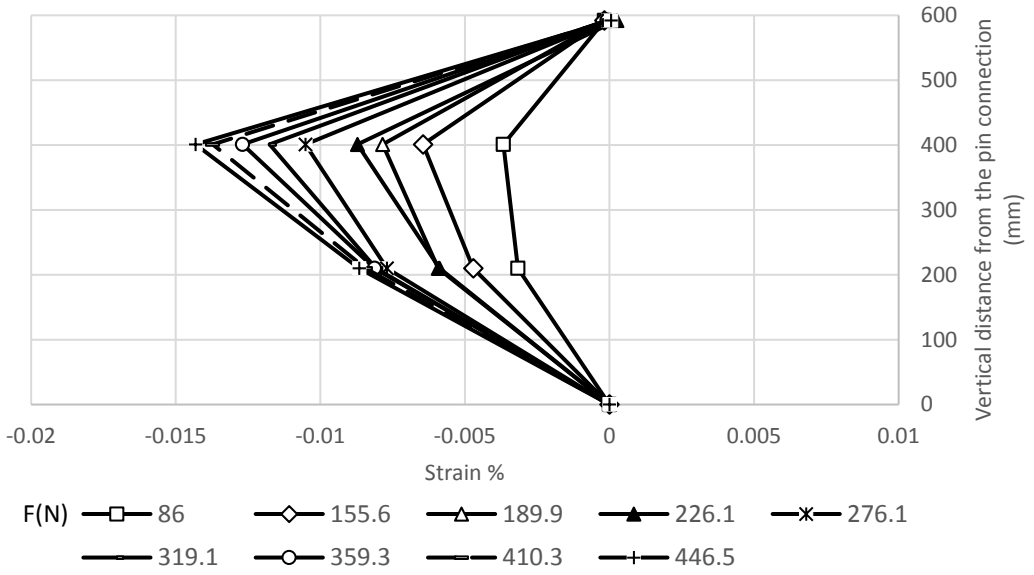

Figure 4.9 Strains along the compressive side of the pile in Test H1 L1 S1 C1 D3 pile offset = 381 mm).

Based on the strain data, the stress and moment of the compressive side of the pile were calculated and reported in Section A.2.2 in Appendix A.

Figures 4.7, 4.8, and 4.9 show that the maximum strains along the compressive side of the pile occurred at 400 mm above the pin connection. This maximum strains in these three tests were almost the same. However, tensile strains developed in the lower part of the compressive side of the pile when the pile had a small offset. This case occurred because There was a multifunction in the strain gauges at that position.

The strains along the tensile side of the pile in Tests H1 L1 S1 C1 **D1**, H1 L1 S1 C1 **D2**, and H1 L1 S1 C1 **D3** are shown in Figures 4.10, 4.11, and 4.12, respectively. Same as the compressive side, the stresses and moments were calculated based on the measured strains along the tensile side of the pile and are included in Section A.2.2 in Appendix A.

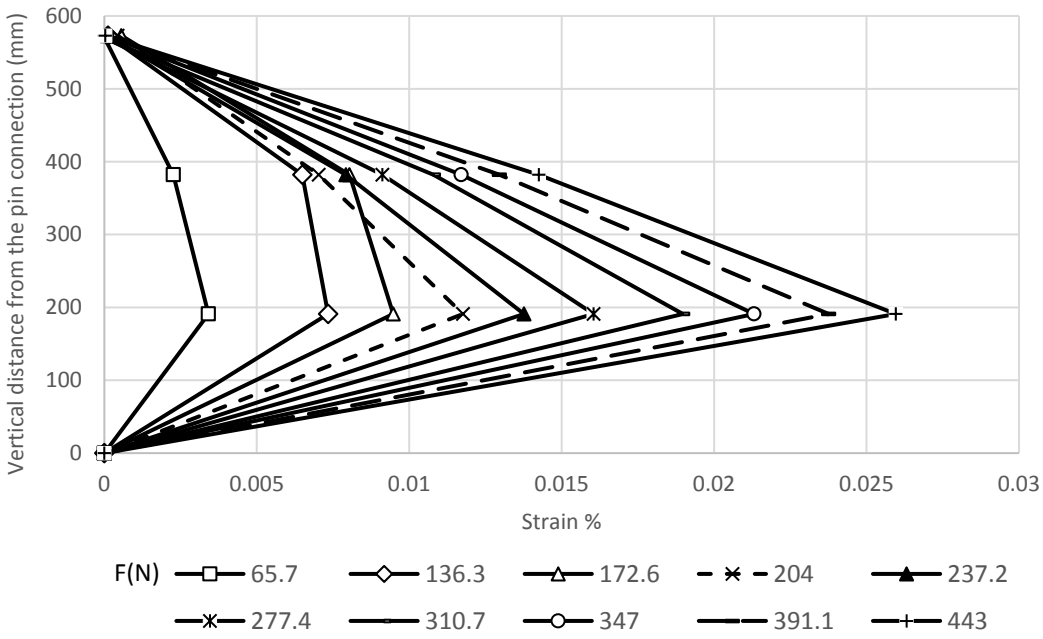

Figure 4.10 Strains along the tensile side of the pile in Test 1-1 (pile offset = 127 mm).

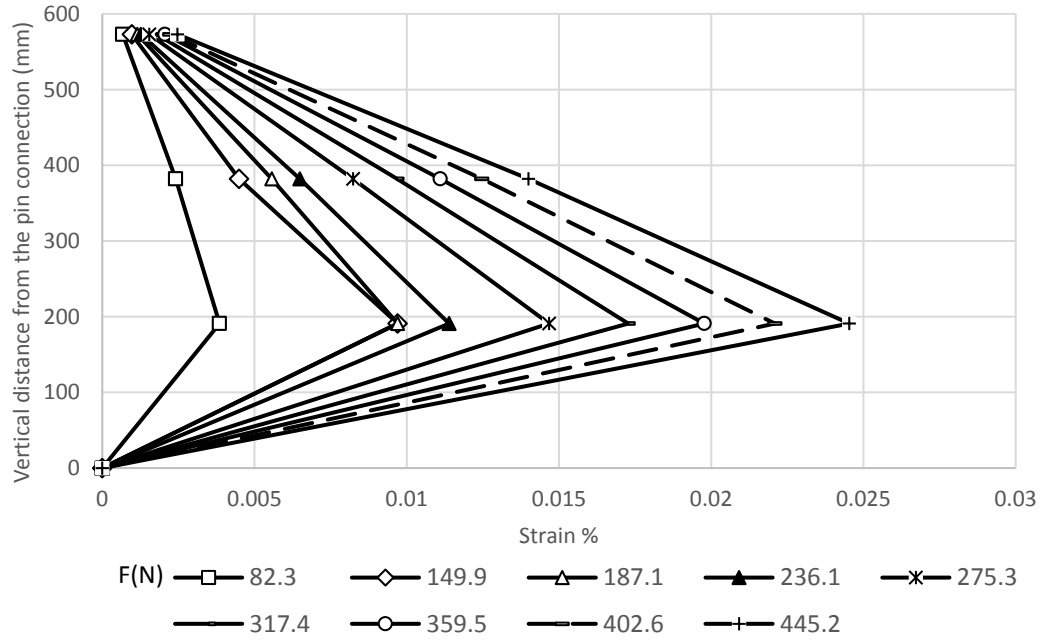

Figure 4.11 Strains along the tensile side of the pile in Test 2-1 (pile offset = 254 mm).

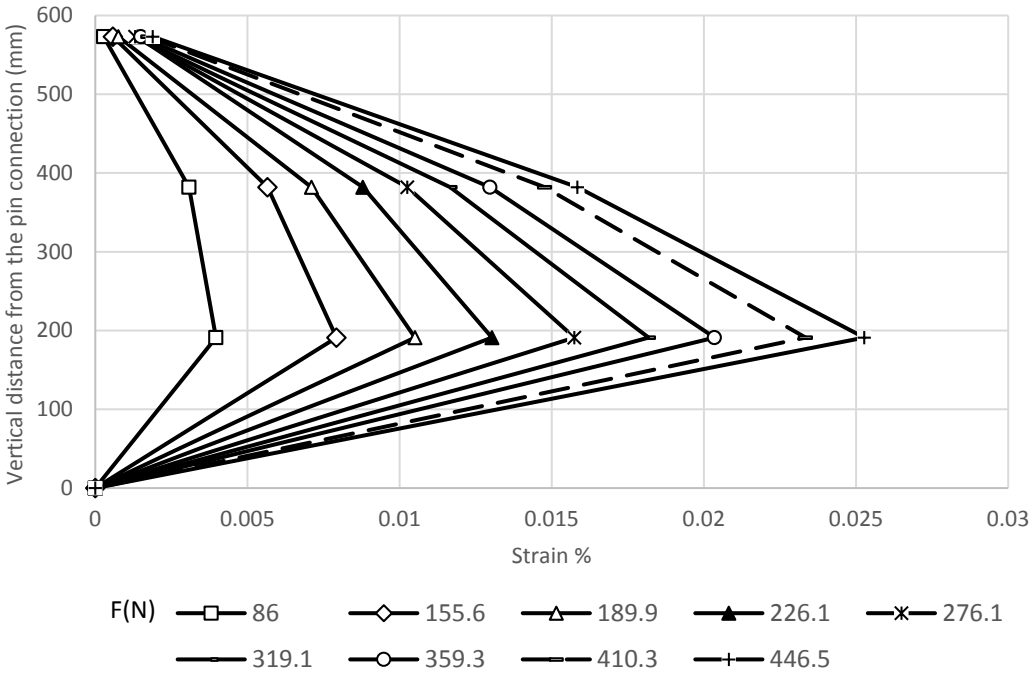

Figure 4.12 Strains along the tensile side of the pile in Test 3-1 pile offset = 381 mm).

Figures 4.10, 4.11, and 4.12 show that the maximum strains along the tensile side of the pile occurred at 200 mm above the pin connection.

4.2.3. Deflection of pile

Figures 4.13, 4.14, and 4.15 present the deflections of the pile under lateral load in Tests H1 L1 S1 C1 **D1**, H1 L1 S1 C1 **D2**, and H1 L1 S1 C1 **D3**, respectively. These deflections were calculated using the strain data of the compressive side of the pile. These curves shows that the deflections decreased by an increase of the pile offset, especially at the load close to the failure.

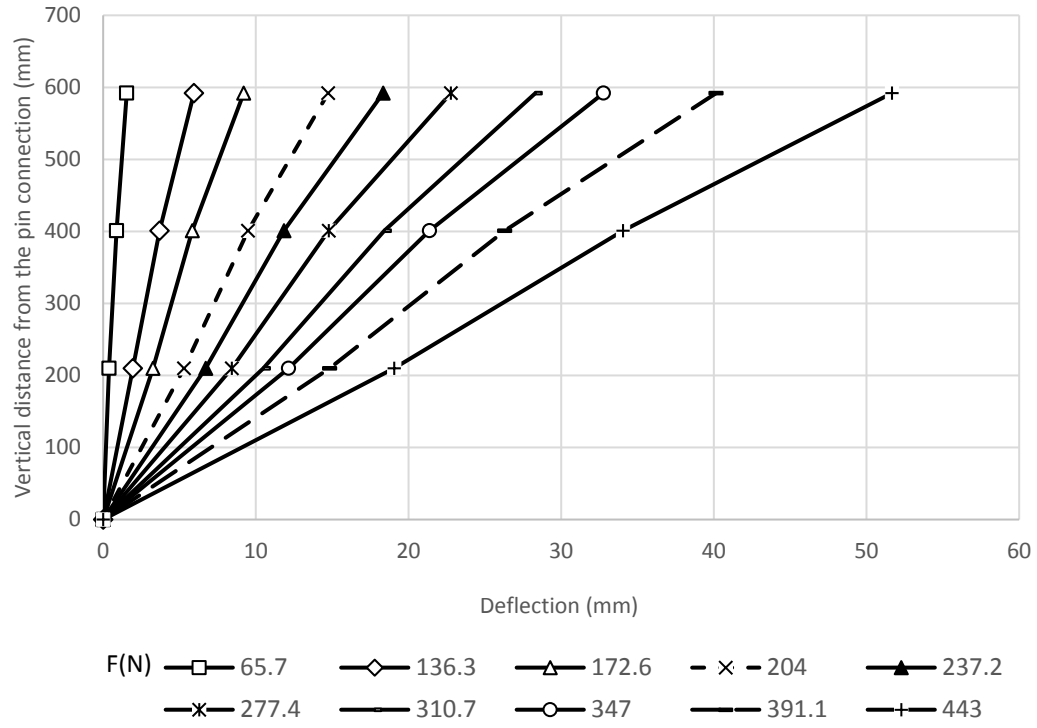

Figure 4.13 Deflections of the pile in Test 1-1 (pile offset = 127 mm).

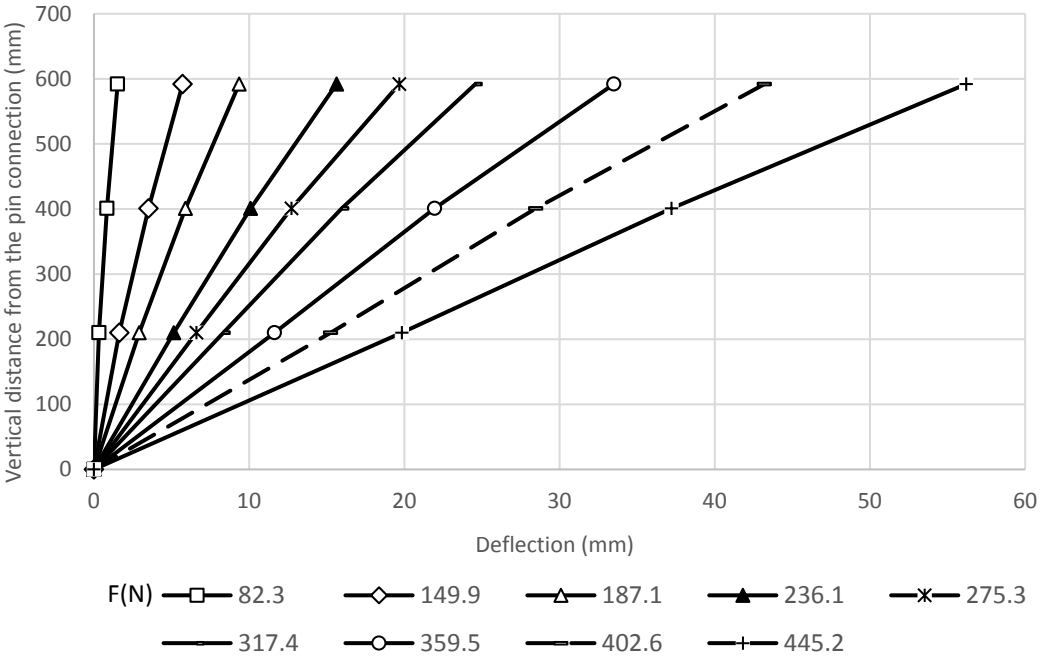

Figure 4.14 Deflections of the pile in Test 2-1 (pile offset = 254 mm).

.

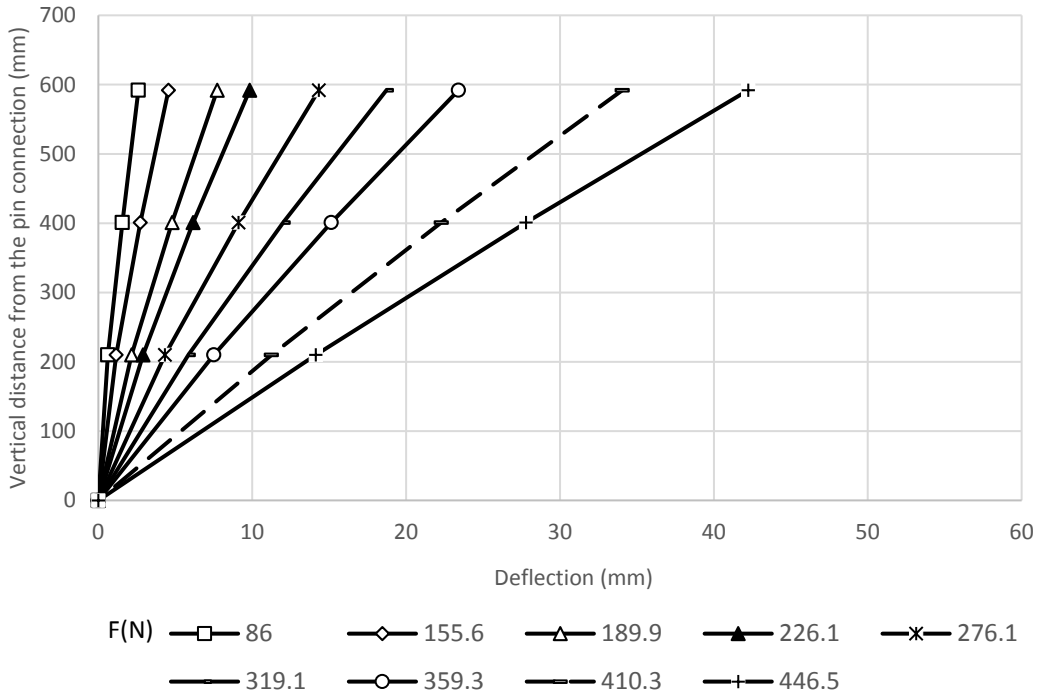

Figure 4.15 Deflections of the pile in Test 3-1 (pile offset = 381 mm).

4.2.4. Strain of geogrid

In each test, the strains of two geogrid layers were monitored using strain gauges. Figures 4.16, 4.17, and 4.18 show the strains of the geogrid in the transverse direction at the elevation of 360 mm in Tests H1 L1 S1 C1 **D1**, H1 L1 S1 C1 **D2**, and H1 L1 S1 C1 **D3**, respectively. In addition, the strains of the geogrid layer at the elevation of 180 mm in the three tests are shown in Section A.2.3 of Appendix A.

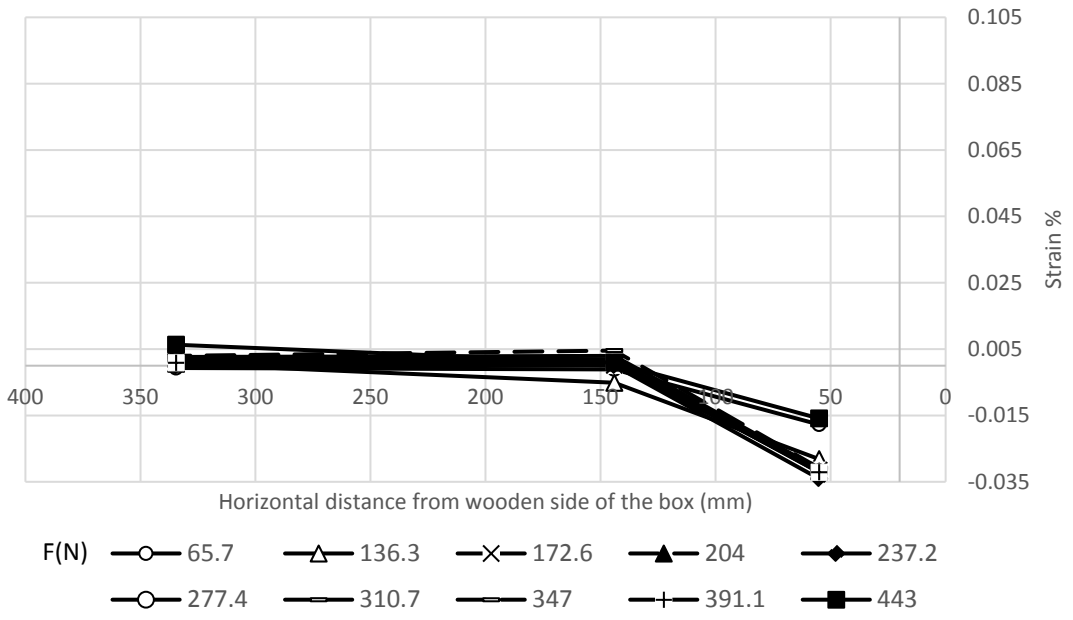

Figure 4.16 Strains of the geogrid layer in the transverse direction at 360 mm from the wall base (Test 1-1 with pile offset = 127 mm).

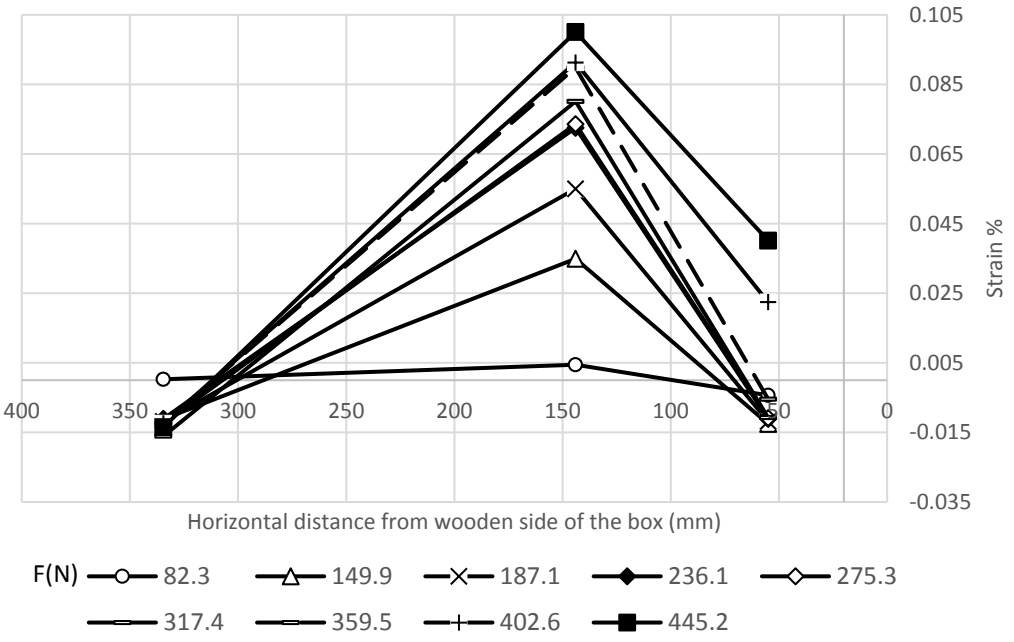

Figure 4.17 Strains of the geogrid layer in the transverse direction at 360 mm from the wall base (Test 2-1 with pile offset = 254 mm).

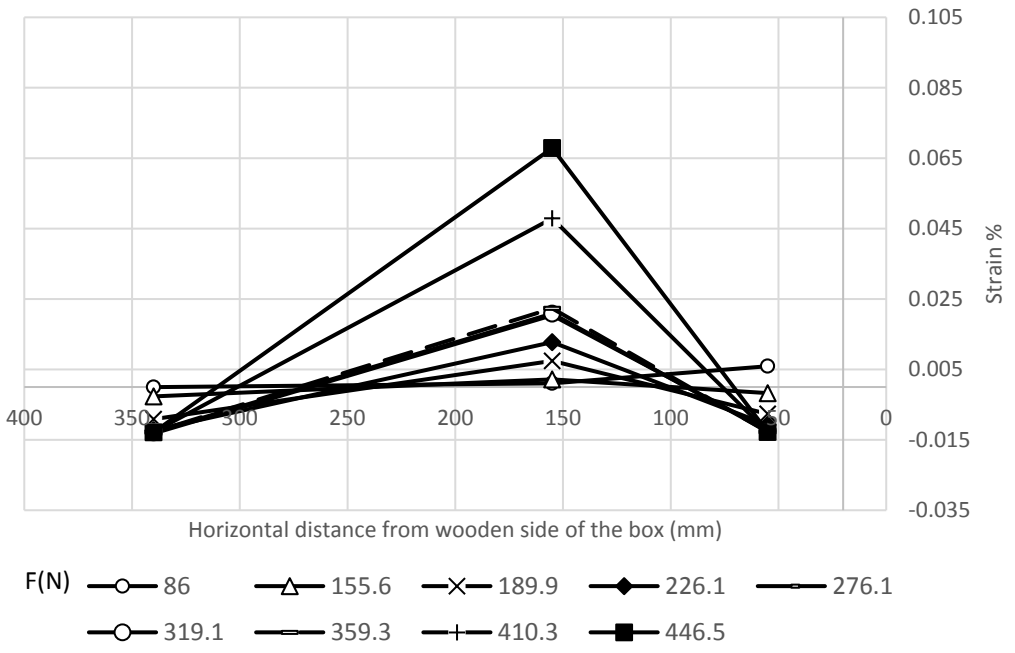

Figure 4.18 Strains of the geogrid layer in the transverse direction at 360 mm from the wall base (Test H2 L2 S1 C1 D1 with pile offset = 381 mm).

The maximum strains in the transverse direction were located in front of the pile in Tests H1 L1 S1 C1 **D2** and H1 L1 S1 C1 **D3**. The strains in the transverse direction in Test H1 L1 S1 C1 **D1** were small as compared with those in other tests. This small strain resulted from the pile close to the wall so that which the short geogrid layer could not function as soil reinforcement.

On the other hand, Figures 4.19, 4.20, and 4.21 show the strains in the longitudinal direction at the elevation of 360 mm in Tests H1 L1 S1 C1 **D1**, H1 L1 S1 C1 **D2**, and H1 L1 S1 C1 **D3**, respectively. All the strain data for the geogrid layer in the longitudinal direction at the elevation of 180 mm from the base of the wall are shown in Section A.2.3 of Appendix A.

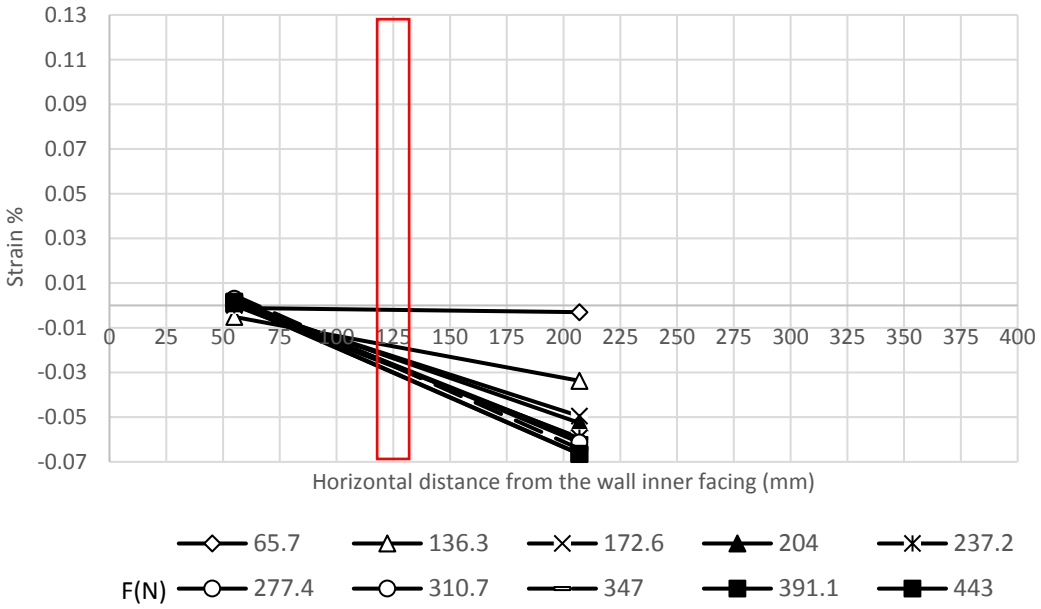

Figure 4.19 Strains of the geogrid layer in the longitudinal direction at 360 mm from the wall base (Test 1-1 with pile offset = 127 mm).

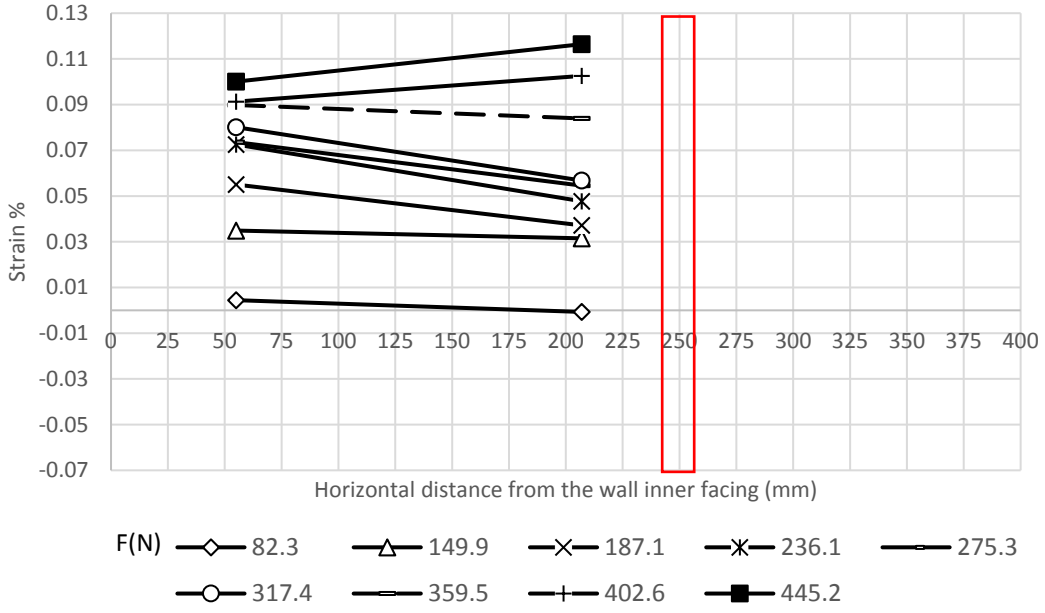

Figure 4.20 Strains of the geogrid layer in the longitudinal direction at 360 mm from the wall base (Test 2-1 with pile offset = 254 mm with pile offset = 254 mm).

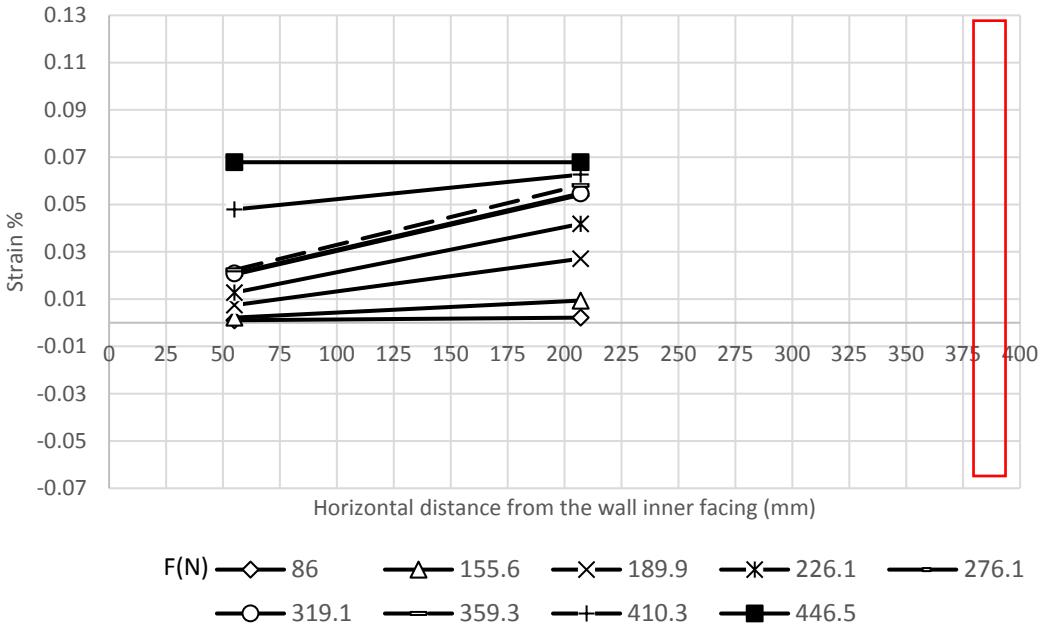

Figure 4.21 Strains of the geogrid layer in the longitudinal direction at 360 mm from the wall base (Test 3-1 with pile offset = 381 mm).

The tensile strains in the longitudinal direction increased along the geogrid layer by an increase of the load in Tests H1 L1 S1 C1 **D2** and H1 L1 S1 C1 **D3**.

4.3. High walls with regular reinforcement length

This section includes the test data for three categories of tests as mentioned in Chapter 3. Each category has three high wall tests with the same parameters except the pile offset.

4.3.1. Category 1

This category includes the data of Tests H2 L2 S2 C1 **D1**, H2 L2 S2 C1 **D2**, and H2 L2 **S2** C1 D3. The spacing between the geogrid layers in this category was 135 mm for the bottom layers and 185 mm for the uppermost layer.

Deflection of wall facing

The deflections of the wall facing along the vertical centerline in Tests H2 L2 S2 C1 **D1**, H2

L2 S2 C1 **D2**, and H2 L2 S2 C1 **D3** are shown in Figures 4.22, 4.23, and 4.24, respectively.

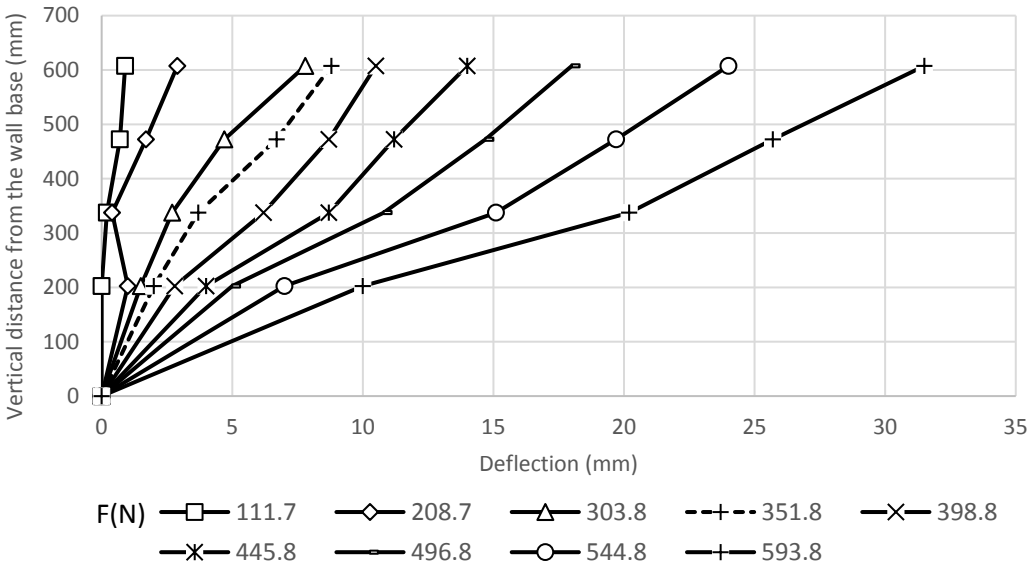

Figure 4.22 Wall facing deflections along the vertical centerline in Test H2 L2 S2 C1 D1 (pile offset = 127 mm).

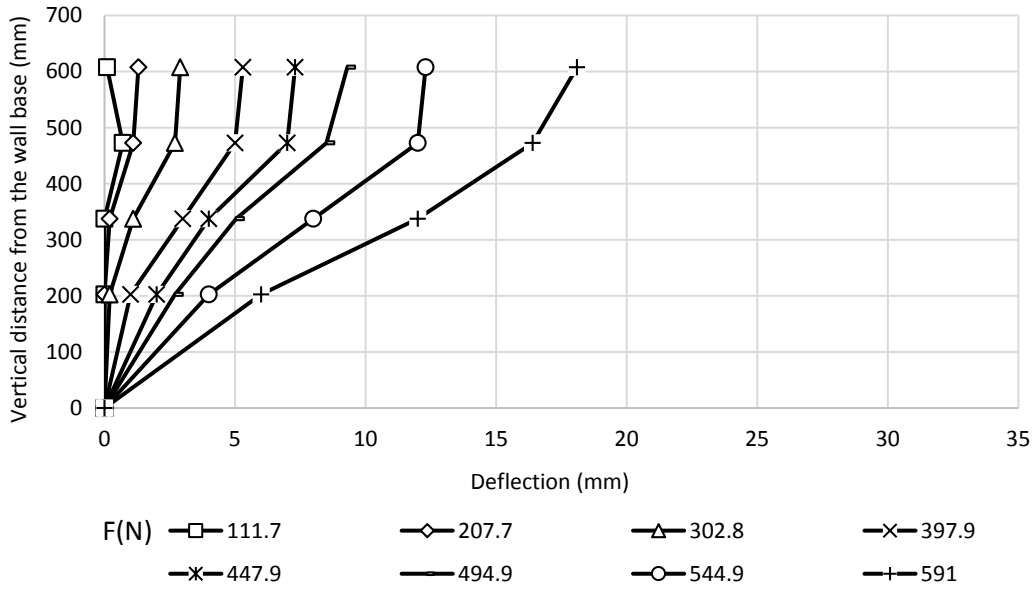

Figure 4.23 Wall facing deflections along the vertical centerline in Test H2 L2 S2 C1 D2 (pile offset = 254 mm).

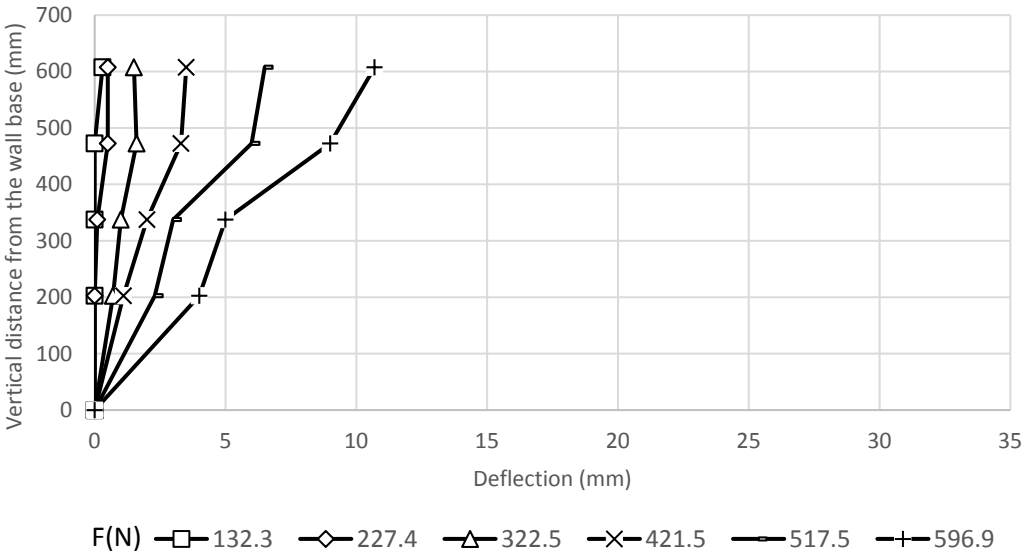

Figure 4.24 Wall facing deflections along the vertical centerline in Test H2 L2 S2 C1 D3 (pile offset = 381 mm).

An increase of the pile offset reduced the deflections of the wall facing. The maximum deflection occurred at 84.4% of the wall height, at which the transverse deflection profiles are shown in Figures 4.25, 4.26, and 4.27.

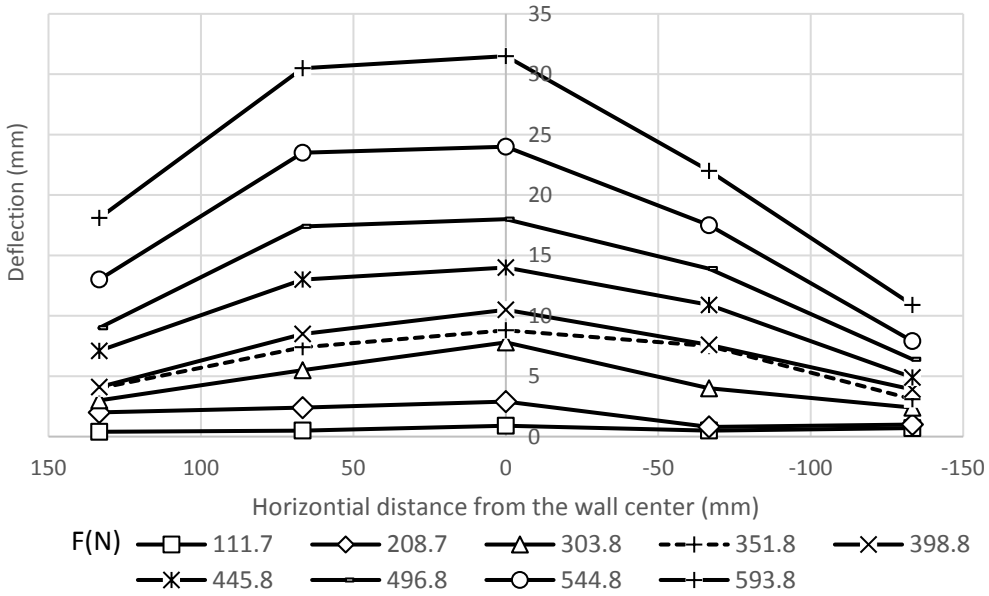

Figure 4.25 Transverse deflection profile at 607.5 mm from the wall base in Test H2 L2 S2 C1 D1 (pile offset = 127 mm).

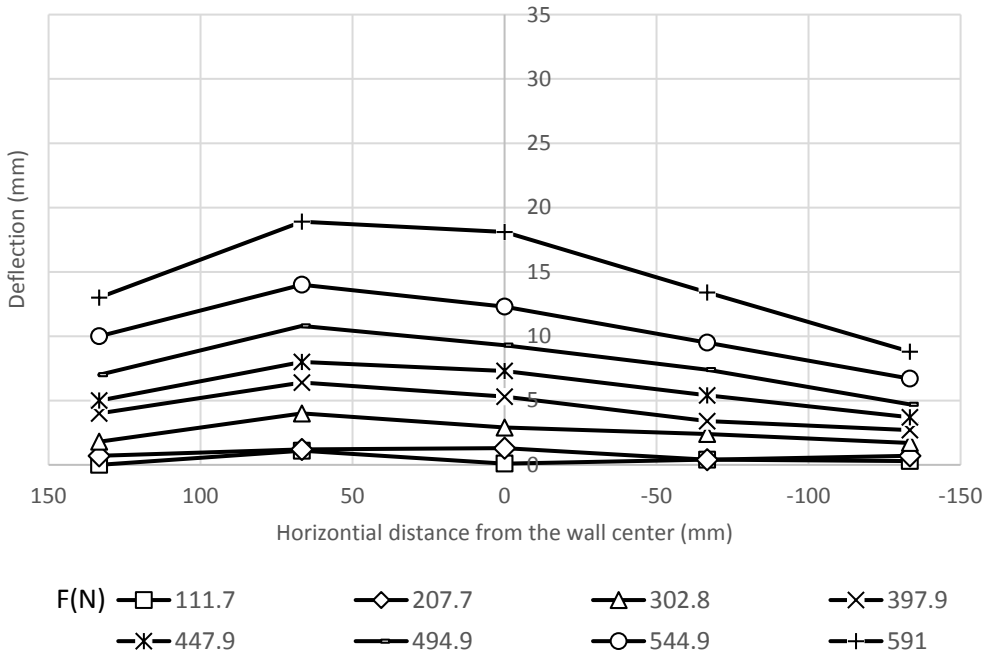

Figure 4.26 Transverse deflection profile at 607.5 mm from the wall base in Test H2 L2 S2 C1 D2 (pile offset = 254 mm).

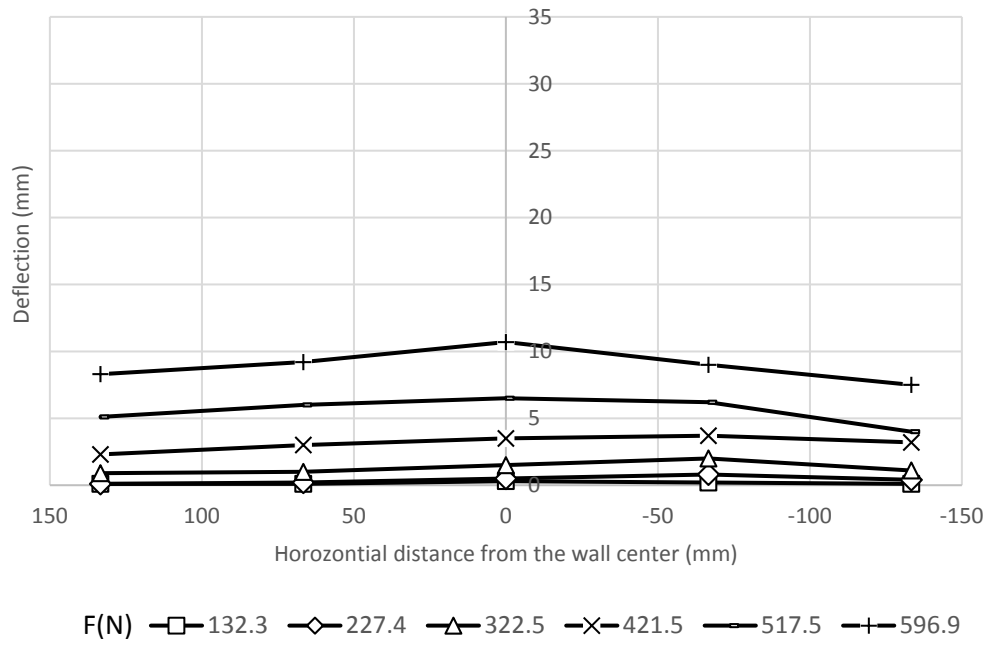

Figure 4.27 Transverse deflection profile at 607.5 mm from the wall base in Test H2 L2 S2 C1 D3 (pile offset = 381 mm).

Figures 4.5, 4.6, 4.7 show the maximum deflections occurred close to the middle of the wall. Furthermore, the transverse deflection profiles became more uniform by an increase of the pile offset. Other transverse deflection profiles at wall heights of 472.5, 337.5, and 202.5 mm are shown in Section A.3.1 of Appendix A.

Strain, stress, and moment of pile

The strains along the compressive side of the pile in Tests H2 L2 S2 C1 **D1**, H2 L2 S2 C1 **D2**, and H2 L2 S2 C1 **D3**.are presented in Figures 4.28, 4.29, and 4.30, respectively. The data for the stresses and the moments along the compressive side of the pile are shown in Section A.3.1. of Appendix A.

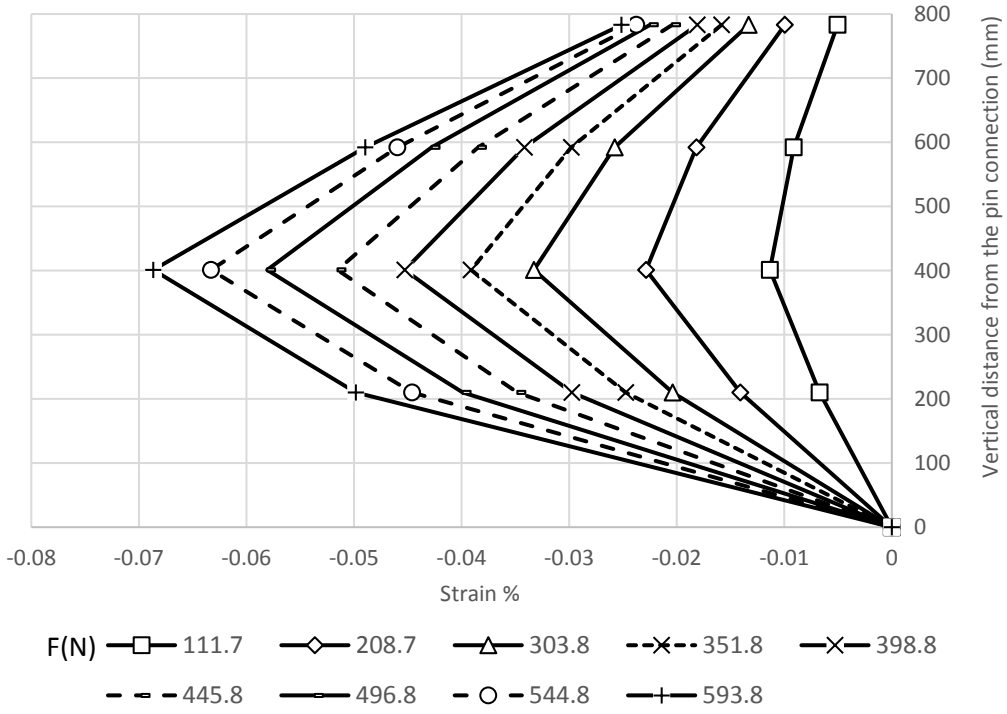

Figure 4.28 Strains along the compressive side of the pile in Test H2 L2 S2 C1 D1 (pile offset = 127 mm).

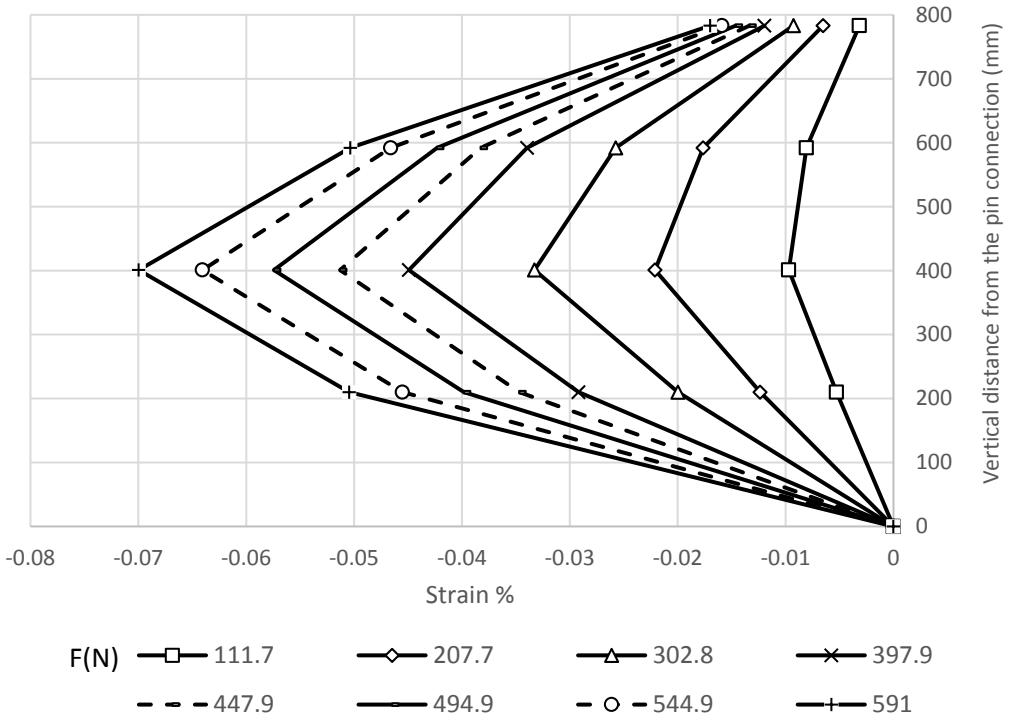

Figure 4.29 Strains along the compressive side of the pile in Test H2 L2 S2 C1 D2 (pile offset = 254 mm).

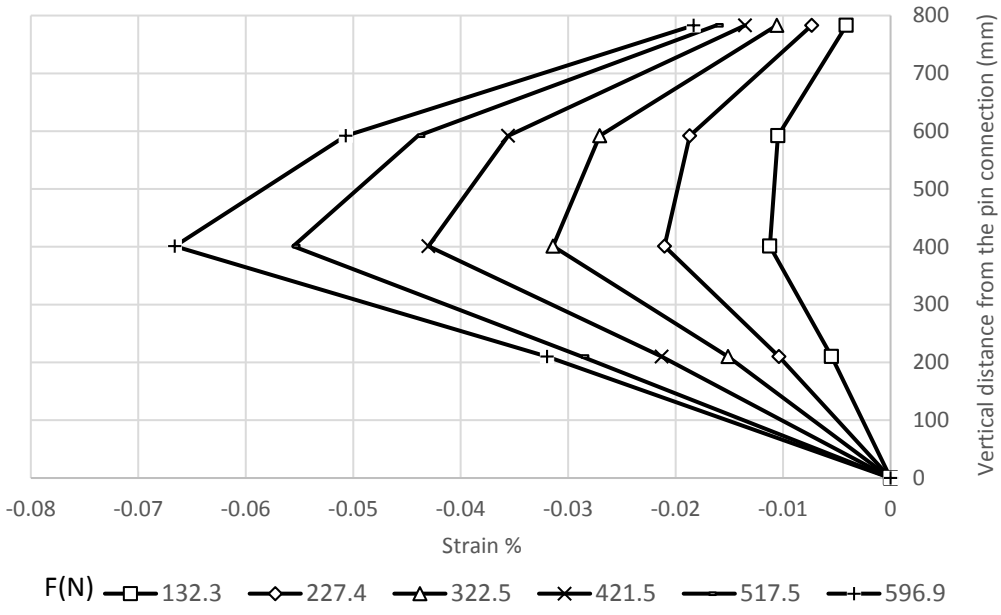

Figure 4.30 Strains along the compressive side of the pile in Test H2 L2 S2 C1 D3 (pile offset = 381 mm).

The maximum strains and moments along the compressive side of the pile occurred at 400 mm above the pin connection; however, the differences in their values among these three tests are small. On the other hand, the strains along the tensile side of the pile in Tests H2 L2 S2 C1 D1, H2 L2 S2 C1 D2, and H2 L2 S2 C1 D3 are presented in Figures 4.30, 4.31, and 4.32, respectively.

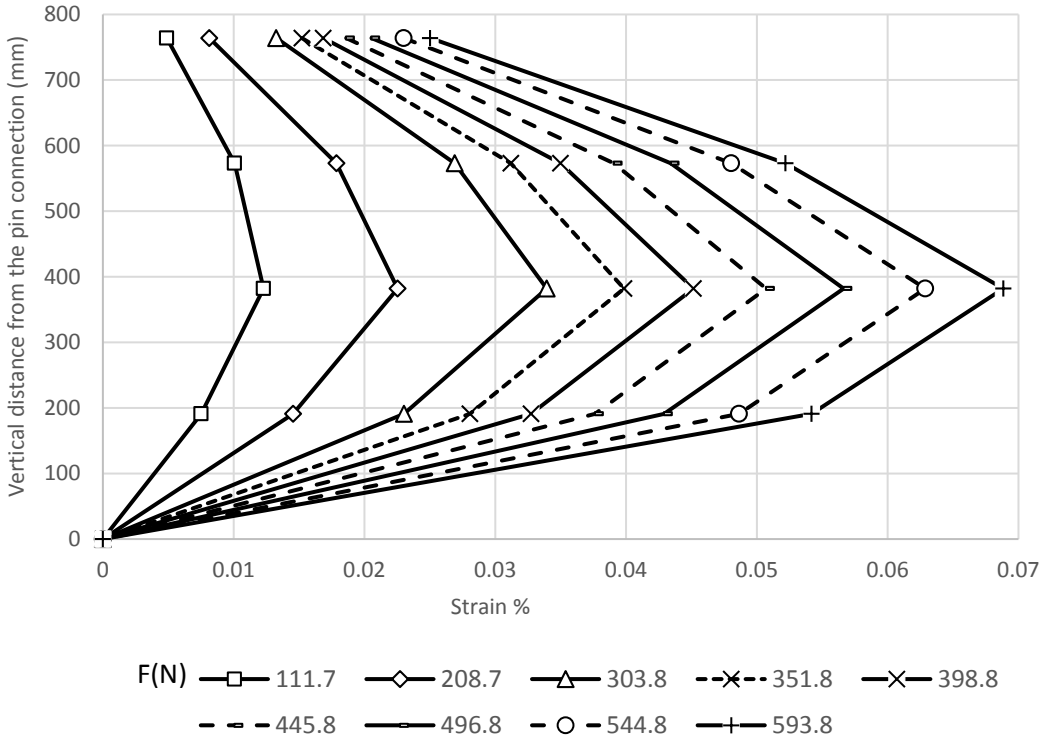

Figure 4.31 Strains along the tensile side of the pile in Test H2 L2 S2 C1 D1 (pile offset = 127 mm).

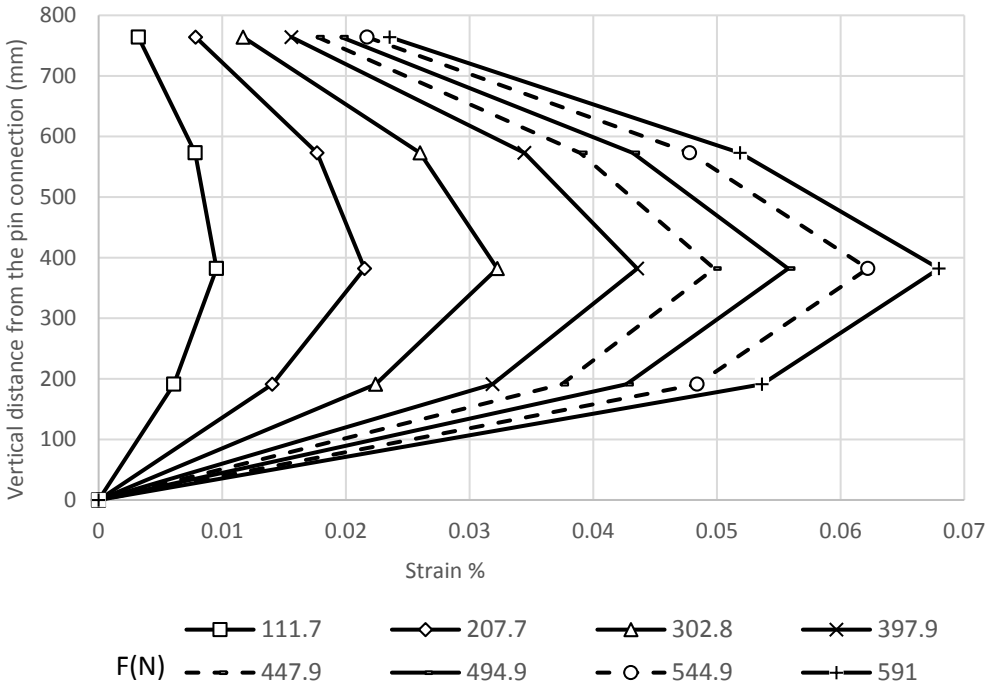

Figure 4.31 Strains along the tensile side of the pile in Test H2 L2 S2 C1 D2 (pile offset = 254 mm).

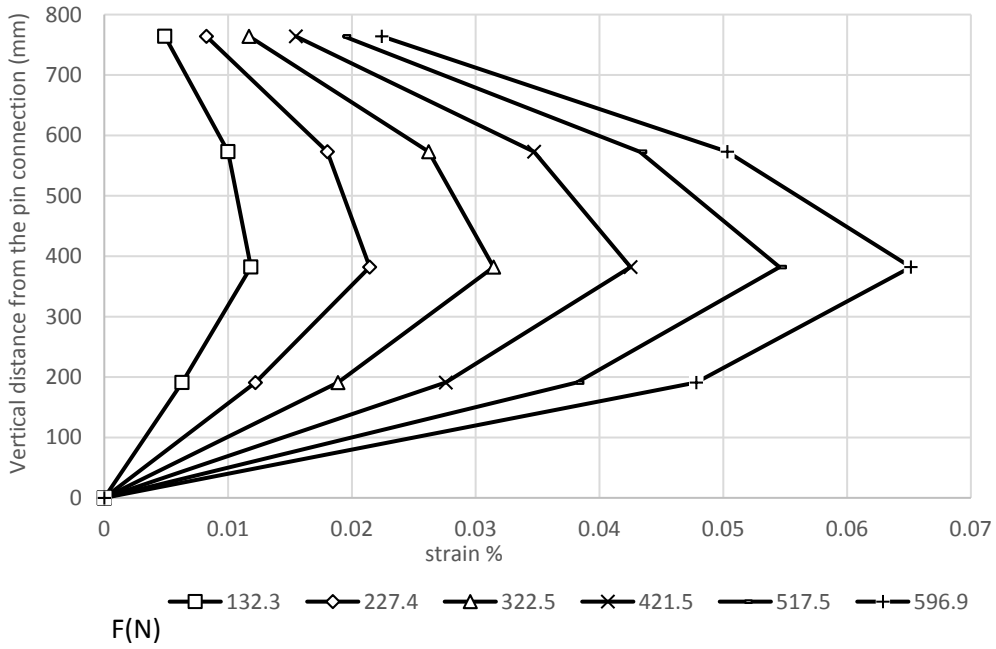

Figure 4.32 Strains along the tensile side of the pile in Test H2 L2 S2 C1 D3 (pile offset = 381 mm).

All the stress and moment data along the tensile side are shown in Section A.3.1. of Appendix A. The magnitudes and distributions of the strains and moments in the tensile side are similar to those in the compressive side.

Deflection of pile

The deflections of the pile under lateral loads in Tests H2 L2 S2 C1 **D1**, H2 L2 S2 C1 **D2**, and H2 L2 S2 C1 **D3**.are shown in Figures 4.33, 4.34, and 4.35 respectively. These figures show that an increase of the plie offset reduced the deflections of the pile. Moreover, the pile shows some flexibility with the increase of the lateral load in these three tests.

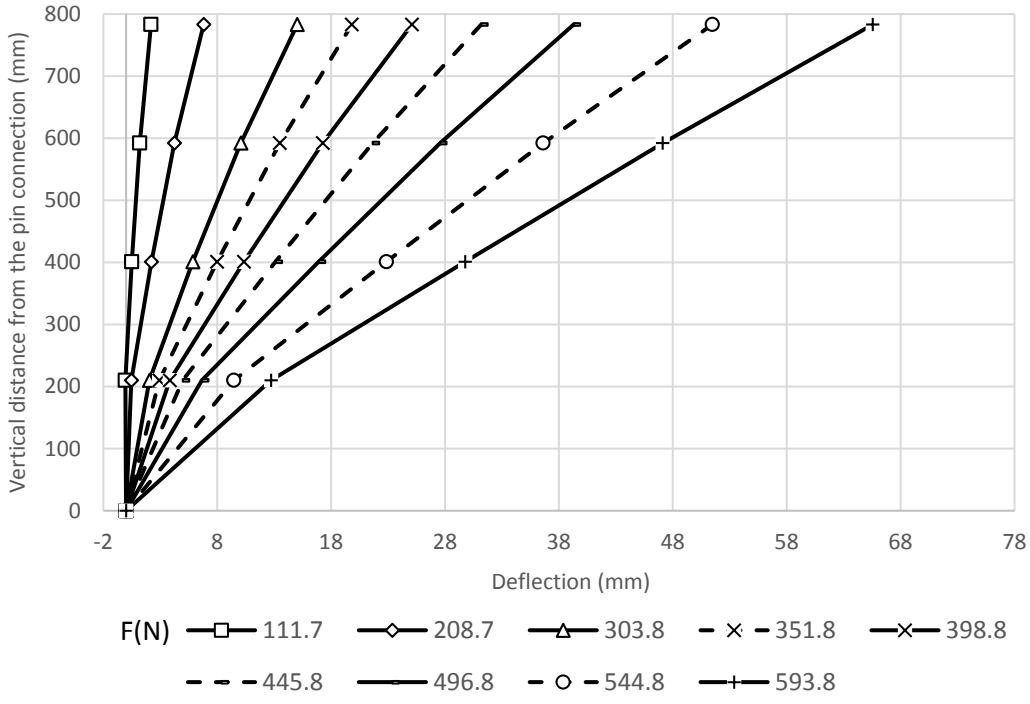

Figure 4.33 Deflections of the pile in Test H2 L2 S2 C1 D1 (pile offset = 127 mm).

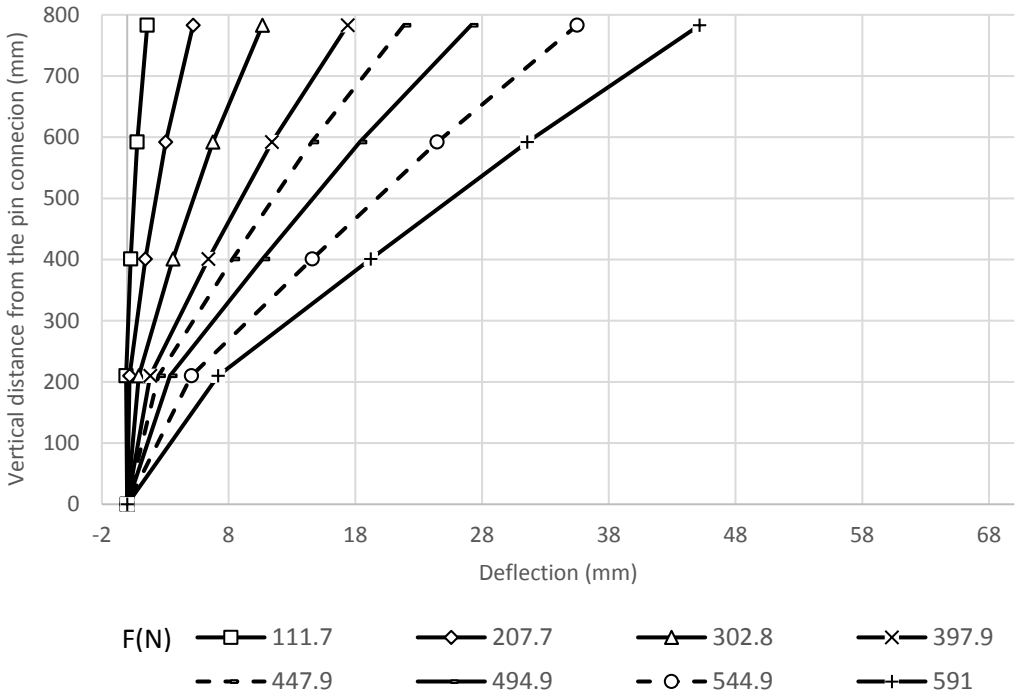

Figure 4.34 Deflections of the pile in Test H2 L2 S2 C1 D2 (pile offset = 254 mm).

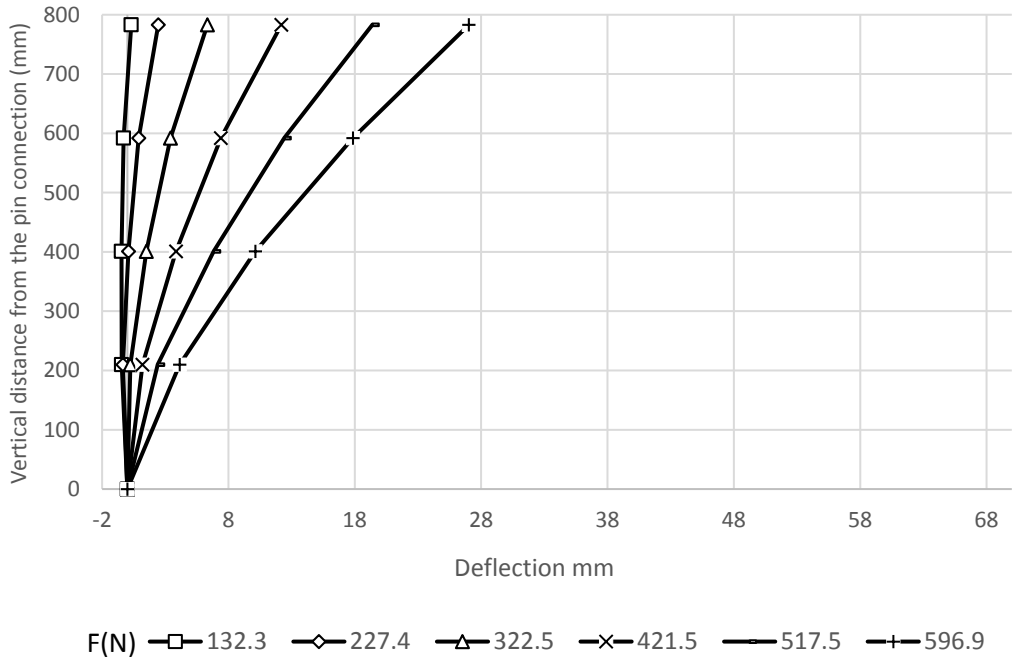

Figure 4.35 Deflections of the pile in Test H2 L2 S2 C1 D3 (pile offset = 381 mm).

Strain of geogrid

The strain distributions of four geogrid layers in the longitudinal direction were obtained. Figures 4.36, 4.37, and 4.38 show the strain distributions at the elevation of 540 mm from the wall base for Tests H2 L2 S2 C1 **D1**, H2 L2 S2 C1 **D2**, and H2 L2 S2 C1 **D3**., respectively. The tensile strains near to the pile location were large in the tests with pile offsets at 2d and 4d because the pile at these offsets was within the high tension zone of the geogrid. On the other hand, a compressive strain was observed near the pile with an offset at 6d because the pile was far from the wall facing and near the end of the geogrid layer. The strain distributions of the geogrid layers at the elevations of 405, 270, and 135 mm are presented in Section A.3.1 of Appendix A.

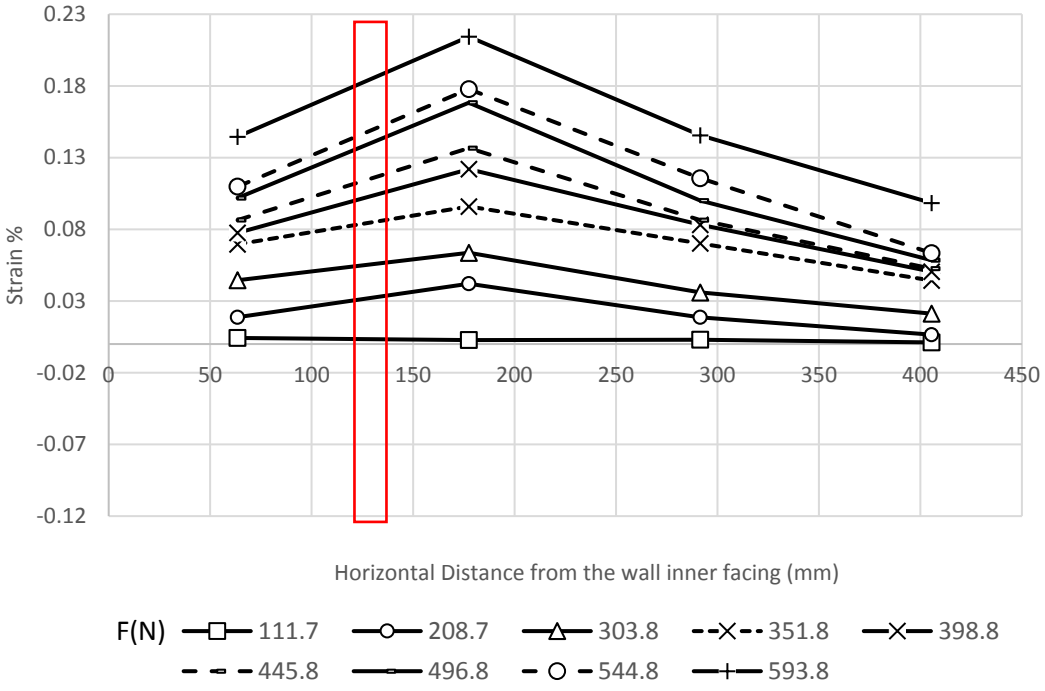

Figure 4.36 Strains of the geogrid layer in the longitudinal direction at 540 mm from the wall base (Test H2 L2 S2 C1 D1 with pile offset = 127 mm).

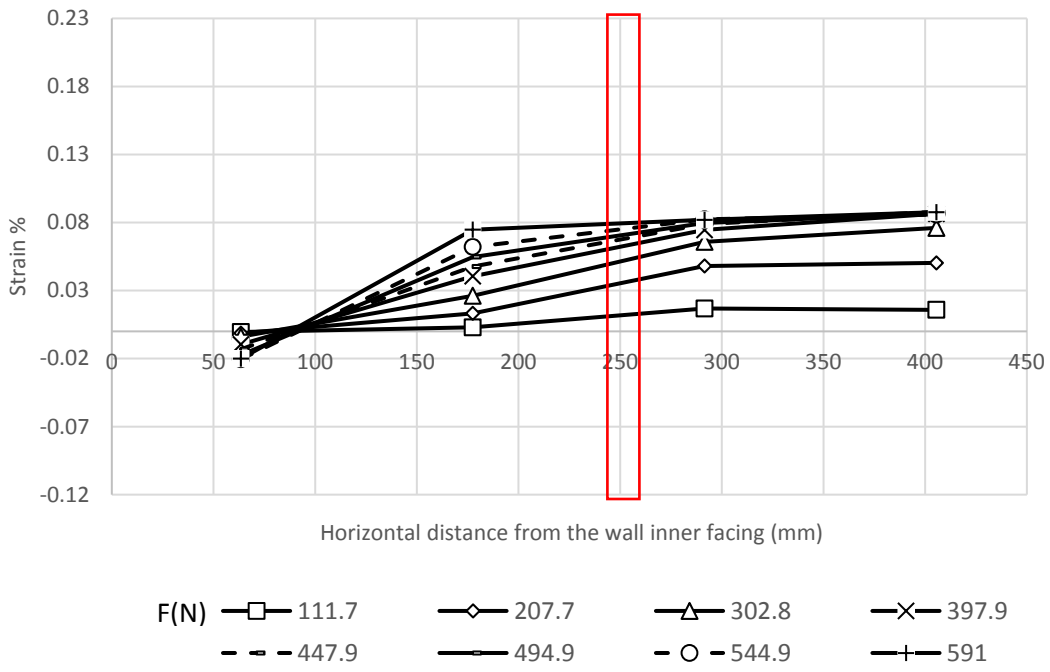

Figure 4.37 Strains of the geogrid layer in the longitudinal direction at 540 mm from the wall base (Test H2 L2 S2 C1 D2 with pile offset = 254 mm).

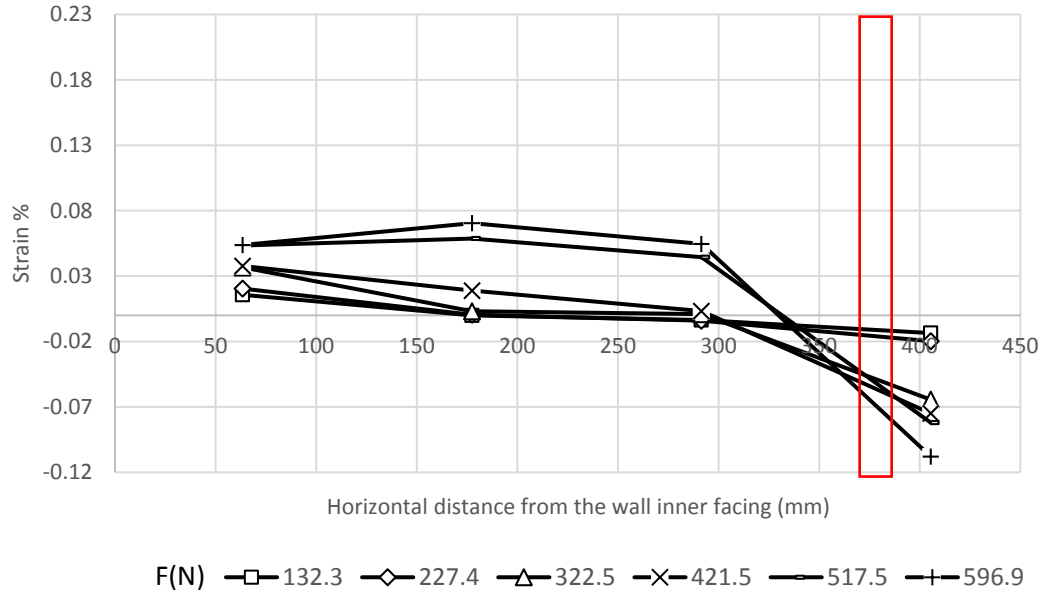

Figure 4.38 Strains of the geogrid layer in the longitudinal direction at 540 mm from the wall base (Test H2 L2 S2 C1 D3 with pile offset = 381 mm).

Pressure behind wall facing

Figures 4.39, 4.40, and 4.41 present the pressure distribution behind the wall facing in Tests H2 L2 S2 C1 **D1**, H2 L2 S2 C1 **D2**, and H2 L2 S2 C1 **D3**., respectively.

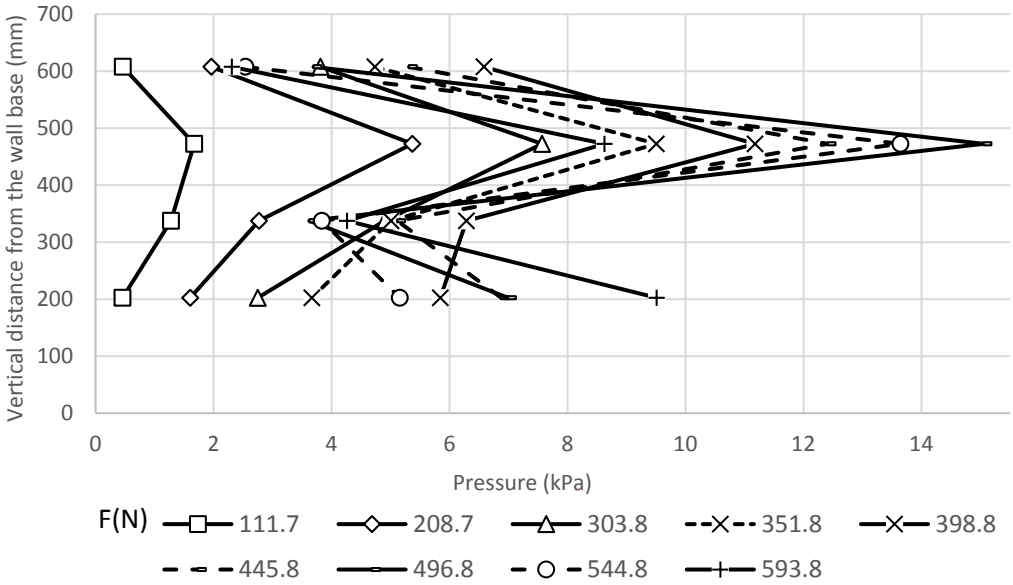

Figure 4.39 Pressures behind the wall facing along the vertical centerline in Test H2 L2 S2 C1 D1 (pile offset = 127 mm).

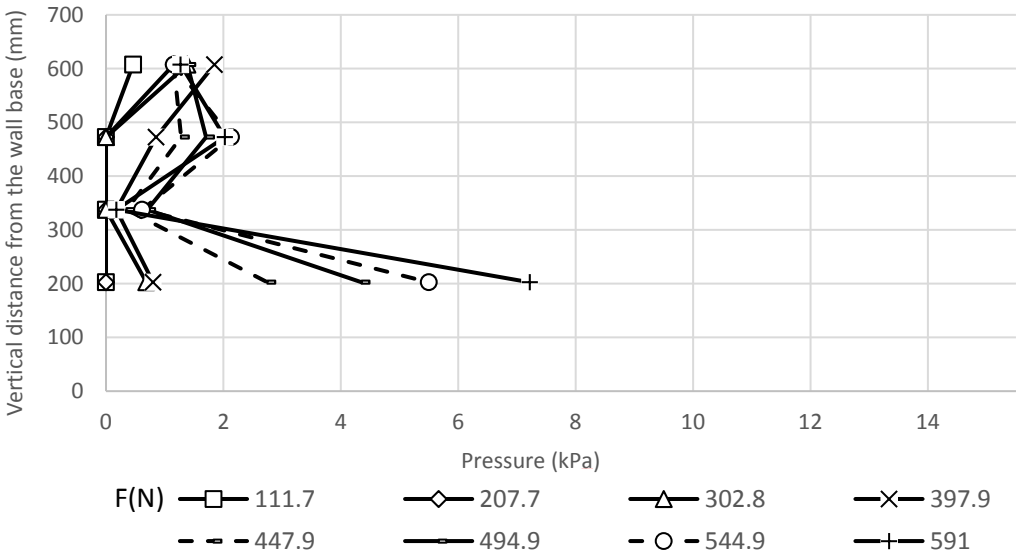

Figure 4.40 Pressures behind the wall facing along the vertical centerline in Test H2 L2 S2 C1 D2 (pile offset = 254 mm).

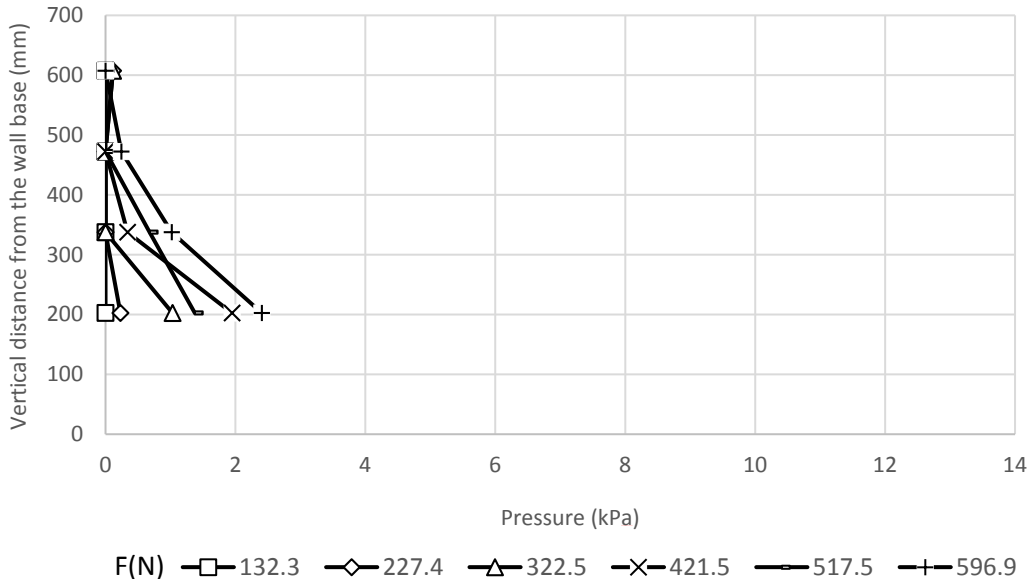

Figure 4.41 Pressures behind the wall facing along the vertical centerline in Test H2 L2 S2 C1 D3 (pile offset = 381 mm).

A high pressure zone was located at 65.5% of the wall height in the test with a small pile offset as shown in Figure 4.39. The pressures in this zone decreased by an increase of the pile offset as shown in Figures 4.40 and 4.41. Moreover, the pressure behind the lower part of the wall near the base was high because of the high overburden stress.

The pressure distributions behind the wall facing in the transverse direction at the elevation of 472.5 mm from the wall base are shown in Figures 4.42, 4.43, and 4.44 for H2 L2 S2 C1 **D1**, H2 L2 S2 C1 **D2**, and H2 L2 S2 C1 **D3**., respectively. In addition, the pressure distributions behind the wall facing in the transverse direction at the elevation of 202.5 mm from the wall base are shown in Figures 4.45, 4.46, and 4.47 for the same tests. Other pressure distributions in the transverse direction at the elevations of 607.5 and 337.5 mm from the wall base are shown in Section A.3.1 in Appendix A.

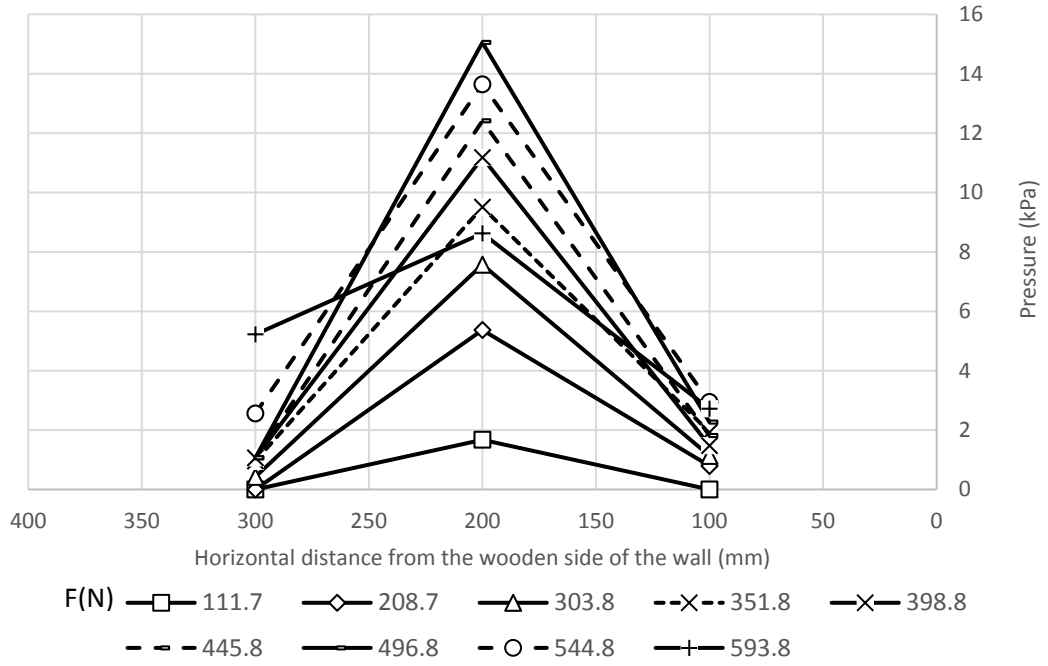

Figure 4.42 Pressure distributions in the transverse direction at the elevation of 472.5 mm from the wall base in Test H2 L2 S2 C1 D1 (pile offset = 127 mm).

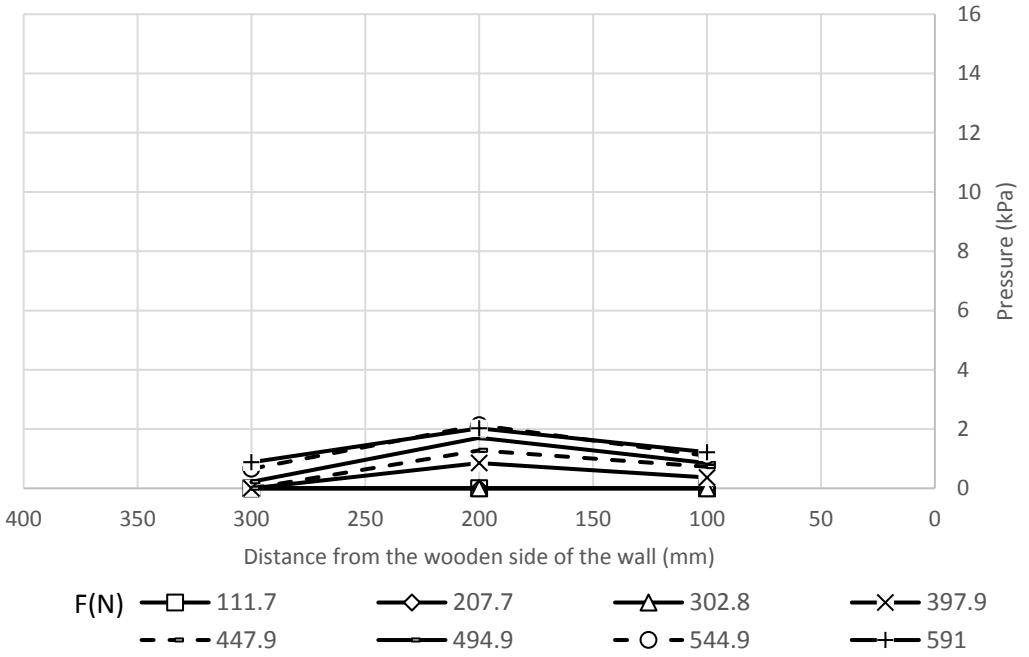

Figure 4.43 Pressure distributions in the transverse direction at the elevation of 472.5 mm from the wall base in Test H2 L2 S2 C1 D2 (pile offset = 254 mm).

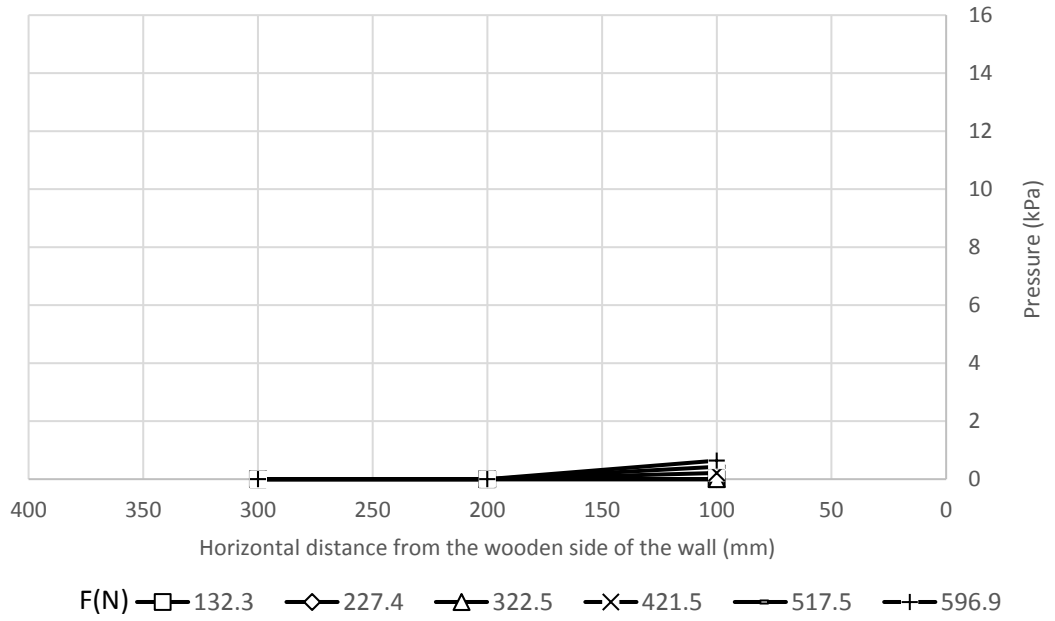

Figure 4.44 Pressure distributions in the transverse direction at the elevation of 472.5 mm from the wall base in Test H2 L2 S2 C1 D3 (pile offset = 381 mm).

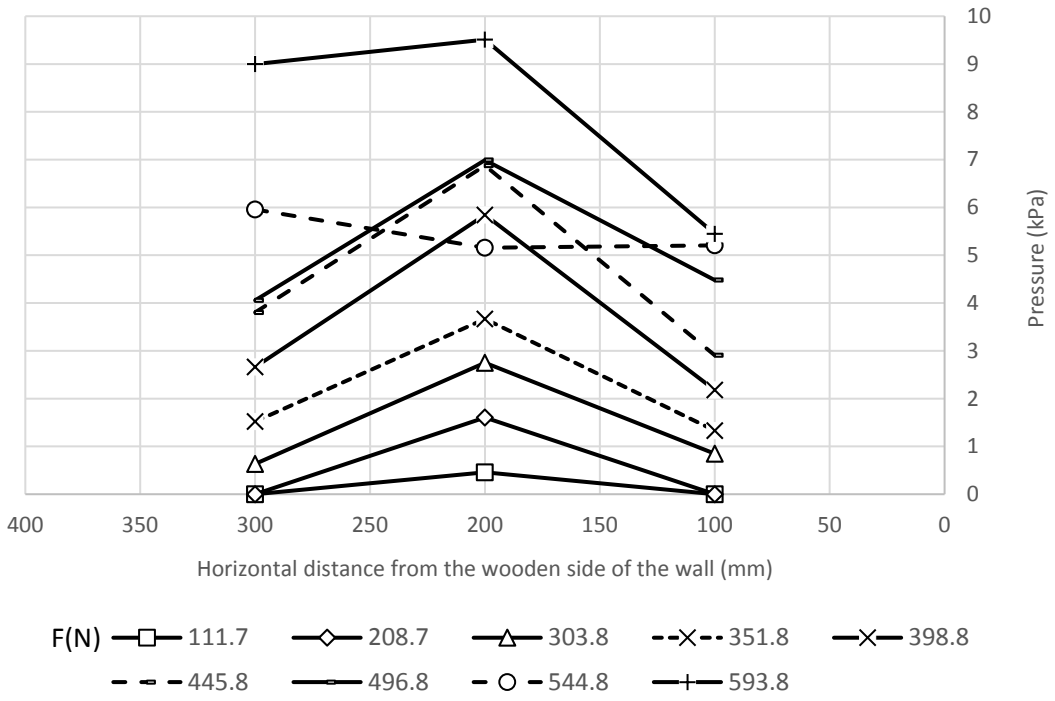

Figure 4.45 Pressure distributions in the transverse direction at the elevation of 202.5 mm from the wall base in Test H2 L2 S2 C1 D1 (pile offset = 127 mm).

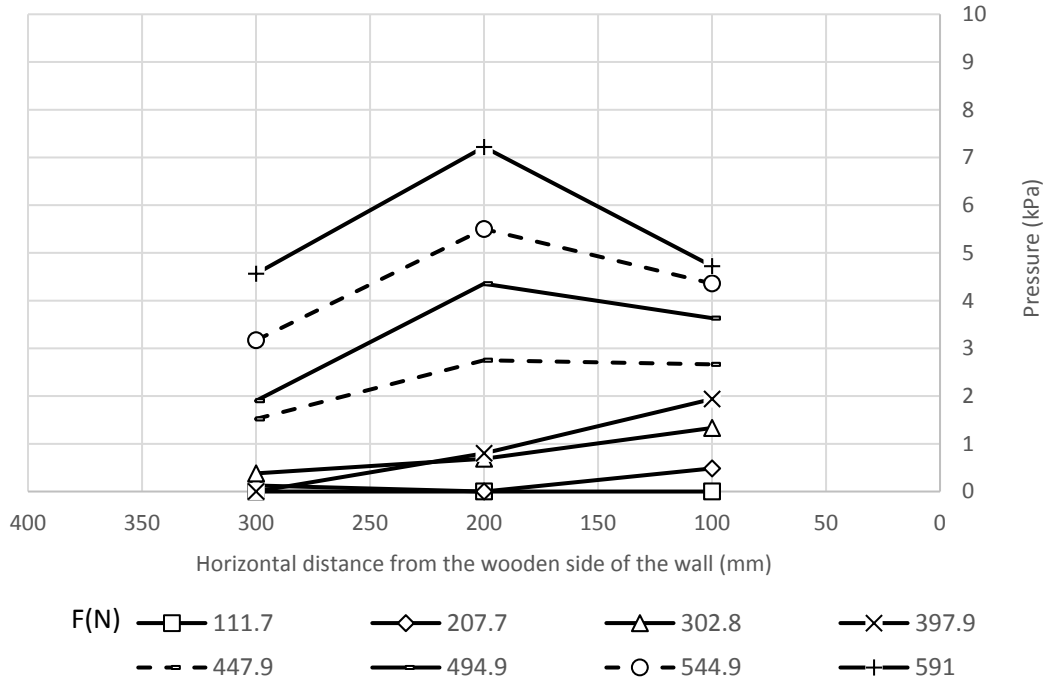

Figure 4.46 Pressure distributions in the transverse direction at the elevation of 202.5 mm from the wall base in Test H2 L2 S2 C1 D2 (pile offset = 254 mm).

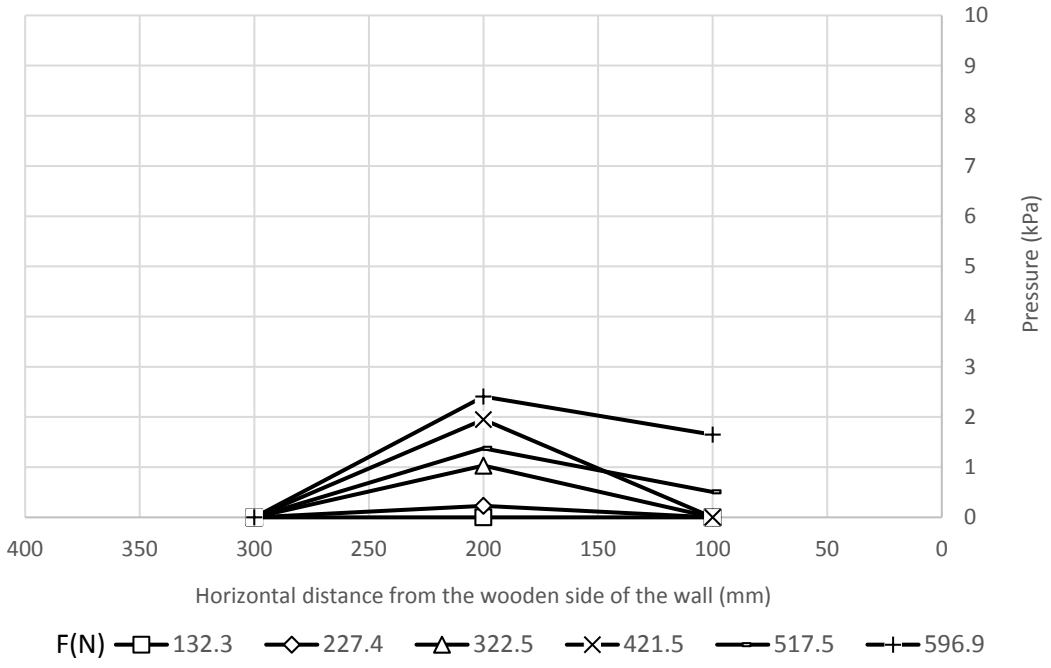

Figure 4.47 Pressure distributions in the transverse direction at the elevation of 202.5 mm from the wall base in Test H2 L2 S2 C1 D3 (pile offset = 381 mm).

4.3.2. Category 2

This category includes the data of Tests H2 L2 S1 C1 **D1**, H2 L2 S1 C1 **D2**, and H2 L2 S1 C1 **D3**. The spacing between the geogrid layers in this category was 90 mm with mechanical connection

Deflection of wall facing

The deflections the wall facing along the vertical centerline of in Tests H2 L2 S1 C1 **D1**, H2 L2 S1 C1 **D2**, and H2 L2 S1 C1 **D3** are shown in Figures 4.48, 4.49, and 4.50, respectively.

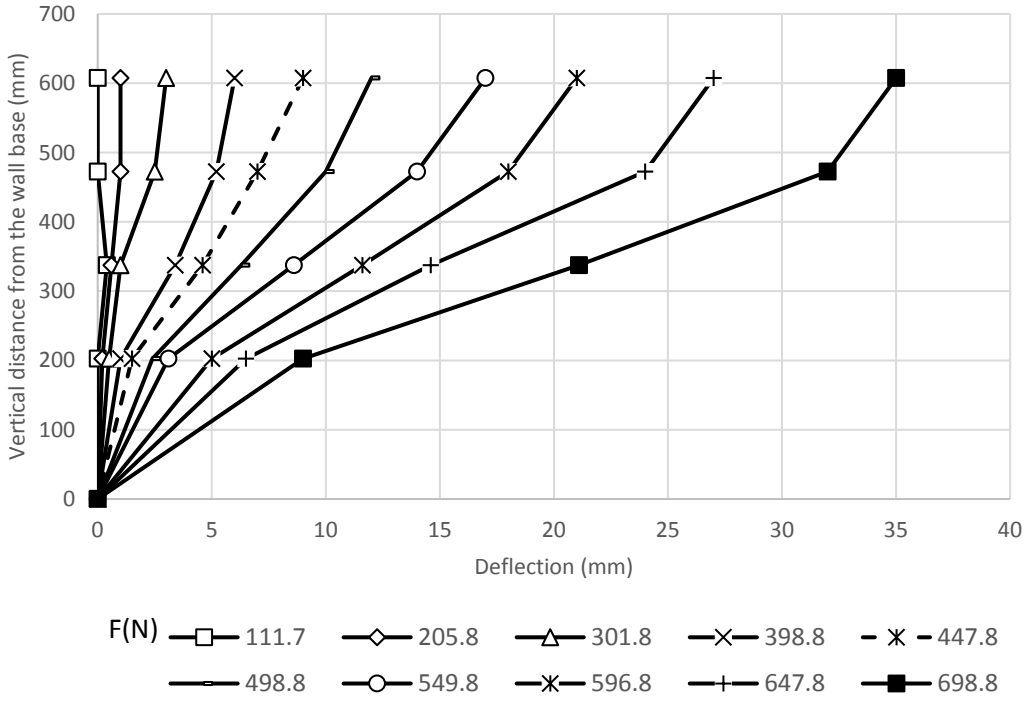

Figure 4.48 Wall facing deflections along the vertical centerline in Test H2 L2 S1 C1 D1 (pile offset = 127 mm).

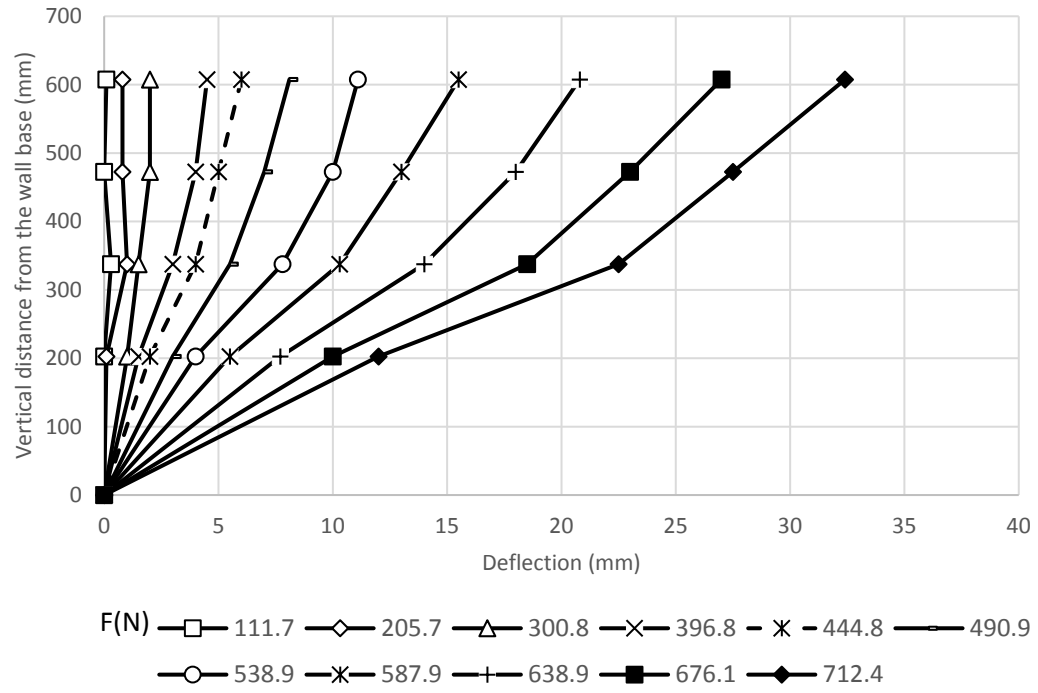

Figure 4.49 Wall facing deflections along the vertical centerline in Test H2 L2 S1 C1 D2 (pile offset = 254 mm).

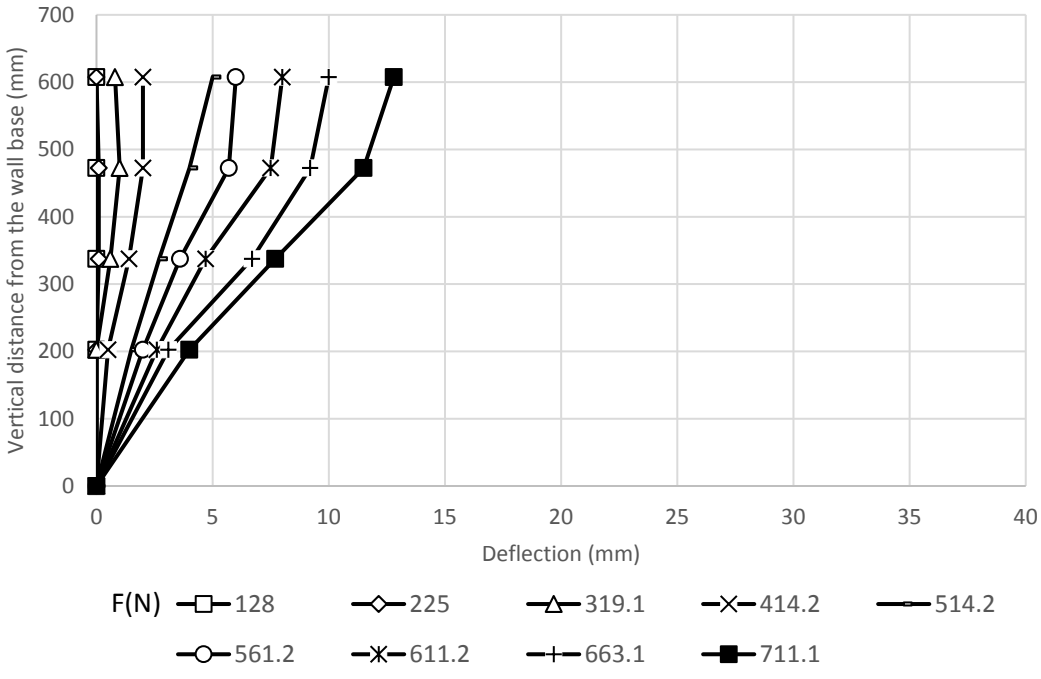

Figure 4.50 Wall facing deflections along the vertical centerline in Test H2 L2 S1 C1 D3 (pile offset = 381 mm).

From Figures 4.48, 4.49, and 4.50, the behavior of the wall facing deflections along the vertical centerline is similar to the behavior that shown in Category 1. The transverse deflection profiles at the maximum deflection location are shown in Figures 4.51, 4.52, and 4.53.

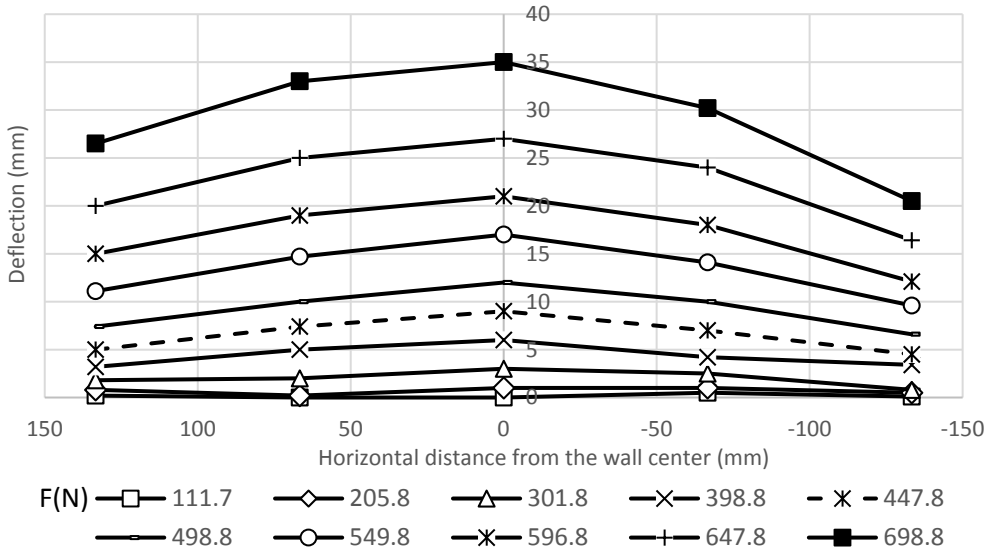

Figure 4.51 Transverse deflection profile at 607.5 mm from the wall base in Test H2 L2 S1 C1 D1 (pile offset = 127 mm).

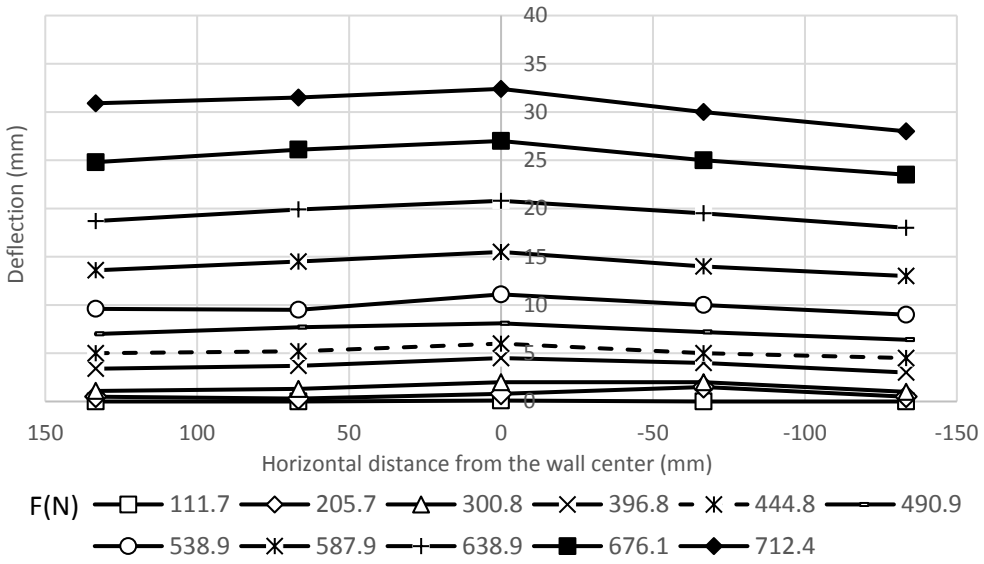

Figure 4.52 Transverse deflection profile at 607.5 mm from the wall base in Test H2 L2 S1 C1 D2 (pile offset = 254 mm).

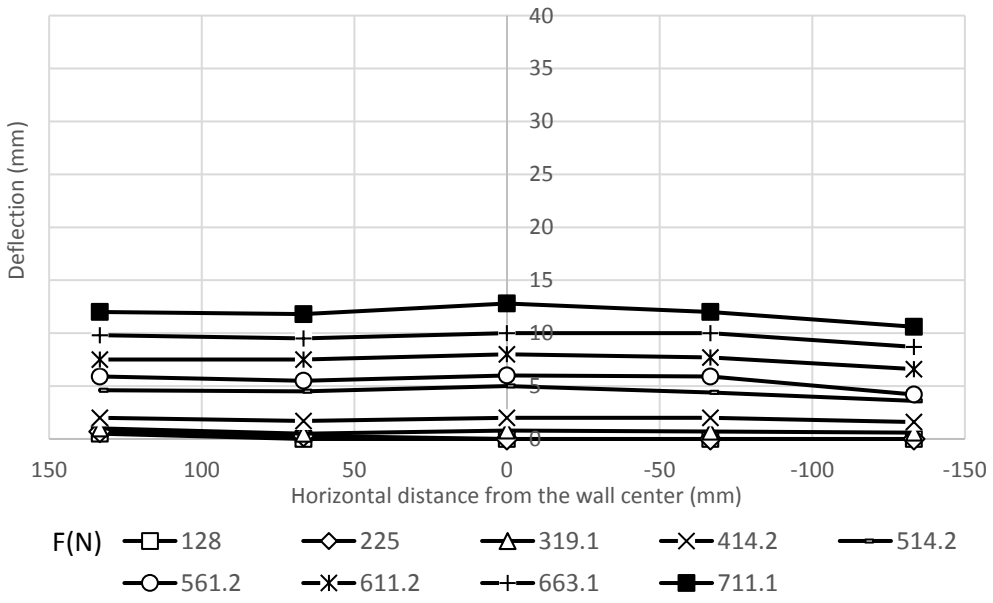

Figure 4.53

Figure 4.53 Transverse deflection profile at 607.5 mm from the wall base in Test H2 L2 S1 C1 D3 (pile offset = 381 mm).

The transverse deflection profiles of the wall facing in this category are similar to those for Category 1. However, the transverse deflection profiles at the elevations of 472.5, 337.5, and 202.5 mm from the wall base are shown in Section A.3.2. of Appendix A.

Strain, stress, and moment of pile

The strains along the compressive side of the pile in Tests H2 L2 S1 C1 **D1**, H2 L2 S1 C1 **D2**, and H2 L2 S1 C1 **D3** are presented in Figures 4.54, 4.55, and 4.56, respectively. The data for the stresses and the moments along the compressive side of the pile are shown in Section A.3.2. of Appendix A.

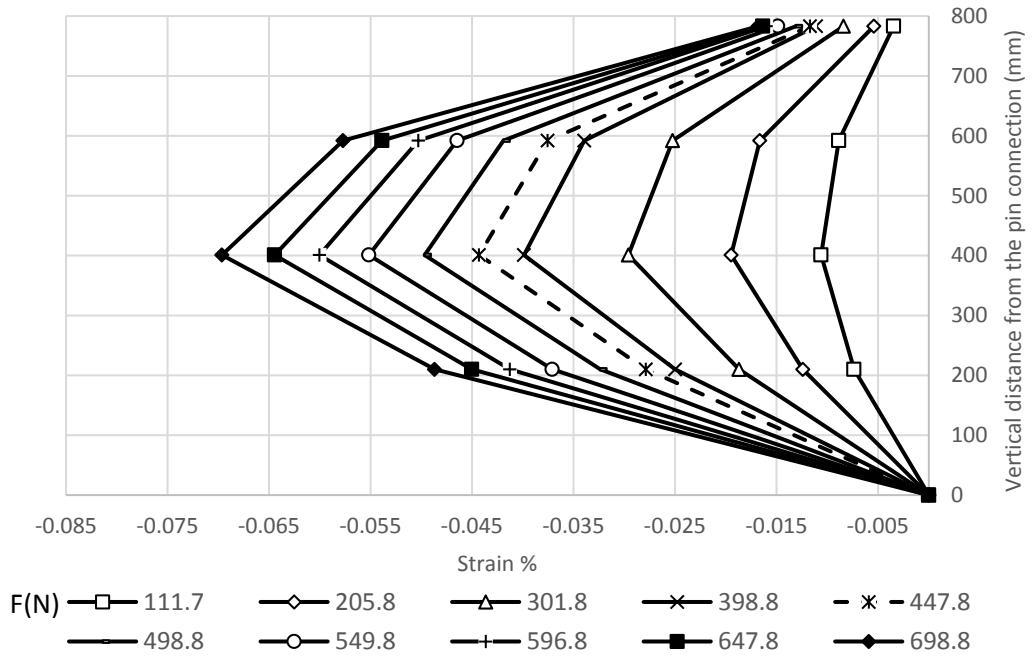

Figure 4.54 Strains along the compressive side of the pile in Test H2 L2 S1 C1 D1 (pile offset =127 mm).

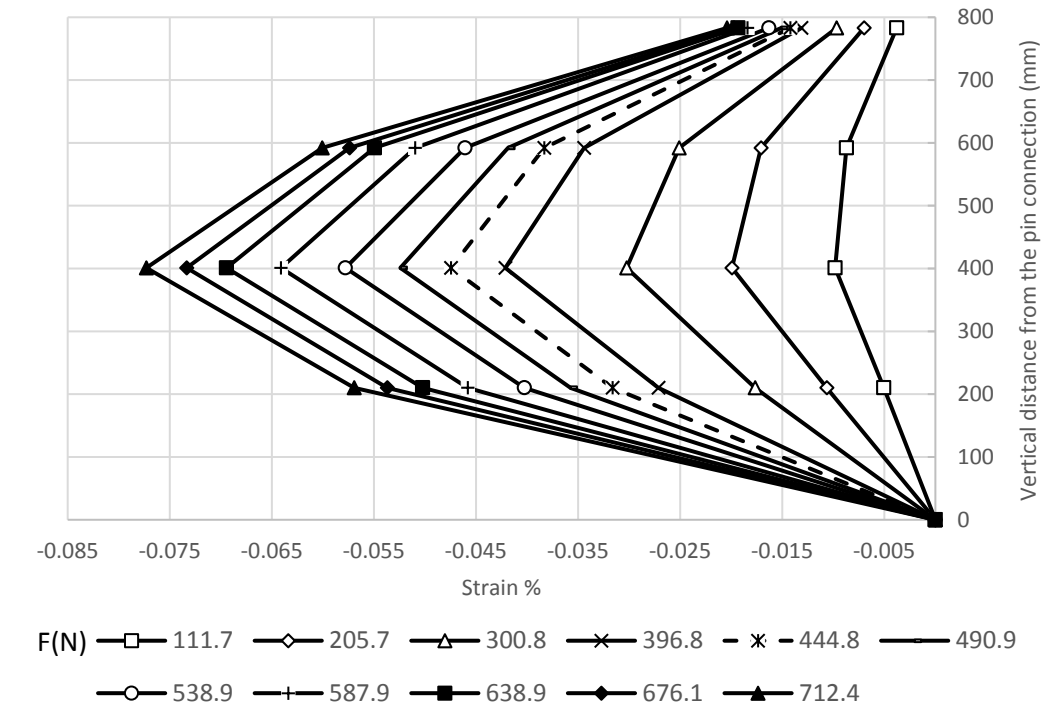

Figure 4.55 Strains along the compressive side of the pile in Test H2 L2 S1 C1 D2 (pile offset =254 mm).

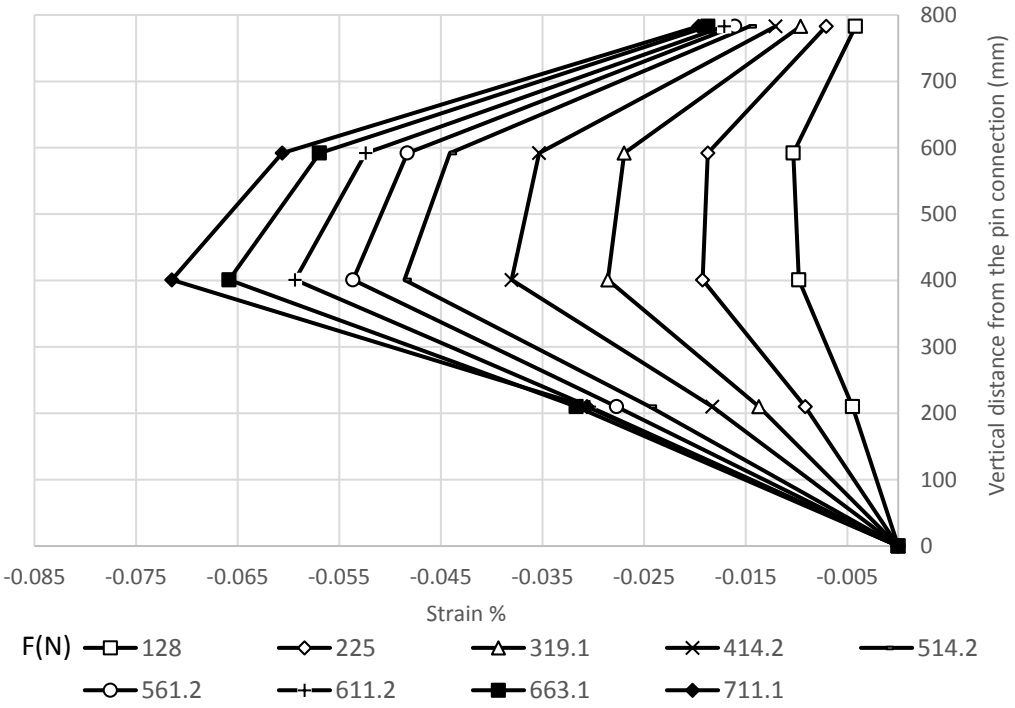

Figure 4.56 Strains along the compressive side of the pile in Test H2 L2 S1 C1 D3 (pile offset = 381 mm).

The strains along the tensile side of the pile in Tests H2 L2 S1 C1 **D1**, H2 L2 S1 C1 **D2**, and H2 L2 S1 C1 **D3**are presented in Figures 4.57, 4.58, and 4.59, respectively. All the data of the stresses and moments along the tensile side are shown in Section A.3.2. of Appendix A. However, the strains and the moments in the compressive and tensile sides are similar to those for Category 1.

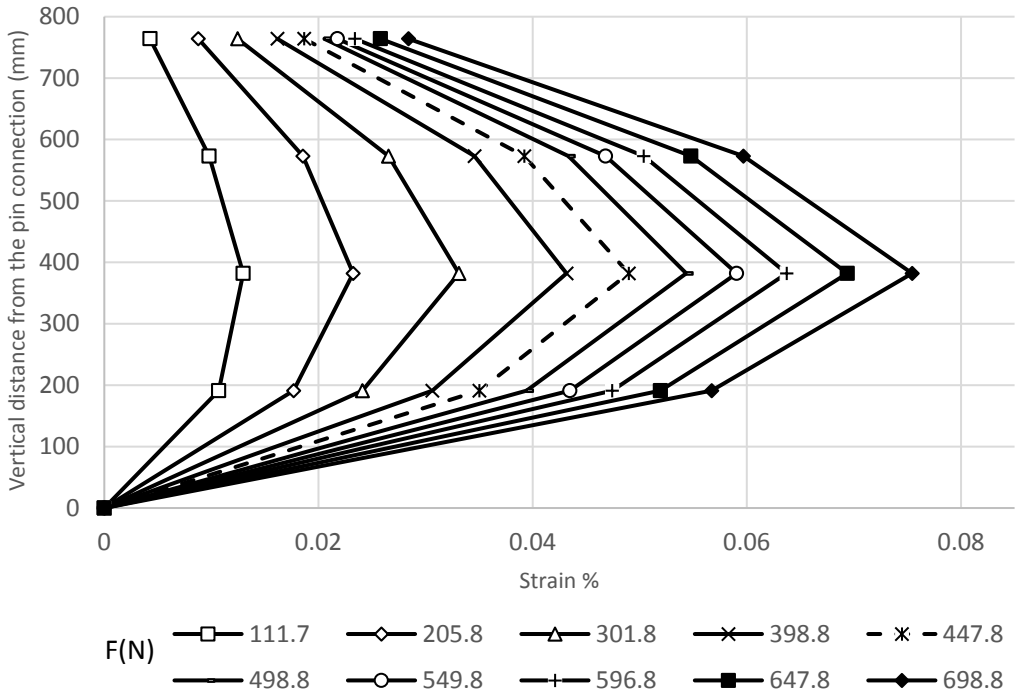

Figure 4.57 Strains along the tensile side of the pile in Test H2 L2 S1 C1 D1 (pile offset =127 mm).

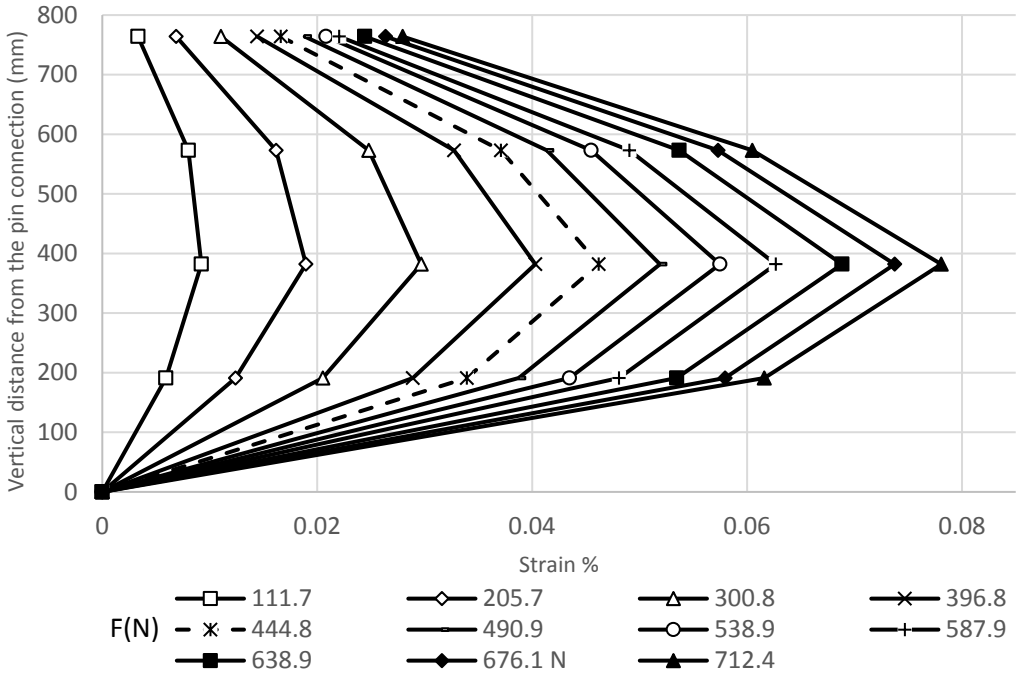

Figure 4.58 Strains along the tensile side of the pile in Test H2 L2 S1 C1 D2 (pile offset =254 mm).

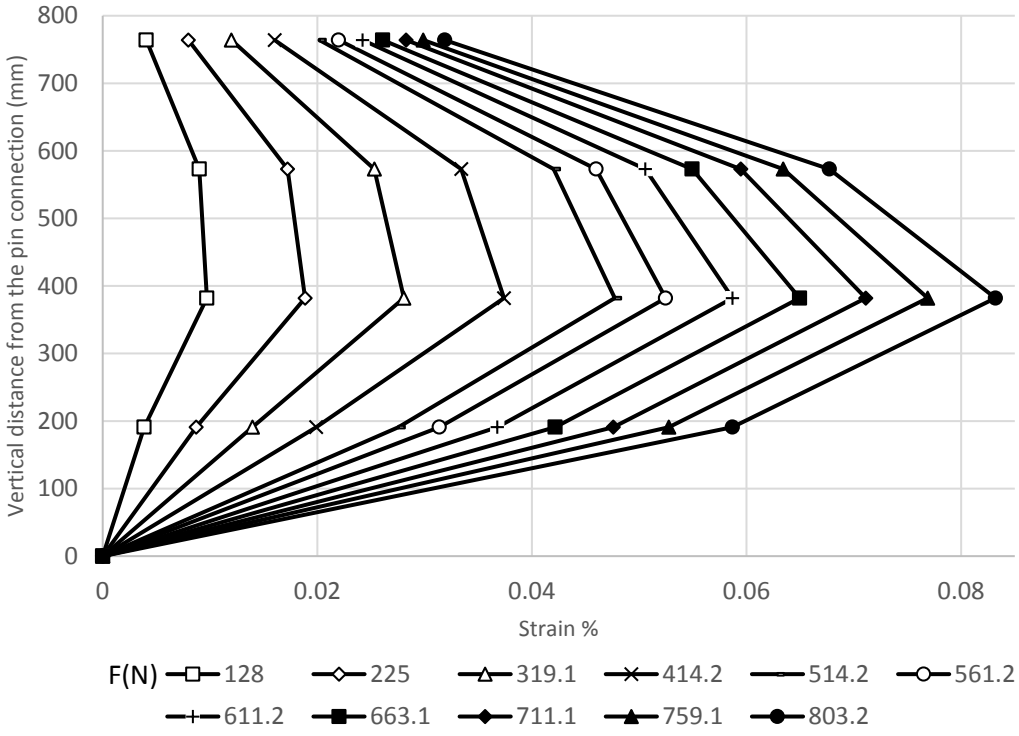

Figure 4.59 Strains along the tensile side of the pile in Test H2 L2 S1 C1 D3 (pile offset =381 mm).

Deflection of pile

The deflections of the pile are shown in Figures 4.60, 4.61, and 4.62 for Tests H2 L2 S1 C1 **D1**, H2 L2 S1 C1 **D2**, and H2 L2 S1 C1 **D3**, respectively. Similar to Category 1, the deflections of the pile in this category decreased by an increase of the pile offset.

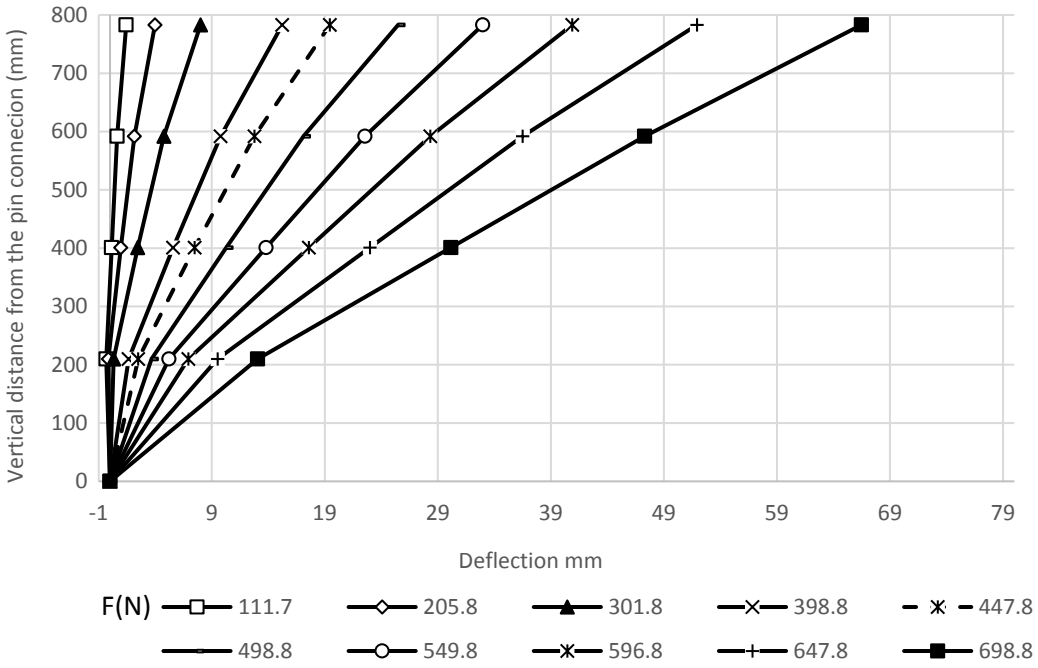

Figure 4.60 Deflections of the pile in Test H2 L2 S1 C1 D1 (pile offset =127 mm).

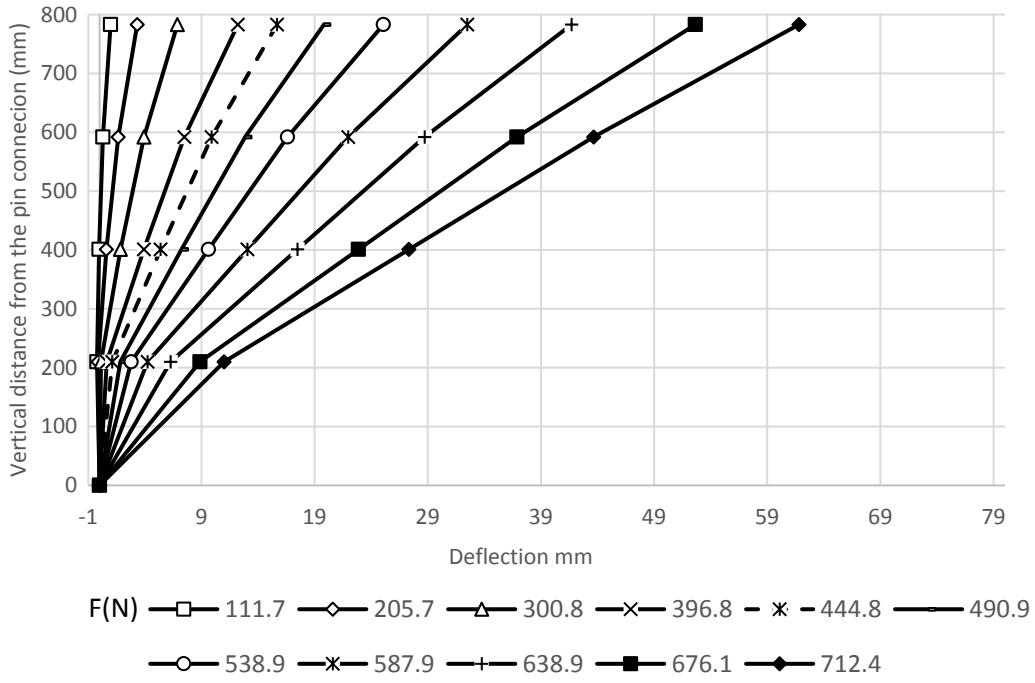

Figure 4.61 Deflections of the pile in Test H2 L2 S1 C1 D2 (pile offset =254 mm).

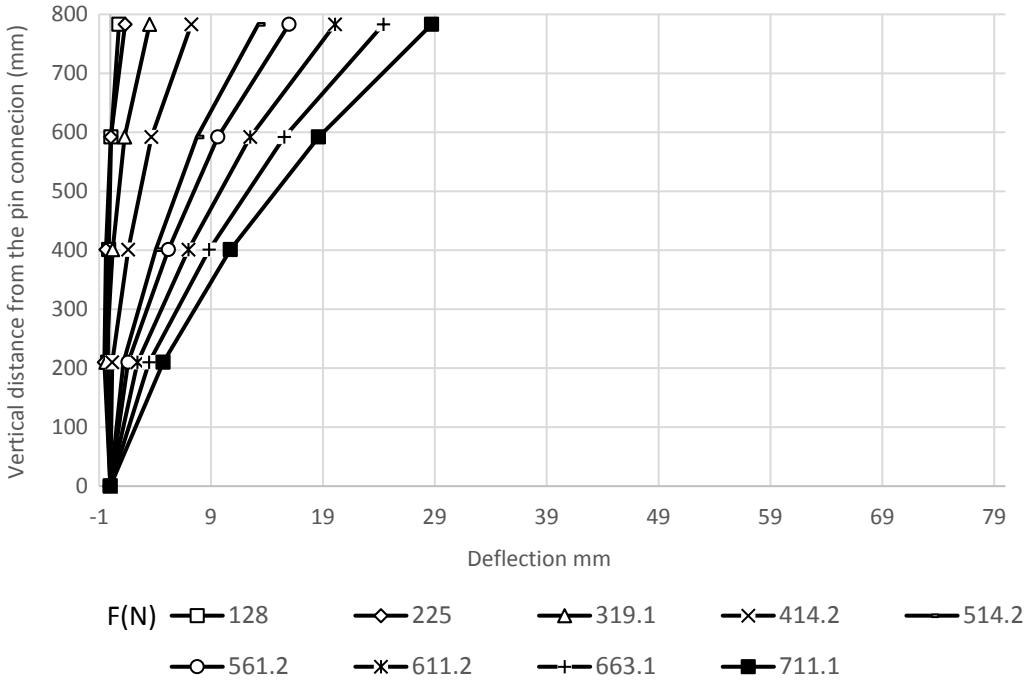

Figure 4.62 Deflections of the pile in Test H2 L2 S1 C1 D3 (pile offset =381 mm).

Strain of geogrid

In the high wall tests, the strains of four geogrid layers in the longitudinal direction were measured using strain gauges. The geogrid strains at the elevation of 630 mm for Tests H2 L2 S1 C1 **D1**, H2 L2 S1 C1 **D2**, and H2 L2 S1 C1 **D3** are shown in Figures 4.63, 4.64, and 4.65, respectively. The strain distribution of the geogrid layer in this category is similar to that shown in Category 1. The strains of the geogrid layers at the elevations of 450, 270, and 90 mm from the wall base for the same tests are presented in Section A.3.2.in Appendix A.

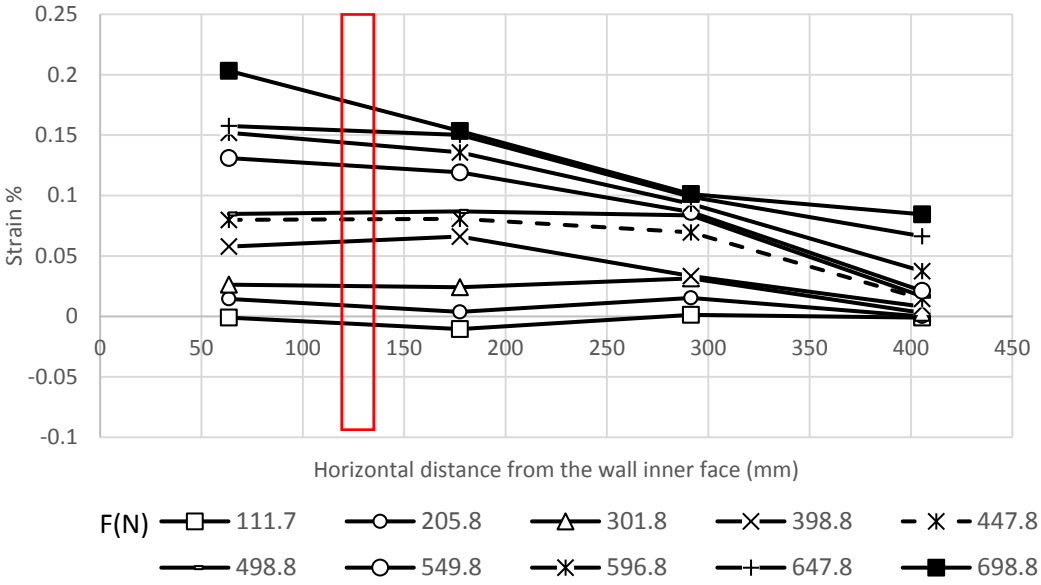

Figure 4.63 Strains of the geogrid layer in the longitudinal direction 630 mm from the wall base in Test H2 L2 S1 C1 D1 (pile offset =127 mm).

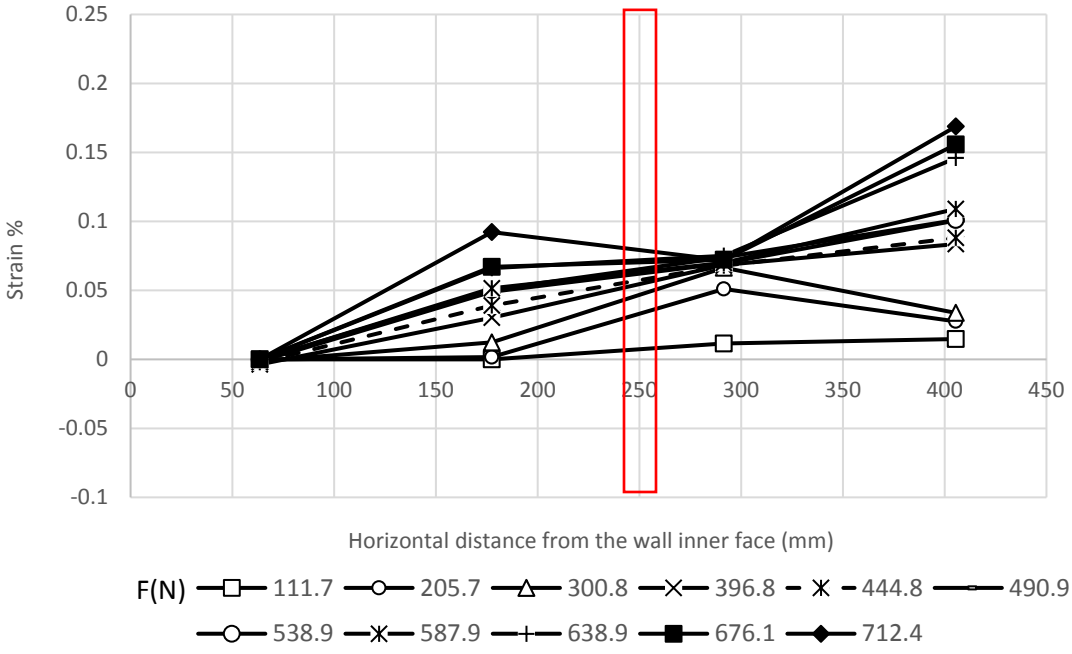

Figure 4.64 Strains of the geogrid layer in the longitudinal direction at 630 mm from the wall base in Test H2 L2 S1 C1 D2 (pile offset =254 mm)..

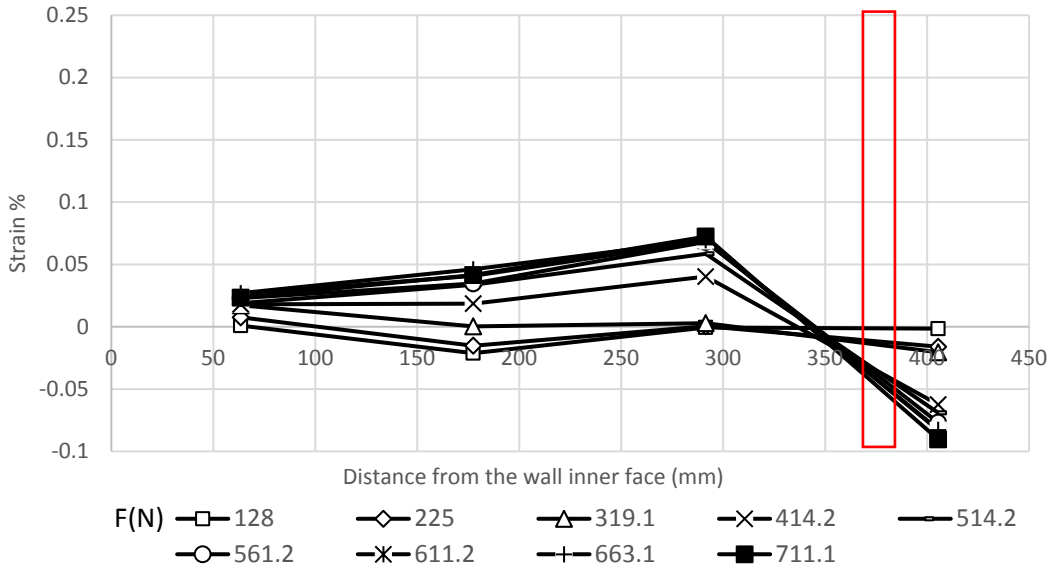

Figure 4.65 Strains of the geogrid layer in the longitudinal direction at 630 mm from the wall base in Test H2 L2 S1 C1 D3 (pile offset =381 mm).

Pressure behind wall facing

Figures 4.66, 4.67, and 4.68 present the pressure distributions behind the wall facing in Tests H2 L2 S1 C1 **D1**, H2 L2 S1 C1 **D2**, and H2 L2 S1 C1 **D3**, respectively.

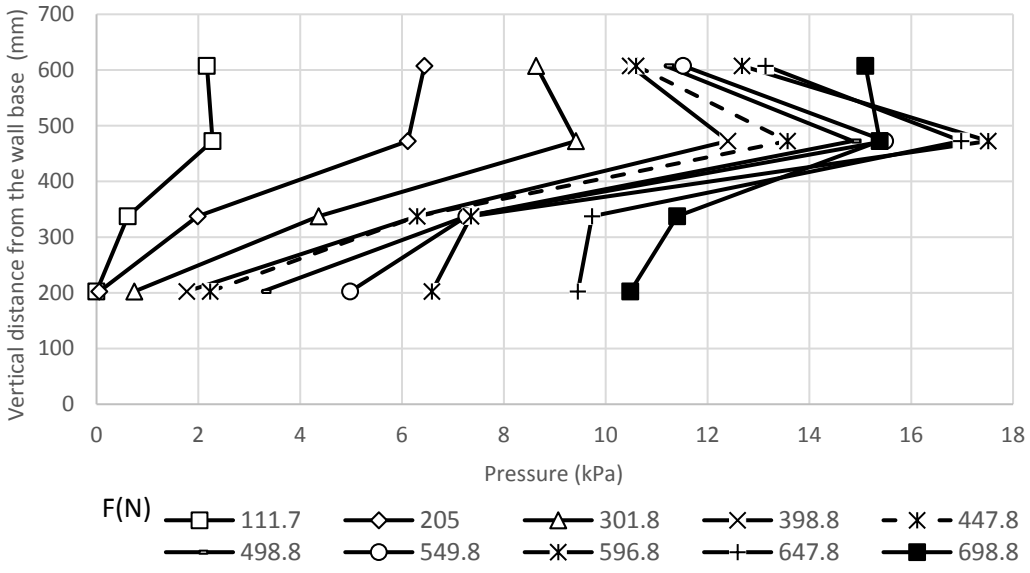

Figure 4.66 Pressures behind the wall facing along the vertical centerline in Test H2 L2 S1 C1 D1 (pile offset = 127 mm).

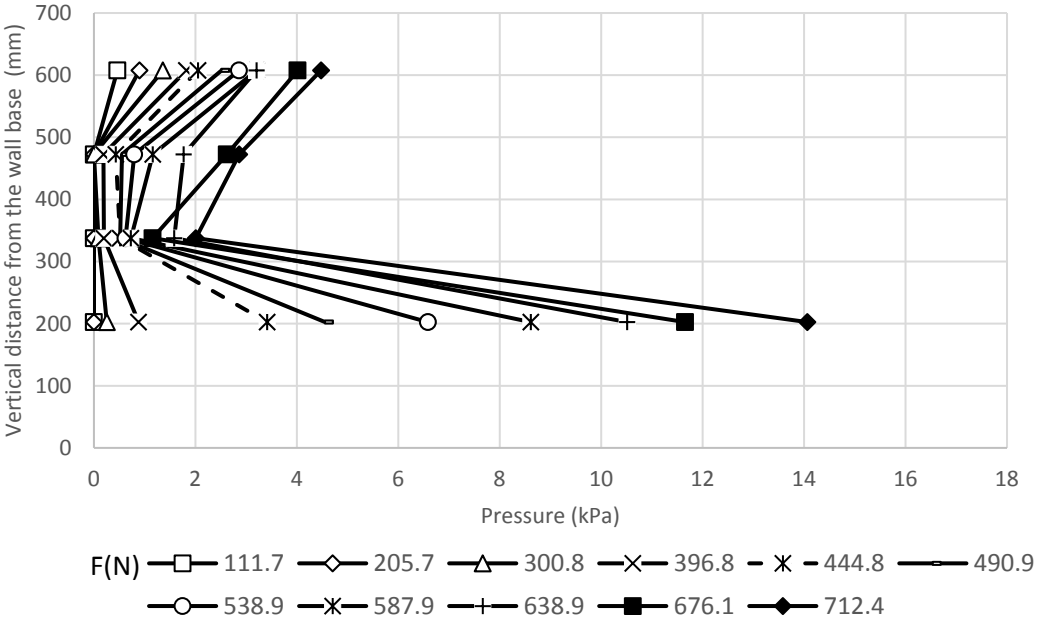

1. **Figure 4.67 Pressures behind the wall facing along the vertical centerline in Test H2 L2 S1 C1 D2 (pile offset = 254 mm).**

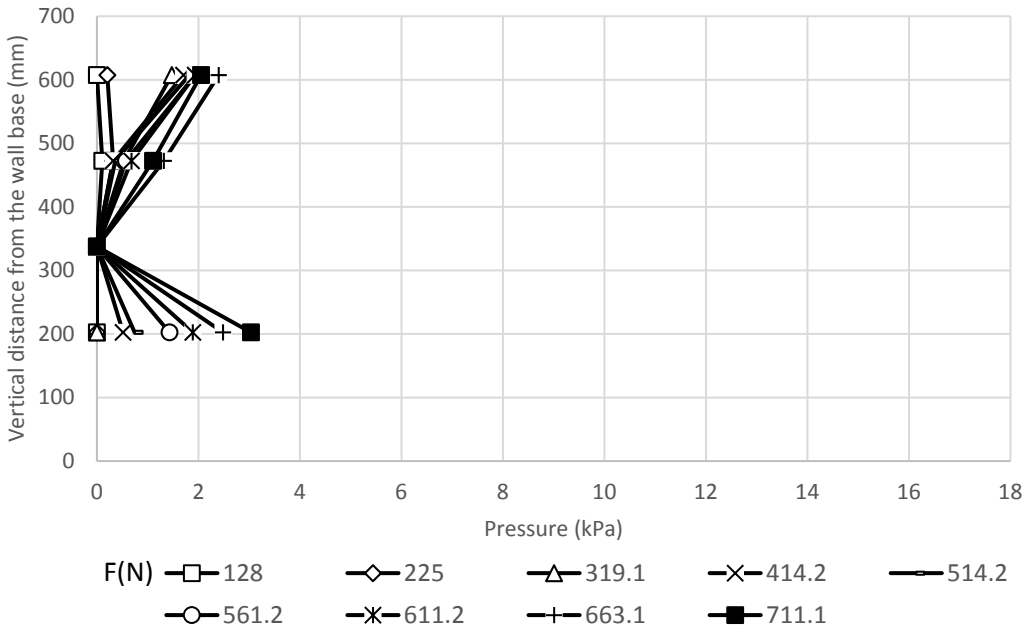

Figure 4.68 Pressures behind the wall facing along the vertical centerline in Test H2 L2 S1 C1 D3 (pile offset = 381 mm).

Figures 4.66, 4.67, and 4.68 show that the pressure distributions in this category are similar to those in Category 1. One exception is that the pressures behind the upper part of the wall were high in these three tests of this category because of the decrease in the spacing between the geogrid layers

The transverse pressure distributions behind the wall facing at the elevation of 472.5 mm from the wall base are as shown in Figures 4.69, 4.70, and 4.71 for Tests H2 L2 S1 C1 **D1**, H2 L2 S1 C1 **D2**, and H2 L2 S1 C1 **D3**, respectively. For the same tests, the transverse pressure distributions behind the wall facing at the elevation of 202.5 mm from the wall base are shown in Figures 4.72, 4.73, and 4.74. Other transverse pressure distributions at the elevations of 607.5 and 337.5 mm are included in Section A.3.2.in Appendix A.

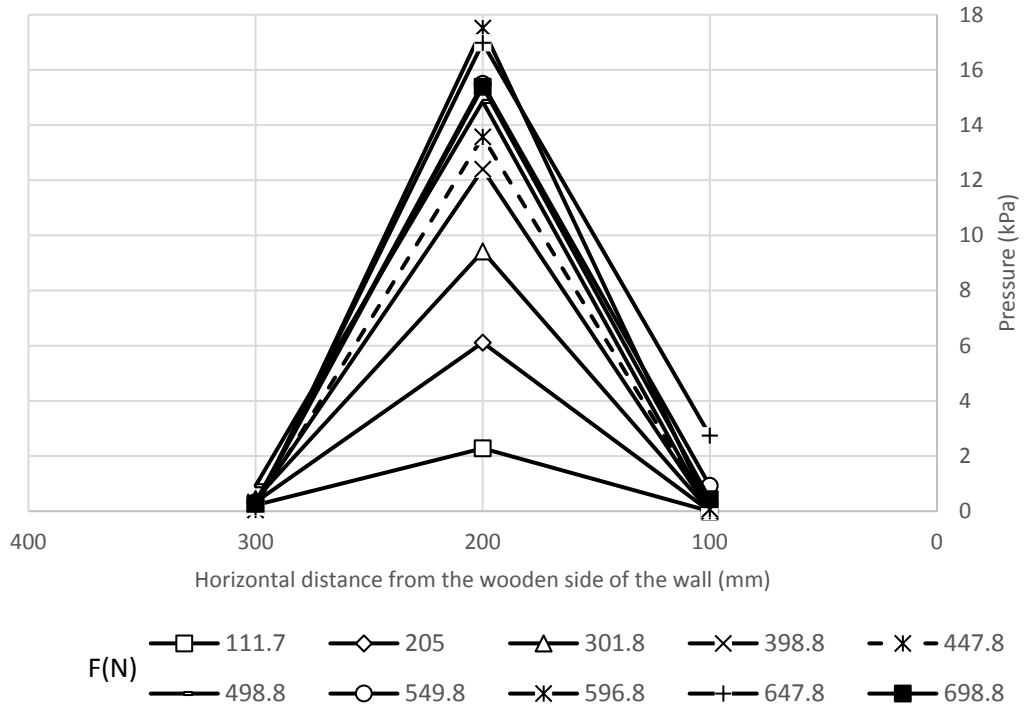

Figure 4.69 Pressure distributions in the transverse direction at the elevation of 472.5 mm from the wall base in Test H2 L2 S1 C1 D1 (pile offset = 127 mm).

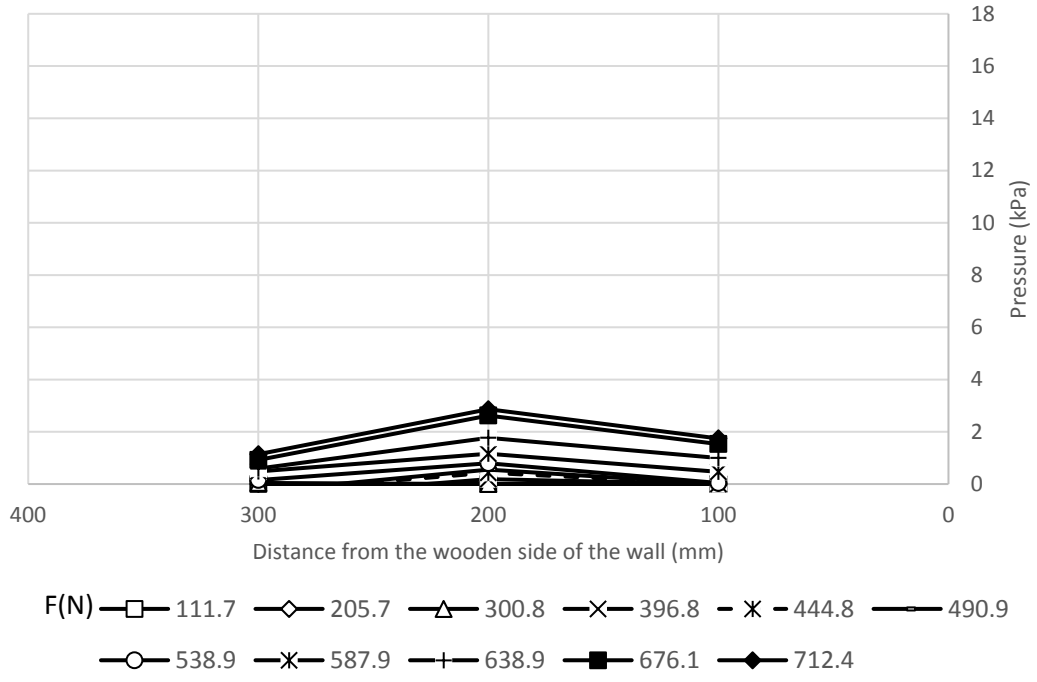

Figure 4.70 Pressure distributions in the transverse direction at the elevation of 472.5 mm from the wall base in Test H2 L2 S1 C1 D2 (pile offset = 254 mm).

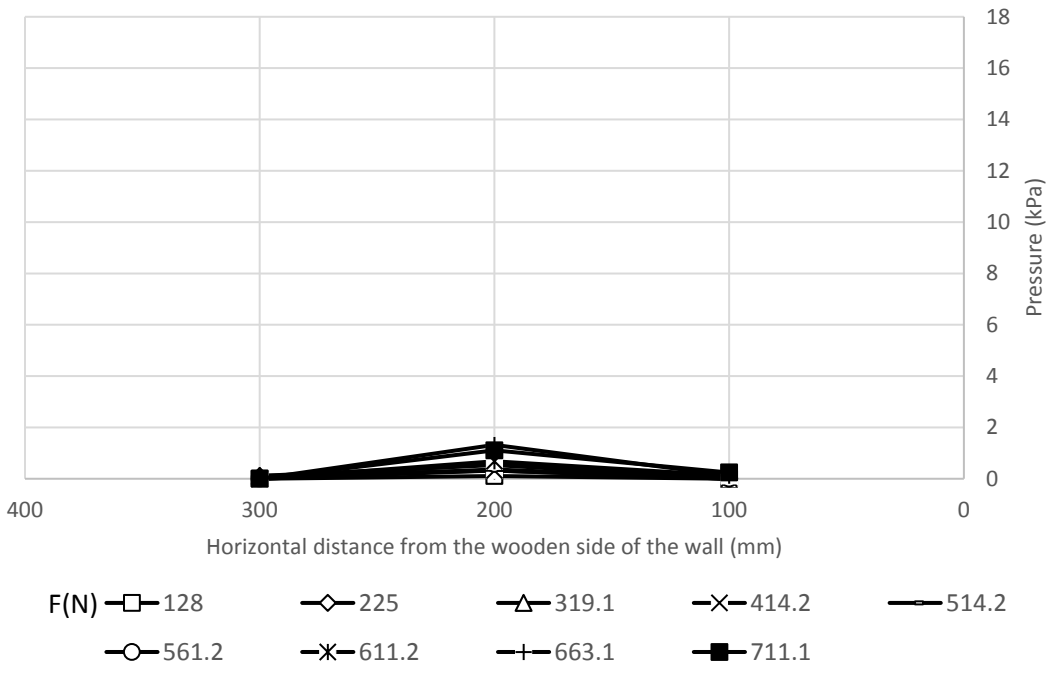

Figure 4.71 Pressure distributions in the transverse direction at the elevation of 472.5 mm from the wall base in Test H2 L2 S1 C1 D3 (pile offset = 381 mm).

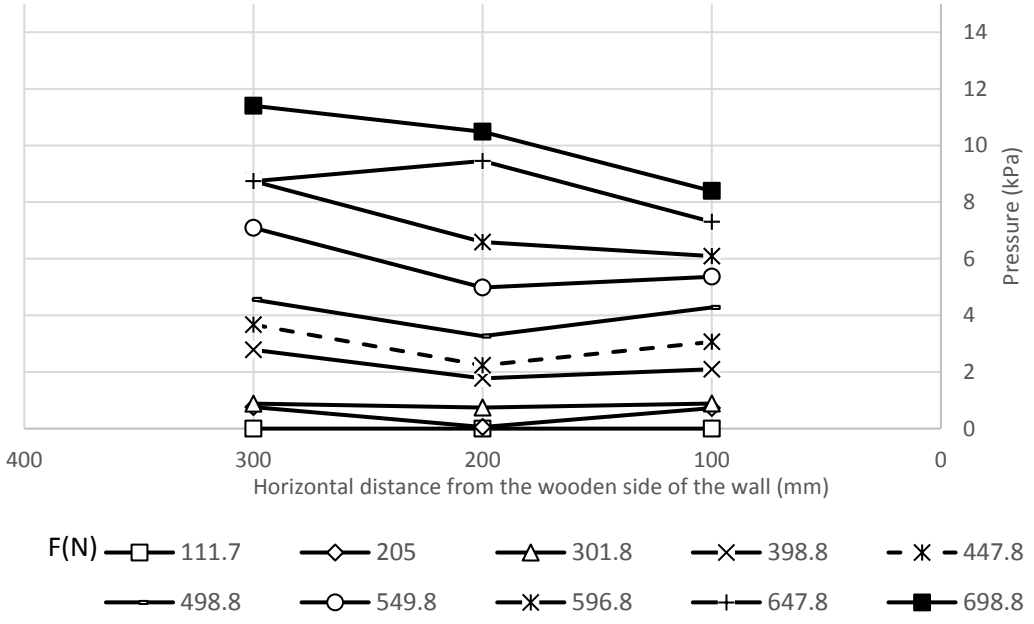

Figure 4.72 Pressure distributions in the transverse direction at the elevation of 337.5 mm from the wall base in Test H2 L2 S1 C1 D1 (pile offset = 127 mm).

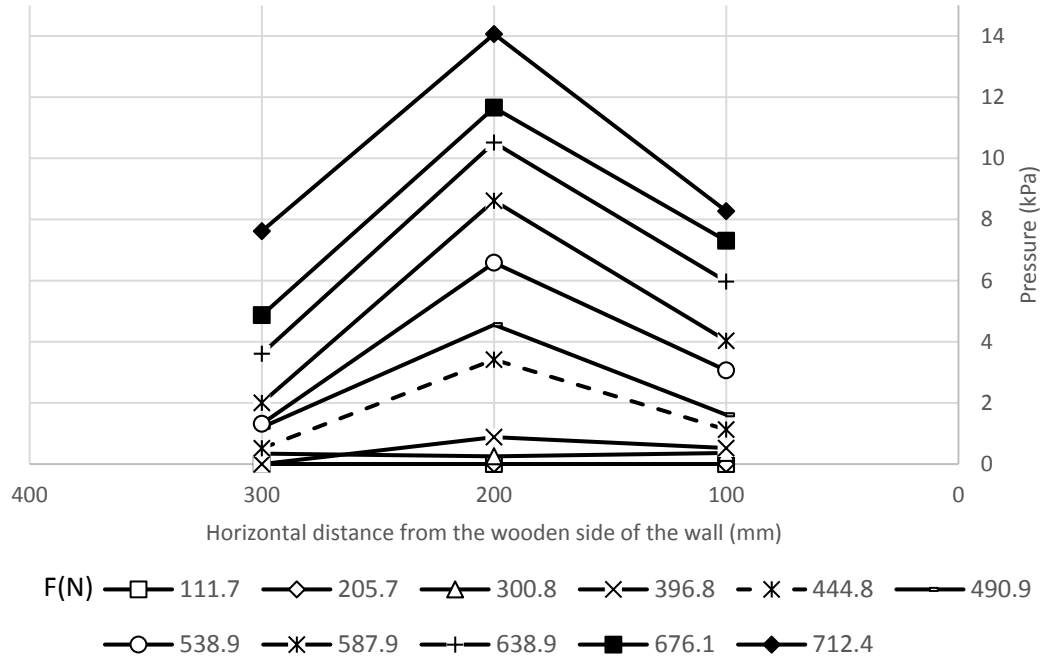

Figure 4.73 Pressure distributions in the transverse direction at the elevation of 337.5 mm from the wall base in Test H2 L2 S1 C1 D2 (pile offset = 254 mm).

Figure 4.74 Pressure distributions in the transverse direction at the elevation of 337.5 mm from the wall base in Test H2 L2 S1 C1 D3 (pile offset = 381 mm).

4.3.3. Category 3

This category includes the data from Tests H2 L2 S1 C2 D1, H2 L2 S1 C2 D2, and H2 L2 S1 C2 D3. The tests of this category had the same parameters as those in Category 2 except for the connection type.

Deflection of wall facing

The deflections along the centerline of the wall facing in Tests H2 L2 S1 C2 D1, H2 L2 S1 C2 D2, and H2 L2 S1 C2 D3 are shown in Figures 4.75, 4.76, and 4.77, respectively.

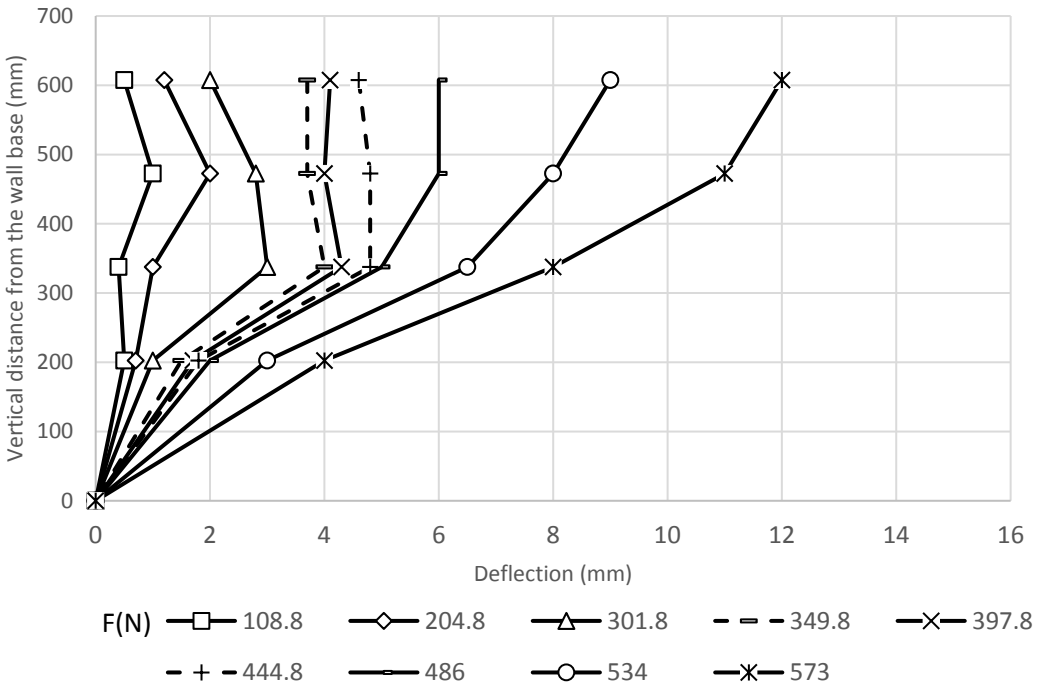

Figure 4.75 Wall facing deflections along the vertical centerline in Test H2 L2 S1 C2 D1 (pile offset = 127 mm).

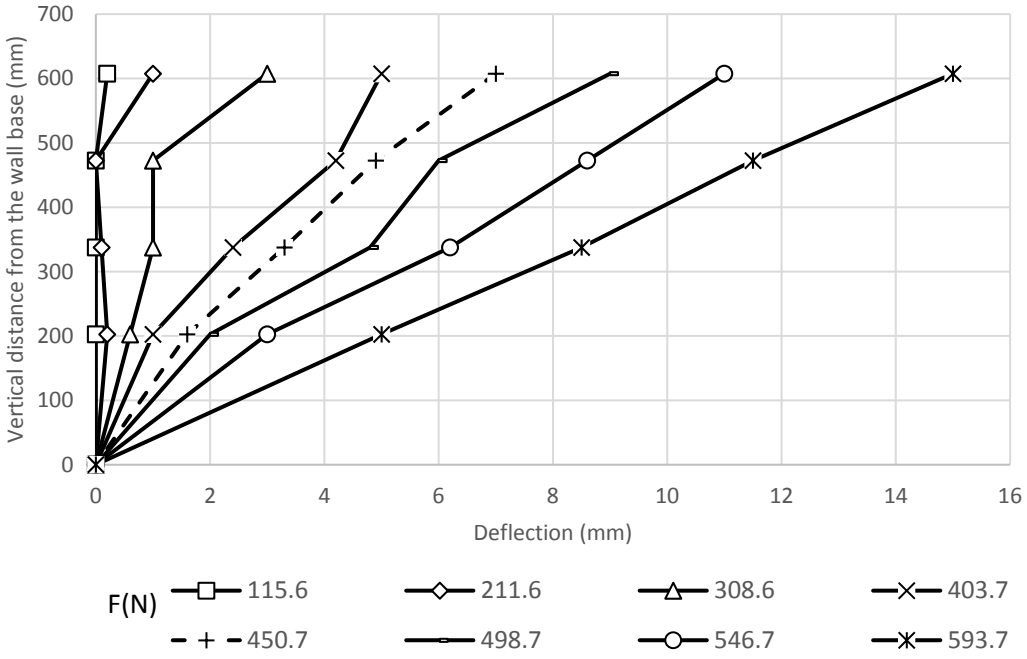

Figure 4.76 Wall facing deflections along the vertical centerline in Test H2 L2 S1 C2 D2 (pile offset = 254 mm).

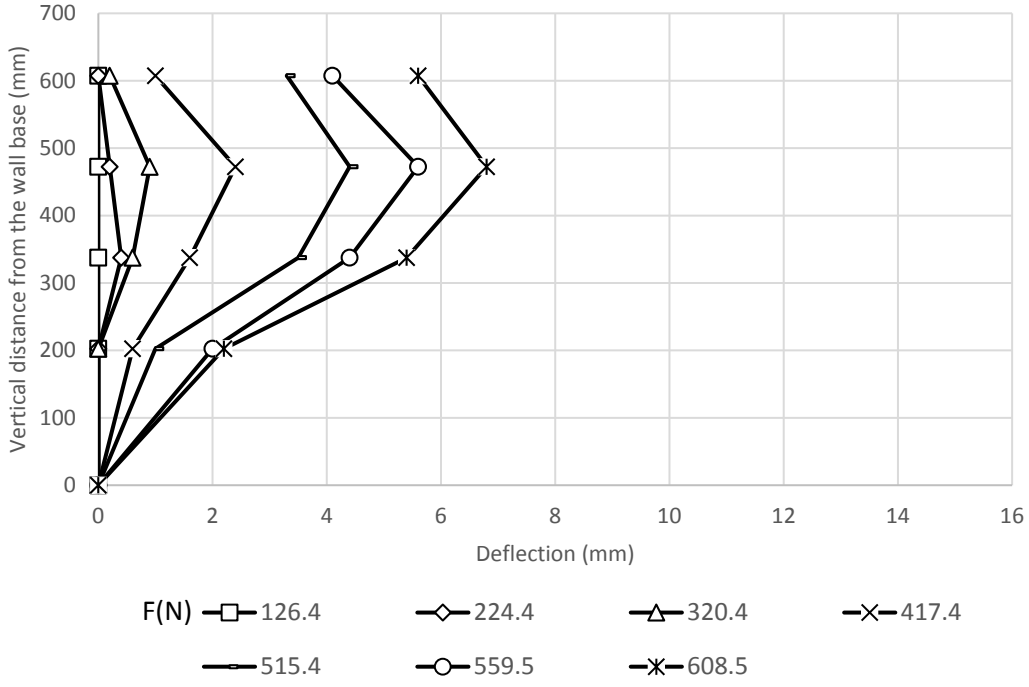

Figure 4.77 Wall facing deflections along the vertical centerline in Test H2 L2 S1 C2 D3 (pile offset = 381 mm).

From the previous figures, the deflection along the centerline of the wall facing in this category has the same behavior that shown in Category 1 of Group 2. An important notice should be mentioned here that the loading steps of Tests H2 L2 S1 C2 **D2** and H2 L2 S1 C2 **D3** are higher than the loading steps in H2 L2 S1 C2 **D1**. For the same tests, the transverse deflection profiles at the maximum deflection location are shown in Figures 4.78, 4.79 and 4.80. the transverse deflection distribution in these figures have the same trend that shown in Category 1 of Group 2.

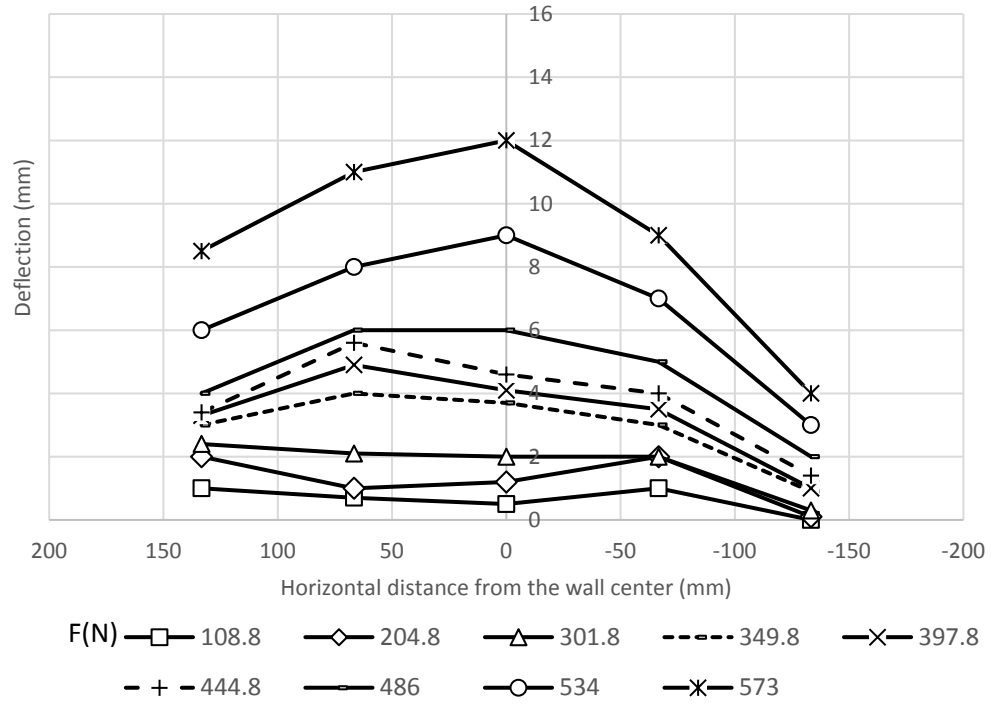

Figure 4.78 Transverse deflection profile at 607.5 mm from the wall base in Test H2 L2 S1 C2 D1 (pile offset = 127 mm).

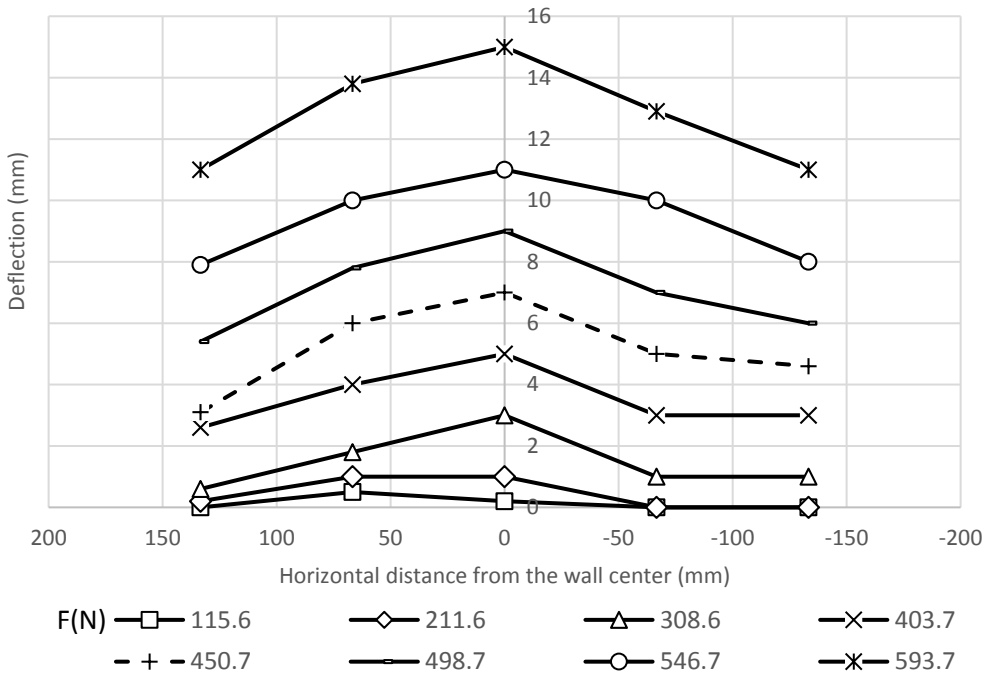

Figure 4.79 Transverse deflection profile at 607.5 mm from the wall base in H2 L2 S1 C2 D2 (pile offset = 254 mm).

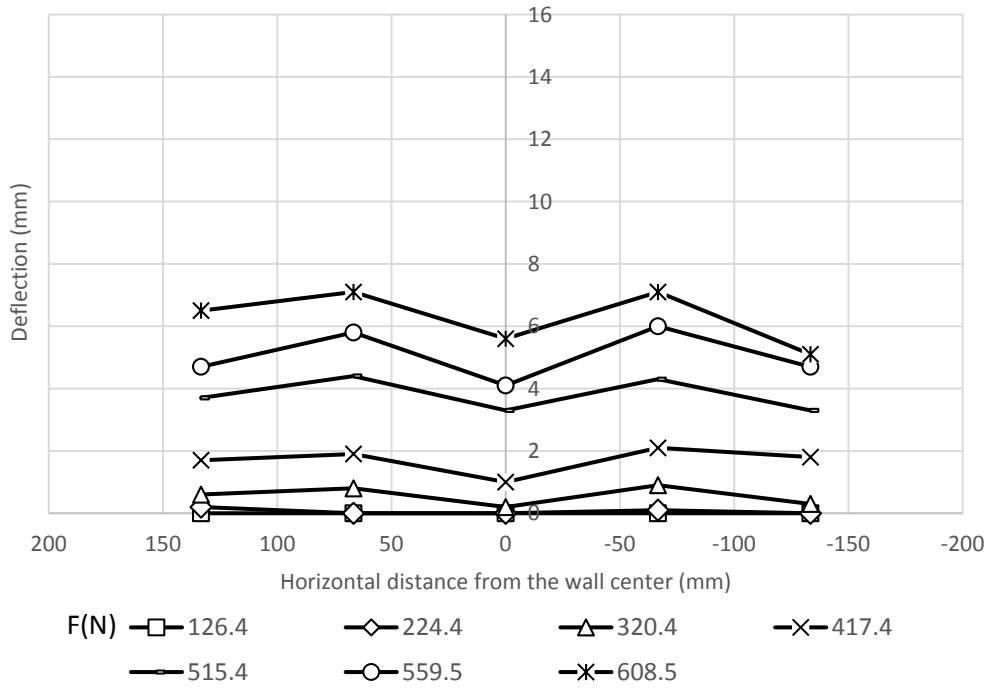

Figure 4.80 Transverse deflection profile at 607.5 mm from the wall base in Test H2 L2 S1 C2 D3 (pile offset = 381 mm).

The transverse deflection profiles of the wall facing at 472.5 mm, 337.5 mm, and 202.5 mm from the wall base for Tests H2 L2 S1 C2 D1, H2 L2 S1 C2 D2, and H2 L2 S1 C2 D3 are shown in section A.3.3. of appendix A.

Strain, stress, and moment of pile

The strains along the compressive side of the pile in Tests H2 L2 S1 C2 D1, H2 L2 S1 C2 D2, and H2 L2 S1 C2 D3 are presented in Figures 4.81, 4.82, and 4.82, respectively. The data figures for the stress and the moment along the compressive side of the pile are shown in section A.3.3. of appendix A.

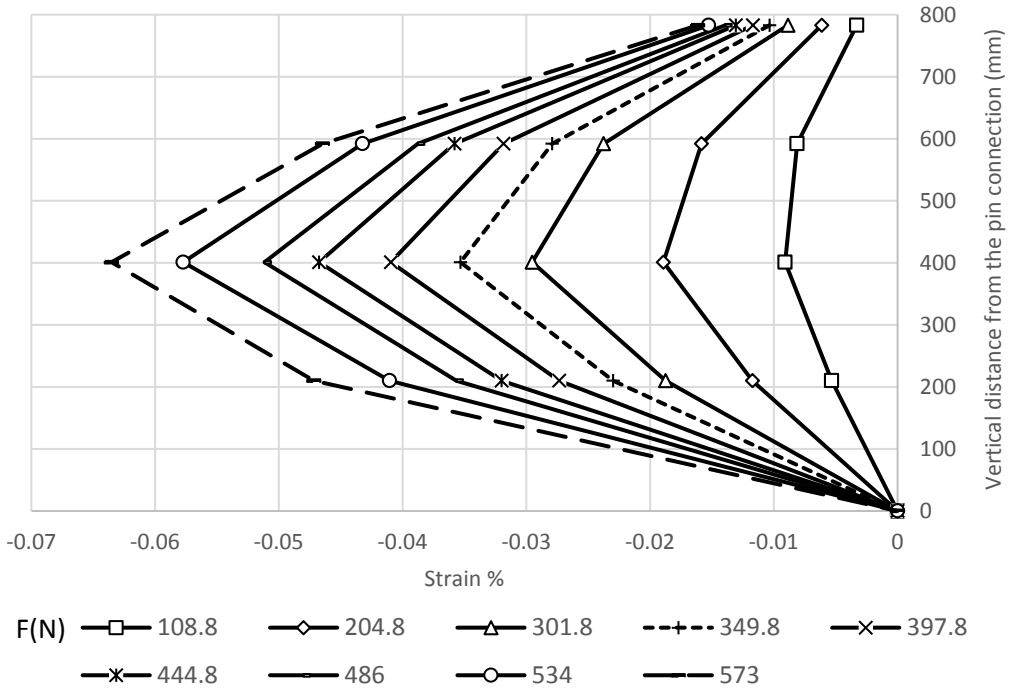

Figure 4.81 Strains along the compressive side of the pile in Test H2 L2 S1 C2 D1 (pile offset = 127 mm).

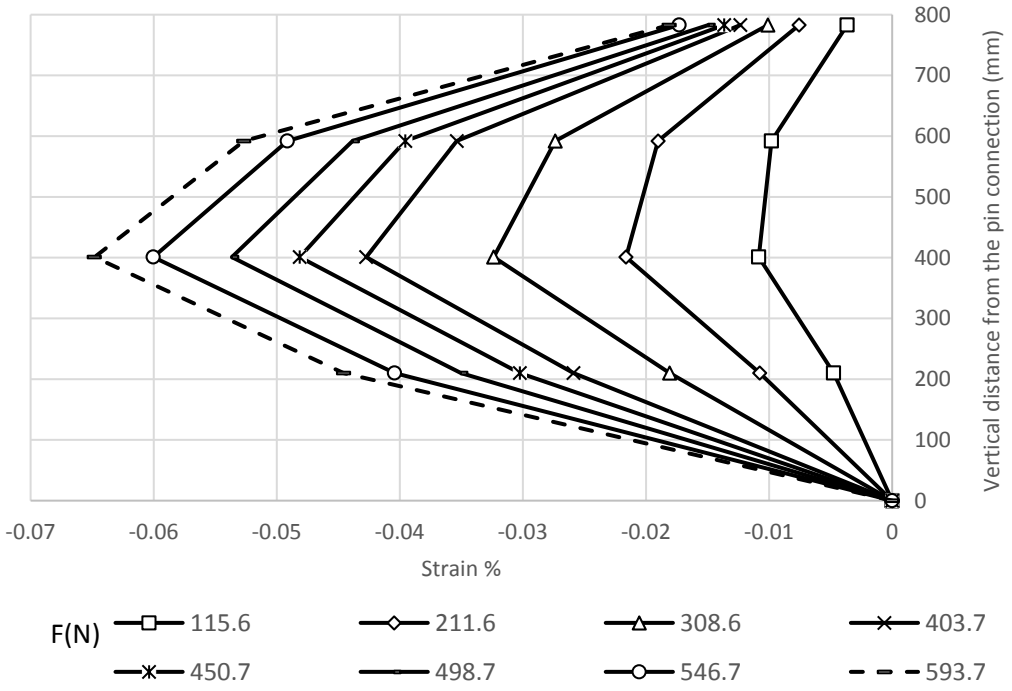

Figure 4.82 Strains along the compressive side of the pile in Test H2 L2 S1 C2 D2 (pile offset = 254 mm).

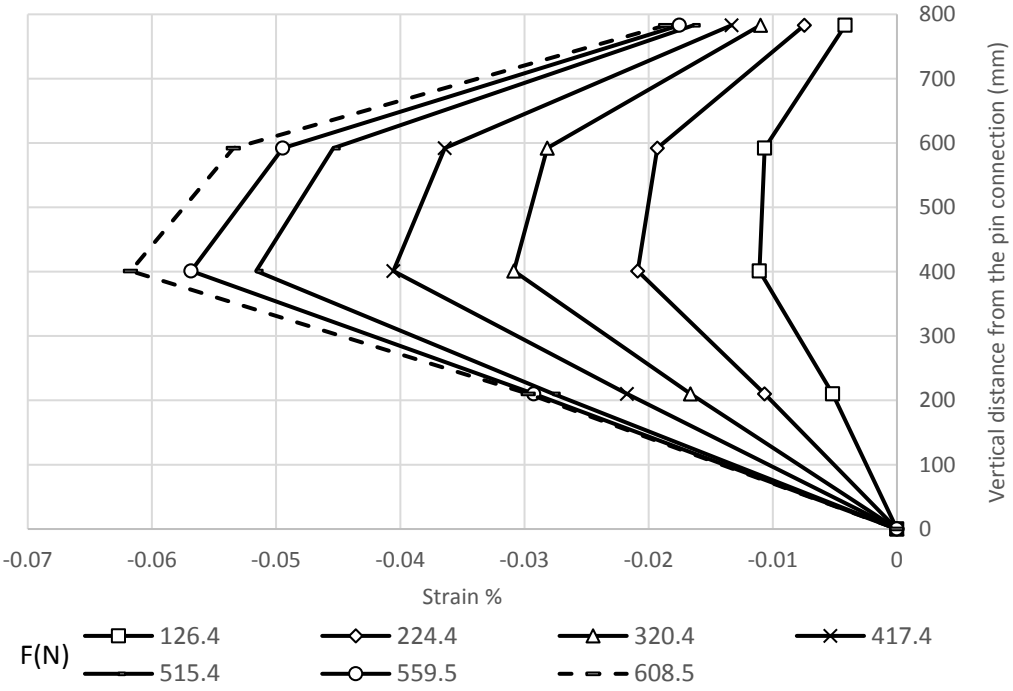

Figure 4.83 Strains along the compressive side of the pile in Test H2 L2 S1 C2 D3 (pile offset = 381 mm).

The strains along the tensile side of the pile in Tests H2 L2 S1 C2 D1, H2 L2 S1 C2 D2, and H2 L2 S1 C2 D3 are presented in Figures 4.84, 4.85, and 4.86, respectively. All the data figures for the stress and moment along the tensile side are shown in section A.3.3. of Appendix A. The strain and the moment in the compressive and tensile sides have the same behavior that shown in Category 1 of Group 2.

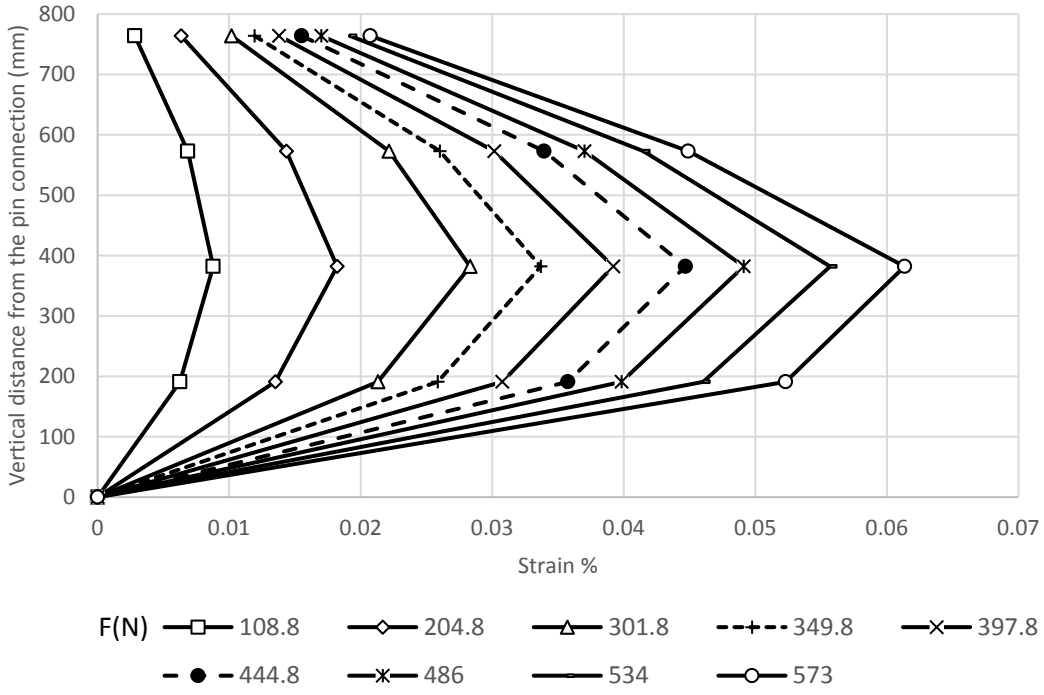

Figure 4.84 Strains along the tensile side of the pile in Test H2 L2 S1 C2 D1 (pile offset = 127 mm).

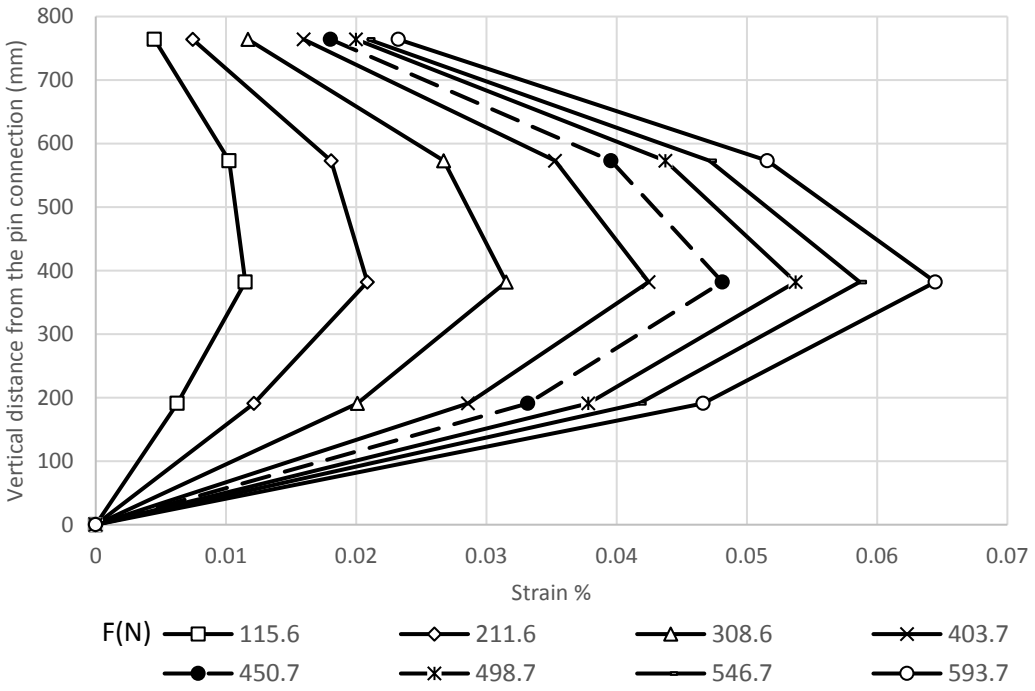

Figure 4.85 Strains along the tensile side of the pile in Test H2 L2 S1 C2 D2 (pile offset = 254 mm).

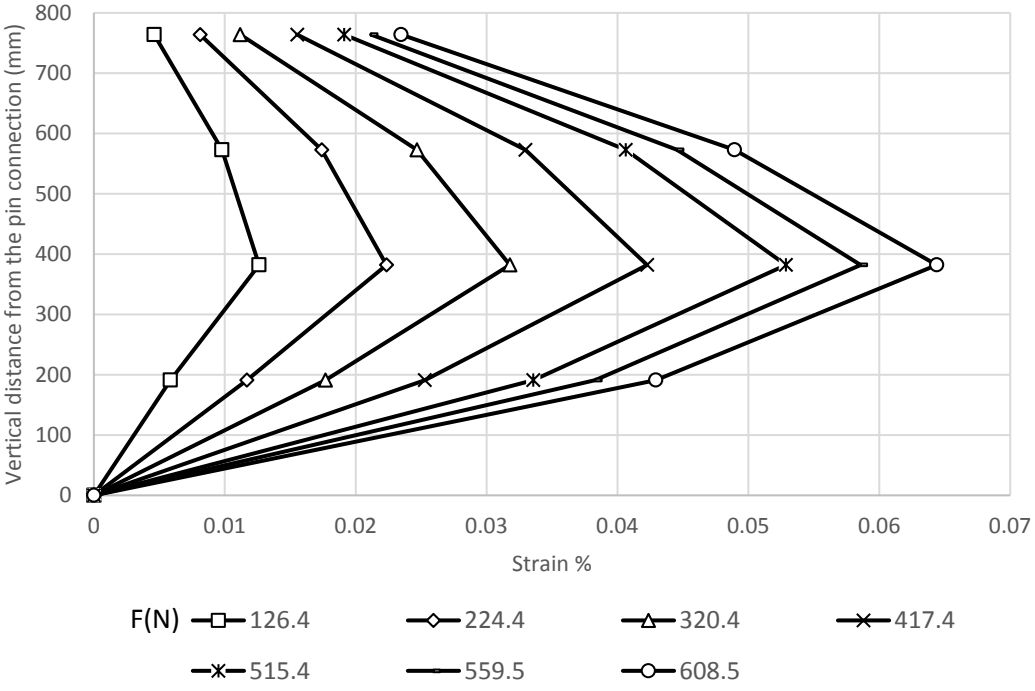

Figure 4.86 Strains along the tensile side of the pile in Test H2 L2 S1 C2 D3 (pile offset = 381 mm).

Deflection of pile

The deflections of the pile are shown in Figures 4.87, 4.88, and 4.89 for Tests H2 L2 S1 C2 D1, H2 L2 S1 C2 D2, and H2 L2 S1 C2 D3, respectively. These deflections have the same behavior that shown in Category 1 of Group 2.

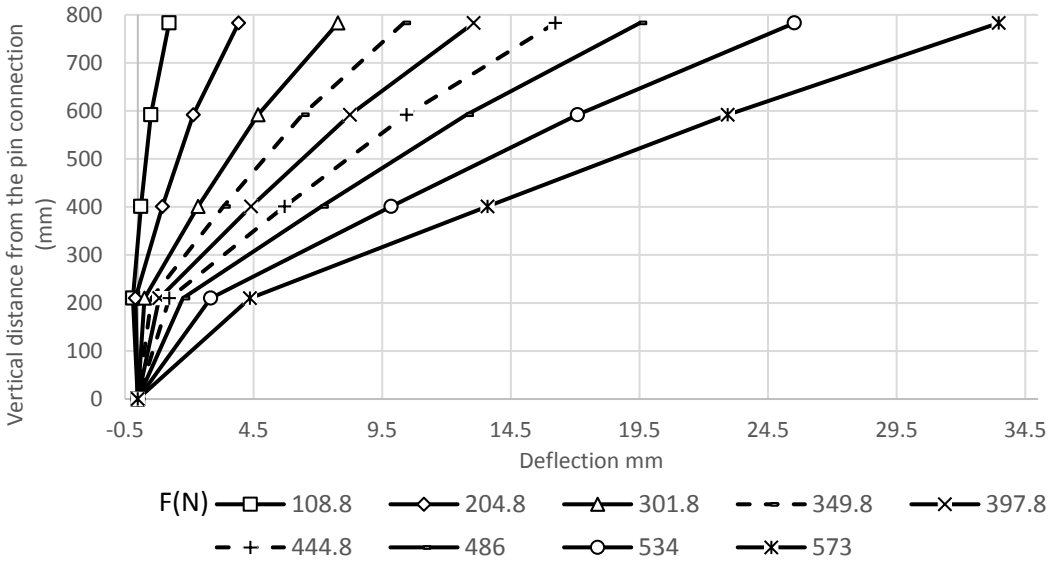

Figure 4.87 Deflections of the pile in Test H2 L2 S1 C2 D1 (pile offset = 127 mm).

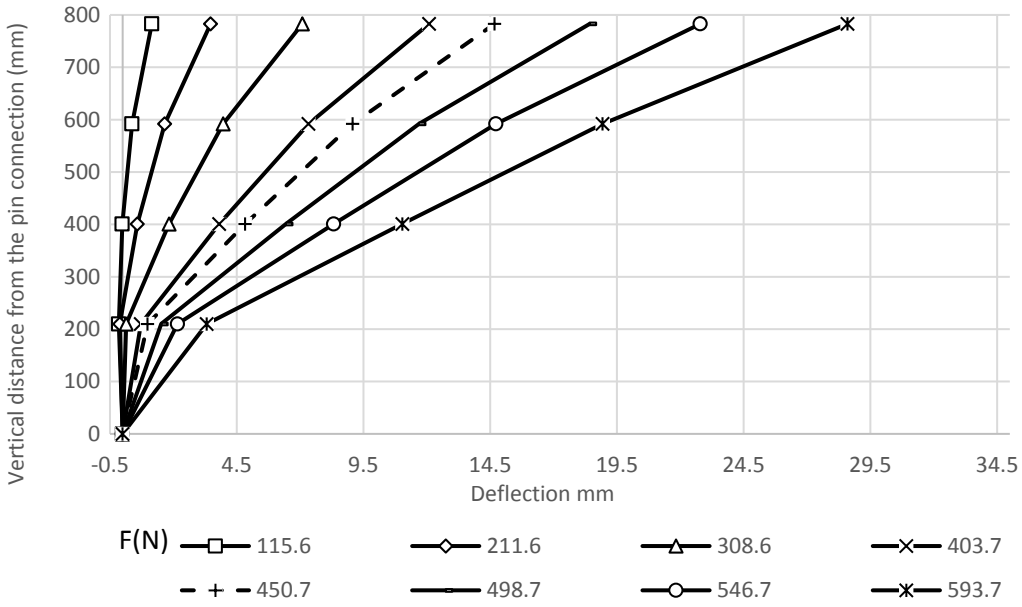

Figure 4.88 Deflections of the pile in Test H2 L2 S1 C2 D2 (pile offset = 254 mm).

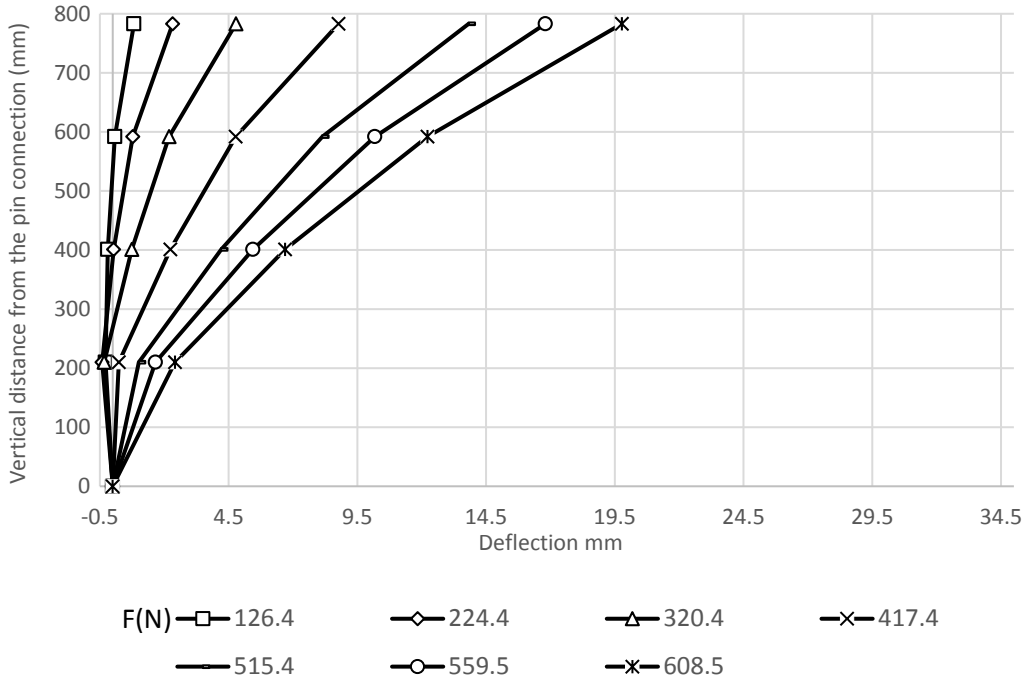

Figure 4.89 Deflections of the pile in Test H2 L2 S1 C2 D3 (pile offset = 381 mm).

Strain of geogrid

The longitudinal strain in the geogrid layer at height equal to 630 mm from wall base for Tests H2 L2 S1 C2 D1, H2 L2 S1 C2 D2, and H2 L2 S1 C2 D3 are shown in Figures 4.90, 4.91, and 4.92, respectively. For the same tests, the strains of the geogrid layers at 450 mm, 270 mm, and 90 mm from the wall base are presented in section A.3.3. of appendix A. The behavior of the strain and moment distributions is similar to the behavior that shown in Category 1 of Group 2.

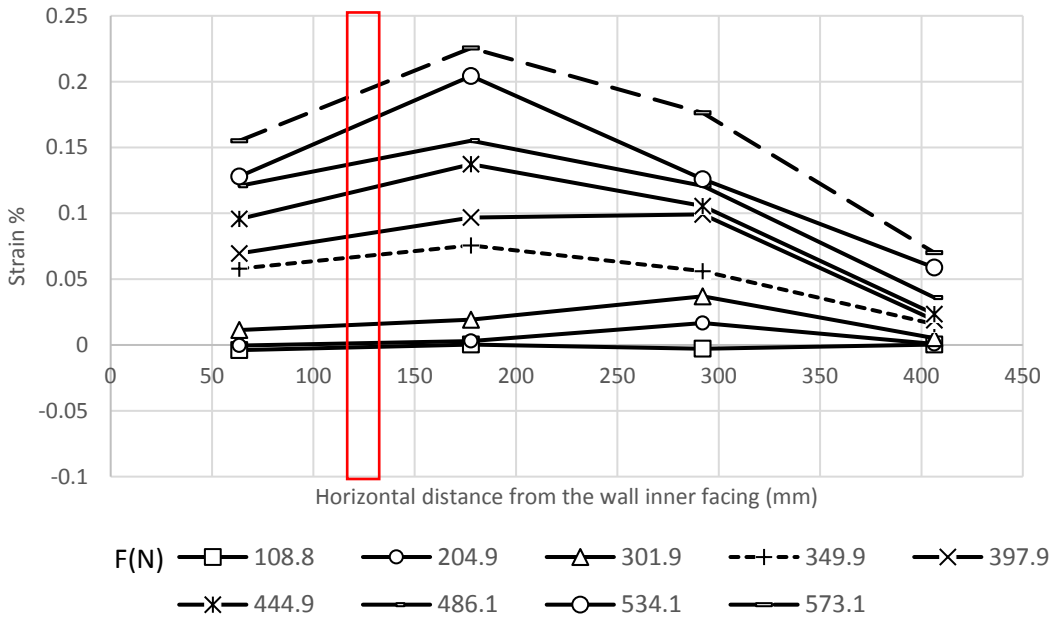

Figure 4.90 Strains of the geogrid layer in the longitudinal direction at 630 mm from the wall base (Test H2 L2 S1 C2 D1 with pile offset = 127 mm).

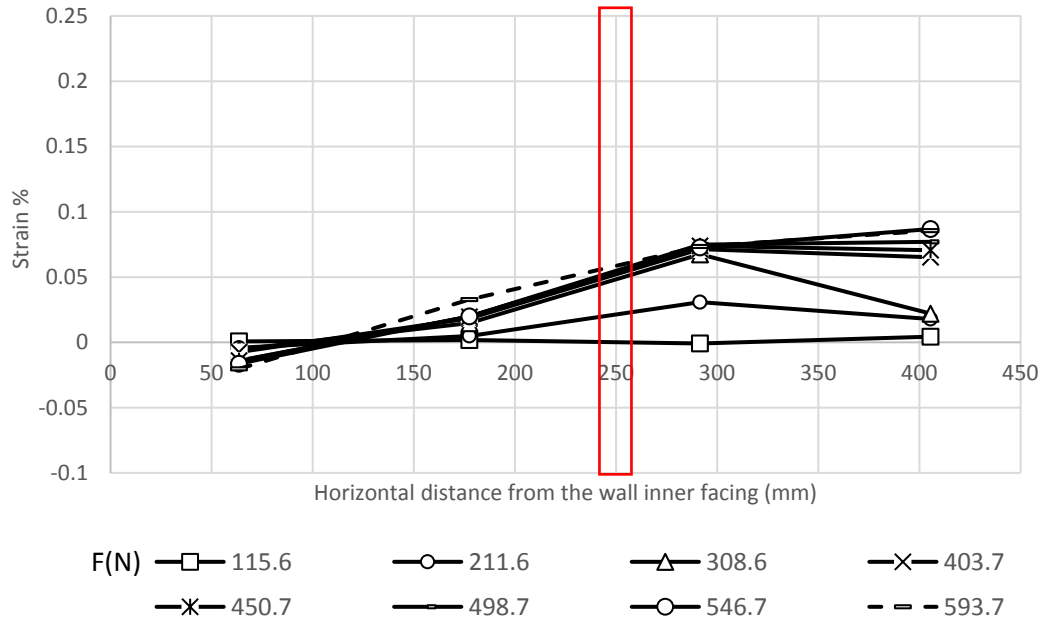

Figure 4.91 Strains of the geogrid layer in the longitudinal direction at 630 mm from the wall base (Test H2 L2 S1 C2 D2 with pile offset = 254 mm).

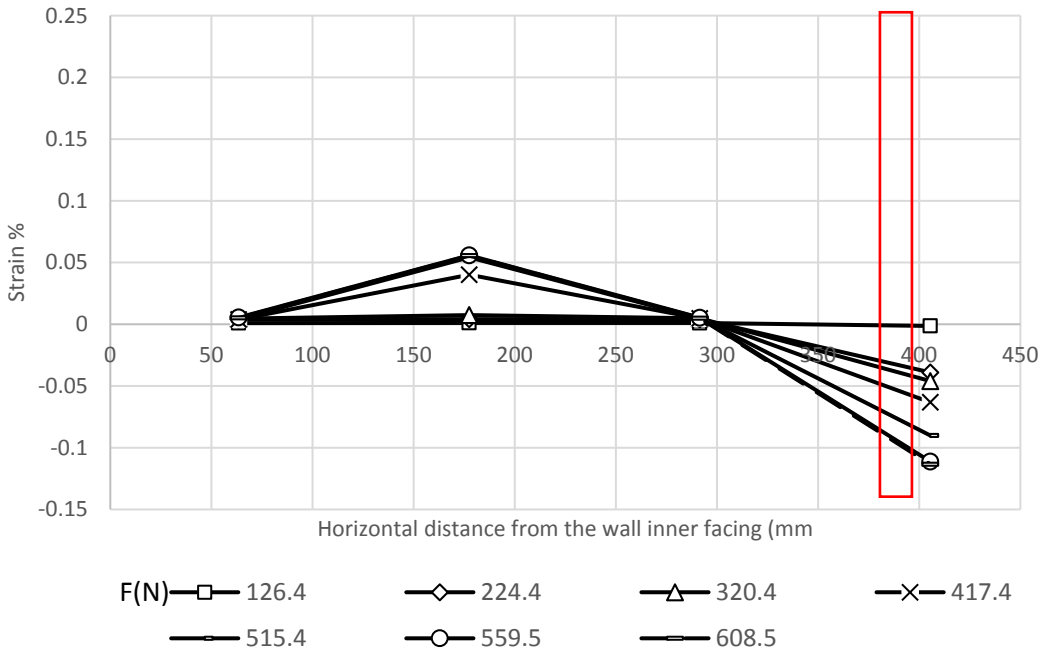

Figure 4.92 Strains of the geogrid layer in the longitudinal direction at 630 mm from the wall base (Test H2 L2 S1 C2 D3 with pile offset = 381 mm).

Pressure behind wall facing

Figures 4.93, 4.94, and 4.95 present the pressure distributions behind the wall facing in Tests H2 L2 S1 C2 D1, H2 L2 S1 C2 D2, and H2 L2 S1 C2 D3, respectively.

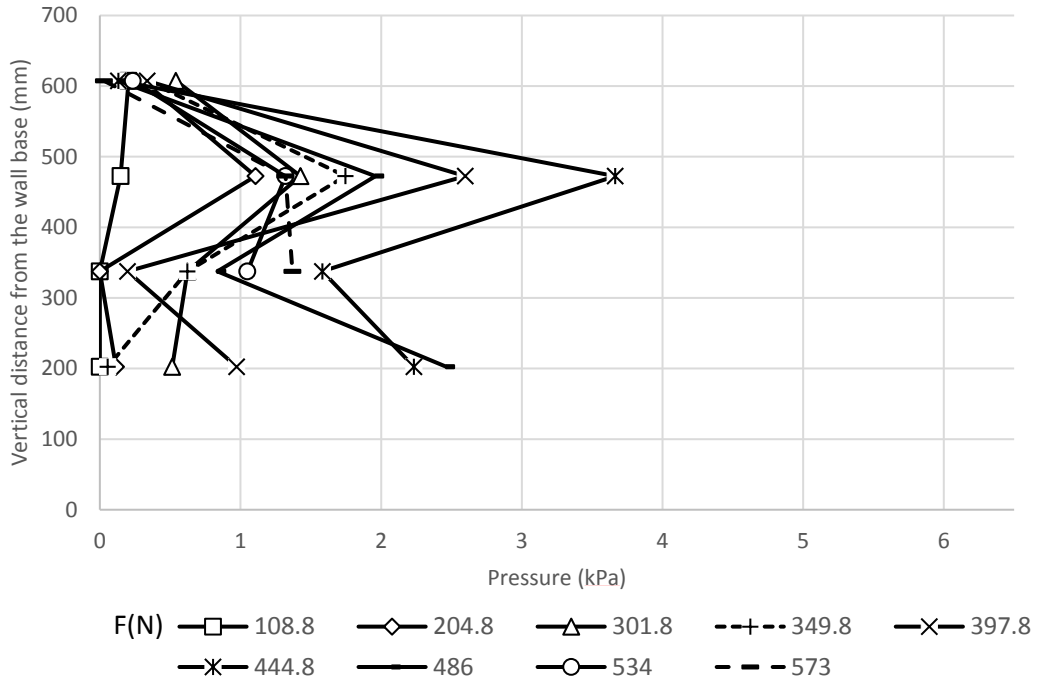

Figure 4.93 Pressures behind the wall facing along the vertical centerline in Test H2 L2 S1 C2 D1 (pile offset = 127 mm).

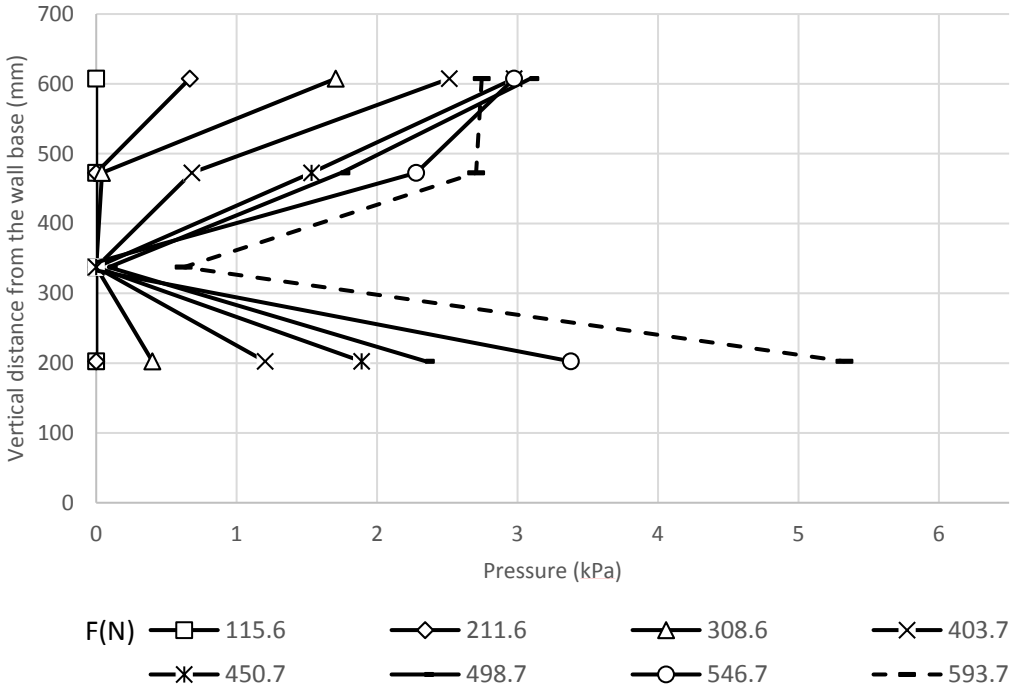

Figure 4.94 Pressures behind the wall facing along the vertical centerline in Test H2 L2 S1 C2 D2 (pile offset = 254 mm).

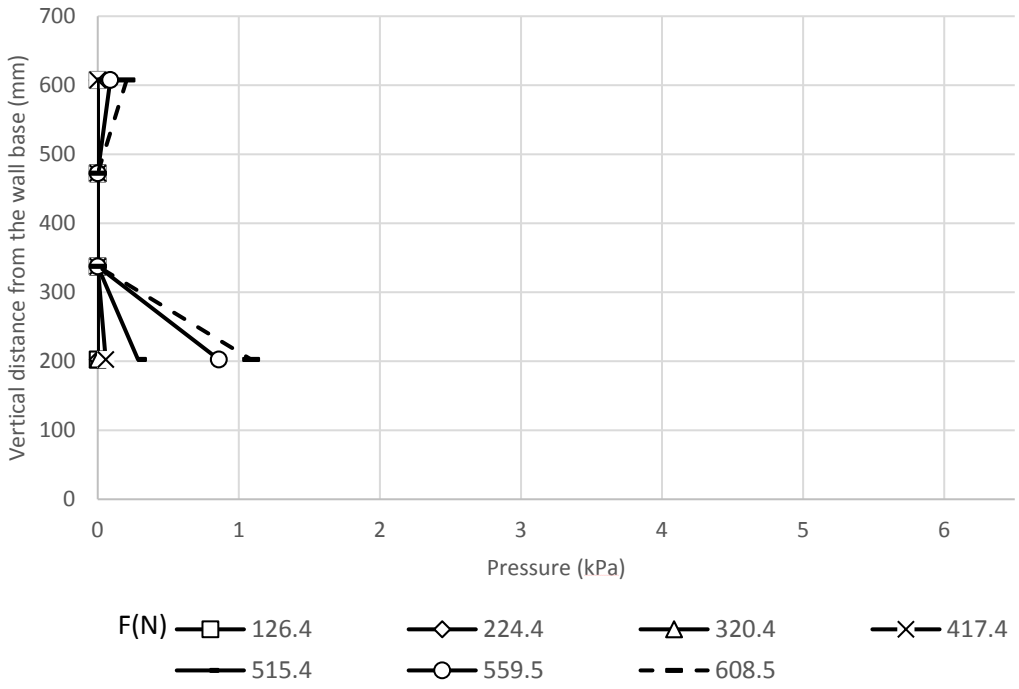

Figure 4.95 Pressures behind the wall facing along the vertical centerline in Test H2 L2 S1 C2 D3 (pile offset = 381 mm).

The transverse pressure distributions behind the wall facing for Tests H2 L2 S1 C2 D1, H2 L2 S1 C2 D2, and H2 L2 S1 C2 D3 at 472.5 mm from the wall base are shown in Figures 4.96, 4.97, and 4.98, respectively. For the same tests, the transverse pressure distributions behind the wall facing at 202.5 mm from the wall base are shown in Figures 4.99, 4.100, and 4.101. The other transverse pressure distributions at the elevations of 607.5 mm and 337.5 mm are included in section A.3.3. of appendix A. The behavior of the pressure distributions is similar to the behavior that shown in Category 2 of Group 2. However, there is a decreasing in the pressure distributions of the Tests H2 L2 S1 C2 D1 at the final loading steps as shown in Figures 4.93 and 4.94. Reaching the failure may be the reason behind the pressure decreasing. In the test with a pile offset equal to (4d), a high pressure zone is induced behind the upper end of the wall facing because of using the frictional connection.

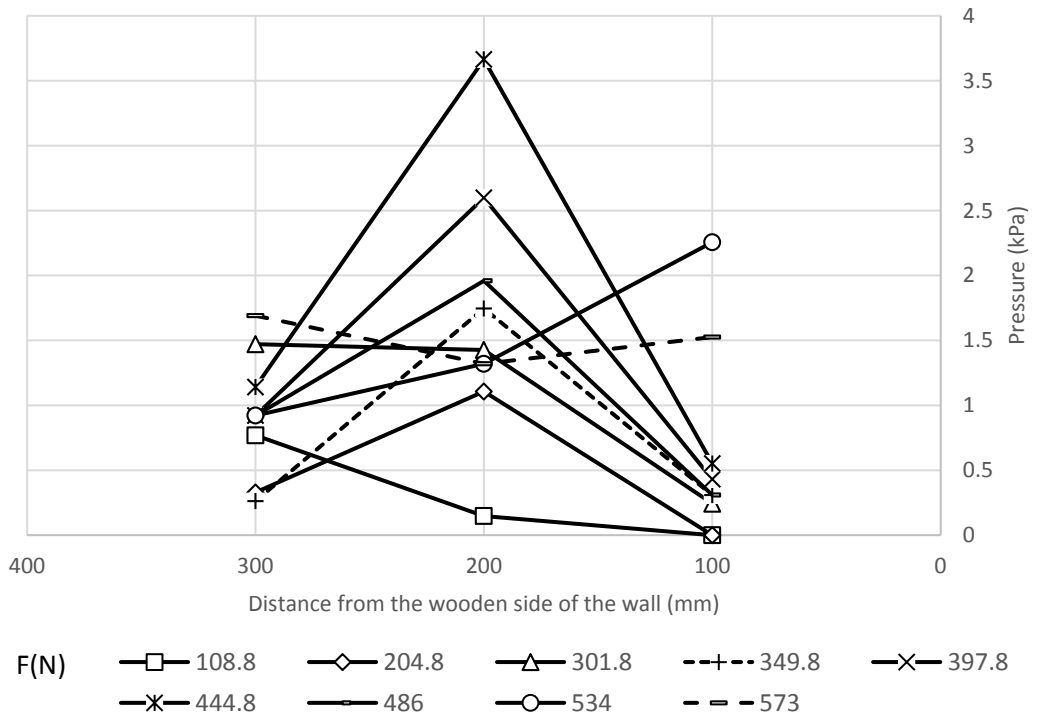

Figure 4.96 Pressure distributions in the transverse direction at the elevation of 472.5 mm from the wall base in Test H2 L2 S1 C2 D1 (pile offset = 127 mm).

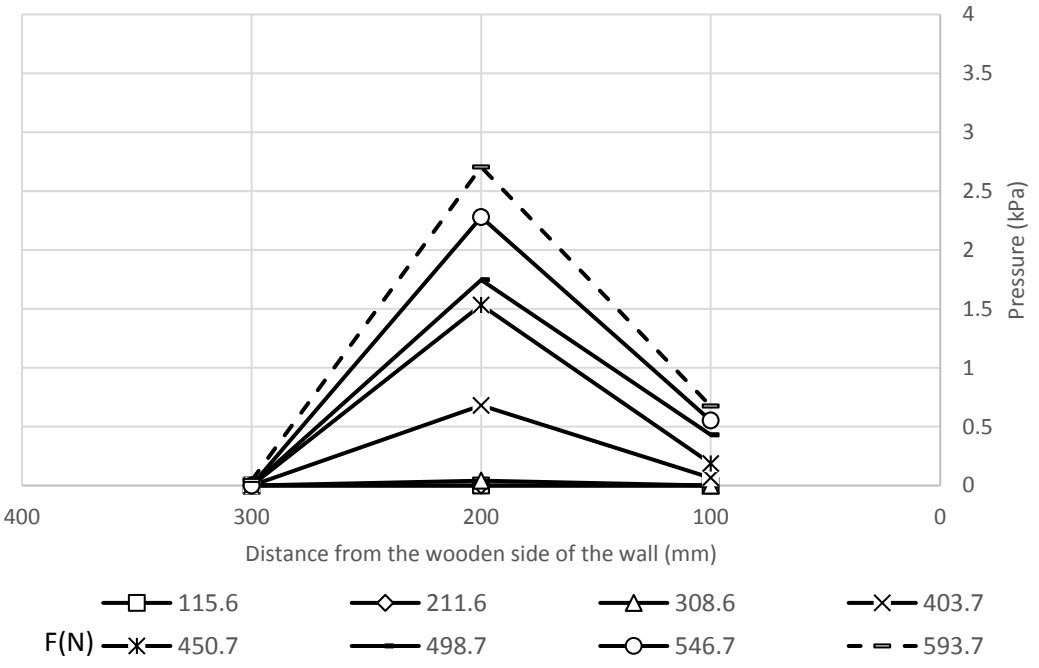

Figure 4.97 Pressure distributions in the transverse direction at the elevation of 472.5 mm from the wall base in Test H2 L2 S1 C2 D2 (pile offset = 254 mm).

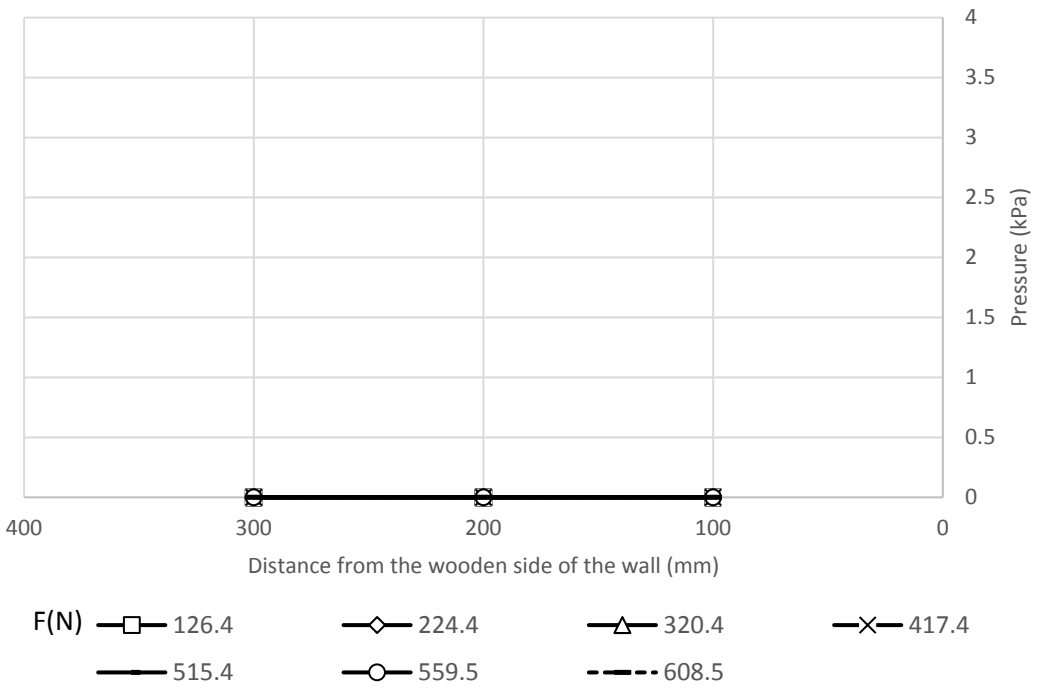

Figure 4.98 Pressure distributions in the transverse direction at the elevation of 472.5 mm from the wall base in Test H2 L2 S1 C2 D3 (pile offset = 381 mm).

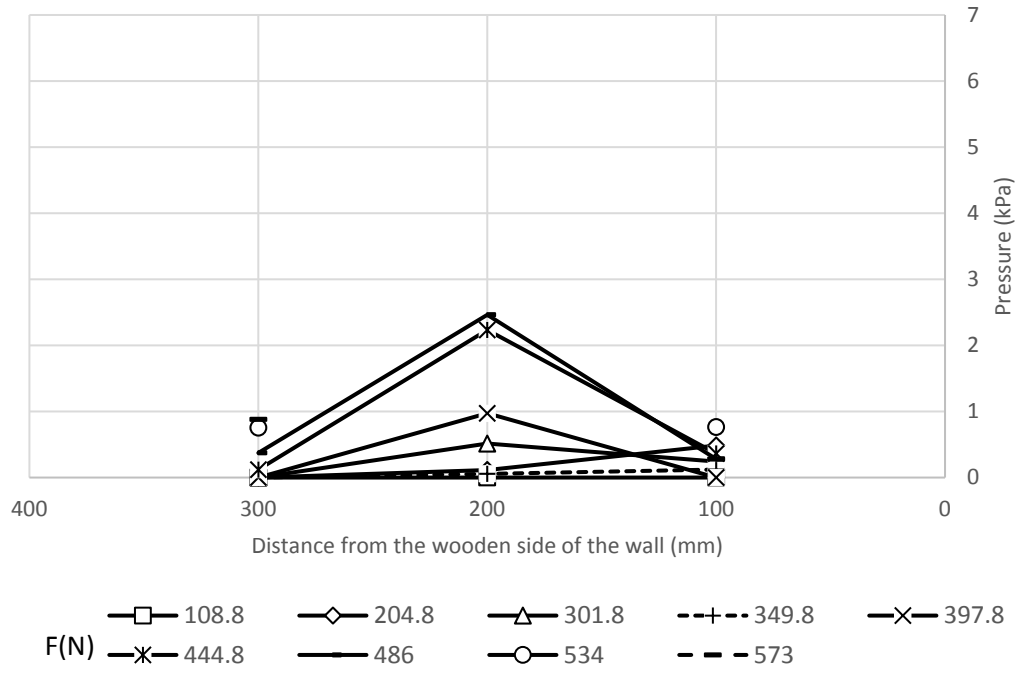

Figure 4.99 Pressure distributions in the transverse direction at the elevation of 202.5 mm from the wall base in Test H2 L2 S1 C2 D1 (pile offset = 127 mm).

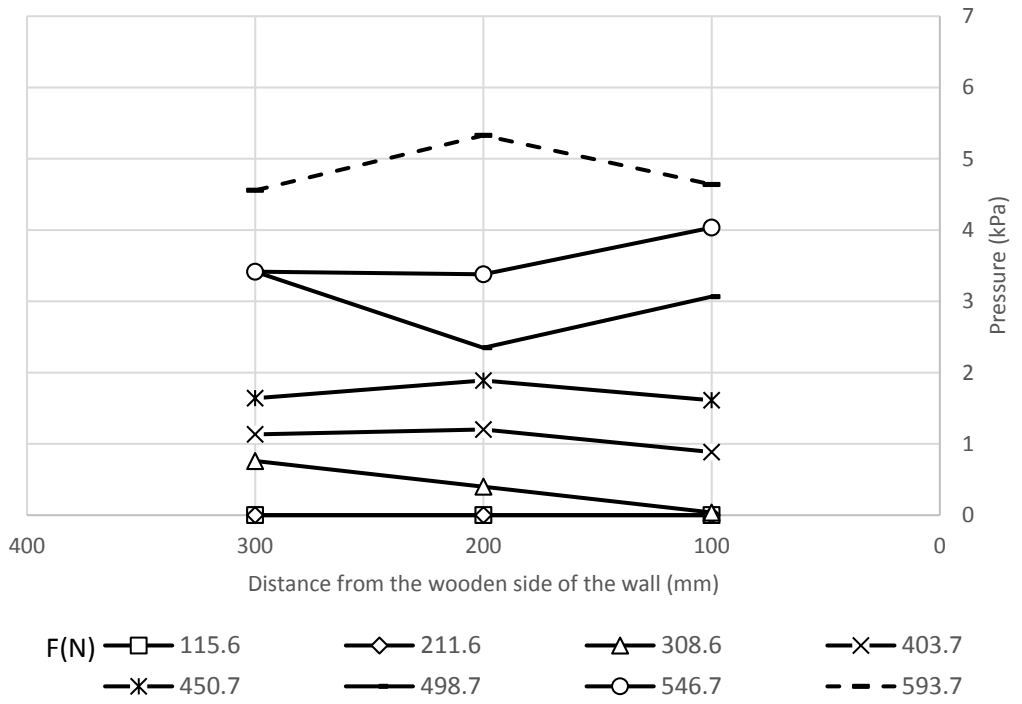

Figure 4.100 Pressure distributions in the transverse direction at the elevation of 202.5 mm from the wall base in Test H2 L2 S1 C2 D2 (pile offset = 254 mm).

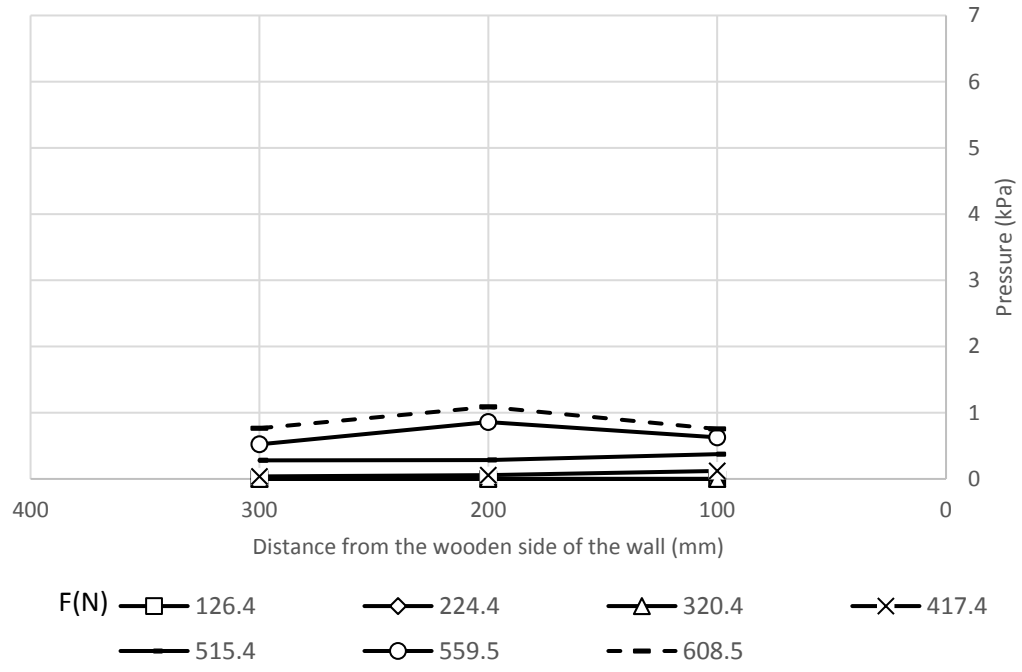

Figure 4.101 Pressure distributions in the transverse direction at the elevation of 202.5 mm from the wall base in Test H2 L2 S1 C2 D3 (pile offset = 381 mm).

4.4. High walls with long reinforcement length

This group includes three categories as was mentioned in Chapter 3. Each category has two high wall tests with the same parameters except for pile offset. The differences between this group the second group is that the reinforcement length is higher and there are no tests with 2d pile offset.

4.4.1. Category 1

This category includes the data figures for Tests H2 L3 S2 C1 **D2** and H2 L3 S2 C1 **D3**. The spacing between the geogrid layers in this category is equal to 135 mm for the bottom layers and 185 mm for the upmost layer.

Deflection of wall facing

The deflections along the center line of the wall facing in Tests H2 L3 S2 C1 **D2** and H2 L3 S2 C1 **D3** are shown in Figures 4.102 and 4.103, respectively. From these figures, the deflection distributions at the pile offset of 4d are higher than the deflection distributions at the pile offset 6d.

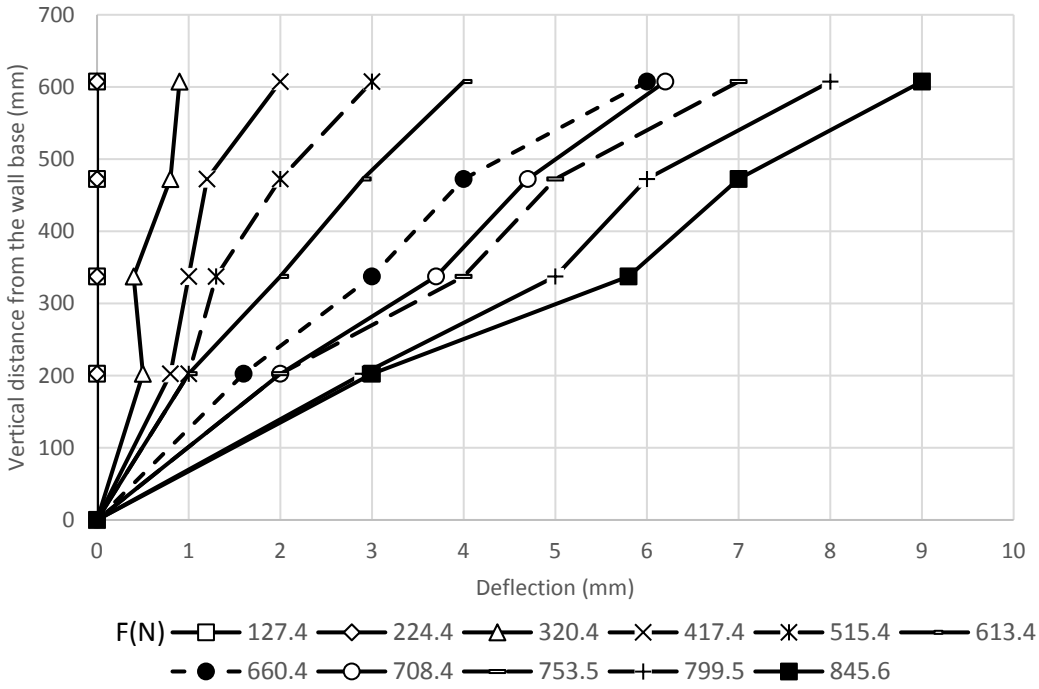

Figure 4.102 Wall facing deflections along the vertical centerline in Test H2 L3 S2 C1 D2 (pile offset = 254 mm).

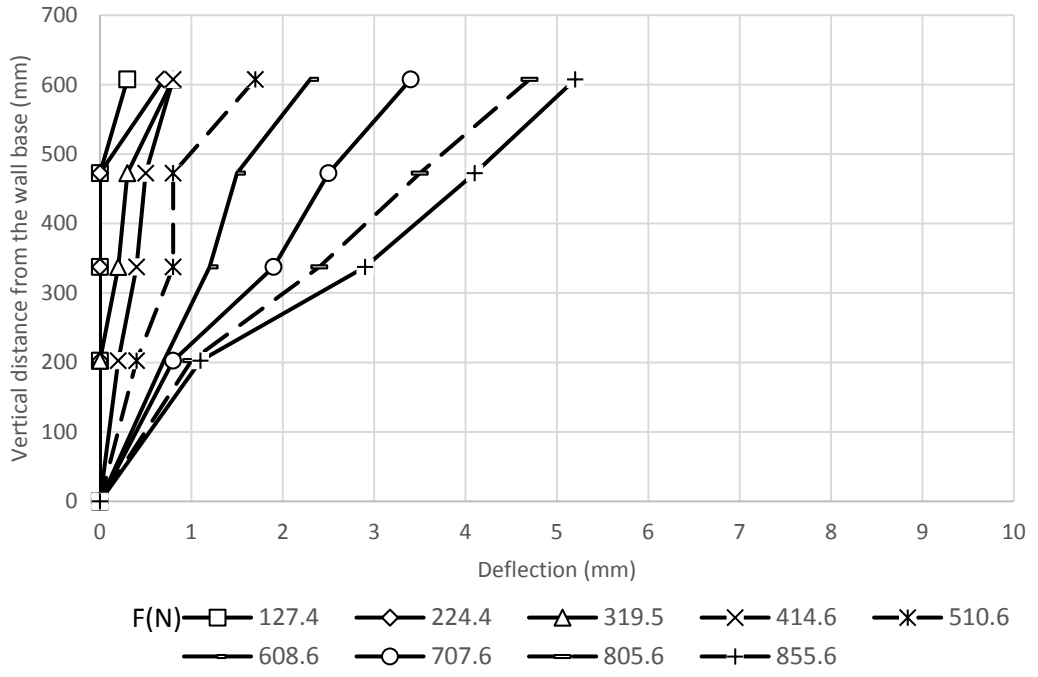

Figure 4.103 Wall facing deflections along the vertical centerline in Test H2 L3 S2 C1 D3 (pile offset = 381 mm).

As the same as Group 2, the maximum deflection occurs at 84.4% of the wall height, and the transverse deflection profiles at this location are shown in Figures 4.104 and 4.105.

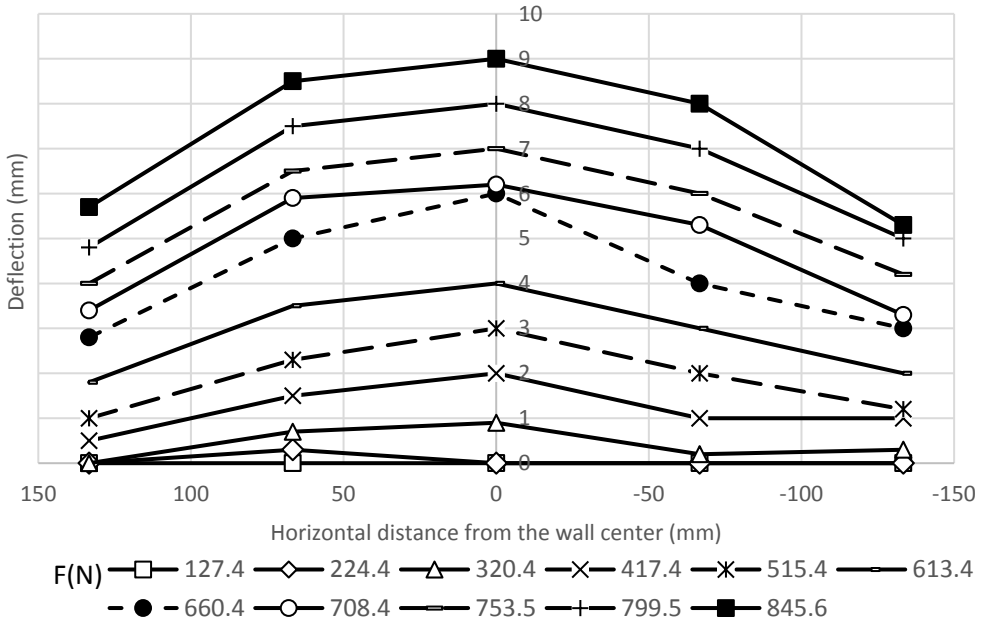

Figure 4.104 Transverse deflection profile at 607.5 mm from the wall base in Test H2 L3 S2 C1 D2 (pile offset = 254 mm).

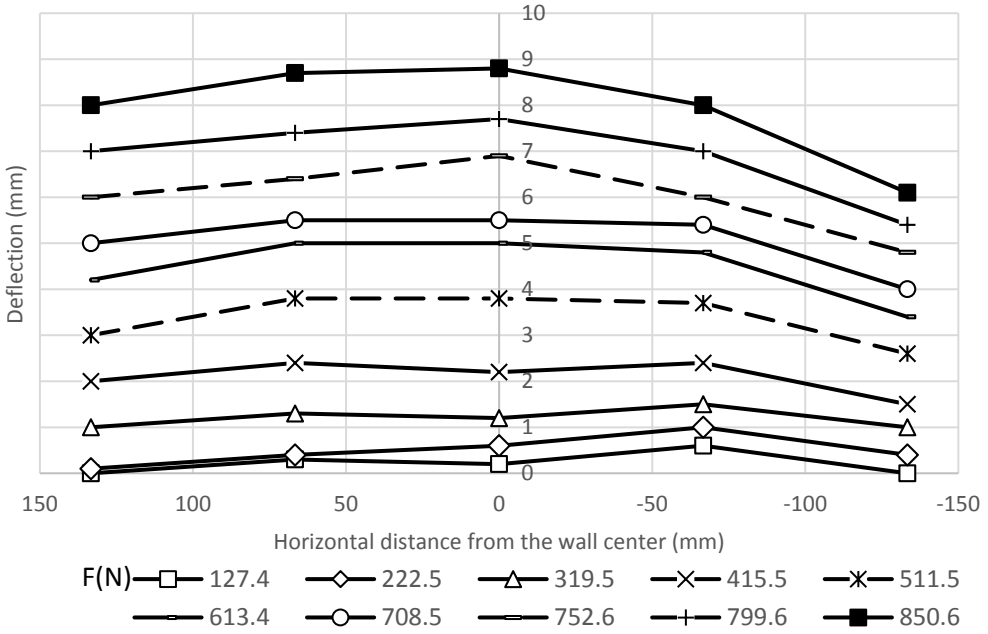

Figure 4.105 Transverse deflection profile at 607.5 mm from the wall base in Test H2 L3 S2 C1 D3 (pile offset = 381 mm).

The transverse deflection distributions are approximately uniform in Figures 4.104 and 4.105 because of the large distance between the pile and the wall facing. For Tests H2 L3 S2 C1 **D2** and H2 L3 S2 C1 **D3**. The transverse deflection profiles of the wall facing at 472.5 mm, 337.5 mm, and 202.5 mm from the wall base are shown in section A.4.1. of Appendix A.

Strain, stress, and moment of pile

The strains along the compressive side of the pile in Tests H2 L3 S2 C1 **D2** and H2 L3 S2 C1 **D3** are presented in Figures 4.106 and 4.107, respectively. For the same tests, the data figures for the stress and the moment along the compressive side of the pile are shown in section A.4.1. of appendix A.

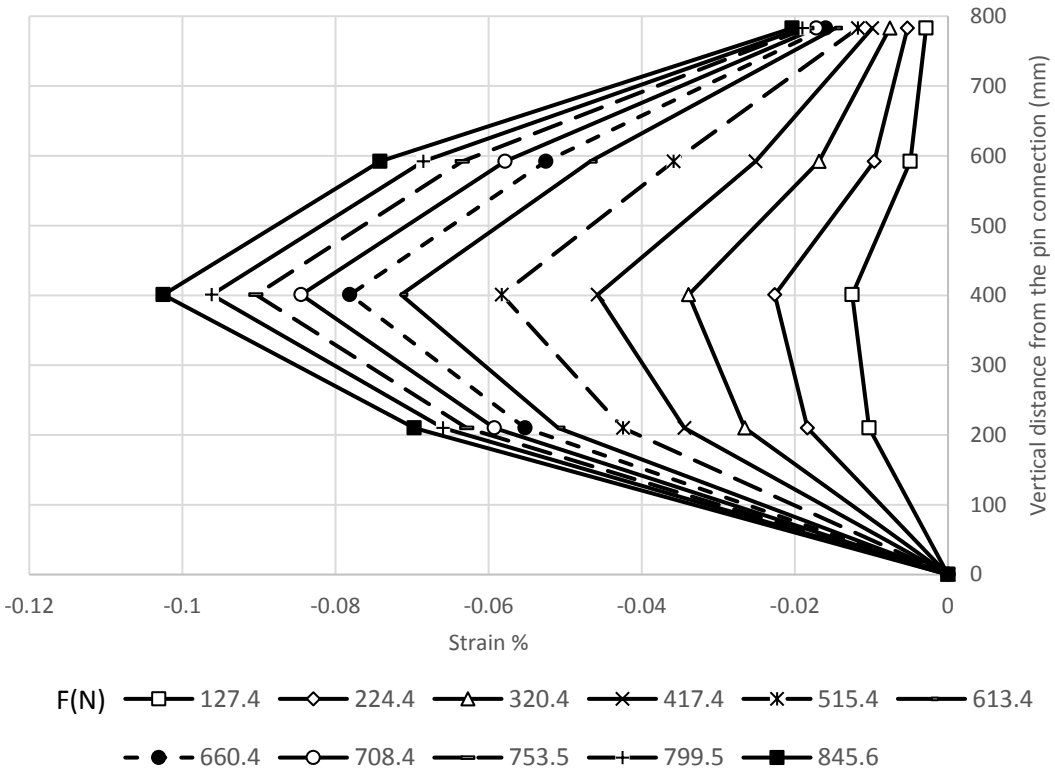

Figure 4.106 Strains along the compressive side of the pile in Test H2 L3 S2 C1 D2 (pile offset = 254 mm).

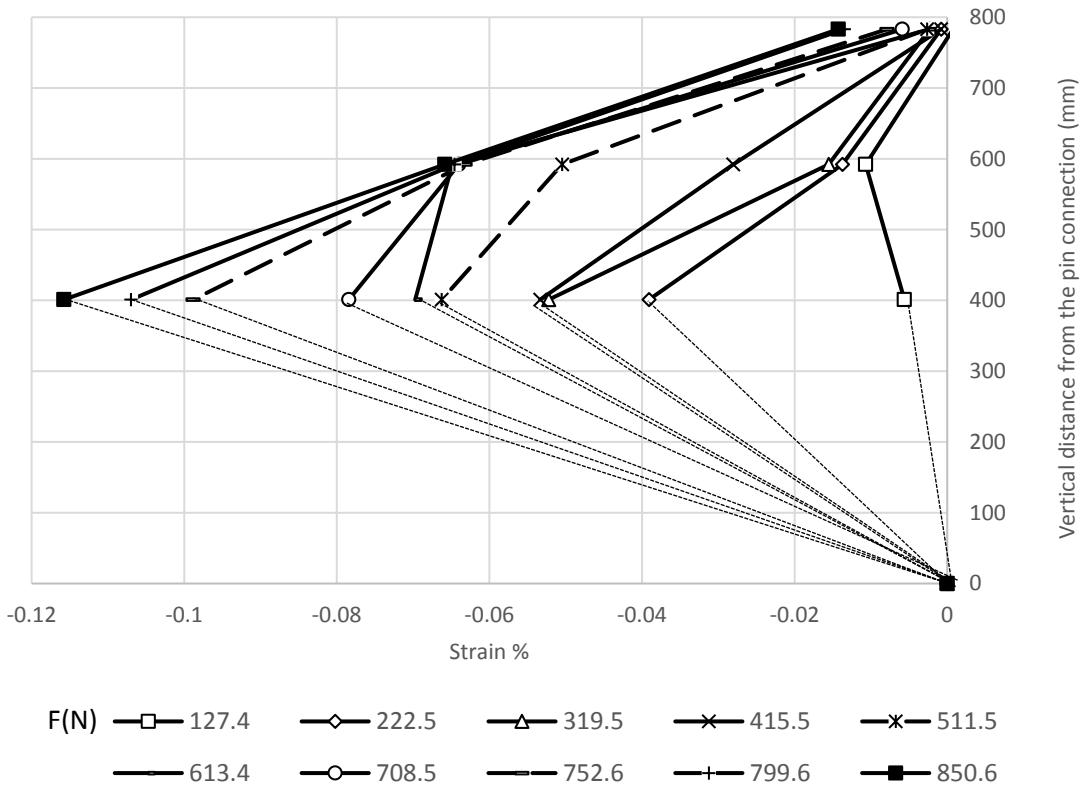

Figure 4.107 Strains along the compressive side of the pile in Test H2 L3 S2 C1 D3 (pile offset = 381 mm).

The strains along the tensile side of the pile in Tests H2 L3 S2 C1 **D2** and H2 L3 S2 C1 **D3** are presented in Figures 4.108 and 4.109, respectively. All the data figures for the stress and moment along the tensile side is shown in section A.4.1. of Appendix A.

For the compressive and the tensile side, the maximum strains are located at 400 mm from the wall base for both pile sides. In addition, the increasing in the strain distributions during the loading steps are not uniform in the test with higher pile offset. Furthermore, the difference between maximum strains of the two tests is significantly higher.

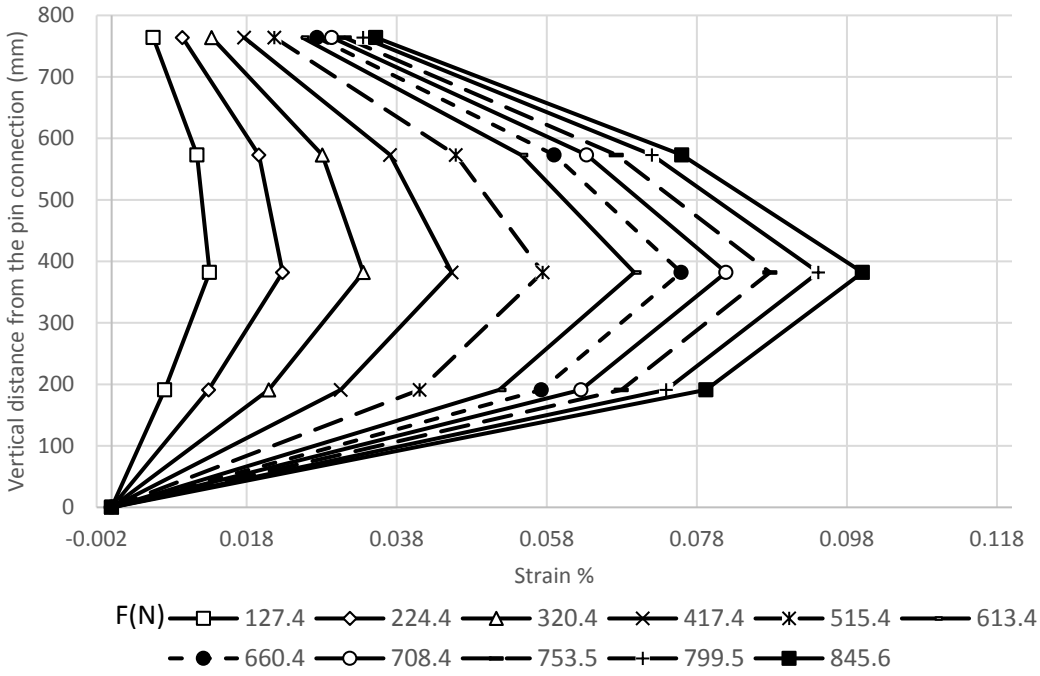

Figure 4.108 Strains along the tensile side of the pile in Test H2 L3 S2 C1 D2 (pile offset = 254 mm).

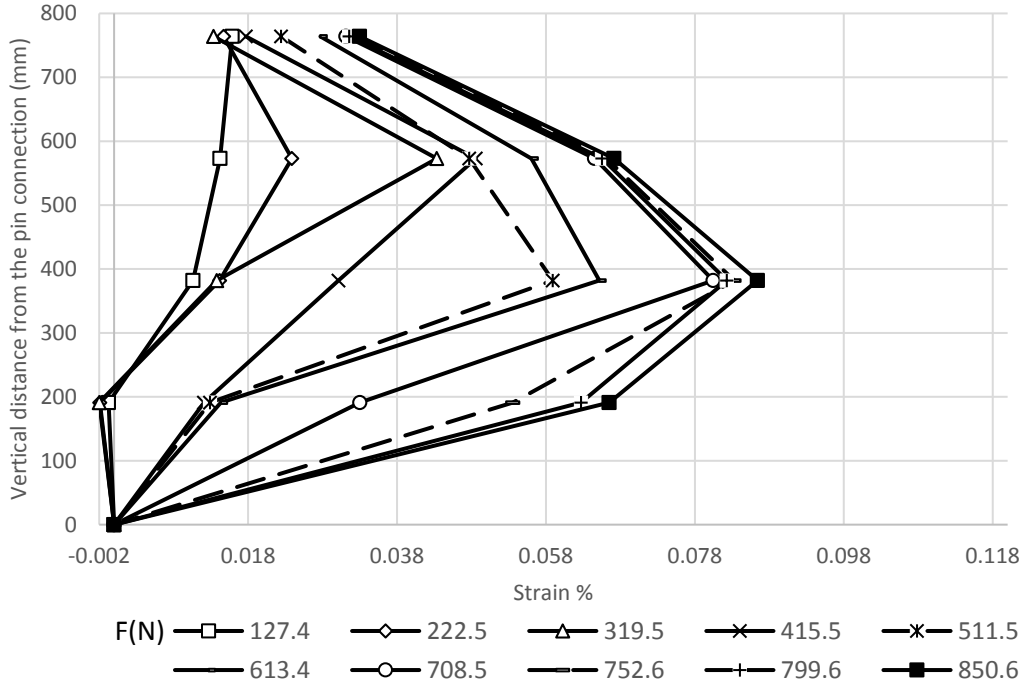

Figure 4.109 Strains along the tensile side of the pile in Test H2 L3 S2 C1 D3 (pile offset = 381 mm).

Deflection of pile

The deflections of the pile are shown in Figures 4.110 and 4.111 for Tests H2 L3 S2 C1 **D2** and H2 L3 S2 **C1** D3, respectively. From these figures, a higher deflection distributions occur when the pile is closer to the wall facing. Moreover, the pile in this group behaves more flexible than Group 2.

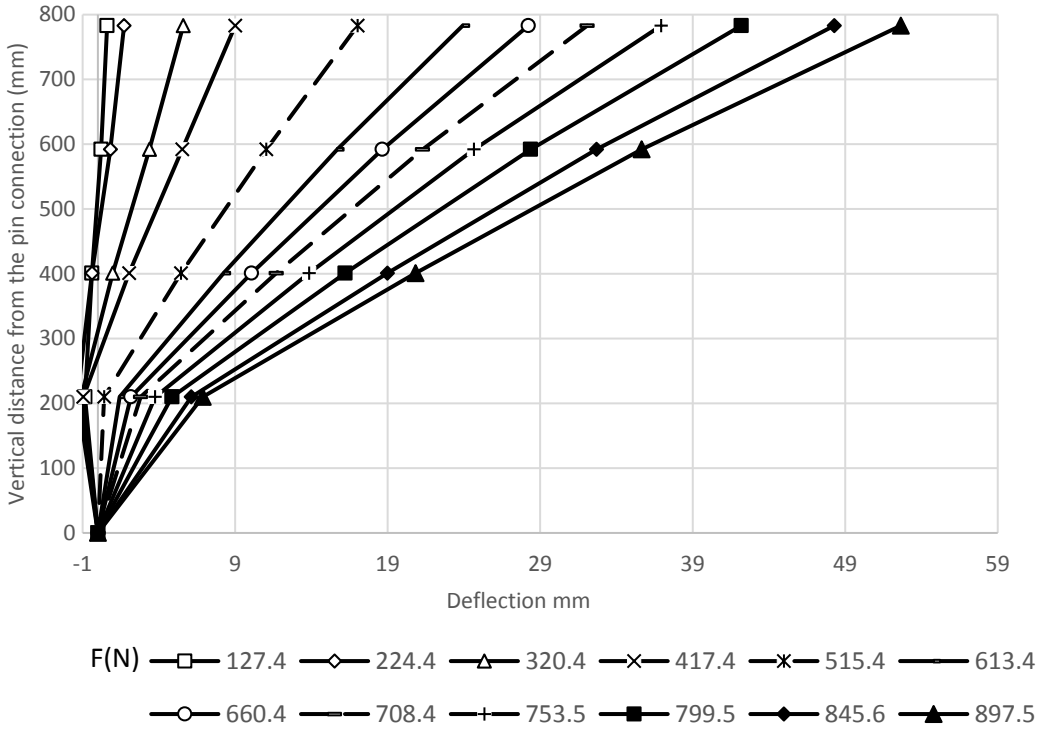

Figure 4.110 Deflections of the pile in Test H2 L3 S2 C1 D2 (pile offset = 254 mm).

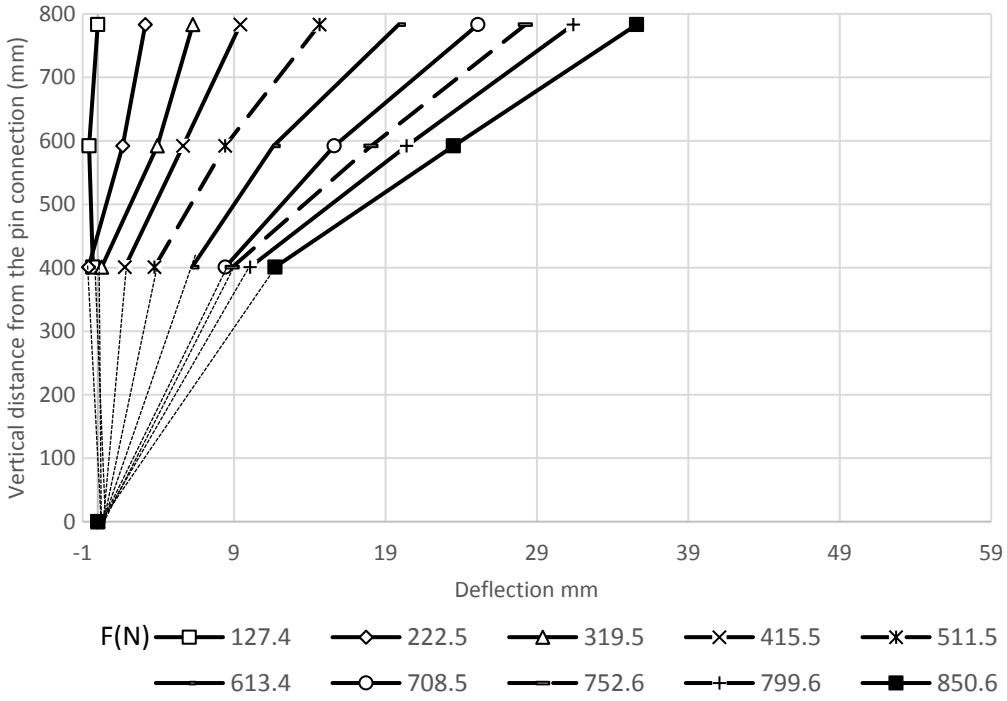

Figure 4.111 Deflections of the pile in Test H2 L3 S2 C1 D3 (pile offset = 381 mm).

Strain of geogrid

The longitudinal strains in the geogrid layer at height equal to 540 mm from the wall base for Tests H2 L3 S2 C1 **D2** and H2 L3 S2 C1 **D3** are shown in Figures 4.112 and 4.113, respectively. For the same tests, the strains of the geogrid layers at 405 mm, 270 mm, and 135 mm from the wall base are presented in section A.4.1. of Appendix A.

The maximum strains are near to the pile location for the two offset. In fact, it behind the pile in the small offset and in front of the pile in the big offset. In the pile offset of 6d, the tensile strain at the end of the geogrid is high. On the other hand, the tensile strains are almost zero at the end of the geogrid at the pile offset of 2d. Therefore, the strain at the end of the long reinforcement increased by an increase of the pile offset.

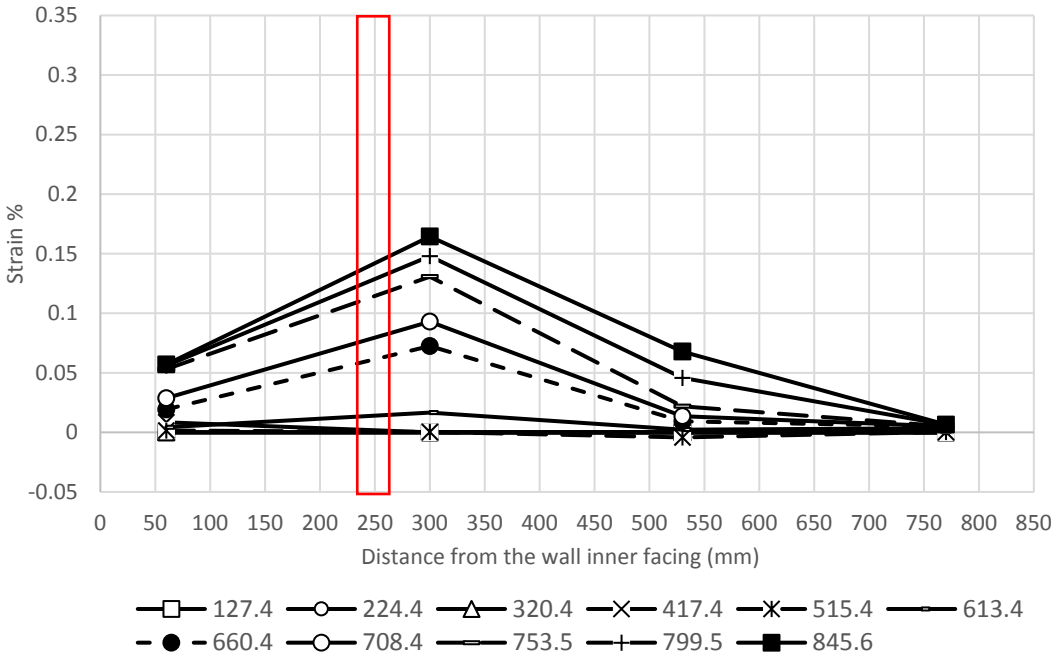

Figure 4.112 Strains of the geogrid layer in the longitudinal direction at 540 mm from the wall base (Test H2 L3 S2 C1 D2 with pile offset = 254 mm).

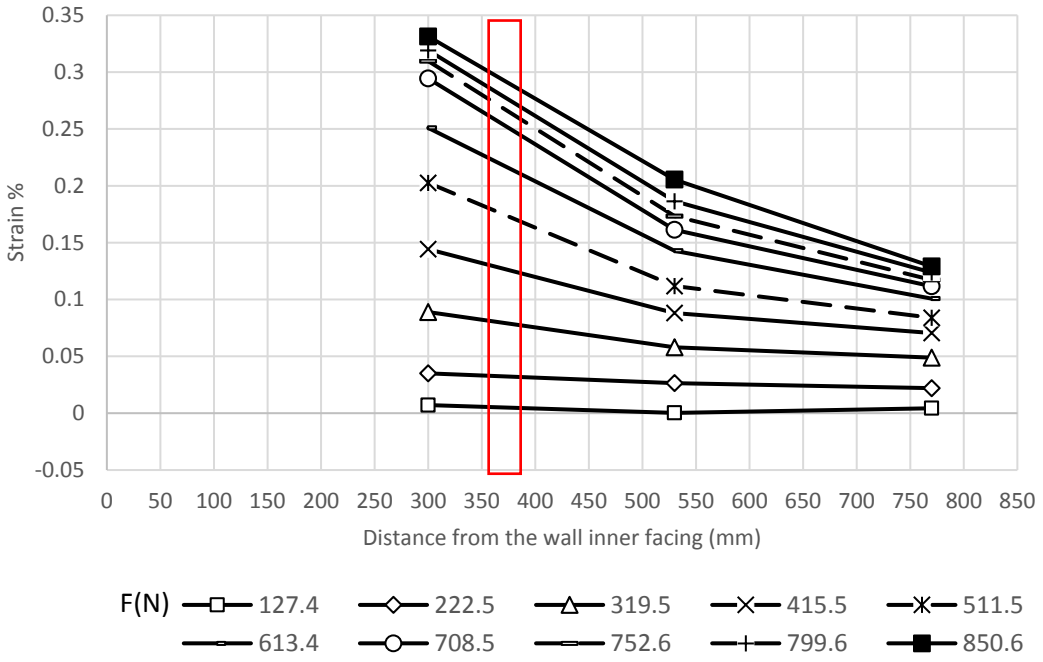

Figure 4.113 Strains of the geogrid layer in the longitudinal direction at 540 mm from the wall base (Test H2 L3 S2 C1 D3 with pile offset = 381 mm).

Pressure behind wall facing

Figures 4.114, and 4.115 present the pressure distributions behind the wall facing in Tests H2 L3 S2 C1 **D2** and H2 L3 S2 C1 **D3**, respectively.

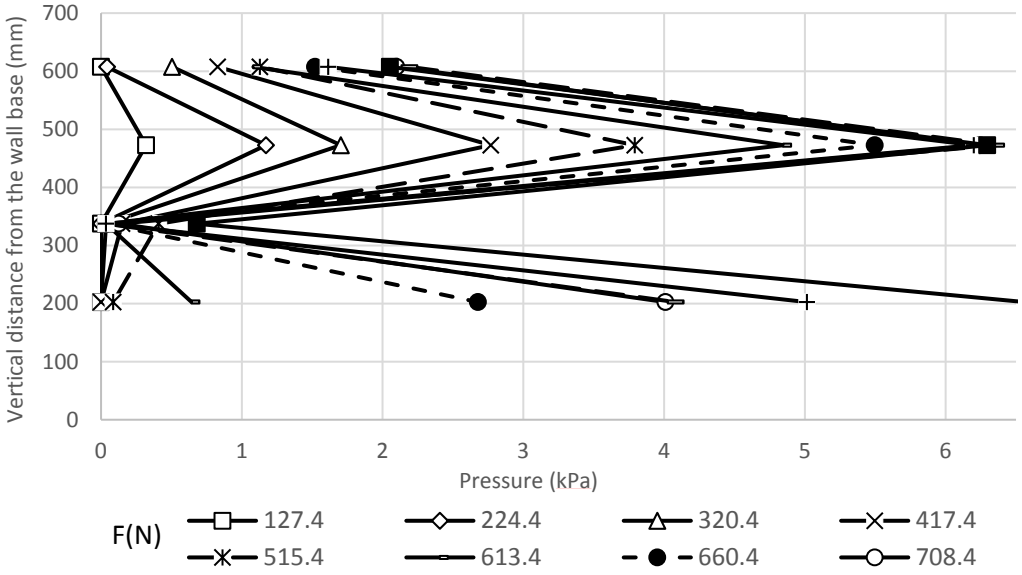

Figure 4.114 Pressures behind the wall facing along the vertical centerline in Test H2 L3 S2 C1 D2 (pile offset = 254 mm).

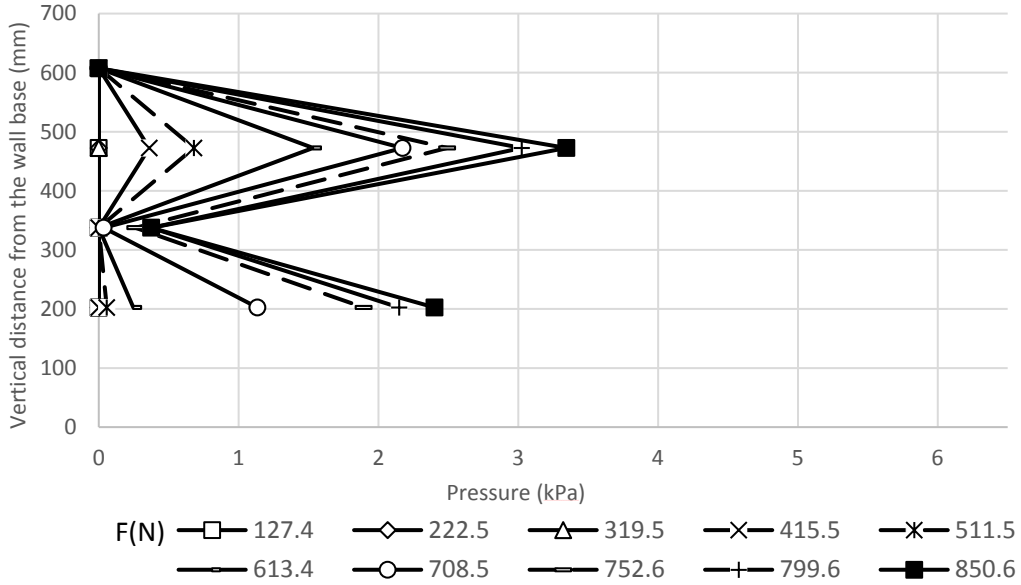

Figure 4.115 Pressures behind the wall facing along the vertical centerline in Test H2 L3 S2 C1 D3 (pile offset = 381 mm).

As the same as the other groups, high pressure zones occur behind the upper and lower part of the wall facing as shown in the previous figures. Both of them decreases by increasing of the pile offset. The transverse pressure distribution behind the wall facing at 472.5 mm from the wall base are as shown in Figures 4.116, and 4.117 for Tests H2 L3 S2 C1 **D2** and H2 L3 S2 C1 **D3**, respectively. For the same tests, the transverse pressure distributions behind the wall facing at 202.5 mm from the wall base are also shown in Figures 4.118 and 4.119. The other transverse pressure distributions at the elevations of 607.5 mm and 337.5 mm are included in section A.4.1. of appendix A.

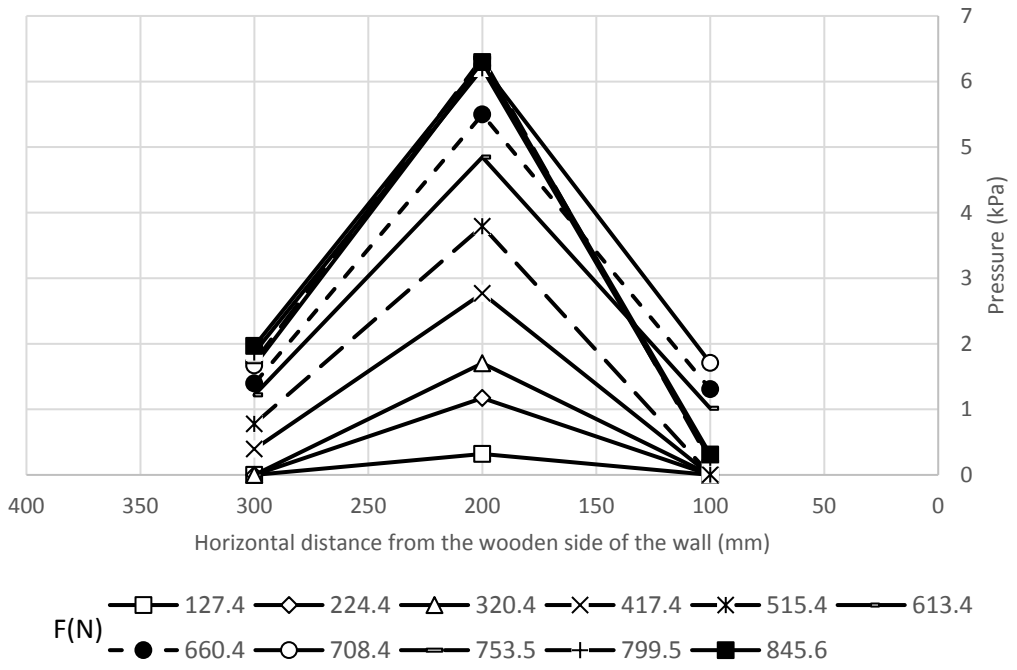

Figure 4.116 Pressure distributions in the transverse direction at the elevation of 472.5 mm from the wall base in Test H2 L3 S2 C1 D2 (pile offset = 254 mm).

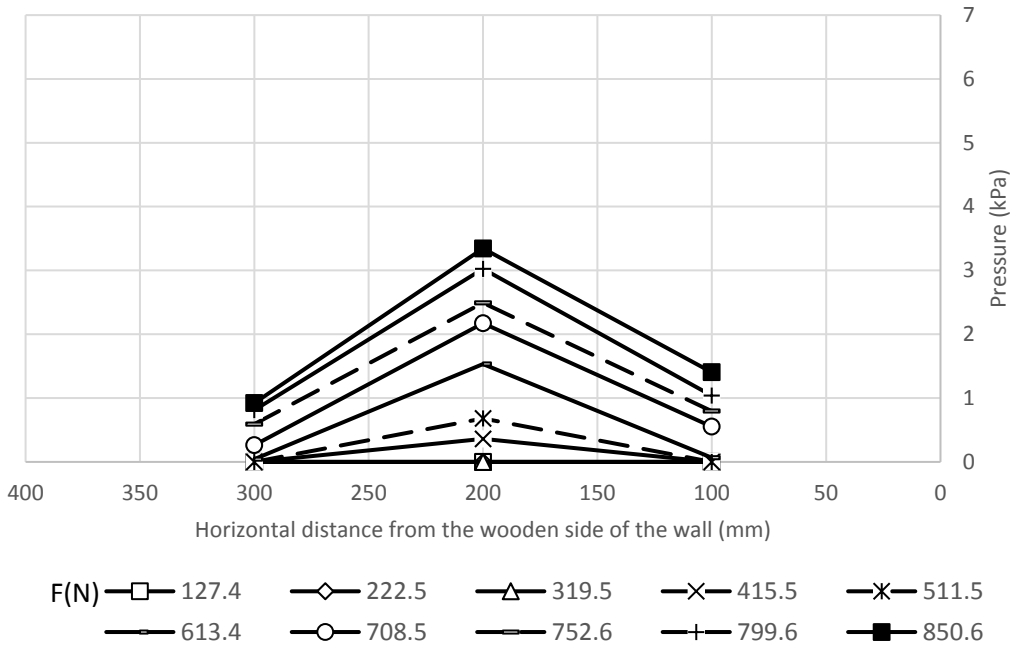

Figure 4.117 Pressure distributions in the transverse direction at the elevation of 472.5 mm from the wall base in Test H2 L3 S2 C1 D3 (pile offset = 381 mm).

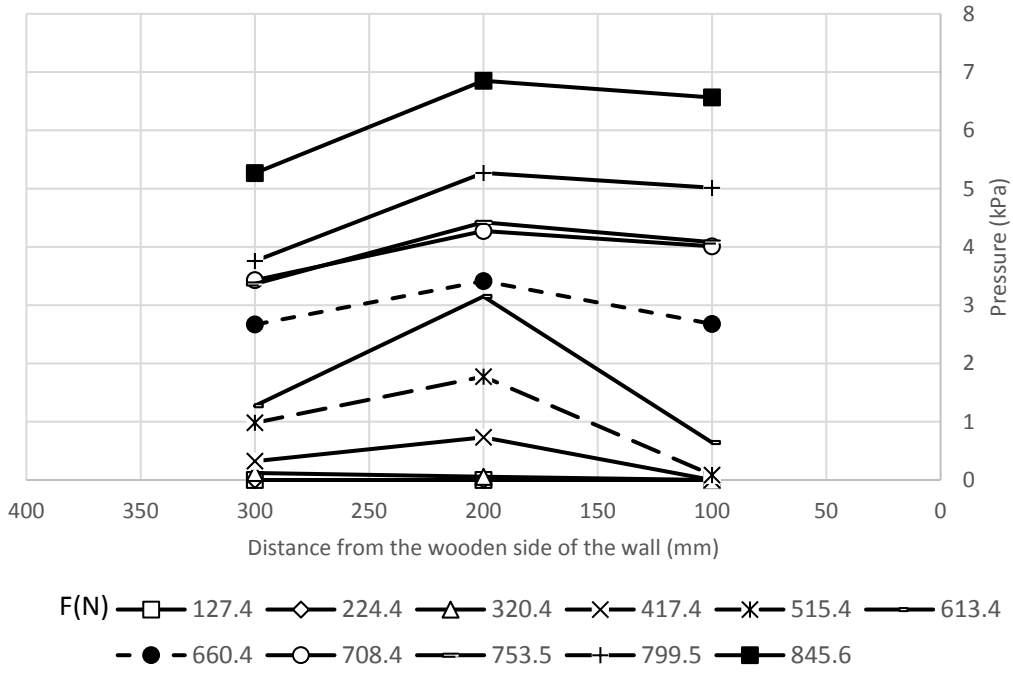

Figure 4.118 Pressure distributions in the transverse direction at the elevation of 202.5 mm from the wall base in Test H2 L3 S2 C1 D2 (pile offset = 254 mm).

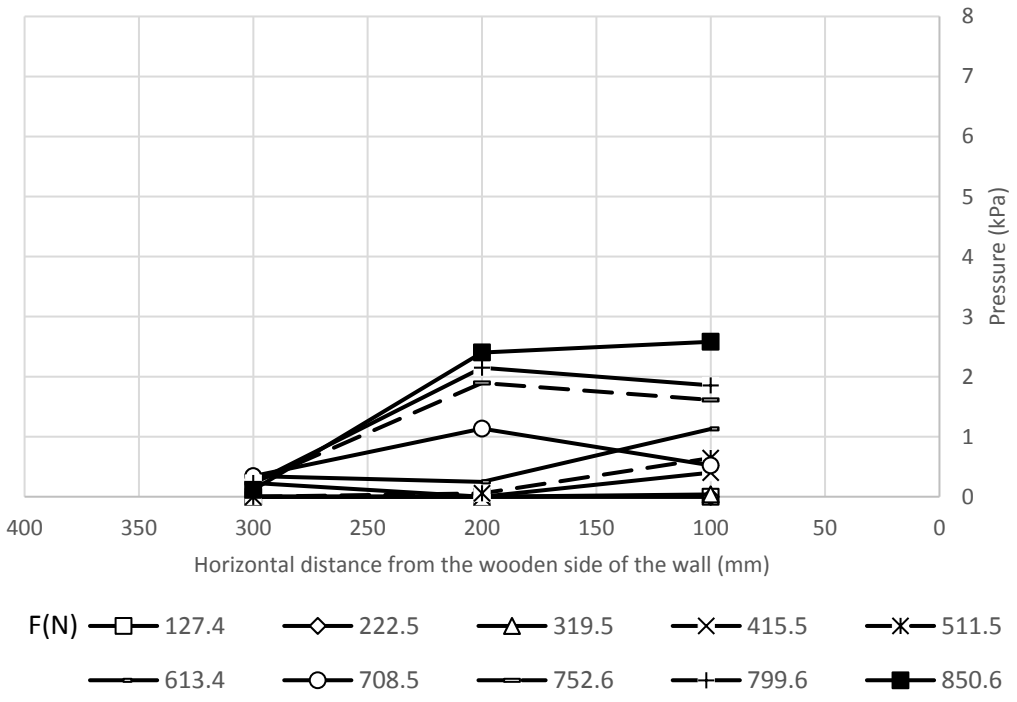

Figure 4.119 Pressure distributions in the transverse direction at the elevation of 202.5 mm from the wall base in Test H2 L3 S2 C1 D3 (pile offset = 381 mm).

4.4.2. Category 2

This category includes the data figures for Tests H2 L3 S1 C1 D2 and H2 L3 S1 C1 D3. A smaller spacing was used between the reinforcement layers.

Deflection of wall facing

The deflections along the centerline of the wall facing in Tests H2 L3 S1 C1 **D2** and H2 L3 S1 C1 **D3** are shown in Figures 4.120 and 4.121, respectively. By observing these figures, the behavior of deflection is similar to the deflection behavior that shown in Category 1 of Group 3.

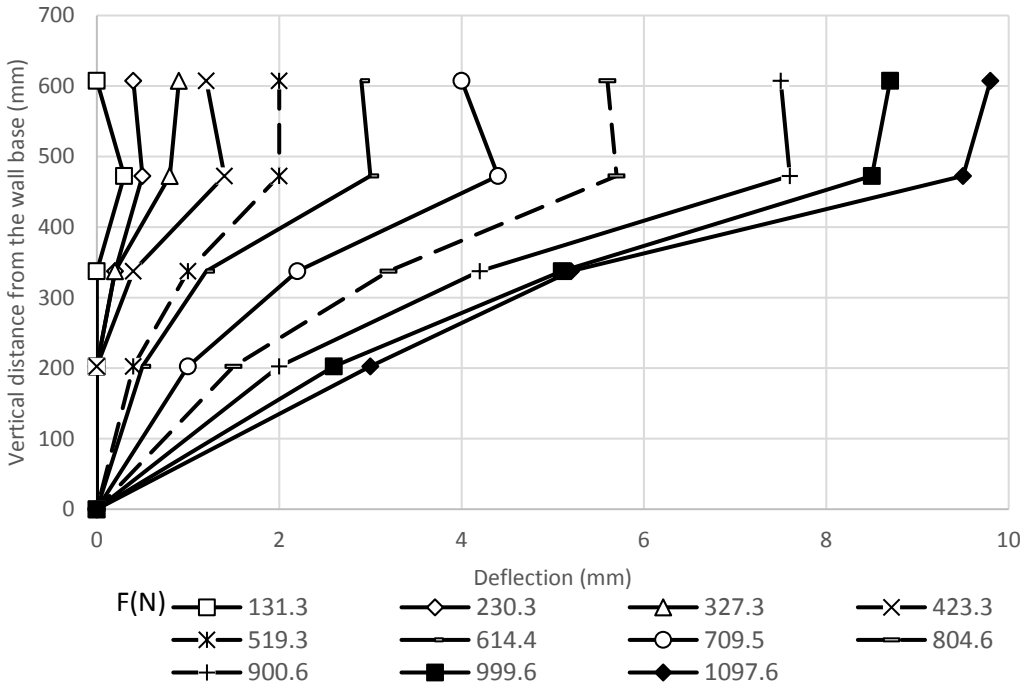

Figure 4.120 Wall facing deflections along the vertical centerline in Test H2 L3 S1 C1 D2 (pile offset = 254 mm).

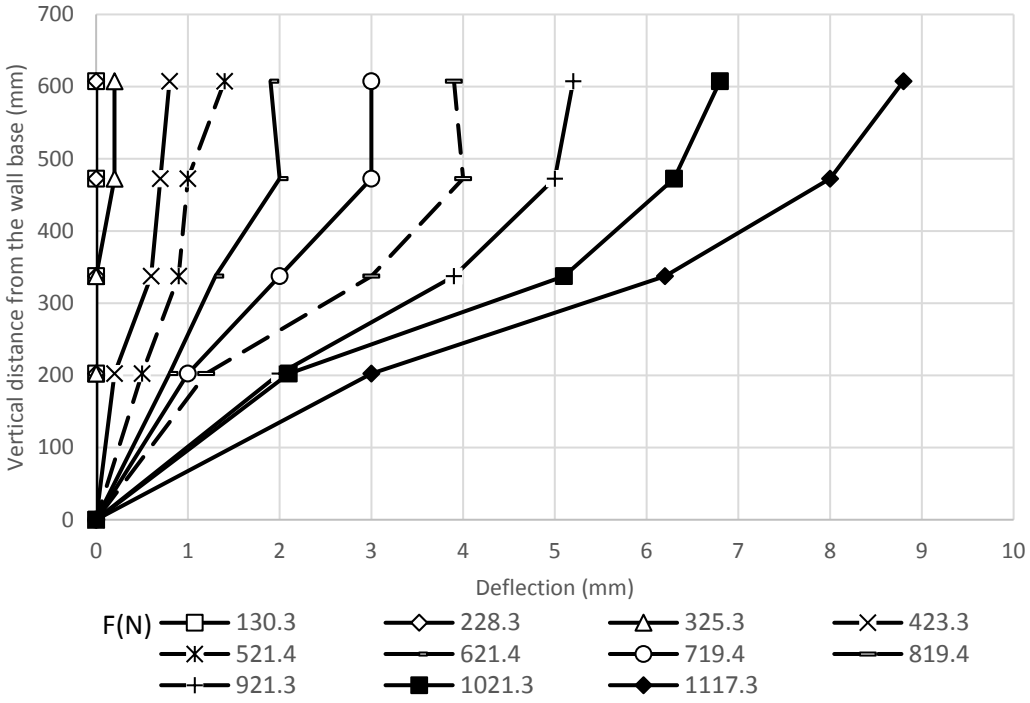

Figure 4.121 Wall facing deflections along the vertical centerline in Test H2 L3 S1 C1 D3 (pile offset = 381 mm)

In the two tests of this category, the maximum deflections occur at the center of the wall or near to it as shown in the transverse deflection profile of the wall facing at 607.5 mm from the wall base in Figures 4.122 and 4.123.

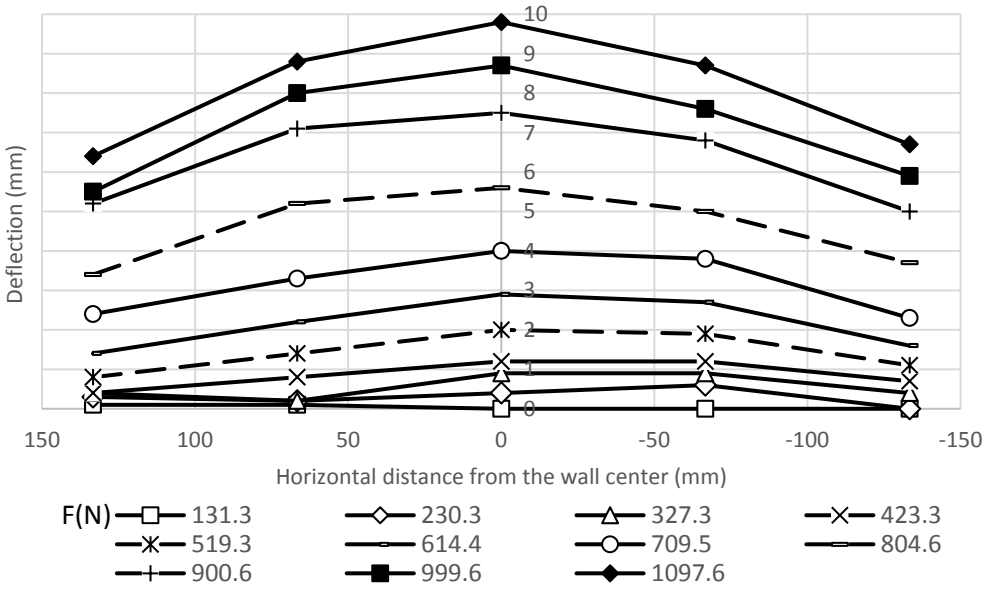

Figure 4.122 Transverse deflection profile at 607.5 mm from the wall base in Test H2 L3 S1 C1 D2 (pile offset = 254 mm).

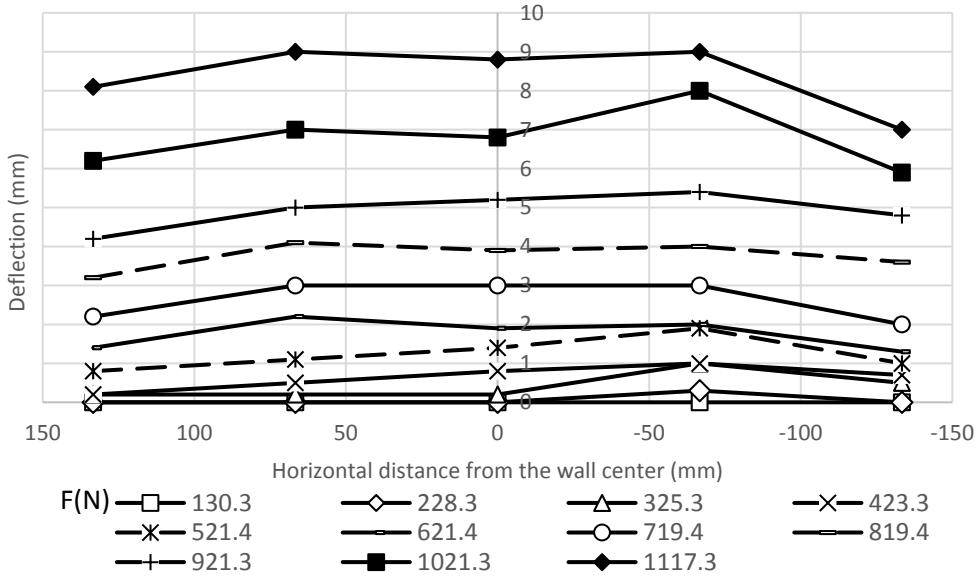

Figure 4.123 Transverse deflection profile at 607.5 mm from the wall base in Test H2 L3 S1 C1 D3 (pile offset = 381 mm).

The transverse deflection profiles of the wall facing at 472.5 mm, 337.5 mm, and 202.5 mm from the wall base for Tests H2 L3 S1 C1 **D2** and H2 L3 S1 C1 **D3** are shown in section A.4.2. of appendix A.

Strain, stress, and moment of pile

The strains along the compressive side of the pile in Tests H2 L3 S1 C1 **D2** and H2 L3 S1 C1 **D3** are presented in Figures 4.124 and 4.125 respectively. For the same tests, the data figures for the stress and the moment along the compressive side of the pile are shown in section A.4.2. of Appendix A.

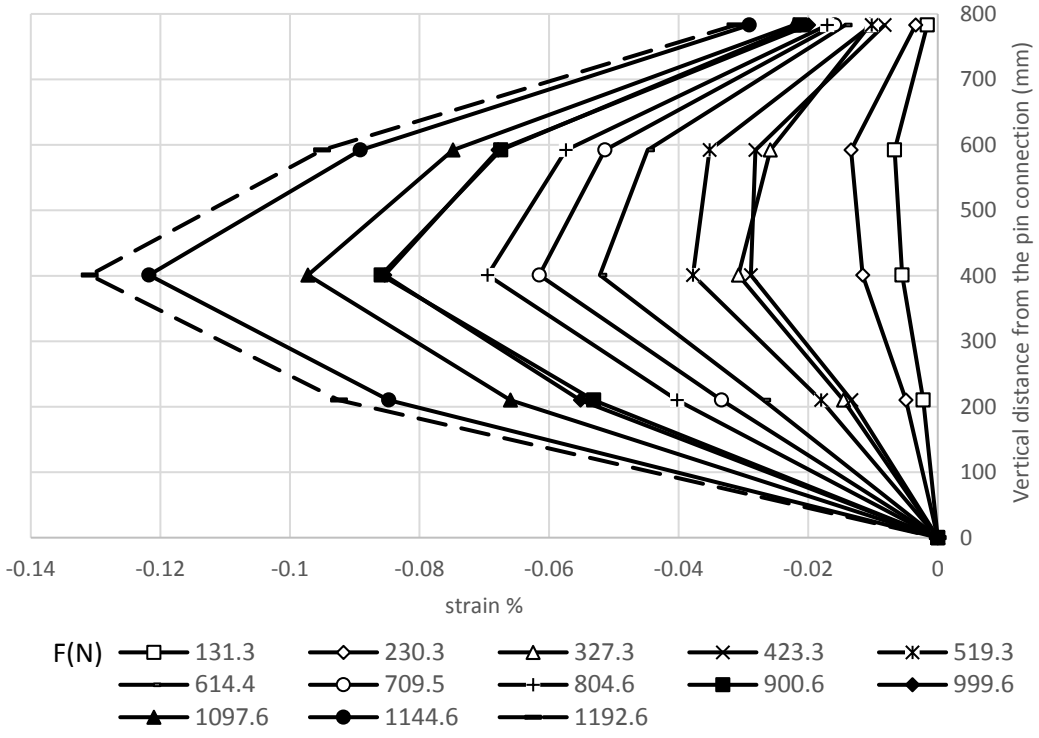

Figure 4.124 Strains along the compressive side of the pile in Test H2 L3 S1 C1 D2 (pile offset = 254 mm).

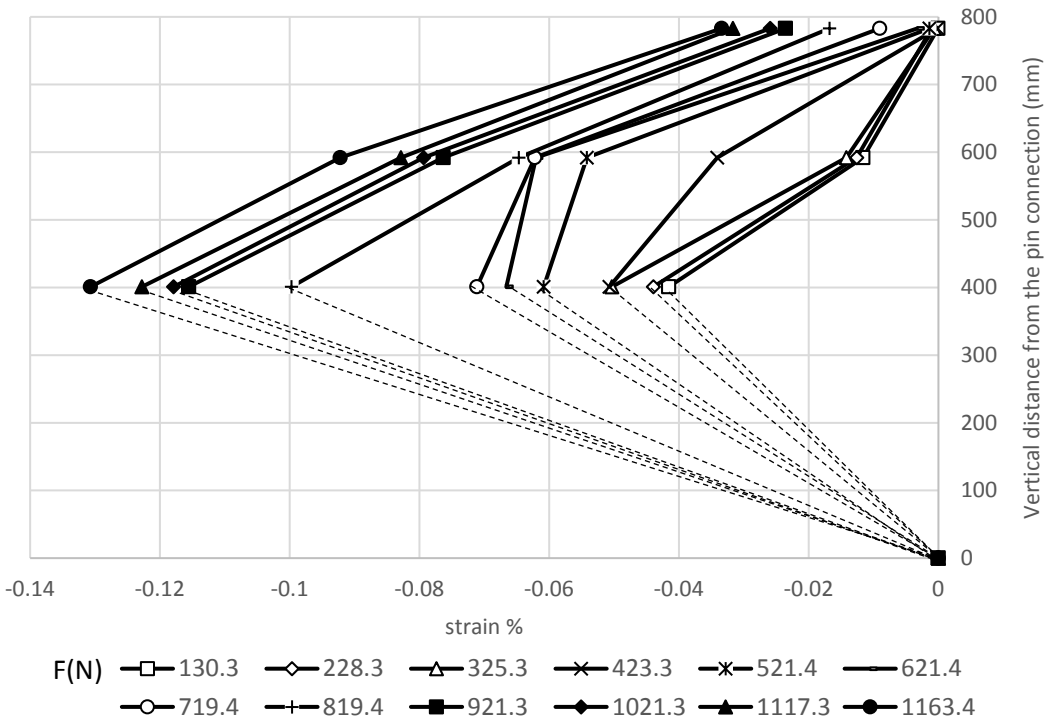

Figure 4.125 Strains along the compressive side of the pile in Test H2 L3 S1 C1 D3 (pile offset = 381 mm).

The strains along the tensile side of the pile in Tests H2 L3 S1 C1 **D2** and H2 L3 S1 C1 **D3** are presented in Figures 4.126 and 4.127, respectively. All the data figures for the stress and moment along the tensile side are shown in section A.4.2. of Appendix A.

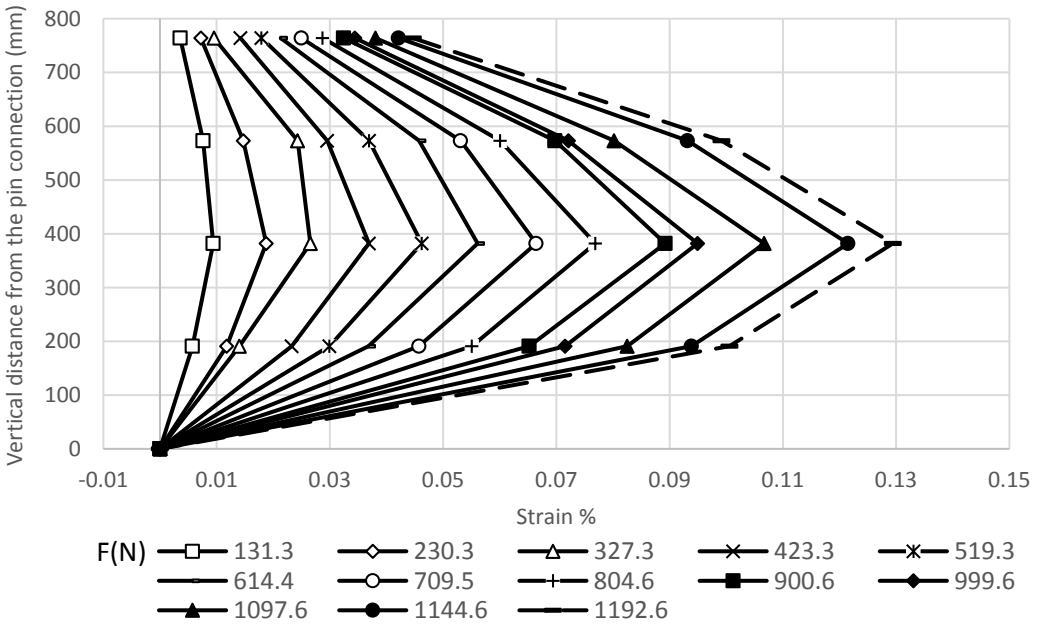

Figure 4.126 Strains along the tensile side of the pile in Test H2 L3 S1 C1 D2 (pile offset = 254 mm).

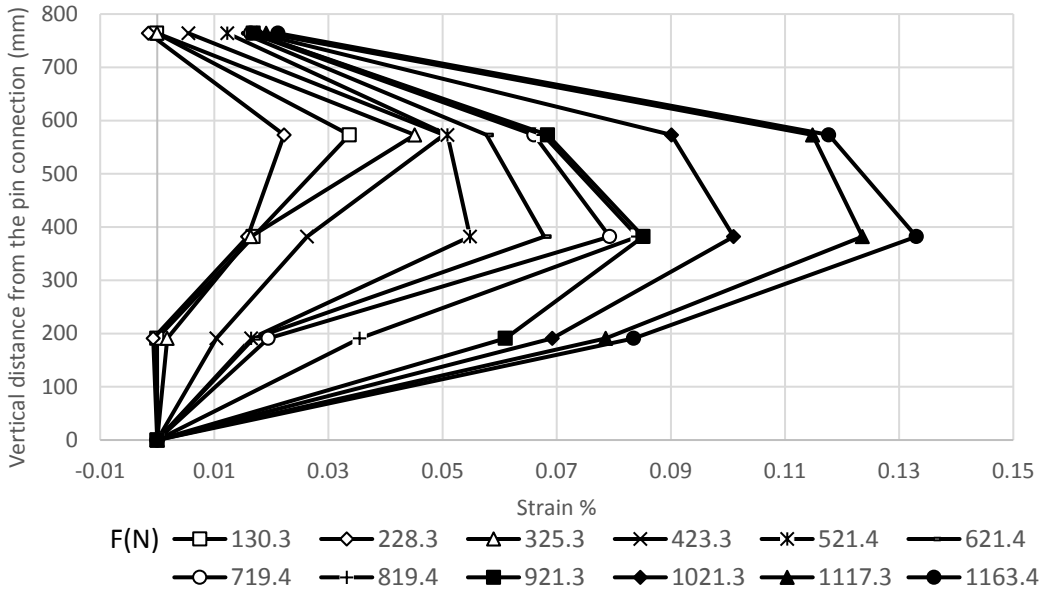

Figure 4.127 Strains along the tensile side of the pile in Test H2 L3 S1 C1 D3 (pile offset = 381 mm).

For the two tests, the behavior of the strain of the compressive and tensile sides of the pile are similar to the behavior that shown in Category 1 of Group 3.

Deflection of pile

The deflections of the pile are shown in Figures 4.128 and 4.129 for Tests H2 L3 S1 C1 **D2** and H2 L3 S1 C1 **D3**, respectively. As the same as the behavior of Category 1 of Group 3, the pile deflection in the two tests decreased by an increase of the distance between the pile and the wall.

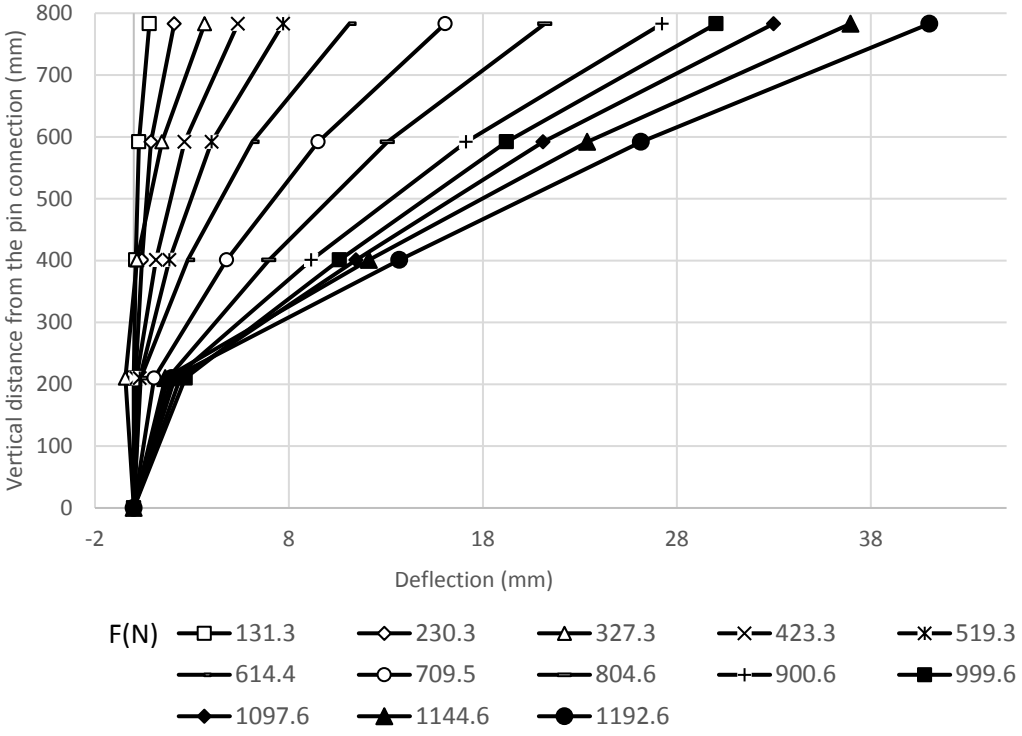

Figure 4.128 Deflections of the pile in Test H2 L3 S1 C1 D2 (pile offset = 254 mm).

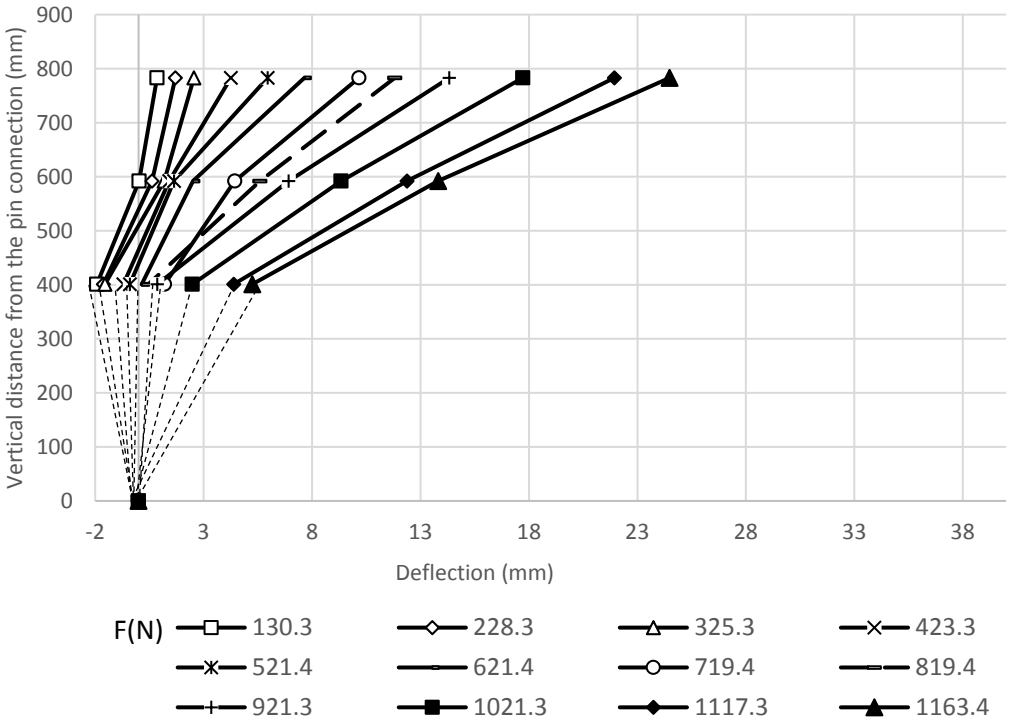

Figure 4.129 Deflections of the pile in Test H2 L3 S1 C1 D3 (pile offset = 381 mm).

Strain of geogrid

The longitudinal strains in the geogrid layer at height equal to 630 mm from the wall base for Tests H2 L3 S1 C1 **D2** and H2 L3 S1 C1 **D3** are shown in Figures 4.130 and 4.131, respectively. For the same tests, the strains of the geogrid layers at 450 mm, 270 mm, and 90 mm from the wall base are presented in section A.4.2. of appendix A. the strain along this geogrid layer for the two tests are similar to the behavior that shown in Category 1 of Group 3

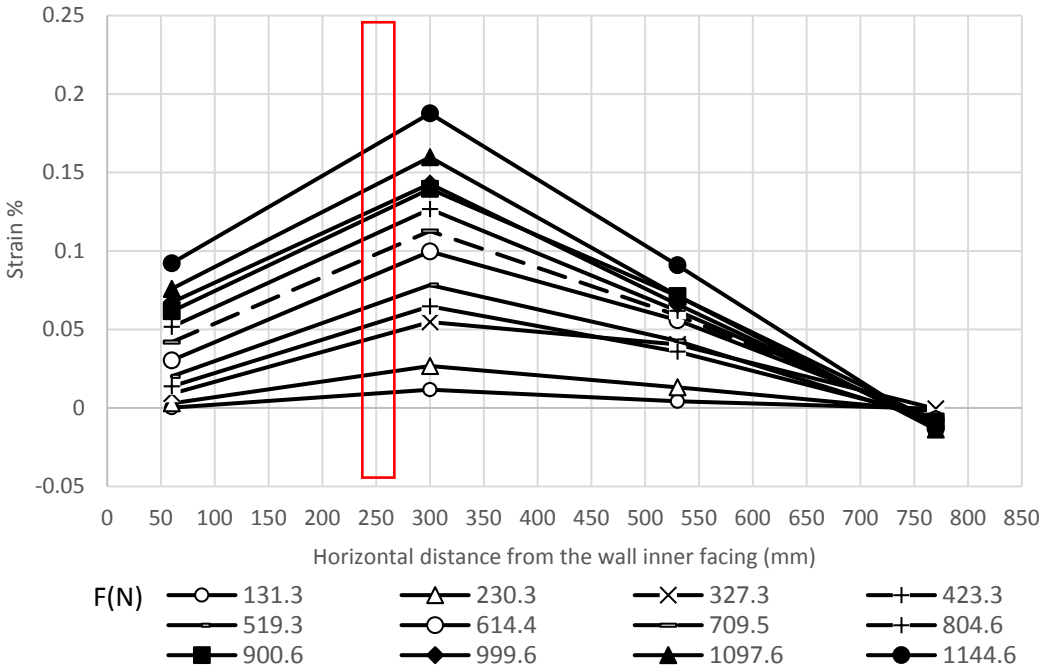

Figure 4.130 Strains of the geogrid layer in the longitudinal direction at 630 mm from the wall base (Test H2 L3 S1 C1 D2 with pile offset = 254 mm).

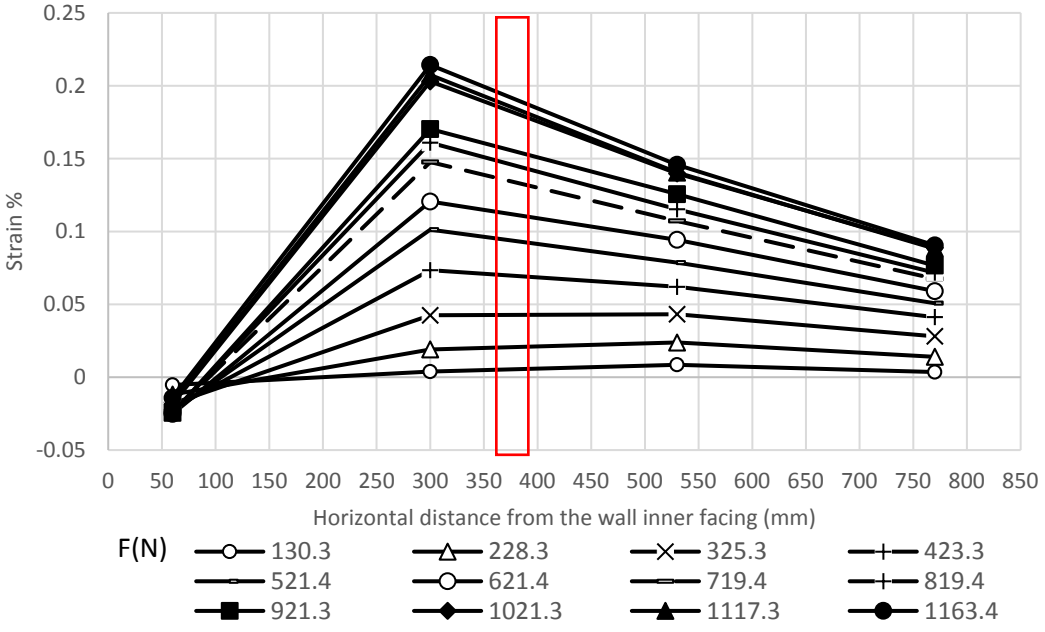

Figure 4.131 Strains of the geogrid layer in the longitudinal direction at 630 mm from the wall base (Test H2 L3 S1 C1 D3 with pile offset = 381 mm).

Pressure behind wall facing

Figures 4.132 and 4.133 present the pressure distributions behind the wall facing in Tests H2 L3 S1 C1 **D2** and H2 L3 S1 C1 **D3**, respectively.

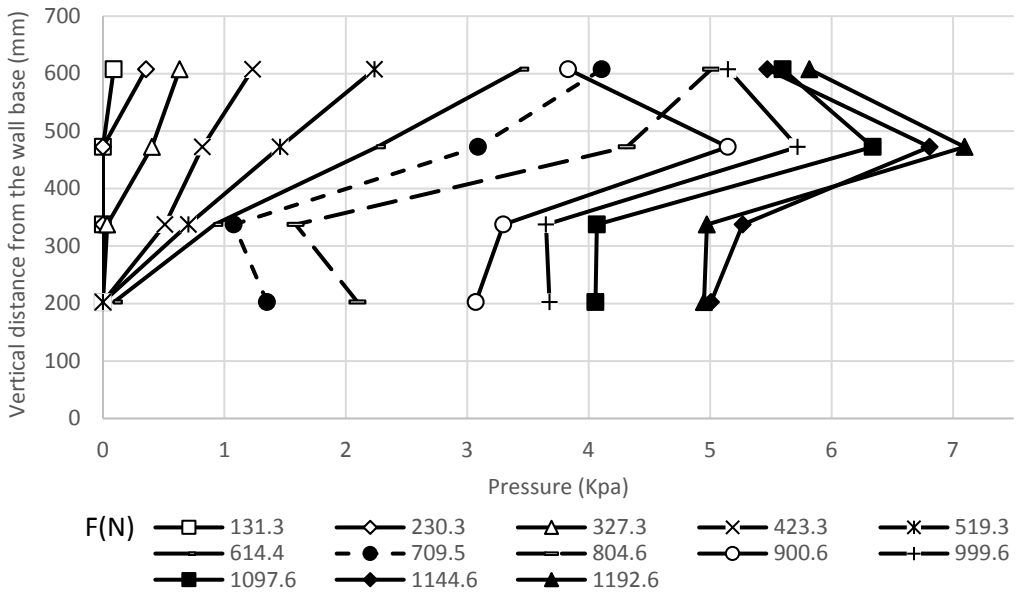

Figure 4.132 Pressures behind the wall facing along the vertical centerline in Test H2 L3 S1 C1 D2 (pile offset = 254 mm).

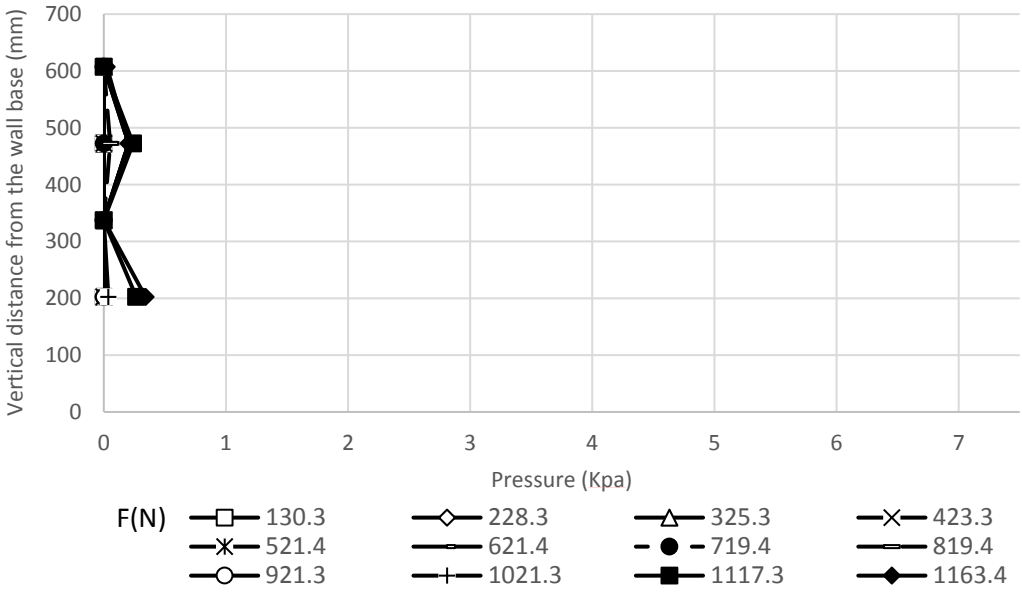

Figure 4.133 Pressures behind the wall facing along the vertical centerline in Test H2 L3 S1 C1 D3 (pile offset = 381 mm).

From the previous figures, the pressures are high behind the wall in the tests with the small pile offset while they are extremely low in tests with large pile offset because of the small spacing between the long reinforcement layers. The transverse pressure distributions behind the wall facing at 472.5 mm from the wall base are as shown in Figures 4.134, and 4.135 for Tests H2 L3 S1 C1 **D2** and H2 L3 S1 C1 **D3**, respectively. For the same tests, he transverse pressure distributions behind the wall facing at 202.5 mm from the wall base are also shown in Figures 4.136 and 4.137. The other transverse pressure distributions at the heights of 607.5 mm and 337.5 mm are included in section A.4.2. of appendix A.

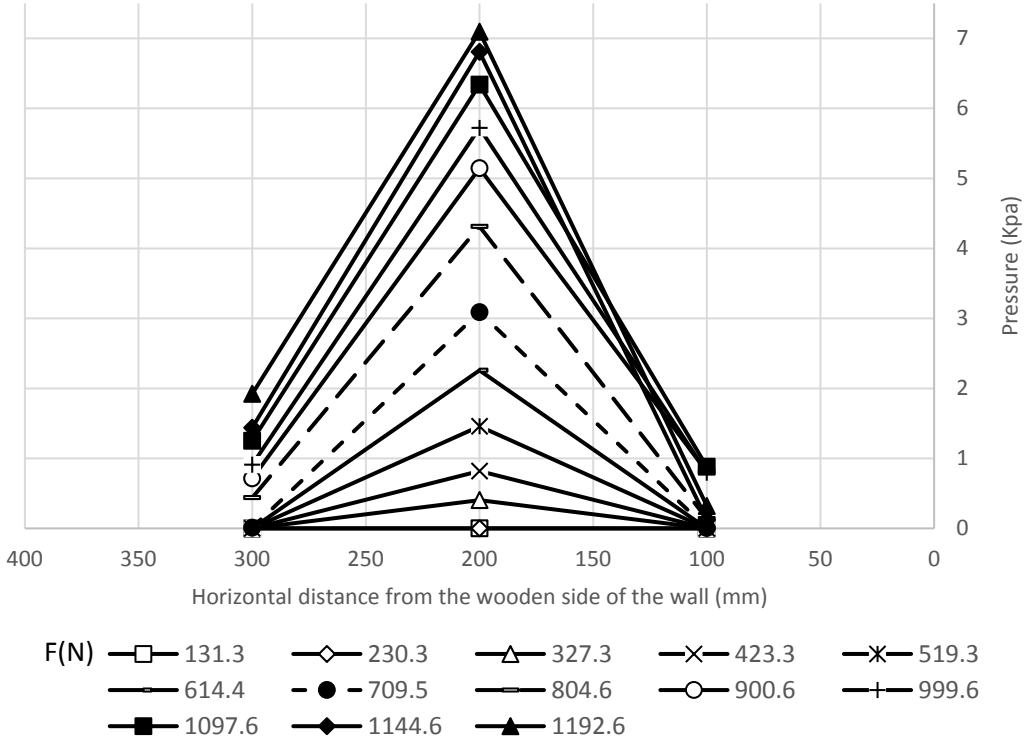

Figure 4.134 Pressure distributions in the transverse direction at the elevation of 472.5 mm from the wall base in Test H2 L3 S1 C1 D2 (pile offset = 254 mm).

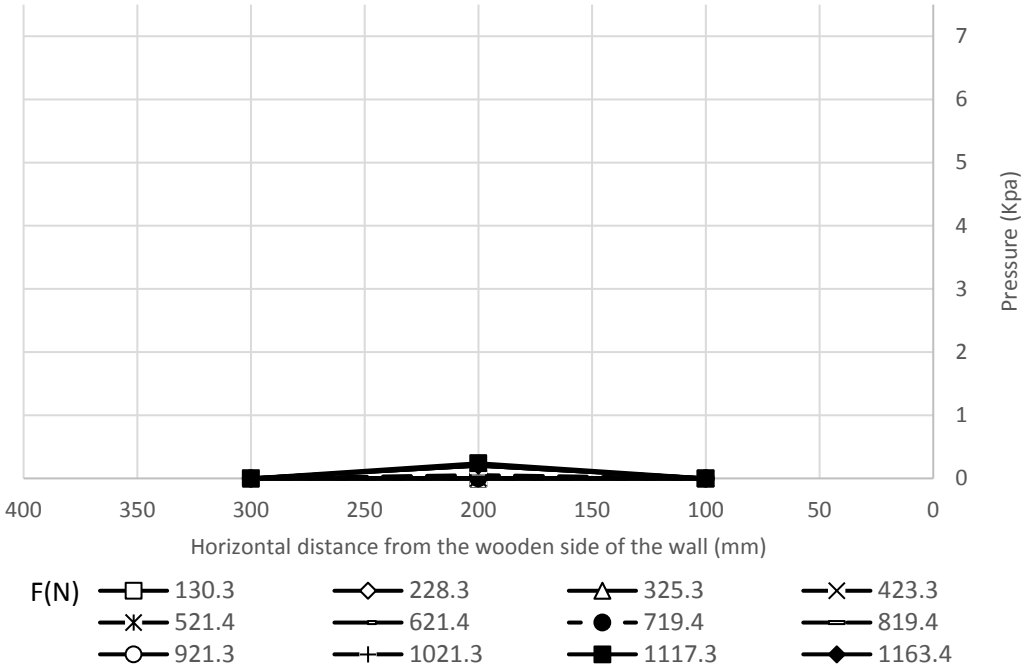

Figure 4.135 Pressure distributions in the transverse direction at the elevation of 472.5 mm from the wall base in Test H2 L3 S1 C1 D3 (pile offset = 381 mm).

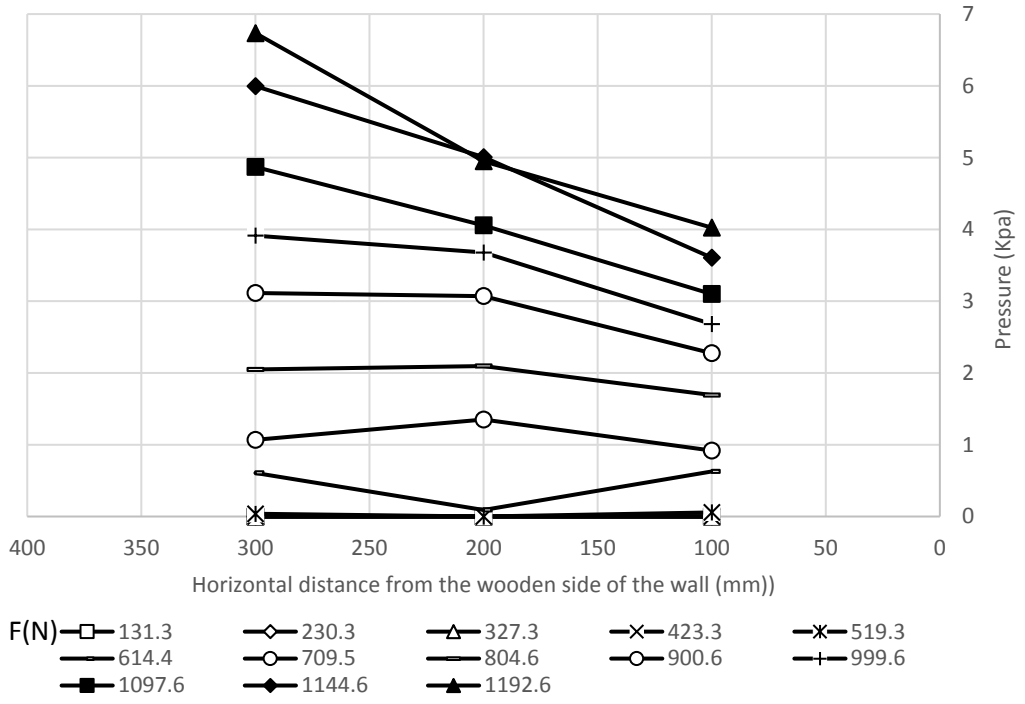

Figure 4.136 Pressure distributions in the transverse direction at the elevation of 202.5 mm from the wall base in Test H2 L3 S1 C1 D2 (pile offset = 254 mm).

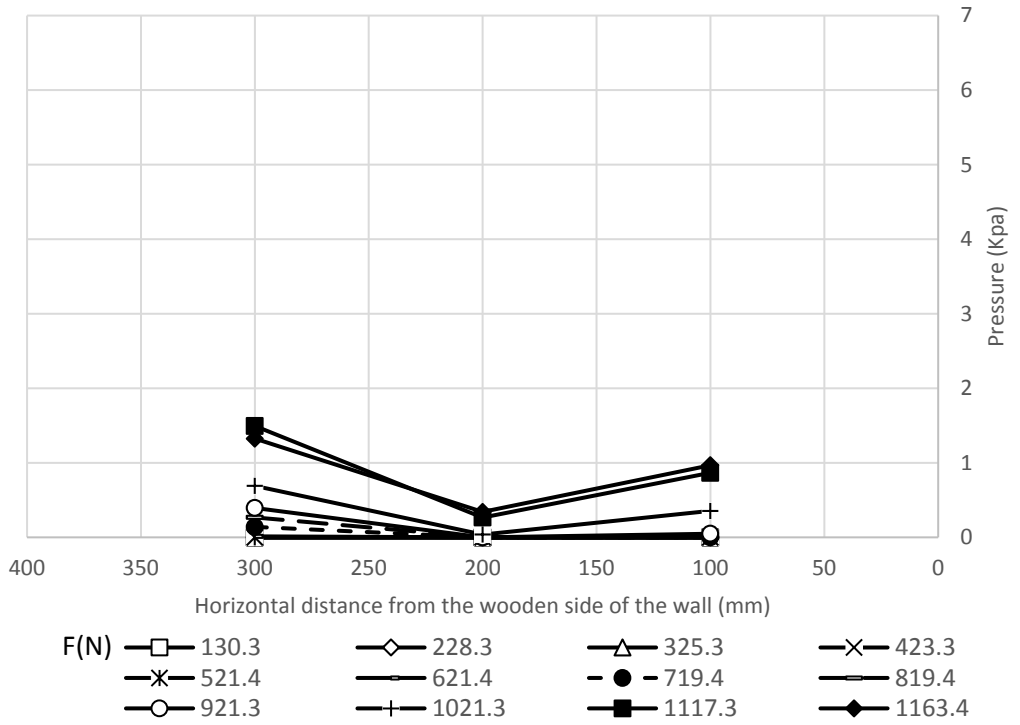

Figure 4.137 Pressure distributions in the transverse direction at the elevation of 202.5 mm from the wall base in Test H2 L3 S1 C1 D3 (pile offset = 381 mm).

4.4.3. Category 3

This category includes the data figures for Tests H2 L3 S1 C2 D2 and H2 L3 S1 C2 D3. A frictional connection type was used in the tests of these category, and all the other parameters are the same as Category 2 of Group 3.

Deflection of wall facing

The deflections along the center line of the wall facing in Tests H2 L3 S1 C2 **D2** and H2 L3 S1 C2 **D3** are shown in Figures 4.138 and 4.139, respectively. The behavior of this deflection in the two pile offsets is similar to the corresponding behavior in the previous categories.

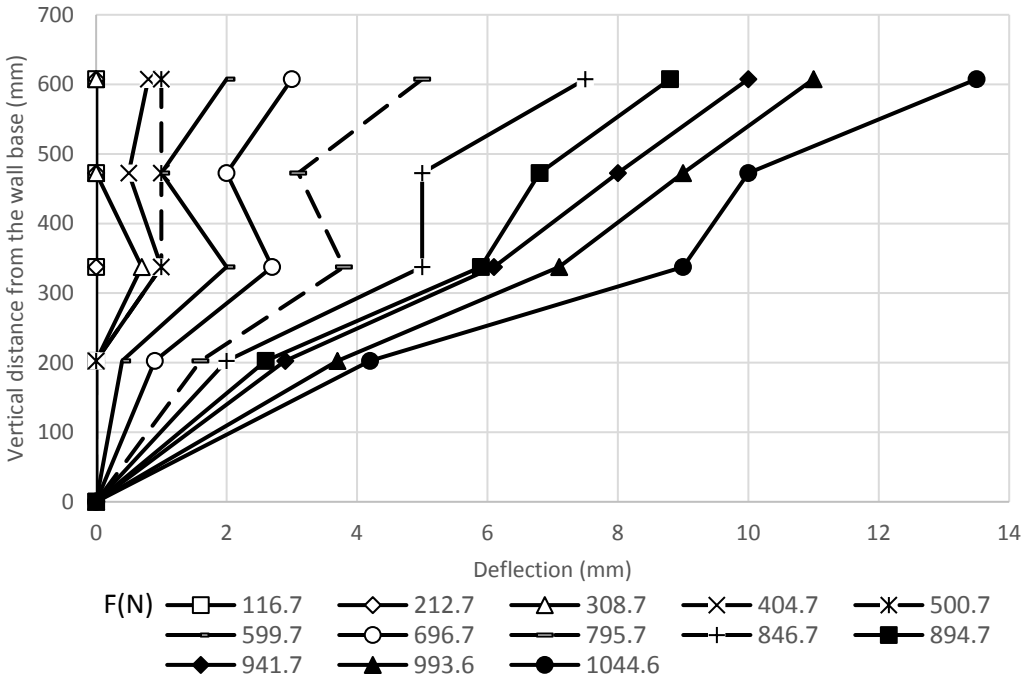

Figure 4.138 Wall facing deflections along the vertical centerline in Test H2 L3 S1 C2 D2 (pile offset = 254 mm).

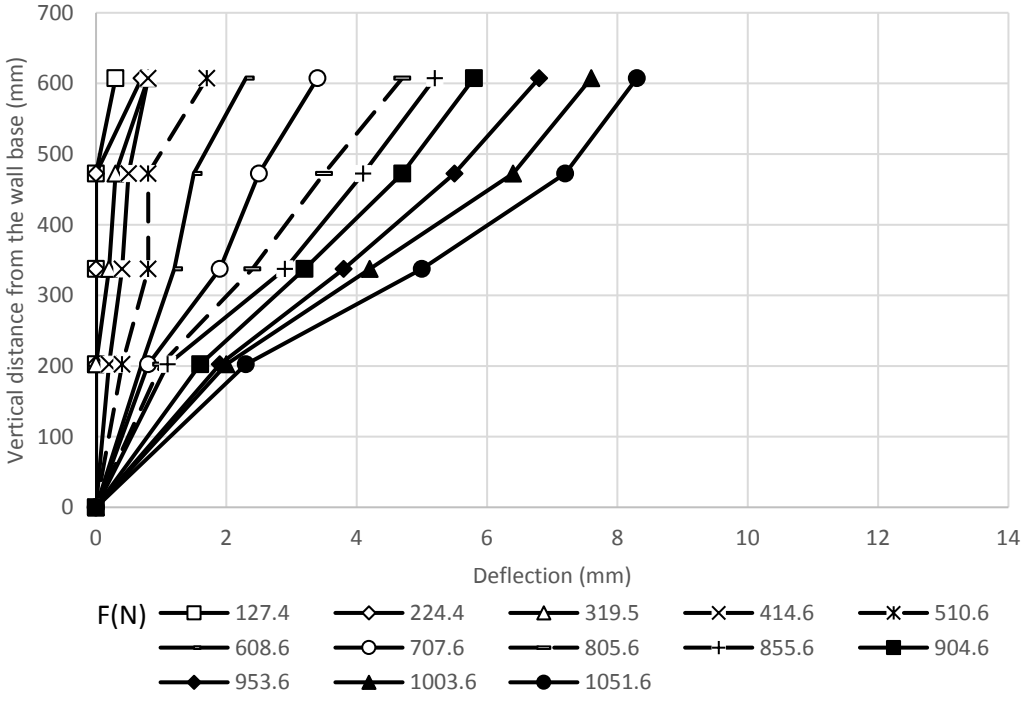

Figure 4.139 Wall facing deflections along the vertical centerline in Test H2 L3 S1 C2 D3 (pile offset = 381 mm).

Figures 4.140 and 4.141 present the transverse deflection profiles of the wall facing for Tests H2 L3 S1 C2 D2 and H2 L3 S1 C2 D3, respectively. In fact, the elevation of these profiles is about 84.4% of the wall height, which is the maximum deflection location.

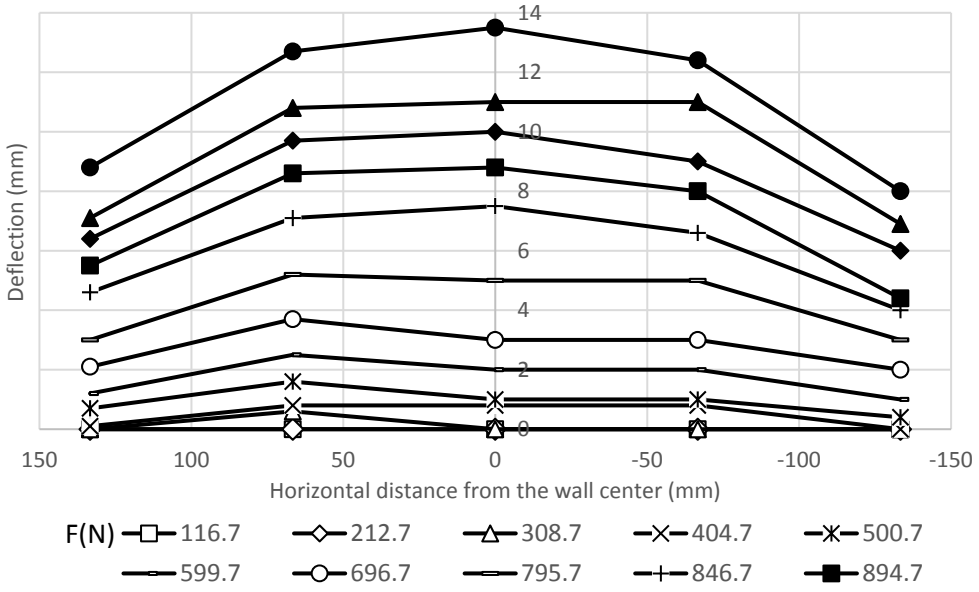

Figure 4.140 Transverse deflection profile at 607.5 mm from the wall base in Test H2 L3 S1 C2 D2 (pile offset = 254 mm).

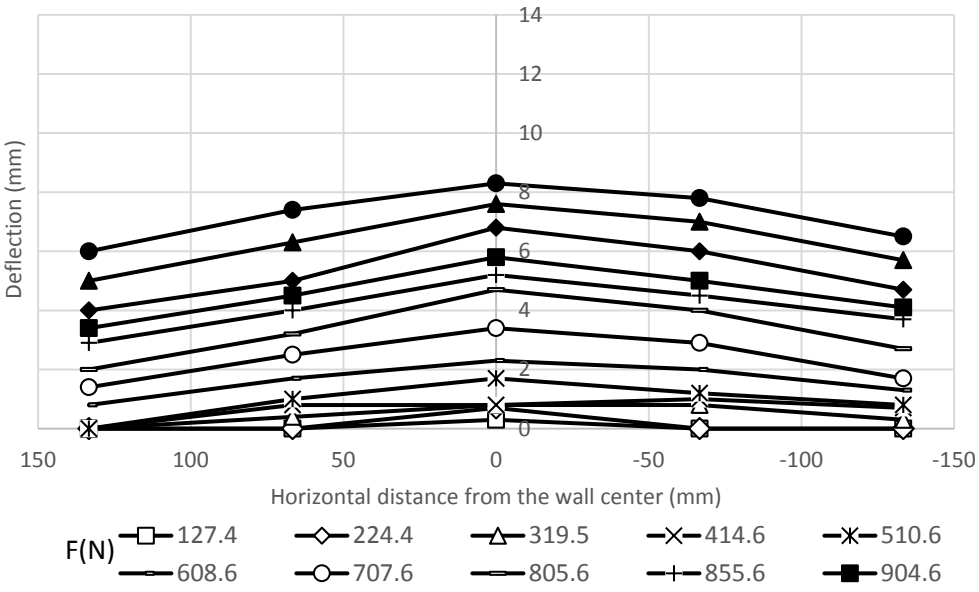

Figure 4.141 Transverse deflection profile at 607.5 mm from the wall base in Test H2 L3 S1 C2 D3 (pile offset = 381 mm).

In general, the behavior of the transverse deflections in the two tests is similar to the behavior that shown in the previous categories. However, the transverse deflection profiles of the wall facing at 472.5 mm, 337.5 mm, and 202.5 mm from the wall base for Tests H2 L3 S1 C2 D2 and H2 L3 S1 C2 D3 are shown in section A.4.3. of Appendix A.

Strain, stress, and moment of pile

The strains along the compressive side of the pile in Tests H2 L3 S1 C2 **D2** and H2 L3 S1 C2 **D3** is presented in Figures 4.142 and 4.143 respectively. For the same tests, the data figures for the stress and the moment along the compressive side of the pile are shown in section A.4.3. of appendix A.

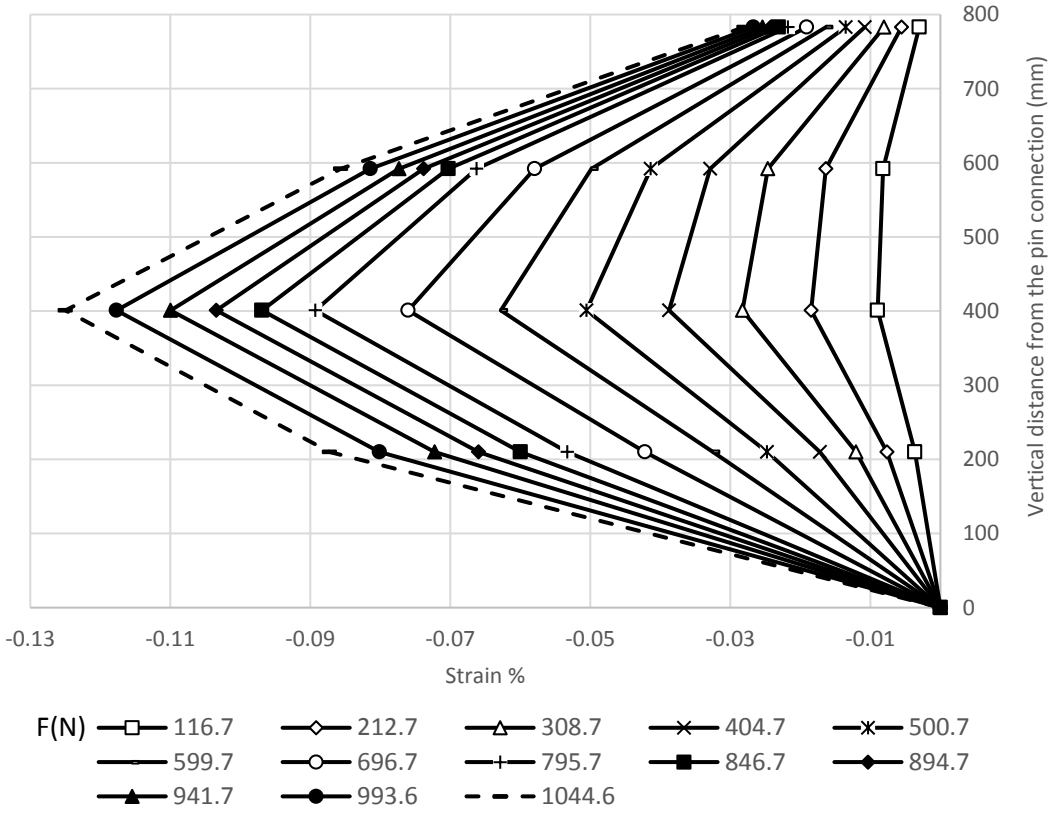

Figure 4.142 Strains along the compressive side of the pile in Test H2 L3 S1 C2 D2 (pile offset = 254 mm).

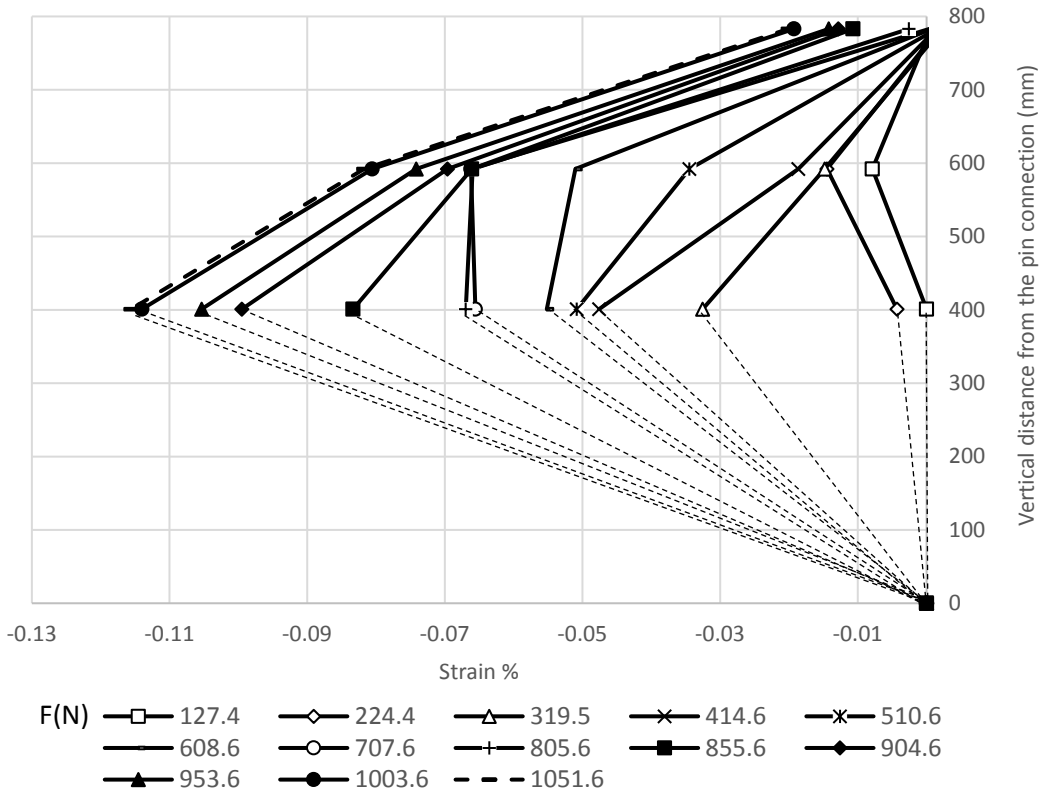

Figure 4.143 Strains along the compressive side of the pile in Test H2 L3 S1 C2 D3 (pile offset = 381 mm).

The strains along the tensile side of the pile in Tests H2 L3 S1 C2 **D2** and H2 L3 S1 C2 **D3** are presented in Figures 4.144 and 4.145, respectively. All the data figures of the stress and moment along the tensile side is shown in section A.4.3. of Appendix A. In both sides of the pile, the strain and moment distributions of the tests of this category have similar behavior as that shown in the previous categories.

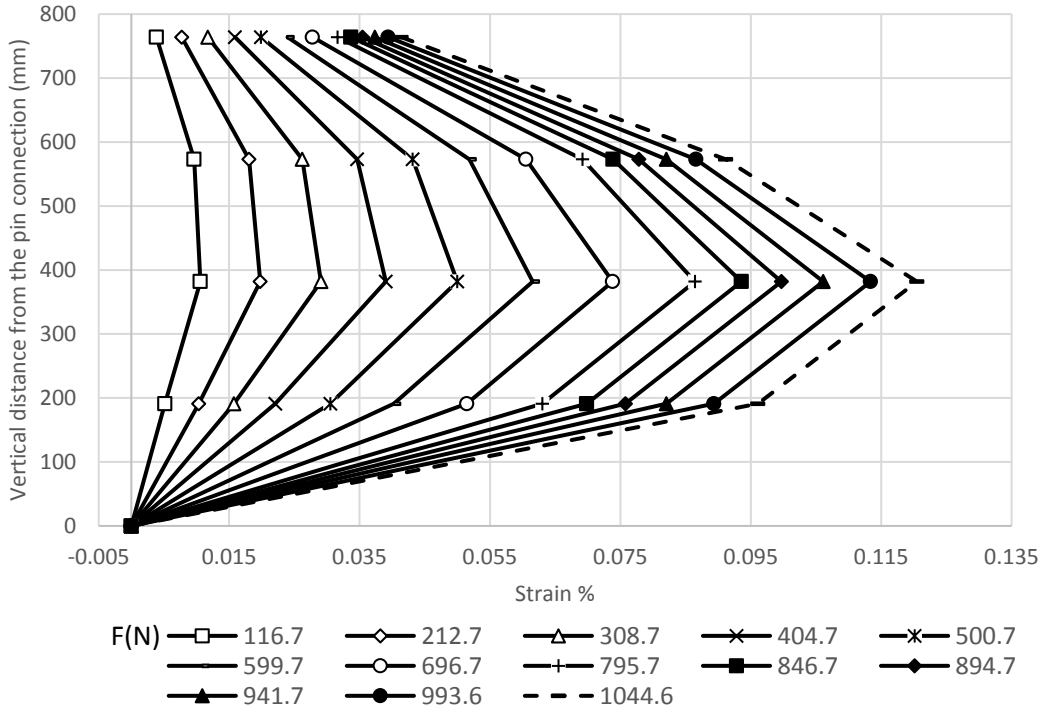

Figure 4.144 Strains along the tensile side of the pile in Test H2 L3 S1 C2 D2 (pile offset = 254 mm).

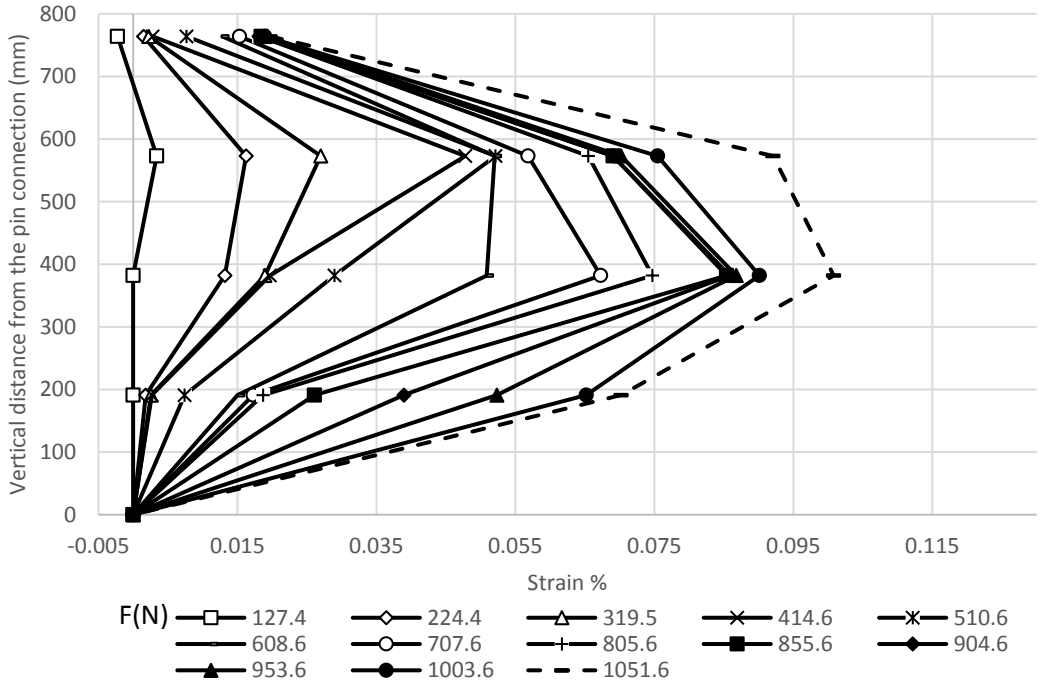

Figure 4.145 Strains along the tensile side of the pile in Test H2 L3 S1 C2 D3 (pile offset = 381 mm).

Deflection of pile

The deflections of the pile are shown in Figures 4.146 and 4.147 for Tests H2 L3 S1 C2 **D2** and H2 L3 S1 C2 **D3**, respectively. These figures show the same behavior that shown in the other categories

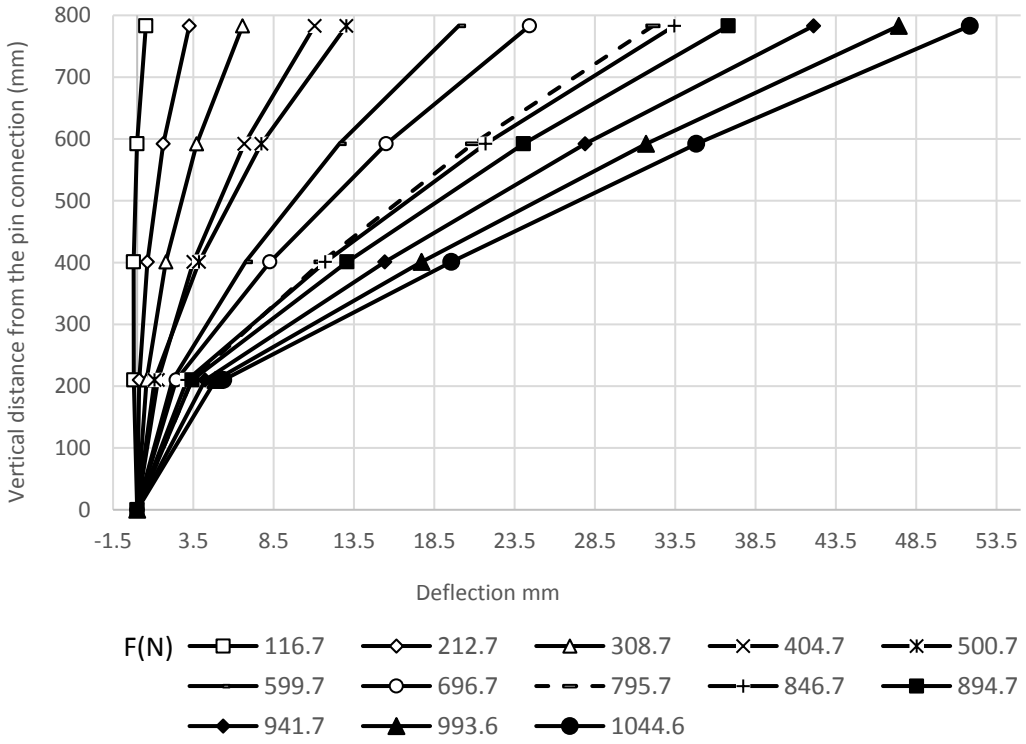

Figure 4.146 Deflections of the pile in Test H2 L3 S1 C2 D2 (pile offset = 254 mm).

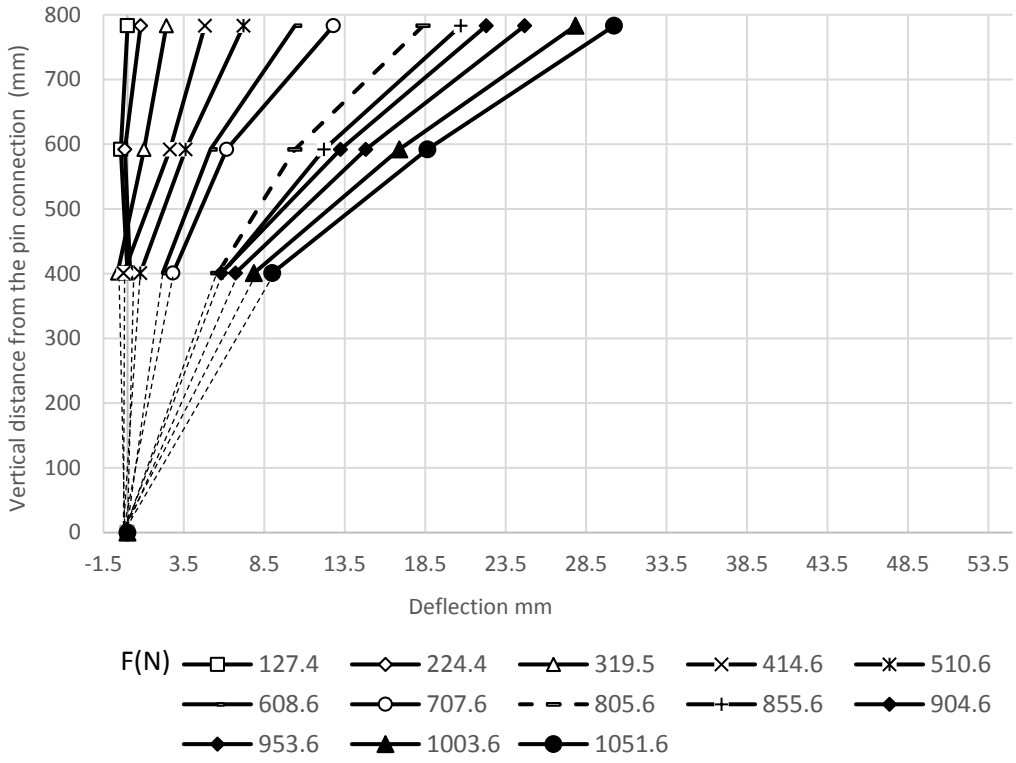

Figure 4.147 Deflections of the pile in Test H2 L3 S1 C2 D3 (pile offset = 254 mm).

Strain of geogrid

The longitudinal strains in the geogrid layer at elevation equal to 630 mm from the wall base for Tests H2 L3 S1 C2 **D2** and H2 L3 S1 C2 **D3** are shown in Figures 4.148 and 4.149, respectively. For the same tests, the strains of the geogrid layers at 450 mm, 270 mm, and 90 mm from the wall base are presented in Section A.4.3. of Appendix A.

As the same as the pervious categories, the tensile strains are higher near to the pile location for the both offsets. In addition, the tensile strains at the end of the geogrid layer increased by an increase of the pile offset as shown in Figures 4.148 and 4.149.

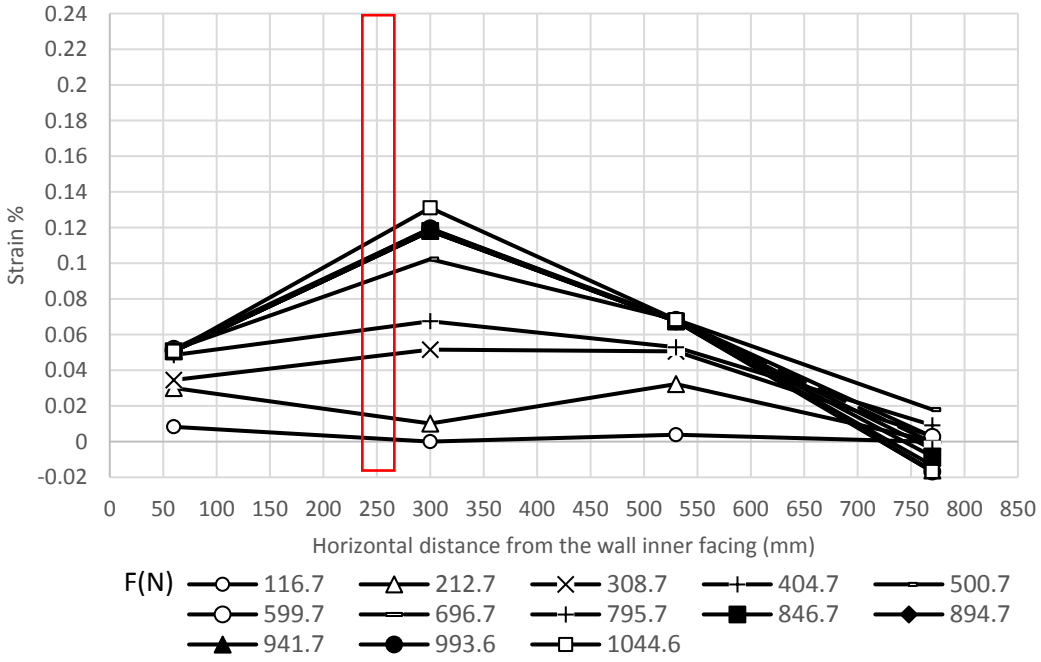

Figure 4.148 Strains of the geogrid layer in the longitudinal direction at 630 mm from the wall base (Test H2 L3 S1 C2 D2 with pile offset = 254 mm).

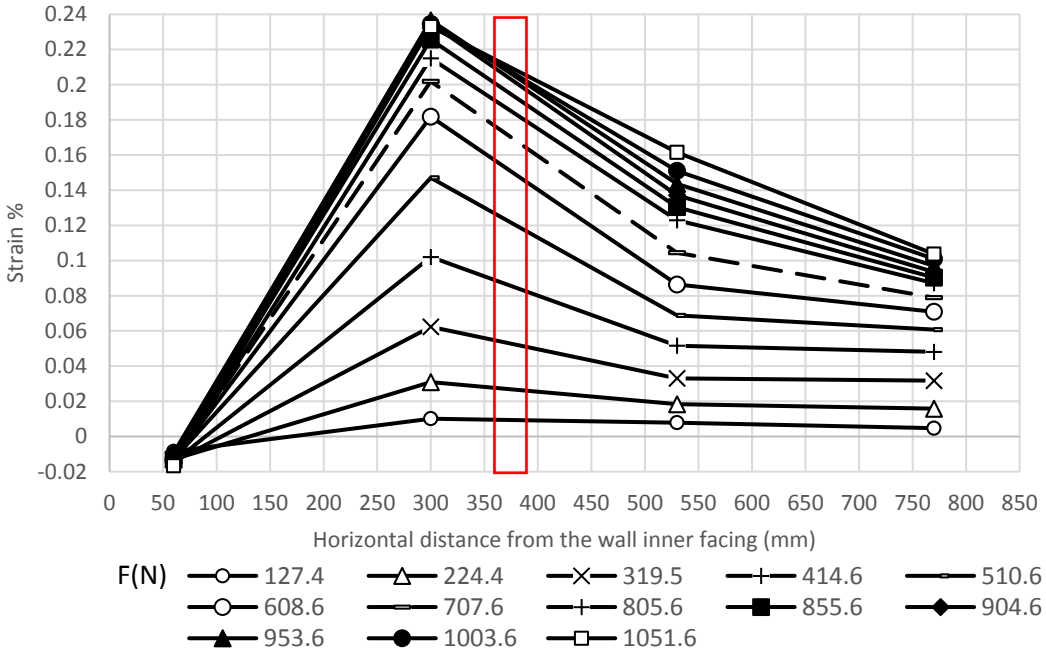

Figure 4.149 Strains of the geogrid layer in the longitudinal direction at 630 mm from the wall base (Test H2 L3 S1 C2 D3 with pile offset = 381 mm).

Pressure behind wall facing

Figures 4.150 and 4.151 present the pressure distributions behind the wall facing in Tests H2 L3 S1 C2 **D2** and H2 L3 S1 C2 **D3**, respectively.

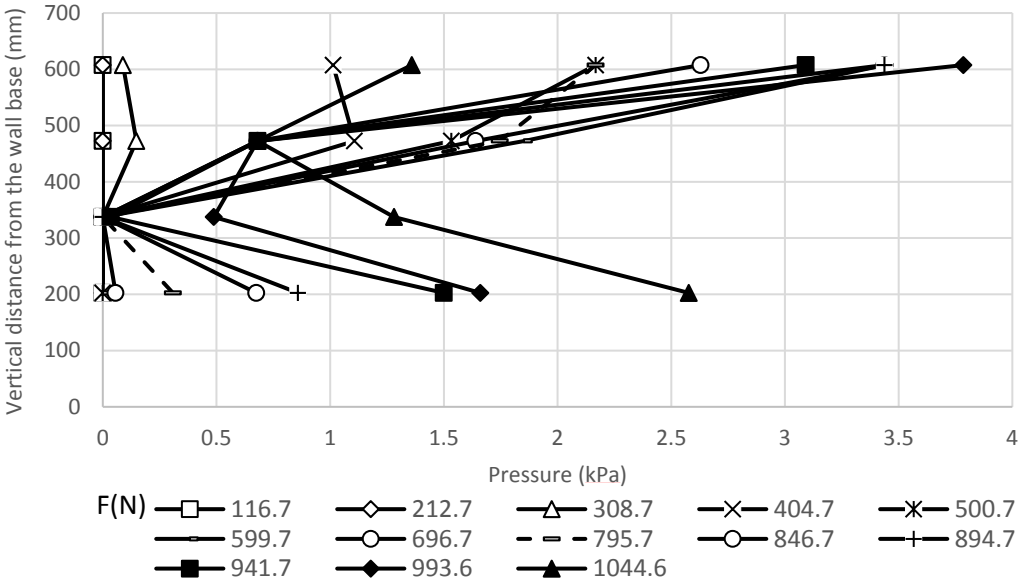

Figure 4.150 Pressures behind the wall facing along the vertical centerline in Test H2 L3 S1 C2 D2 (pile offset = 254 mm).

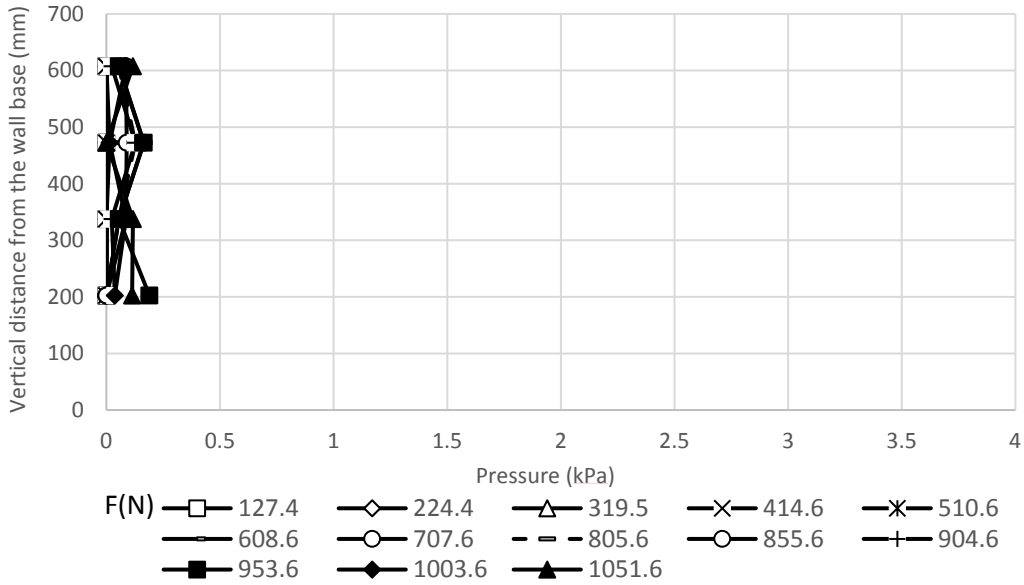

Figure 4.151 Pressures behind the wall facing along the vertical centerline in Test H2 L3 S1 C2 D3 (pile offset = 381 mm).

The same behavior of the pressure distributions that shown in Category 2 of Group 3 is apply on the tests of this category. However, a high pressure zone is noticed behind the upper end of the wall facing due using the frictional connection. The transverse pressure distributions behind the wall facing at 472.5 mm from the wall base are as shown in Figures 4.152, and 4.153 for Tests H2 L3 S1 C2 **D2** and H2 L3 S1 C2 **D3**, respectively. For the same tests, the transverse pressure distributions behind the wall facing at 202.5 mm from the wall base are also shown in Figures 4.154 and 4.155. The other transverse pressure distributions at the elevation of 607.5 mm and 337.5 mm are included in section A.4.3. of Appendix A.

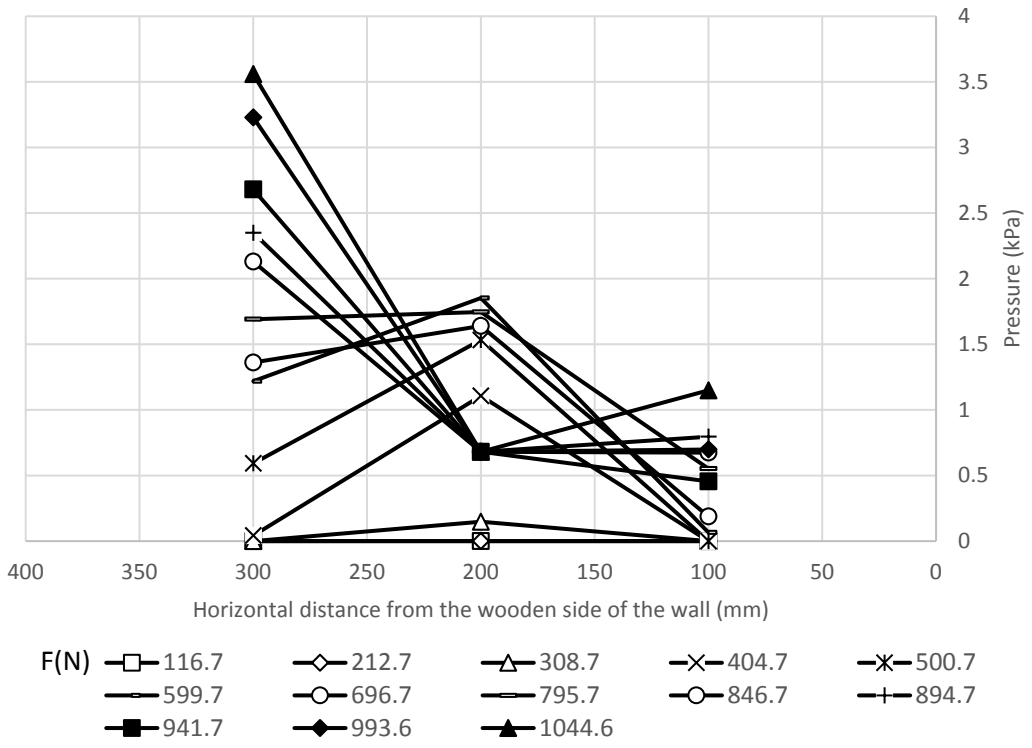

Figure 4.152 Pressure distributions in the transverse direction at the elevation of 472.5 mm from the wall base in Test H2 L3 S1 C2 D2 (pile offset = 254 mm).

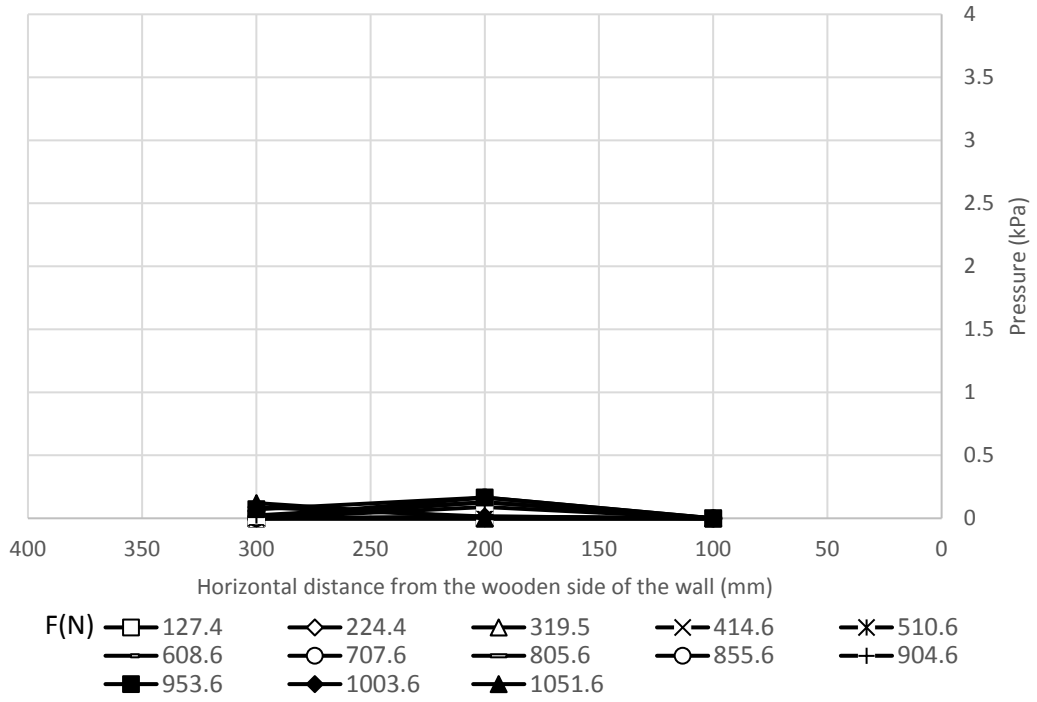

Figure 4.153 Pressure distributions in the transverse direction at the elevation of 472.5 mm from the wall base in Test H2 L3 S1 C2 D3 (pile offset = 381 mm).

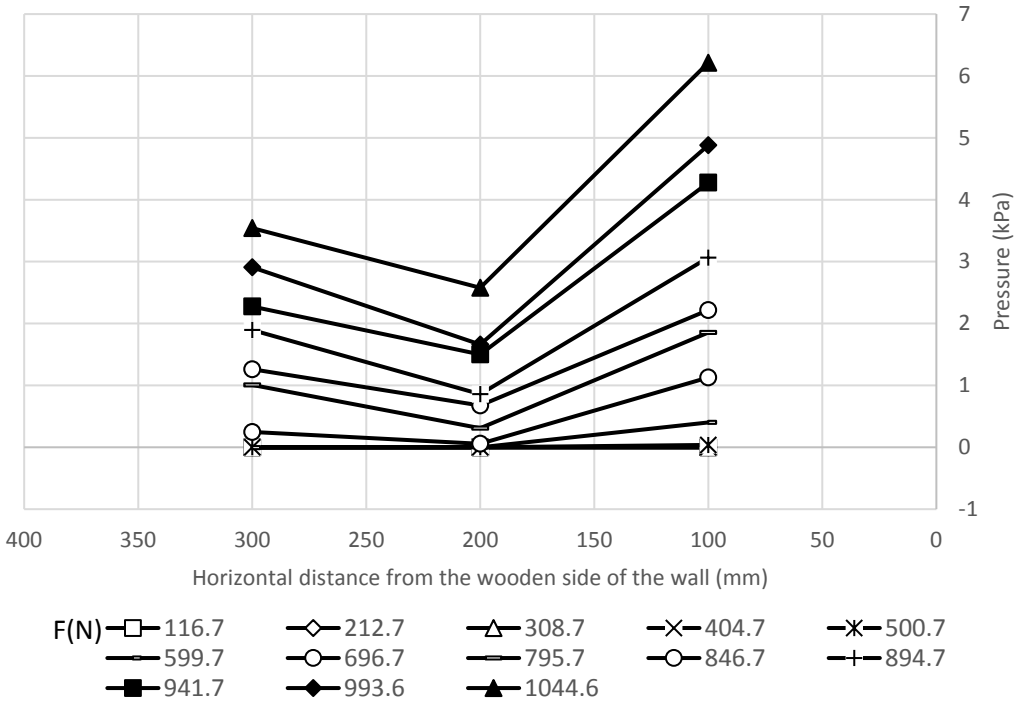

Figure 4.154 Pressure distributions in the transverse direction at the elevation of 202.5 mm from the wall base in Test H2 L3 S1 C2 D2 (pile offset = 254 mm).

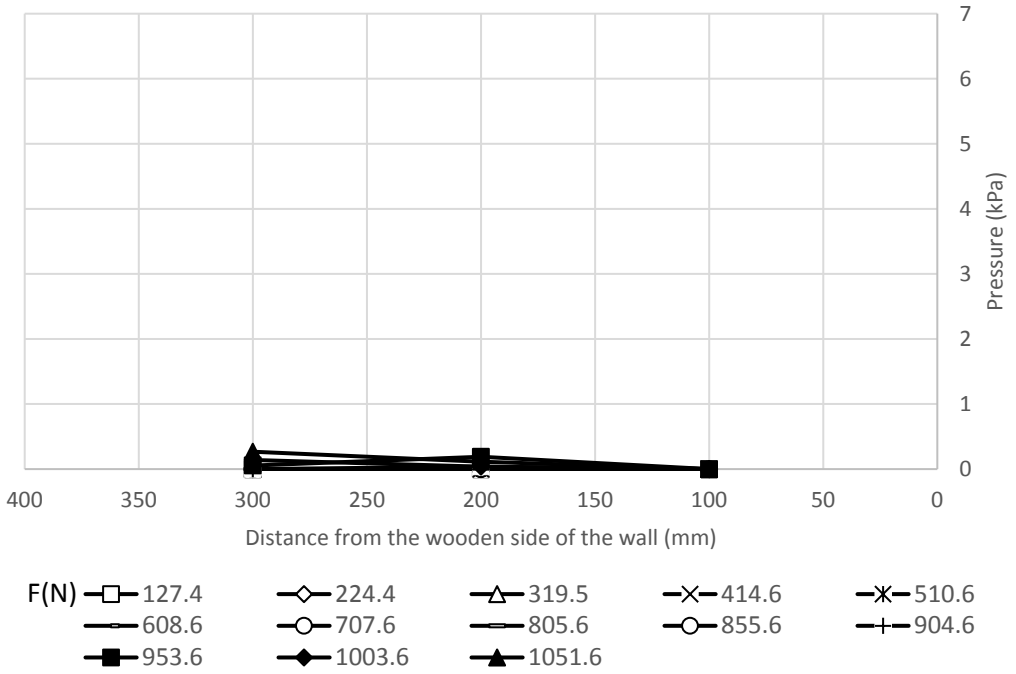

Figure 4.155 Pressure distributions in the transverse direction at the elevation of 202.5 mm from the wall base in Test H2 L3 S1 C2 D3 (pile offset = 381 mm).

Chapter 5 Data Analyses

5.1 Introduction

The test data reported in Chapter four is analyzed and compared in the three main sections of this chapter. Section one includes the data analysis of one comparison set of the test data based on the change in the wall height and the reinforcement length in the model MSE walls. The second section presents the analyses of five comparison sets considering the change in two parameters of soil reinforcement. The last section shows the analyses of two comparison sets considering the change in the connection type between the wall facing and the soil reinforcement.

In Chapter four, the tests were classified into several groups and categories to summarize the test data with different pile offsets. The test data for piles at three offsets are combined into each group in this chapter considering the ultimate lateral load capacities of the pile. This capacity was obtained following the recommendation of Broms (1964). Broms (1964) considered the lateral load that induces a pile lateral deflection equal to 20% of the pile diameter as the ultimate lateral load capacity. Then, every two groups were organized in a specific set and compared by changing at least one influence factor. For a comparing purpose, a specific lateral load was chosen for each set to evaluate the result change between these two groups. The magnitude of this load was close to the average value of the ultimate lateral load capacities of the tests in the comparison set.

5.2. Effect of wall height and reinforcement length

One comparison set with two groups of tests is considered in this section. The main variable between these groups is the wall height. However, by changing the wall height, the reinforcement length should be changed as well according to the reinforcement length to wall height ratio of 0.7. All the information about these two groups in Set 1 is shown in Table 5.2.

Table 5.1 Detials of Set 1

Tests	Ultimate Lateral Load N	Wall Height H, mm	Layer length L, mm	Layer spacing S, mm	Offset D, mm	Connection Type	Group designation
H1 L1 S1 C1 D1	192	450	315	90	127 (2d)	Mechanical	Group 1 or **H1 L1** S1 C1 D123
H1 L1 S1 C1 D2	212.6				254 (4d)		
H1 L1 S1 C1 D3	258.6				381 (6d)		
H2 L2 S1 C1 D1	368	720	504	90	127 (2d)		Category 2 of Group 2 or **H2 L2** S1 C1 D123
H2 L2 S1 C1 D2	405				254 (4d)		
H2 L2 S1 C1 D3	504				381 (6d)		

The ultimate lateral load capacities of the piles were determined from the load-displacement curves at the lateral deflection equal to 20% of the pile diameter as mentioned earlier. Figure 5.1 (a) presents the load-displacement curves at the elevation of 592 mm from the pin connection of the tests in Group **H1 L1** S1 C1 D123 while Figure 5.1 (b) presents the load-displacement curves at the elevation of 783 mm from the pin connection of the tests in Group **H2 L2** S1 C1 D123.

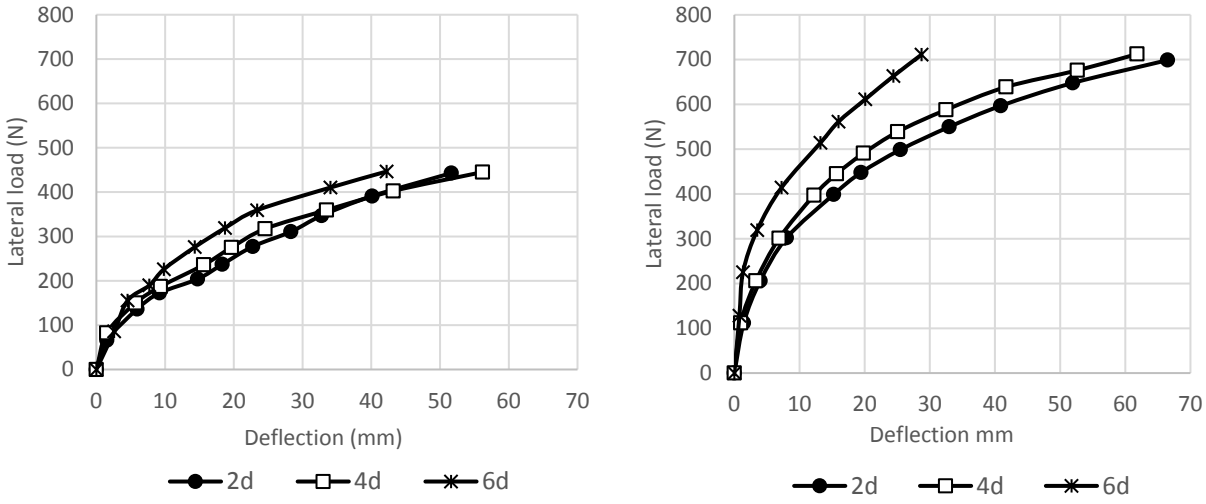

(a) (b)

Figure 5.1 Load-displacement curves of Set 1: (a) Group H1 L1 S1 C1 D123 and (b) Group H2 L2 S1 C1 D123.

In each group, an increase of the pile offset increased the ultimate lateral load capacity of the pile. On the other hand, an increase of the wall height from 450 mm in Group H1 **L1** S1 C1 D123 to 720 mm in Group H2 **L2** S1 C1 D123 increased the pile capacity by approximately 92% in both tests with pile offsets 4d and 6d.

For comparison purposes, the lateral load of 300 N was selected. Using this load, different types of data were analyzed in order to investigate the effect of the wall height and the reinforcement length. The comparison data in this section include the deflections of the wall facing and the strains of the reinforcement layers in addition to the strains, stresses, moments, and deflections of the pile.

5.2.1. Deflection of wall facing

The deflections of the wall facing along the vertical centerline in Group **H1 L1** S1 C1 D123 and Group **H2 L2** S1 C1 D123 are shown in

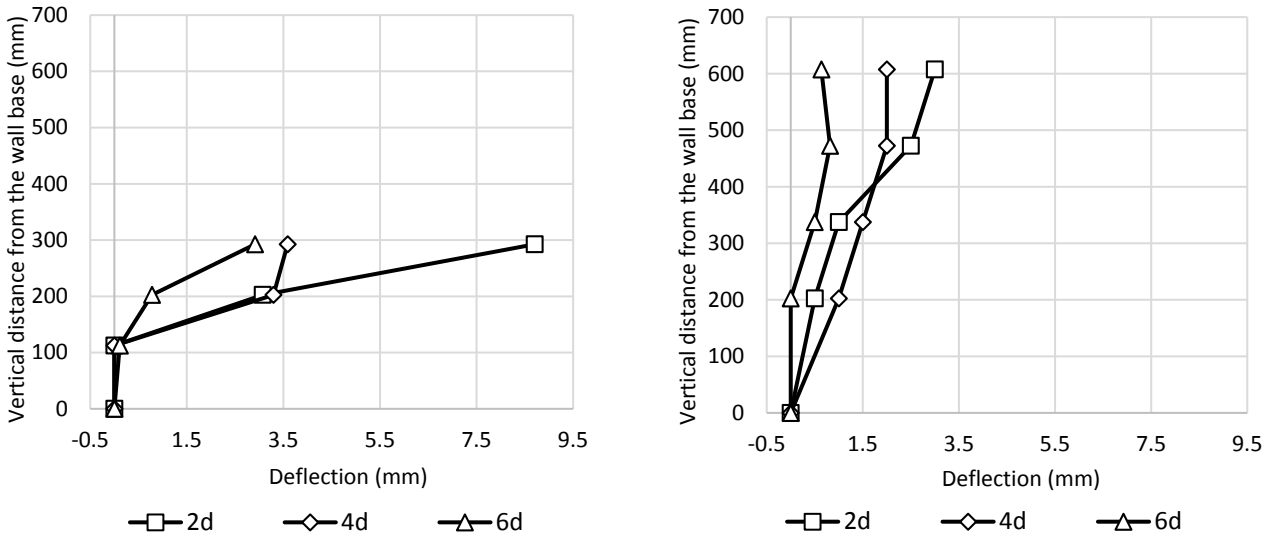

Figure 5.2 Deflections of the wall facing along the vertical centerline at a lateral load of 300 N in: (a) Group H1 L1 S1 C1 D123 and (b) Group H2 L2 S1 C1 D123.

Figure 5.2 shows that a decrease of the pile offset increased the maximum deflection of the wall facing along the vertical centerline in each group. At the elevation equal to 65% of the wall height, the deflections of the wall facing in Group **H1 L1** S1 C1 D123 are larger than those in Group **H2 L2** S1 C1 D123 at the same corresponding offsets. An increase of the wall height as well as an increase of the reinforcement length decreased the wall deflection. Figure 5.3 presents

the Transverse deflection of the wall facing at 65% of the wall height. As shown from Figure 5.3 (b), the transverse deflection of the pile was more uniform by the increase of the wall height.

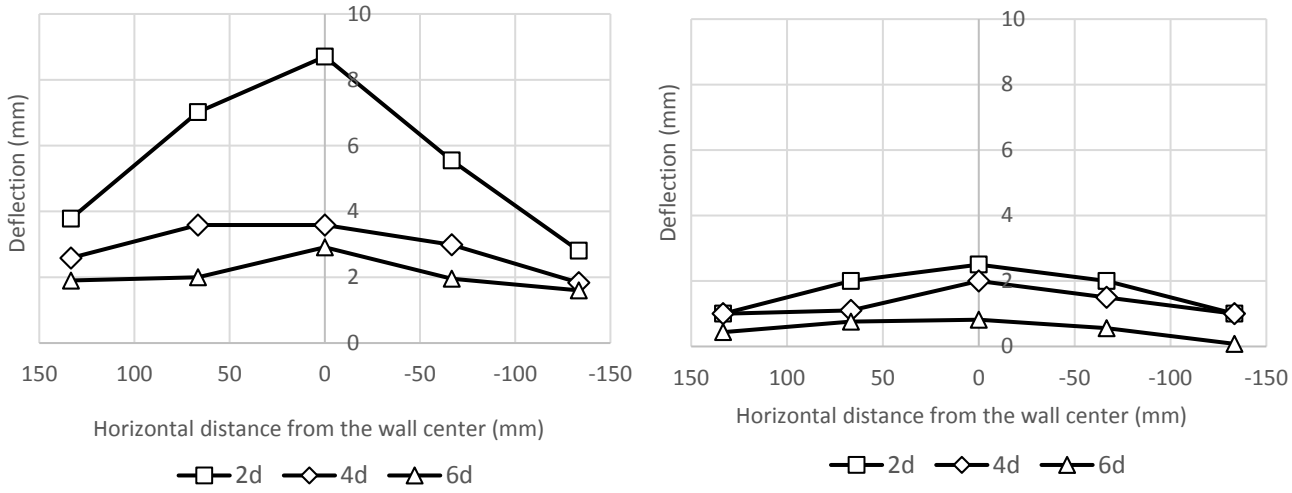

(a) (b)

Figure 5.3 Transverse deflections of the wall facing at a load of 300 N in: (a) Group H1 L1 S1 C1 D123 and (b) Group H2 L2 S1 C1 D123.

5.2.2. Strain, stress, and moment of pile

The strains of the laterally loaded pile in Group **H1 L1** S1 C1 D123 and Group **H2 L2** S1 C1 D123 are shown in Figure 5.4. On the compressive side of the pile, the maximum strains of the two groups occurred at an elevation equal to 44% of the pile height. This height was located within the top part of the wall facing for the tests in Group **H1 L1** S1 C1 D123 and at the middle part of the wall facing for the tests of Group **H2 L2** S1 C1 D123.

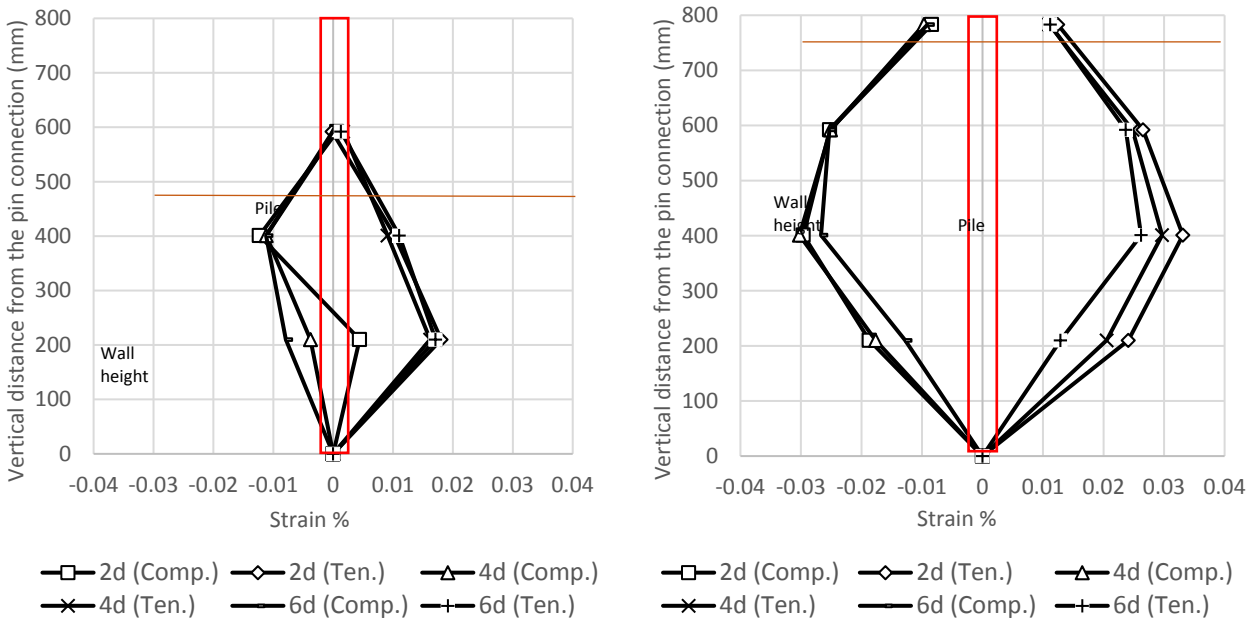

Figure 5.4 Strains of the laterally loaded pile at a load of 300 N in: (a) Group (H1 L1 S1 C1 D123) (b) Group (H2 L2 S1 C1 D123).

The location of the maximum tensile strain on the tensile side of the pile in Group **H1 L1** S1 C1 D123 was about 22% of the pile height. On the other hand, the location of the tensile strain in Group **H2 L2** S1 C1 D123 was about 44% of the pile height. Both locations were in the middle part of the wall in each group. The tension strain in the lower part of the pile's compressive side of Test **H1 L1** S1 C1 D1 is due a defect in the strain gauge at that location.

Furthermore, the strains along the compressive and tensile sides of the pile in Group **H1 L1** S1 C1 D123 were lower than those in Group **H2 L2** S1 C1 D123. Moreover, the values of the maximum compressive and tensile strains in all tests of Group **H1 L1** S1 C1 D123 were the same as shown in Figure 5.4 (a). On the other hand, there were slight differences in these strains for the tests of Group **H2 L2** S1 C1 D123 in Figure 5.4 (b). These differences are probably because of the small variation in the soil resistance against the pile lateral deflection.

The stresses and moments of the laterally loaded pile of Group **H1 L1** S1 C1 D123 and Group **H2 L2** S1 C1 D123 are shown in Figure 5.5 and 5.6, respectively. The same behavior observed in Figure 5.4 is shown in these two figures.

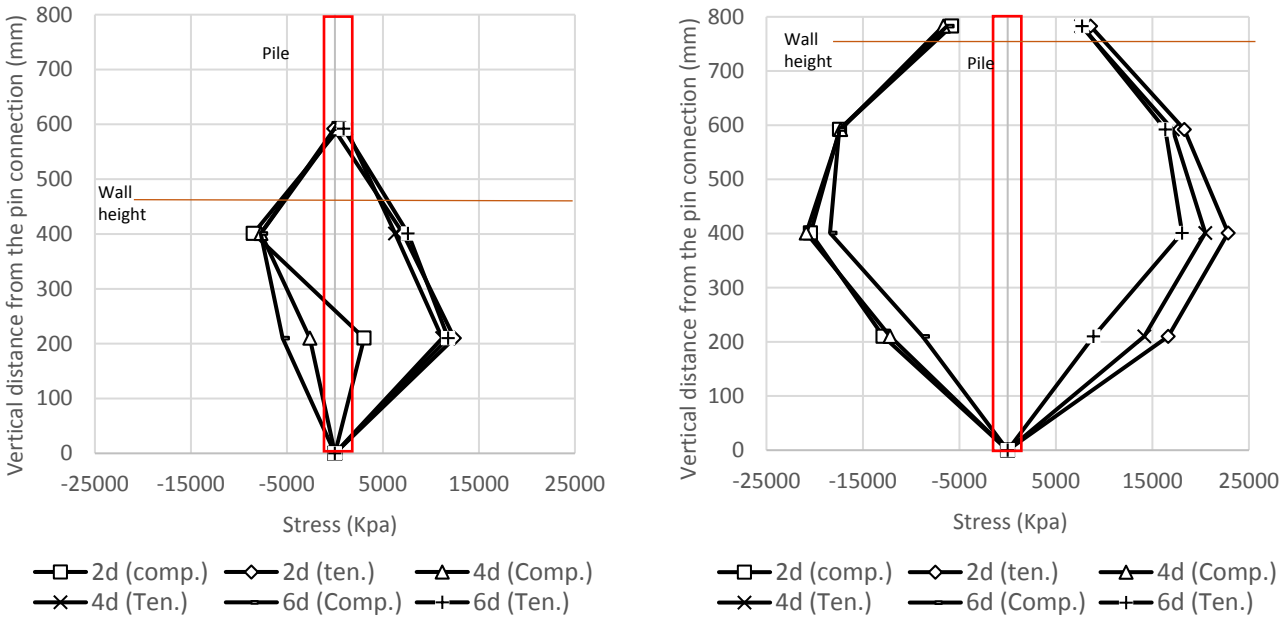

(a) (b)

Figure 5.5 Stresses of the laterally loaded pile at a load of 300 N in: (a) Group (H1 L1 S1 C1 D123) (b) Group (H2 L2 S1 C1 D123).

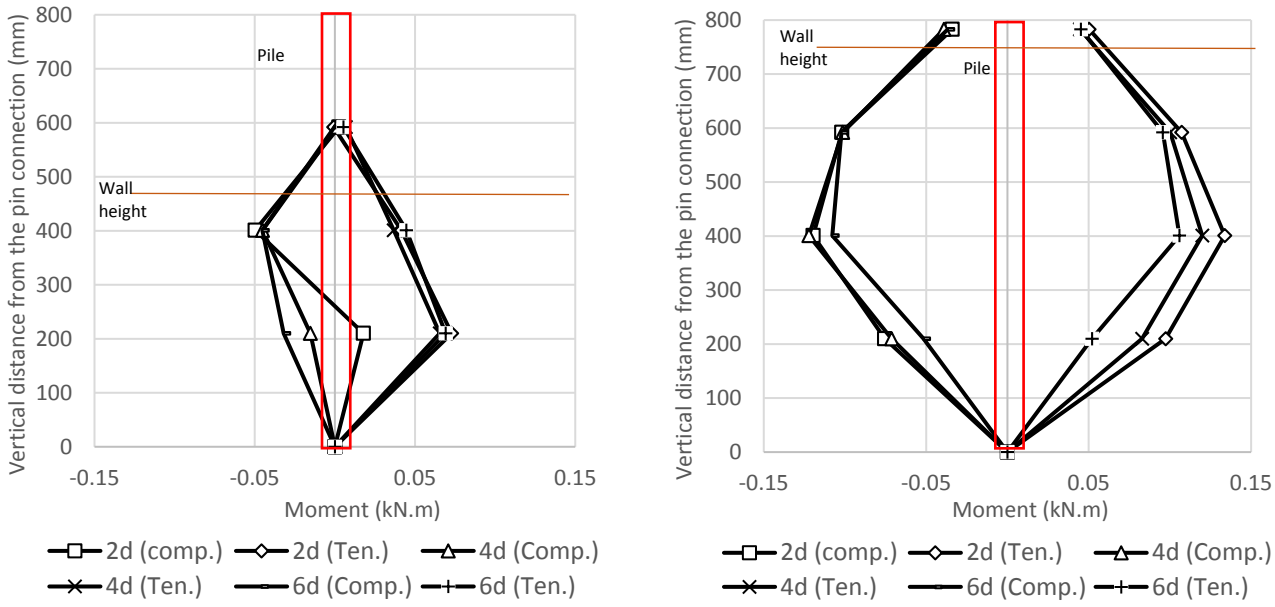

Figure 5.6 Moments of the laterally loaded pile at a load of 300 N in: (a) Group (H1 L1 S1 C1 D123) (b) Group (H2 L2 S1 C1 D123).

5.2.3. Strain of geogrid

From Figure 3.19 in Chapter 3, the strain gauges for the geogrid layers were organized into gauge Groups G1 and G2 for the low height wall tests and gauges Groups G1, G2, G3, and G4 for the high wall tests. In this section, the strain data of Groups **H1 L1** S1 C1 D123 and **H2 L2** S1 C1 D123 are analyzed using two approaches. The first approach considers the data of one gauges group with different pile offsets. The second approach includes the data of one pile offset with different gauge groups.

Figures 5.7 and 5.8 present the strains of the geogrid layers using the first analysis approach. At 12% of the reinforcement length, the strains of the gauges group G1 for both Groups **H1 L1** S1 C1 D123 and **H2 L2** S1 C1 D123 are shown in Figure 5.7 (a) and (b). Figure 5.8 (a) shows the strain distribution of gauge group G2 at 67% of the reinforcement length in Group H1 L1 S1

C1 D123. On the other hand, Figure 5.8 (b) presents the strain distribution of gauge group G3 at 57% of the reinforcement length in Group **H2 L2** S1 C1 D123.

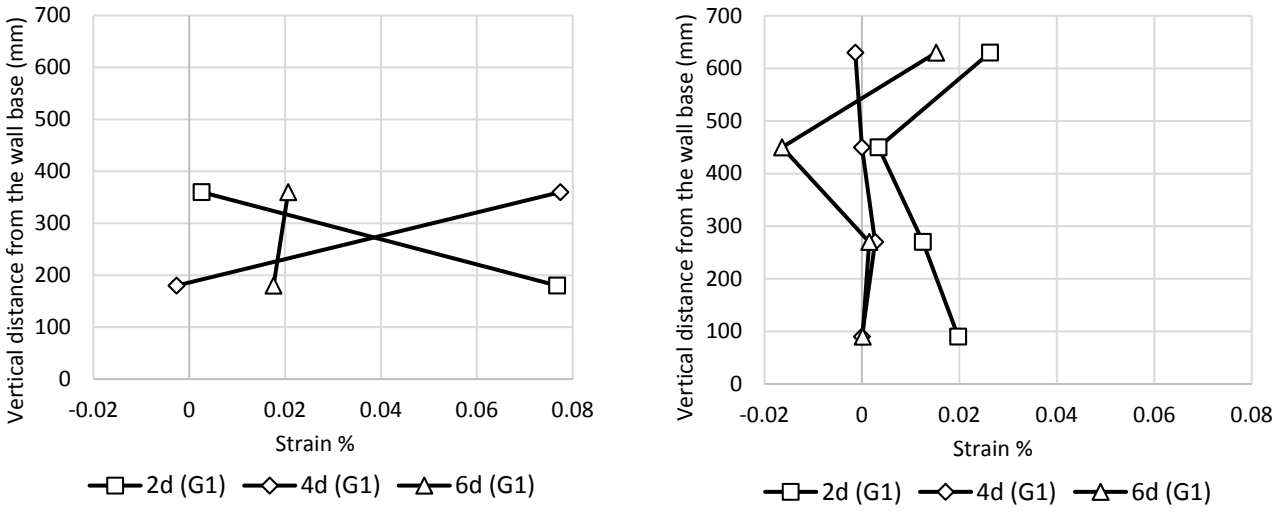

(a) (b)

Figure 5.7 Strains of the geogrid layers at a load of 300 N in: (a) gauge group (G1) in Group (H1 L1 S1 C1 D123) and (b) gauge group (G1) in Group (H2 L2 S1 C1 D123).

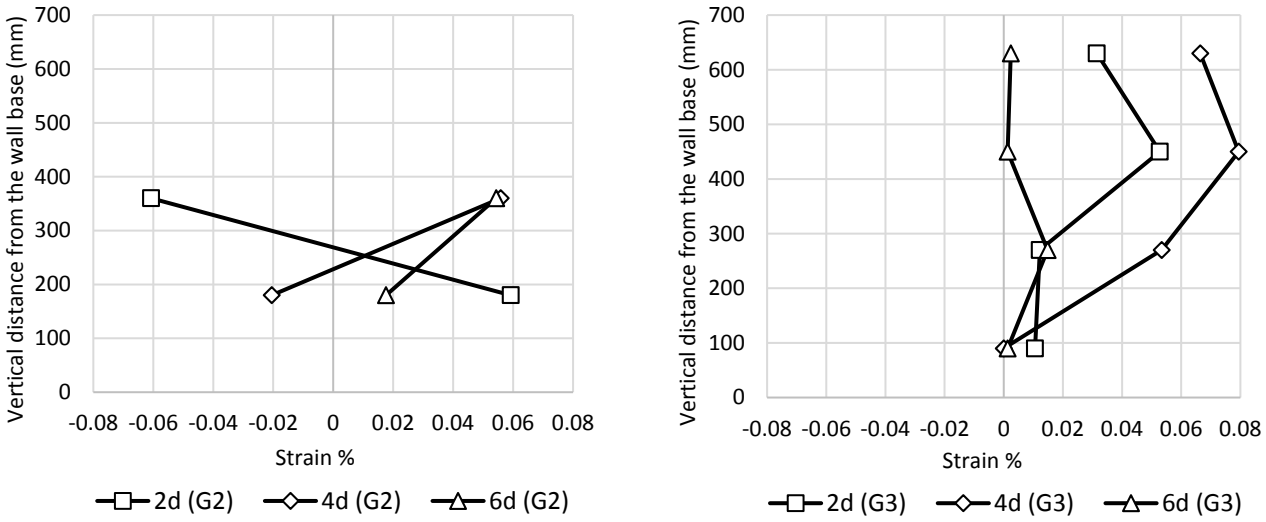

(a) (b)

Figure 5.8 Strains of the geogrid layers at a load of 300 N in: **(a) gauge group (G2) in group (H1 L1 S1 C1 D123) and (b) gauges group (G3) in group (H2 L2 S1 C1 D123).**

Figure 5.7 (a) and Figure 5.8 (a) show that low tensile strains were recorded on the top geogrid layers for the small pile offset. This lower strain occurred because of the bending of the reinforcement at that location due to the large pile deflection and the small distance between the pile and the wall.

In general, the tensile strains of gauge Group G1 at the smallest pile offset were higher than those at the larger pile offsets as shown in Figure 5.7 (a) and (b). This behavior occurred because of the pile proximity to gauge Group G1). At the same pile offset in the two Groups **H1 L1** S1 C1 D123 and **H2 L2** S1 C1 D123, the maximum tensile strains in Group **H1 L1** S1 C1 D123 were higher than those in Group **H2 L2** S1 C1 D123. By reducing the wall height, the soil resistance to the lateral deflection of the pile decreased. Therefore, the geogrid layers experienced more tensile strains or stresses to resist the deflection of the wall facing.

For Group **H2 L2** S1 C1 D123, the tensile strains in gauge Group G3 were higher at the pile offset of 4d than those at other pile offsets because of the pile proximity to the location of this gauge group. For Group **H1 L1** S1 C1 D123, the tensile strains of gauge Group G2 for the two pile offsets 4d and 6d were higher in the upmost layer and lower in the lower geogrid layer. This behavior is due to the larger deflection of the pile behind the upper part of the wall, which induced a high strain in the geogrid layer around the deflected pile.

By using the second analysis approach, the strain data can be presented as shown in Figures 5.9, 5.10, and 5.11. The same gauge groups from the first analysis approach are chosen to compare the strain behavior between Group **H1 L1** S1 C1 D123 and Group **H2 L2** S1 C1 D123.

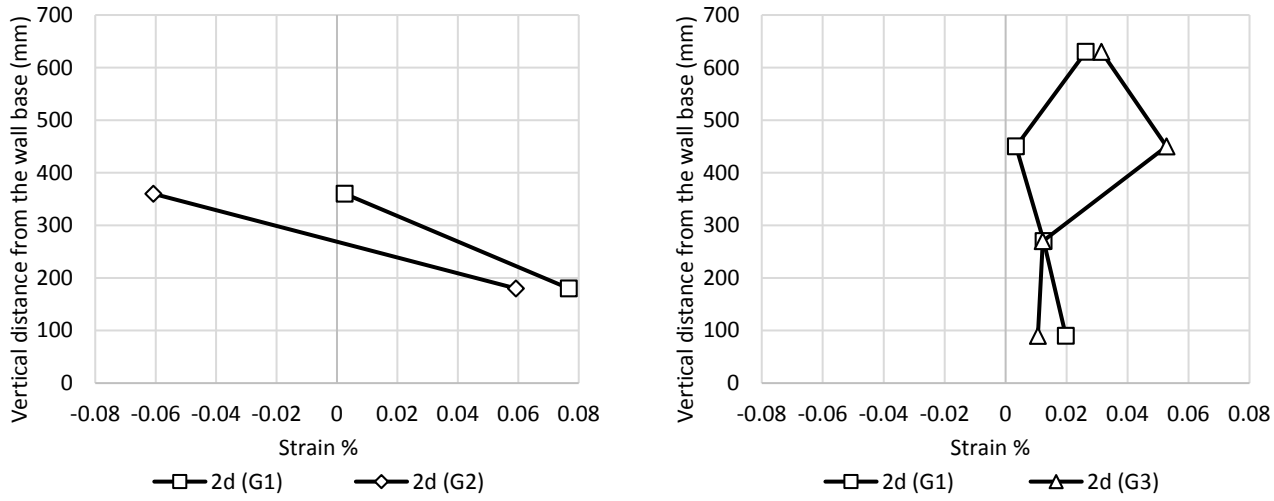

(a) (b)

Figure 5.9 Strains of the geogrid layer at a load of 300 N at: (a) pile offset 2d in group (H1 L1 S1 C1 D123) and (b) pile offset (2d) in group (H2 L2 S1 C1 D123).

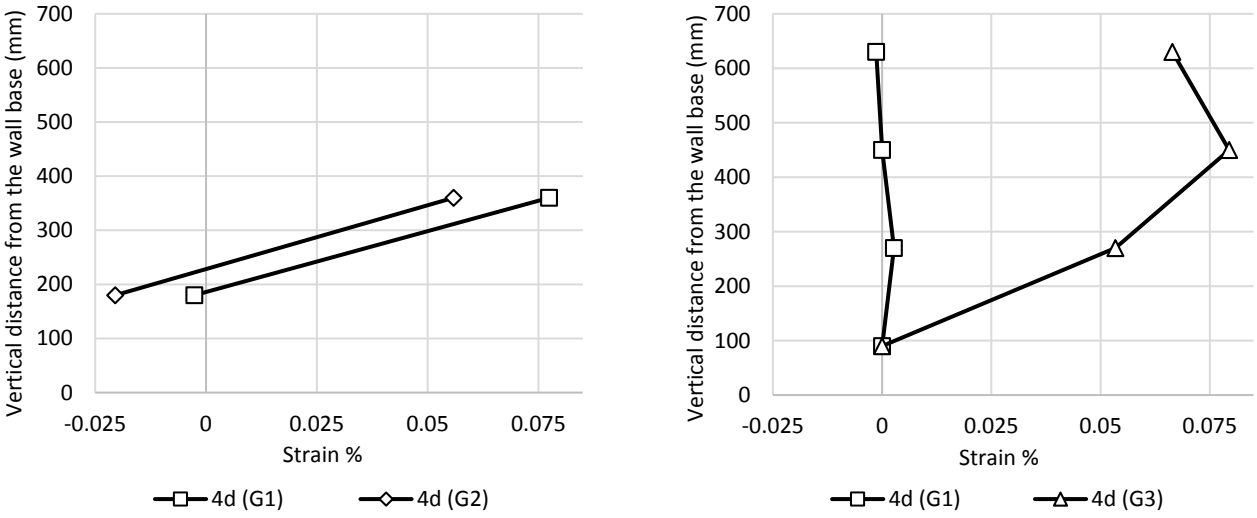

(a) (b)

Figure 5.10 Strains of the geogrid layer at a load of 300 N at: (a) pile offset 4d of group (H1 L1 S1 C1 D123) and (b) pile offset 4d of group (H2 L2 S1 C1 D123).

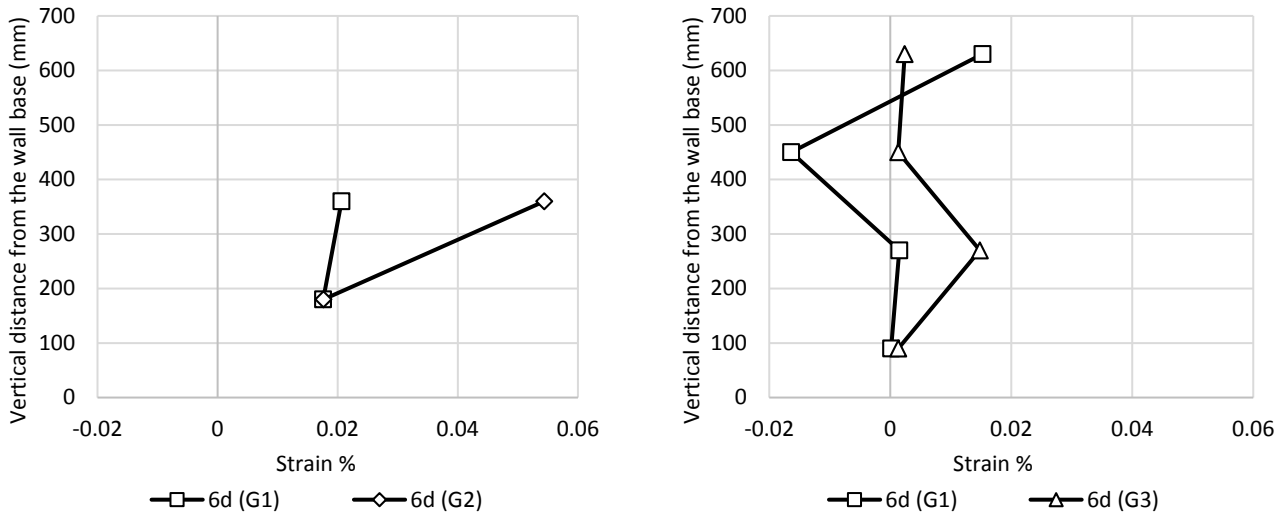

Figure 5.11 Strains of the geogrid layer at a load of 300 N at: (a) pile offset 6d in Group (H1 L1 S1 C1 D123) and (b) pile offset (6d) in Group (H2 L2 S1 C1 D123).

Figures 5.9 (b), 5.10 (b), and 5.11 (b) show that the tensile strains in gauge group G3 were larger than those in gauge Group G1. The reason behind this behavior is that the part of the geogrid layer behind the pile was subjected to large tensile strains or higher stresses due to the deflections of the pile and the MSE wall.

On the other hand, the tensile strains in gauge group G2 were smaller than those in gauge group G1 as shown in Figures 5.9 (a) and 5.10 (a) . For Group H1 L1 S1 C1 D123, there was no enough reinforcement length to develop high resistance to the friction force with the soil. Therefore, the tensile strain decreased by increasing the distance from the wall facing. However, Figures 5.11 (a) shows an opposite case. The tensile strains in gauge group G2 were larger than those in gauge group G1. This irregular case is probably due to the location of the pile at the offset of 6d, which was behind the MSE wall system as shown in Figure 3.26 (C).

5.3. Effect of reinforcement spacing and length

Two important parameters, reinforcement spacing and length, have been considered in this section in order to investigate their effects.

5.3.1. Reinforcement spacing

In order to determine the effect of reinforcement spacing, two comparison sets with different reinforcement lengths were analyzed. Set 2 has the regular reinforcement length of 0.7 H while Set 3 has the long reinforcement length of 1.25 H. Each of these sets has two groups with one key variable, which is the vertical spacing of the geogrid layers.

Set 2 High wall with regular reinforcement length and mechanical connection

All the information about the tests in this set is shown in Table 5.3. Each one of the two groups in this set includes three tests. For each corresponding pile offset in the table, the only variable parameter is the vertical spacing between the geogrid layers

Table 5.2 Detials of Set 2

Tests	Ultimate Lateral Load N	Wall Height H, mm	Layer length L, mm	Layer spacing S, mm	Offset D, mm	Connection Type	Group designation
H2 L2 S2 C1 D1	278	720	504	135	127 (2d)	Mechanical	Category 1 of Group 2 or H2 L2 **S2** C1 D123
H2 L2 S2 C1 D2	335				254 (4d)		
H2 L2 S2 C1 D3	430				381 (6d)		
H2 L2 S1 C1 D1	368	720	504	90	127 (2d)		Category 2 of Group 2 or H2 L2 **S1** C1 D123
H2 L2 S1 C1 D2	405				254 (4d)		
H2 L2 S1 C1 D3	504				381 (6d)		

The ultimate lateral load capacities of the piles in Groups H2 L2 **S2** C1 D123 and H2 L2 **S1** C1 D123 are listed in Table 5.3. These capacities were obtained from the load-displacement curves shown in Figure 5.12.

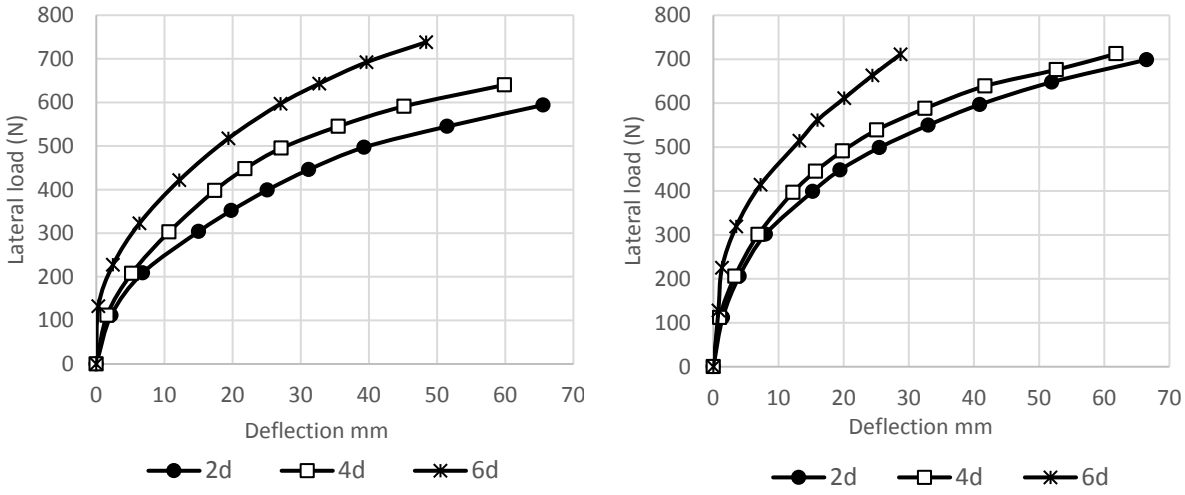

Figure 5.12 Load-Displacement curves of Set 2 in: (a) Group (H2 L2 S2 C1 D123) and (b) Group (H2 L2 S1 C1 D123).

The ultimate lateral load capacity of the pile increased by an increase of the pile offset. On the other hand, the reinforcement spacing was reduced from 135 mm in the tests of Group H2 L2 **S2** C1 D123 to 90 mm in the tests of Group H2 L2 **S1** C1 D123. The pile capacities increased by approximately 32%, 20%, and 17% at pile offsets of 2d, 4d, and 6d, respectively when the reinforcement spacing decreased. However, the chosen comparison load for this set was 400 N, and all the data of the two groups were analyzed by considering this load.

Deflection of wall facing

The deflections of the wall facing along the vertical centerline of Group H2 L2 S2 C1 D123 and Group H2 L2 S1 C1 D123 are shown in Figure 5.13.

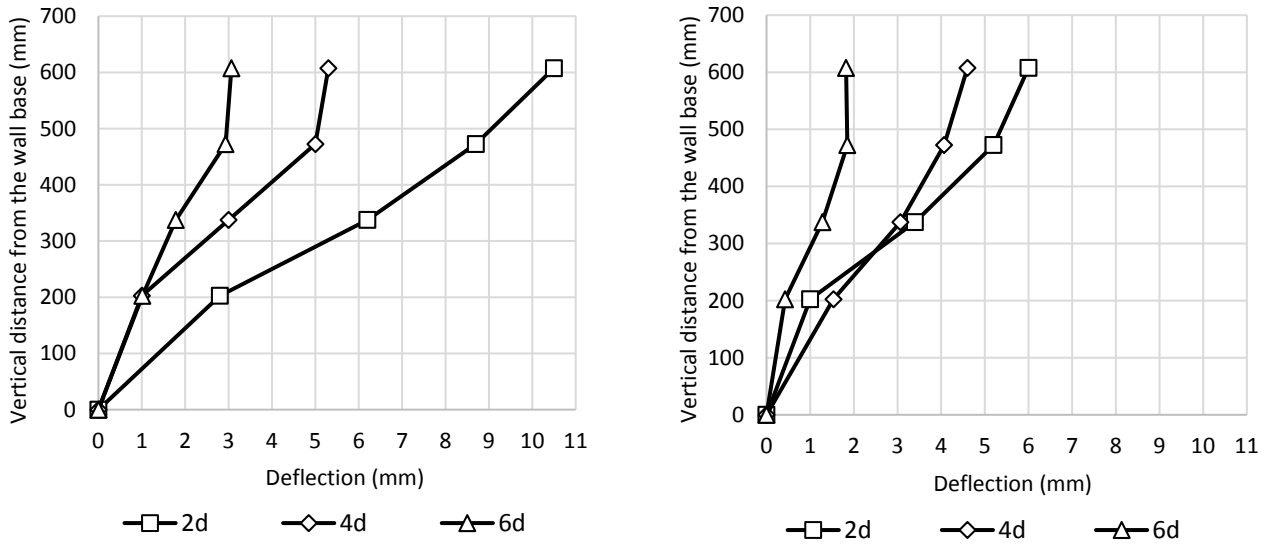

(a) (b)

Figure 5.13 Deflections of the wall facing along the vertical centerline at a load of 400 N in: (a) Group (H2 L2 S2 C1 D123) (b) Group (H2 L2 S1 C1 D123).

The deflections of the wall facing along the vertical centerline in each group increased by a decrease of the pile offset. This behavior is observed from Figure 5.13, especially for the wall part that had a large deflection. On the other hand, Figure 5.14 presents the Transverse deflections of the wall for the two groups at an elevation of 84% of the wall height. At each corresponding offset, the maximum deflections of Group H2 L2 **S2** C1 D123 were larger than those of Group H2 L2 **S1** C1 D123. By reducing the spacing, more reinforcement layers can be used and more resistance to the wall deflection can be obtained.

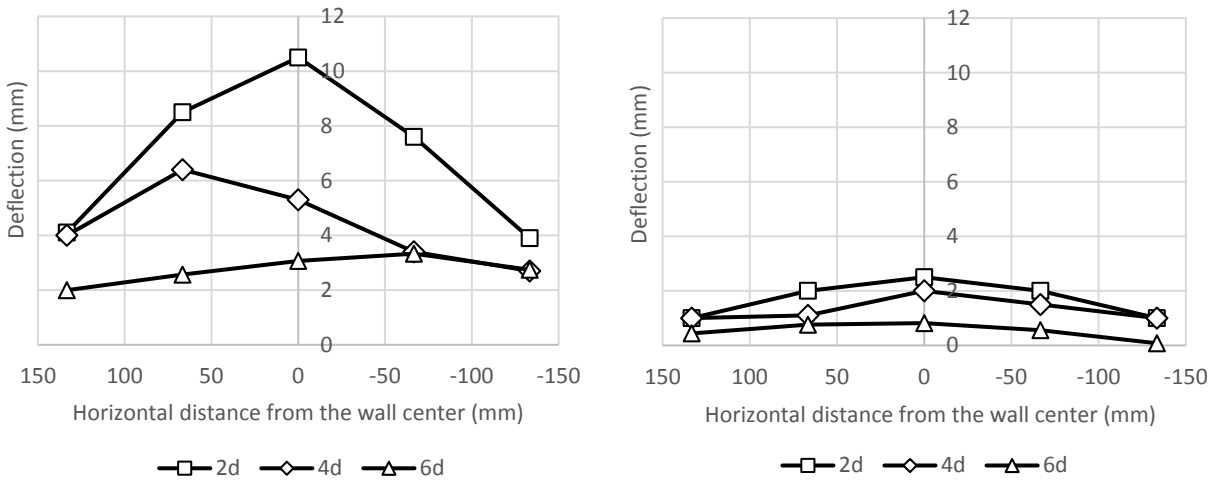

(a) (b)

Figure 5.14 transverse distribution of the wall deflections at 84% of the wall height and a load of 400 N in: (a) Group (H2 L2 S2 C1 D123) and (b) Group (H2 L2 S1 C1 D123).

Strain, Stress, and moment of the pile.

Figure 5.15 presents the strains of the laterally loaded pile of Group H2 L2 S2 C1 D123 and Group H2 L2 S1 C1 D123. The maximum compressive and tensile strains occurred at an elevation of 44% of the pile height. Figures 5.15 (a) and (b) show that the change in the reinforcement spacing between the two groups did not cause a substantial change in the maximum compressive and tensile strains of the two group. However, one exception is shown in Figure 5.15 (a) for the compressive strain of Group H2 L2 S1 C1 D123. There are small differences between the maximum compressive strains at different pile offsets due to the variation of the soil resistance during the tests. The same behavior applies to the stress and moment of the pile as shown in Figures 5.16 and 5.17.

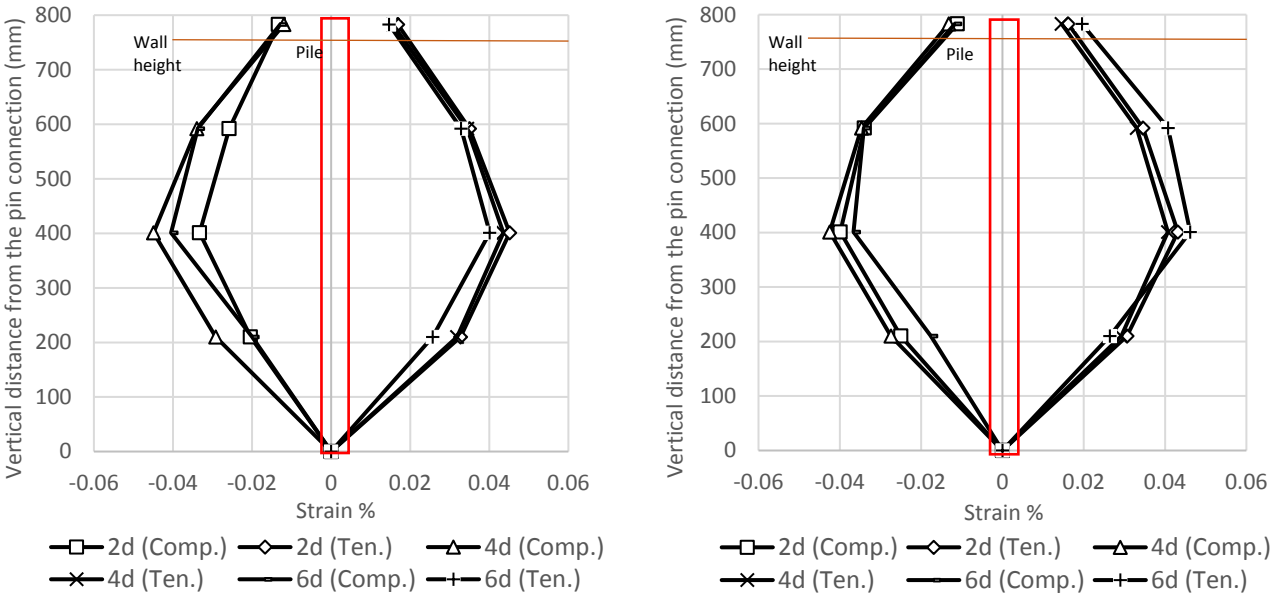

(a) (b)

Figure 5.15 Strains of the laterally loaded pile at a load of 400 N in: (a) Group (H2 L2 S2 C1 D123) and (b) Group (H2 L2 S1 C1 D123).

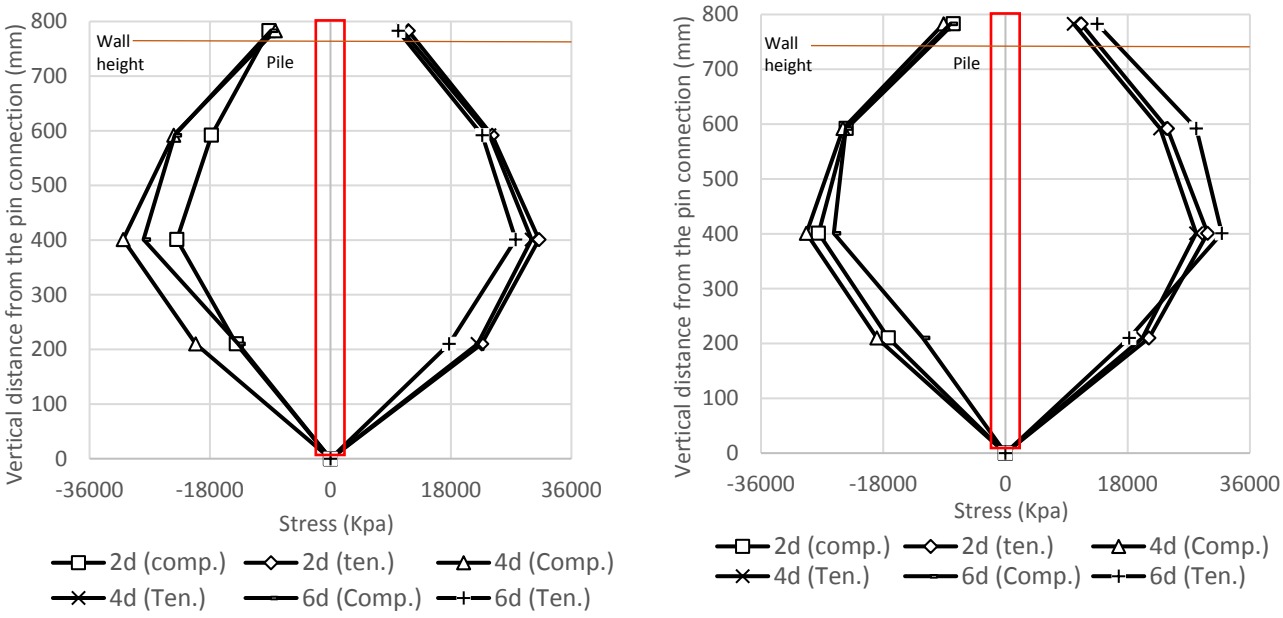

(a) (b)

Figure 5.16 Stresses of the laterally loaded pile at a load of 400 N in: (a) Group (H2 L2 S2 C1 D123) and (b) Group (H2 L2 S1 C1 D123).

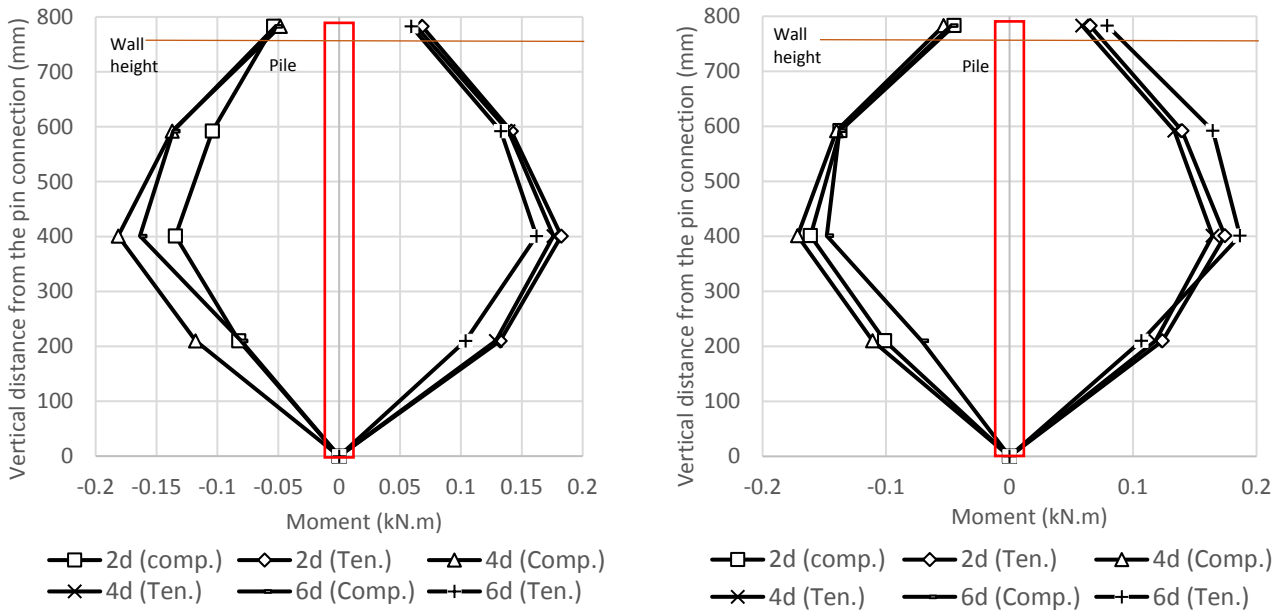

(a) (b)

Figure 5.17 Moments of the laterally loaded pile at load of 400 N in: (a) Group (H2 L2 S2 C1 D123) and (b) Group (H2 L2 S1 C1 D123).

Strain of geogrid

The same analysis approaches that were used in Set 1 are considered in this set. Figures 5.18, 5.19, 5.20, and 5.21 show the strains using the first analysis approach while Figures 5.22, 5.23, and 5.24 show the strains using the second analysis approach.

For the Groups H2 L2 **S2** C1 D123 and H2 L2 **S1** C1 D123, the strains of gauge goups G1 and G2 were the highest at the pile offset of 2d as shown in Figures 5.18 and 5.19. Large strains are observed from Figures 5.18 and 5.19 at the pile offset of 2d because the pile location was between gauge groups G1 and G2 as shown in Figure 3.16 (a). The same observation is shown in Figures 5.20 and 5.21 but for the pile offset of 4d. In this case, the pile location was between gauge groups G3 and G4 as shown in Figure 3.16 (b).

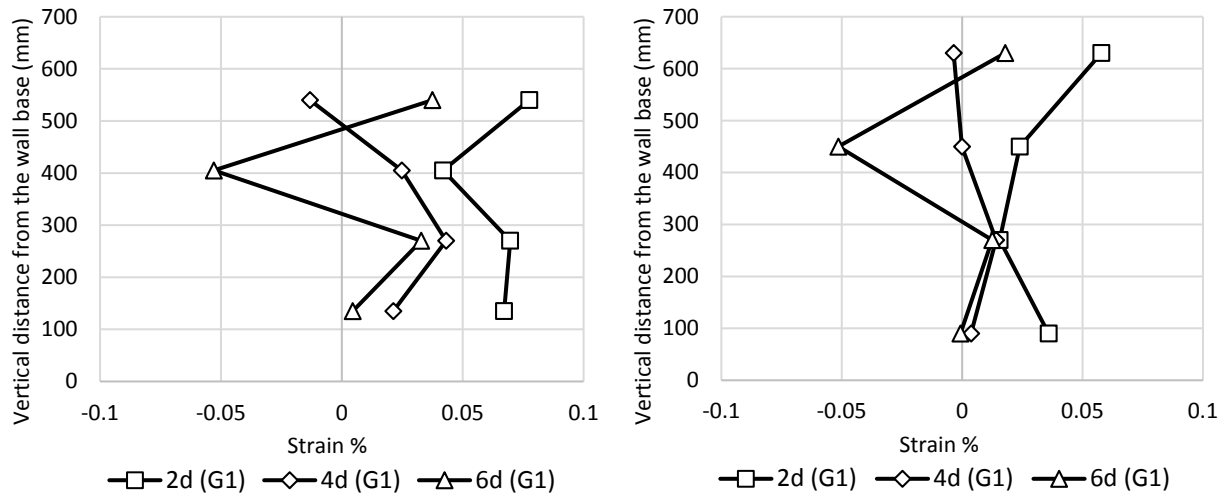

(a) (b)

Figure 5.18 Strains of the geogrid layers at a load of 400 N in: (a) Gauge group (G1) of Group (H2 L2 S2 C1 D123) and (b) Gauge group (G1) of Group (H2 L2 S1 C1 D123).

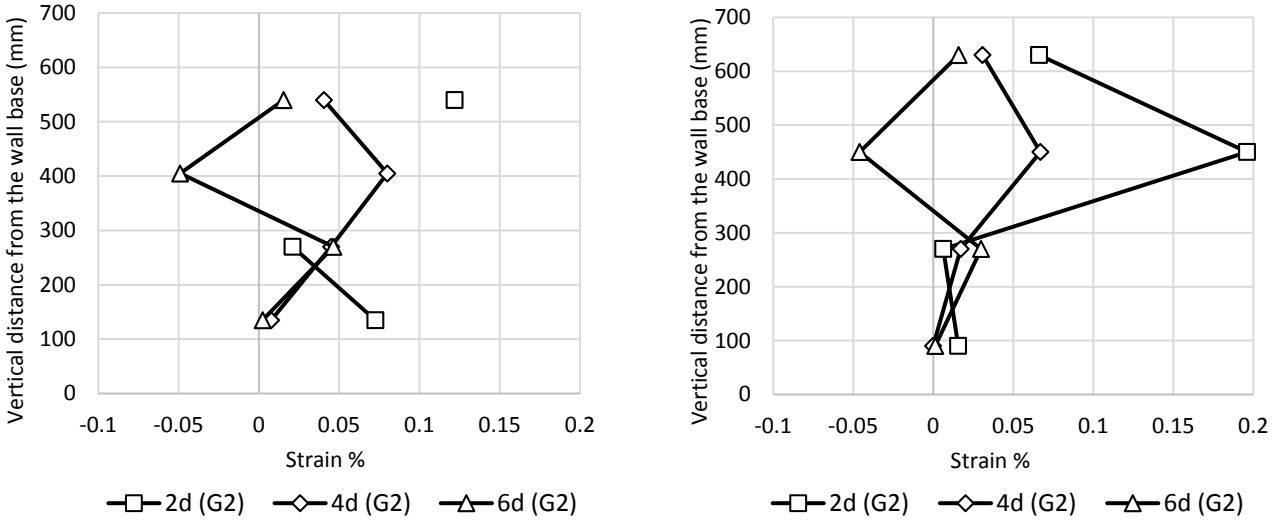

(a) (b)

Figure 5.19 Strains of the geogrid layers at a load of 400 N in: (a) Gauge group (G2) of Group (H2 L2 S2 C1 D123) and (b) Gauge group (G2) of Group (H2 L2 S1 C1 D123).

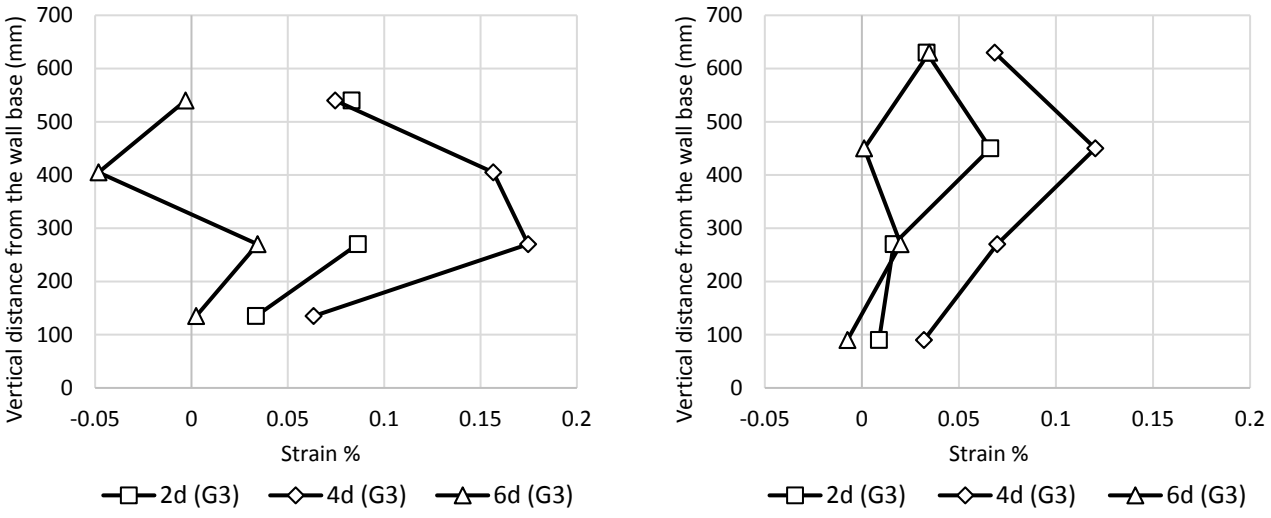

(a) (b)

Figure 5.20 Strains of the geogrid layers at a load of 400 N in: (a) Gauge group (G3) of Group (H2 L2 S2 C1 D123) and (b) Gauge group (G3) of Group (H2 L2 S1 C1 D123).

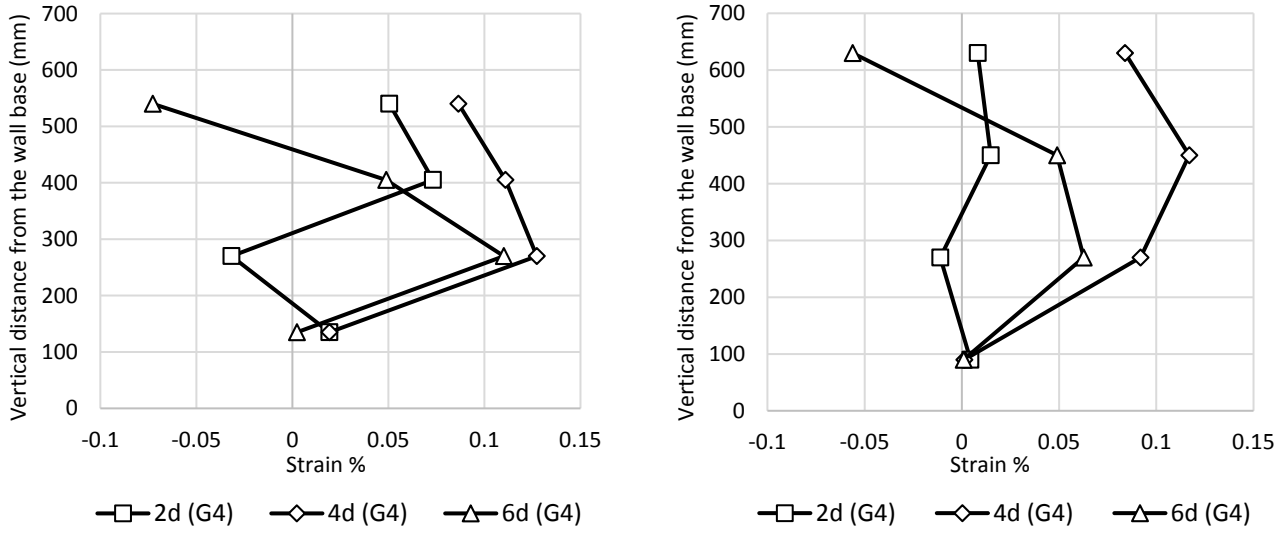

(a) (b)

Figure 5.21 Strains of the geogrid layers at a load of 400 N in: (a) Gauge group (G4) of Group (H2 L2 S2 C1 D123) (b) Gauge group (G4) of Group (H2 L2 S1 C1 D123).

At the same pile offsets in the two groups, the maximum tensile strains of Group H2 L2 **S2** C1 D123 were larger than those of Group H2 L2 **S1** C1 D123. This difference is because of the large reinforcement spacing between the layers of Group H2 L2 **S2** C1 D123. By increasing of the spacing, the number of the reinforcement layers decreased. Thus, the tensile strain increased for all the reinforcement layers.

As have mentioned earlier, the strains in Figures 5.22, 5.23, and 5.24 were analyzed using the second analysis approach. From these figures, the strain distribution at a specific pile offset depends on the distance between the pile offset and the location of the gauge group. For the pile offsets of 2d, 4d, and 6d, the largest strains were recorded by gauge groups G2, G3 and G4, respectively. Moreover, Figures 5.22, 5.23, and 5.24 also show that the maximum tensile strains of Group H2 L2 **S2** C1 D123 were larger than those of Group H2 L2 **S1** C1 D123.

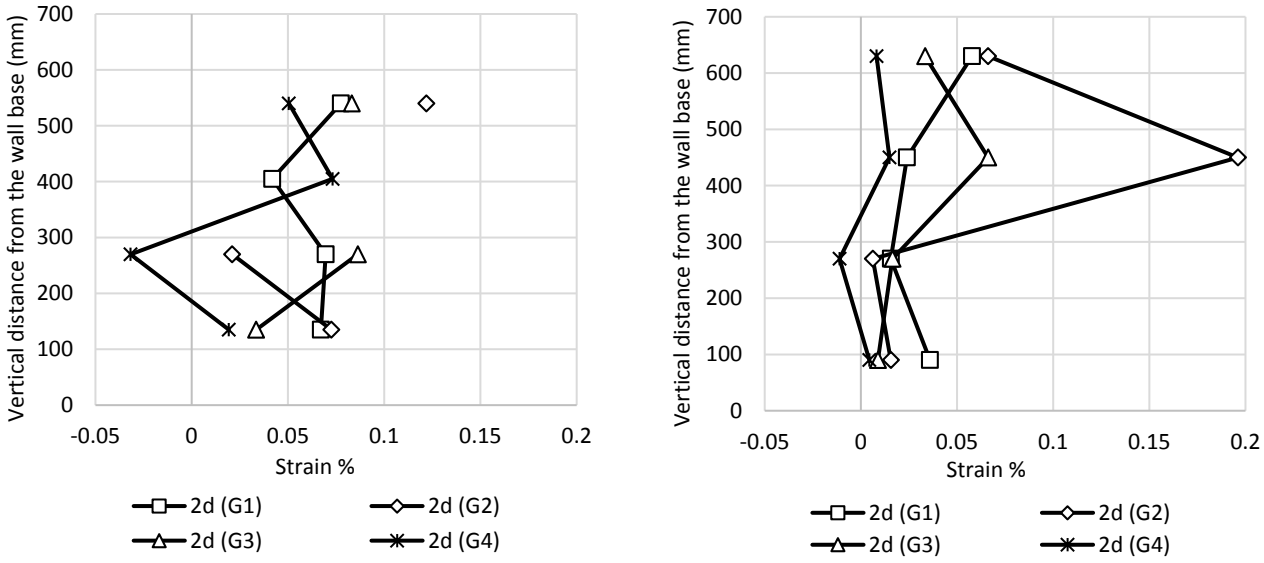

Figure 5.22 Strains of the geogrid layers at a load of 400 N at: (a) Pile offset (2d) of Group (H2 L2 S2 C1 D123) and (b) Pile offset (2d) of Group (H2 L2 S1 C1 D123).

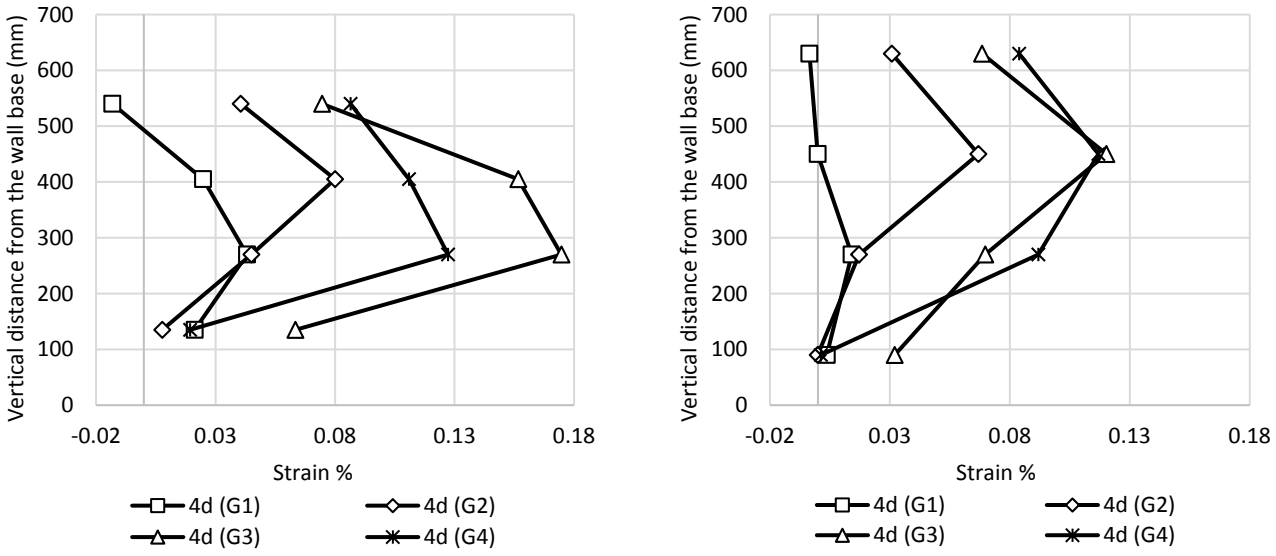

(a) (b)

Figure 5.23 Strains of the geogrid layers at a load of 400 N at: (a) Pile offset (4d) of Group (H2 L2 S2 C1 D123) and (b) Pile offset (4d) of Group (H2 L2 S1 C1 D123).

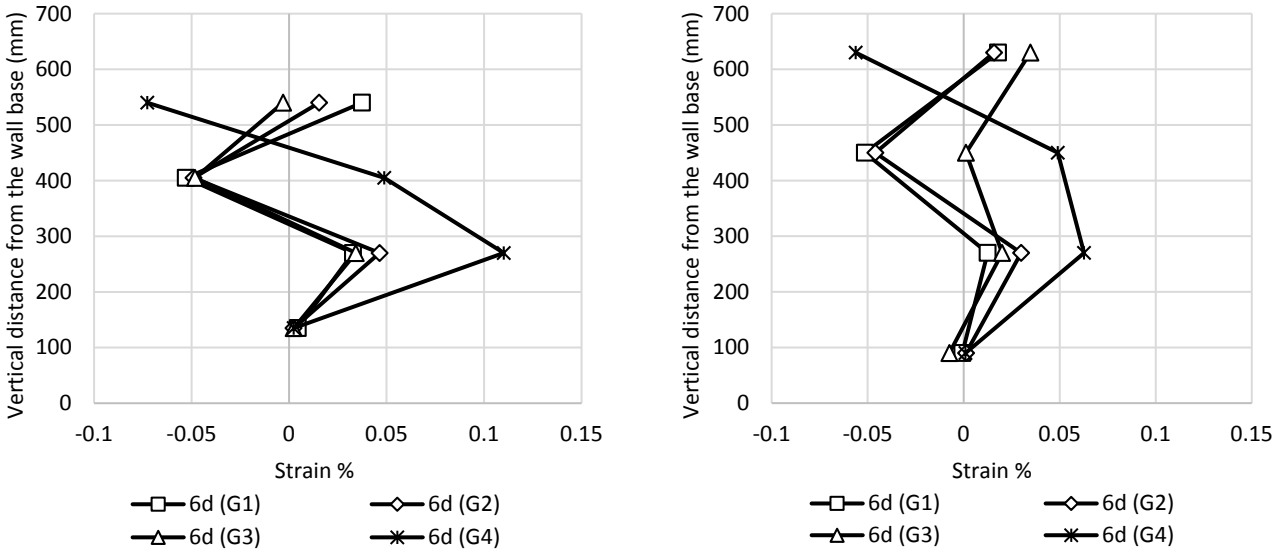

(a) (b)

Figure 5.24 Strains of the geogrid layers at a load of 400 N at: (a) Pile offset (6d) of Group (H2 L2 S2 C1 D123) (b) Pile offset (6d) of Group (H2 L2 S1 C1 D123).

Pressure behind the wall facing.

Figure 5.25 shows the earth pressure behind the wall facing along the centerline of Group H2 L2 **S2** C1 D123 and Group H2 L2 **S1** C1 D123 while Figure 5.26 shows the transverse distribution of the pressure of the two group at 65.5% of the wall height.

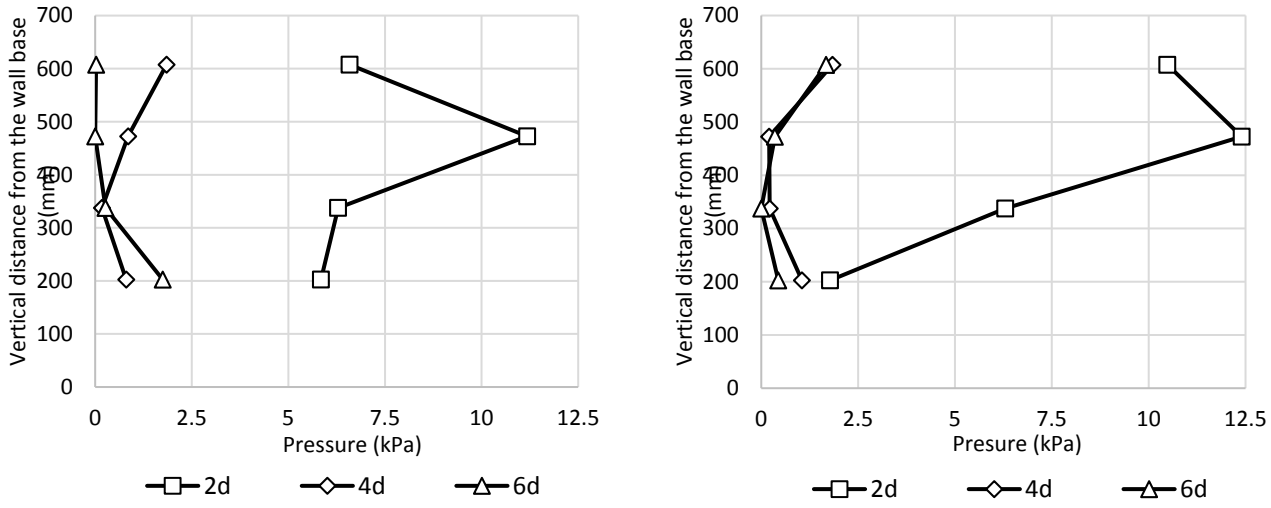

(a) (b)

Figure 5.25 Pressure behind the wall facing at a load of 400 N: (a) Group (H2 L2 S2 C1 D123) (b) Group (H2 L2 S1 C1 D123).

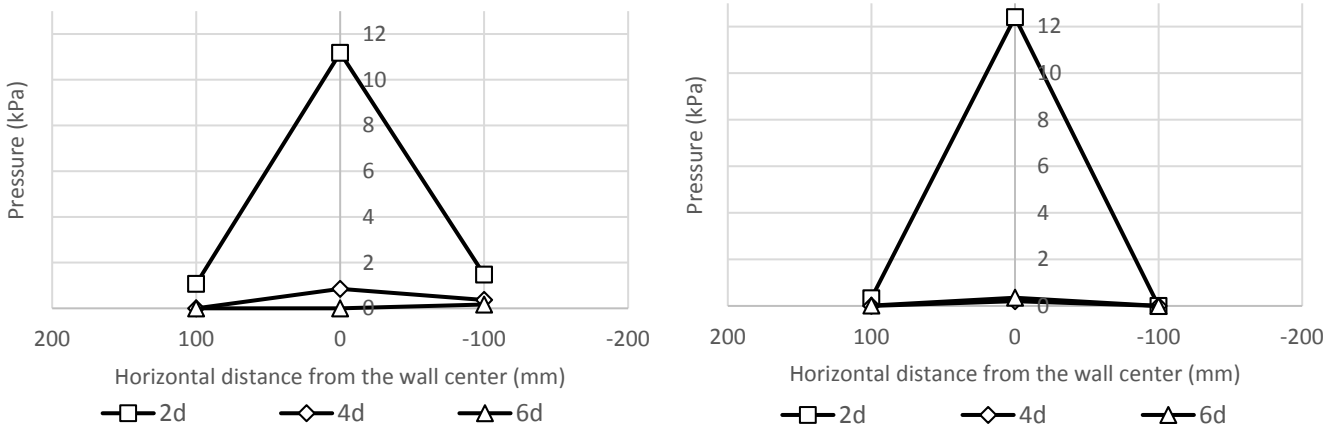

(a) (b)

Figure 5.26 Transverse distribution of the pressures at 65.5% of the wall height and load of 400 N in: (a) group (H2 L2 S2 C1 D123) and (b) group (H2 L2 S1 C1 D123).

For the two groups of this set, the pressures at the pile offset 2d were higher than those at other pile offsets as shown in Figure 5.25. This large pressure difference is due to the pile proximity to the wall facing at that offset.

At the pile offset 2d, a high pressure zone developed at 65.5% of the wall height. This zone resulted from the high soil resistance to the large deflection of the laterally loaded pile. In fact, the soil at that location was compressed and the overburden weight below this high pressure zone was reduced. As a result, the lateral earth pressure decreased below 65.5% of the wall height. Then, another high pressure zone developed behind the bottom part of the wall specifically in the group with large reinforcement spacing. The developing of this pressure is due to the increase of the overburden weight after the first high pressure zone. For the pile offsets of 4d and 6d, the location of the high pressure zones behind the upper part of the wall moved higher than 65.5% of the wall height because of the large distance between the wall facing and these offsets.

Even though the deflections of the wall facing of Group H2 L2 **S2** C1 D123 were larger than Group H2 L2 **S1** C1 D123, the difference between the maximum pressures for these groups was small. The change in the deflections of the two groups was not because of the magnitude of the pressure behind the facing. It was due to the change in number of the geogrid layers.

Set 3 High wall with long reinforcement length and mechanical connection

This set includes the analyses of Groups H2 L3 **S2** C1 D23 and H2 L3 **S1** C1 D23. Each group of them includes two tests as shown in Table 5.4. Similar to the previous set, the variable parameter between the two groups of this set is the spacing between the geogrid layers. However, the length of the reinforcement was longer than that in the tests of Set 2. Also, only the two large pile offsets are considered in this set.

Table 5.3 Detials of Set 3

Tests	Ultimate Lateral Load N	Wall Height H, mm	Layer length L, mm	Layer spacing S, mm	Offset D, mm	Connection Type	Group designation
H2 L3 S2 C1 D2	405	720	900	135	254 (4d)	Mechanical	Category 1 of Group 3 or H2 L3 **S2** C1 D23
H2 L3 S2 C1 D3	473				381 (6d)		
H2 L3 S1 C1 D2	660	720	900	90	254 (4d)		Category 2 of Group 3 or H2 L3 **S1** C1 D23
H2 L3 S1 C1 D3	870				381 (6d)		

The load-displacement curves of the pile in Groups H2 L3 **S2** C1 D23 and H2 L3 **S1** C1 D23 are shown in Figures 5.27

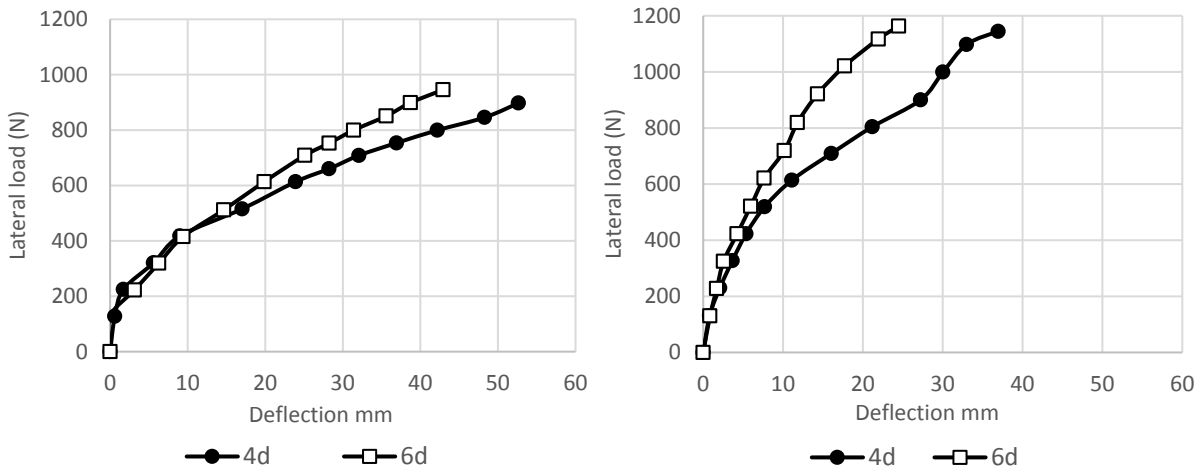

Figure 5.27 Load -Displacement curves of Set 3 in: (a) Group (H2 L3 S2 C1 D23) and (b) Group (H2 L3 S1 C1 D23)

The pile capacity behavior in this set is the same as the behavior of Set 2. By reducing the spacing of the geogrid layers, the pile capacity increased by 63% and 84% at the pile offsets of 4d and 6d, respectively. These percentages are higher than those of Set 2 because the wall was more stable due the long reinforcement length. The chosen comparison load for this set was 600 N, and all the data of the two groups were analyzed at this load.

Deflection of wall facing

The deflection distributions of the wall facing along the vertical centerline of Group H2 L3 S2 C1 D23 and Group H2 L3 S1 C1 D23 are shown in Figure 5.28.

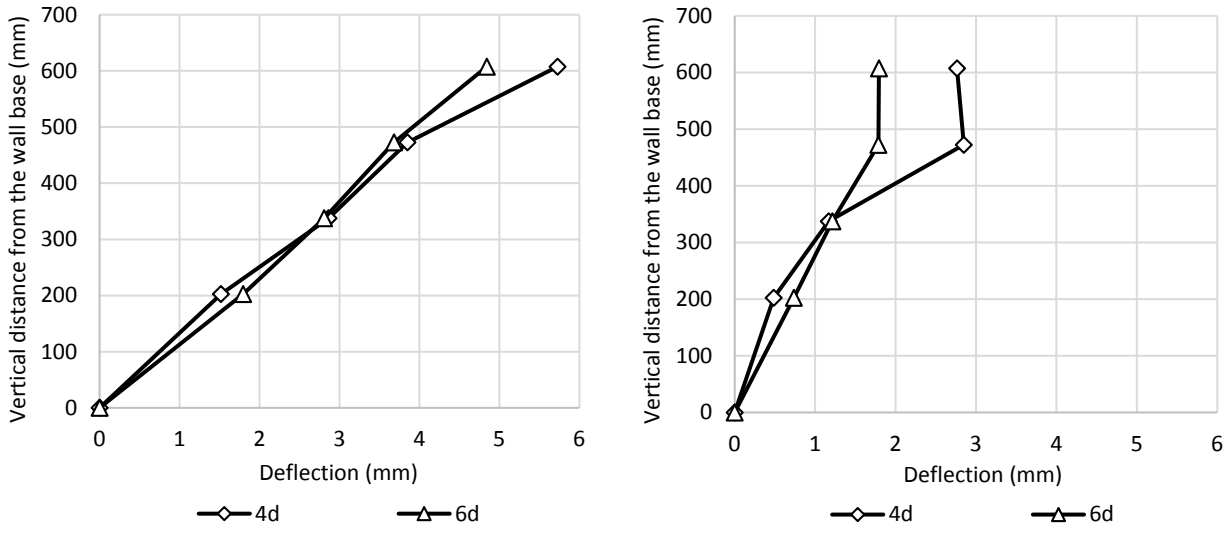

Figure 5.28 Deflections of the wall facing at the vertical centerline at a load of 600 N in: (a) Group (H2 L3 S2 C1 D23) and (b) Group (H2 L3 S1 C1 D23).

Figure 5.28 shows the similar deflection behavior as that shown in the groups of Set 2 at pile offsets 4d and 6d. The difference between the wall deflections in each group was small because both offsets were far from the wall facing. On the other hand, Figure 5.29 presents the Transverse distribution of the wall facing deflection at the maximum wall deflection. The deflection distribution of the wall facing in this figure is more uniform than that at the large pile offset. This behavior is due to the large distance between the pile and wall facing. From both Figure 5.28 and Figure 5.29, the maximum deflection at each pile offset of Group H2 L3 **S2** C1

D23 was higher than the maximum deflection at the corresponding pile offset of Group H2 L3 **S1** C1 D23 because of the large spacing of the first group.

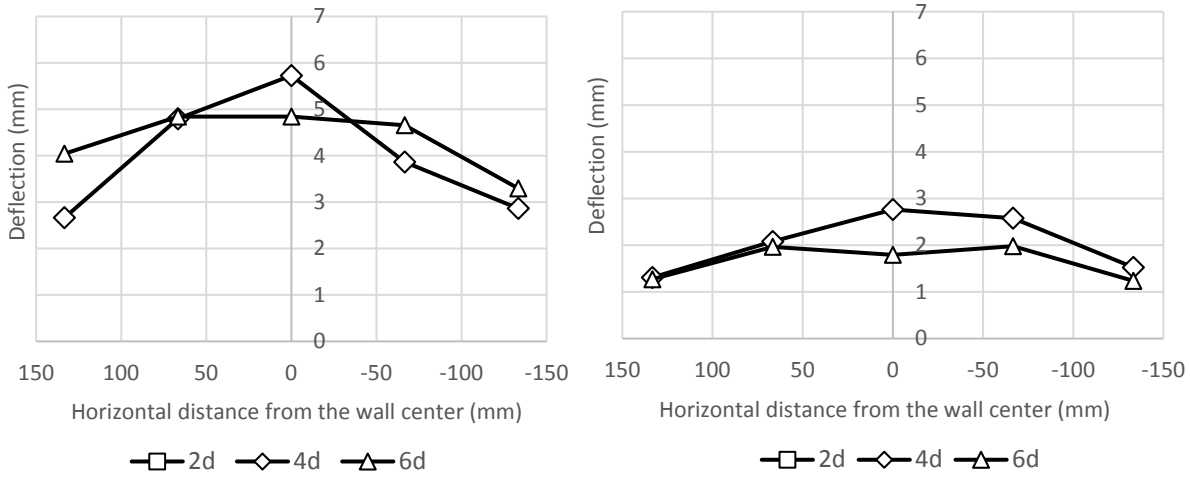

(a) (b)

Figure 5.29 Transverse distribution of the wall facing deflection at 84% of the wall height and load of 600 N in: (a) Group (H2 L3 S2 C1 D23) and (b) Group (H2 L3 S1 C1 D23).

Strain, Stress, and moment of the pile

Figure 5.30 presents the strains of the laterally loaded pile of Group H2 L3 **S2** C1 D23 and Group H2 L3 **S1** C1 D23. Similar to Set 2, the maximum strains in the compressive and tensile sides of the pile for the two groups occurred at 44% of the pile height. The maximum strains increased by 19% on the tensile side and 31% on the compressive side of the pile by increasing the offset from 4d to 6d for Group H2 L3 **S1** C1 D23 as shown in Figure 5.30 (b. This increase is because of the high soil resistance due to the decrease of the spacing between the reinforcement layers. On the other hand, the difference in the maximum strains in the both sides of the pile for Group H2 L3 **S2** C1 D23 was small at the pile offsets of 4d and 6d. However, similar behavior applies to the stress and moment of the pile as shown in Figures 5.31 and 5.32.

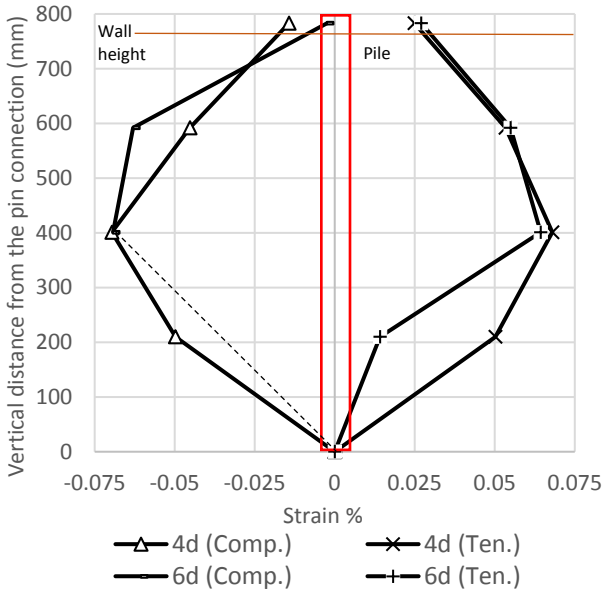

(a)

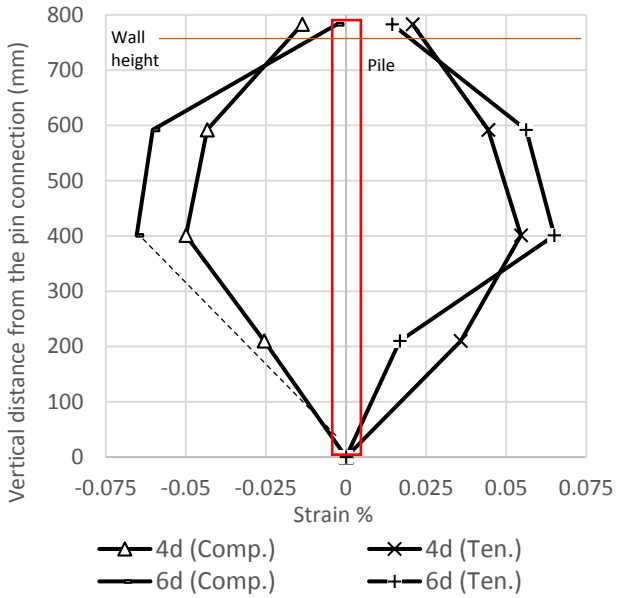

(b)

Figure 5.30 Strains of the laterally loaded pile at a load of 600 N in: (a) Group (H2 L3 S2 C1 D23) and (b) Group (H2 L3 S1 C1 D23).

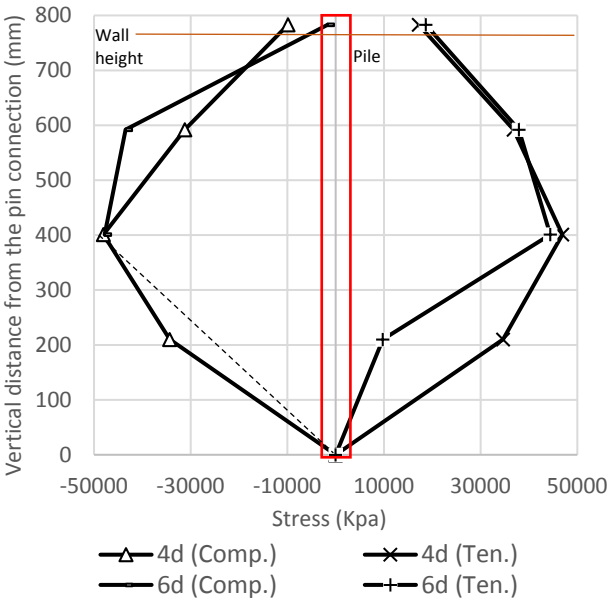

(a)

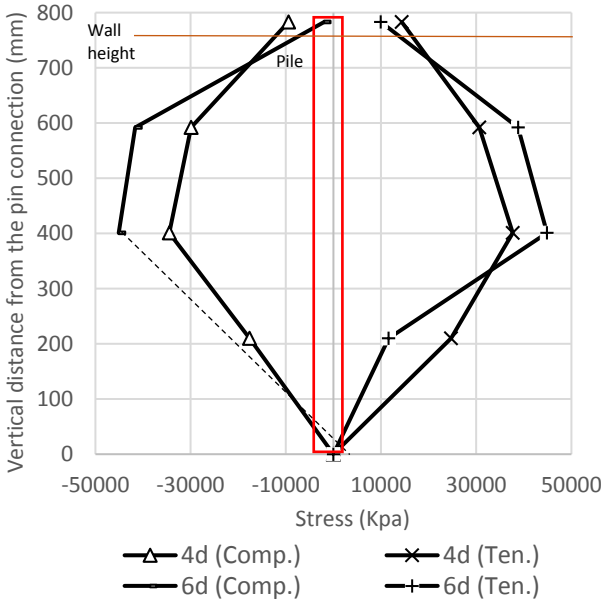

(b)

Figure 5.31 Stresses of the laterally loaded pile at a load of 600 N in: (a) Group (H2 L3 S2 C1 D23) and (b) Group (H2 L3 S1 C1 D23).

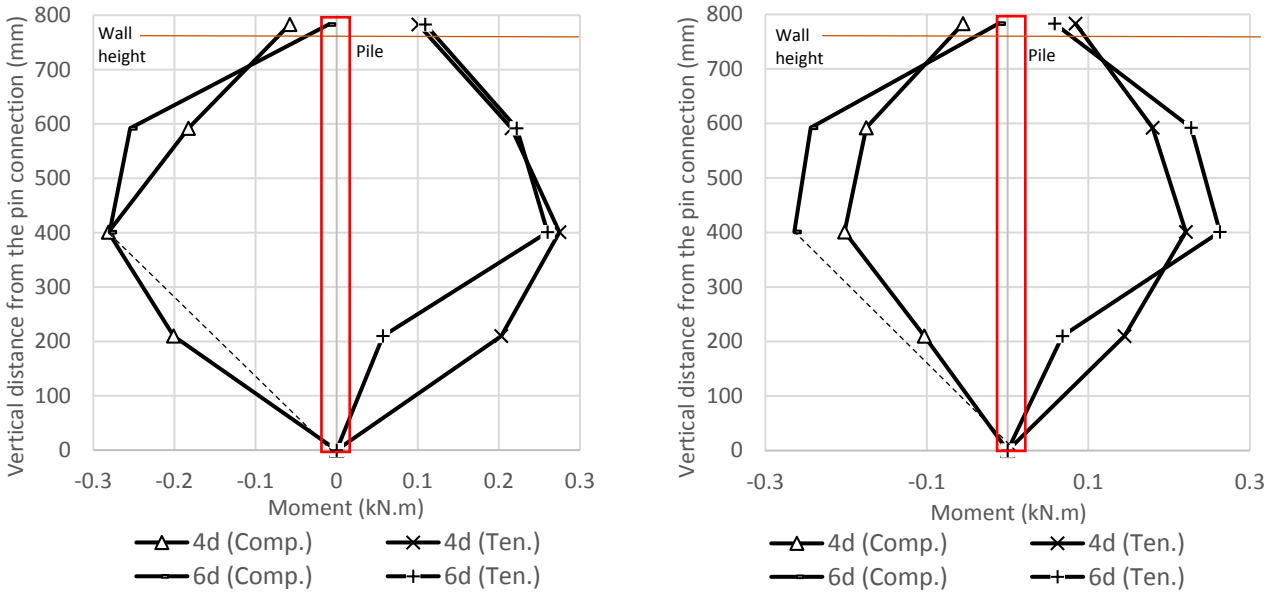

(a) (b)

Figure 5.32 Moments of the laterally loaded pile at a load of 600 N in: (a) Group (H2 L3 S2 C1 D23) and (b) Group (H2 L3 S1 C1 D23).

Strain of geogrid

In this set, the positions of the gauge groups were different than those in Set 2 as shown in Figure 3.19 (c). Therefore, the pile proximity to the gauge groups changed at each pile offset. Figures 5.33, 5.34, 5.35, and 5.36 show the strains using the first analysis approach while Figures 5.37, and 5.38 show the strains using the second analysis approach.

For Group H2 L3 **S2** C1 D23, the strains of gauges groups G1 were low and similar at the pile offsets of 4d and 6d as shown in Figures 5.33 (a). On the contrary, the strains were large and dissimilar for gauge group G2 at the same pile offsets as shown in Figures 5.34 (a). The strains of gauge groups G3 and G4 for the same group were the highest at the pile offset of 6d as shown in Figures 5.35 (a), and 5.36 (a), respectively.

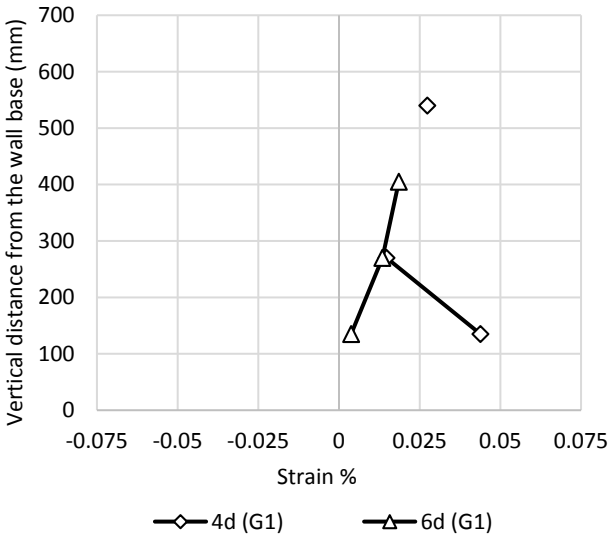

(a)

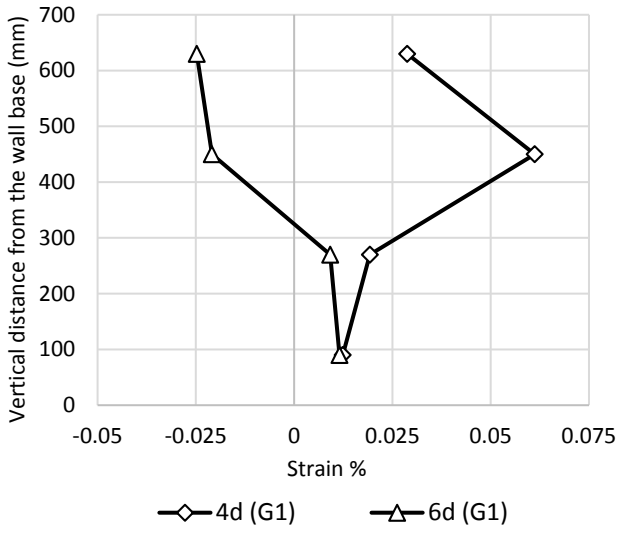

(b)

Figure 5.33 Strains of the geogrid layers at a load of 600 N in: (a) Gauge group (G1) of Group (H2 L3 S2 C1 D23) and (b) Gauge group (G1) of Group (H2 L3 S1 C1 D23).

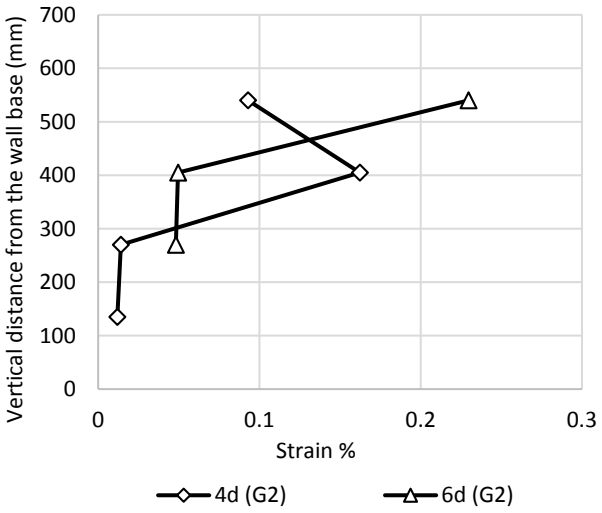

(a)

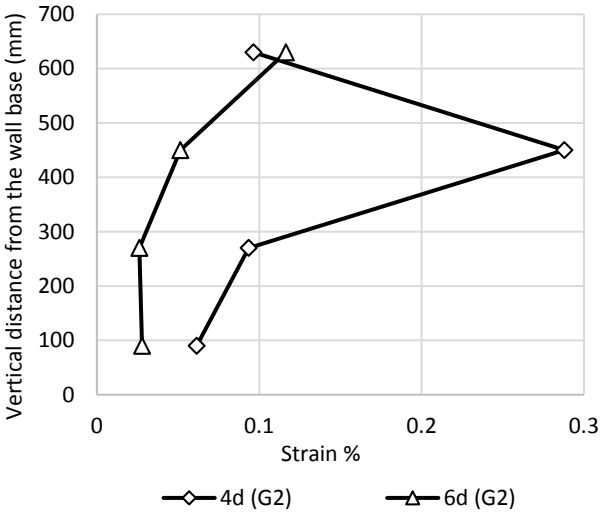

(b)

Figure 5.34 Strains of the geogrid layers at a load of 600 N in: (a) Gauge group (G2) of Group (H2 L3 S2 C1 D23) and (b) Gauge group (G2) of Group (H2 L3 S1 C1 D23).

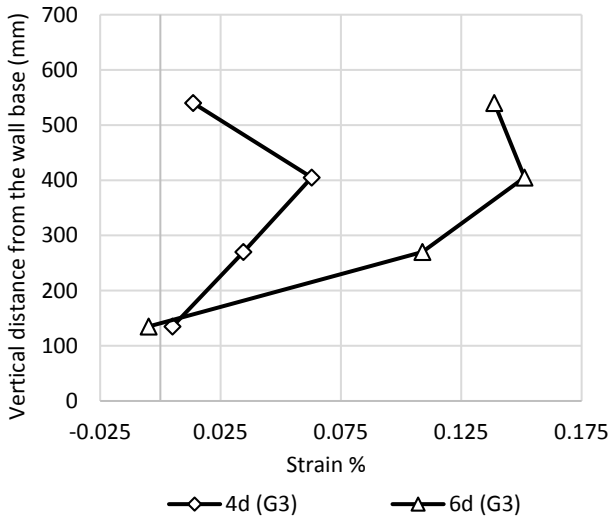

(a)

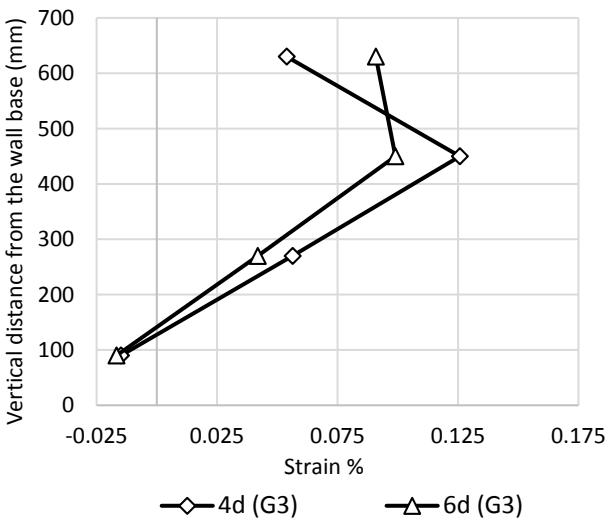

(b)

Figure 5.35 Strains of the geogrid layers at a load of 600 N in: (a) Gauge group (G3) of Group (H2 L3 S2 C1 D23) and (b) Gauge group (G3) of Group (H2 L3 S1 C1 D23).

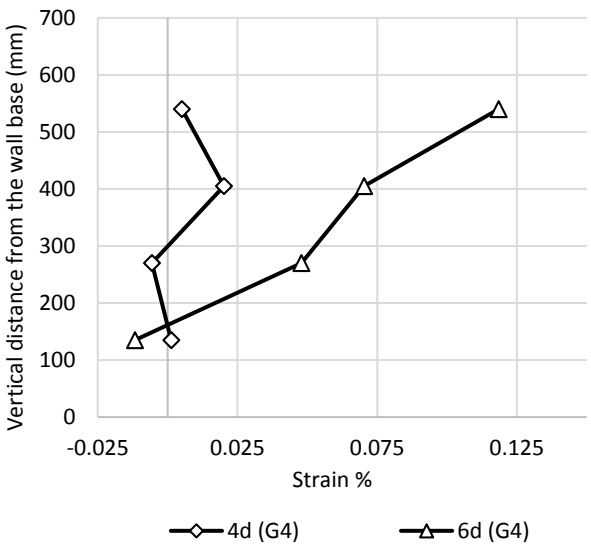

(a)

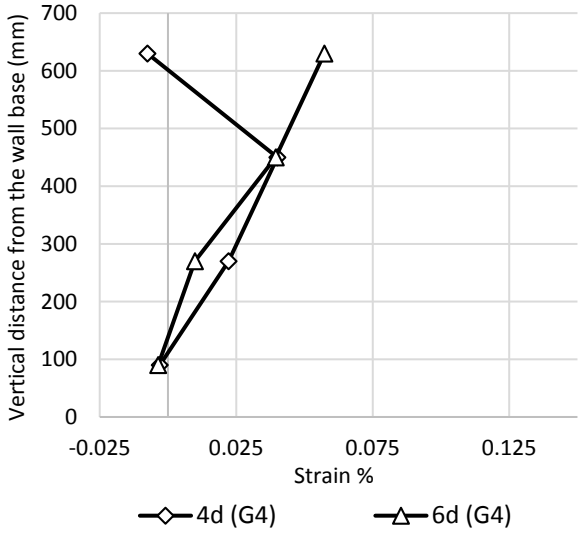

(b)

Figure 5.36 Strains of the geogrid layers at a load of 600 N in: (a) Gauge Group (G4) of group (H2 L3 S2 C1 D23) and (b) Gauge group (G4) of Group (H2 L3 S1 C1 D23).

On the other hand, the strains of gauges groups G1 in Group H2 L3 **S1** C1 D23 were the highest at the pile offset of 4d as shown in Figures 5.33 (b). The same trend applies to the gauge groups G2, G3 and G4 as shown in Figures 5.34 (b), 5.35 and 5.36 (b), respectively. However, the strains of the upmost layer in gauges groups G2, G3 and G4 were low at the pile offset of 4d. In fact, the pressure and the deflection at that location were high. Therefore, the reinforcement layer may experience a pullout failure because of the large wall deflection at that height.

The strain distributions shown in Figures 5.37 and 5.38 depend on the second analysis approach. For the pile offset of 4d, the larger strains were recorded by gauge group G2 in both Groups H2 L3 **S2** C1 D23 and H2 L3 **S1** C1 D23. This gauge group was near the location of the pile at that offset as shown in figure 3.17 (a). Moreover, the highest strains at the pile offset of 6d were recorded by gauge group G3 and G4, but the maximum strains were recorded by gauge group G3. In this case, the pile was located between these two gauge groups as shown in Figure 3.17 (b).

In general, the maximum tensile strains should be higher in the geogrid layers with large reinforcement spacing as mentioned in Set 2. This behavior is shown in Figure 5.38 for the pile offset of 6d while it is not shown in Figure 5.37 for the pile offset of 4d. The reason is due to the long reinforcement length. In fact, the position of the pile at the offset of 4d was near to the wall, and it was not within the high tension zone of the geogrid. On the other hand, the position of the pile at the offset of 6d was in the middle of the reinforcement length. Thus, it was within the high tension zone of the long geogrid layers. Therefore, high strains were induced inside the reinforcement layers due to the lateral deflections of the pile and the wall as well.

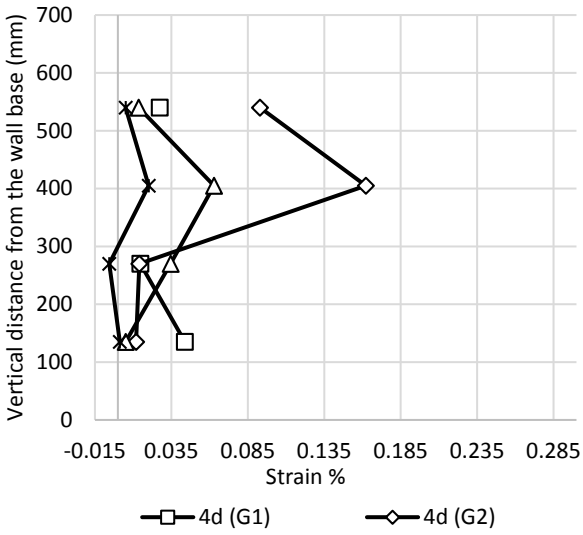

(a)

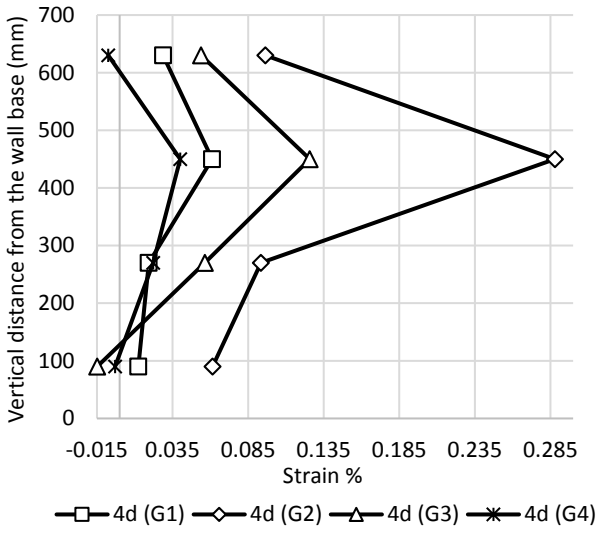

(b)

Figure 5.37 Strains of the geogrid layers at a load of 600 N at: (a) Pile offset (4d) of Group (H2 L3 S2 C1 D23) and (b) Pile offset (4d) of Group (H2 L3 S1 C1 D23).

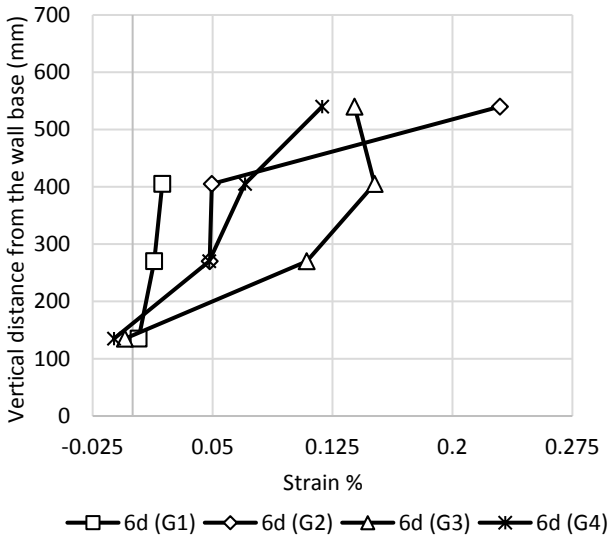

(a)

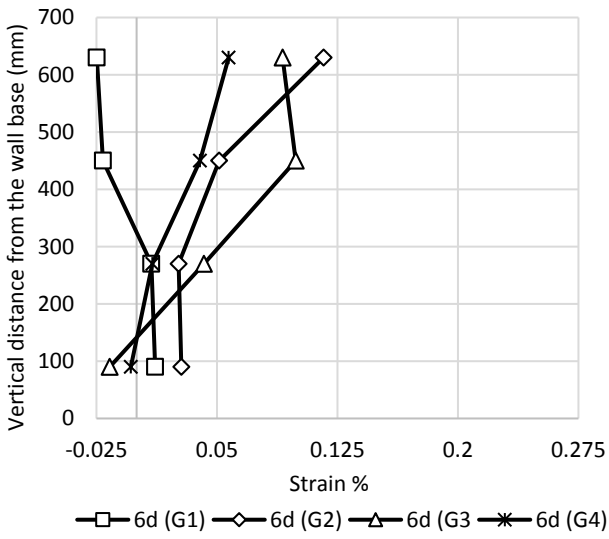

(b)

Figure 5.38 Strains of the geogrid layers at load of 600 N at: (a) Pile offset (6d) of Group (H2 L3 S2 C1 D23) and (b) Pile offset (6d) of Group (H2 L3 S1 C1 D23).

Pressure behind the wall facing.

Figure 5.38 shows the pressure behind of the wall facing along the vertical centerline of Groups H2 L3 **S2** C1 D23 and H2 L3 **S1** C1 D23 while Figure 5.39 presents the transverse distribution of the pressure of the two groups at 65.5% of the wall height. In each group, the pressure behind the wall facing along the vertical centerline of decreased by increasing of the pile offset. Furthermore, the maximum pressures in Group H2 L3 **S2** C1 D23 were higher than those in Group H2 L3 **S1** C1 D23 due to the large spacing between the geogrid layers in the first group.

The behavior of the pressure distribution for Group H2 L3 **S2** C1 D23 is similar to that of Set 2. At the small pile offset, the maximum pressures occurred at 65.5% of the wall height as shown in Figure 5.38 (a). By reducing the reinforcement spacing in Group H2 L3 **S1** C1 D23, the location of the maximum pressure for the small pile offset moved to higher than 65.5% of the wall as shown in Figure 5.38 (b). The soil resistance to the lateral pile deflection increased by a decrease of the spacing between the reinforcement layers. Therefore, the pile deflected at an elevation near the top surface of the wall more than that at the lower elevation. Thus, the induced pressures increased behind the wall facing at an elevation of higher than 65.5% of the wall height.

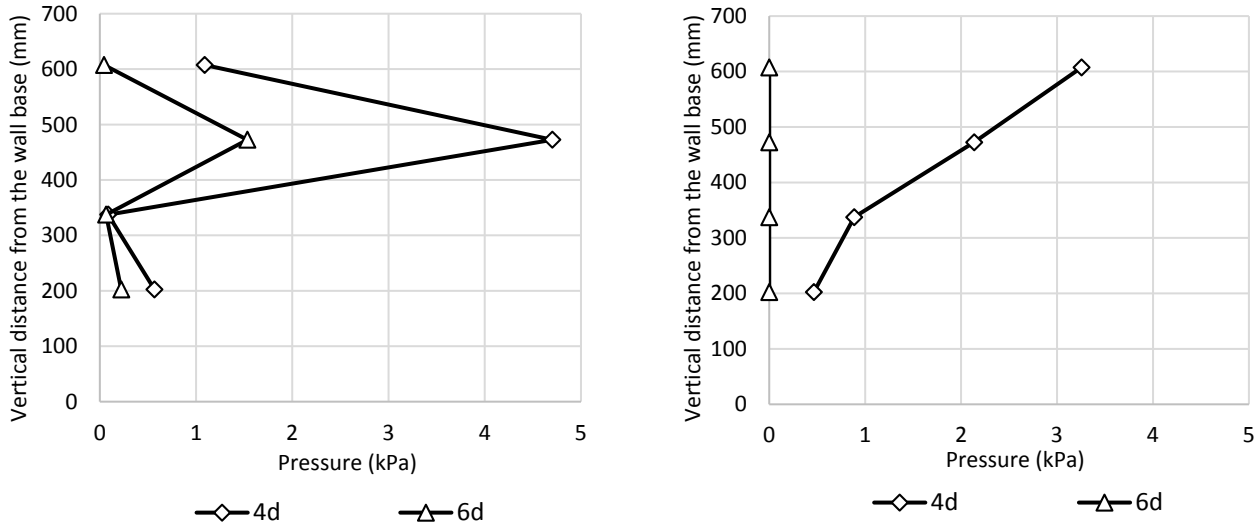

Figure 5.39 Pressures behind the wall facing at a load of 600 N in: (a) Group (H2 L3 S2 C1 D23) and (b) Group (H2 L3 S1 C1 D23).

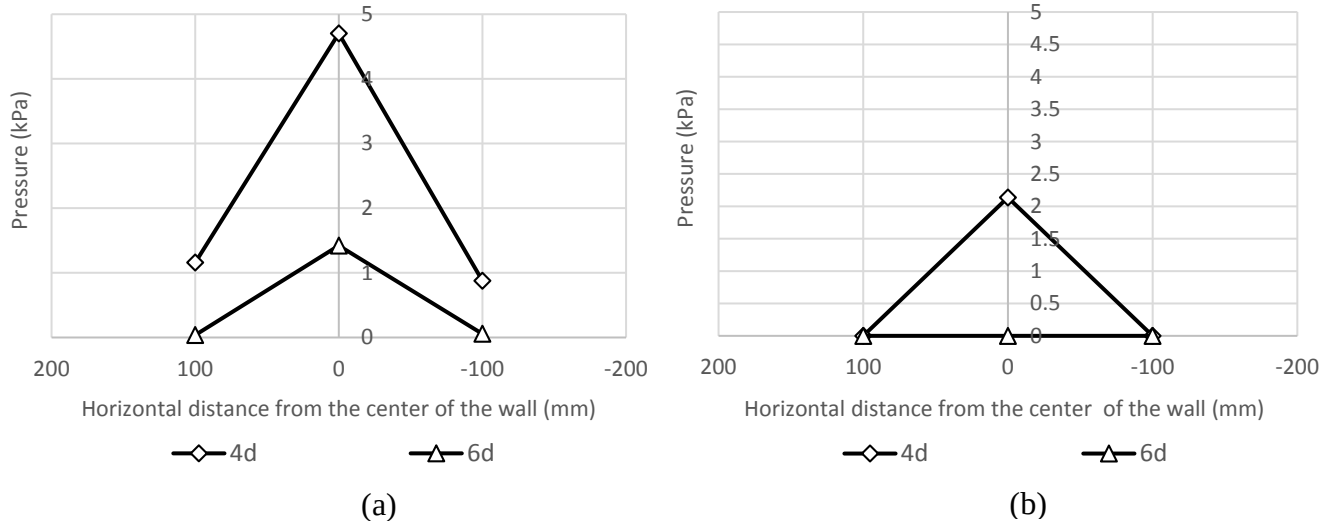

Figure 5.40 Transverse distribution of the pressures at 65.5% of the wall height and a load of 400 N in: (a) Group (H2 L3 S2 C1 D23) and (b) Group (H2 L3 S1 C1 D23).

5.3.2. Reinforcement length

Three comparison sets were organized and analyzed to investigate the effect of the length of the geogrid layers. The first set is Set 4, which includes the large spacing of 135 mm with mechanical connection between the wall facing and the reinforcement. The second set is Set 5. This set includes the small spacing of 90 mm with mechanical connection. The final set is Set 6. The spacing between the geogrid layers in this set was equal to 90 mm, and the connection was frictional connection.

Set 4 High wall with large reinforcement spacing and mechanical connection

Table 5.5 presents the parameter information of the two groups that are analyzed in this set.

Table 5.4 Detials of Set 4

Tests	Ultimate Lateral Load N	Wall Height H, mm	Layer length L, mm	Layer spacing S, mm	Offset D, mm	Connection Type	Group designation
H2 L2 S2 C1 D2	335	720	504	135	254 (4d)	Mechanical	Category 1 of Group 2 or H2 **L2** S2 C1 D23
H2 L2 S2 C1 D3	430				381 (6d)		
H2 L3 S2 C1 D2	405	720	900	135	254 (4d)		Category 1 of Group 3 or H2 **L3** S2 C1 D23
H2 L3 S2 C1 D3	473				381 (6d)		

The lateral pile deflections in Group H2 **L2** S2 C1 D23 are shown in Figure 5.41 (a). On the other hand, the lateral pile deflections in Group H2 **L3** S2 C1 D23 are shown in Figure 5.41 (b).

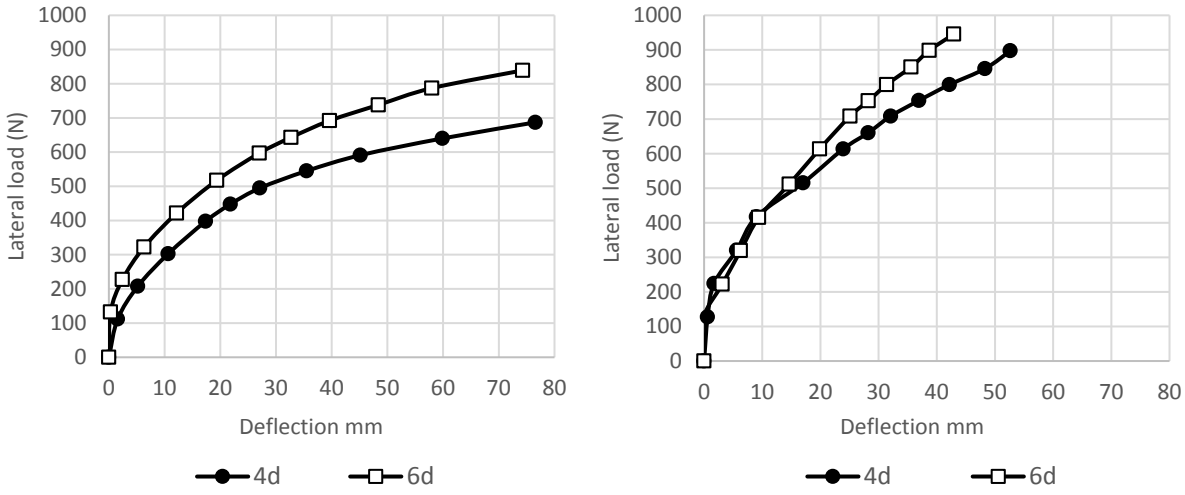

(a) (b)

Figure 5.41 Load-Displacement curves of Set 4: (a) Group (H2 L2 S2 C1 D23) and (b) Group (H2 L3 S2 C1 D23).

For each group, the ultimate lateral load capacities of the pile increased by an increase of the pile offset. Furthermore, the length of the geogrid layers decreased from 504 mm in the tests of Group H2 **L2** S2 C1 D23 to 900 mm in the tests of Group H2 **L3** S2 C1 D23. This decrease caused an increase in the pile capacities by approximately 21% and 16% at pile offsets of 4d and 6d, respectively. However, the chosen comparison load for this set was equal to 400 N, and all data of the two groups were analyzed at this load.

Deflection of wall facing

The deflection distributions of the wall facing along the vertical centerline for the tests of Groups H2 L2 S2 C1 D23 and H2 L3 S2 C1 D23 are shown in Figure 5.42. In each group, the deflections of the wall facing increased by a decrease of the pile offset.

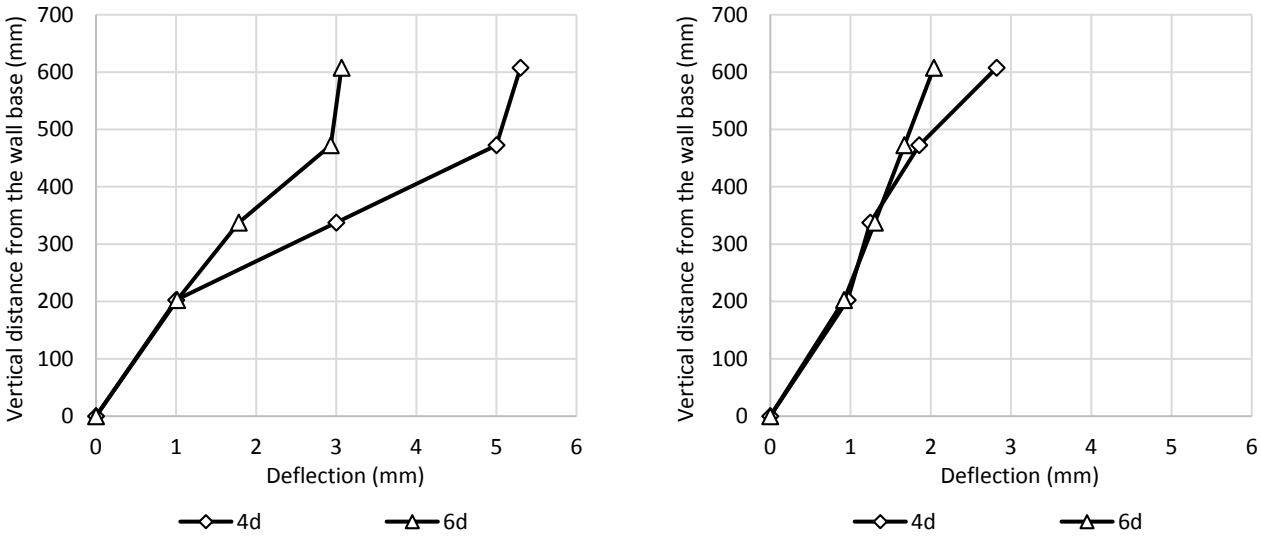

(a) (b)

Figure 5.42 Deflections of the wall facing along the vertical centerline at a load of 400 N in: (a) Group (H2 L2 S2 C1 D23) and (b) Group (H2 L3 S2 C1 D23).

Figure 5.41 shows that the maximum deflections occurred at 84% of the wall height. At the pile offset of 4d, the maximum deflections of the tests of Group H2 L2 S2 C1 D23 were larger than those of the tests of Group H2 L3 S2 C1 D23. The same behavior applies to the pile offset of 6d. Thus, the increase in the length of geogrid layer caused more resistance to the wall deflection. This behavior is also shown in the transverse deflections of the wall for the two groups in Figure 5.43. In addition, more uniform deflection is shown in this figure with the pile offset of 6d because the pile was far from the wall facing.

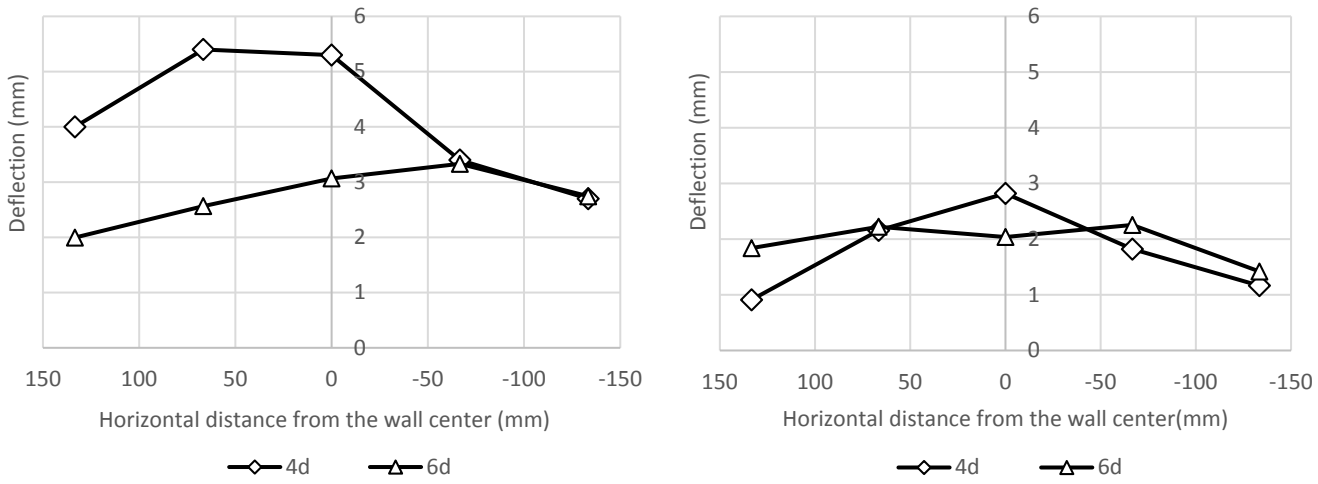

(a) (b)

Figure 5.43 Transverse distributions of the wall deflections at 84% of the wall height and a load of 400 N in: (a) Group H2 L2 S2 C1 D23 and (b) Group H2 L3 S2 C1 D23.

Strain, stress, and moment of the pile

For both sides of the pile, the maximum strains were almost the same at the two pile offsets of Group H2 **L2** S2 C1 D23 as shown in Figure 5.44 (a). By increasing the reinforcement length in Group H2 **L3** S2 C1 D23, the pile faced more resistance from the geogrid layers in addition to the increased resistance from the soil mass in front of the pile. Thus, the maximum strains at the pile offset of 6d became larger especially on the compressive side as shown in Figure 5.44 (b).

The maximum strains in the compressive and tensile sides of the pile occurred at an elevation equal to 44% of the pile height for Group H2 **L2** S2 C1 D23. At the comparison load of 400 N, the locations of the maximum strains on the tensile side of the pile of Group H2 **L3** S2 C1 D23 were higher than 44% of the wall height. However, this location returned to the regular height by increasing the loading step as shown in Figure A.146 in Appendix A. Figures 5.45 and 5.46 for the stress and moment show the same trend as Figure 5.44.

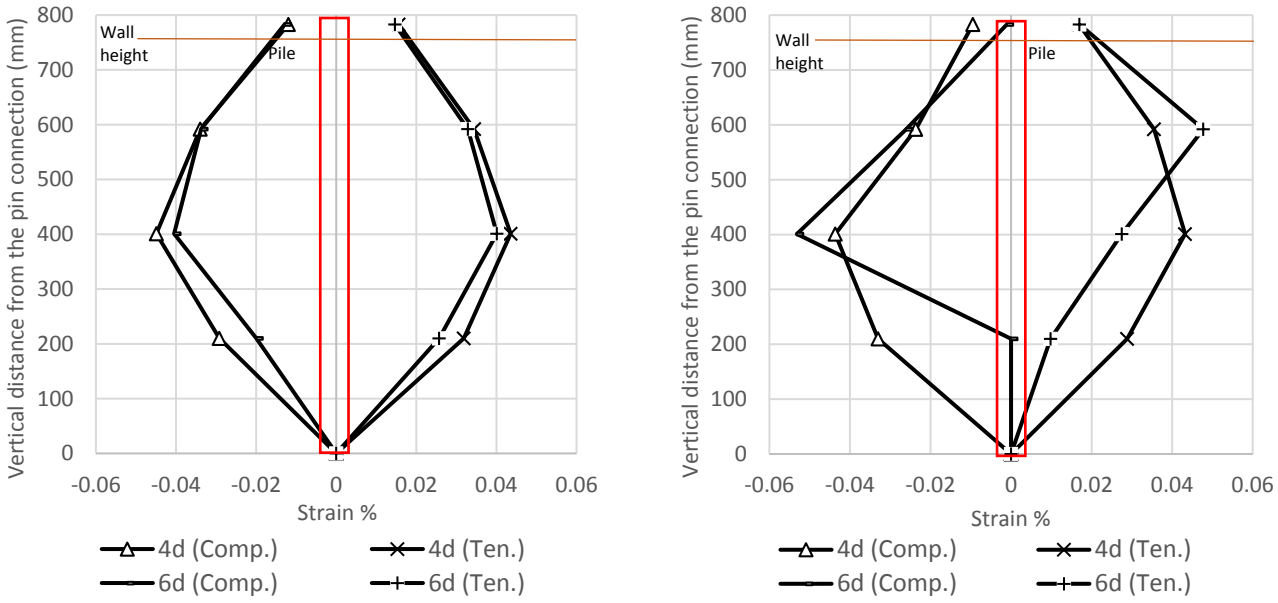

(a) (b)

Figure 5.44 Strains of the laterally loaded pile at a load of 400 N in: (a) Group (H2 L2 S2 C1 D23) and (b) Group (H2 L3 S2 C1 D23).

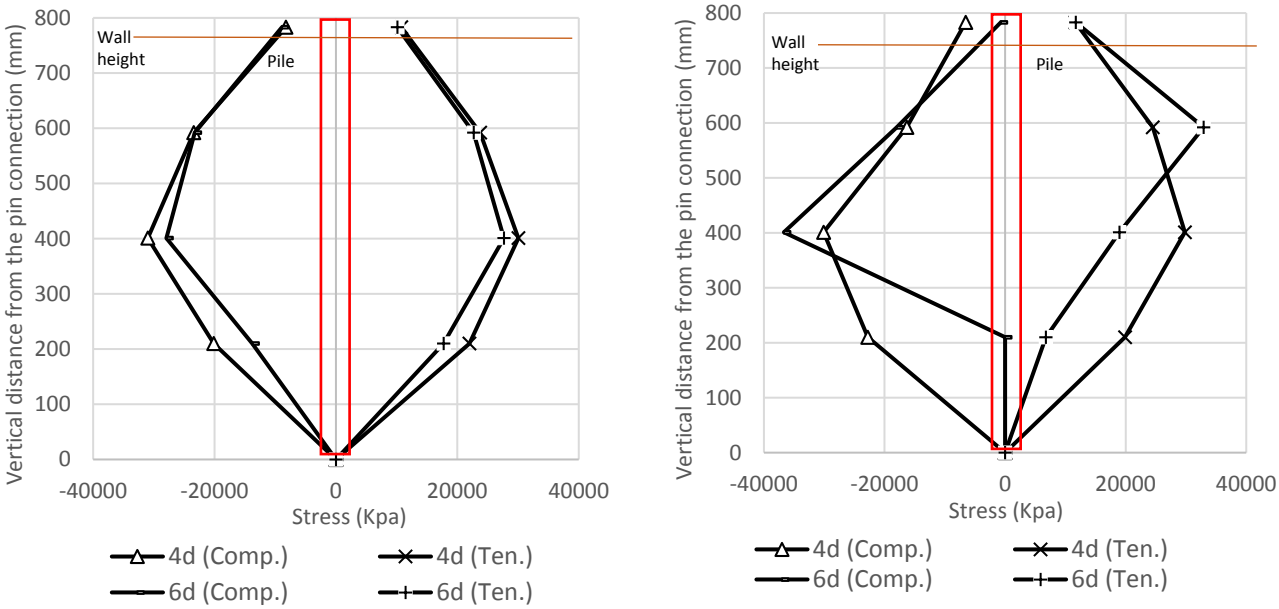

(a) (b)

Figure 5.45 Stresses of the laterally loaded pile at a load of 400 N in: (a) Group (H2 L2 S2 C1 D23) and (b) Group (H2 L3 S2 C1 D23).

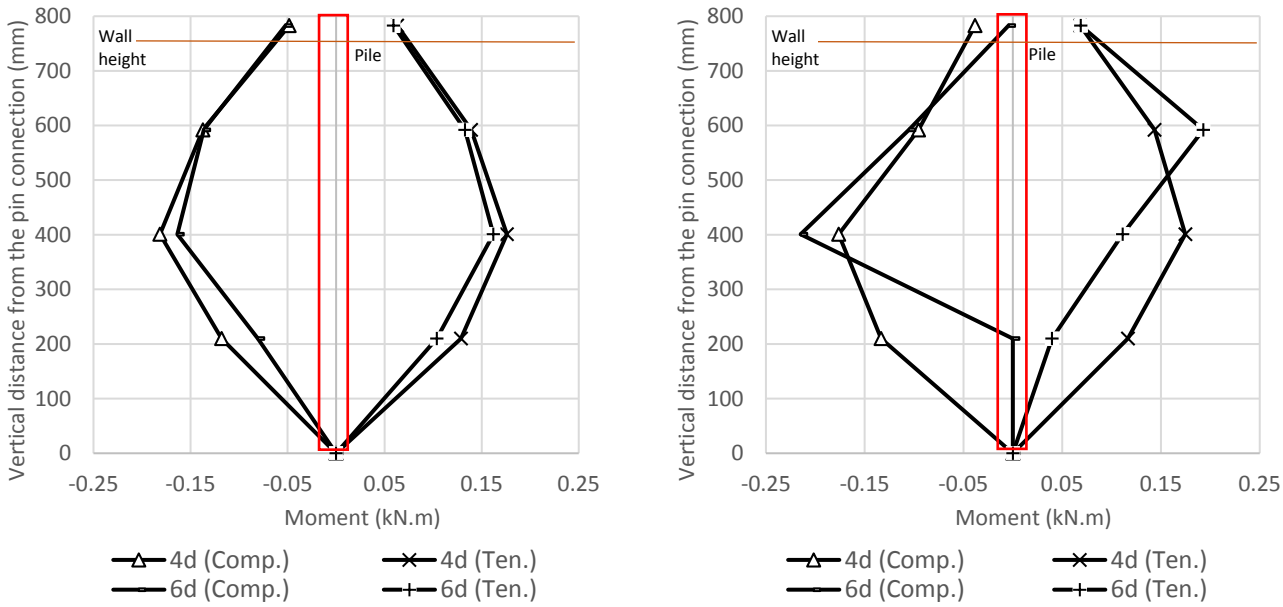

(a) (b)

Figure 5.46 Moments of the laterally loaded pile at a load of 400 N in: (a) Group (H2 L2 S2 C1 D23) and (b) Group (H2 L3 S2 C1 D23).

Strain of the geogrid

Figures 5.47, 5.48, 5.49, and 5.50 show the strain analysis by using the first analysis approach. On the other hand, Figures 5.51, and 5.52 show the strain distributions by using the second analysis approach.

For Group H2 **L2** S2 C1 D23, the pile location at the pile offset of 4d was at the same location of gauges group G3, and between gauges groups G2 and G4. Therefore, the strain distributions were the highest at the pile offset of 4d as shown in Figures 5.47 (a), 5.48 (a), 5.49 (a) and 5.50 (a).

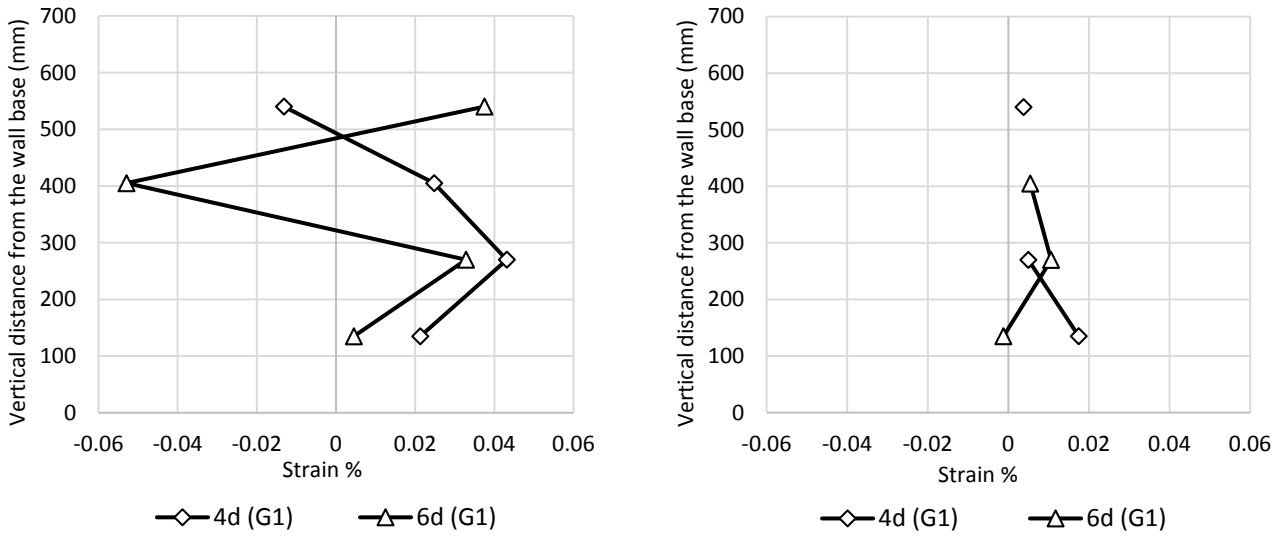

(a) (b)

Figure 5.47 Strains of the geogrid layers at a load of 400 N: (a) Gauges group (G1) of Group (H2 L2 S2 C1 D23) (b) Gauges group (G1) of Group (H2 L3 S2 C1 D23).

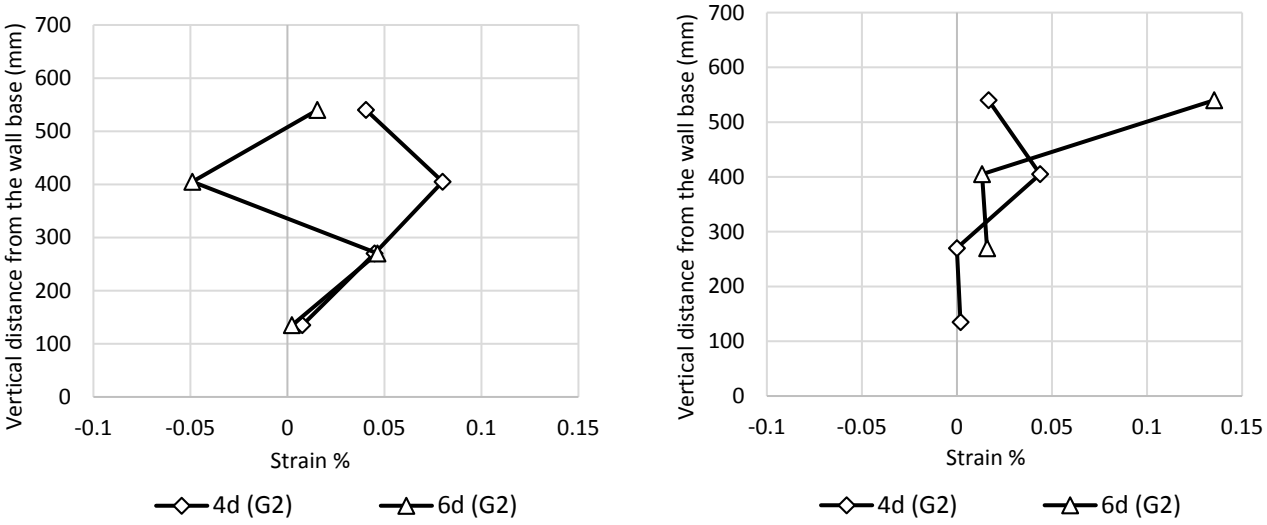

(a) (b)

Figure 5.48 Strains of the geogrid layers at a load of 400 N: (a) Gauges group (G2) of Group (H2 L2 S2 C1 D23) (b) Gauges group (G2) of Group (H2 L3 S2 C1 D23).

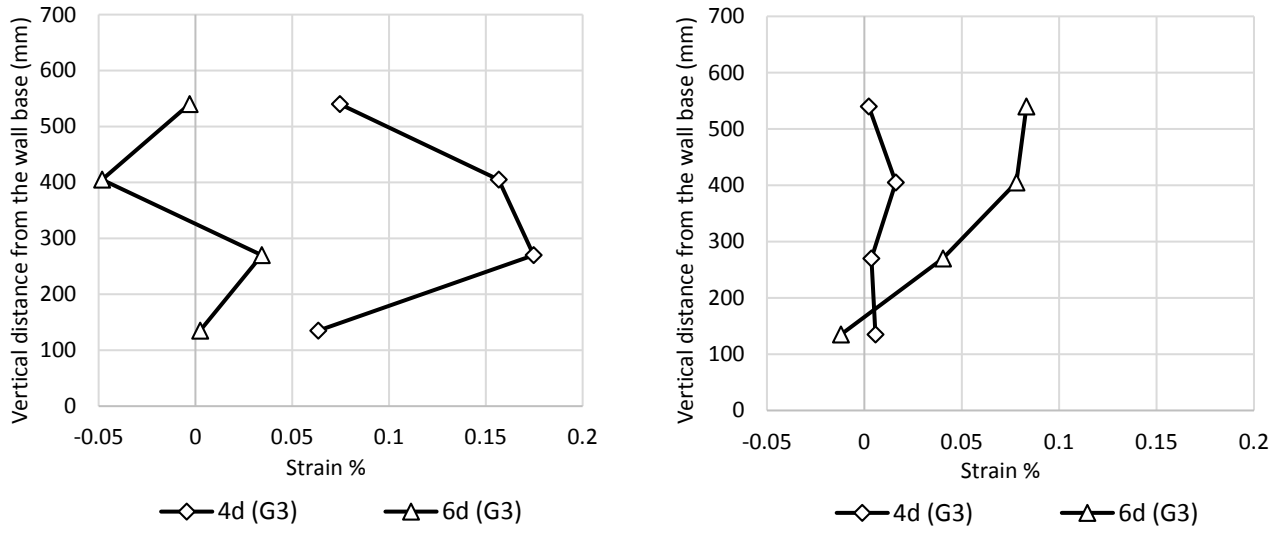

(a) (b)

Figure 5.49 Strains of the geogrid layers at a load of 400 N: (a) Gauges group (G3) of Group (H2 L2 S2 C1 D23) (b) Gauges group (G3) of Group (H2 L3 S2 C1 D23).

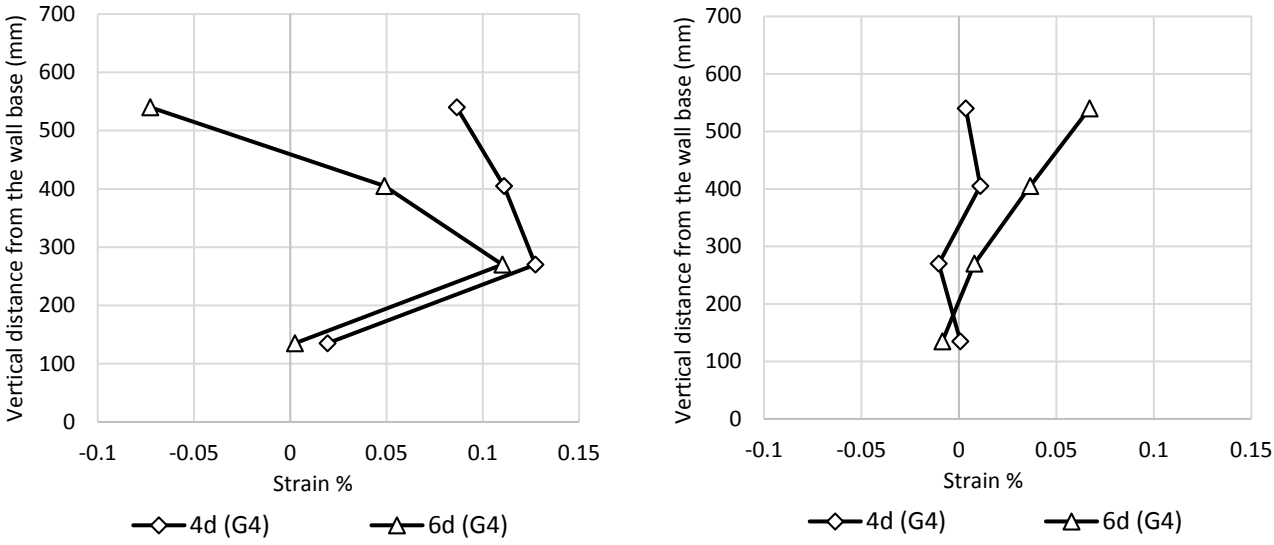

(a) (b)

Figure 5.50 Strains of the geogrid layers at a load of 400 N: (a) Gauges group (G4) of Group (H2 L2 S2 C1 D23) (b) Gauges group (G4) of Group (H2 L3 S2 C1 D23).

For Group H2 **L3** S2 C1 D23, The strain distributions of gauges group G1 was low for the two pile offsets as shown in Figure 5.47 (b) . On the other hand, the pile location at (6d) was between gauges groups G2 and G4. Thus, the strain distributions of the gauges groups G2, G3, and G4 were the highest at the pile offset of 6d as shown in Figures 5.48 (b), 5.49 (b) and 5.50 (b), respectively.

Because the two groups of this set have different reinforcement length, the strain distributions at each pile offset depend on the pile proximity to position of each gauges group. Thus, Figure 5.51 and 5.52 show the order of strain distributions of the tests of the two groups of this set based on the pervious reason. From Figure 5.51 (a), the strain distributions of gauges groups G3 and G4 were the higher because the pile location was beside G3 and in front of G4 at the offset of 4d. From Figure 5.52 (b), the strain distributions of gauges groups G2 and G3 were the higher because the pile location was beside G2 and in front of G3 at the offset of 4d. The same trend is observed for the strain distributions of the two groups at the offset of 6d as shown in Figure 5.52.

At the pile offset of 4d, the maximum tensile strain of all gauges groups of Group H2 **L2** S2 C1 D23 were higher than the corresponding maximum tensile strain of Group H2 **L3** S2 C1 D23 as shown in Figure 5.51. In fact, the pile at the offset of 4d is located within the high tension strain zone of the geogrid layers with regular length. As a result, the lateral load from the pile causes more strain in the geogrid layers. On the other hand, the strain distribution of Group H2 **L3** S2 C1 D23 increased by an increase of the pile offset from 4d to 6d as shown in Figure 5.51 (b) and 5.52 (b). The reason is that the pile location at the offset of 6d was within the high tension zone of the long geogrid layers.

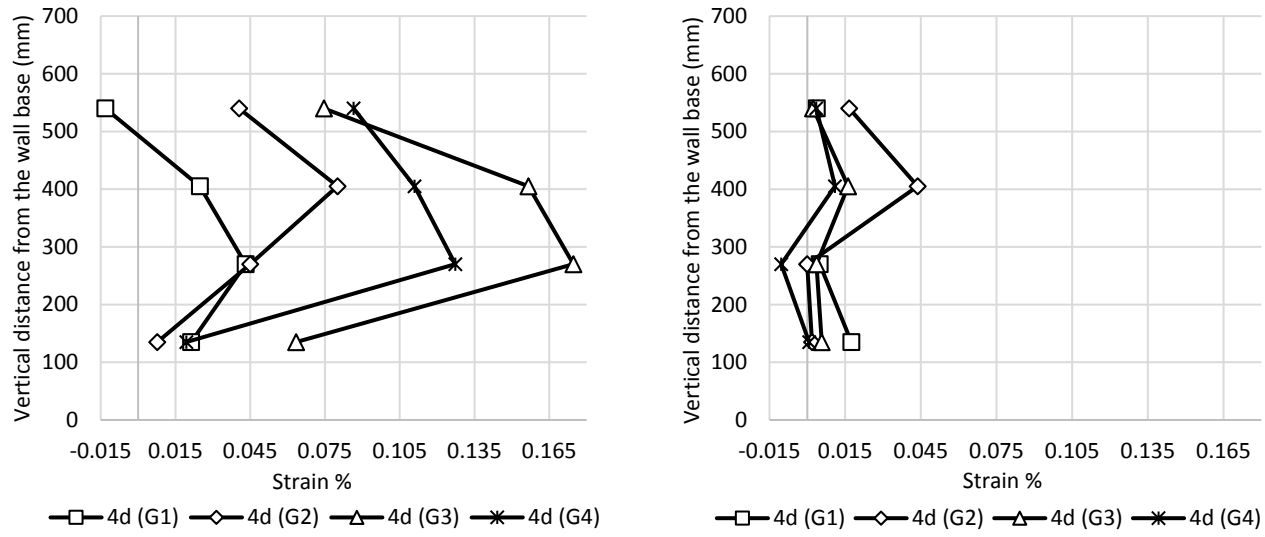

(a) (b)

Figure 5.51 Strains of the geogrid Layers at a load of 400 N: (a) Pile offset (4d) of Group (H2 L2 S2 C1 D23) (b) Pile offset (4d) of Group (H2 L3 S2 C1 D23).

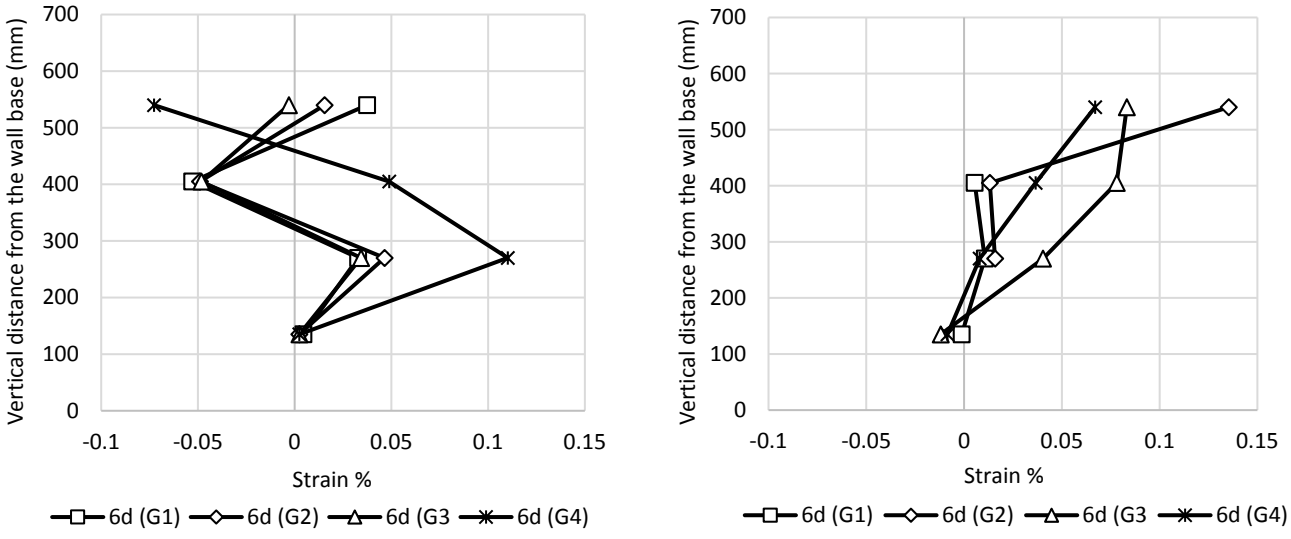

(a) (b)

Figure 5.52 Strains of the geogrid layers at a load of 400 N: (a) Pile offset (6d) of Group (H2 L2 S2 C1 D23) (b) Pile offset (6d) of Group (H2 L3 S2 C1 D23).

Pressure behind the wall facing

Figure 5.53 shows the pressure distribution behind the wall facing along the vertical centerline in Groups H2 **L2** S2 C1 D23 and H2 **L3** S2.C1 D23. Two high-pressure zones are shown in Figure 5.53 (a) while only one high-pressure zone at 65.5% of the wall height is shown in Figure 5.53 (b). Thus, the pressures at the bottom of the wall increased by reducing the length of the geogrid layers when the pile offset was large. However, at each corresponding pile offset, the maximum pressure of the tests of Group H2 **L3** S2 C1 D23 was higher than that of the tests of Group H2 **L2** S2 C1 D23 because longer reinforcement reduced wall facing deflection so that the earth pressure was increased.

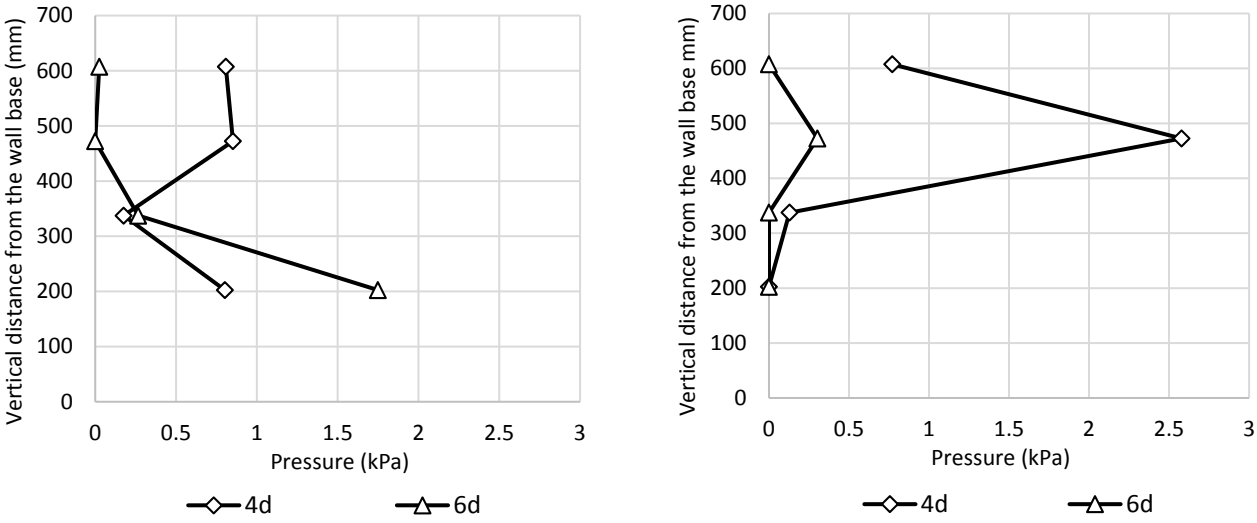

(a) (b)

Figure 5.53 Pressures behind the wall facing at a load of 400 N in: (a) Group H2 L2 S2 C1 D23 and (b) Group H2 L3 S2 C1 D23.

Figure 5.54 presents the transverse distribution of the pressure of Groups H2 **L3** S2 C1 D23 and H2 **L3** S C1 D23 at 65.5% of the wall height. This Figure shows the position of the

maximum pressure and the behavior of the transverse pressure distribution in each group. In fact, this distribution becomes more uniform by increasing of the pile offset.

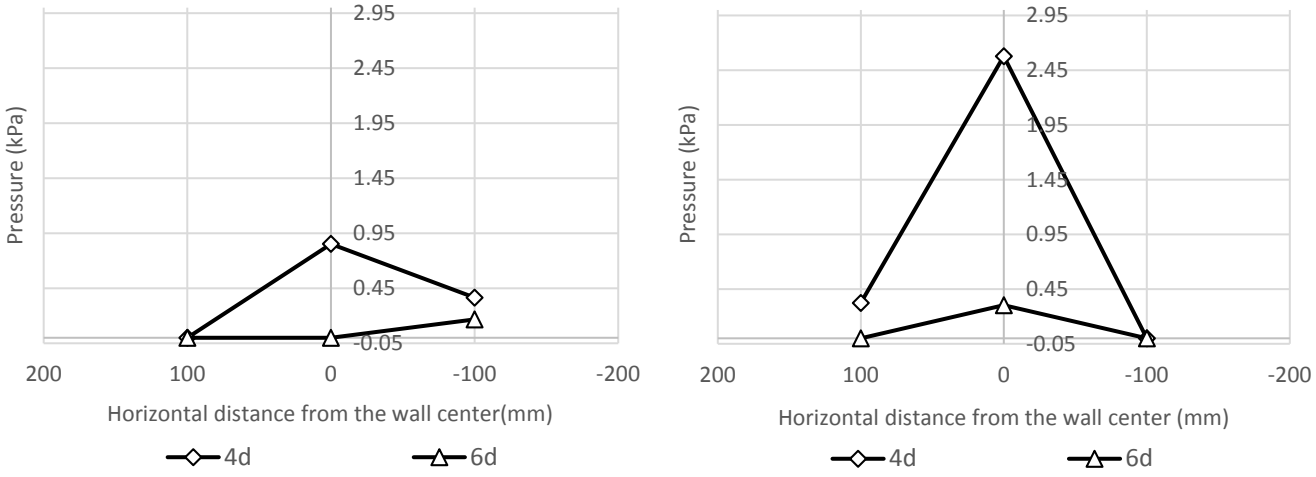

Figure 5.54 Transverse distribution of the pressure at 65.5% of the wall height and a load of 400 N: (a) Group H2 L2 S2 C1 D23 (b) Group H2 L3 S2 C1 D23.

Set 5 High wall with small reinforcement spacing and mechanical connection

Table 5.6 presents the information about the parameters of the two groups that were analyzed in this set. The load deflection curves of the tests of Groups H2 **L2** S1 C1 D23 and H2 **L3** S1 C1 D23 are shown in Figures 5.55.

Table 5.5 Details of Set 5

Tests	Ultimate Lateral Load N	Wall Height H, mm	Layer length L, mm	Layer spacing S, mm	Offset D, mm	Connection Type	Comparison Groups
H2 L2 S1 C1 D2	405	720	504	90	254 (4d)	Mechanical	Category 2 of Group 2 or H2 **L2** S1 C1 D23
H2 L2 S1 C1 D3	504				381 (6d)		
H2 L3 S1 C1 D2	660	720	900	90	254 (4d)		Category 2 of Group 3 or H2 **L3** S1 C1 D23
H2 L3 S1 C1 D3	890				381 (6d)		

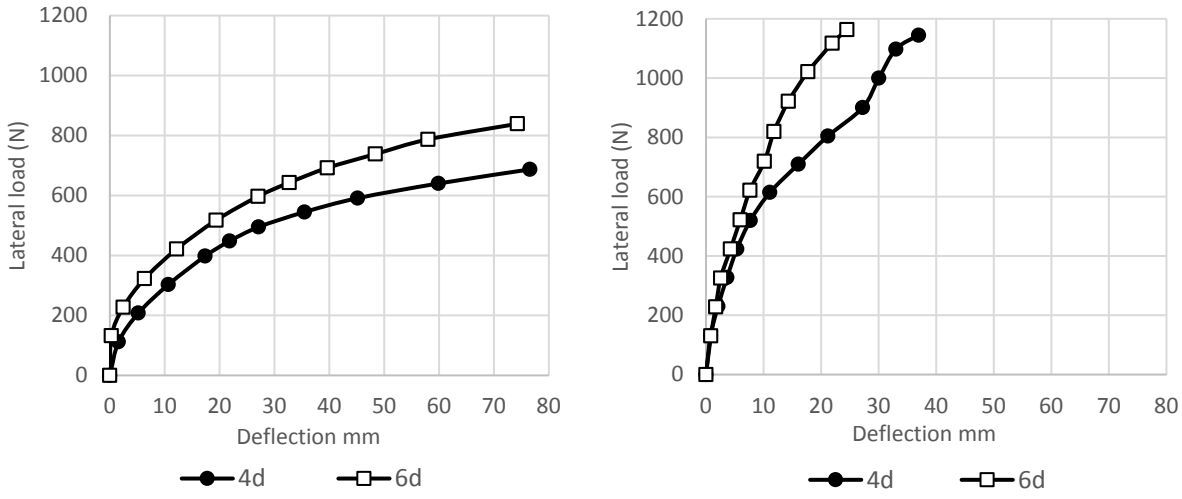

(a) (b)

Figure 5.55 Load -Displacement curves of Set 5: (a) Group (H2 L2 S1 C1 D23) and (b) Group (H2 L3 S1 C1 D23).

The load-displacement behavior of the groups of this set is similar to the load-displacement behavior that shown in Set 4. The reinforcement length of Group H2 **L2** S1 C1 D23 is equal to 504 mm while The reinforcement length of Group H2 **L3** S1 C1 D23 is equal to 900 mm. This increase in the reinforcement length causes increasing in the pile capacity by 63% and 76.5% at pile offsets of 4d and 6d, respectively. A load of 600 N is chosen to analyze the data of the two groups of this section.

Deflection of wall facing

The deflection distributions at the vertical centerline of the wall facing of Group H2 **L2** S C1 D23 and Group H2 **L3** S1 C1 D23 are shown in Figure 5.56. On the other hand, the distributions of the transverse deflection of the wall for the two groups are shown in figure 5.57. The behavior of the deflection distribution at the vertical centerline and cross-section of the wall is similar to the behavior that shown in Set 4.

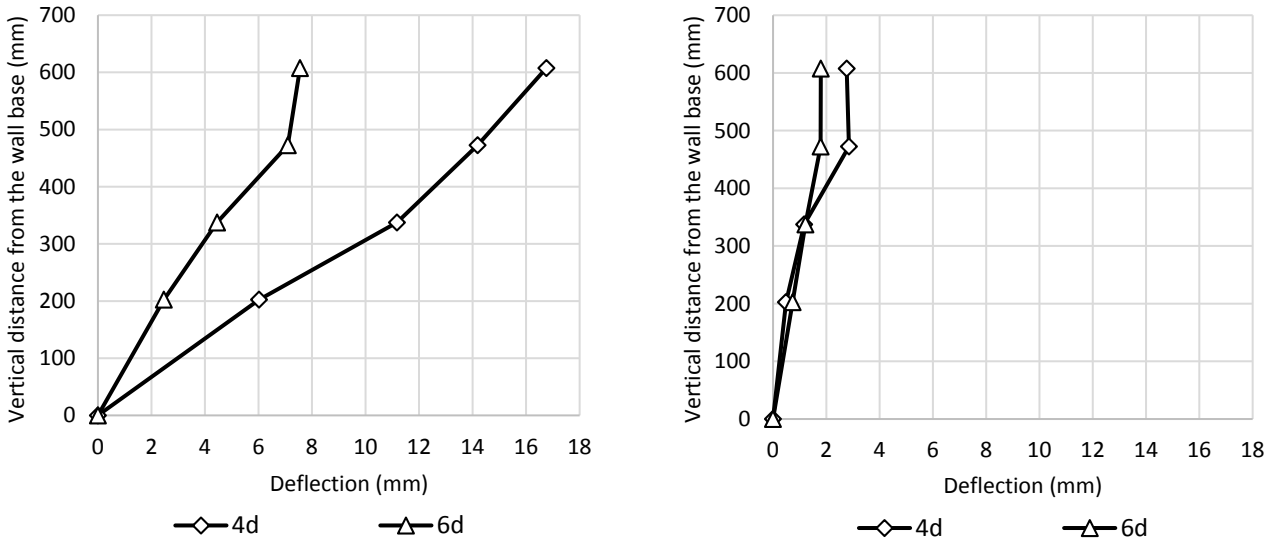

(a) (b)

Figure 5.56 Deflections of the wall facing along the vertical centerline at a load of 600 N in: (a) Group (H2 L2 S1 C1 D23) and (b) Group (H2 L3 S1 C1 D23).

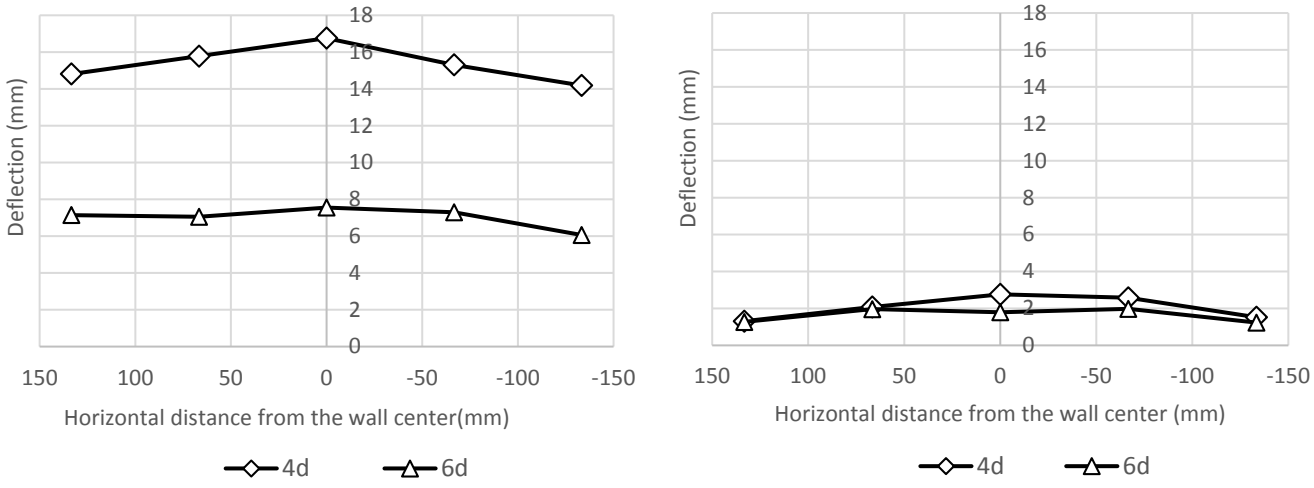

(a) (b)

Figure 5.57 Transverse distributions of the wall deflections at 84% of the wall height and a load of 600 N in: (a) Group (H2 L2 S1 C1 D23) and (b) Group (H2 L3 S1 C1 D23).

Strain, Stress, and moment of the pile

The strain, stress, and moment along the pile are shown in Figures 5.58, 5.59, and 5.60, respectively. Their behaviors are similar to the behavior that are shown in tests of Set 4. For all tests of the two groups, the maximum strain in the two side occurs at 44% of the pile height. From Figure 5.58 (b), the maximum compressive and tensile strains at the pile offset of 6d) were higher than the maximum compressive and tensile strains at the pile offset of 4d. The reason behind this differences the increasing of the soil resistance due to the increasing of the soil mass in front of the deflected pile. Also, the small spacing and the long reinforcement have an important rule to increase the soil resistance.

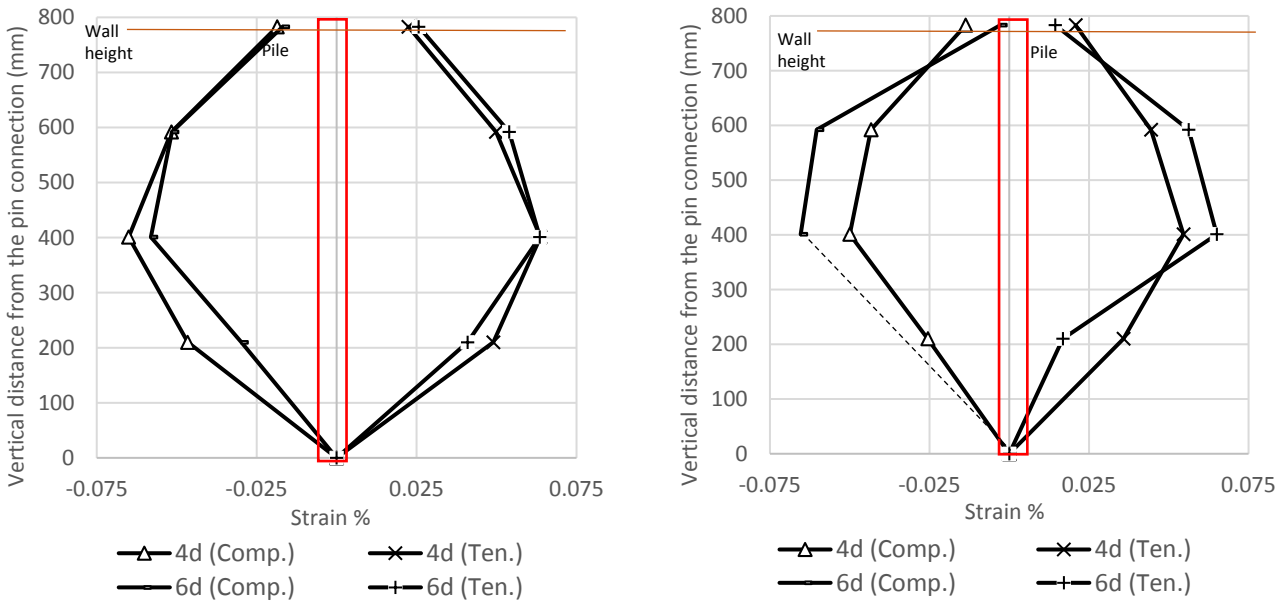

(a) (b)

Figure 5.58 Strains of the laterally loaded pile at a load of 600 N in: (a) Group (H2 L2 S1 C1 D23) and (b) Group (H2 L3 S1 C1 D23).

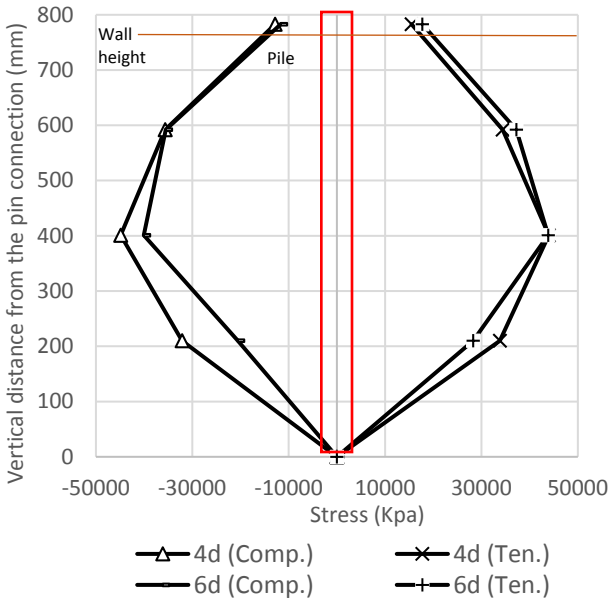

(a)

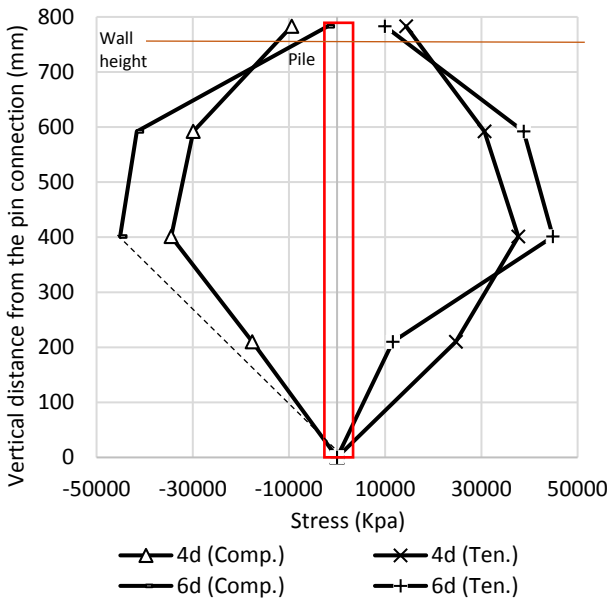

(b)

Figure 5.59 Stresses of the laterally loaded pile at a load of 600 N in: (a) Group (H2 L2 S1 C1 D23) and (b) Group (H2 L3 S1 C1 D23).

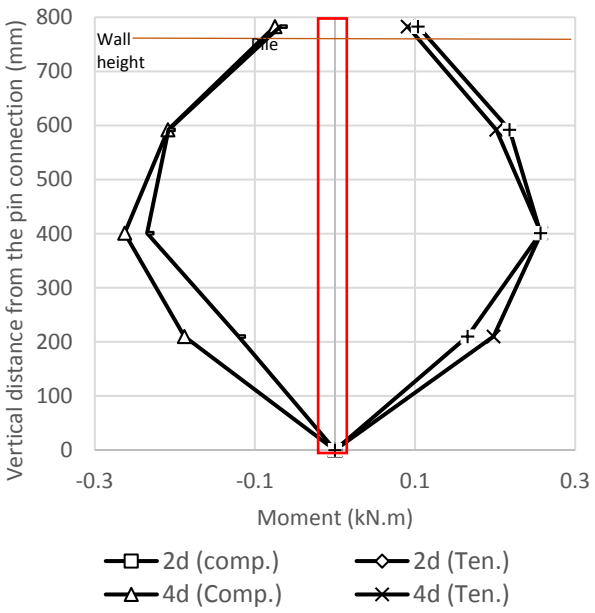

(a)

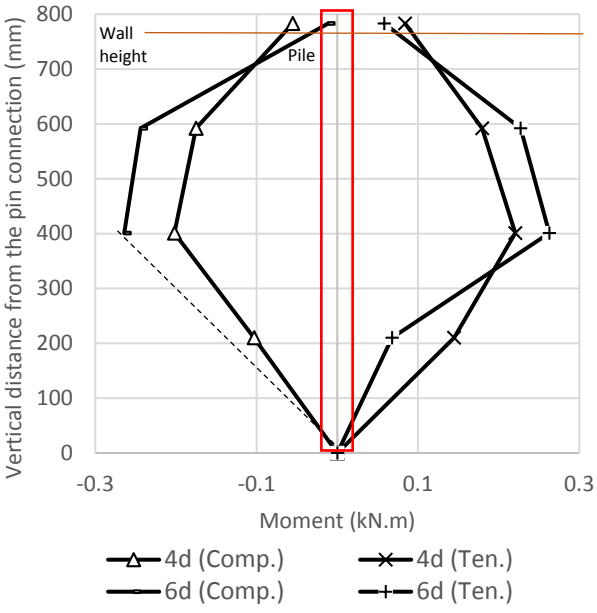

(b)

Figure 5.60 Moments of the laterally loaded pile at a load of 600 Nin: (a) Group (H2 L2 S1 C1 D23) and (b) Group (H2 L3 S1 C1 D23).

Strain of the geogrid

The same two analysis approaches are used in this set. Figures 5.61, 5.62, 5.63, and 5.64 show the strain by using the first analysis approach. On the other hand, Figures 5.65, and 5.66 show the strain by using the second analysis approach.

The gauges groups of the tests of this set have the same position as the gauges groups of the tests of Set 4. Therefore, the behavior of the strain distribution of the two groups of this set is similar to the behavior of the strain distribution of Set 4. However, the spacing between the geogrid layers of the test of the set was smaller than it in the tests of Set 4. As a result, the strain distribution of Group H2 **L2** S1 C1 D23 decreased and the strain distribution of Group H2 **L3** S1 C1 D23 increased at the pile offset of 4d as shown in the figures below.

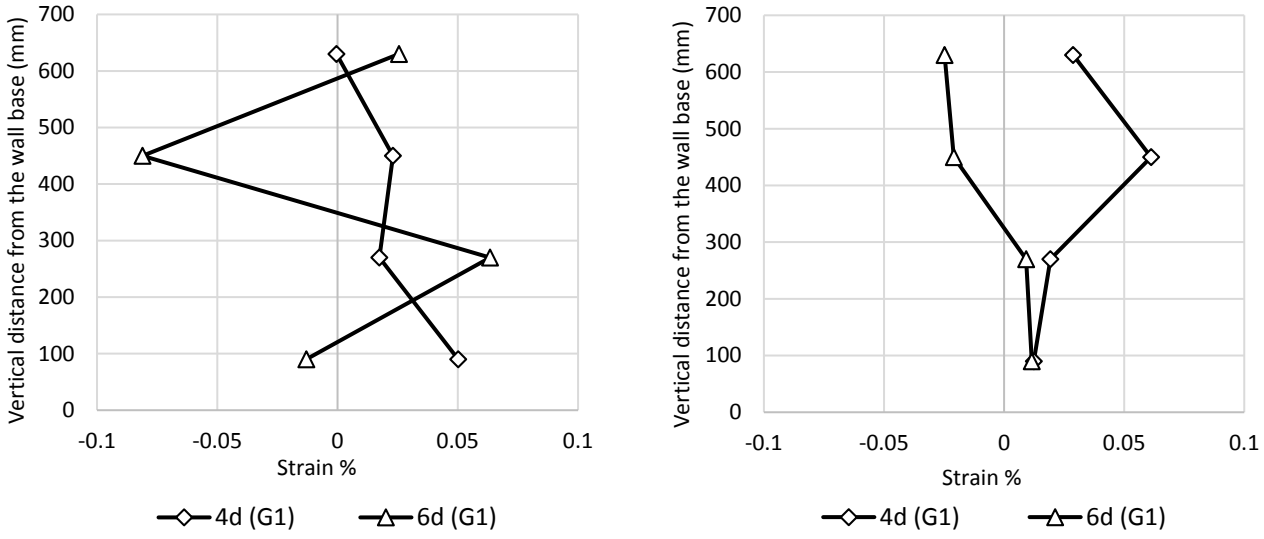

(a) (b)

Figure 5.61 Strains of the geogrid layers at a load of 600 N in: (a) Gauges group (G1) of Group (H2 L2 S1 C1 D23) and (b) Gauges group (G1) of Group (H2 L3 S1 C1 D23).

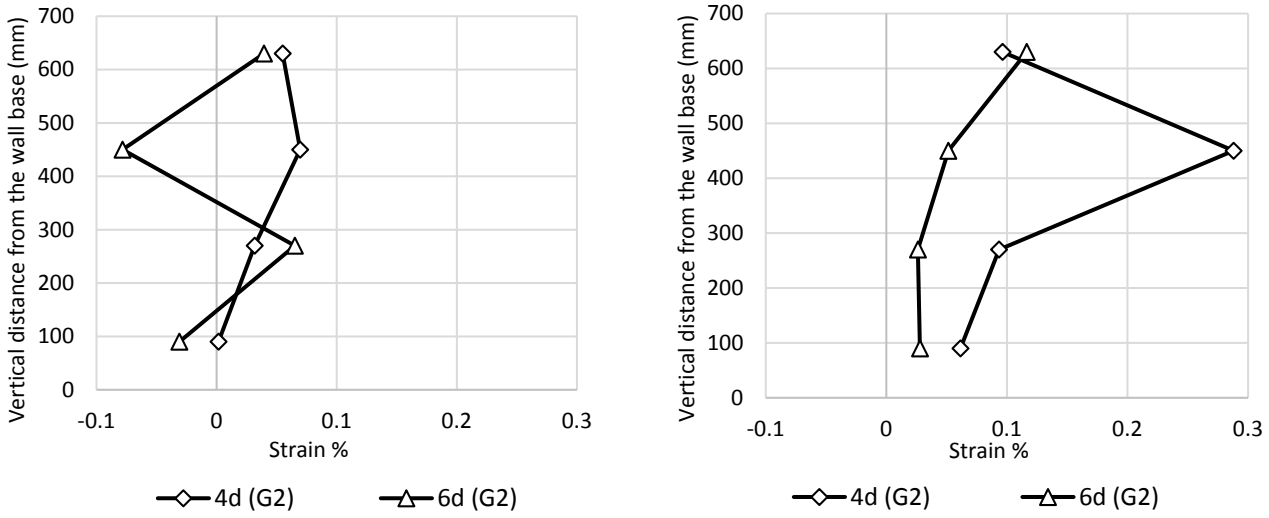

(a) (b)

Figure 5.62 Strains of the geogrid layers at a load of 600 N in: (a) Gauges group (G2) of Group (H2 L2 S1 C1 D23) and (b) Gauges group (G2) of Group (H2 L3 S1 C1 D23).

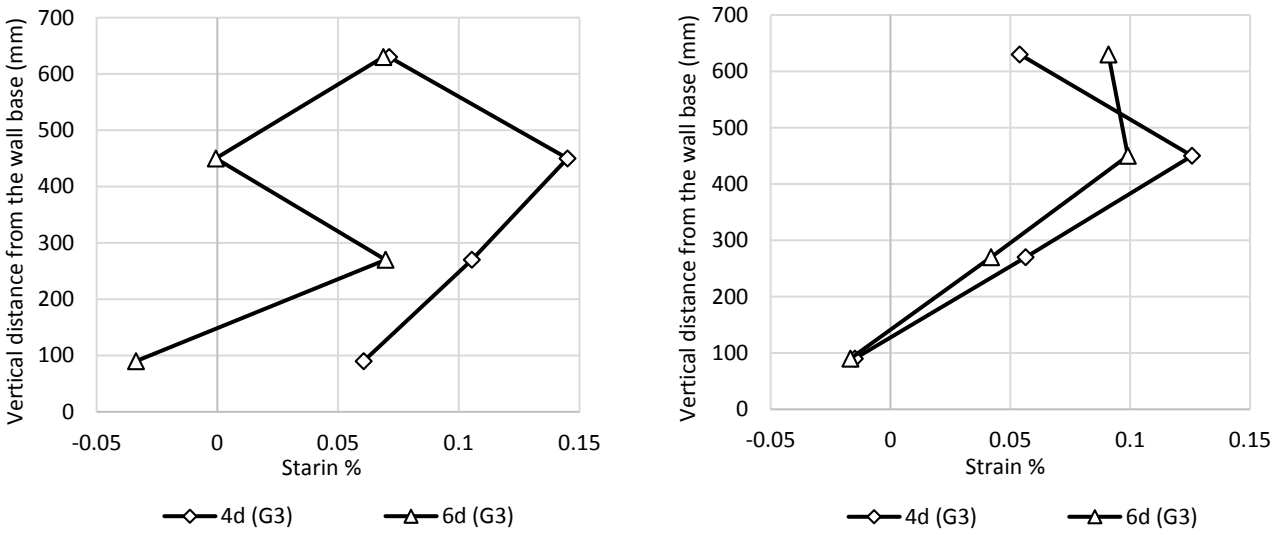

(a) (b)

Figure 5.63 Strains of the geogrid layers at a load of 600 N in: (a) Gauges group (G3) of Group (H2 L2 S1 C1 D23) and(b) Gauges group (G3) of Group (H2 L3 S1 C1 D23).

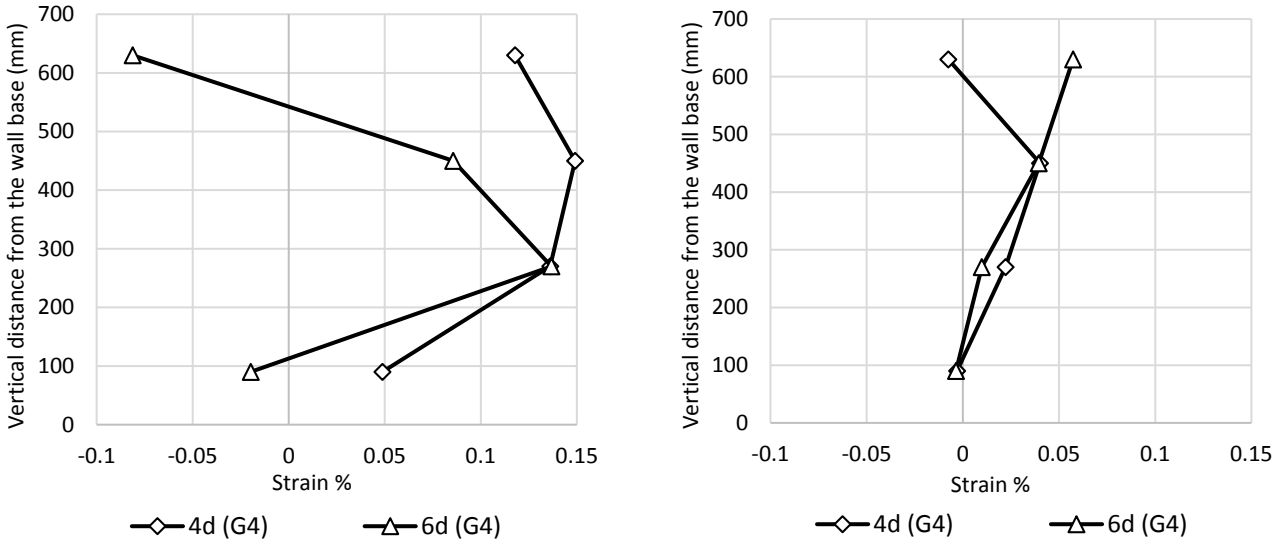

(a) (b)

Figure 5.64 Strains of the geogrids at a load of 600 N in: (a) Gauges group (G4) of Group (H2 L2 S1 C1 D23) and (b) Gauges group (G4) of Group (H2 L3 S1 C1 D23).

For the second analysis approach, the behavior in each group is similar to the behavior that in Set 4. However, the strain distributions of the all gauges groups of Group H2 **L3** S1 C1 D23 at the pile offset 4d were high as shown in Figure 5.64 (b). This high distribution may due the decreasing in the spacing between the reinforcement layers. For Figure 5.65, the behavior is the same as Set 4.

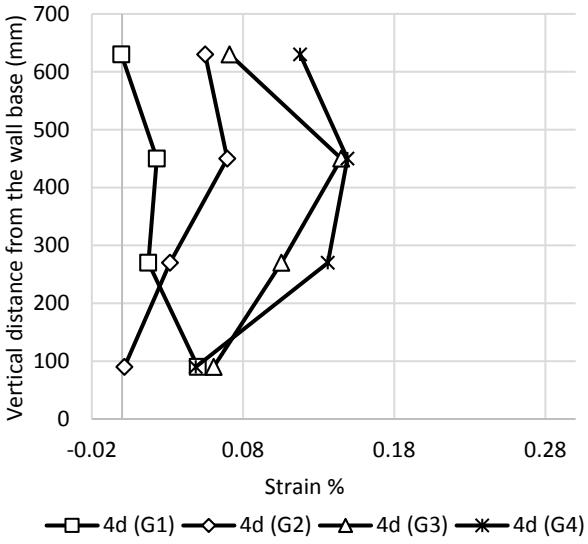

(b)

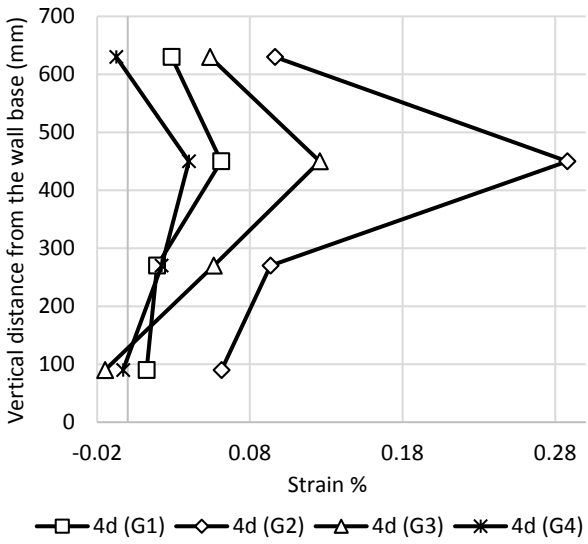

(b)

Figure 5.65 Strains of the geogrid layers at a load of 600 N in: (a) Pile offset (4d) of Group (H2 L2 S1 C1 D23) and (b) Pile offset (4d) of Group (H2 L3 S1 C1 D23).

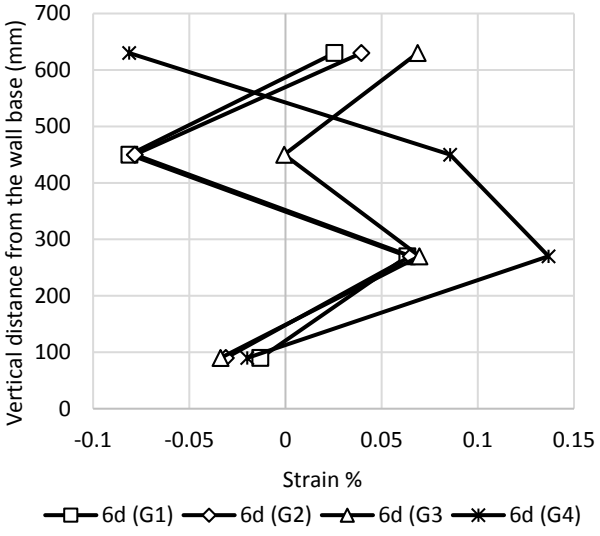

(a)

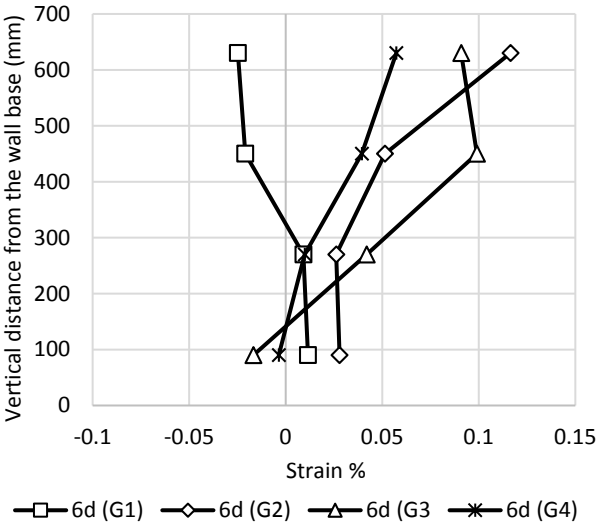

(b)

Figure 5.66 Strains of the geogrids at a load of 600 N in: (a) Pile offset (6d) of Group (H2 L2 S1 C1 D23) and (b) Pile offset (6d) of Group (H2 L3 S1 C1 D23).

Pressure behind the wall facing

Figure 5.67 shows the pressure behind the vertical centerline of the wall facing of groups H2 **L2** S1 C1 D23 and H2 **L3** S1 C1 D23. As the same as Set 4, the pressure behind the vertical centerline of the wall facing in each group increased by decrease of the pile offset. Also, a high-pressure zone occurs at the bottom of the wall facing in the tests of the Group H2 **L2** S1 C1 D23. However, the location of the maximum pressure behind the upper part of the wall moves higher than 65.5% of the wall height due to the small spacing between the geogrid layers.

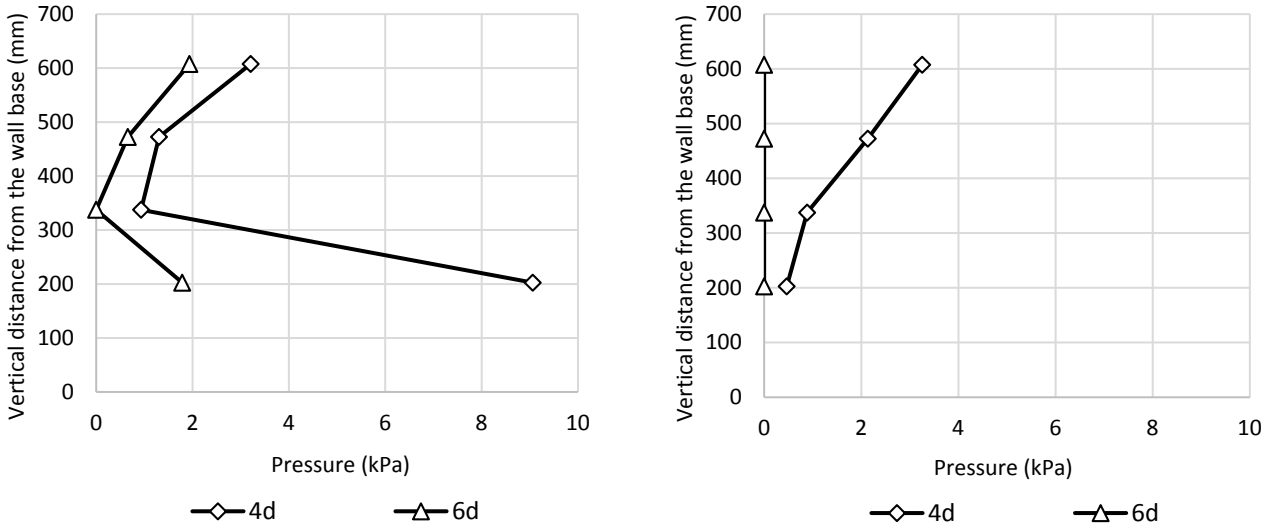

(a)

Figure 5.67 Pressures behind the wall facing at a load of 400 N in: (a) Group (H2 L2 S1 C1 D23) and (b) Group (H2 L3 S1 C1 D23).

Figure 5.68 presents the transverse distribution of the pressure of Groups H2 **L2** S1 C1 D23 and H2 **L3** S1 C1 D23 at 84% of the wall height. As the same as Set 4, the transvese distribution of the pressure becomes more uniform by increasing of the pile offset.

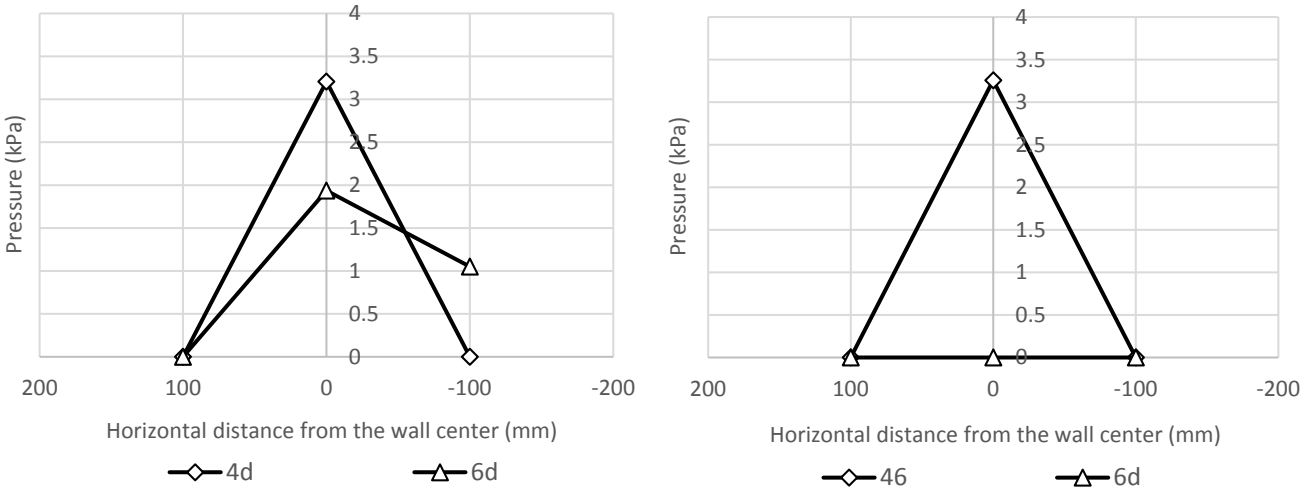

. (a) (b)

Figure 5.68 Transverse distribution of the pressures at 84% of the wall height and a load of 600 N in: (a) Group (H2 L2 S1 C1 D23) and (b) Group (H2 L3 S1 C1 D23).

Set 6 High wall with small reinforcement spacing and frictional connection

Table 5.7 presents the parameters information for the two groups that were analyzed in this set. The load-displacement curves of the tests of Groups H2 **L2** S1 C2 D23 and H2 **L3** S1 C2 D23 are shown in Figures 5.69.

Table 5.6 Details of Set 6

Tests	Ultimate Lateral Load N	Wall Height H, mm	Layer length L, mm	Layer spacing S, mm	Offset D, mm	Connection Type	Comparison Groups
H2 L2 S1 C2 D2	416	720	504	90	254 (4d)	Frictional	Category 3 of Group 2 or H2 **L2** S1 C2 D23
H2 L2 S1 C2 D3	495				381 (6d)		
H2 L3 S1 C2 D2	494	720	900	90	254 (4d)		Category 3 of Group 3 or H2 **L3** S1 C2 D23
H2 L3 S1 C2 D3	707				381 (6d)		

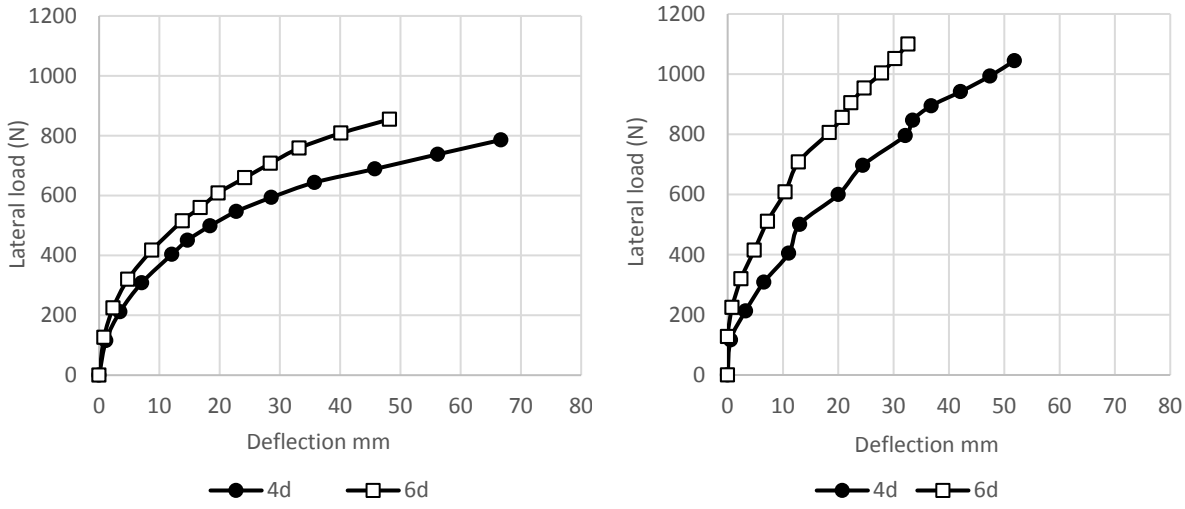

Figure 5.69 Load -Displacement curves of Set 6 in: (a) Group (H2 L2 S1 C2 D23) and (b) Group (H2 L3 S1 C2 D23).

The load-displacement behavior of the groups of this set is similar to The load-displacement behavior that shown in Set 4. The change in the reinforcement length between the tests of Groups H2 **L2** S1 C2 D23 and H2 **L3** S1 C2 D23 causes increasing in the pile capacity by approximately 19% and 43% at the pile offsets of 4d and 6d, respectively. As the same as Set 5, the comparison load in this set is equal to 600 N.

Deflection of wall facing

The deflection distributions at the vertical centerline of the wall facing of Groups H2 **L2** S1 C2 D23 and H2 **L3** S1 C2 D23 are shown in Figure 5.70. On the other hand, the transverse deflection distributions of the wall for the two groups are shown in Figure 5.71. The behavior of the deflection distribution at the vertical centerline and cross-section of the wall is similar to the behavior that shown in Set 5.

.

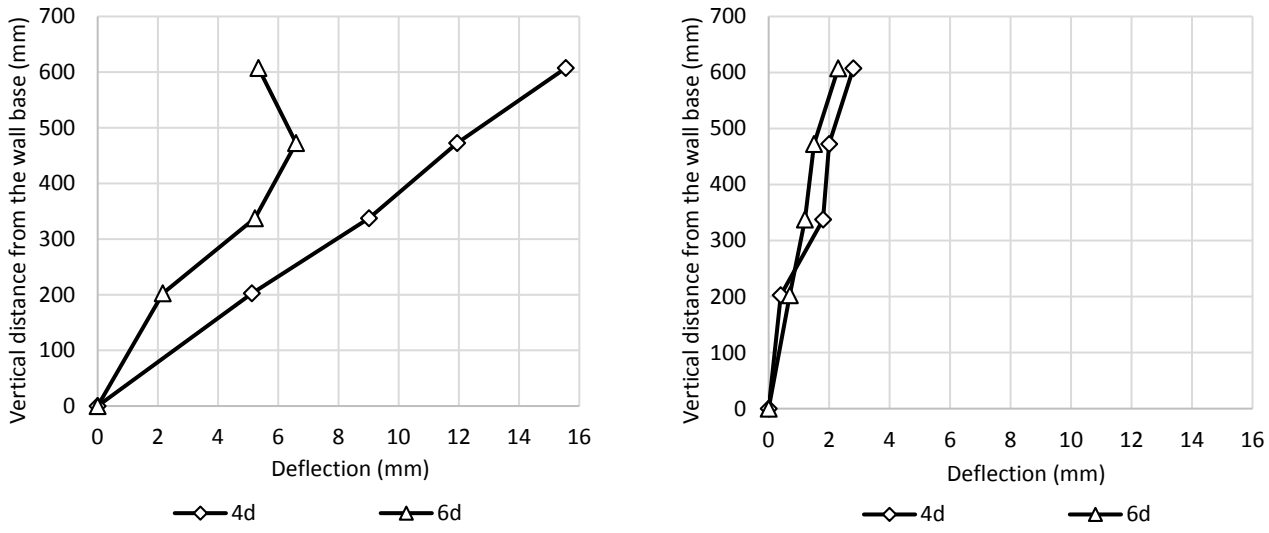

(a) (b)

Figure 5.70 Deflections at the wall facing along the vertical centerline at a load of 600 N in: (a) Group (H2 L2 S1 C2 D23) and (b) Group (H2 L3 S1 C2 D23).

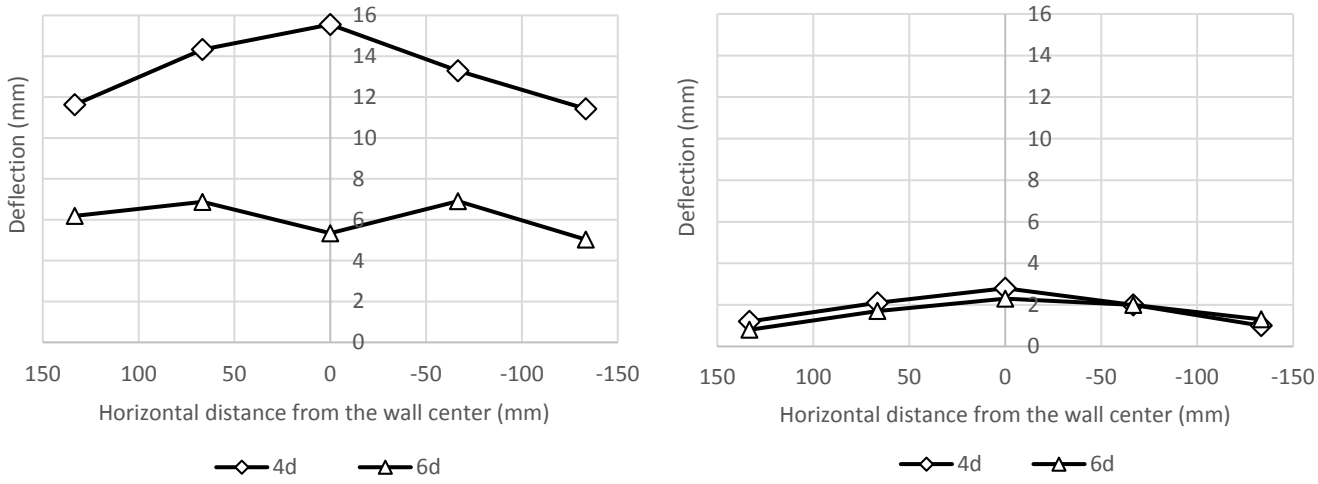

(a) (b)

Figure 5.71 Transverse distribution of the wall deflection at 84% of the wall height and a load of 600 N in: (a) Group (H2 L2 S1 C2 D23) and (b) Group (H2 L3 S1 C2 D23).

Strain, Stress, and moment of the pile

The strain, stress, and moment along the pile are shown in Figures 5.72, 5.73, and 5.74, respectively. Their behaviors are similar to the behaviors that shown in groups of Set 5 with one exception for Group H2 **L3** S1 C2 D23. The maximum compressive and tensile strains at the pile offset of 6d were lower than The maximum compressive and tensile strains at the pile offset of 6d. In fact, the frictional connection provides the reinforcement layer with more freedom to move between the wall blocks. Therefore, no more resistance from the geogrid layers is considered against the pile deflection. Thus, the pile experience lower strain or stress at the pile offset of 6d.

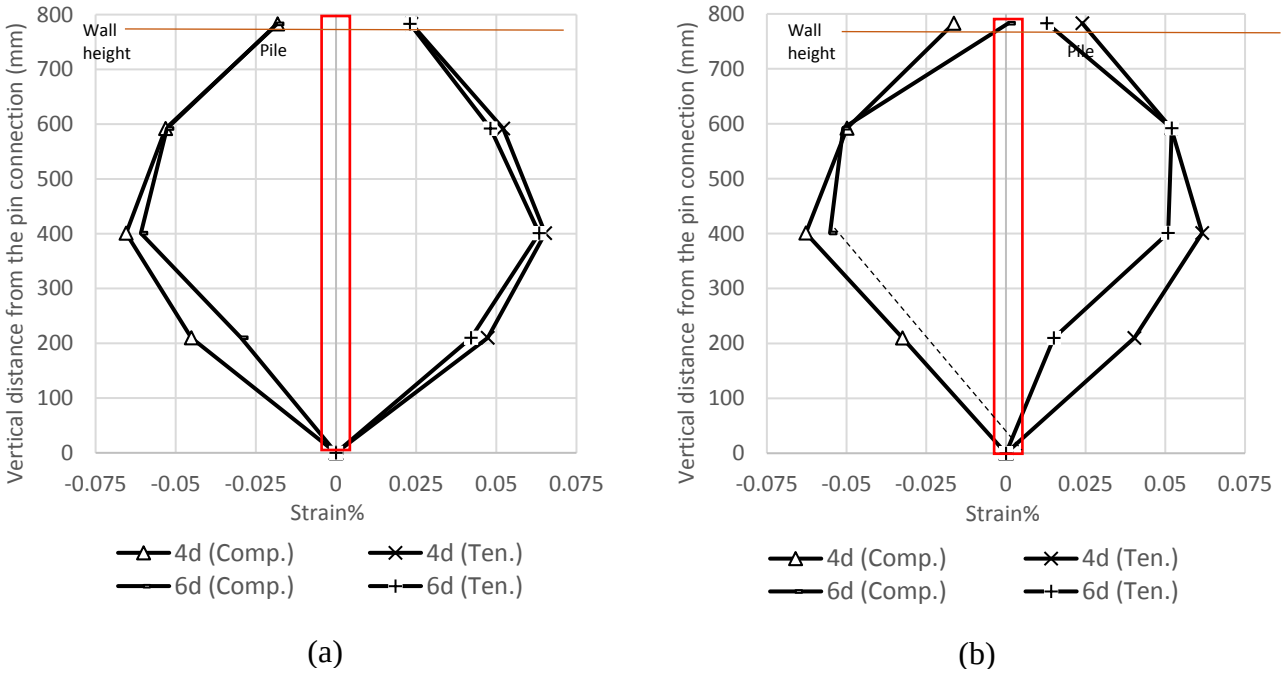

(a) (b)

Figure 5.72 Strains of the laterally loaded pile at a load of 600 N in: (a) Group (H2 L2 S1 C2 D23) and (b) Group (H2 L3 S1 C2 D23).

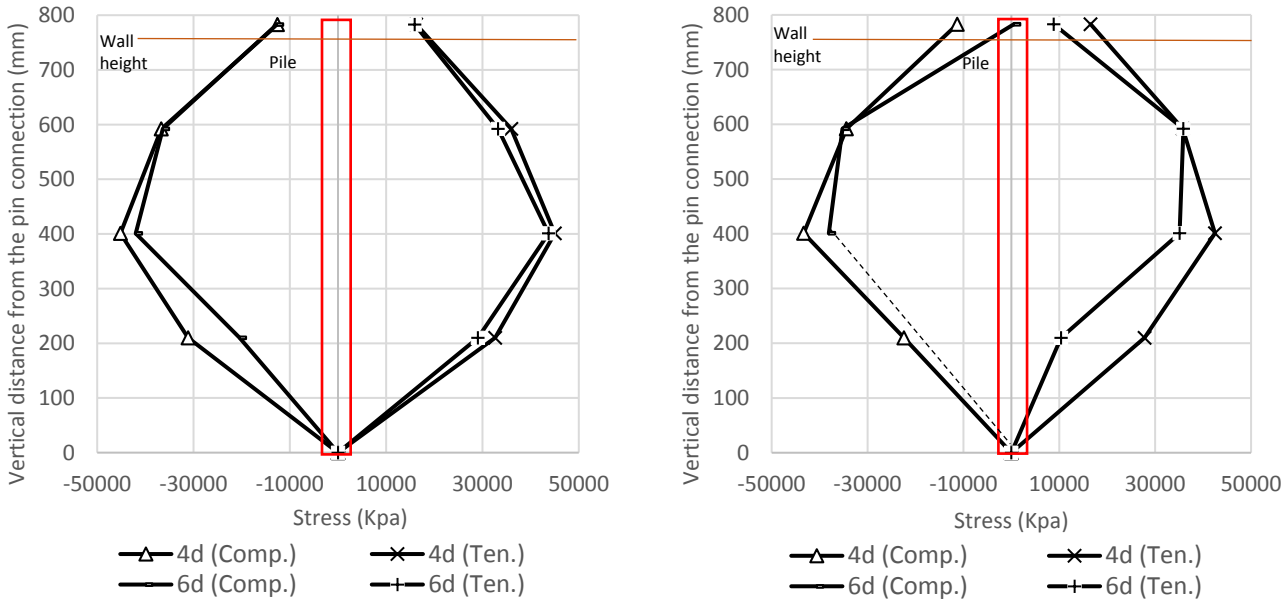

(a) (b)

Figure 5.73 Stresses of the laterally loaded pile at a load of 600 N in: (a) Group (H2 L2 S1 C2 D23) and (b) Group (H2 L3 S1 C2 D23).

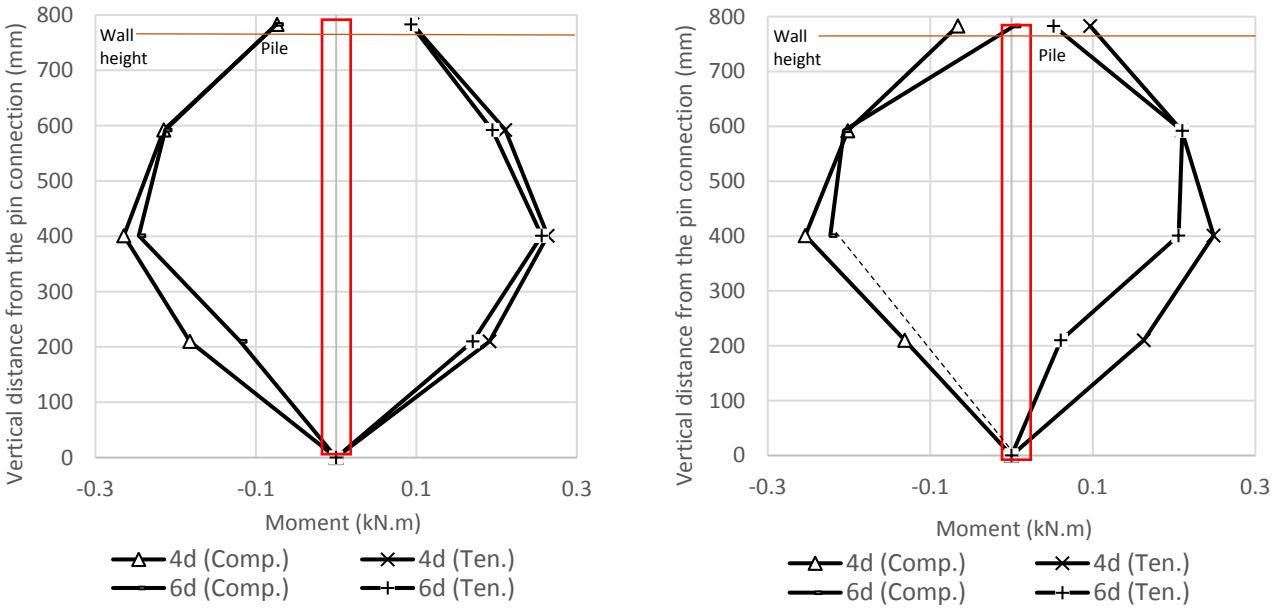

(a) (b)

Figure 5.74 Moments of the laterally loaded pile at a load of 600 N in: (a) Group (H2 L2 S1 C2 D23) and (b) Group (H2 L3 S1 C2 D23).

Strain of the geogrid

Figures 5.75, 5.76, 5.77, and 5.78 show the strain by using the first analysis approach. In addition, Figures 5.79, and 5.80 show the strain by using the second analysis approach. For both of these analysis approaches, the behavior of the strain distribution is the same as the behavior that shown in Set 5.

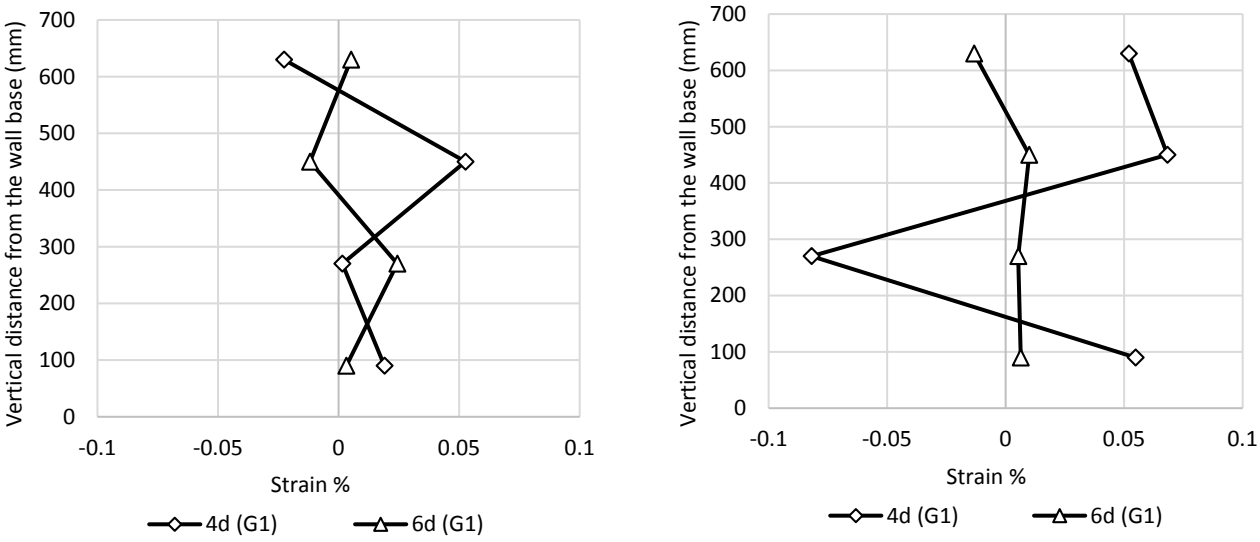

(a) (b)

Figure 5.7574 Strains of the geogrids at load of 600 N in: (a) Gauges group (G1) of Group (H2 L2 S1 C2 D23) and (b) Gauges group (G1) of Group (H2 L3 S1 C2 D23).

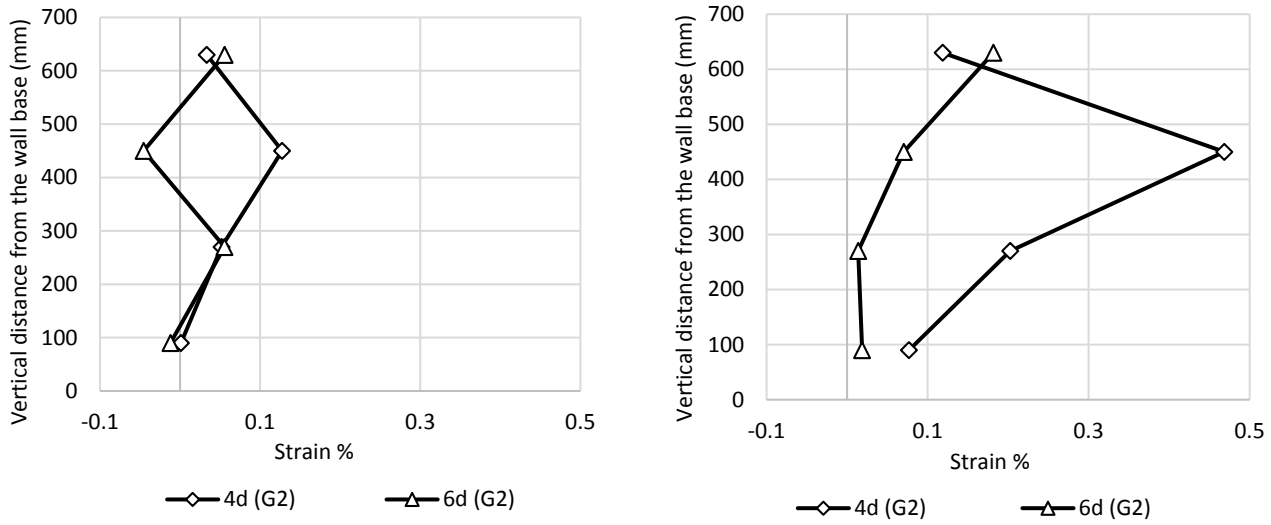

(a) (b)

Figure 5.76 Strains of the geogrids at load of 600 N in: (a) Gauges group (G2) of group (H2 L2 S1 C2 D23) and (b) Gauges group (G2) of group (H2 L3 S1 C2 D23).

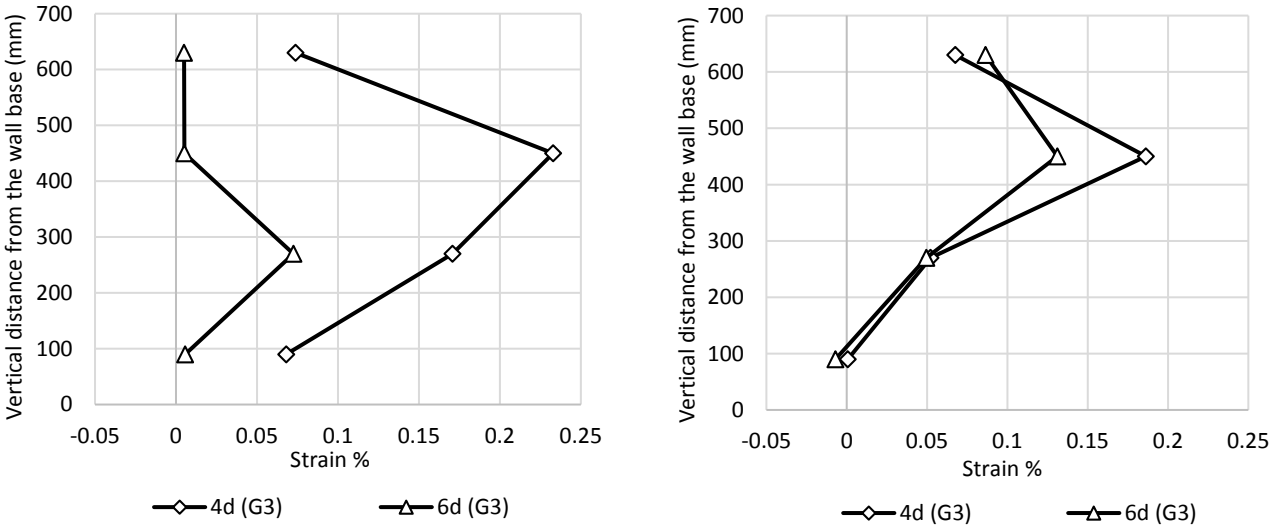

(a) (b)

Figure 5.77 Strains of the geogrid layers at a load of 600 N in: (a) Gauges Group (G3) of Group (H2 L2 S1 C2 D23) and (b) Gauges Group (G3) of Group (H2 L3 S1 C2 D23)

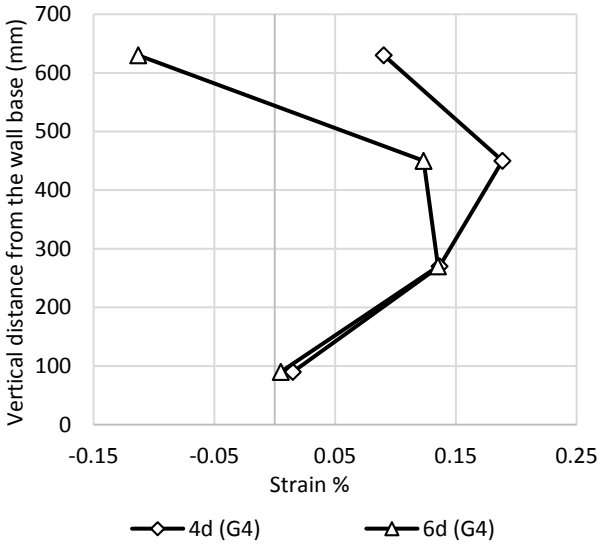

(a)

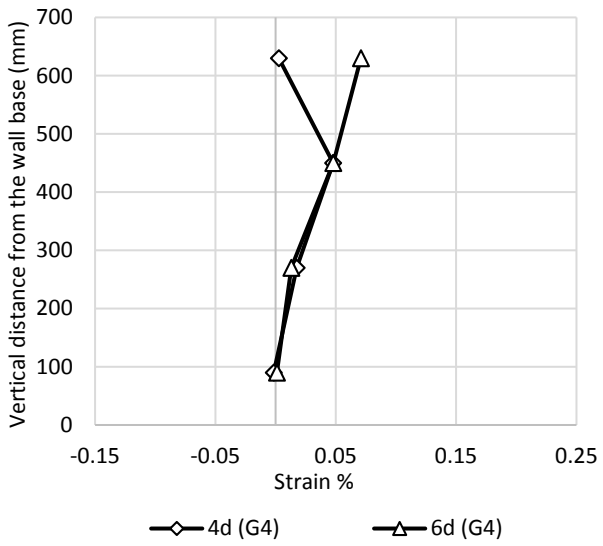

(b)

Figure 5.78 Strains of the geogrid layers at a load of 600 N in: (a) Gauges group (G4) of Group (H2 L2 S1 C2 D23) and (b) Gauges group (G4) of Group (H2 L3 S1 C2 D23).

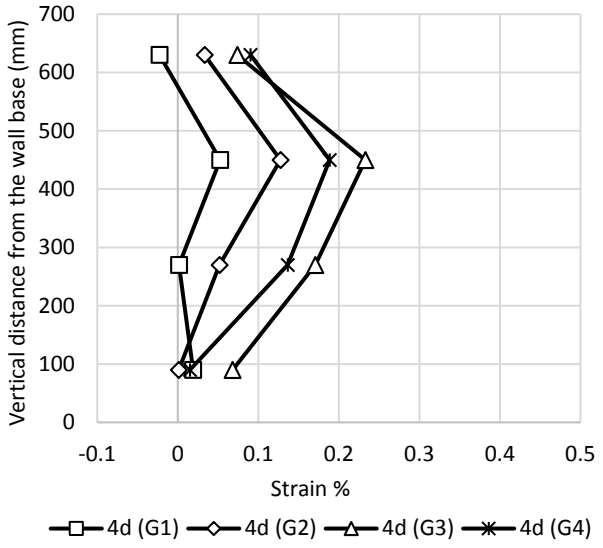

(a)

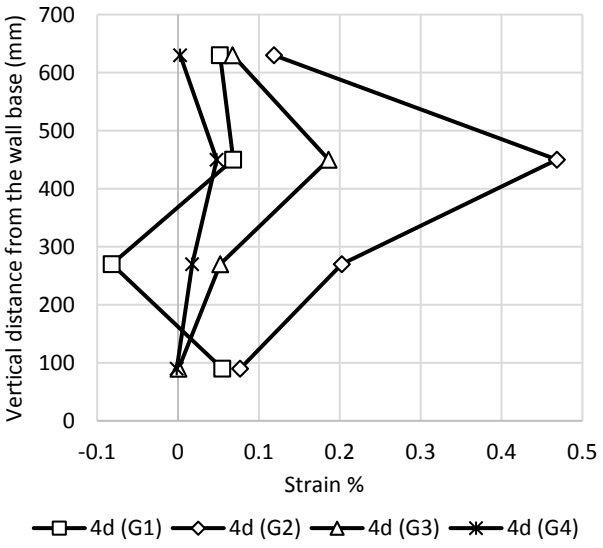

(b)

Figure 5.79 Strains of the geogrid layers at a load of 600 N in: (a) Pile offset (4d) of Group (H2 L2 S1 C2 D23) and (b) Pile offset (4d) of Group (H2 L3 S1 C2 D23).

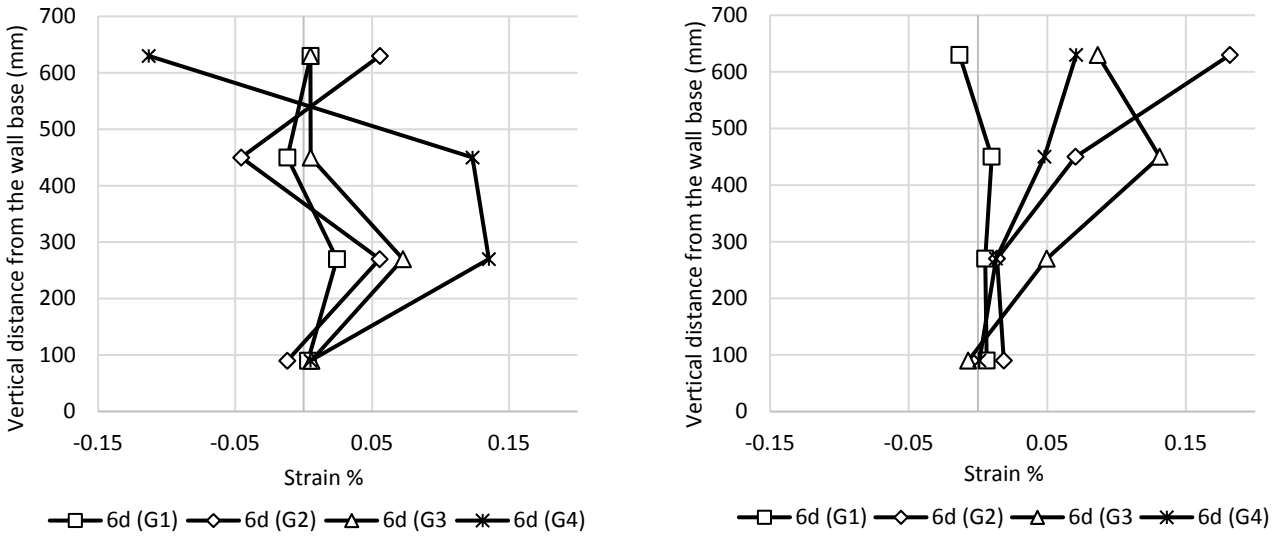

(a) (b)

Figure 5.80 Strains of the geogrids at a load of 600 N in: (a) Pile offset (6d) of Group (H2 L2 S1 C2 D23) and (b) Pile offset (6d) of Group (H2 L3 S1 C2 D23).

Pressure behind the wall facing

Figure 5.81 shows the pressure distributions behind the vertical centerline of the wall facing for Groups H2 **L2** S1 C2 D23 and H2 **L3** S1 C2 D23. On the other hand, Figure 5.82 presents the transverse pressure distributions for Groups H2 **L2** S1 C2 D23 and H2 **L3** S1 C2 D23 at 84% of the wall height. The behavior of the pressure distribution in the both case is similar to the behavior that shown in Set 5.

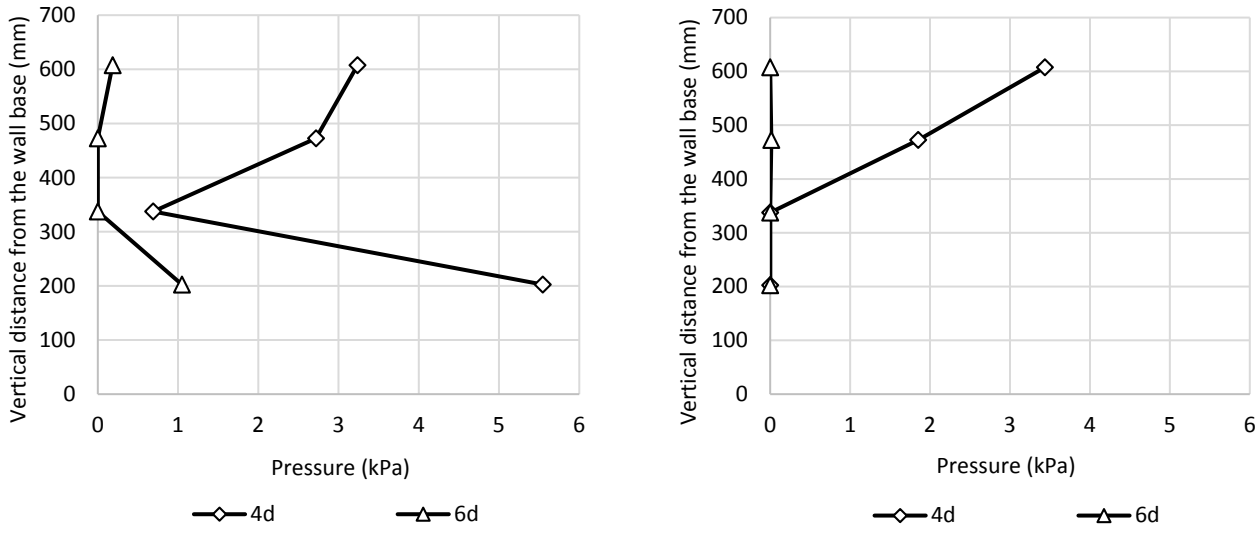

(a) (b)

Figure 5.81 Pressures behind the wall facing at a load of 600 N in: (a) Group (H2 L2 S1 C2 D23) and (b) Group (H2 L3 S1 C2 D23).

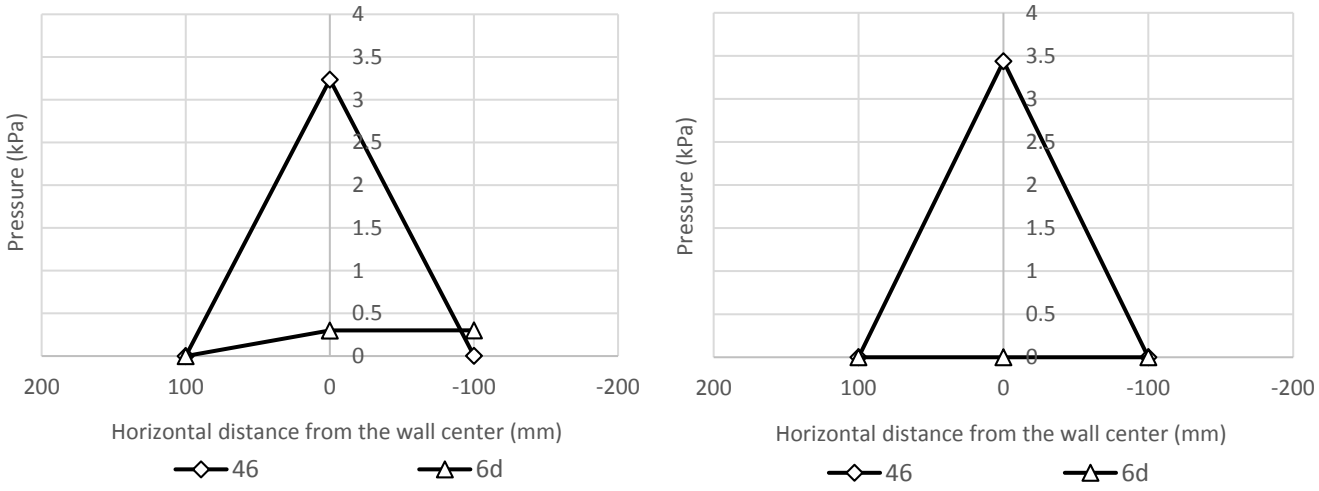

(a) (b)

Figure 5.82 Transverse distribution of the pressure at 84% of the wall height and at a load of 600 N in: (a) Group (H2 L2 S1 C2 D23) and (b) Group (H2 L3 S1 C2 D23).

5.4. Data Comparison due the change in the connection type

Two comparison sets are considered in this section. The first set has the regular reinforcement length while the second set has the long reinforcement length. The main variable in each set was the connection type between the wall facing and reinforcement layers.

Set 7 High wall with regular reinforcement length and small reinforcement spacing

All the information about the tests of this set is shown in Table 5.8. Each one of the two groups of this set includes three tests with three different pile offsets.

Table 5.7 Detials of Set 7.

Tests	Ultimate Lateral Load N	Wall Height H, mm	Layer length L, mm	Layer spacing S, mm	Offset D, mm	Connection Type	Group designation
H2 L2 S1 C1 D1	368	720	504	90	127 (2d)	Mechanical	Category 2 of Group 2 or H2 L2 S1 **C1** D123
H2 L2 S1 C1 D2	405				254 (4d)		
H2 L2 S1 C1 D3	504				381 (6d)		
H2 L2 S1 C2 D1	391	720	504	90	127 (2d)	Frictional	Category 3 of Group 2 or H2 L2 S1 **C2** D123
H2 L2 S1 C2 D2	416				254 (4d)		
H2 L2 S1 C2 D3	494				381 (6d)		

The load-displacement curves of the tests of Group H2 L2 S1 **C1** D123 are shown in Figure 5.83 (a), while The load-displacement curves of the tests of Group H2 L2 S1 **C2** D123 are shown in Figure 5.83 (b).

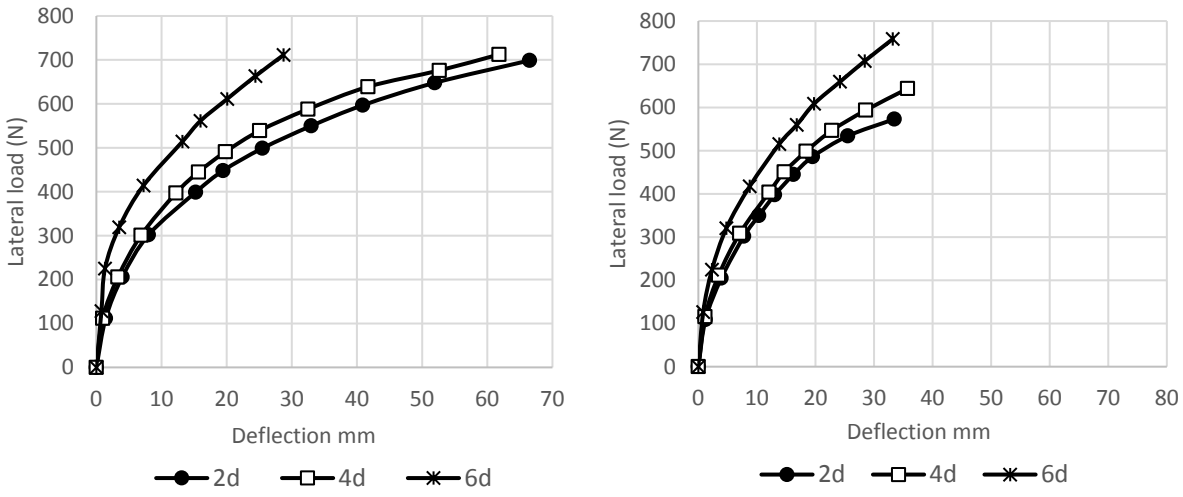

(a) (b)

Figure 5.83 Load -displacement curves of Set 7 in: (a) Group (H2 L2 S1 C1 D123) and (b) Group (H2 L2 S1 C2 D123).

The ultimate lateral load or the capacity of the pile increased by an increase of the pile offset. Even though different connection types were used in this set, there are no significant differences in the values of the pile capacities between the two groups at each corresponding pile offset. However, the comparison load for this set is equal to 400 N.

Deflection of wall facing

The deflection distribution at the vertical centerline of the wall facing of Group H2 L2 S1 **C1** D123 and Group H2 L2 S1 **C2** D123 are shown in Figure 5.84.

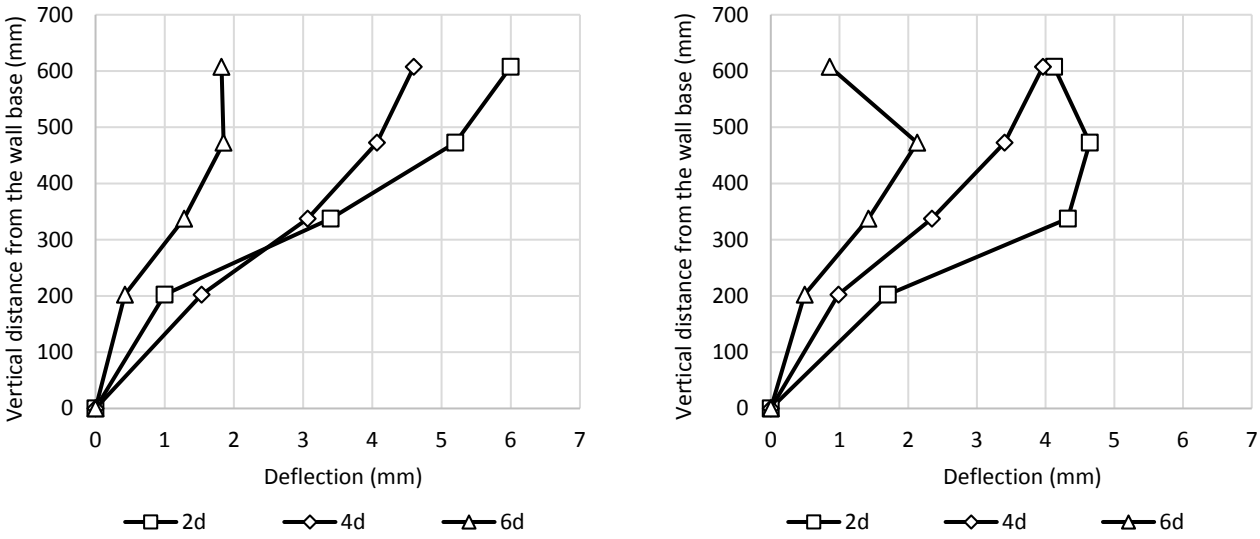

(a) (b)

Figure 5.84 Deflections of the wall facing along the vertical centerline at a load of 400 N in: (a) Group (H2 L2 S1 C1 D123) and (b) Group (H2 L2 S1 C1 D123).

The deflection distribution at the vertical centerline of the wall facing in each group increased by a decrease of the pile offset as shown in Figure 5.84. At a load of 400 N, the maximum deflection occurs at 84% of the wall height in the tests of Group H2 L2 S1 **C1** D123. On the other hand, it occurs at 65.5% of the wall height in the tests of Group H2 L2 S1 **C2** D123 except for the test with 4d pile offset. However, the maximum deflection at the pile offset of 2d returns to the location of 84% when the lateral load increased as shown in Figure 4.73 (a).

Figure 5.85 presents the transverse deflection of the wall for the two groups at 84% of the wall height. It is clear that by increasing the pile offset, the deflection distribution in the transverse section of the wall facing become more uniform

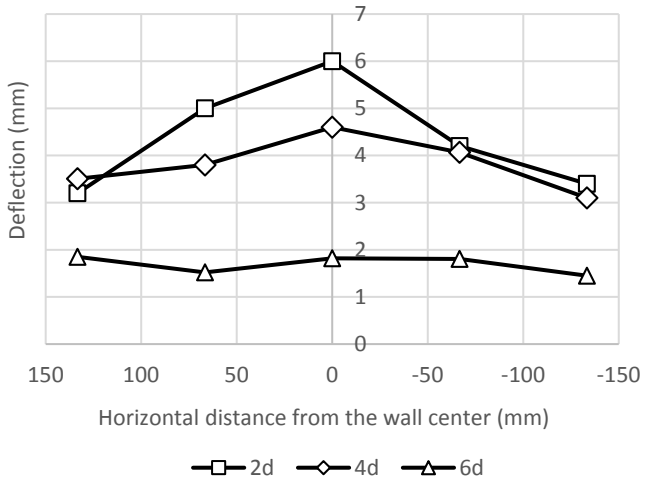

(a)

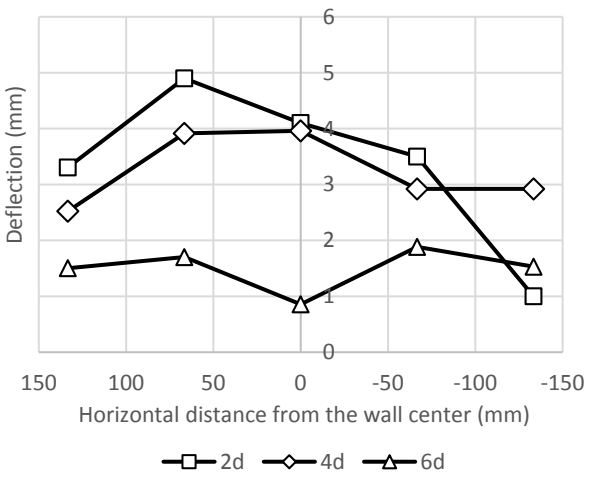

(b)

Figure 5.85 Transverse distribution of the wall deflection at 84% of the wall height and a load of 400 N in: (a) Group (H2 L2 S1 C1 D123) and (b) Group (H2 L2 S1 C1 D123).

Strain, Stress, and moment of the pile:

The strain distributions along the pile for Groups H2 L2 S1 **C1** D123 and H2 L2 S1 **C2** D123 are shown in Figure 5.86. In each group, the maximum compressive and tensile strain locations of the pile were at an elevation equal to 44% of the wall height. As shown in Figure 5.86 (a) and (b), the changing in the connection type between the two groups does not cause a significant change in the values of the maximum tensile and compressive strain. However, Figures 5.87 and 5.88 show the same trend that shown in Figure 5.86.

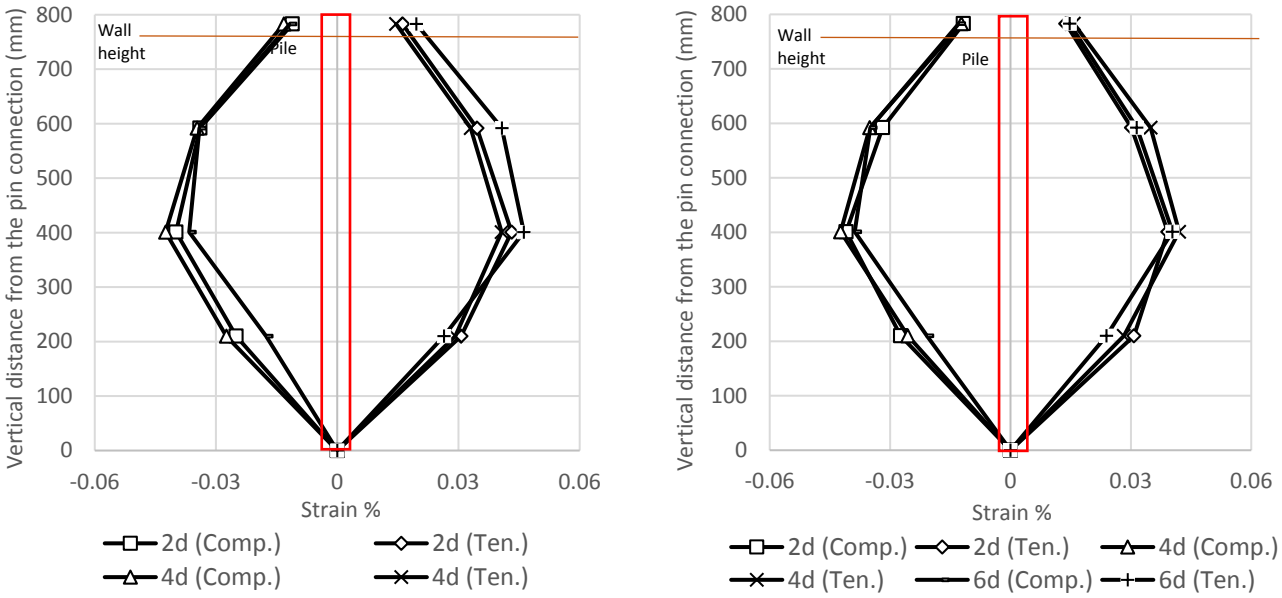

(a) (b)

Figure 5.86 Strains of the laterally loaded pile at a load of 400 N in: (a) Group (H2 L2 S1 C1 D123) and (b) Group (H2 L2 S1 C2 D123).

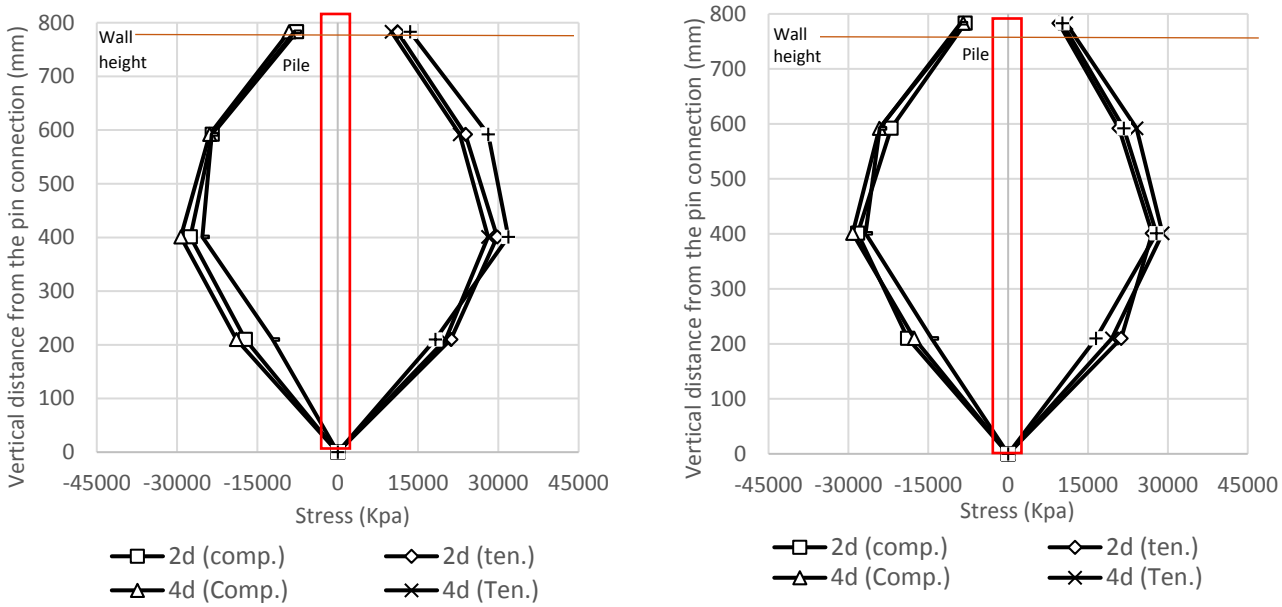

(a) (b)

Figure 5.87 Stresses of the laterally loaded pile at a load of 400 N in: (a) Group (H2 L2 S1 C1 D123) and (b) Group (H2 L2 S1 C2 D123).

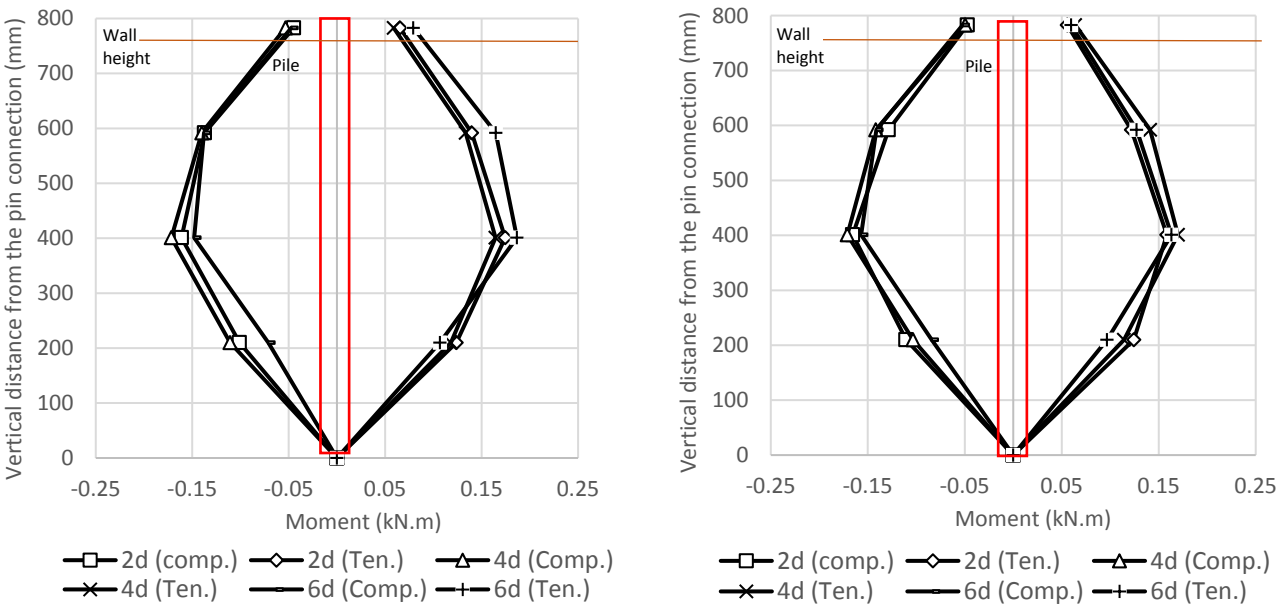

(a) (b)

Figure 5.88 Moments of the laterally loaded pile at a load of 400 N in: (a) Group (H2 L2 S1 C1 D123) and (b) Group (H2 L2 S1 C2 D123).

Strain of the geogrid

The two strain analysis approaches are considered in this set. Figures 5.89, 5.90, 5.91, and 5.92 show the strain distribution by using the first analysis approach. In addition, Figures 5.93, 5.94, and 5.95 show the strain distribution by using the second analysis approach. The behavior of the strain distribution that recorded by each gauges group in Figures 5.89, 5.90, 5.91, and 5.92 is similar to the behavior that shown in the Figures 5.18, 5.19, 5.20, and 5.21 of Set 2, respectively.

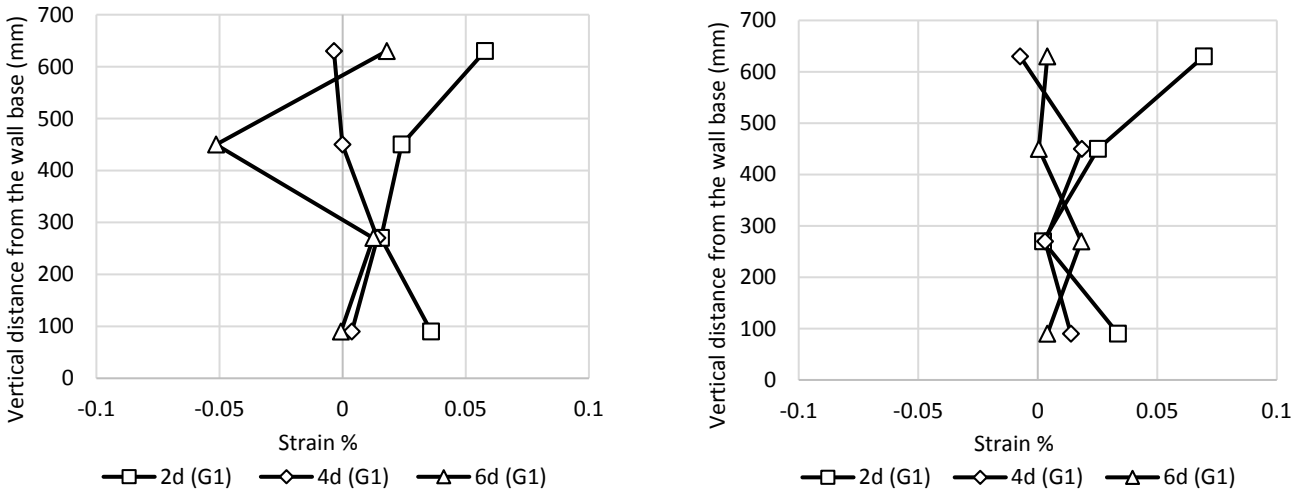

(a) (b)

Figure 5.89 Strains of the geogrids at load of 400 N in: (a) Gauges group (G1) of group (H2 L2 S1 C1 D123) and (b) Gauges group (G1) of group (H2 L2 S1 C2 D123).

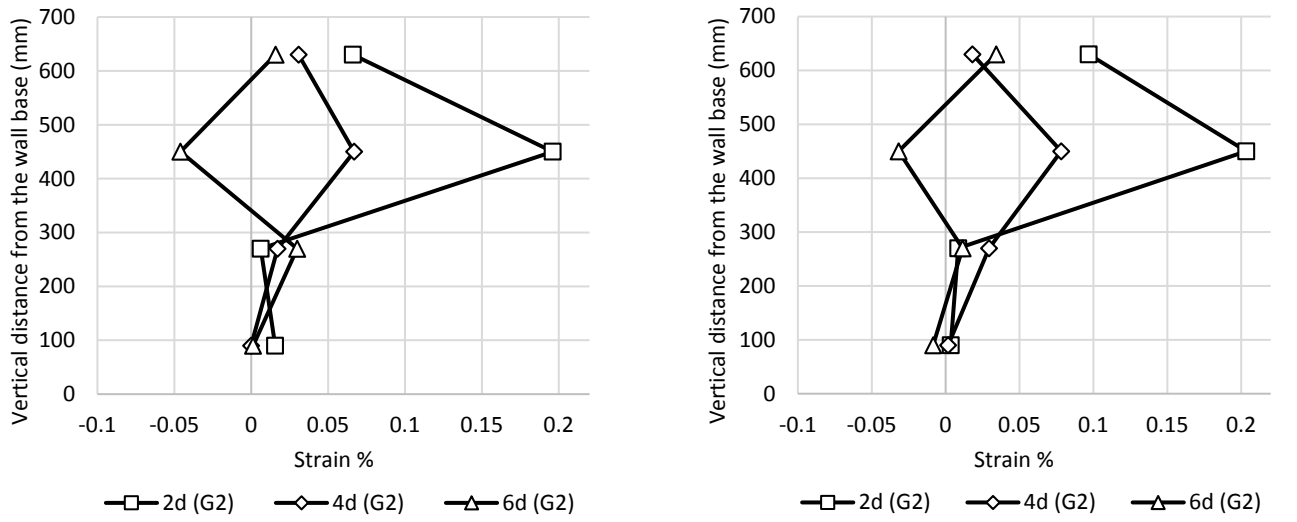

(a) (b)

Figure 5.90 Strains of the geogrids at load of 400 N in: (a) Gauges group (G2) of group (H2 L2 S1 C1 D123) and (b) Gauges group (G2) of group (H2 L2 S1 C2 D123).

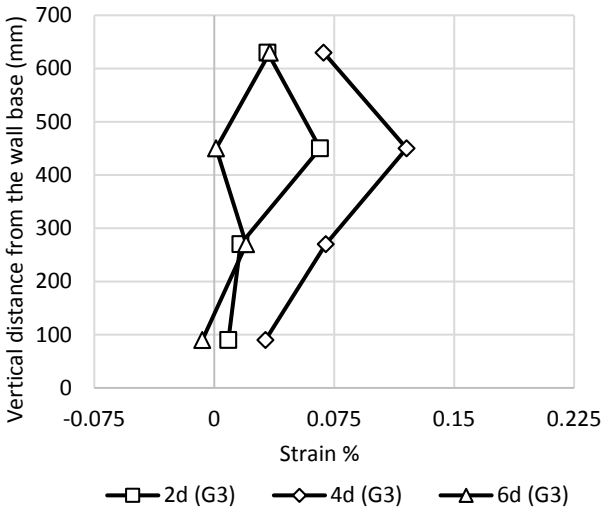

(a)

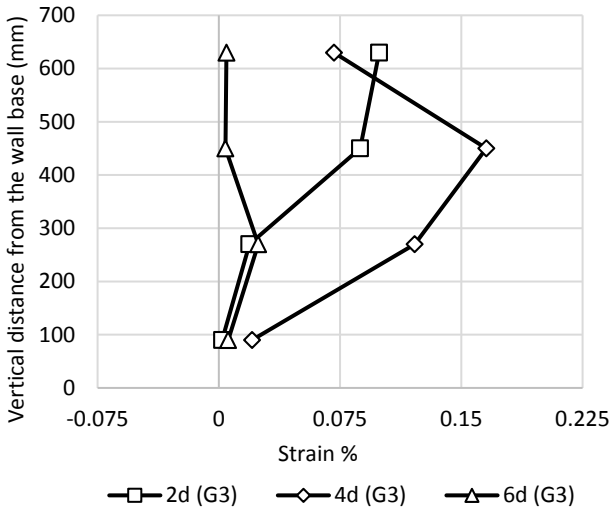

(b)

Figure 5.91 Strains of the geogrid layers at a load of 400 N in: (a) Gauges group (G3) of Group (H2 L2 S1 C1 D123) and (b) Gauges group (G3) of Group (H2 L2 S1 C2 D123).

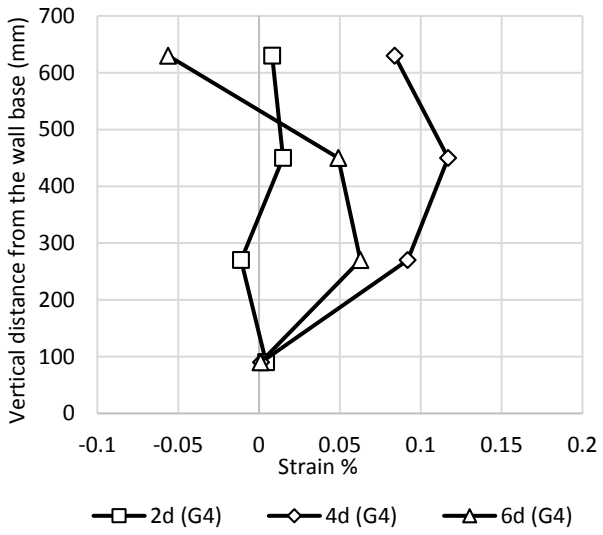

(a)

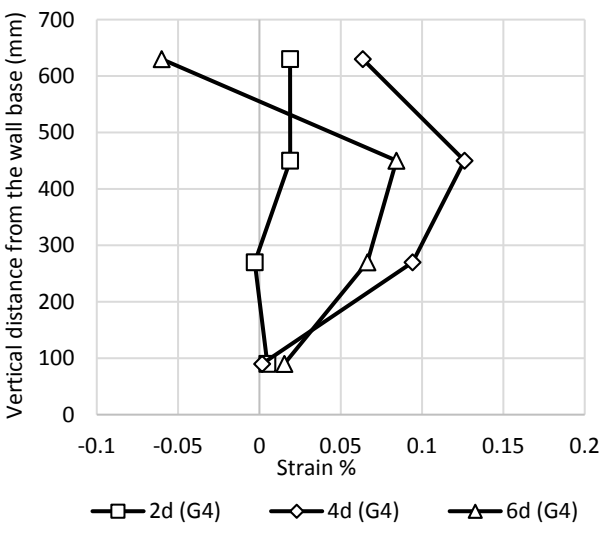

(b)

Figure 5.92 Strains of the geogrids at a load of 400 N in: (a) Gauges group (G4) of Group (H2 L2 S1 C1 D123) and (b) Gauges group (G4) of Group (H2 L2 S1 C2 D123).

In the second analysis approach, the same behavior as that shown in Set 2 applies to the behavior of the strain distributions of this set. For the pile offsets equal to 2d, 4d and 6d, the highest strain distributions were recorded by gauges groups G2, G3, and G4, respectively. At each corresponding gauges group, the difference between the values of the maximum tensile strain in Group H2 L2 S1 **C2** D123 and Group H2 L2 S1 **C1** D123 was insignificant.

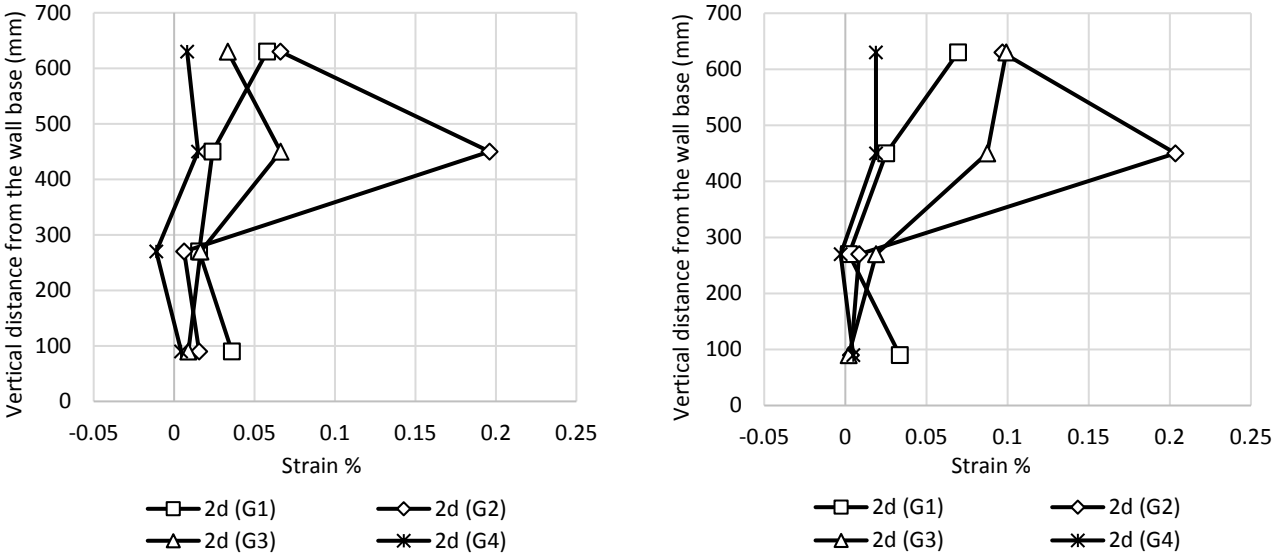

Figure 5.93 Strains of the geogrid layers at load of 400 N in: (a) Pile offset (2d) of Group (H2 L2 S1 C1 D123) and (b) Pile offset (2d) of Group (H2 L2 S1 C2 D123).

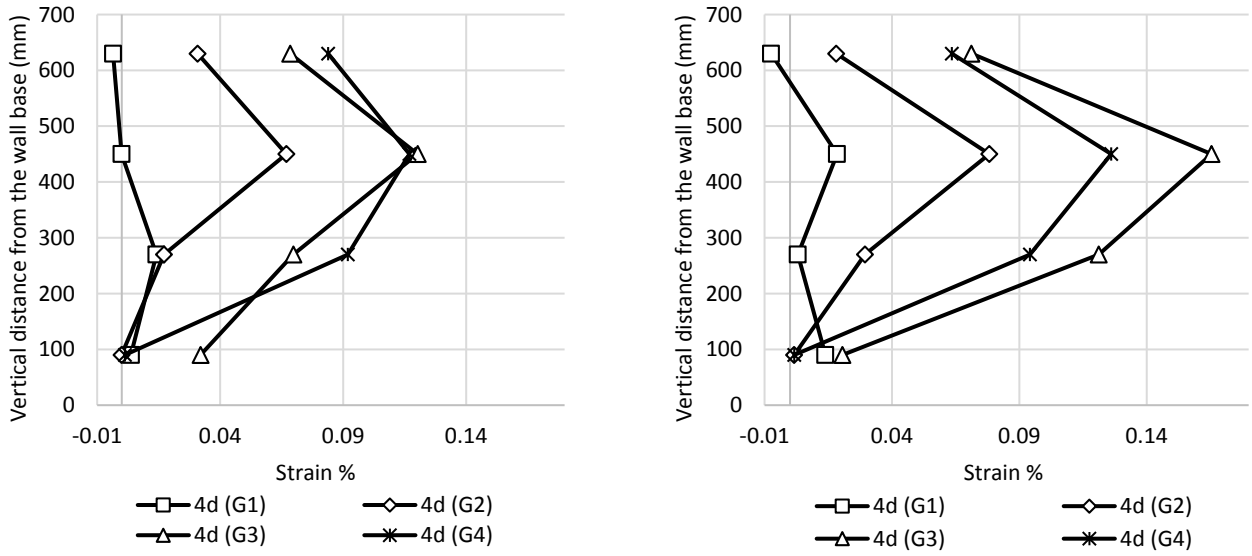

(a) (b)

Figure 5.94 Strains of the geogrid layers at a load of 400 N in: (a) Pile offset (4d) of Group (H2 L2 S1 C1 D123) and (b) Pile offset (4d) of Group (H2 L2 S1 C2 D123).

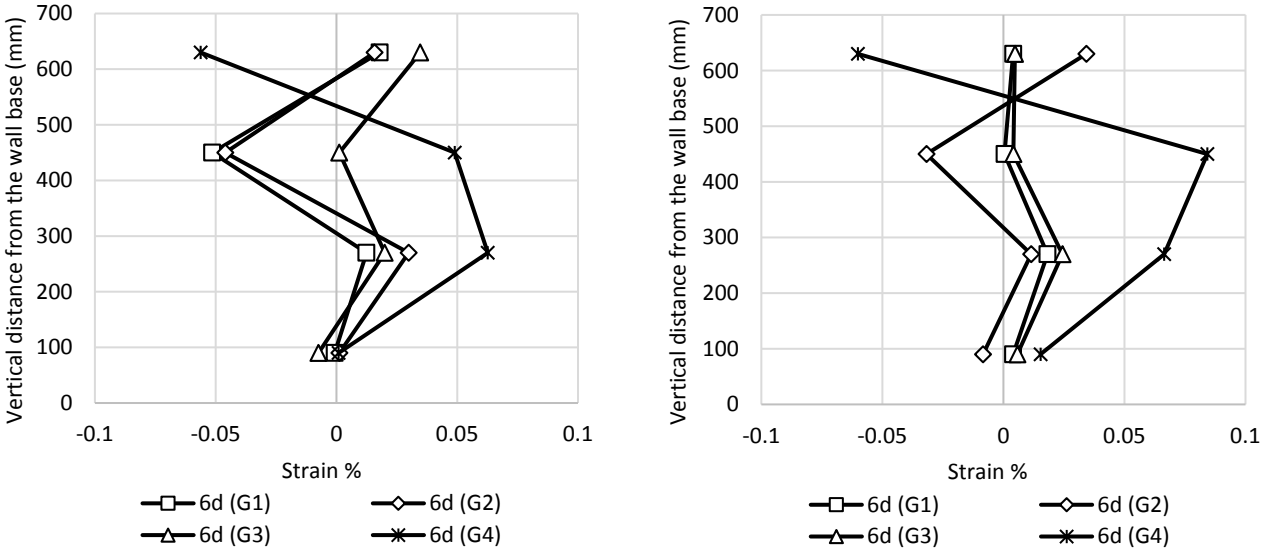

(a) (b)

Figure 5.95 Strains of the geogrid layers at a load of 400 N in: (a) Pile offset (6d) of Group (H2 L2 S1 C1 D123) and (b) Pile offset (6d) of Group (H2 L2 S1 C2 D123).

Pressure behind the wall facing

Figure 5.96 shows the pressure distributions behind the vertical centerline of the wall facing of Groups H2 L2 S1 **C1** D123 and H2 L2 S1 **C2** D123. On the other hand, Figure 5.97 shows the transverse pressure distributions the two group at 65.5% of the wall height.

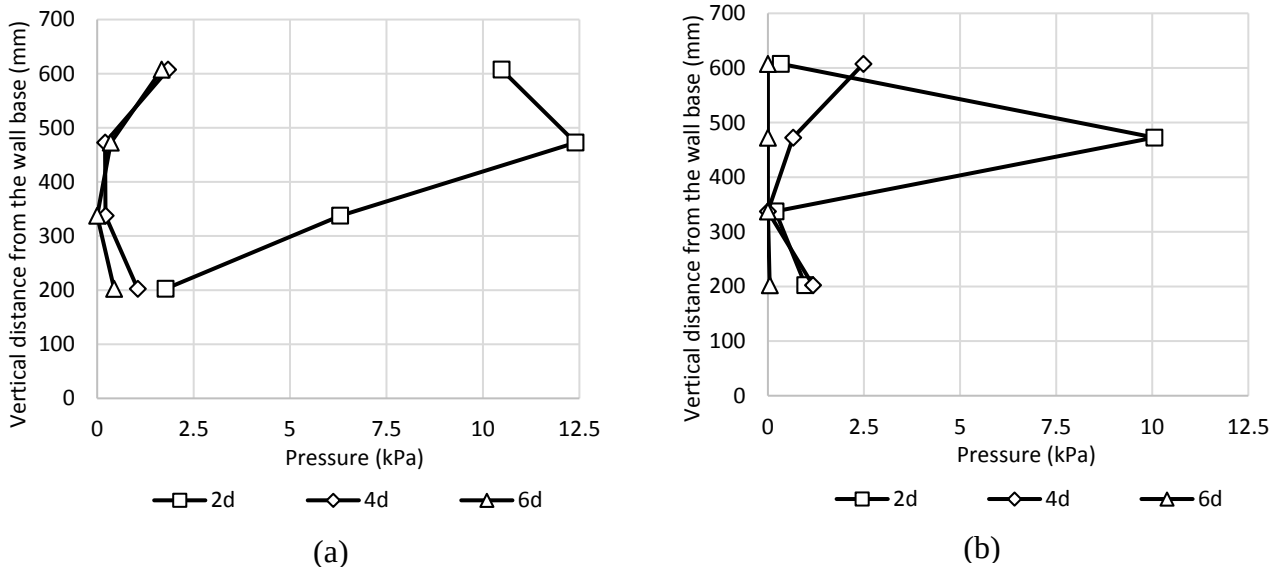

Figure 5.96 Pressure behind the wall facing at a load of 400 N: (a) Group (H2 L2 S1 C1 D123) (b) Group (H2 L2 S1 C2 D123).

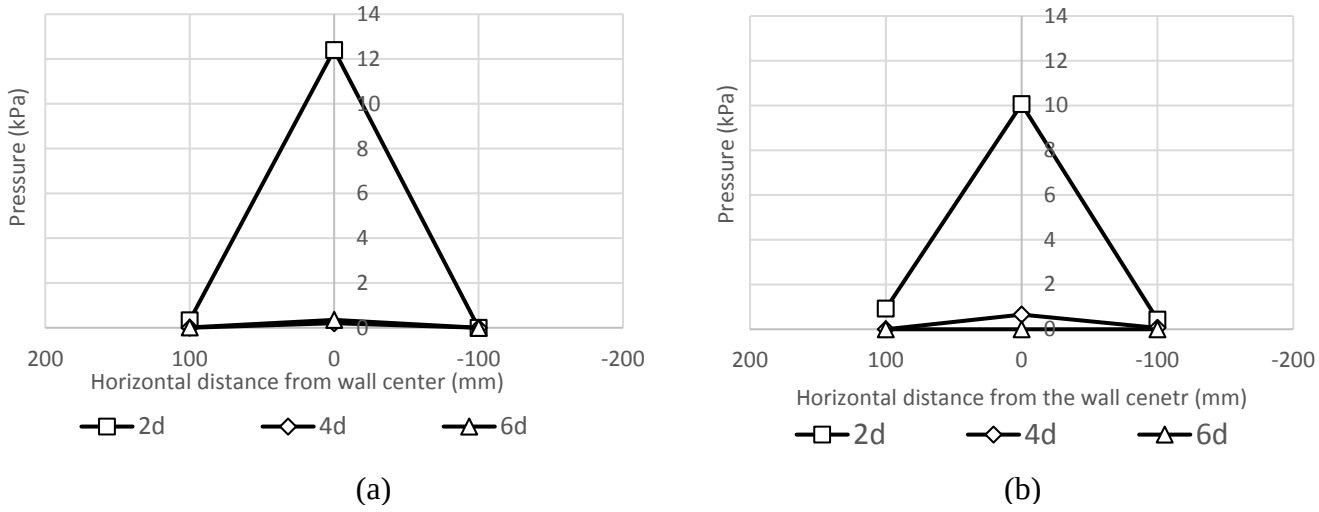

Figure 5.97 Transverse distribution of the pressure at 65.5% of the wall height and a load of 400 N: (a) Group (H2 L2 S1 C1 D123) (b) Group (H2 L2 S1 C2 D123).

In each group, the behavior of the pressure distributions is similar to the behavior that shown in Set 2. At pile offset equal to 2d, the maximum pressure of Group H2 L2 S1 **C1** D123 is higher than the maximum pressure of Group H2 L2 S1 **C2** D123 as shown in Figure 5.96. This small difference in maximum pressure was due to the presence of the mechanical connection in the tests of Group H2 L2 S1 **C1** D123. This connection provides additional resistance to the lateral deflection of the pile. Therefore, more pressure was needed to cause more deflection to the wall.

Set 8 High wall with long reinforcement length and small reinforcement spacing

This set presents the analysis of groups H2 L3 S1 **C1** D23 and H2 L3 S1 **C2** D23. Each group of them includes two tests as shown in Table 5.9. As the same as the Set 7, the variable parameter in this set was the connection type. However, the length of the reinforcement in this set is longer than Set 7, and only the two pile offsets were considered.

Table 5.8 Detailes of Set 8.

Tests	Ultimate Lateral Load N	Wall Height H, mm	Layer length L, mm	Layer spacing S, mm	Offset D, mm	Connection Type	Group designation
H2 L3 S1 C1 D2	660	720	900	90	254 (4d)	Mechanical	Category 2 of Group 3 or H2 L3 S1 **C1** D23
H2 L3 S1 C1 D3	890				381 (6d)		
H2 L3 S1 C2 D2	490	720	900	90	254 (4d)	Frictional	Category 3 of Group 3 or H2 L3 S1 **C2** D23
H2 L3 S1 C2 D3	700				381 (6d)		

The load-displacement curves of the tests of Groups H2 L3 S1 **C1** D23 and H2 L3 S1 **C2** D23 are shown in Figures 5.98.

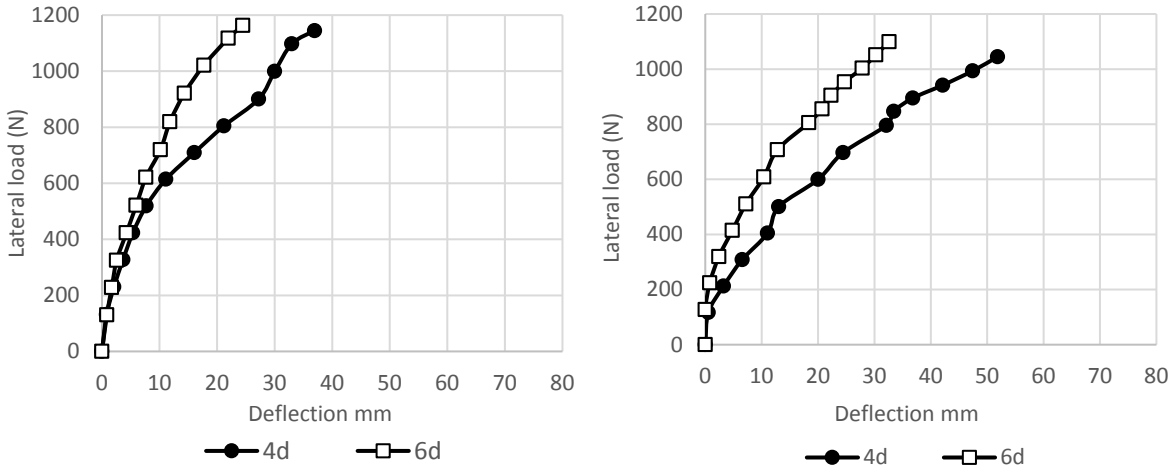

(a) (b)

Figure 5.98 Load -Displacement curves of Set 8 in: (a) Group (H2 L3 S1 C1 D23) and (b) Group (H2 L3 S1 C2 D23).

In each group. the behavior of the lateral deflection of the pile is the same as the behavior that shown in Set 7. On the other hand, by using the mechanical connection instead of the frictional connection, the pile capacity increased by 34.6% and 27% at the pile offsets of 4d and 6d, respectively. These differences were higher than the differences that shown in Set 7 because the wall was more stable due to the high reinforcement length. However, the chosen comparison load for this set is equal to 700 N.

Deflection of wall facing

The deflection at the vertical centerline of the wall facing of Group H2 L3 S1 **C1** D123 and Group H2 L3 S1 **C2** D123 is shown in Figure 5.99. On the other hand, Figure 5.100 presents the transverse deflection of the wall for the two groups at 84% of the wall height. The behavior that shown in Figures 5.99. and 5.100 is similar to the wall deflection behavior that shown in Set 7.

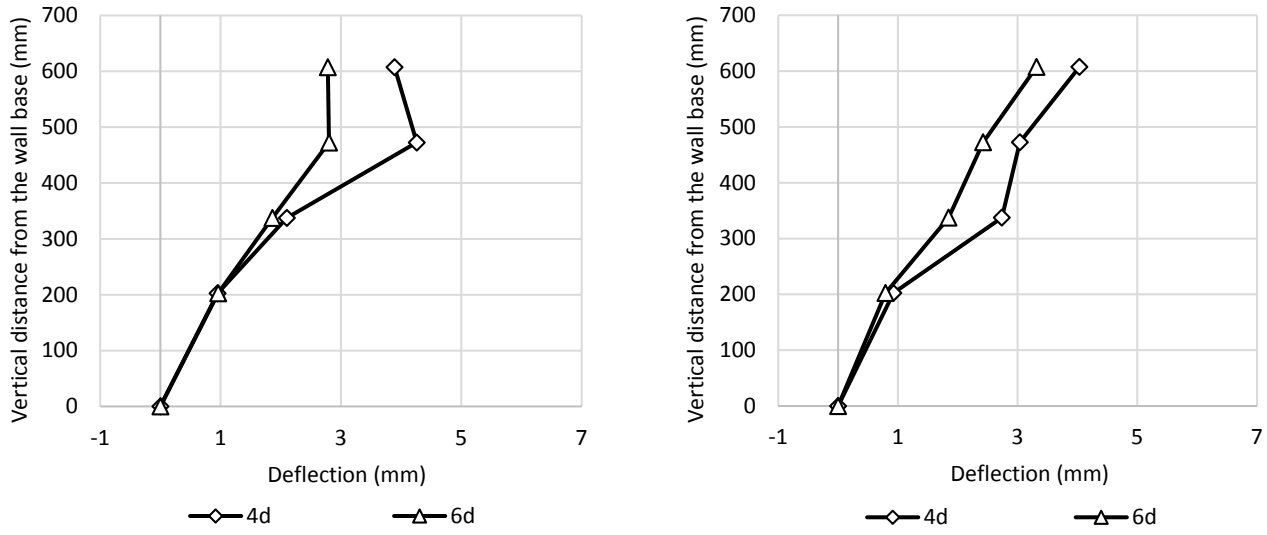

(a) (b)

Figure 5.99 Deflections of the wall facing along the vertical centerline at a load of 700 N in: (a) Group (H2 L3 S1 C1 D23) and (b) Group (H2 L3 S1 C2 D23).

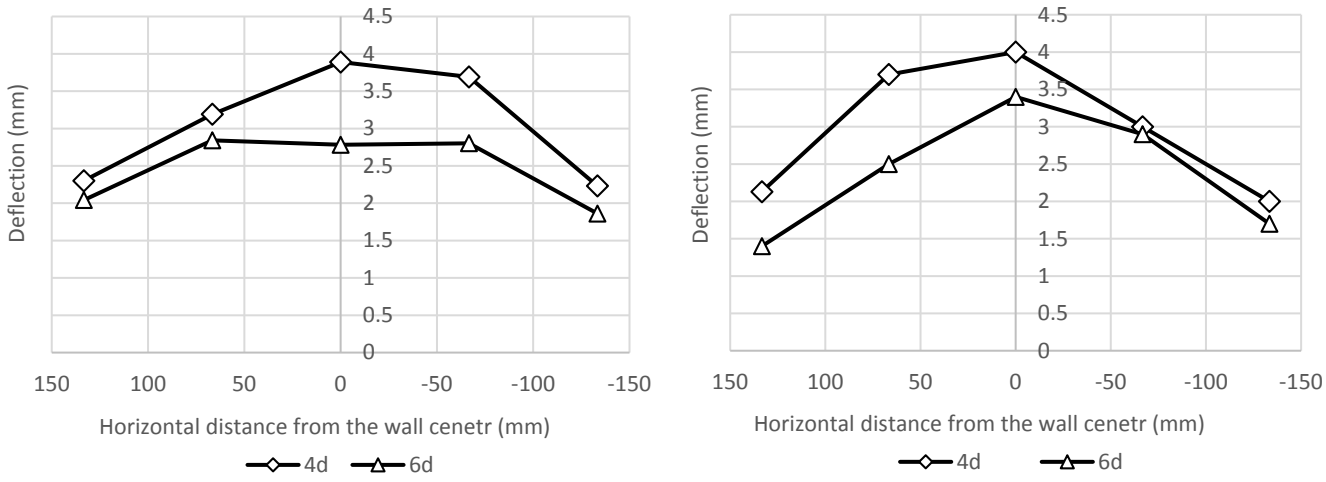

(a) (b)

Figure 5.100 Transverse distribution of the wall deflection at 84% of the wall height and a load of 700 N in: (a) Group (H2 L3 S1 C1 D23) and (b) Group (H2 L3 S1 C2 D23).

Strain, Stress, and moment of the pile

The strain distribution along the pile for Groups H2 L3 S1 C1 D23 and H2 L3 S1 C2 D23

is shown in Figure 5.101. In each group, the maximum strain location for the both pile's sides was at an elevation equal to 44% of the pile height. At the pile offset of 6d, the location of the maximum strain at the compressive side of the pile was higher than 44% of the pile height. This location returns back to 44% of the pile height when the load increased as shown in Figure 4.145. However, the differences in the maximum compressive and tensile strain between the two pile offsets were small for Group H2 L3 S1 **C2** D23. On the other hand, these differences were relatively high for Group H2 L3 S1 **C1** D23 because of the use of the mechanical connection. In fact, the resistance to the pile deflection increased by using this connection. Thus, the strain inside the pile will be increased as well especially for the far pile offset. The same behavior applies to the stress and moment of the pile as shown in Figures 5.102 and 5.103.

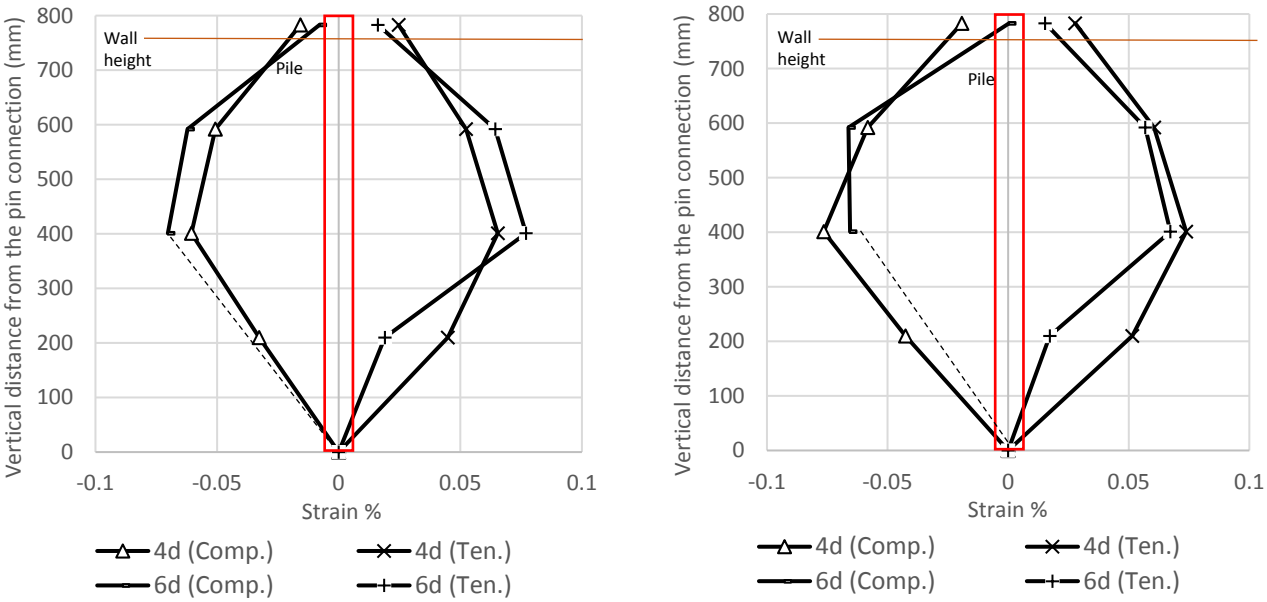

Figure 5.101 Strains of the laterally loaded pile at a load of 700 N in: (a) Group (H2 L3 S1 C1 D23) and (b) Group (H2 L3 S1 C2 D23)

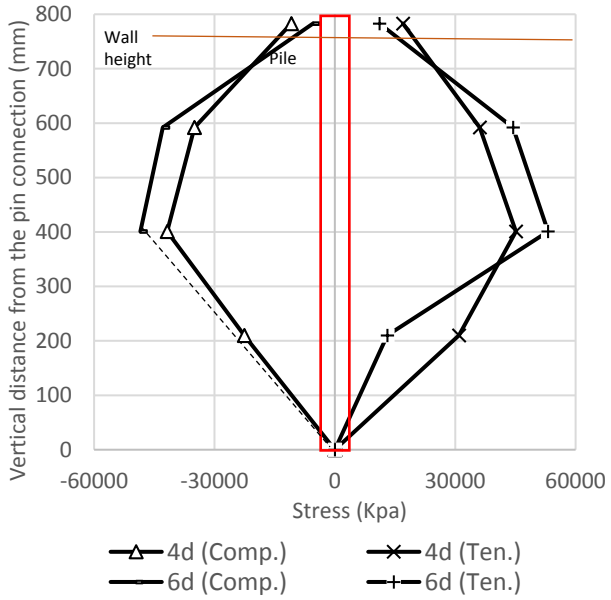

(a)

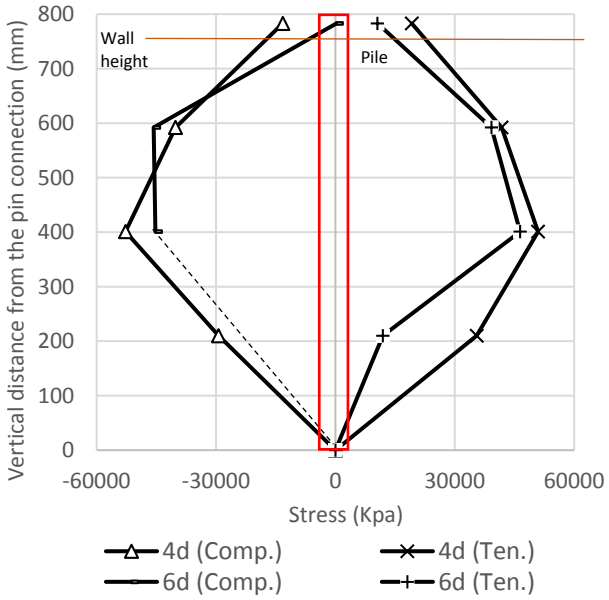

(b)

Figure 5.102 Stresses of the laterally loaded pile at a load of 700 N in: (a) Group (H2 L3 S1 C1 D23) and (b) Group (H2 L3 S1 C2 D23).

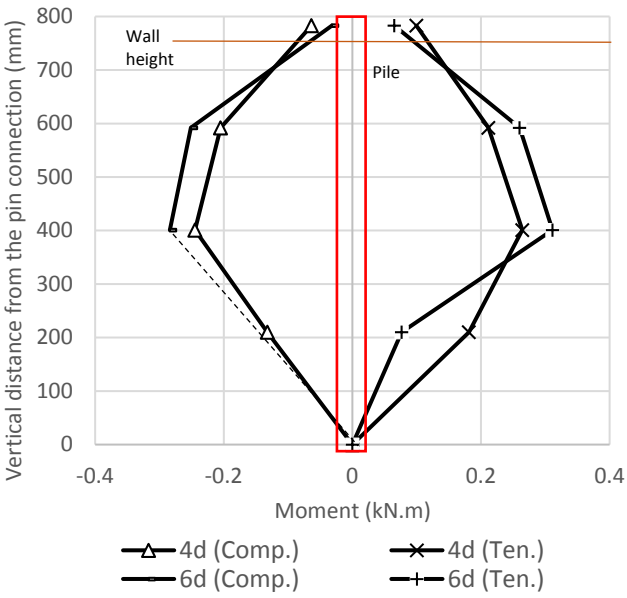

(a)

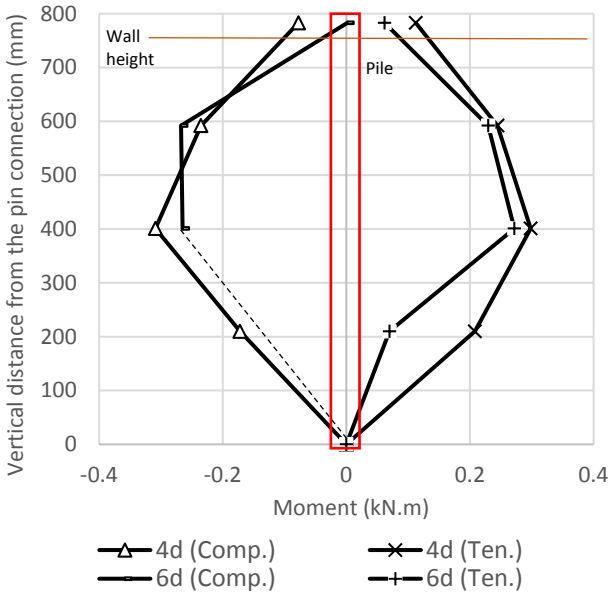

(b)

Figure 5.103 Moments of the laterally loaded pile at a load of 400 N in: (a) Group (H2 L3 S1 C1 D23) and (b) Group (H2 L3 S1 C2 D23).

Strain of the geogrid

Figures 5.104, 5.105, 5.106, and 5.107 show the strain distribution by using the first analysis approach while Figures 5.108 and 5.109 show the strain distribution by using the second analysis approach. For the same spacing between the geogrid, the strain distributions of gauges groups G1, G2, and G3 were the highest at the pile offset of 4d as shown in Figures 5.104, 5.105, and 5.106. the reason is that these gauges group were near to the location of the pile at that offset. For the gauges group G4, both of the pile locations 4d and 6d were near to the location of this gauges group. Therefore, the stain distribution id closed as shown in Figure 5.107.

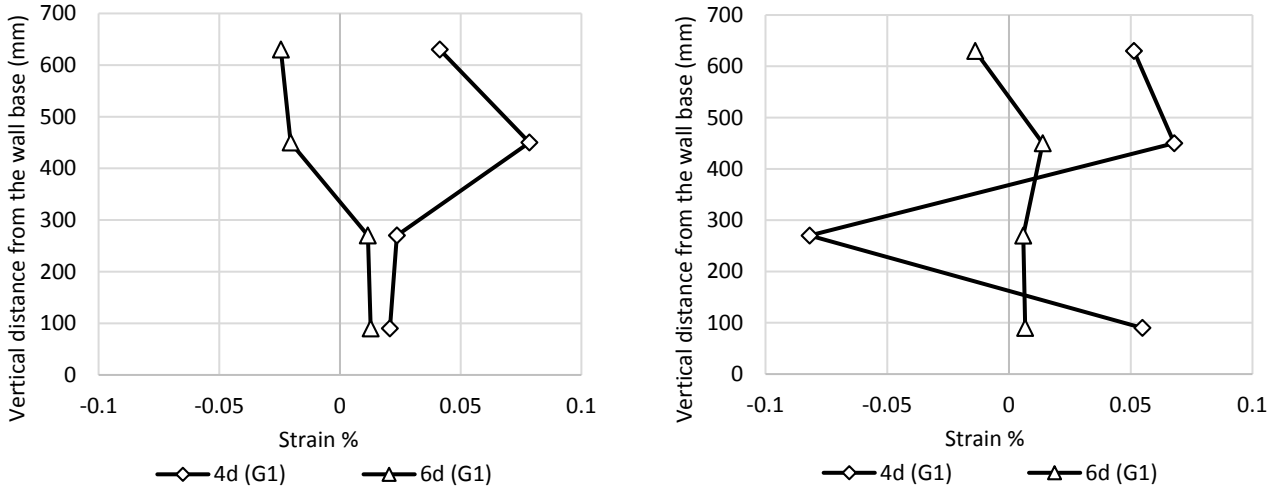

Figure 5.104 Strains of the geogrid layers at a load of 700 N in: (a) Gauges group (G1) of Group (H2 L3 S1 C1 D23) and (b) Gauges group (G1) of Group (H2 L3 S1 C2 D23).

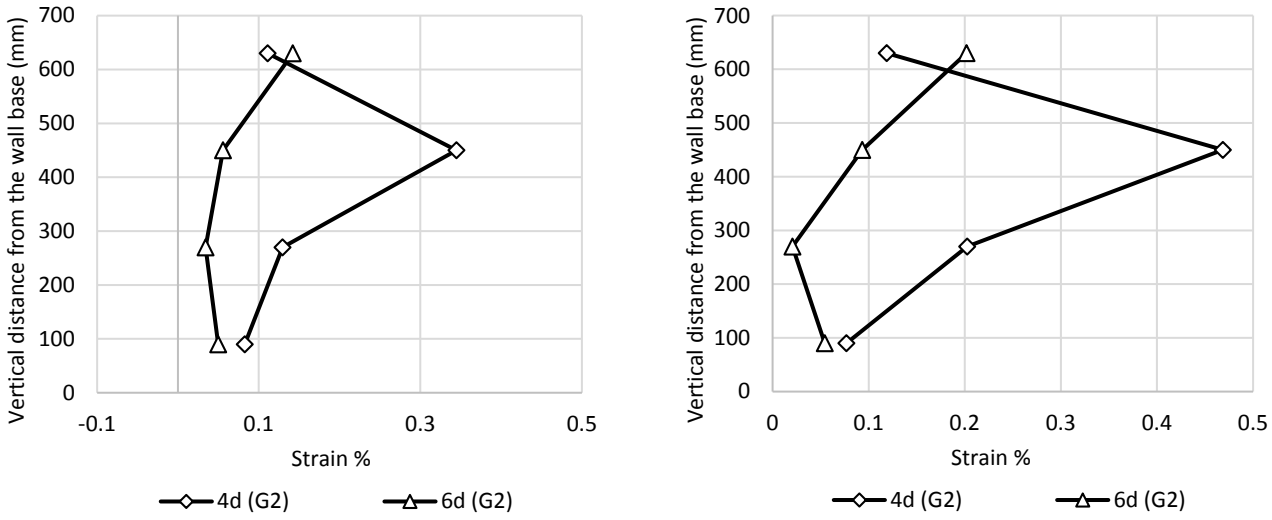

(a) (b)

Figure 5.105 Strains of the geogrid layers at a load of 700 N in: (a) Gauges group (G2) of Group (H2 L3 S1 C1 D23) and (b) Gauges group (G2) of Group (H2 L3 S1 C2 D23).

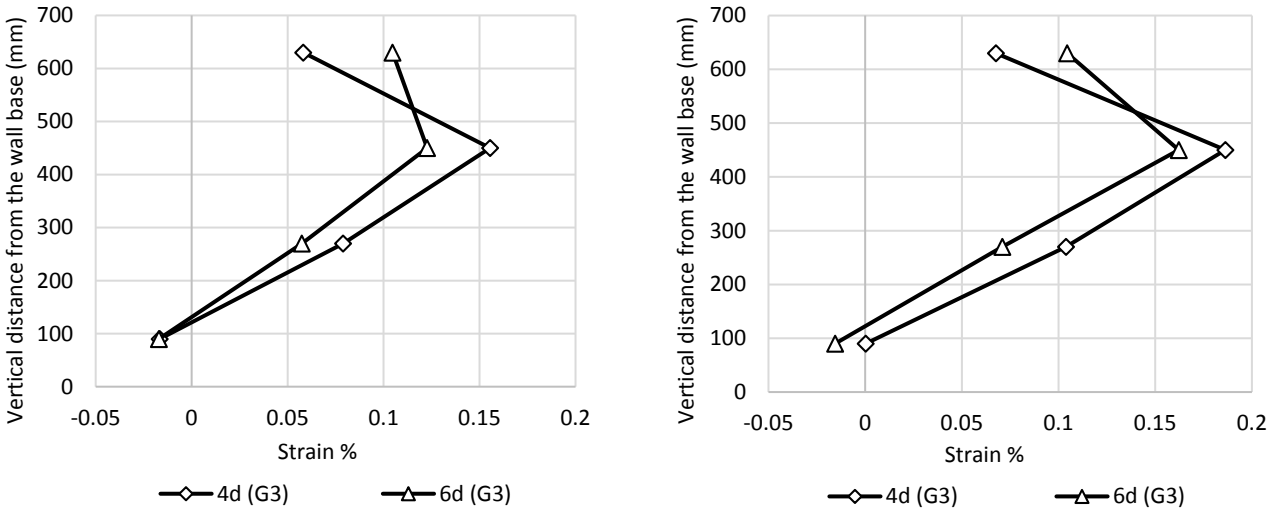

(a) (b)

Figure 5.106 Strains of the geogrid layers at a load of 700 N in: (a) Gauges group (G3) of Group (H2 L3 S1 C1 D23) and (b) Gauges group (G3) of Group (H2 L3 S1 C2 D23).

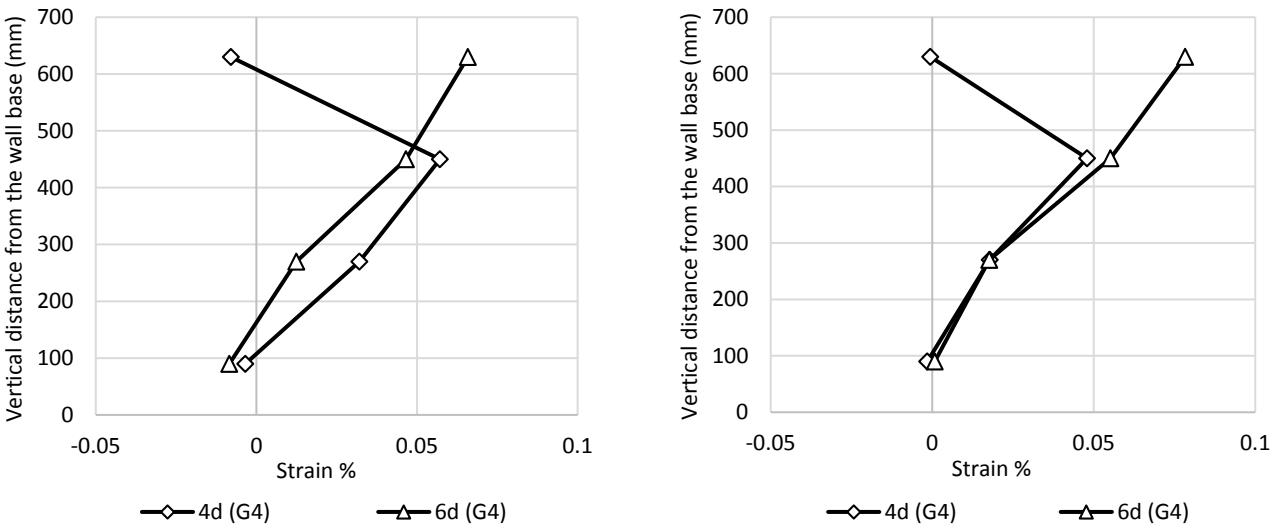

(a) (b)

Figure 5.107 Strains of the geogrid layers at a load of 700 N in: (a) Gauges group (G4) of Group (H2 L3 S1 C1 D23) and(b) Gauges group (G4) of Group (H2 L3 S1 C2 D23).

From Figure 5.108, the tensile strain distribution of gauges group G2 was the highest. The location of this gauges group was next to the pile location at the pile offset of 4d as shown in Figure 3.17 (a). From Figure 5.109, both tensile strain distributions of Gauges groups G2 and G3 were high because the pile was located between these gauges groups as shown in Figure 3.17 (b. However, the differences of the values of the maximum tensile strain between the two groups were insignificant as shown in Figures 5.108, and 5.109.

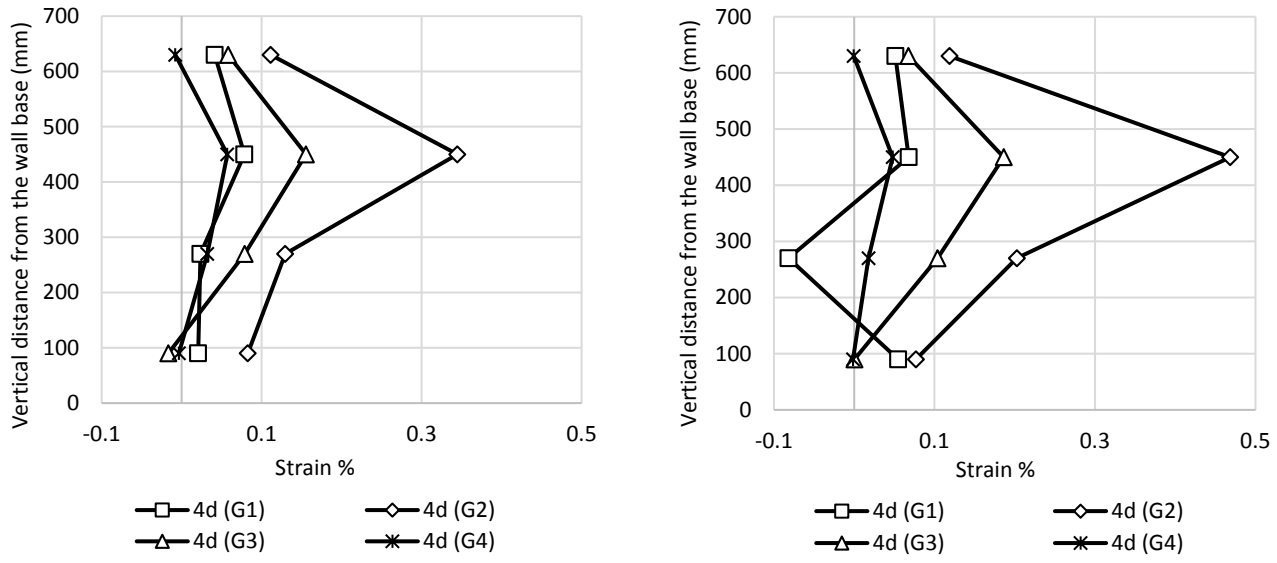

(a) (b)

Figure 5.108 Strains of the geogrid layers at a load of 700 N in: (a) Pile offset (4d) of Group (H2 L3 S1 C1 D123) and (b) Pile offset(6d) of Group (H2 L3 S1 C2 D123).

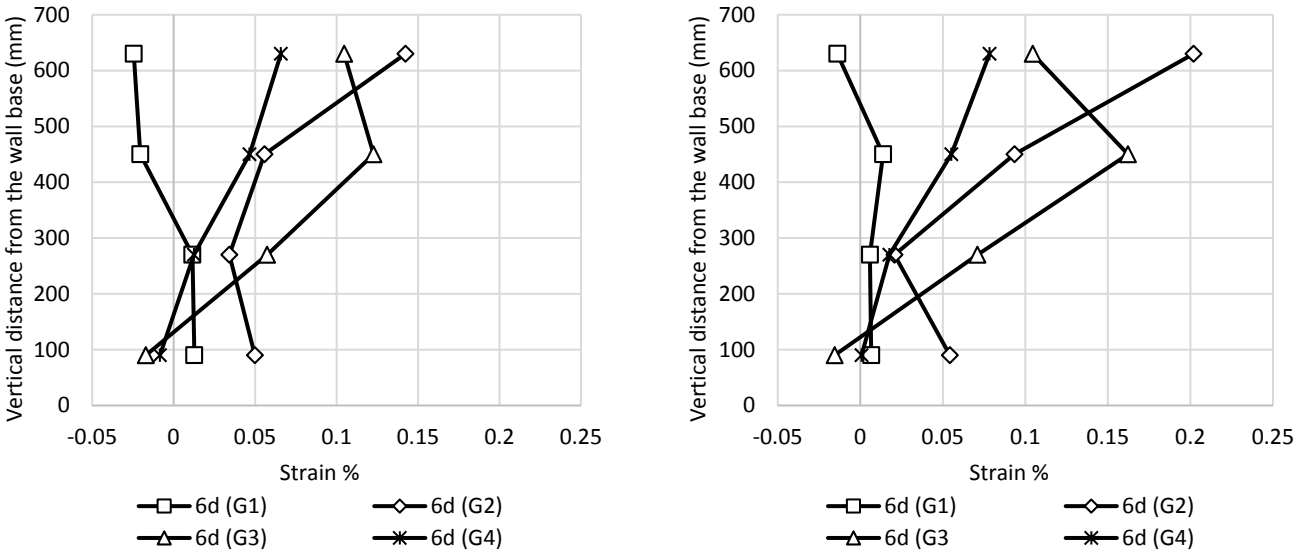

(a) (b)

Figure 5.109 Strains of the geogrid layers at a load of 700 N in: (a) Pile offset (6d) of Group (H2 L3 S1 C1 D23) and (b) Pile offset (6d) of Group (H2 L3 S1 C2 D23).

Pressure behind the wall facing

Figure 5.110 shows the pressure distributions behind the vertical centerline of the wall facing of Groups H2 L3 S1 **C1** D23 and H2 L3 S1 **C2** D23. On the other hand, Figure 5.111 shows the transverse pressure distributions of the two groups at 84% of the wall height.

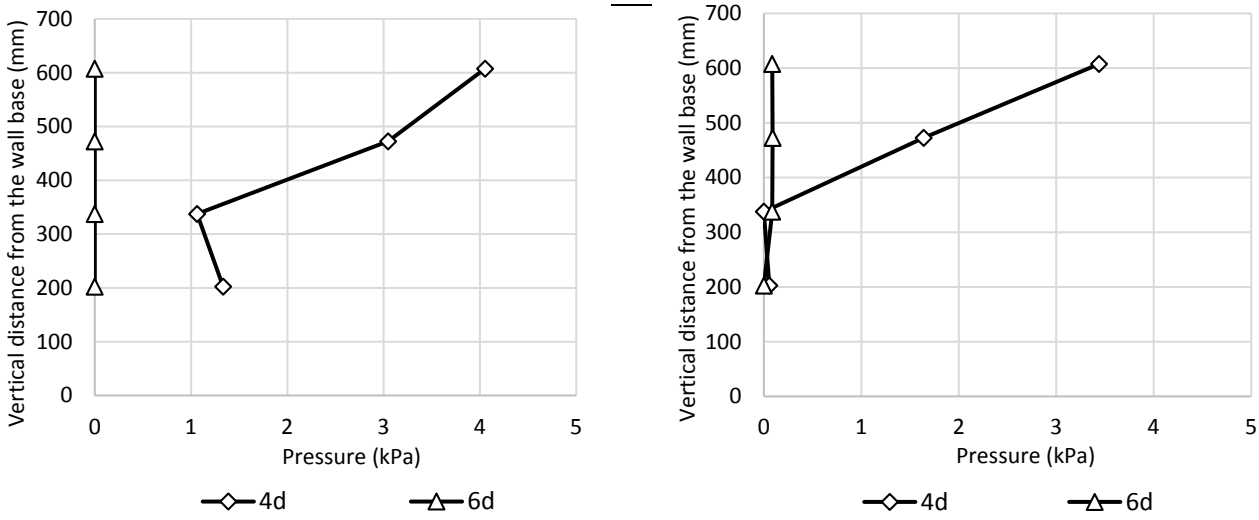

(a) (b)

Figure 5.110 Pressures behind the wall facing at load of 700 N in: (a) Group (H2 L3 S1 C1 D23) and (b) Group (H2 L3 S1 C2 D23).

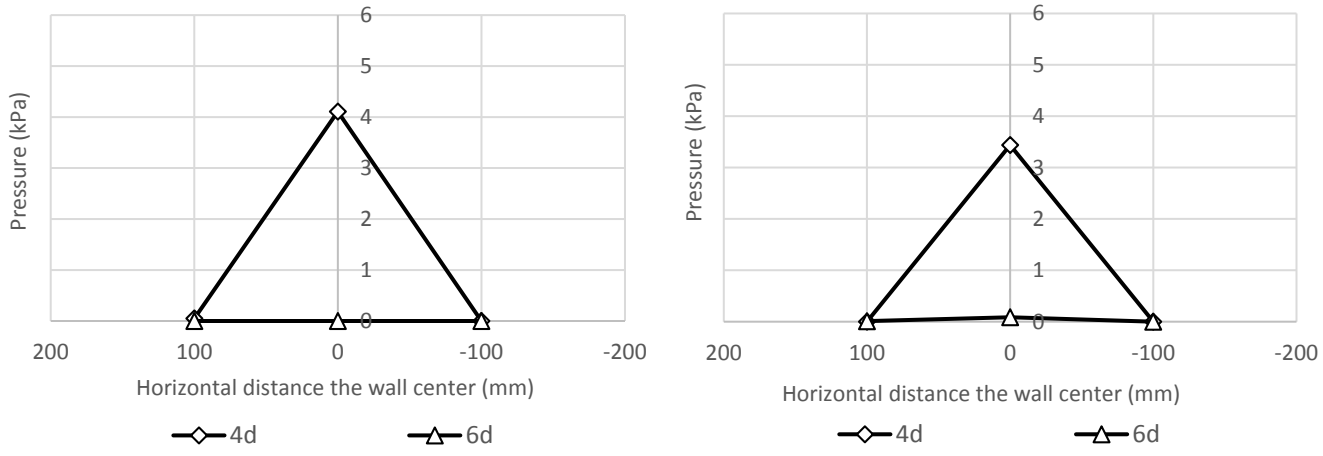

(a) (b)

Figure 5.111 Transverse distribution of the pressures at 84% of the wall height and a load of 700 N in: (a) Group (H2 L3 S1 C1 D23) and (b) Group (H2 L3 S1 C2 D23).

At the pile offsets of 4d and 6d, the behaviors of the pressure distribution at the vertical centerline and transverse profiles were similar to the behavior that shown in Set 7.

Chapter 6 Conclusions

6.1. Introduction

This study investigated the influence factors on the performance of laterally loaded piles in MSE walls. Eighteen model tests were conducted by changing the wall height, the reinforcement length, the pile offset from the wall facing, and the wall connection. Pile and wall deflections, earth pressures behind wall facing, and strains on piles and geogrids were measured. The measured data were reduced and analyzed.

The tests results are first summarized for three test groups of low walls with regular reinforcement length, high walls with regular reinforcement length, and high walls with long reinforcement length. Then, the analysis of the test results is provided for eight comparison sets. Set 1 includes tests with small spacing, mechanical connection, and different wall height and reinforcement length. Set 2 includes high wall tests with regular reinforcement length, mechanical connection, and different reinforcement spacing. Set 3 includes high wall tests with long reinforcement length, mechanical connection, and different reinforcement spacing. Set 4 includes high wall tests with large reinforcement spacing, mechanical connection, and different reinforcement length. Set 5 includes high wall tests with small reinforcement spacing, mechanical connection, and different reinforcement length. Set 6 includes high wall tests with small reinforcement spacing, frictional connection, and different reinforcement length. Set 7 includes high wall tests with small reinforcement spacing, regular reinforcement length, and different wall connection. Set 8 includes high wall tests with small reinforcement spacing, long reinforcement length, and different wall connection. After finishing the analysis conclusion, the overall conclusions are made in the following sections. Finally, the future work is recommended.

6.2. Tests results

6.2.1. Low walls with regular reinforcement length

1. The lateral deflections of the pile and the vertical centerline of the wall facing decreased by the increase of the pile offset. Moreover, the lateral deflection of the wall facing in the transverse direction became more uniform by the increase of the pile offset.
2. The maximum compressive strain of the pile occurred at 44% of the pile height while the maximum tensile strain occurred at 22% of the pile height. This difference resulted from the low wall in front of the pile.
3. The geogrid layers experienced high strains in the longitudinal and transverse directions at the large pile offsets.

6.2.2. High walls with regular reinforcement length

1. The lateral deflections of the pile and the vertical centerline of the wall facing decreased by the increase of the pile offset. In addition, the lateral deflection of the wall facing in the transverse direction became more uniform by the increase of the pile offset.
2. The maximum compressive and tensile strains occurred at 44% of the pile height, which was at the middle of the wall.
3. The tensile strains along the uppermost geogrid layer decreased by the increase of the pile offset.
4. The lateral pressures behind the upper part of the vertical centerline of the wall facing decreased by the increase of the pile offset. Furthermore, the lateral pressures behind

the upper part of the wall in the transverse direction became more uniform by the increase of the pile offset.

6.2.3. High walls with long reinforcement length

1. At the pile offsets of 4d and 6d d is the pile diameter, the lateral deflection of the pile, the lateral deflection of the vertical centerline of the wall facing, the maximum compressive and tensile strains of the pile, and the lateral pressure behind the wall were similar to those mentioned in Section 6.2.2.
2. The high tension zone of the geogrid layers expanded with the increase of the geogrid length. Therefore, the tensile strain along the uppermost geogrid layer increased by the increase of the pile offset.

6.3. Analysis of test results

6.3.1. Effect of wall height

1. An increase of the wall height increased the pile capacity and the maximum compressive and tensile strains of the pile at a higher load.
2. An increase of the wall height reduced the lateral deflection of the vertical centerline of the wall facing and the maximum tensile strain of the geogrids strain profiles. On the other hand, an increase of the wall height increased the uniformity of the lateral deflection of the wall facing in the transverse direction.

6.3.2. Effect of reinforcement parameters

Reinforcement spacing

1. For Sets 2 and 3, a decrease of the reinforcement spacing increased the pile capacity.

2. For Sets 2 and 3, an increase of the reinforcement spacing increased the lateral deflection of the vertical centerline of the wall facing and the maximum tensile strain of the geogrids strain profiles. However, a decrease of the reinforcement spacing increased the uniformity of the lateral deflection of the wall facing in the transverse direction.
3. There was no significant change in the maximum compressive and tensile strains of the pile by changing the reinforcement spacing for Set 2. On the other hand, there was a small change in the maximum compressive and tensile strains of the pile at the pile offset of 4d for Set 3. This change resulted from the increase in the resistance because of the reduction of the reinforcement spacing.
4. There was no significant change in the lateral pressure behind the upper part of the vertical centerline of the wall facing by changing the reinforcement spacing for Set 2. However, an increase of the reinforcement spacing increased the lateral pressure behind the upper part of the vertical centerline of the wall facing for Set 3.

Reinforcement length

1. For Sets 4, 5 and 6, an increase of the reinforcement length increased the pile capacity and decreased the lateral deflection of the vertical centerline of the wall facing. In addition, an increase of the reinforcement length increased the uniformity of the lateral deflection of the wall facing in the transverse direction.
5. The maximum compressive and tensile strains of the pile do not change by changing the reinforcement length of Set 6. Only an increase of the reinforcement length increased the maximum compressive strain at the pile offset of 6d for Set 4. However,

an increase of the reinforcement length resulted in a small decrease in the maximum compressive and tensile strains at the pile offset of 4d for Set 3 of Set 5.

3. An increase of the reinforcement length increased the lateral pressure behind the upper part of the vertical centerline of the wall facing of Set 4. On the other hand, there was no significant change in the lateral pressure behind the upper part of the vertical centerline of the wall facing when the reinforcement length of Sets 4d and 6d was changed.

Facing connection

1. There was no significant change in the pile capacity by changing the connection type for Set 7. However, the use of the frictional connection instead of the mechanical connection resulted in the decrease of the pile capacity for Set 8.
2. There was no significant change in the lateral deflection of the vertical centerline of the wall facing by changing the facing connection type for Set 8.
3. For Sets 7 and 8 there was no significant change in the maximum tensile strain of the geogrids strain profiles by changing the connection type.
4. For Sets 7 and 8 the use of the frictional connection instead of the mechanical connection reduced the lateral pressure behind the upper part of the vertical centerline of the wall facing.

6.4. Overall Conclusions

1. The tensile strain of the geogrid layer was high near to pile location especially when the pile was within the maximum tensile zone of the geogrid.

2. The effect of the wall connection on the pile capacity was related to the length of the reinforcement layers. In fact, an increase of the reinforcement length increased this effect as shown in the capacity comparison between the groups of Set 8.
3. Two high lateral earth pressure zones were induced behind the vertical centerline of the wall facing. A decrease of the pile offset increased the pressure in the high-pressure zone behind the upper part of the wall. In addition, the spacing between the reinforcement layers affected the location of the maximum pressure. On the other hand, the high-pressure zone behind the lower part decreased by the increase of the reinforcement length.

6.5. Future work

The tests conducted in this study were under static load only. Further studies are recommended to investigate the factors influencing performance of a pile within an MSE wall under repeated lateral loading. On the other hand, a single pile was used in the model tests in this study. Tests to examine the effect of pile group is highly recommended. Finally, numerical analyses should be conducted to analyze the test results in this study to gain in-depth knowledge of the behavior of piles in MSE walls.

Refrence

AASHTO (2012). *AASHTO LRFD Bridge Design Specifications*, American Association of State Highway and Transportation Officials, Washington, DC.

Anderson, P. L., and Brabant, K. "Increased use of MSE abutments." *Proc., International Bridge Conference*.

API (1991). "Recommended practice for planning, designing and constructing fixed offshore platforms." *API recommended practice 2A (RP2A)*, API.

Berg, R., Vulova, C., Deaton, H., and Hashash, Y. "Effects of pile driving through a full-height precast concrete panel faced, geogrid-reinforced, mechanically stabilized earth (MSE) wall." *Proc., Case Studies In Earth Retaining Structures*, ASCE, 1-10.

Bowman, E. R. (1958). "Investigation of the lateral resistance to movement of a plate in cohesionless soil." Master of Science in Civil Engineering, University of Texas at Austin.

Briaud, J. L., Smith, T., and Meyer, B. "Using the pressuremeter curve to design laterally loaded piles." *Proc., Offshore Technology Conference*, Offshore Technology Conference.

Broms, B. B. (1964). "Lateral resistance of piles in cohesionless soils." *Journal of the Soil Mechanics and Foundations Division*, 90(3), 123-158.

Broms, B. B. (1964). "Lateral resistance of piles in cohesive soils." *Journal of the Soil Mechanics and Foundations Division*, 90(2), 27-64.

Elias, V., Christopher, B. R., and Berg, R. R. (2001). "Mechanically Stabilized Earth Walls and Reinforced Soil Slopes Design and Construction Guidelines."

FHWA (2001). "Mechanically Stabilized Earth Walls and Reinforced Soil Slopes Design and Construction Guidelines." V. Elias, B. R. Christopher, and R. R. Berg, eds., FHWA.

FHWA (2007). "Mechanically stabilized earth wall abutments for bridge support." I. Zevgolis, and P. L. Bourdeau, eds.West Lafayette, IN

Fleming, W. (1992). "A new method for single pile settlement prediction and analysis." *Géotechnique*(42), 41H2 L2 S1 C2 D125.

Han, J., and Frost, J. (2000). "Load–deflection response of transversely isotropic piles under lateral loads." *International journal for numerical and analytical methods in geomechanics*, 24(5), 509-529.

Hansen, J. B., and Christensen, N. H. (1961). *The Ultimate Resistance of Rigid Piles Against Transversal Forces: Model Tests with Transversally Loaded Rigid Piles in Sand*, Geoteknisk Institut.

Hatch, C. K. (2014). "Lateral Resistance of Piles Near Vertical MSE Abutment Walls." Master of Science, Brigham Young University, Pravo, UT.

Huang, J., Han, J., Parsons, R. L., and Pierson, M. C. (2013). "Refined numerical modeling of a laterally-loaded drilled shaft in an MSE wall." *Geotextiles and Geomembranes*, 37, 61-73.

Huang, J., Parsons, R. L., Han, J., and Pierson, M. (2011). "Numerical analysis of a laterally loaded shaft constructed within an MSE wall." *Geotextiles and Geomembranes*, 29(3), 23H2 L2 S2 C1 D341.

Ismael, O. K. (2014). "Evaluating the Behavior of Laterally Loaded Piles under a Scoured Condition by Model Tests." Master of Science, University of Kansas.

Kulhawy, F. H. (1991). "Drilled shaft foundations." *Foundation engineering handbook*, Springer, 537-552.

Kulhawy, F. H., O'Rourke, T., Stewart, J. P., and Beech, J. (1983). *Transmission Line Structure Foundations for Uplift-compression Loading, Load Test Summaries: Appendix to EPRI Final Report EL-2870*, Electric Power Research Institute.

Nelson, K. R. (2013). "Lateral Resistance of Piles Near Vertical MSE Abutment Walls at Provo Center Street." Master of Science, Brigham Young University, Provo, UT.

Pierson, M., Parsons, R., Han, J., and Brennan, J. (2009). "Capacities and Deflections of Laterally Loaded Shafts Behind Mechanically Stabilized Earth Wall." *Transportation Research Record: Journal of the Transportation Research Board*(2116), 6H2 L3 S1 C1 D29.

Pierson, M. C., Parsons, R. L., Han, J., and Brennan, J. J. (2010). "Laterally loaded shaft group capacities and deflections behind an MSE wall." *Journal of Geotechnical and Geoenvironmental Engineering*, 137(10), 882-889.

Poulos, H. G. (1971). "BEHAVIOR OF LATERALLY LOADED PILES I. SINGLE PILES." *Journal of Soil Mechanics & Foundations Div*.

Price, J. S. (2012). "Lateral Resistance of Piles Near Vertical MSE Abutment Walls." Master of Science, Brigham Young University, Provo, UT.

Reese, L. C., Isenhower, W. M., and Wang, S.-T. (2006). *Analysis and design of shallow and deep foundations*, Wiley Hoboken, NJ.

Rollins, K. M., Price, J. S., and Bischoff, J. (2011). "Lateral Resistance of Piles near Vertical MSE Abutment Walls." *Geo-Frontiers 2011*, American Society of Civil Engineers 3526-3535.

Rollins, K. M., Price, J. S., and Nelson, K. R. (2013). "Lateral Resistance of Piles Near Vertical MSE Abutment Walls." Utah Department of Transportation UT-1X.13

Sandvik, G., and Sowers, G. (1970). *Introductory soil mechanics and foundations*, Macmillan, New York.

Smith, T. D. (1987). "Pile horizontal soil modulus values." *Journal of Geotechnical Engineering*, 113(9), 1040-1044.

Xiao, C., Han, J., and Zhang, Z. (2015). "Experimental study on performance of geosynthetic-reinforced soil model walls on rigid foundations subjected to static footing loading." *Geotextiles and Geomembranes*.

Zhang, L., Silva, F., and Grismala, R. (2005). "Ultimate Lateral Resistance to Piles in Cohesionless Soils." *Journal of Geotechnical & Geoenvironmental Engineering*, 131(1), 78-83.

Appendix A Tests Data

A.1. Introduction

Parts of the data for Groups 1, 2, and 3 have been included in this appendix. Sections one and two represents the data of Groups 1 and 2 respectively while the final section represents the data of Group 3. Sub-sections have been considered in this appendix to show the data of each category in Group 2 and group 3.

A.2. Group 1

A.2.1. Deflection of the wall facing:

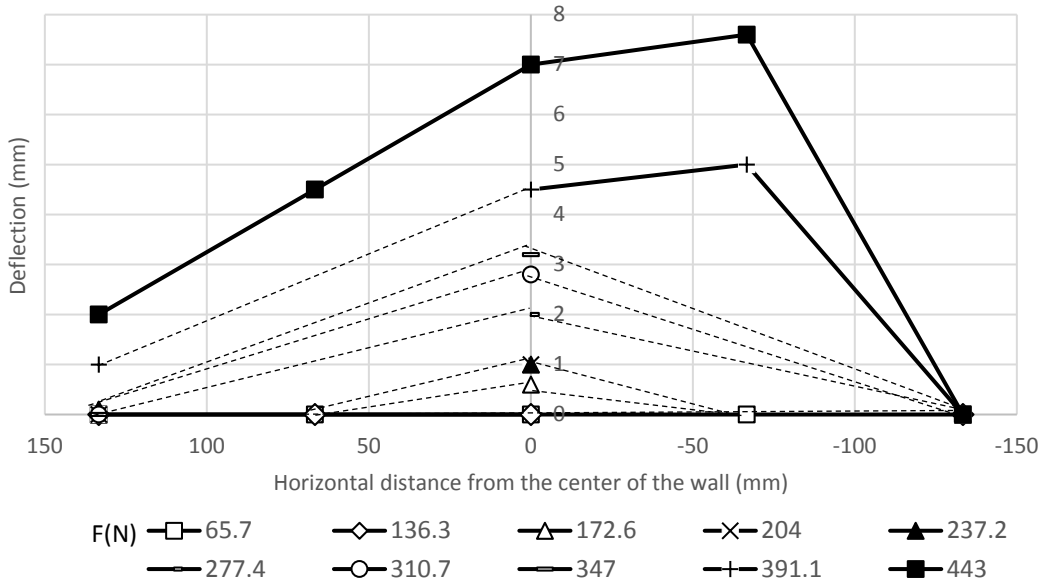

Figure A.1 Transverse deflection profiles at 202.5.5 mm from the wall base for Test H1 L1 S1 C1 D1.

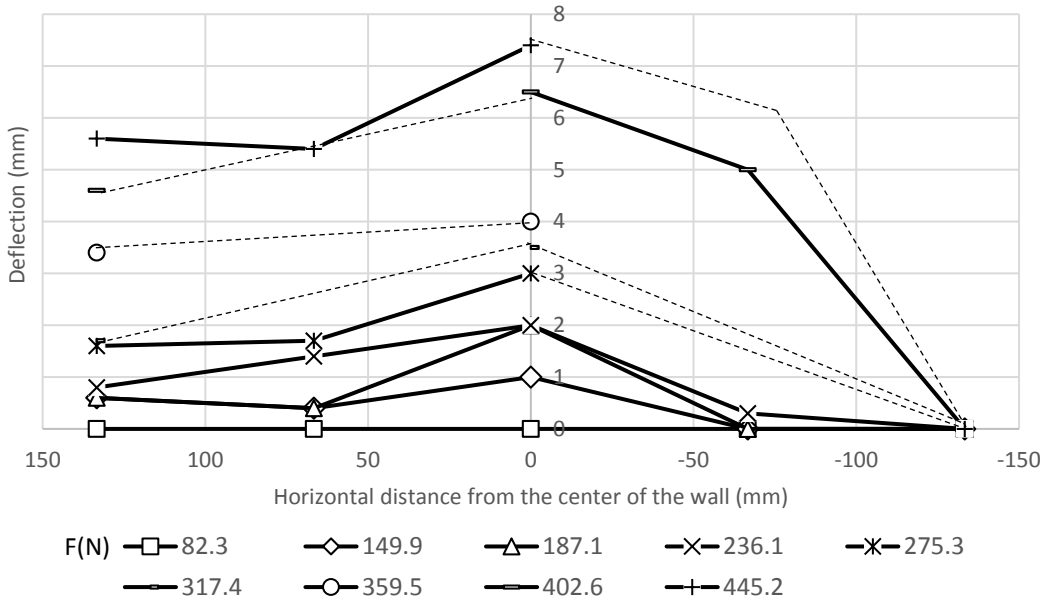

Figure A.2 Transverse deflection profiles at 202.5 mm from the wall base for Test H1 L1 S1 C1 D2.

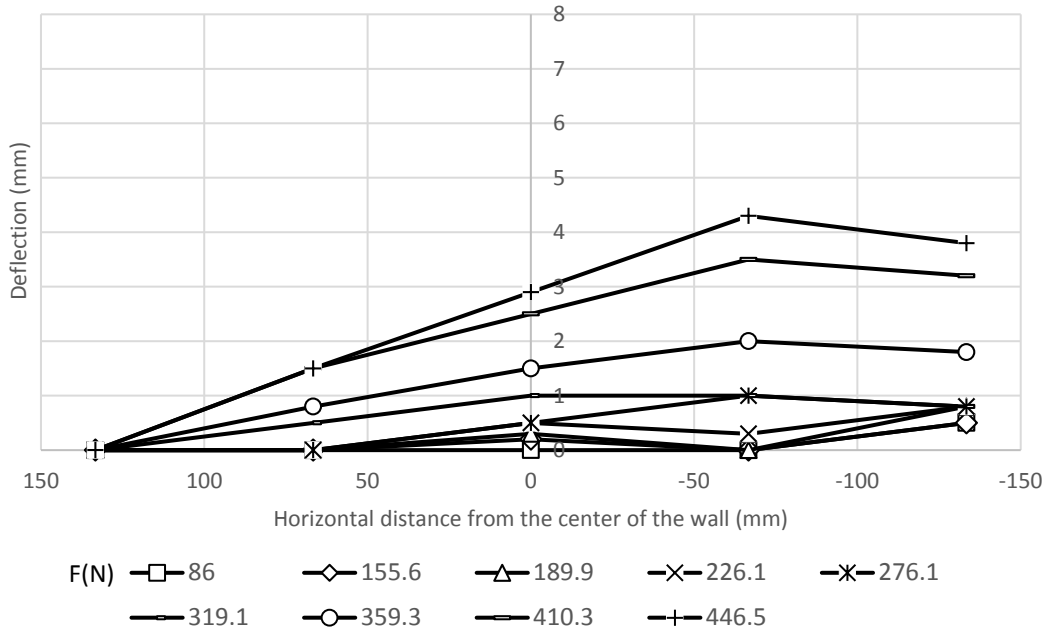

Figure A.3 Transverse deflection profiles at 202.5 mm from the wall base for Test H1 L1 S1 C1 D3.

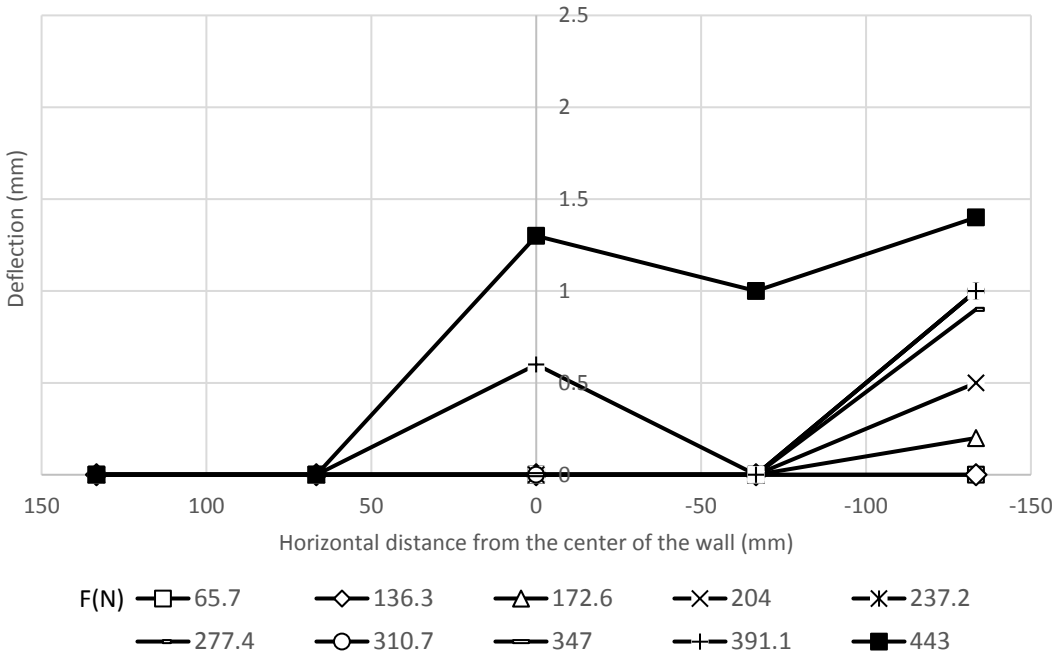

Figure A.4 Transverse deflection profiles at 112.5 mm from the wall base for Test H1 L1 S1 C1 D1.

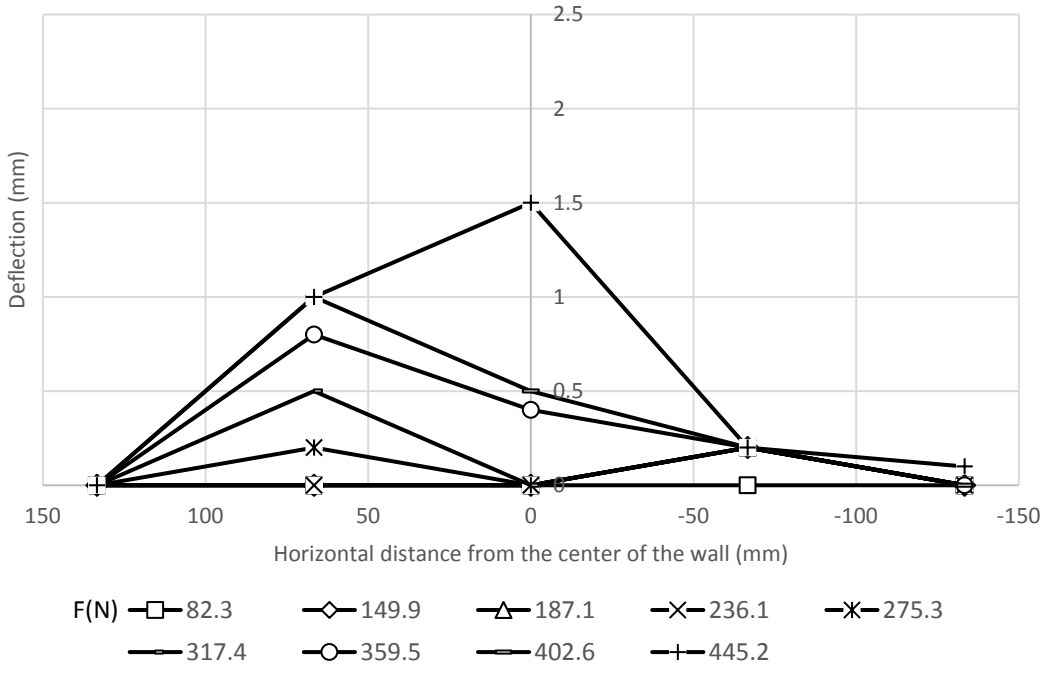

Figure A.5 Transverse deflection profiles at 112.5 mm from the wall base for Test H1 L1 S1 C1 D2.

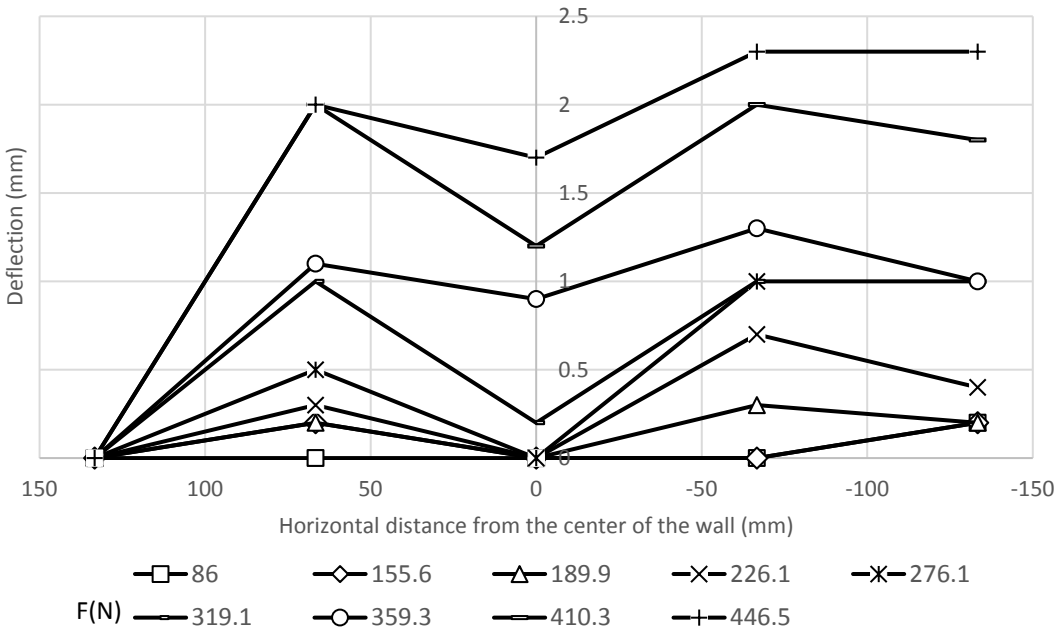

Figure A.6 Transverse deflection profiles at 112.5 mm from the wall base for Test H1 L1 S1 C1 D3.

A.2.2. Stress and moment of the pile:

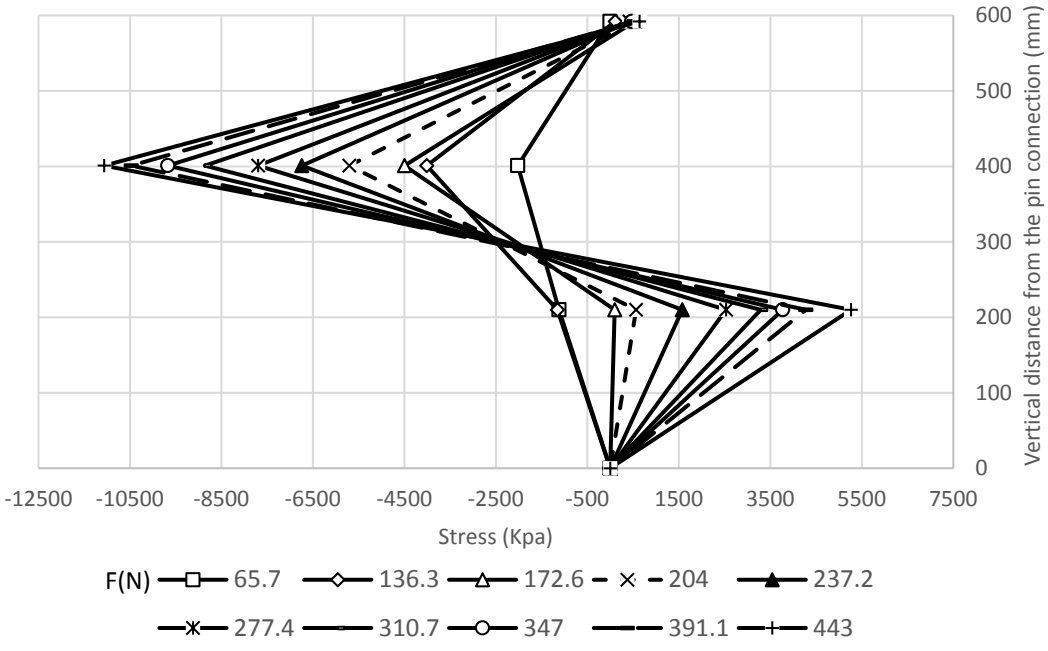

Figure A.7 Stresses along the compressive side of the pile in Test H1 L1 S1 C1 D1.

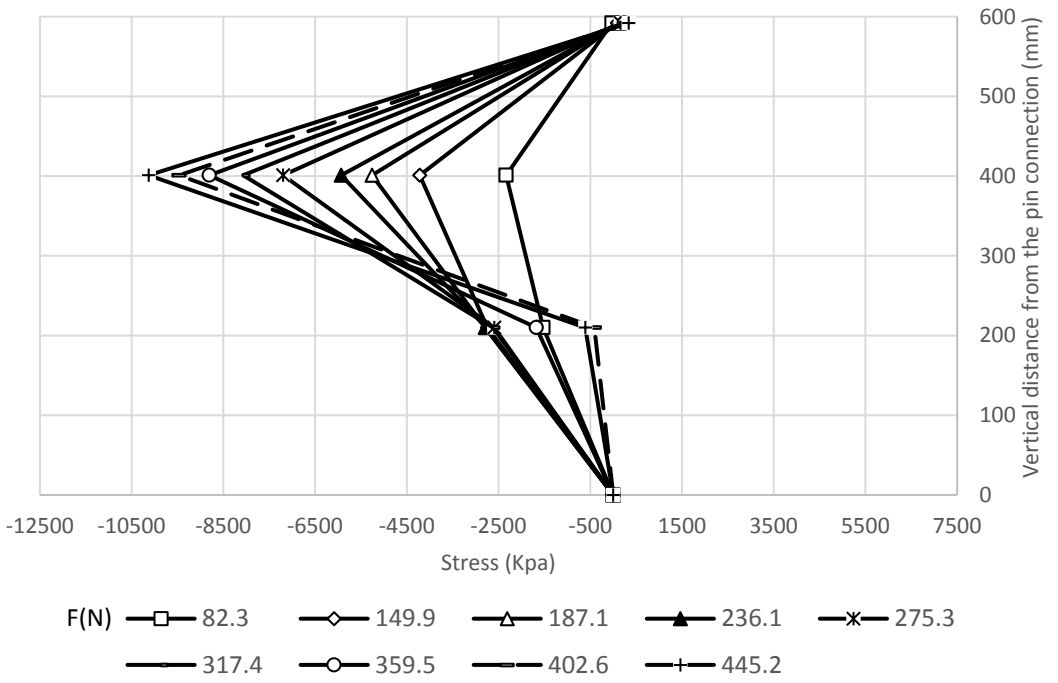

Figure A.8 Stresses along the compressive side of the pile in Test H1 L1 S1 C1 D2.

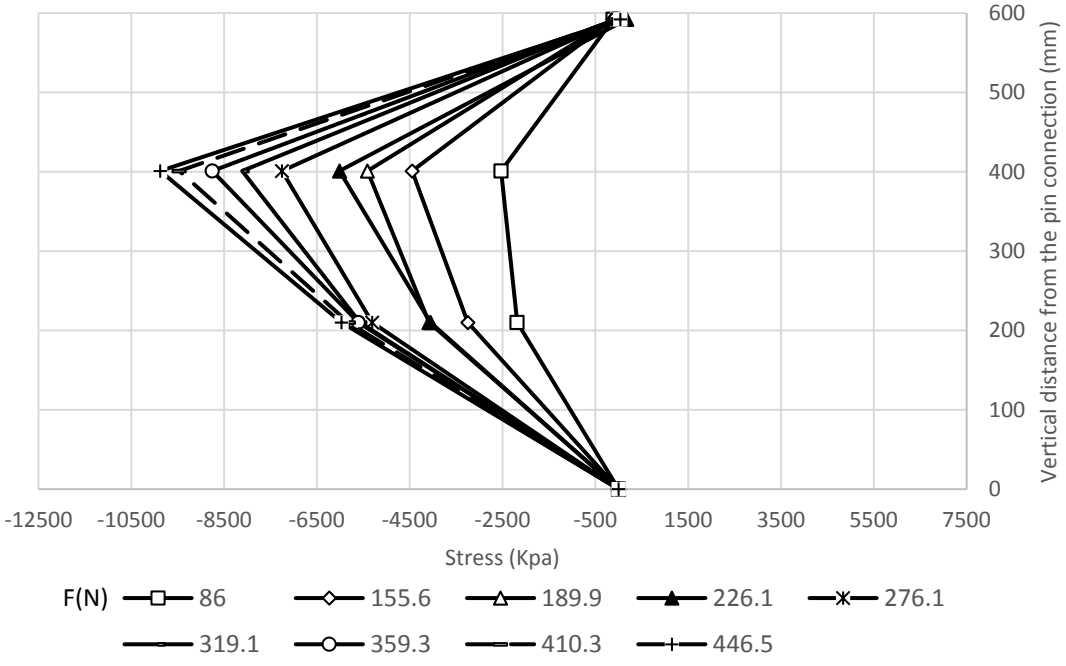

Figure A.9 Stresses along the compressive side of the pile in Test H1 L1 S1 C1 D3.

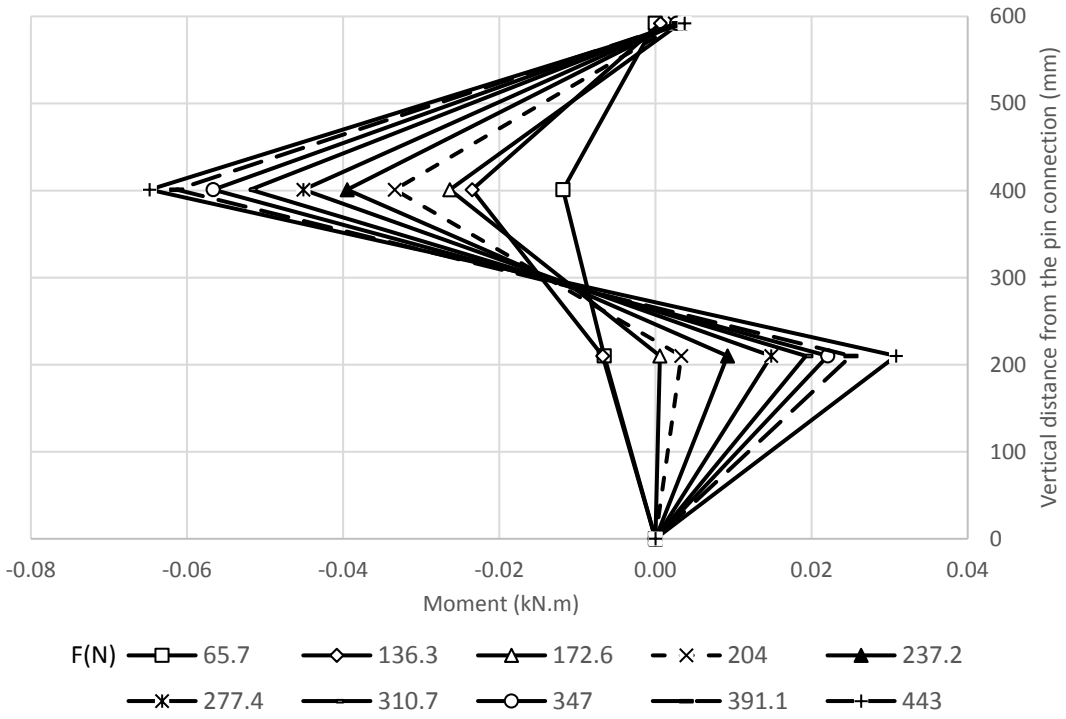

Figure A.10 Moments along the compressive side of the pile in Test H1 L1 S1 C1 D1.

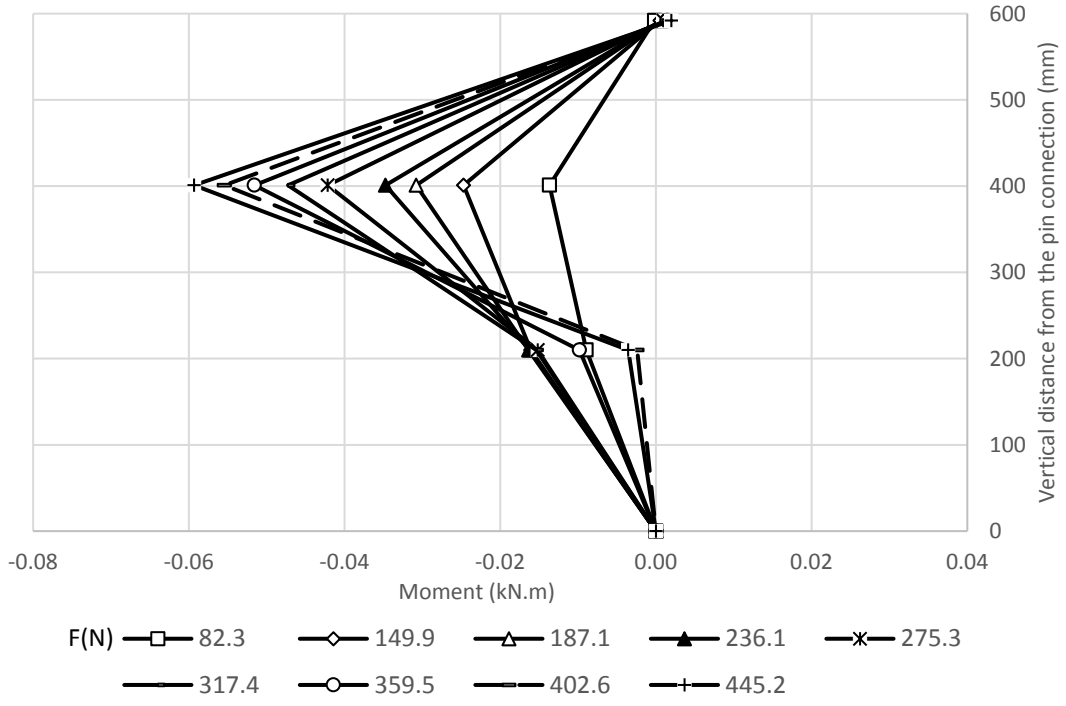

Figure A.11 Moments along the compressive side of the pile in Test H1 L1 S1 C1 D2.

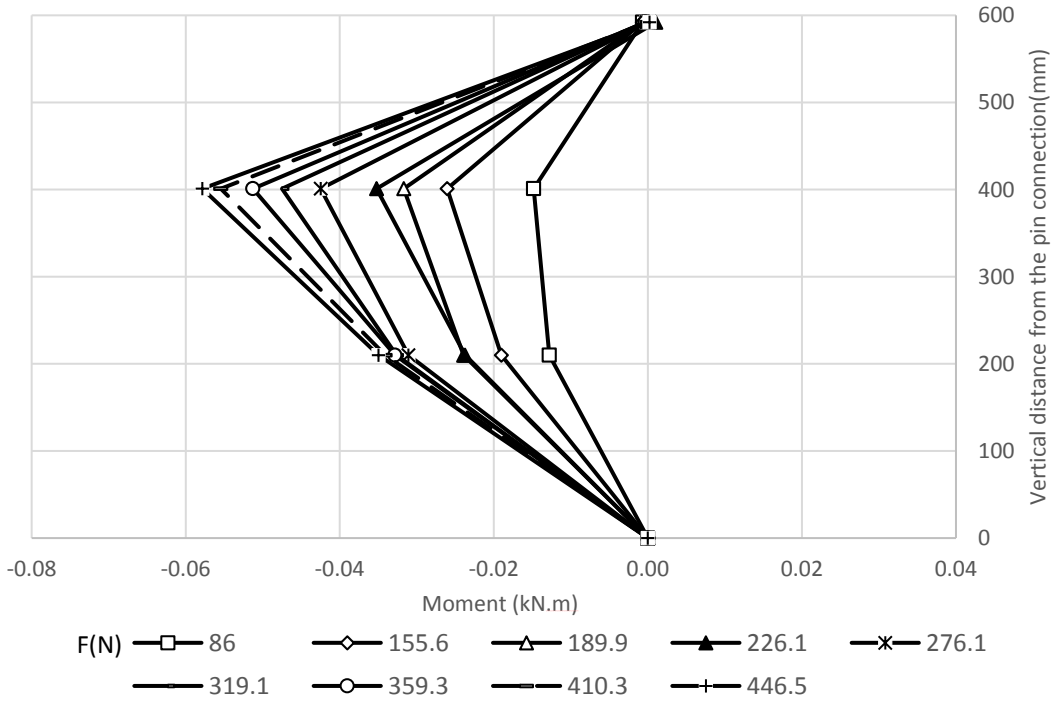

Figure A.12 Moments along the compressive side of the pile in Test H1 L1 S1 C1 D3.

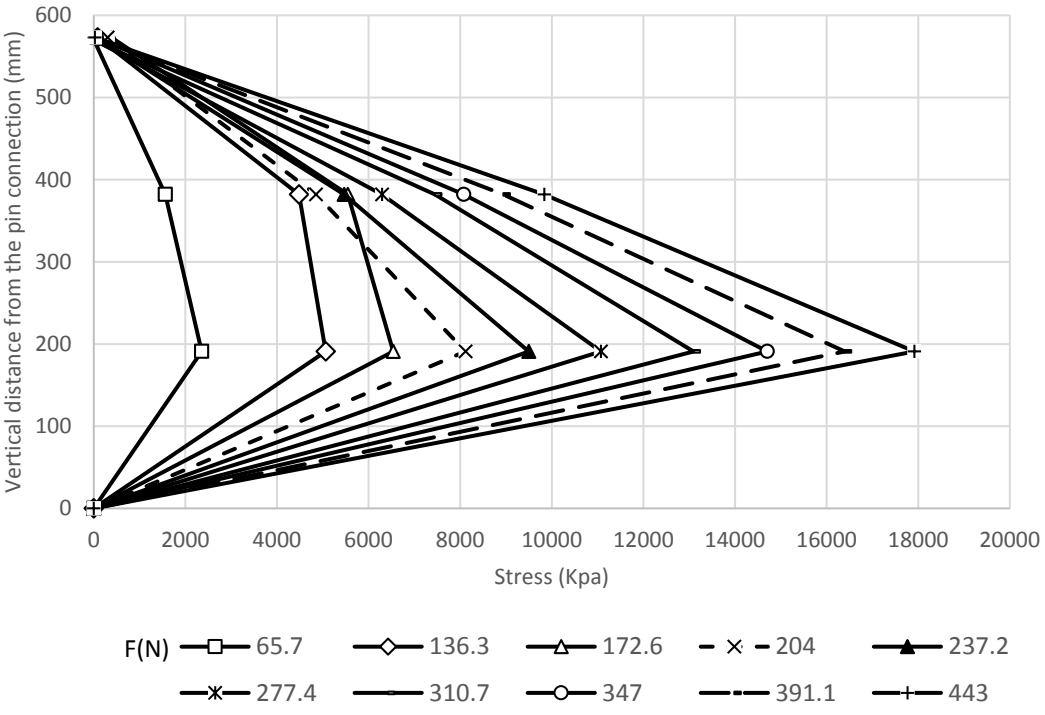

Figure A.13 Stresses along the tensile side of the pile in Test H1 L1 S1 C1 D1.

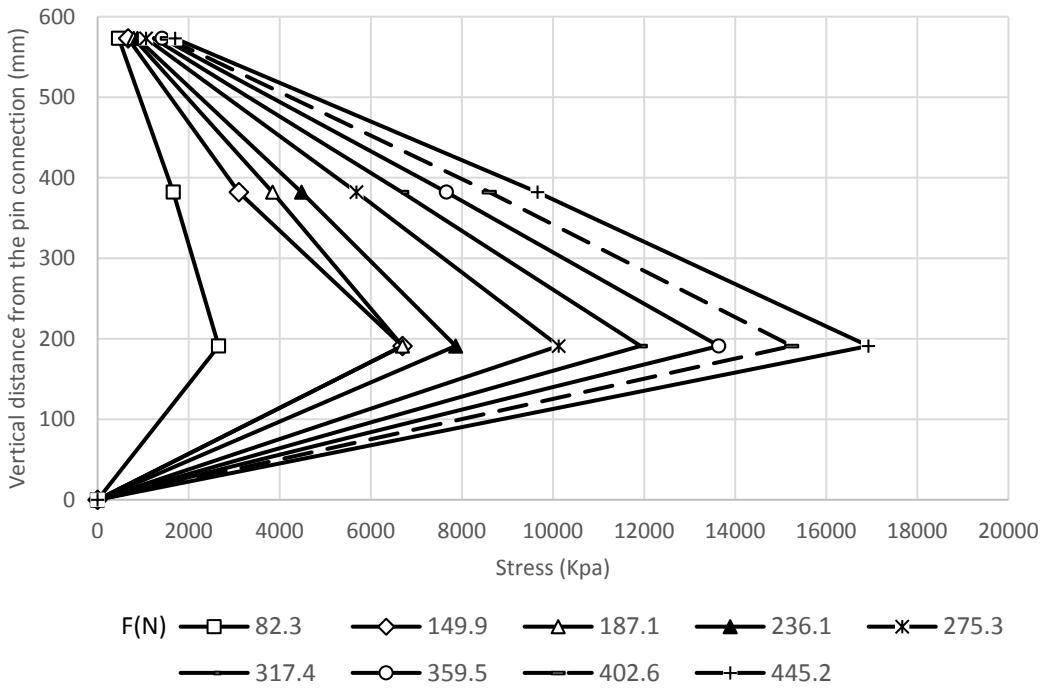

Figure A.14 Stresses along the tensile side of the pile in Test H1 L1 S1 C1 D2.

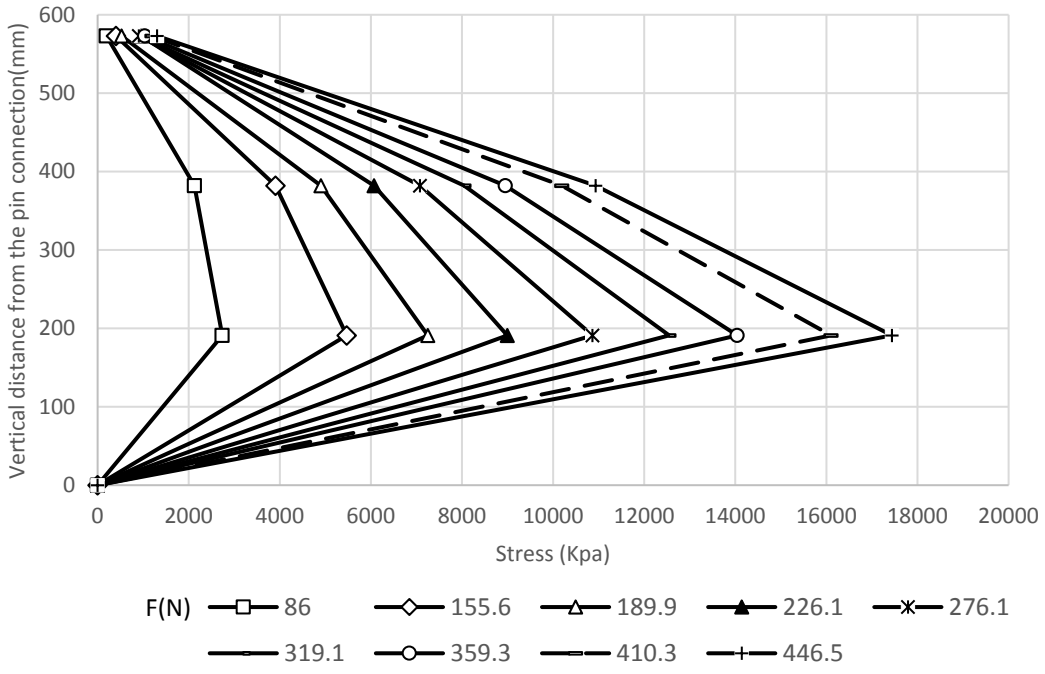

Figure A.15 Stresses along the tensile side of the pile in Test H1 L1 S1 C1 D3.

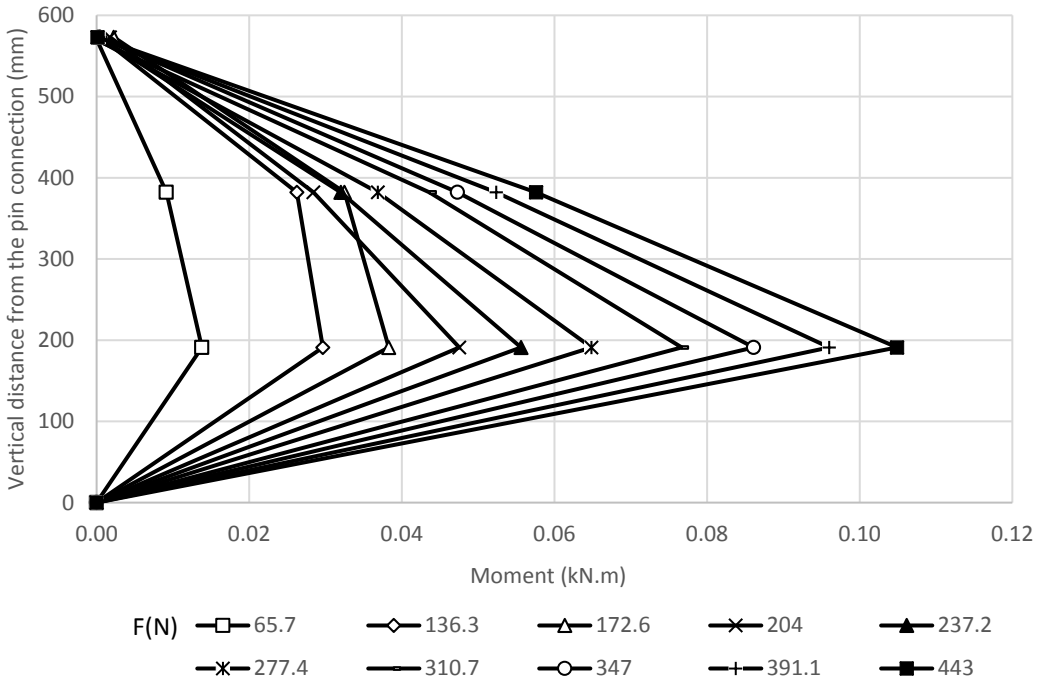

Figure A.16 Moments along the tensile side of the pile in Test H1 L1 S1 C1 D1.

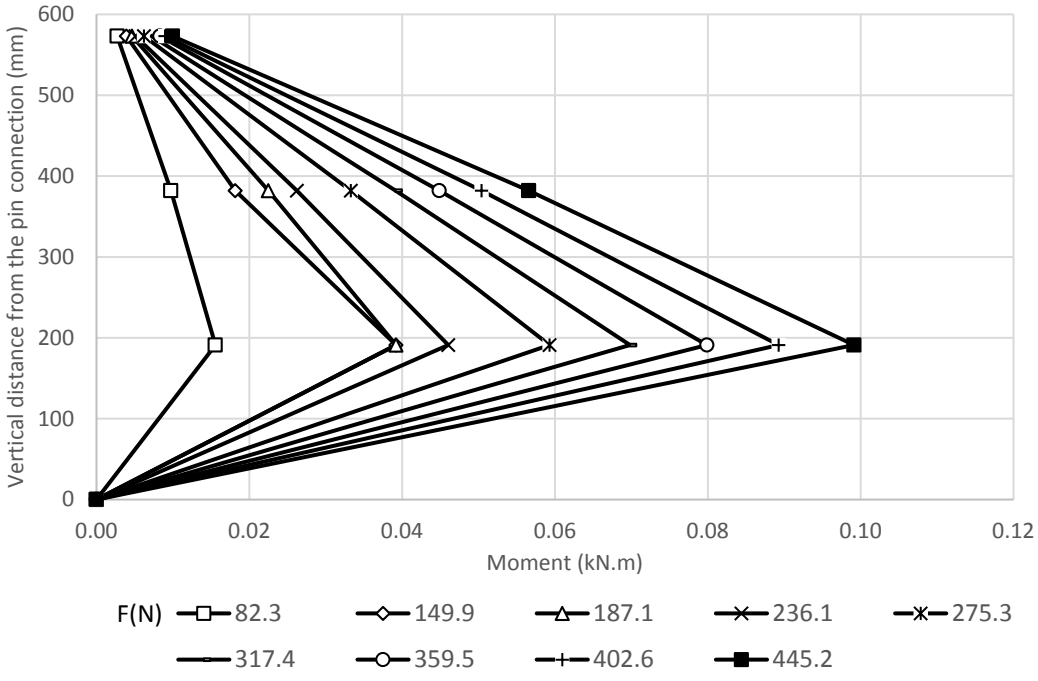

Figure A.17 Moments along the tensile side of the pile in Test H1 L1 S1 C1 D2.

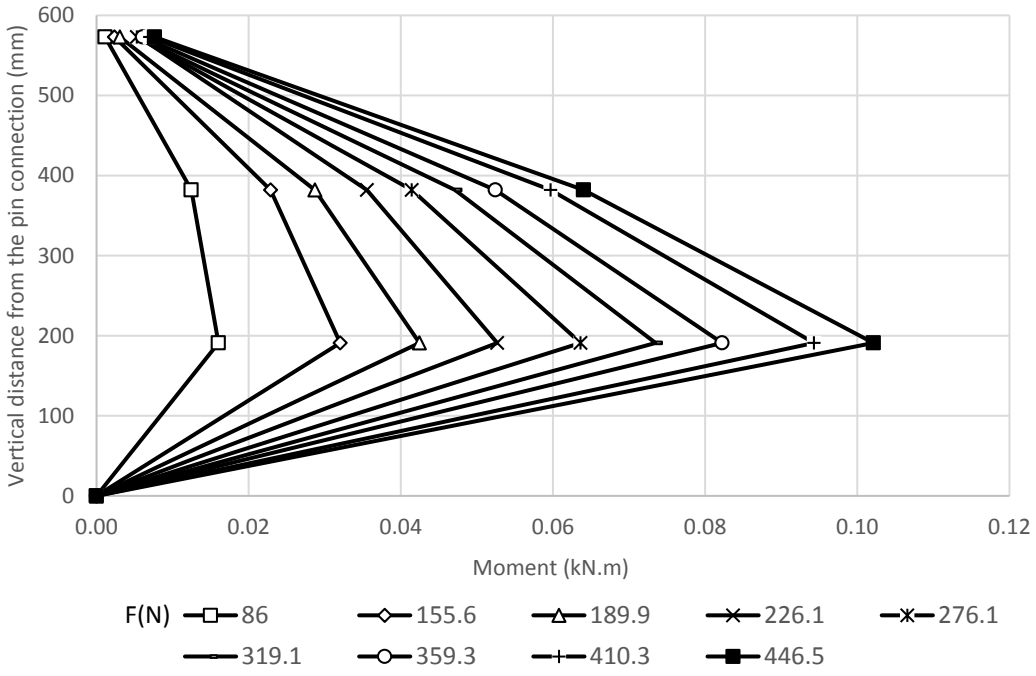

Figure A.18 Moments along the tensile side of the pile in Test H1 L1 S1 C1 D3.

A.2.3. Strain in the geogrid layers:

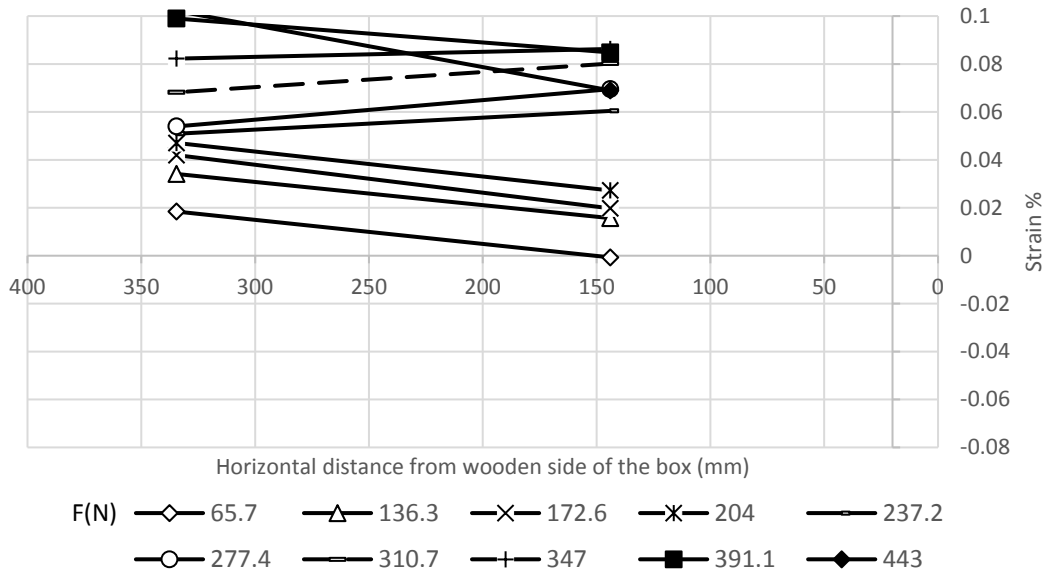

Figure A.19 Strains in the transverse direction of the geogrid layer at 180 mm from the wall base (Test H1 L1 S1 C1 D1).

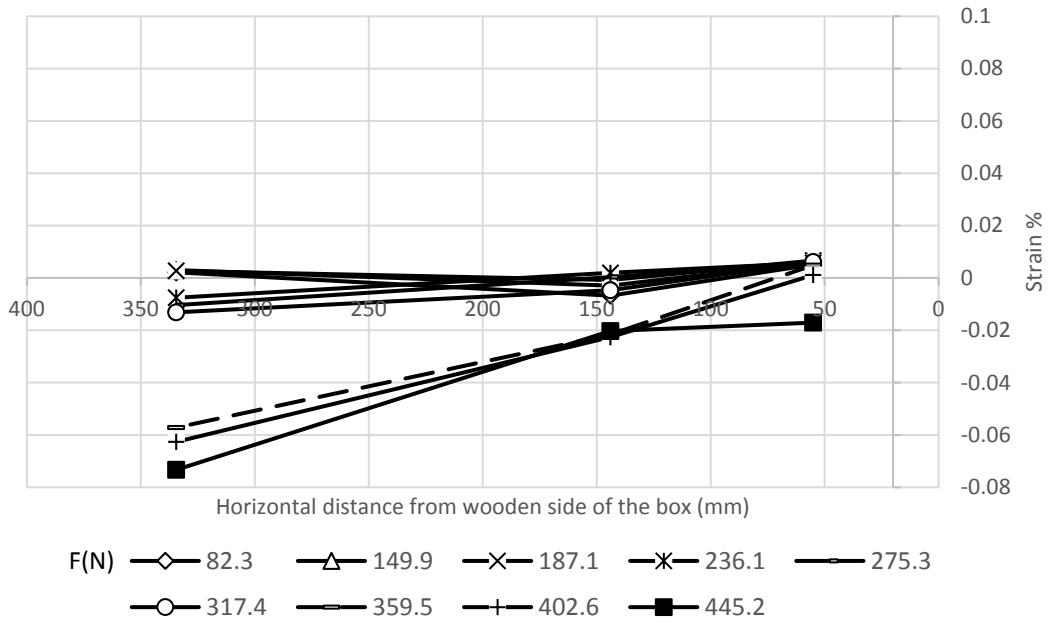

Figure A.20 Strains in the transverse direction of the geogrid layer at 180 mm from the wall base (Test H1 L1 S1 C1 D2).

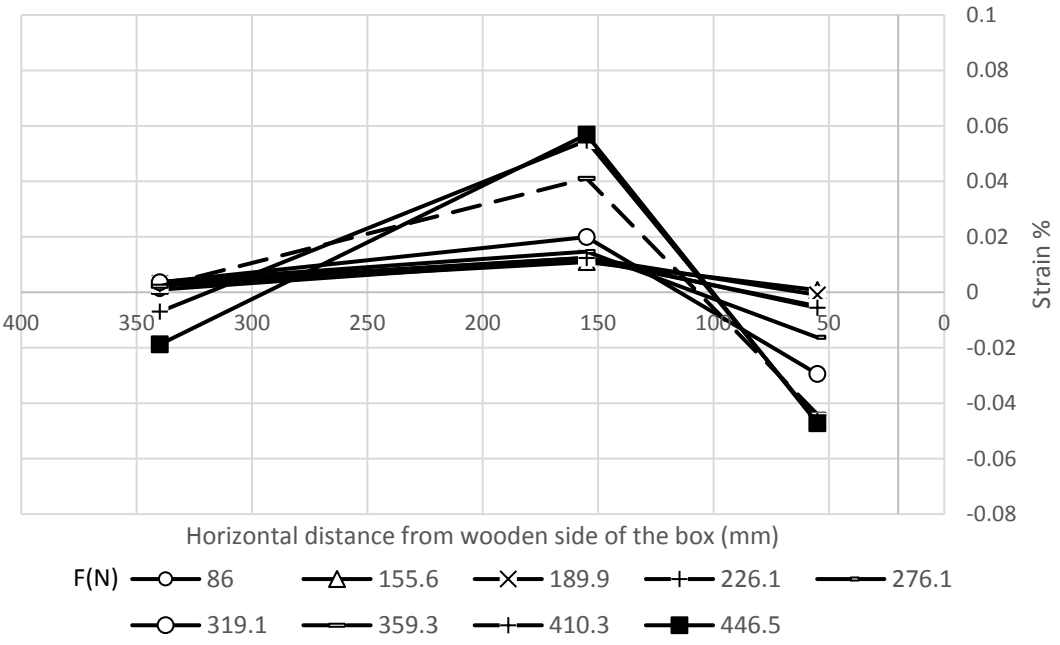

Figure A.21 Strains in the transverse direction of the geogrid layer at 180 mm from the wall base (Test H1 L1 S1 C1 D3).

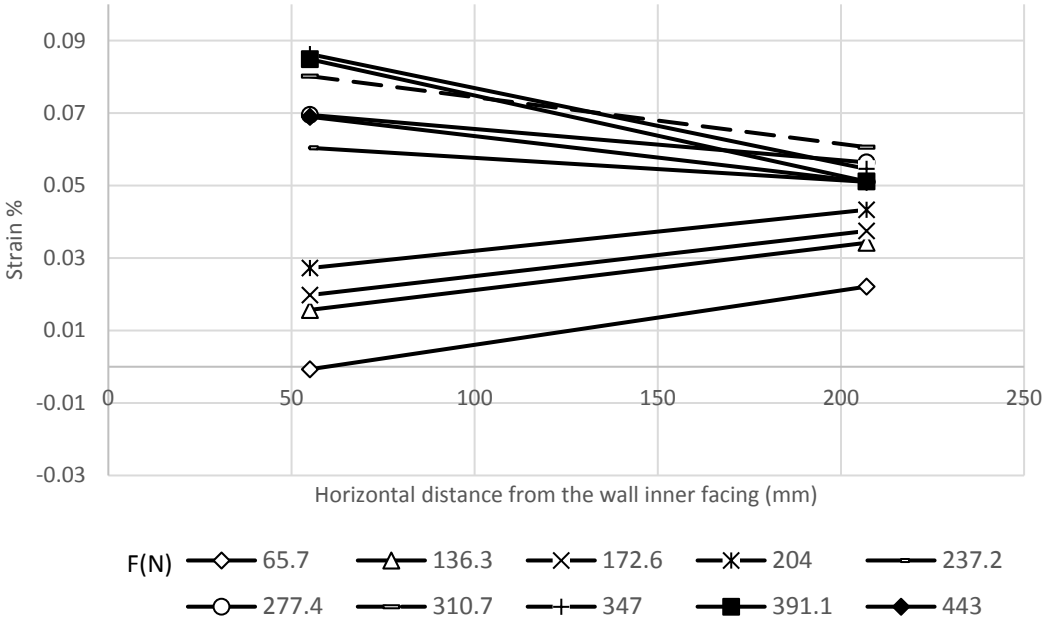

Figure A.22 Strains in the longitudinal direction of the geogrid layer at 180 mm from the wall base (Test H1 L1 S1 C1 D1).

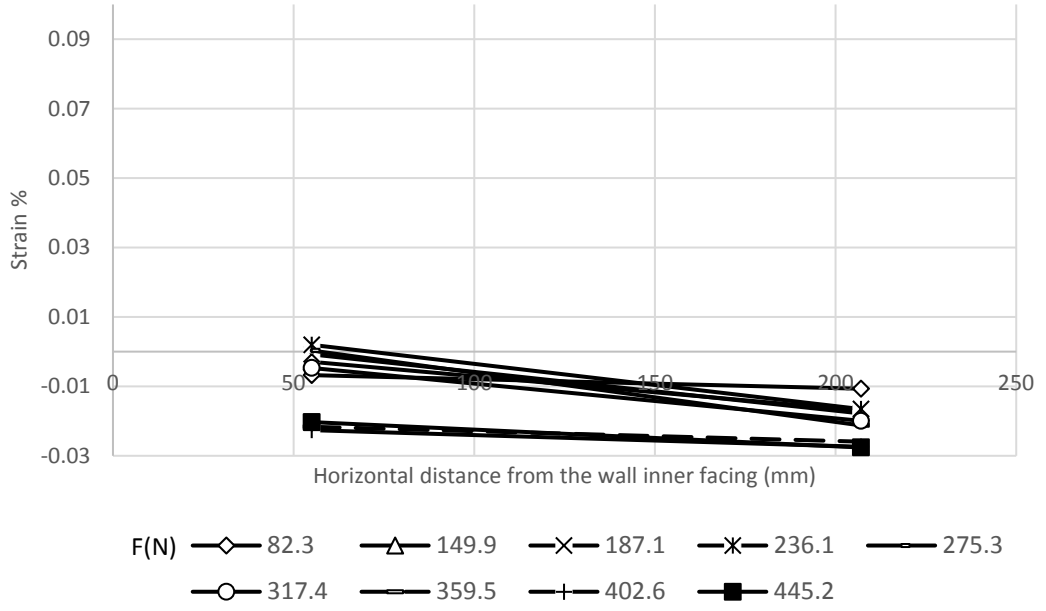

Figure A.23 Strains in the longitudinal direction of the geogrid layer at 180 mm from the wall base (Test H1 L1 S1 C1 D2).

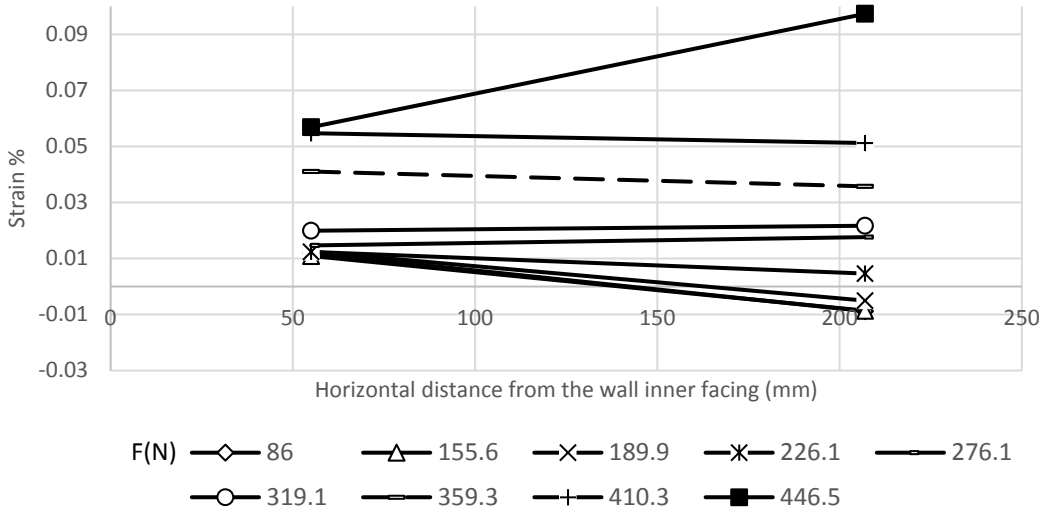

Figure A.24 Strains in the longitudinal direction of the geogrid layer at 180 mm from the wall base (Test H1 L1 S1 C1 D3).

A.3. Group 2

A.3.1. Category 1

Deflection of the wall facing:

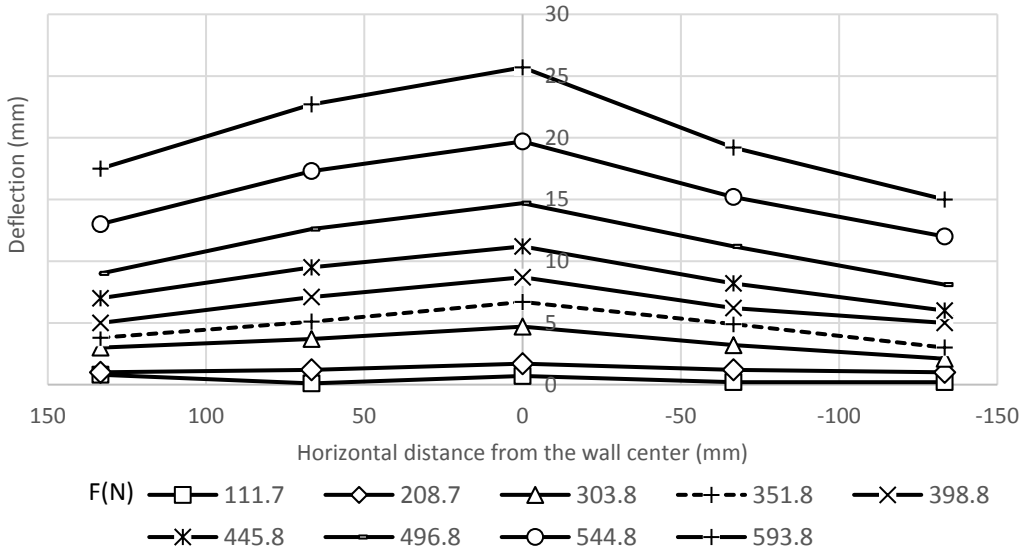

Figure A.25 Transverse deflection profiles at 472.5 mm from the wall base for Test H2 L2 S2 C1 D1.

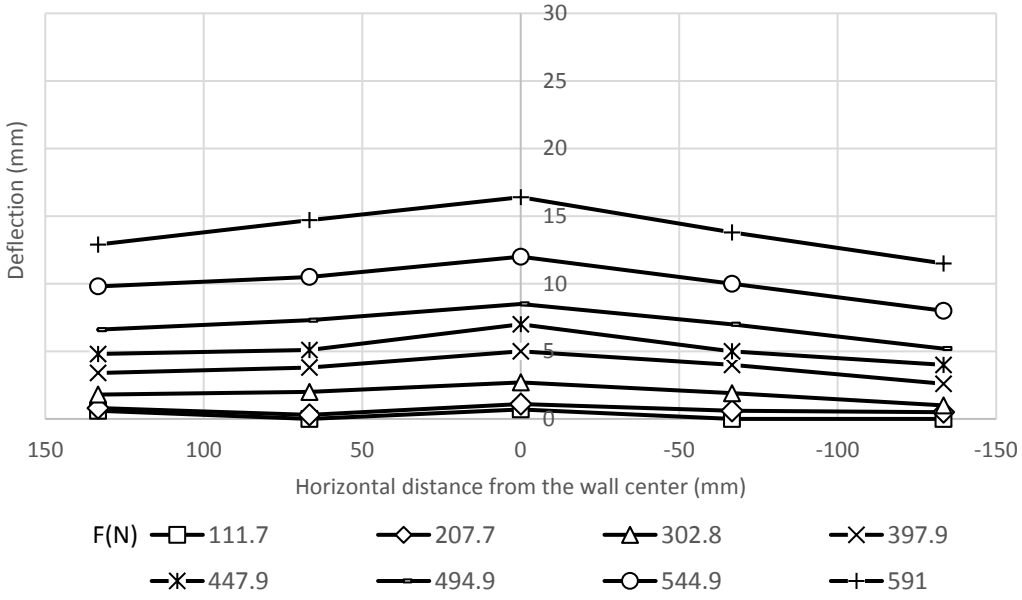

Figure A.26 Transverse deflection profiles at 472.5 mm from the wall base for Test H2 L2 S2 C1 D2.

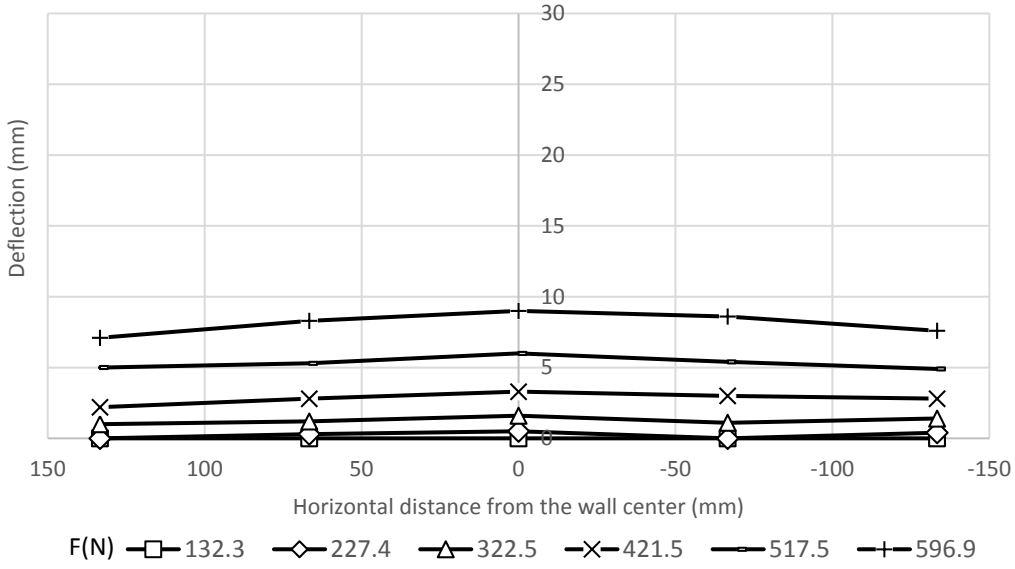

Figure A.27 Transverse deflection profiles at 472.5 mm from the wall base for Test H2 L2 S2 C1 D3.

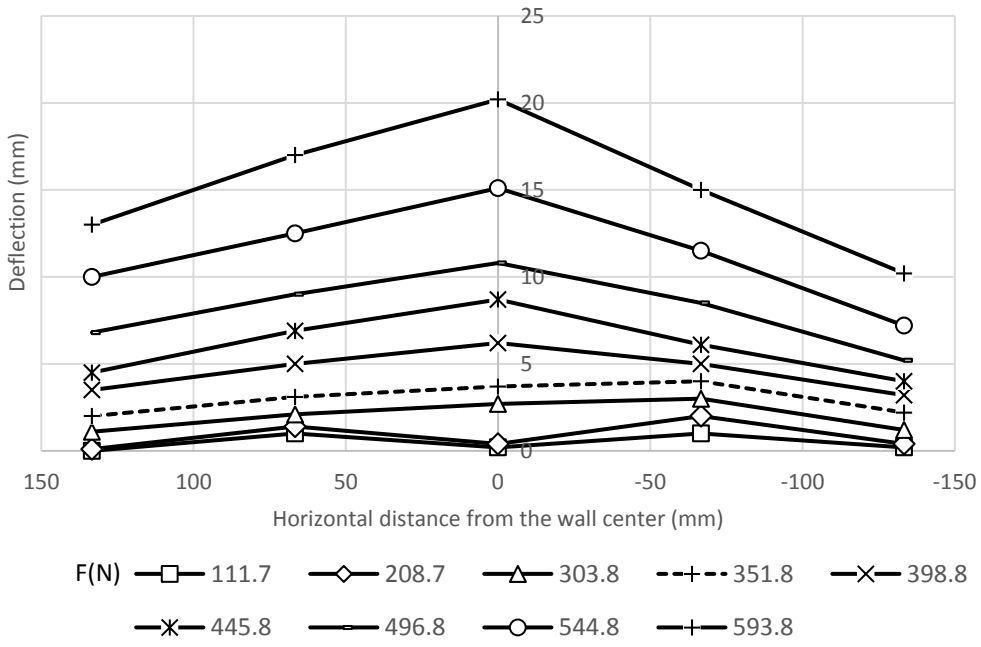

Figure A.28 Transverse deflection profiles at 337.5 mm from the wall base for Test H2 L2 S2 C1 D1.

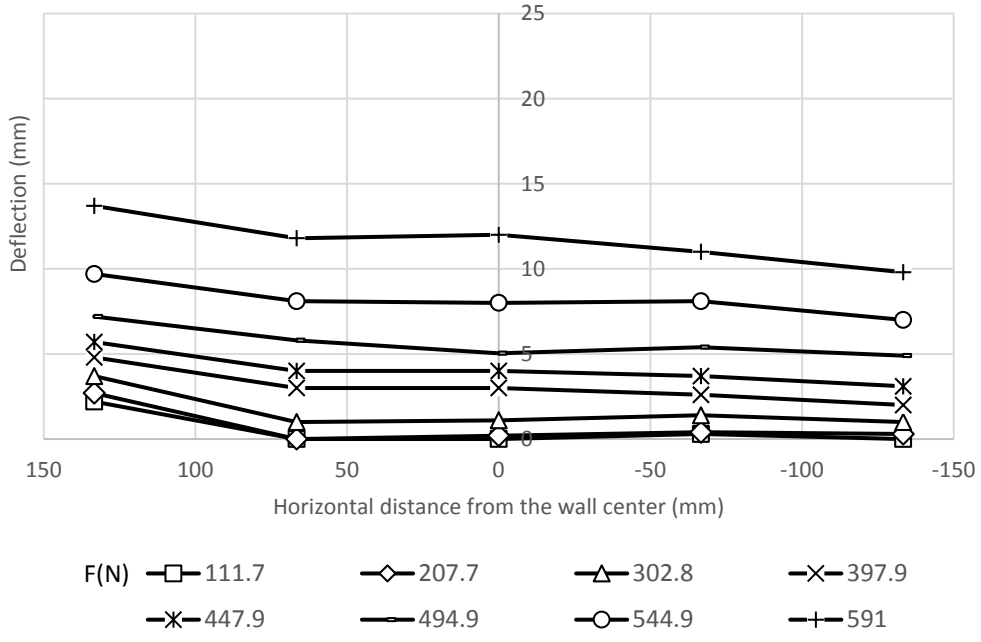

Figure A.29 Transverse deflection profiles at 337.5 mm from the wall base for Test H2 L2 S2 C1 D2.

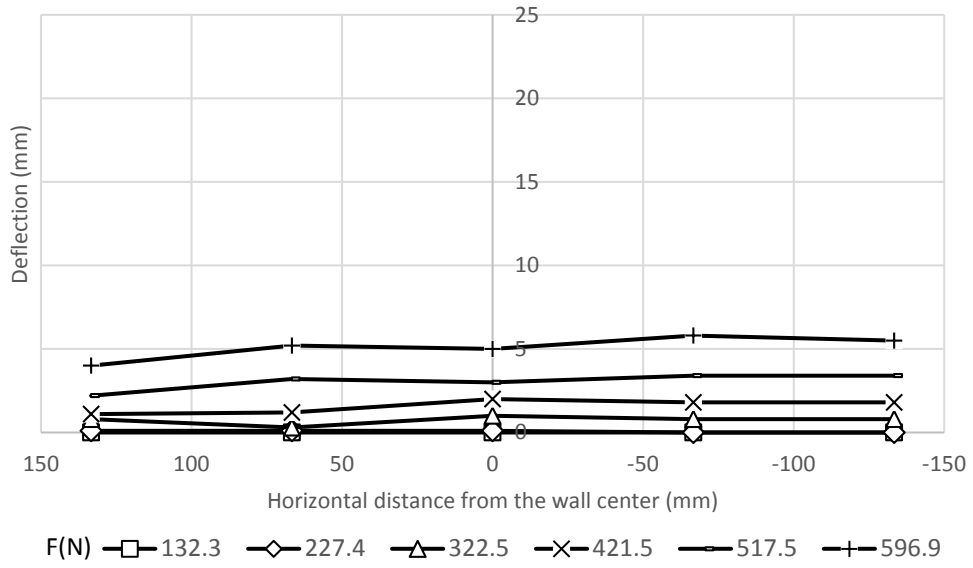

Figure A.30 Transverse deflection profiles at 337.5 mm from the wall base for Test H2 L2 S2 C1 D3.

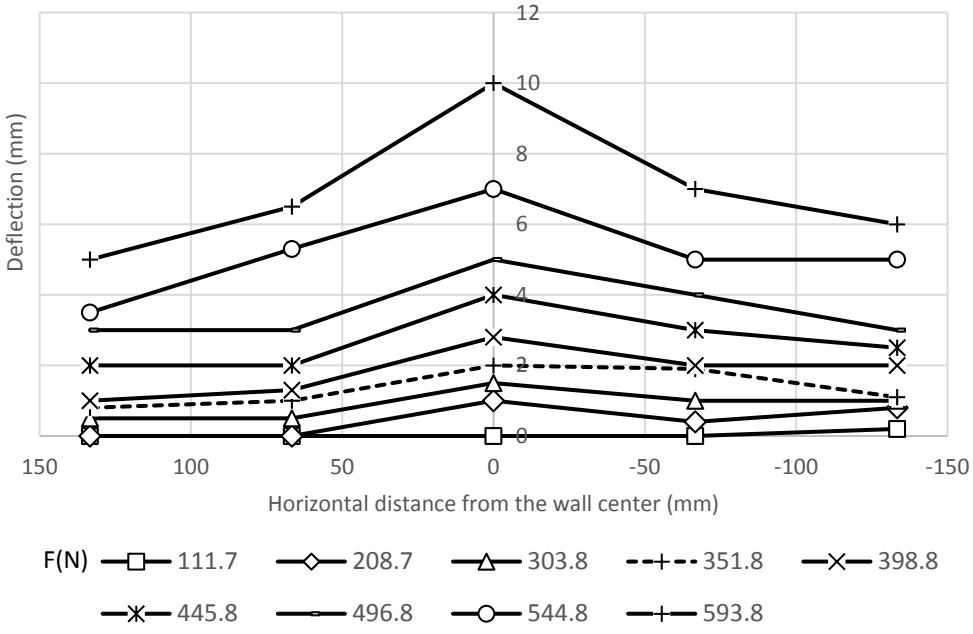

Figure A.31 Transverse deflection profiles at 202.5 mm from the wall base for Test H2 L2 S2 C1 D1.

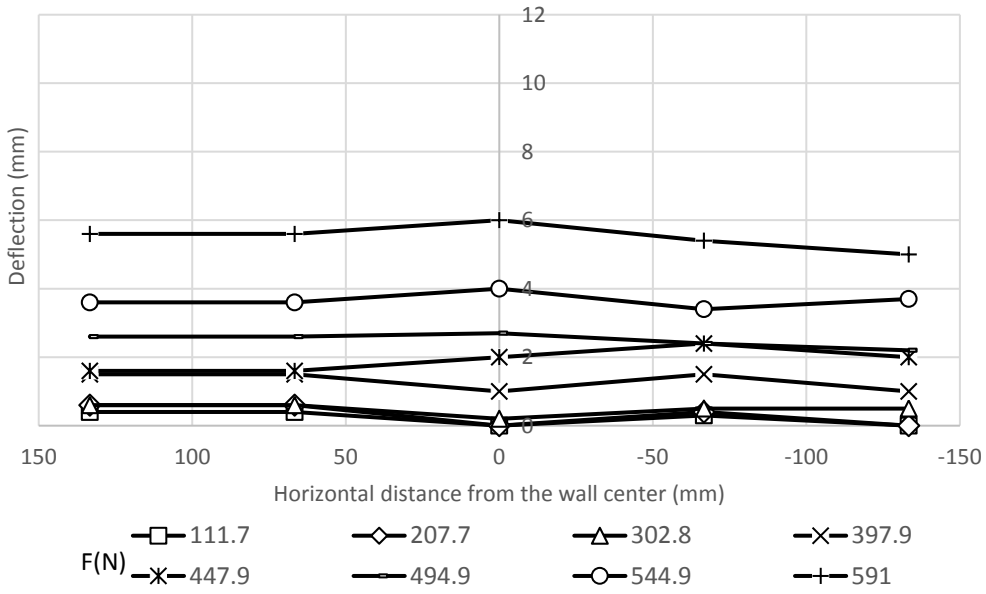

Figure A.32 Transverse deflection profiles at 202.5 mm from the wall base for Test H2 L2 S2 C1 D2.

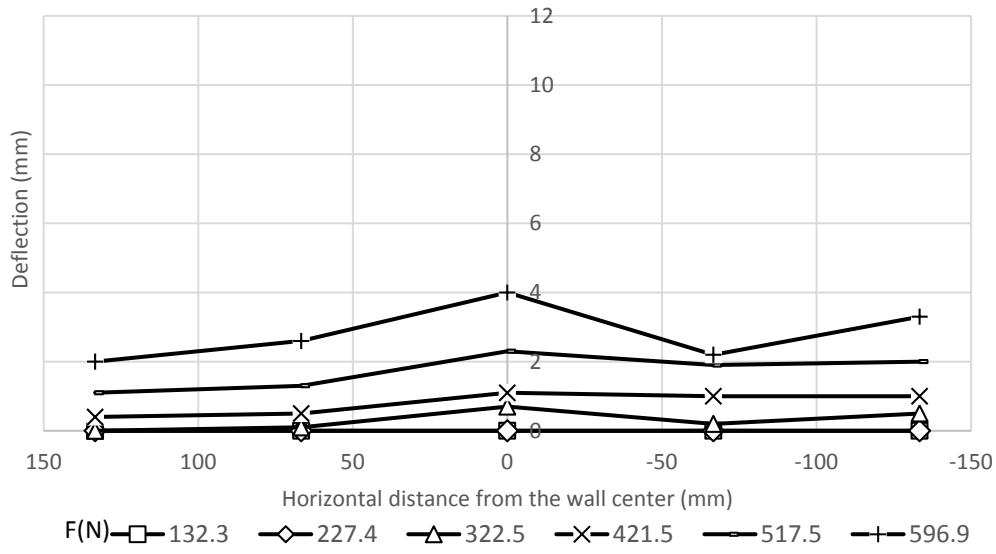

Figure A.33 Transverse deflection profiles at 202.5 mm from the wall base for Test H2 L2 S2 C1 D3.

Stress and moment of the pile:

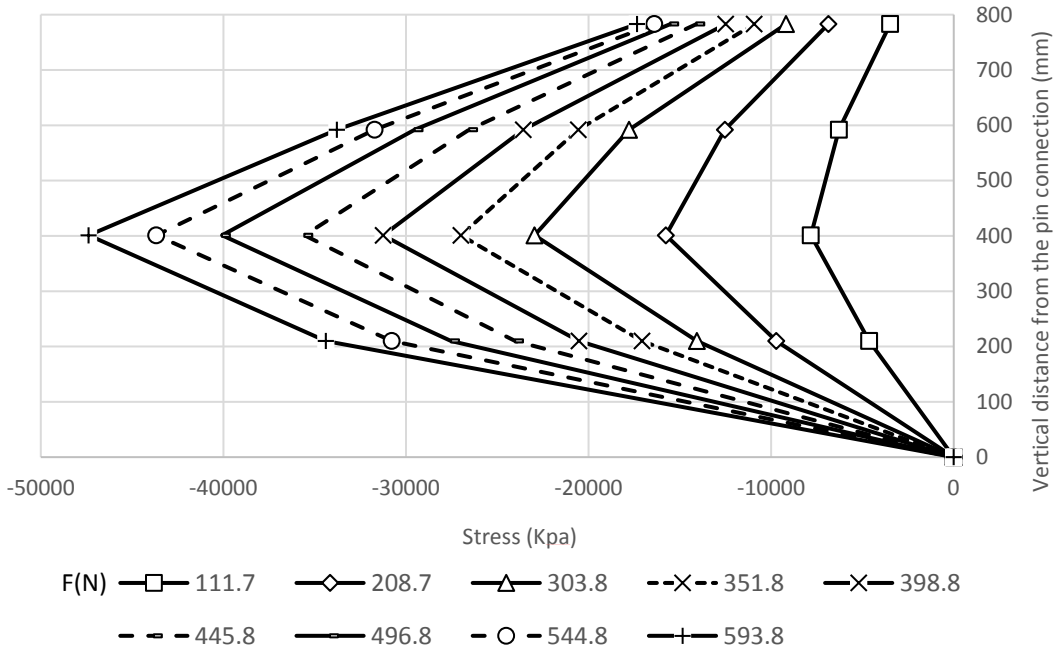

Figure A.34 Stresses along the compressive side of the pile in Test H2 L2 S2 C1 D1.

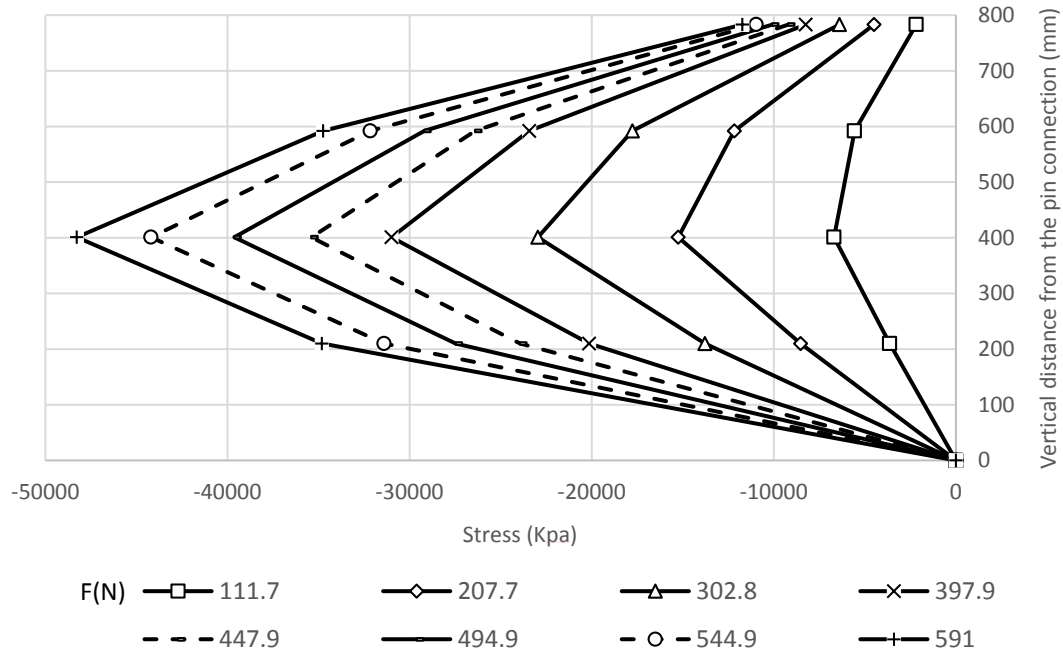

Figure A.35 Stresses along the compressive side of the pile in Test H2 L2 S2 C1 D2.

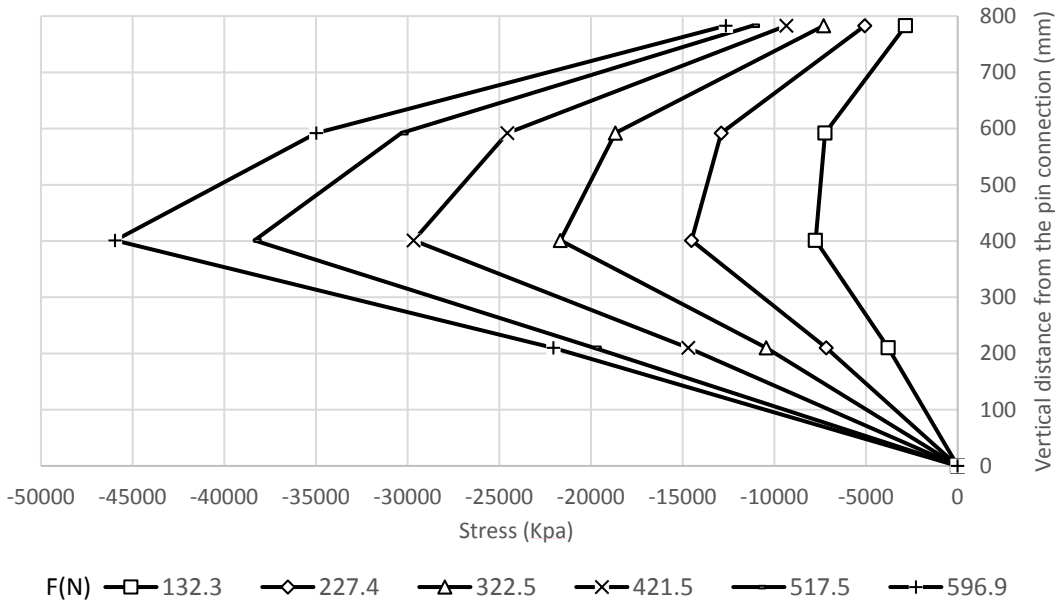

Figure A.36 Stresses along the compressive side of the pile in Test H2 L2 S2 C1 D3.

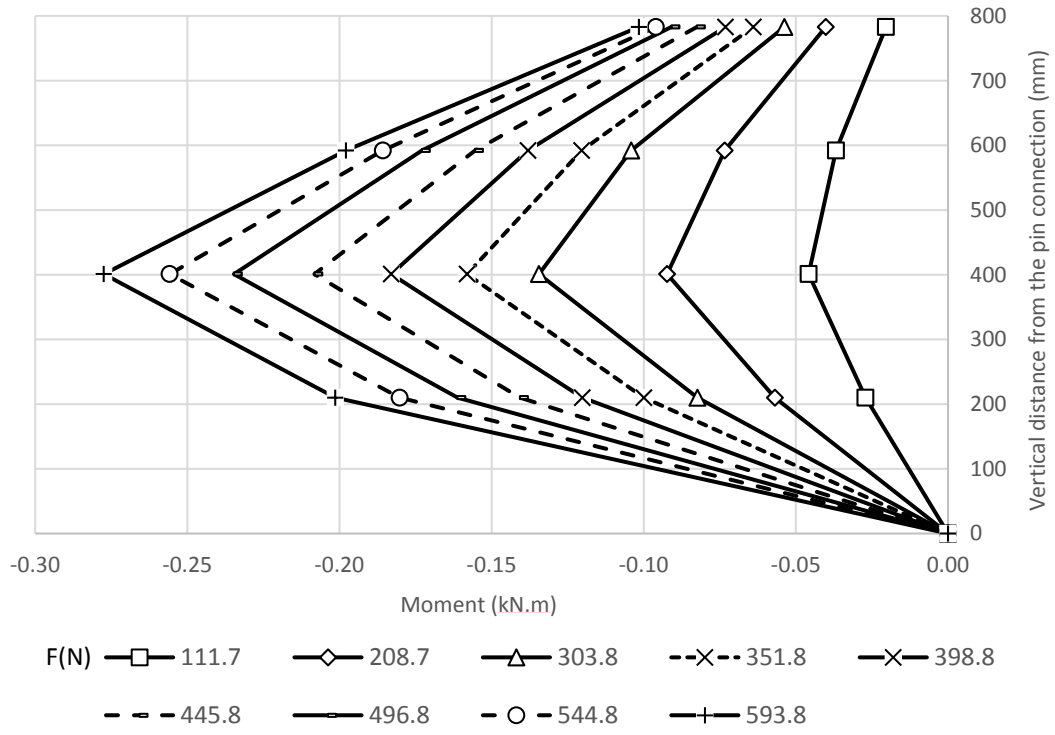

Figure A.37 Moments along the compressive side of the pile in Test H2 L2 S2 C1 D1.

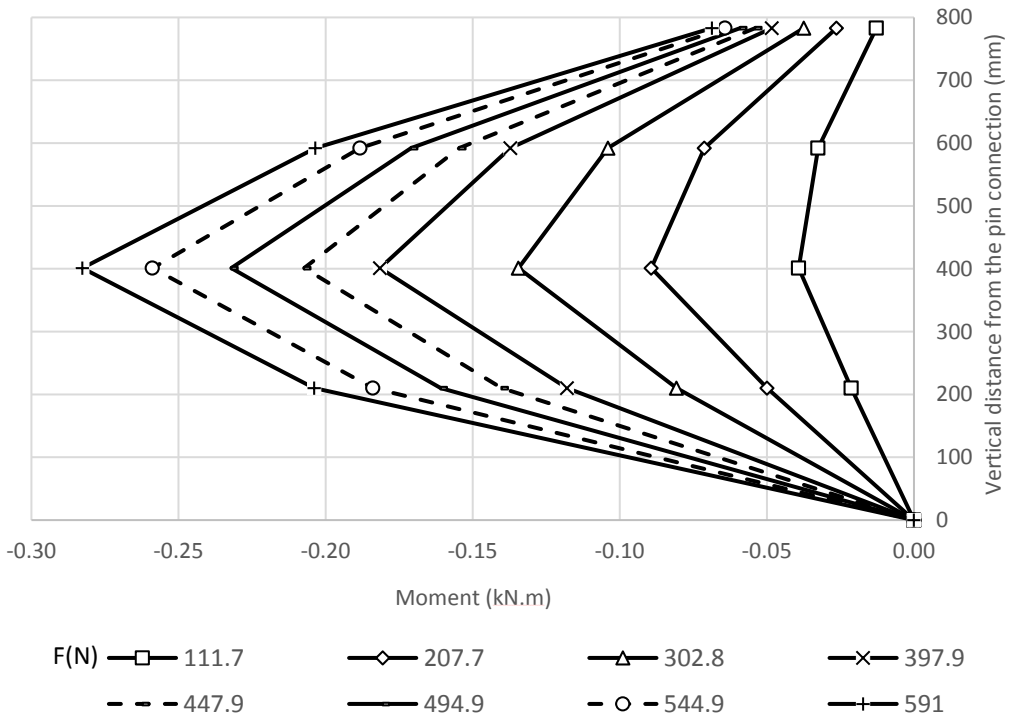

Figure A.38 Moments along the compressive side of the pile in Test H2 L2 S2 C1 D2.

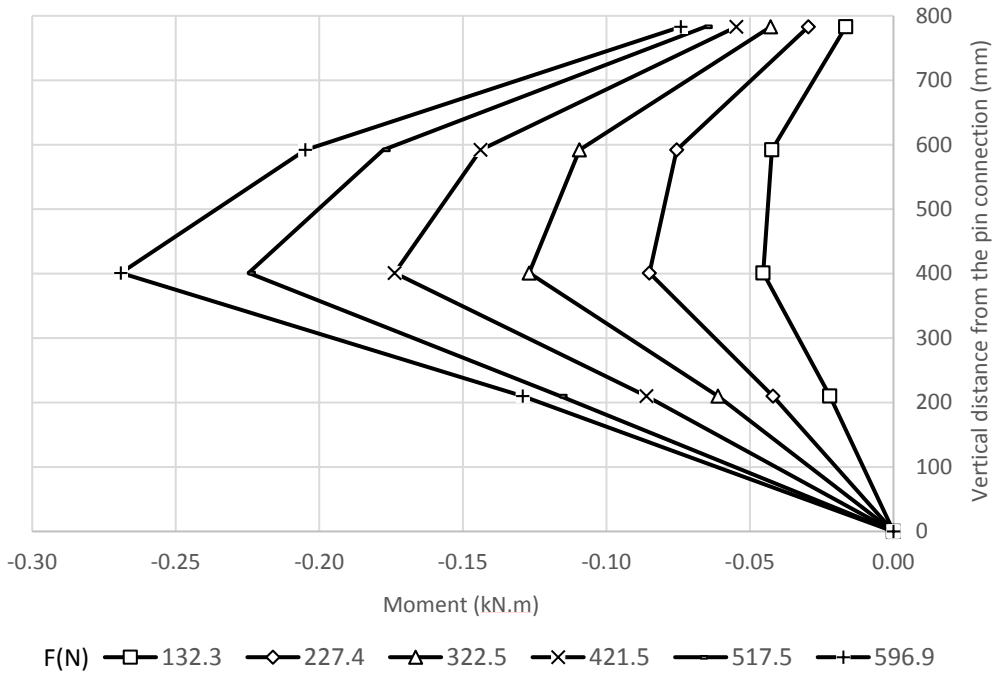

Figure A.39 Moments along the compressive side of the pile in Test H2 L2 S2 C1 D3.

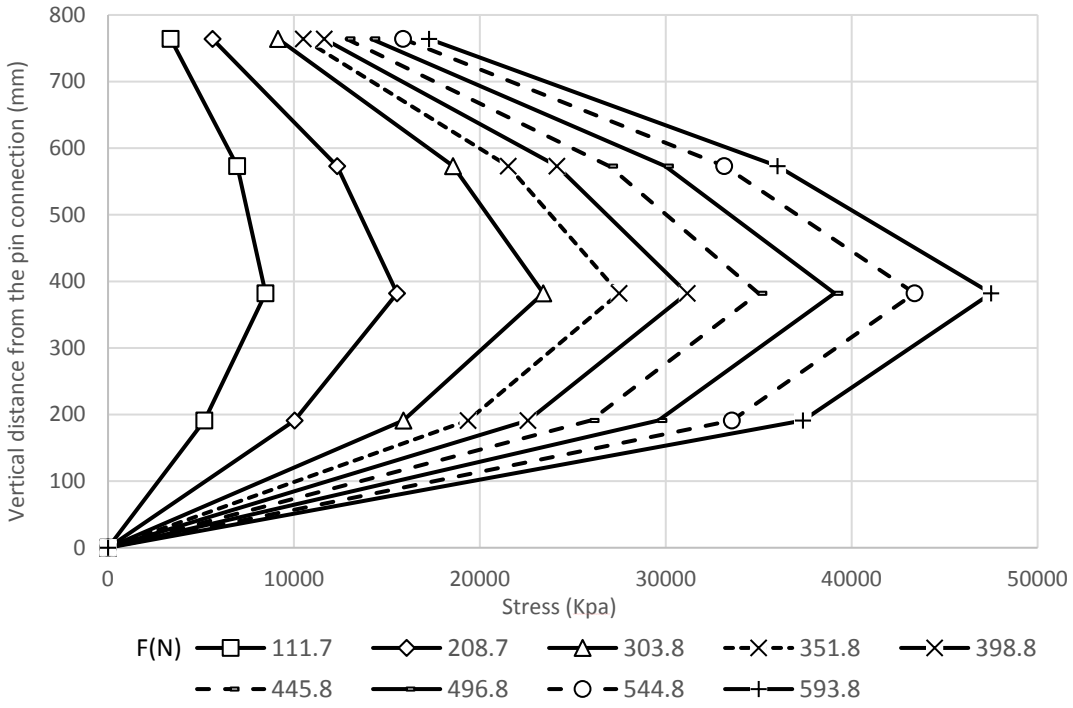

Figure A.40 Stresses along the tensile side of the pile in Test H2 L2 S2 C1 D1.

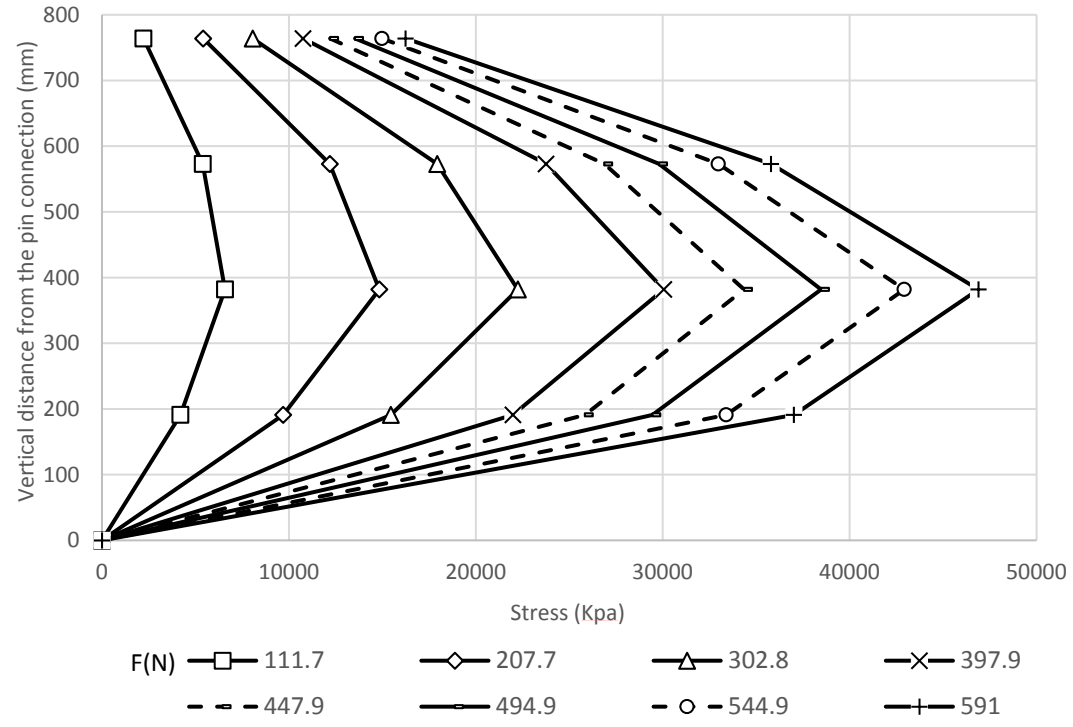

Figure A.41 Stresses along the tensile side of the pile in Test H2 L2 S2 C1 D2.

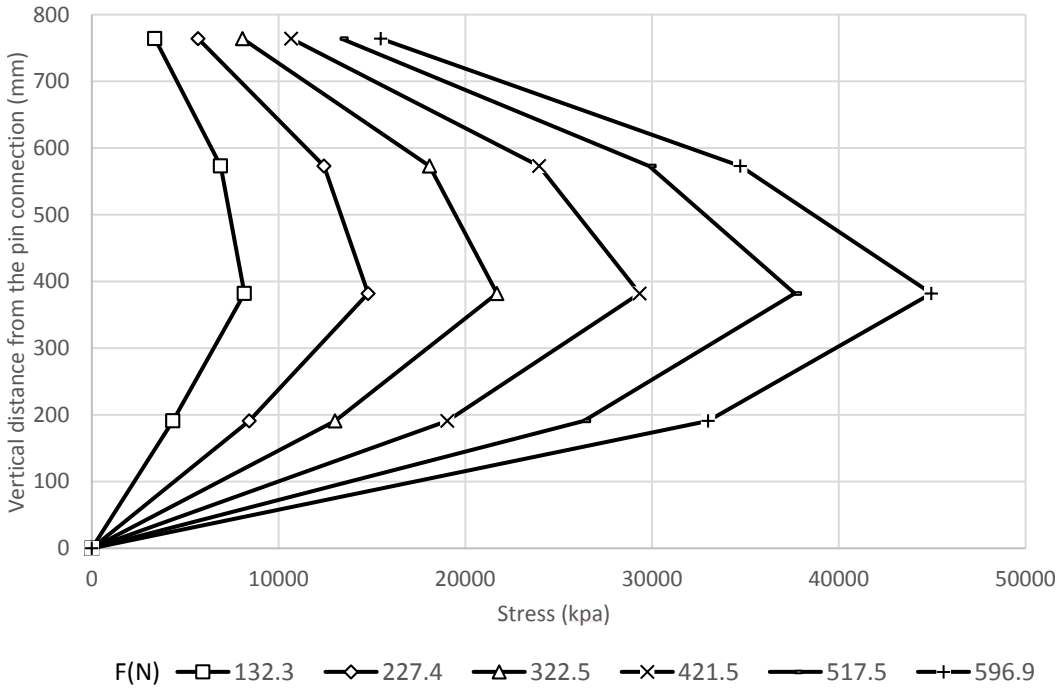

Figure A.42 Stresses along the tensile side of the pile in Test H2 L2 S2 C1 D3.

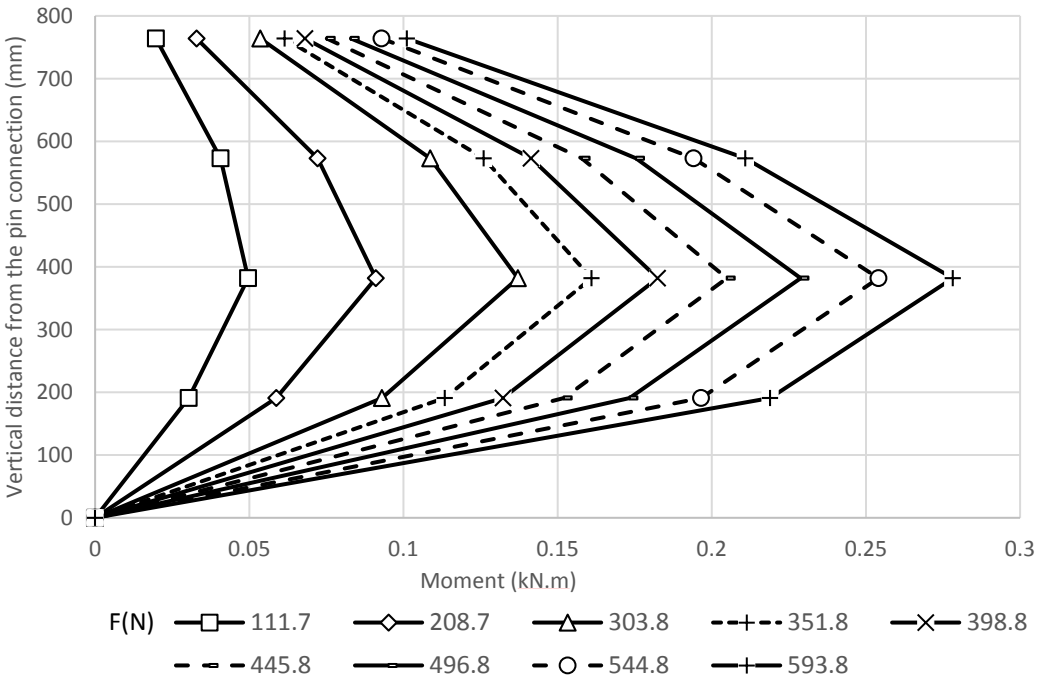

Figure A.43 Moments along the tensile side of the pile in Test H2 L2 S2 C1 D1.

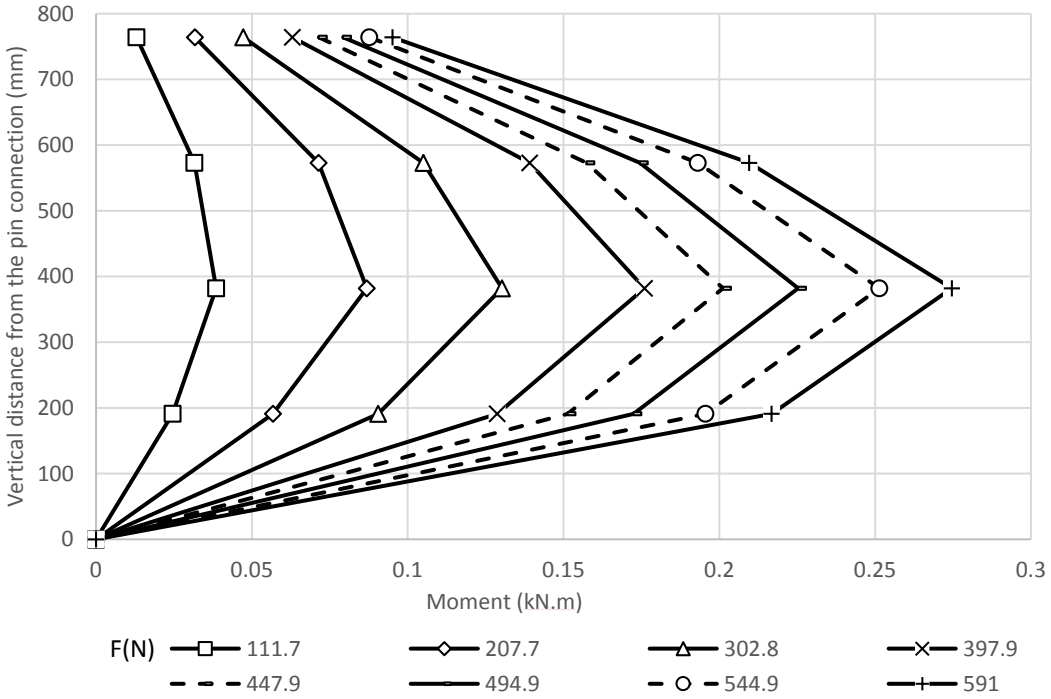

Figure A.44 Moments along the tensile side of the pile in Test H2 L2 S2 C1 D2.

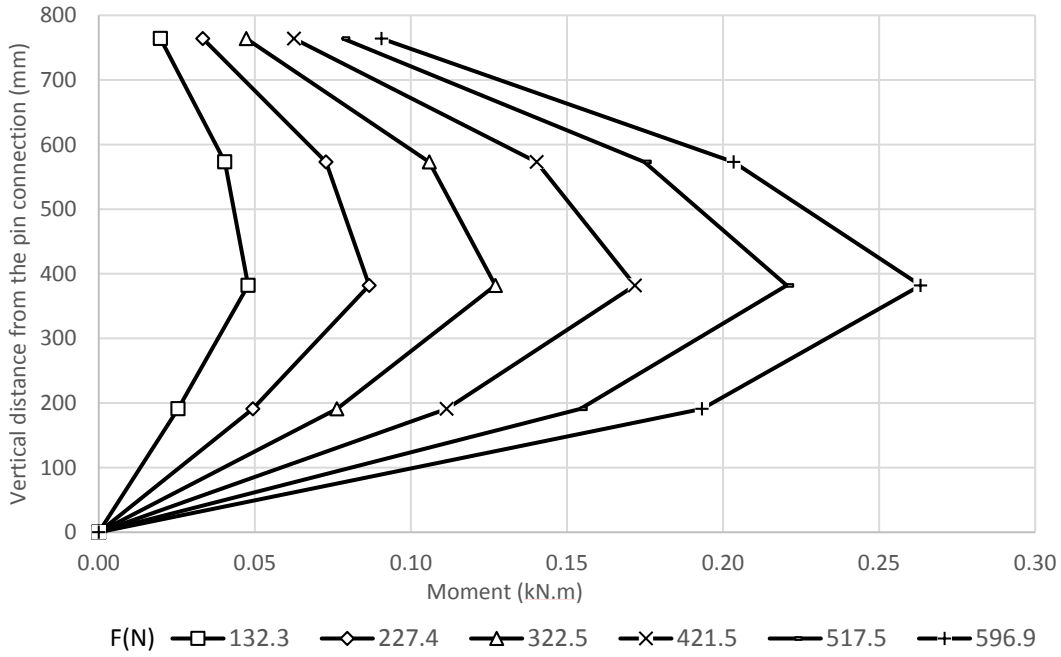

Figure A.45 Moments along the tensile side of the pile in Test H2 L2 S2 C1 D3.

Strain in the geogrid layers:

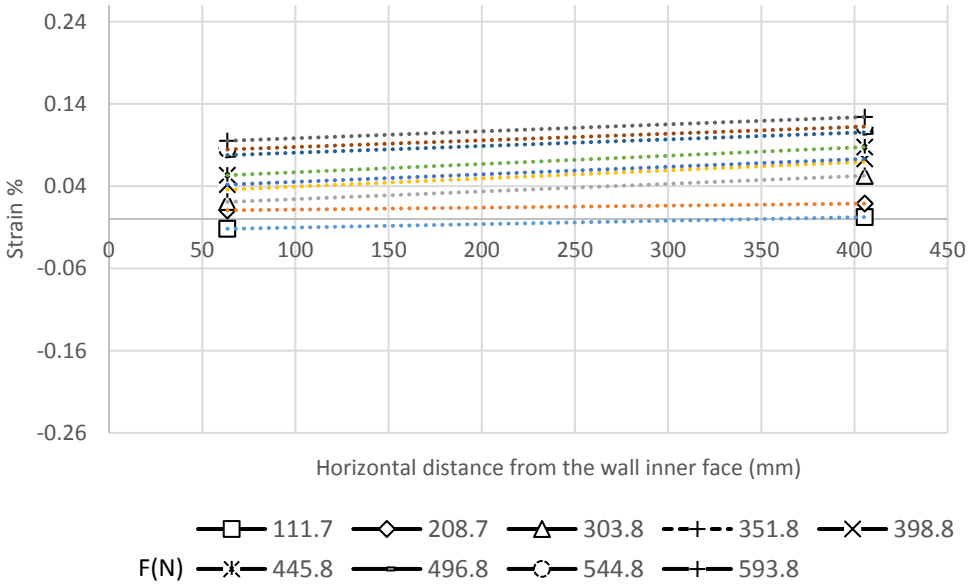

Figure A.46 Strains in the geogrid layer at 405 mm from the wall base (Test H2 L2 S2 C1 D1).

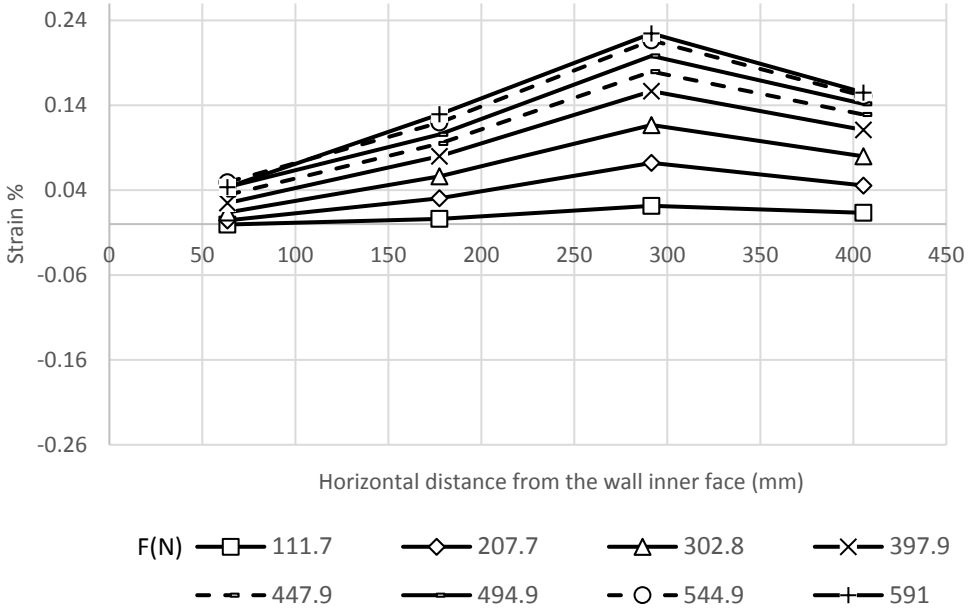

Figure A.47 Strains in the geogrid layer at 405 mm from the wall base (Test H2 L2 S2 C1 D2).

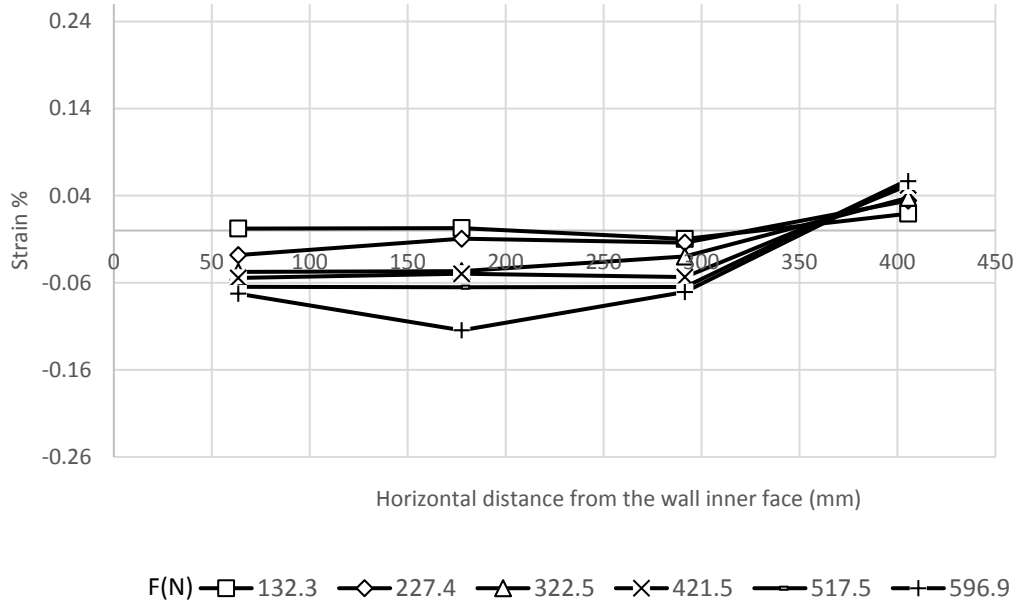

Figure A.48 Strains in the geogrid layer at 405 mm from the wall base (Test H2 L2 S2 C1 D2).

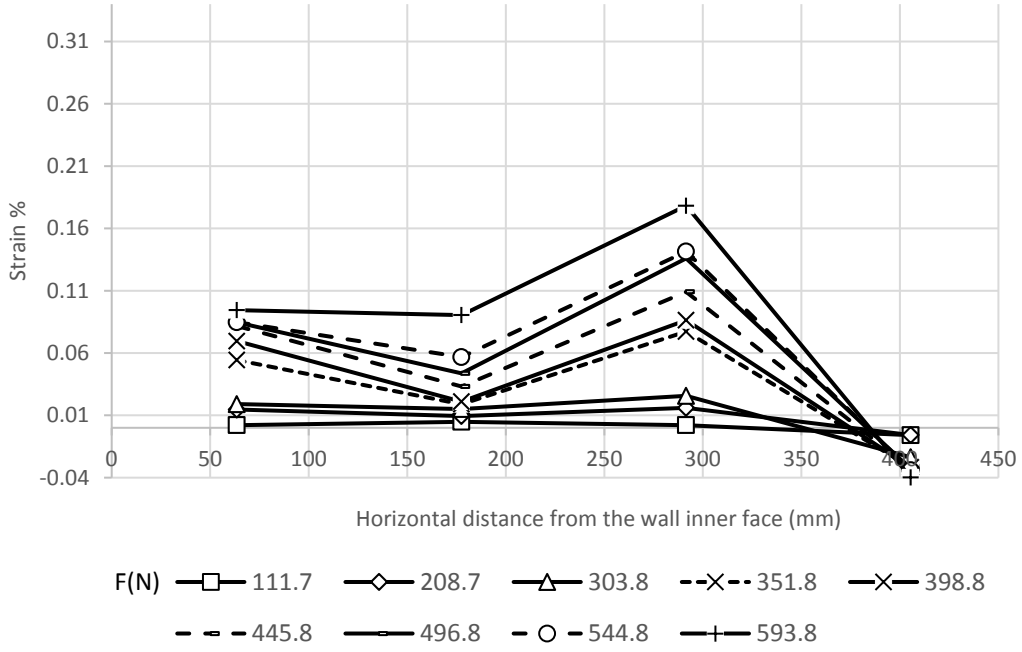

Figure A.49 Strains in the geogrid layer at 270 mm from the wall base (Test H2 L2 S2 C1 D1).

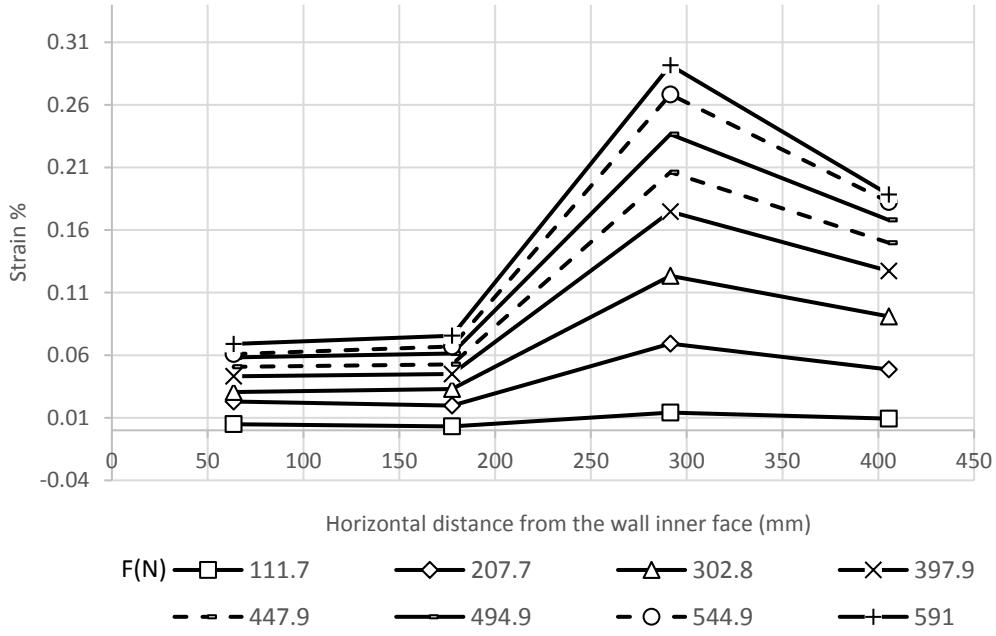

Figure A.50 Strains in the geogrid layer at 270 mm from the wall base (Test H2 L2 S2 C1 D2).

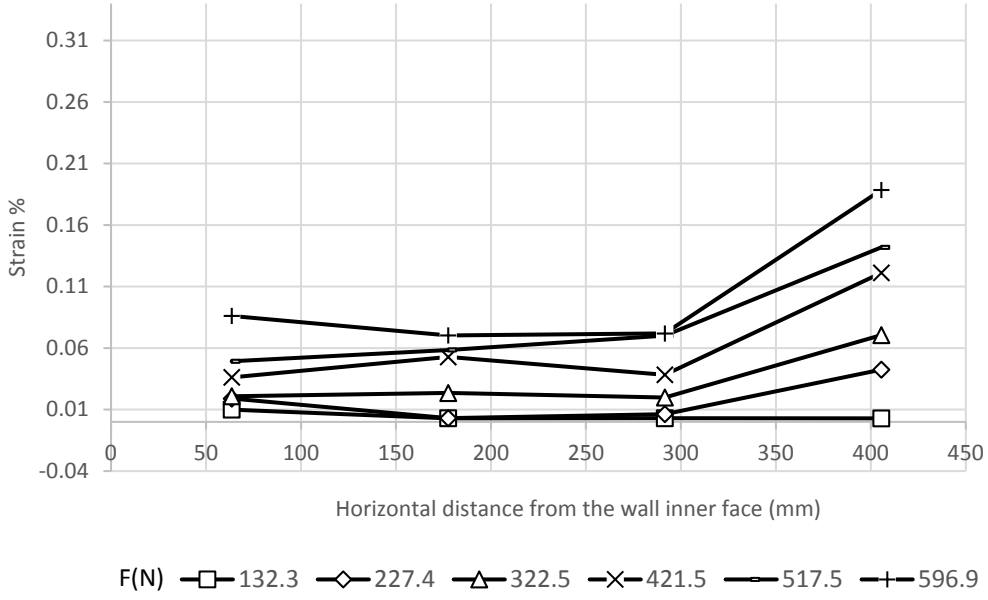

Figure A.51 Strains in the geogrid layer at 270 mm from the wall base (Test H2 L2 S2 C1 D3).

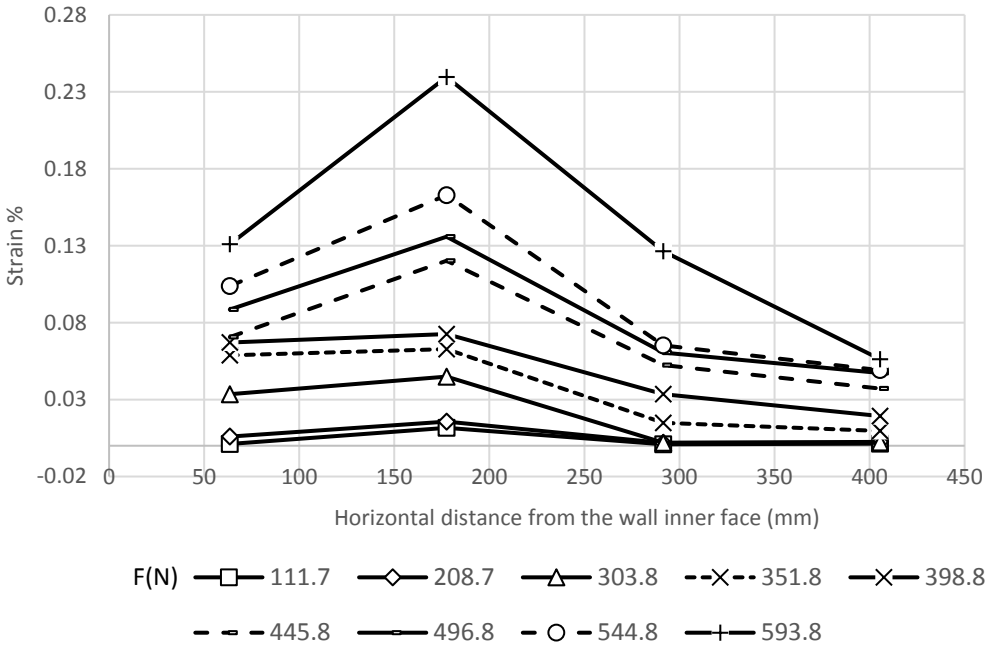

Figure A.52 Strains in the geogrid layer at 135 mm from the wall base (Test H2 L2 S2 C1 D1).

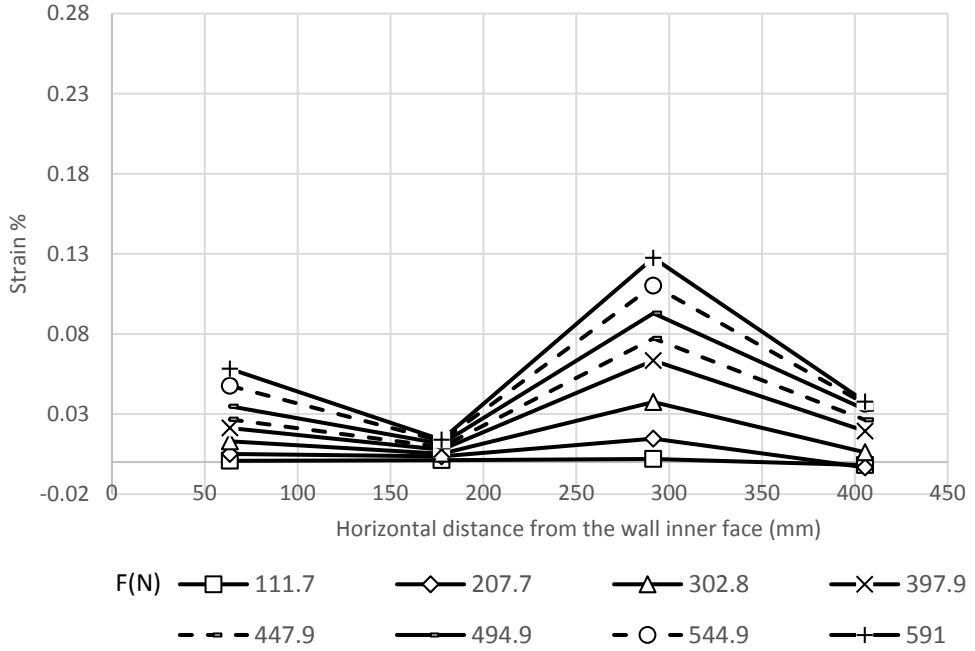

Figure A.53 Strains in the geogrid layer at 135 mm from the wall base (Test H2 L2 S2 C1 D2).

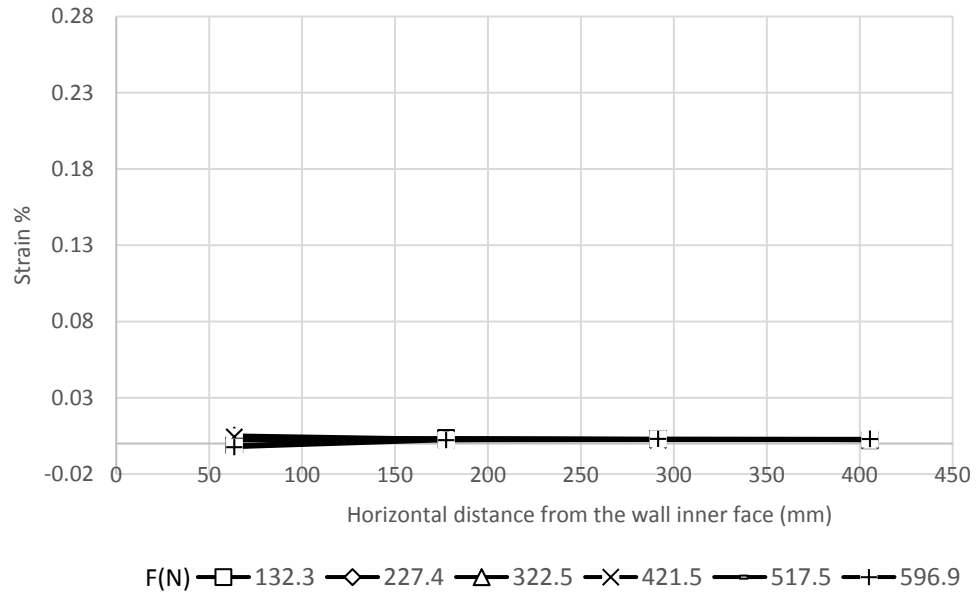

Figure A.54 Strains in the geogrid layer at 135 mm from the wall base (Test H2 L2 S2 C1 D3).

Pressure behind the wall facing:

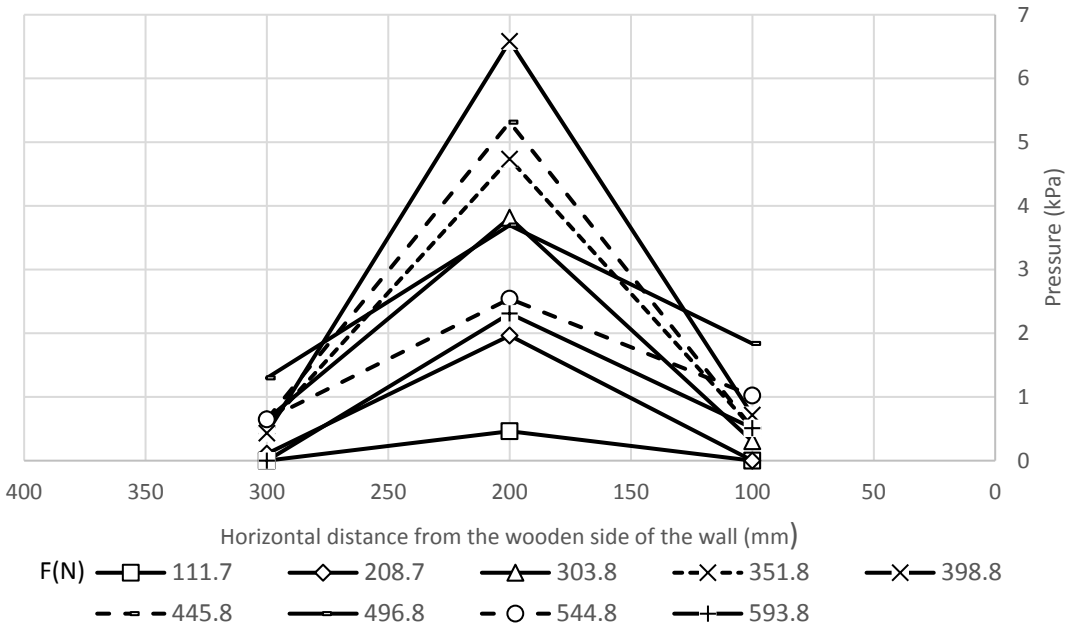

Figure A.55 Transverse pressure distributions at 607.5 mm from the wall base for Test H2 L2 S2 C1 D1.

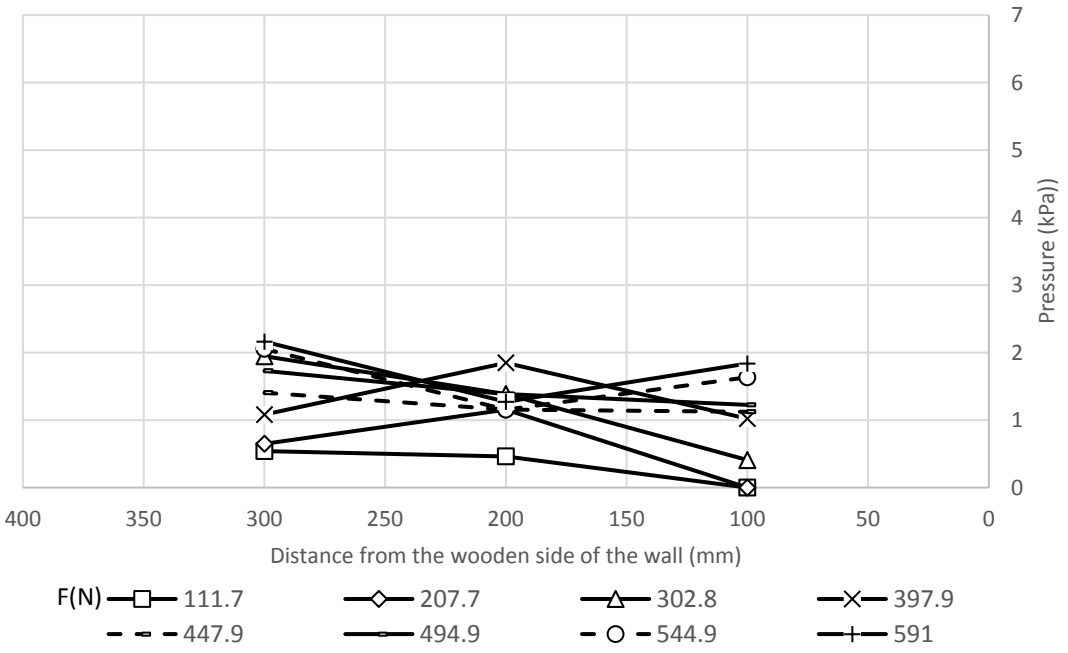

Figure A.56 Transverse pressure distributions at 607.5 mm from the wall base for Test H2 L2 S2 C1 D2.

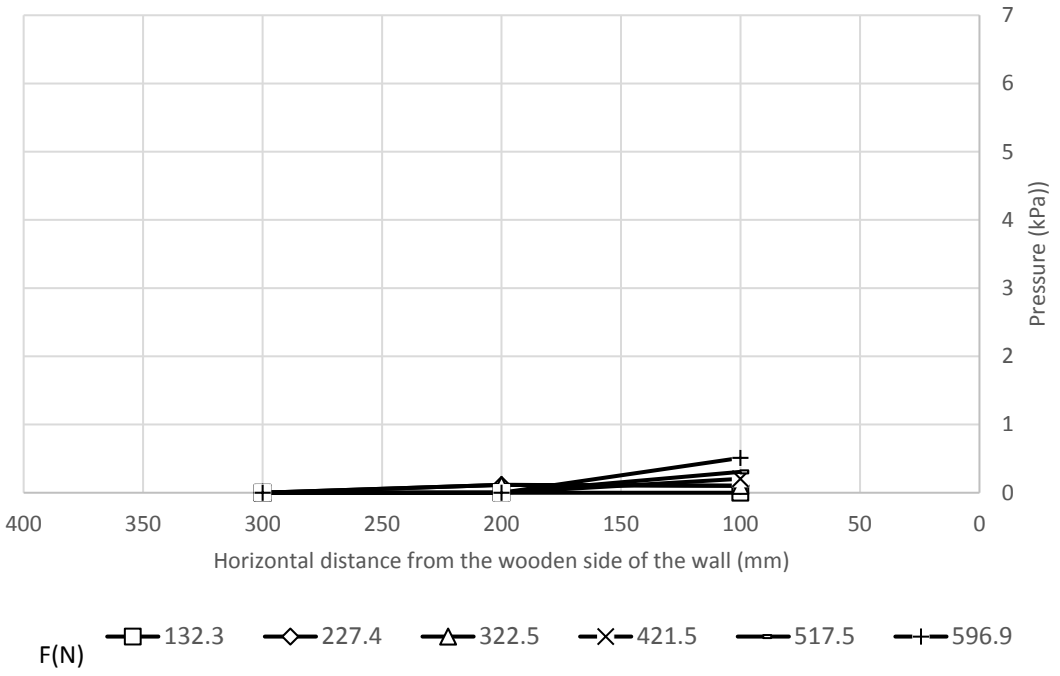

Figure A.57 Transverse pressure distributions at 607.5 mm from the wall base for Test H2 L2 S2 C1 D3.

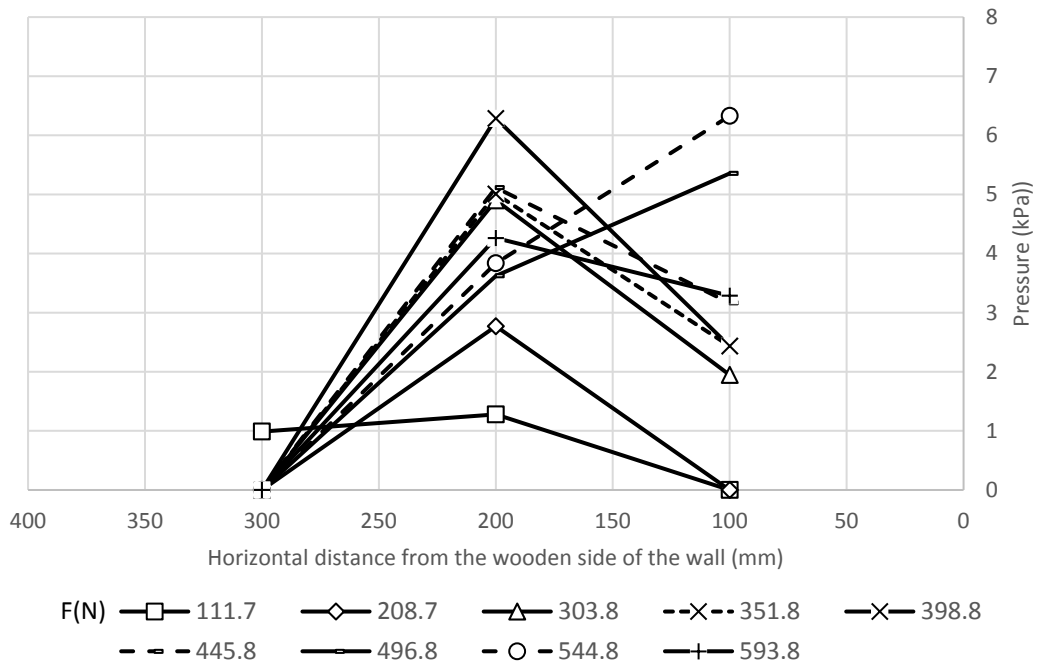

Figure A.58 Transverse pressure distributions at 337.5 mm from the wall base for Test H2 L2 S2 C1 D1.

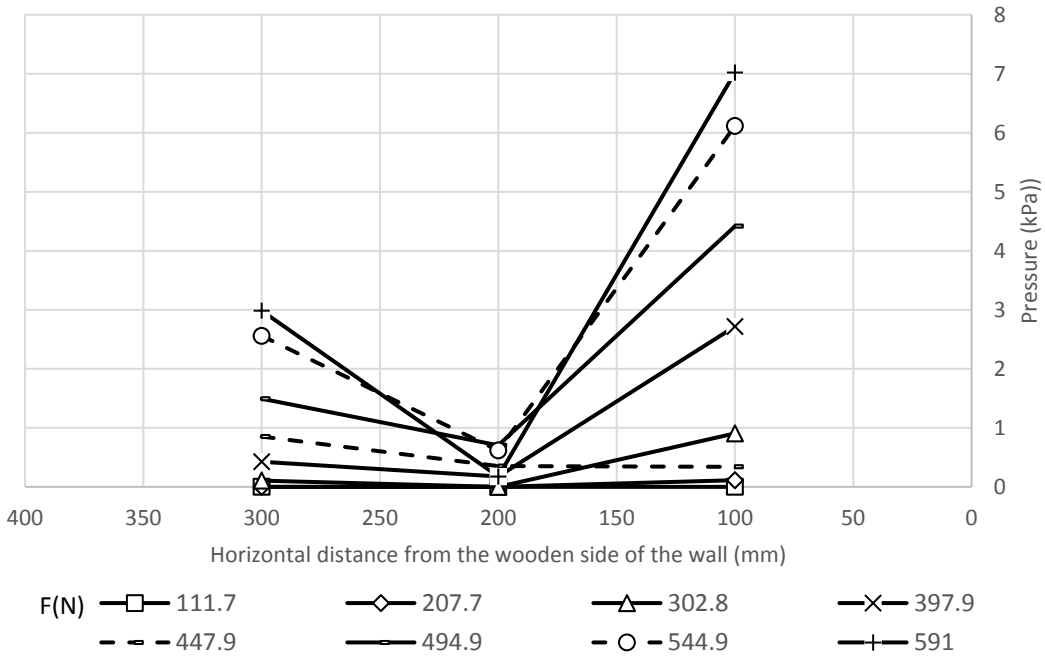

Figure A.59 Transverse pressure distributions at 337.5 mm from the wall base for Test H2 L2 S2 C1 D2.

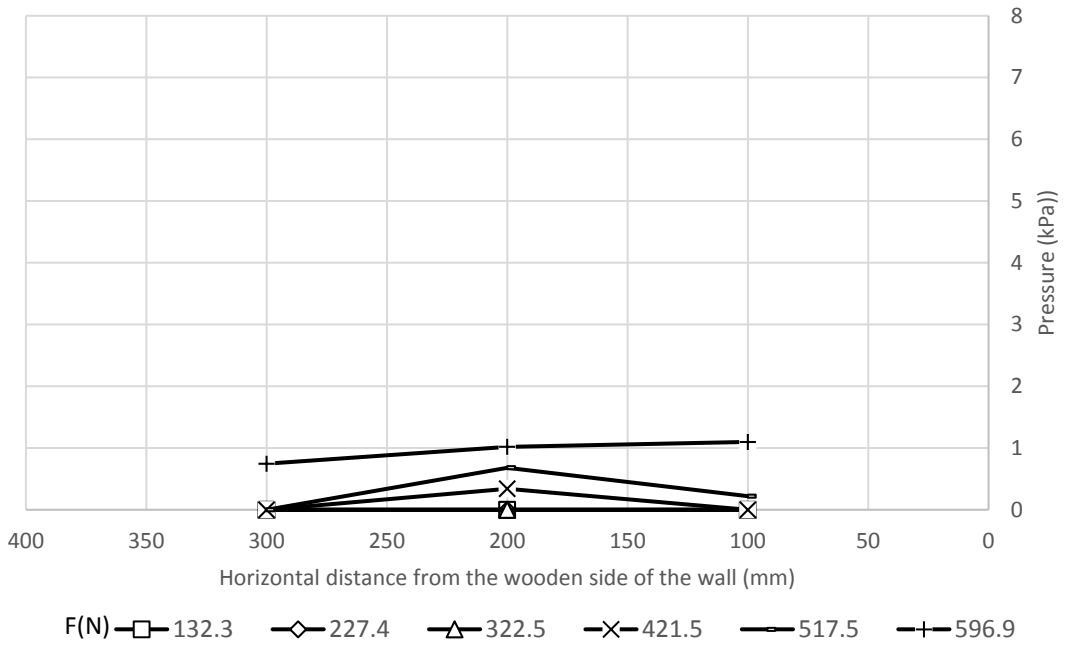

Figure A.60 Transverse pressure distributions at 337.5 mm from the wall base for Test H2 L2 S2 C1 D3.

A.3.2. Category 2

Deflection of the wall facing:

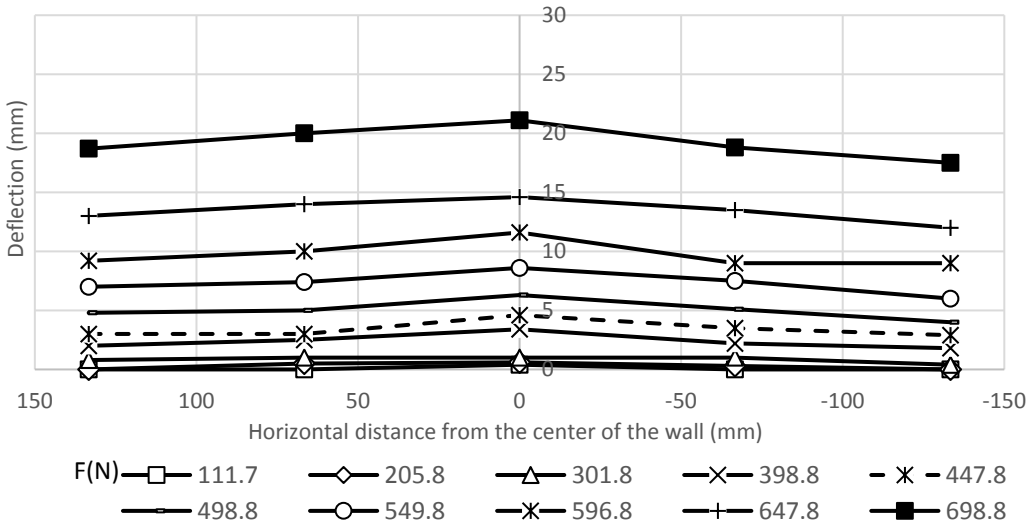

Figure A.61 Transverse deflection profiles at 472.5 mm from the wall base for Test H2 L2 S1 C1 D1.

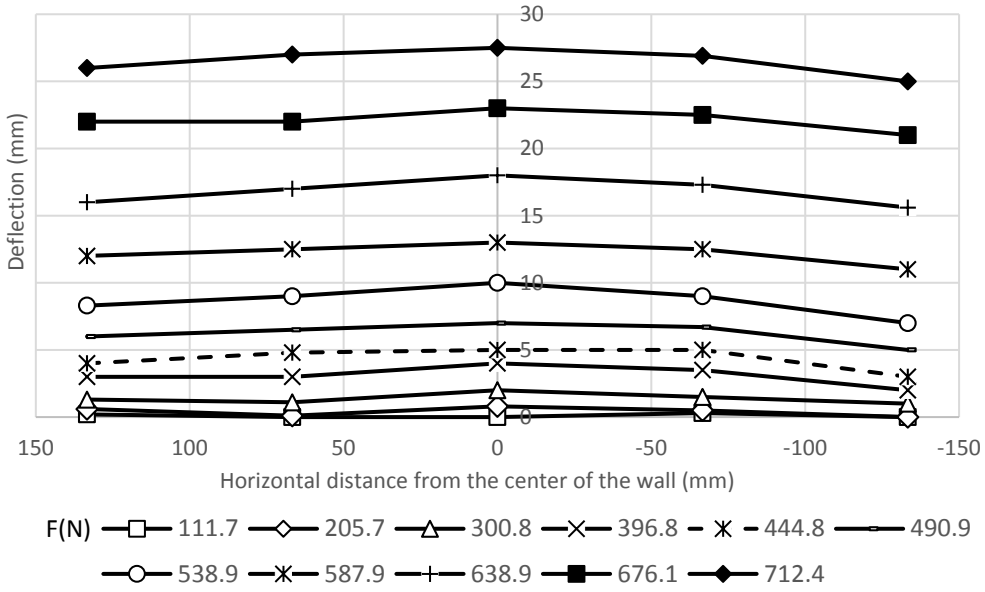

Figure A.62 Transverse deflection profiles at 472.5 mm from the wall base for Test H2 L2 S1 C1 D2.

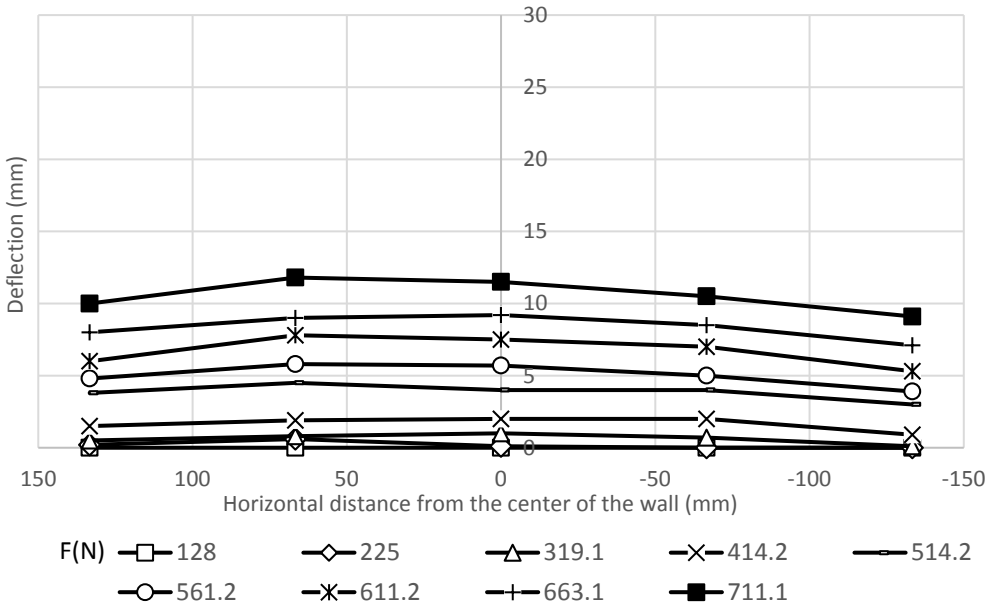

Figure A.63 Transverse deflection profiles at 472.5 mm from the wall base for Test H2 L2 S1 C1 D3.

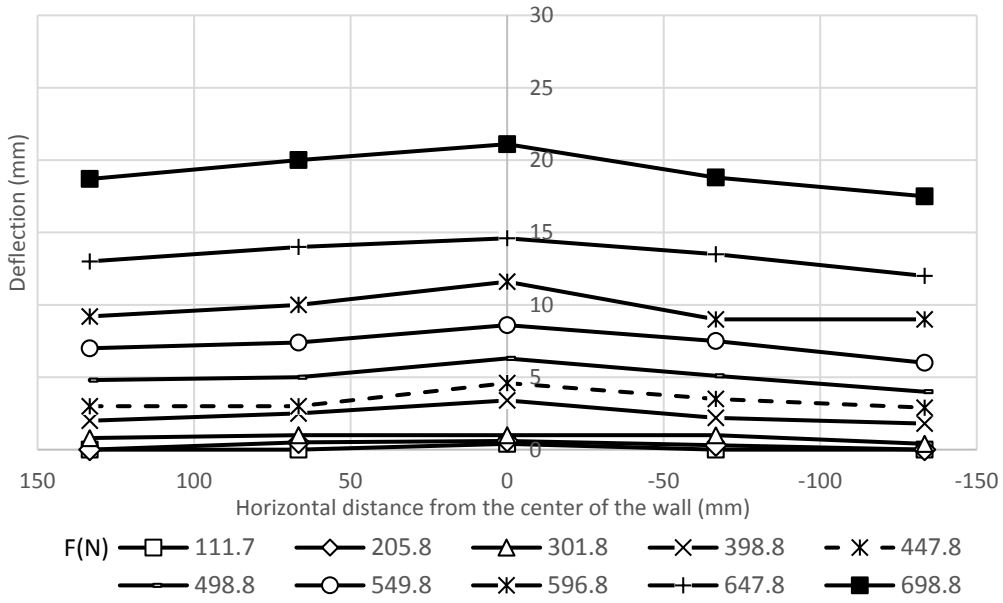

Figure A.64 Transverse deflection profiles at 337.5 mm from the wall base for Test H2 L2 S1 C1 D1.

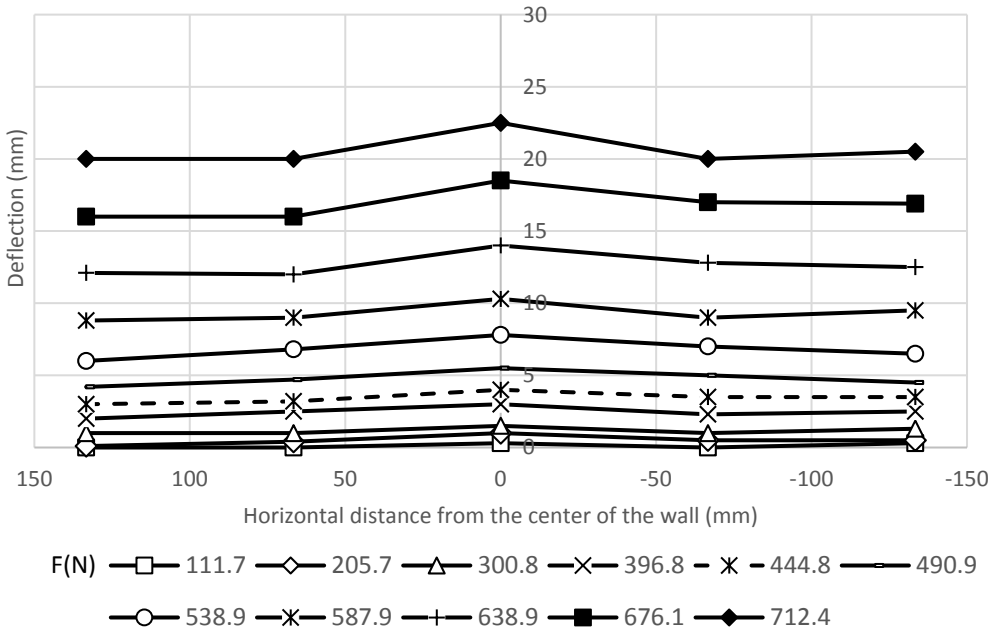

Figure A.65 Transverse deflection profiles at 337.5 mm from the wall base for Test H2 L2 S1 C1 D2.

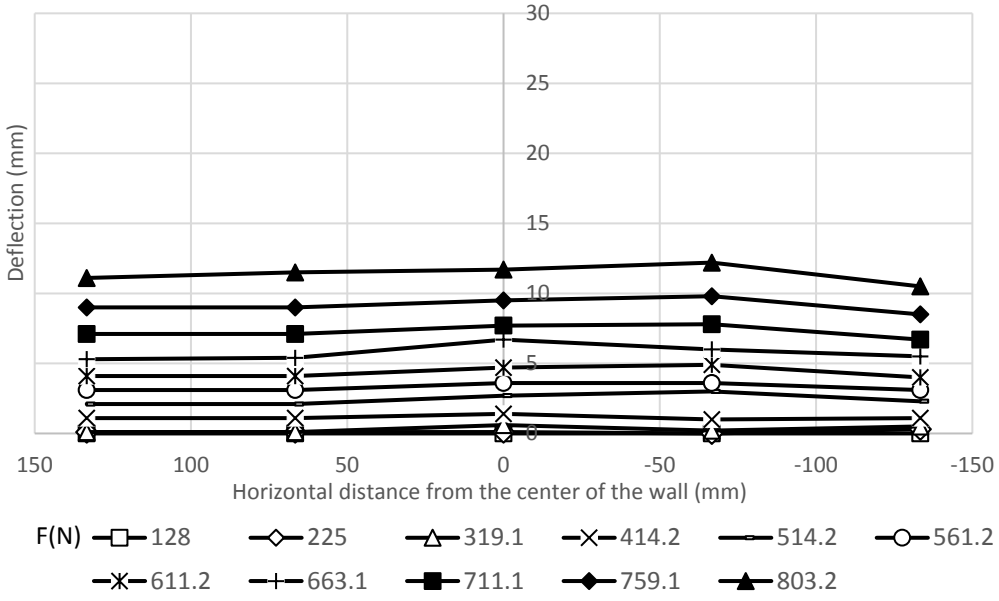

Figure A.66 Transverse deflection profiles at 337.5 mm from the wall base for Test H2 L2 S1 C1 D3.

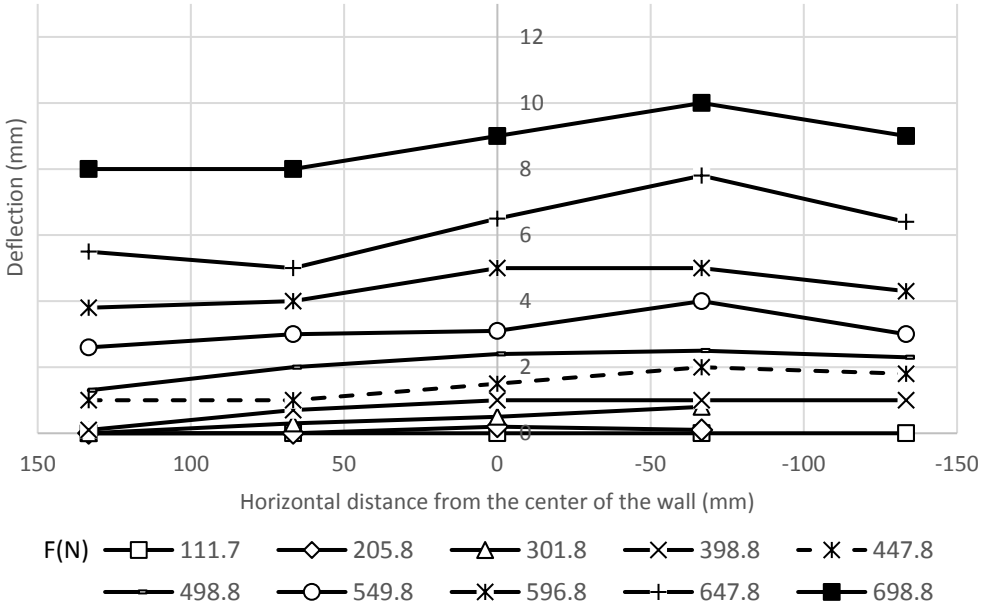

Figure A.67 Transverse deflection profiles at 202.5 mm from the wall base for Test H2 L2 S1 C1 D1.

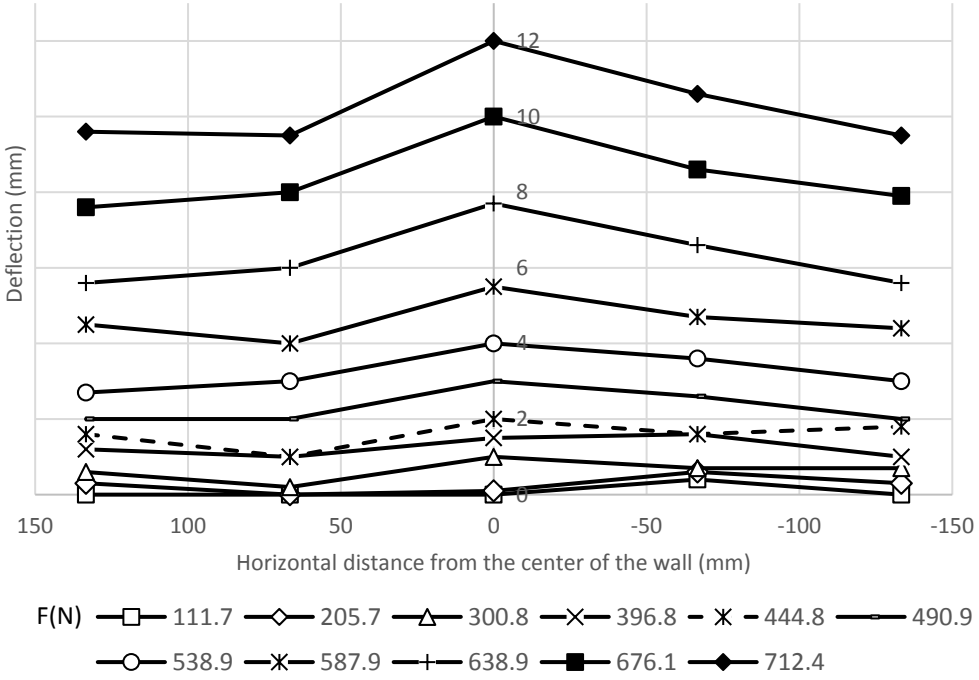

Figure A.68 Transverse deflection profiles at 202.5 mm from the wall base for Test H2 L2 S1 C1 D2.

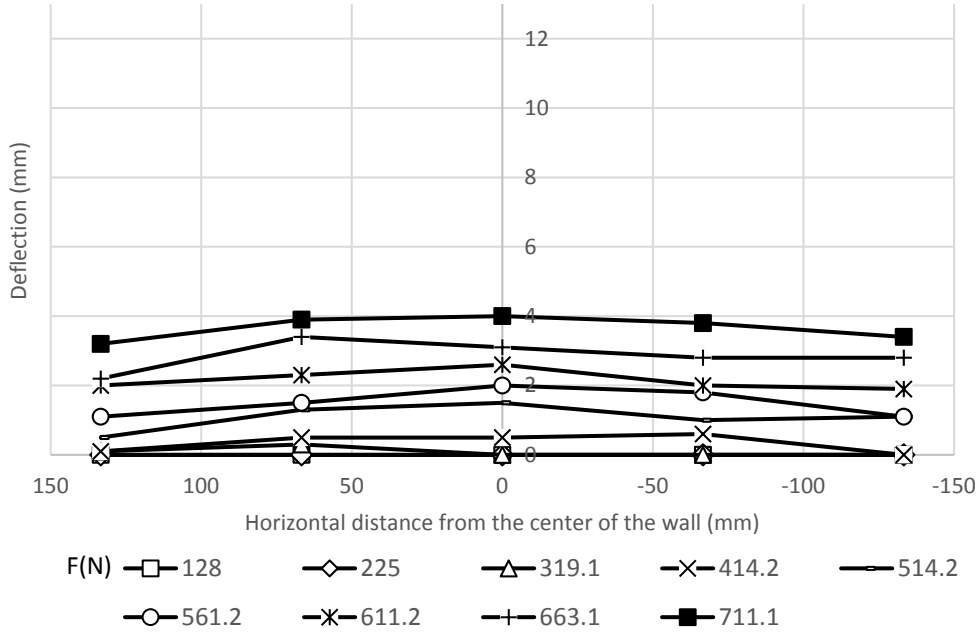

Figure A.69 Transverse deflection profiles at 202.5 mm from the wall base for Test H2 L2 S1 C1 D3.

Stress and moment of the pile:

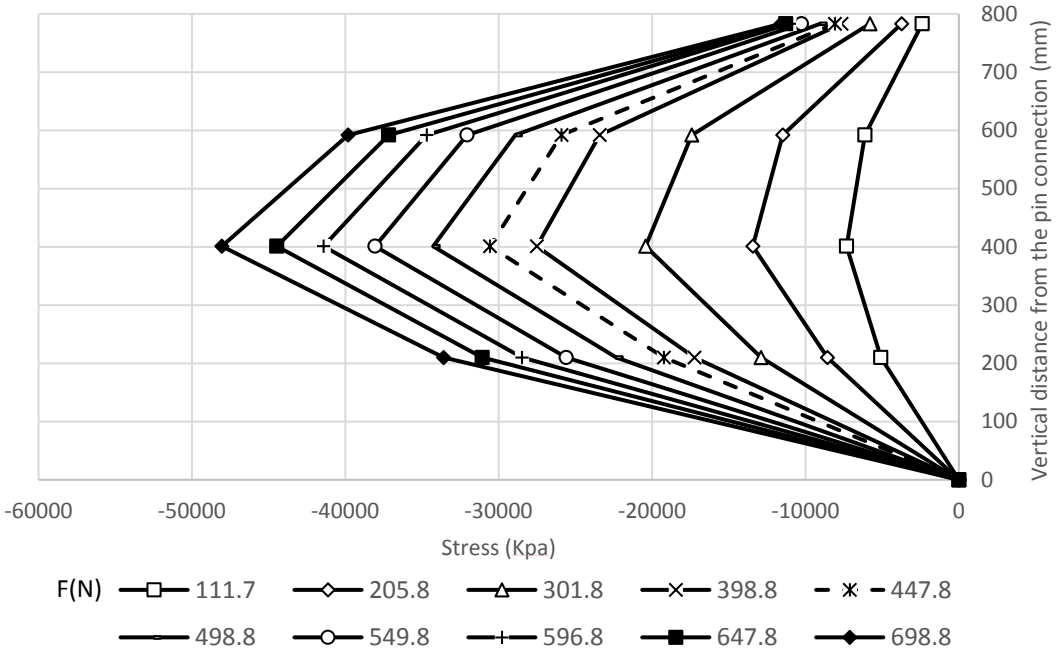

Figure A.70 Stresses along the compressive side of the pile in Test H2 L2 S1 C1 D1.

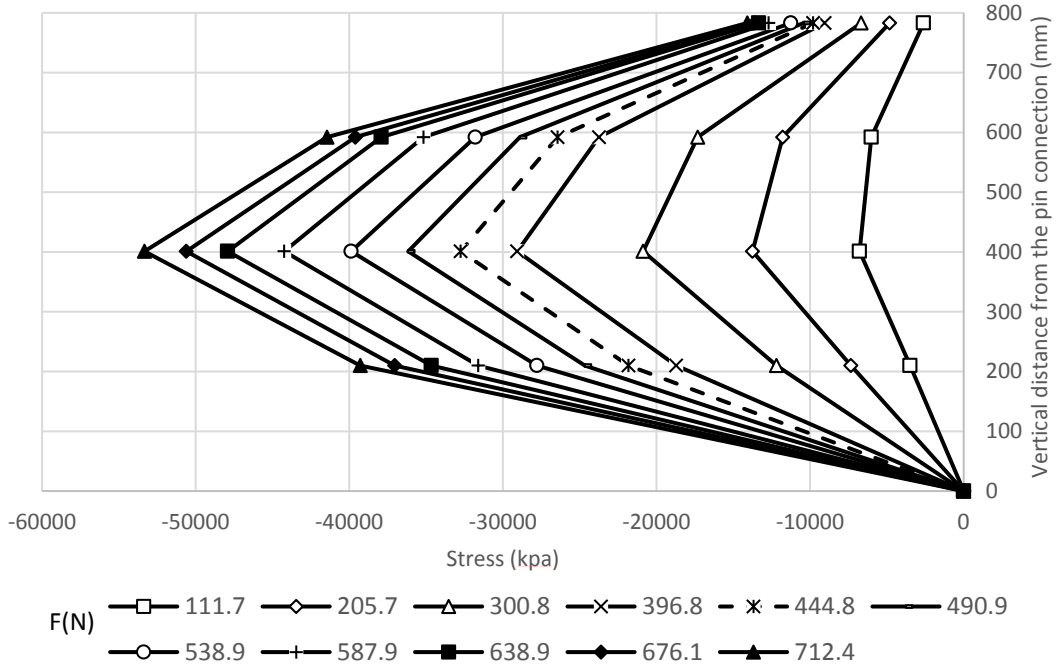

Figure A.71 Stresses along the compressive side of the pile in Test H2 L2 S1 C1 D2.

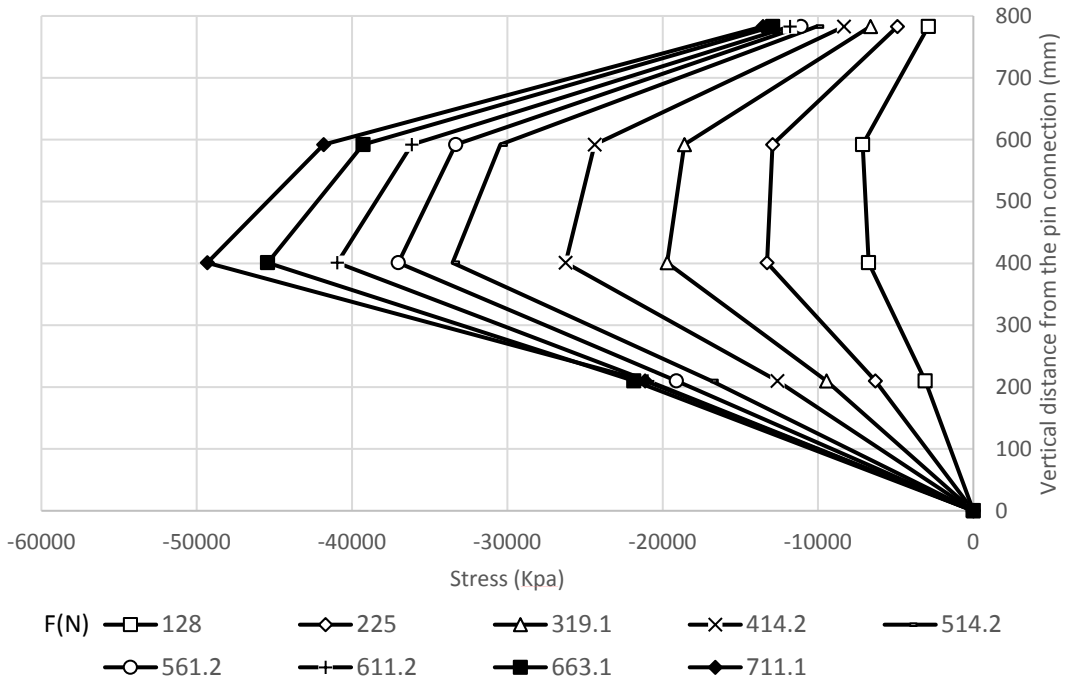

Figure A.72 Stresses along the compressive side of the pile in Test H2 L2 S1 C1 D3.

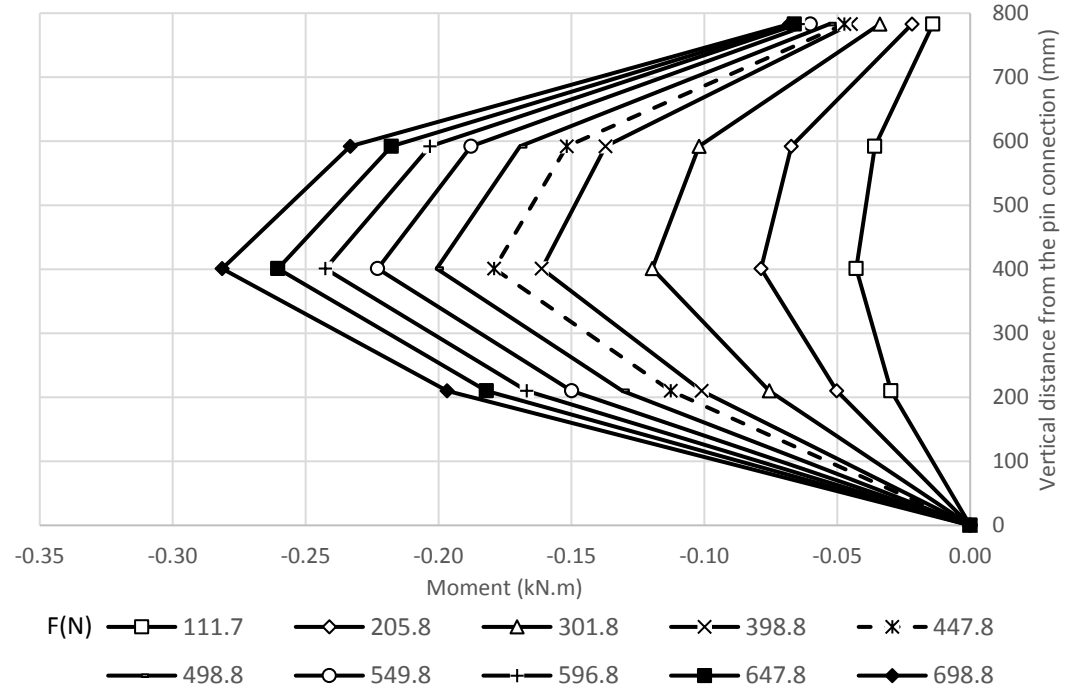

Figure A.73 Moments along the compressive side of the pile in Test H2 L2 S1 C1 D1.

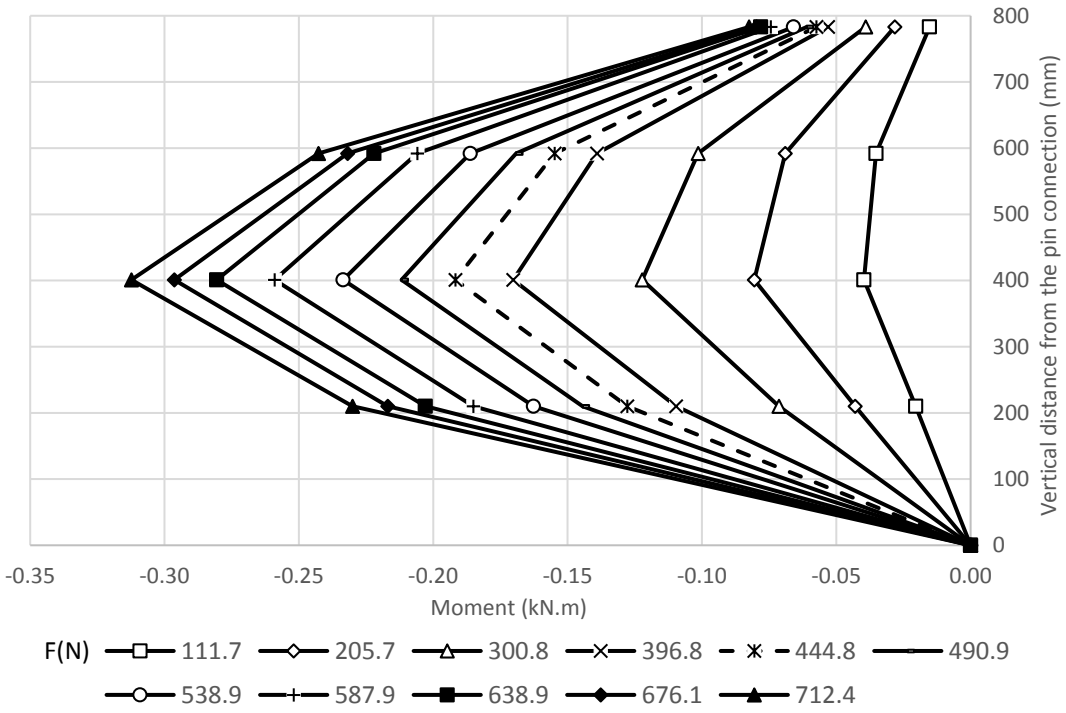

Figure A.74 Moments along the compressive side of the pile in Test H2 L2 S1 C1 D2.

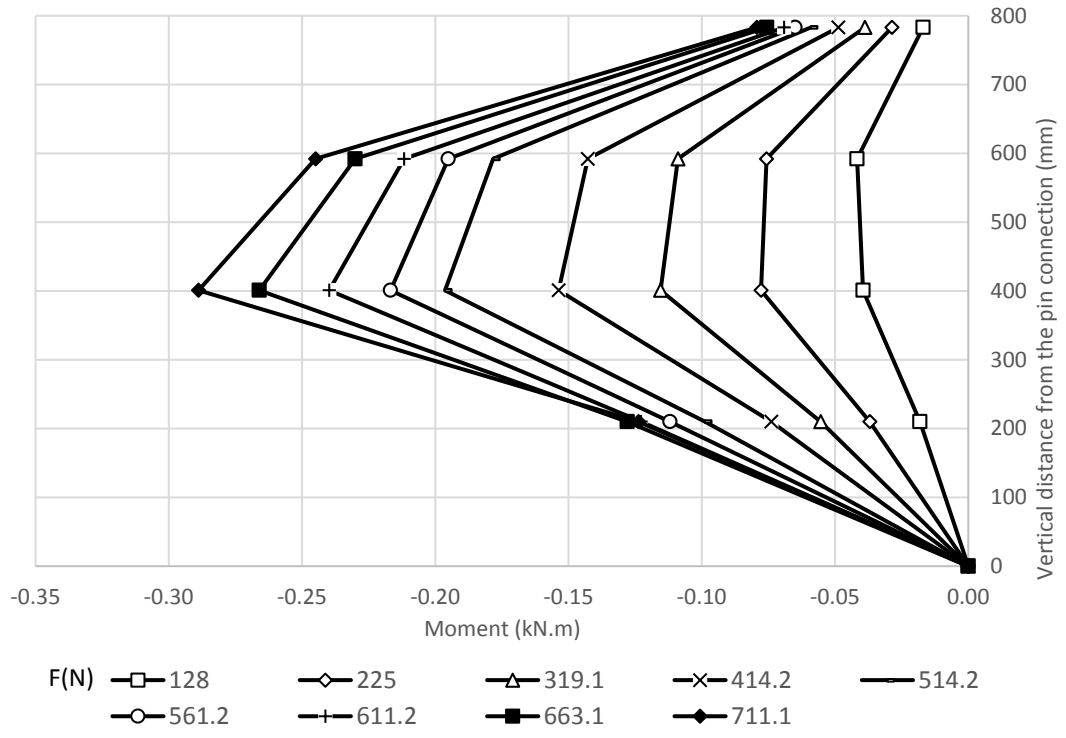

Figure A.75 Moments along the compressive side of the pile in Test H2 L2 S1 C1 D3.

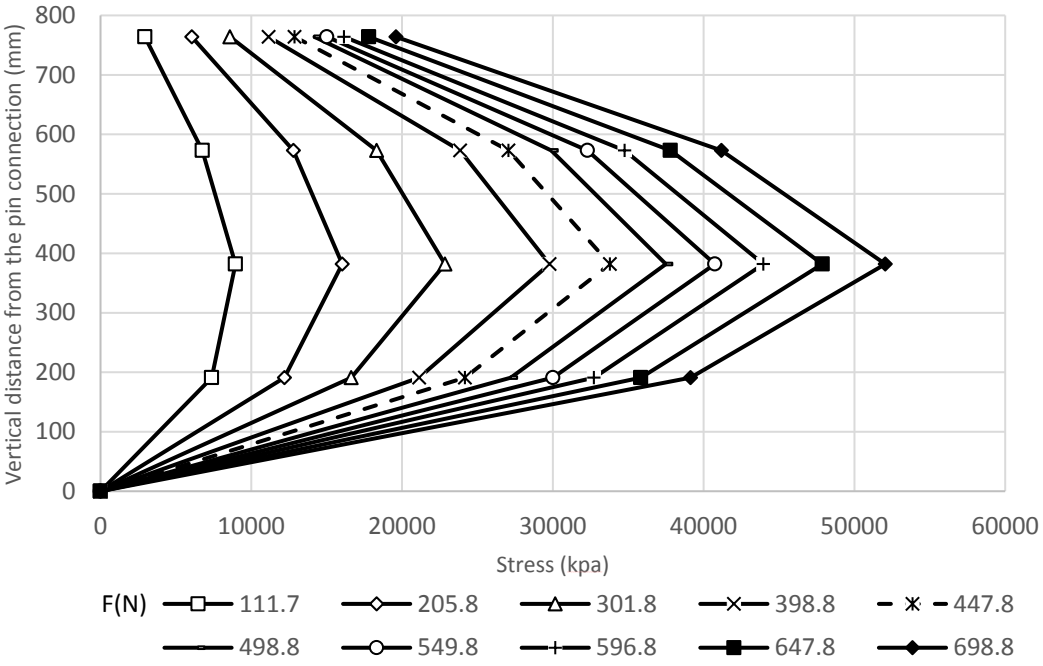

Figure A.76 Stresses along the tensile side of the pile in Test H2 L2 S1 C1 D1.

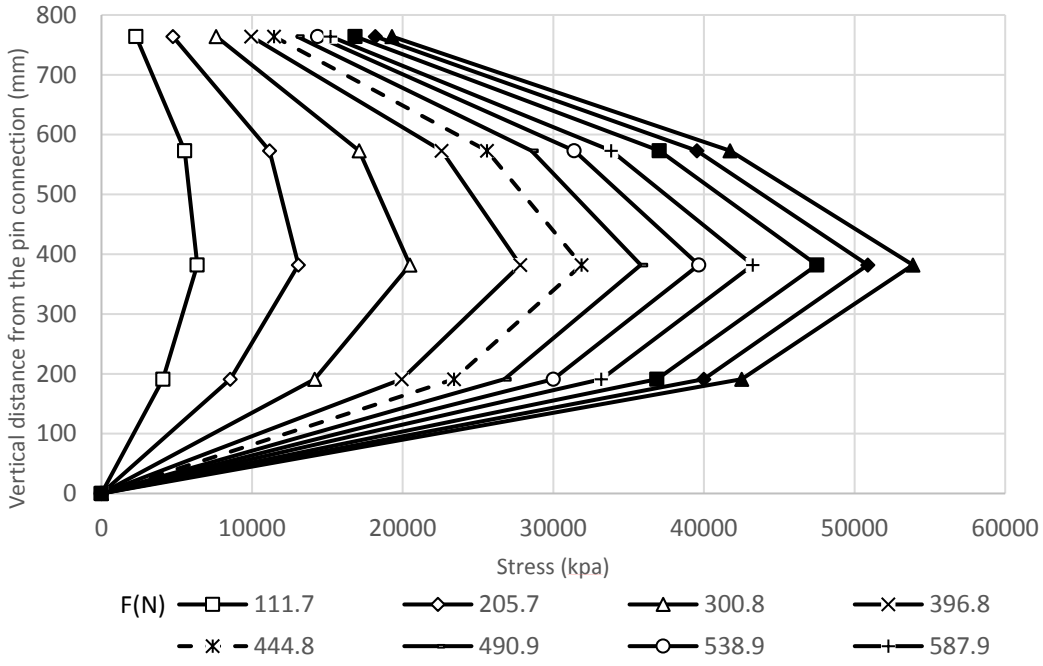

Figure A.77 Stresses along the tension side of the pile in Test H2 L2 S1 C1 D2.

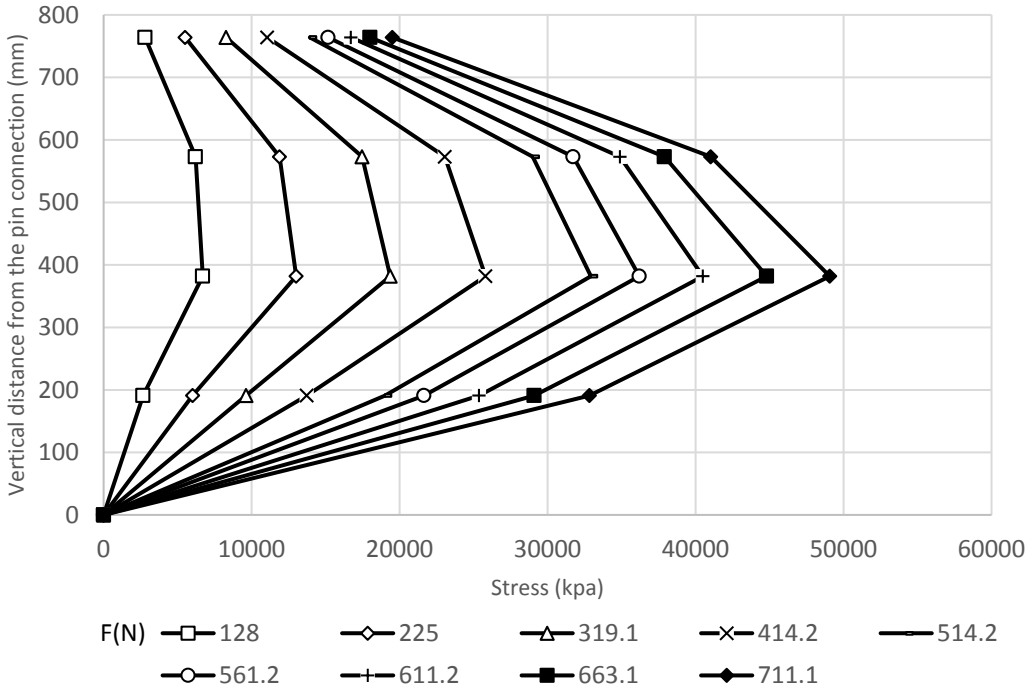

Figure A.78 Stresses along the tensile side of the pile in Test H2 L2 S1 C1 D3.

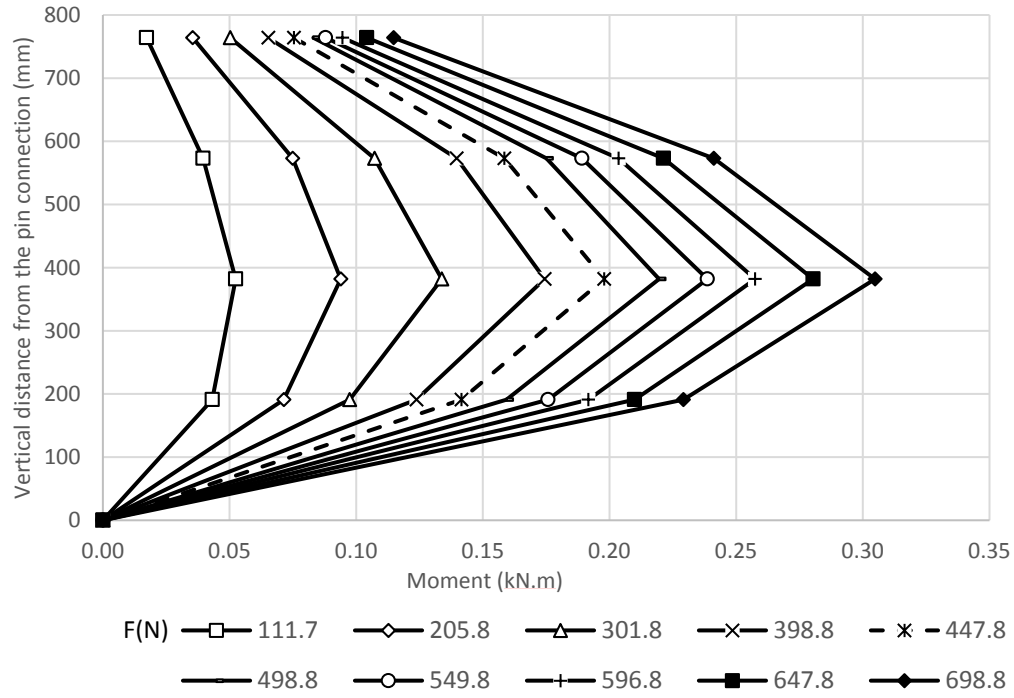

Figure A.79 Moments along the tensile side of the pile in Test H2 L2 S1 C1 D1.

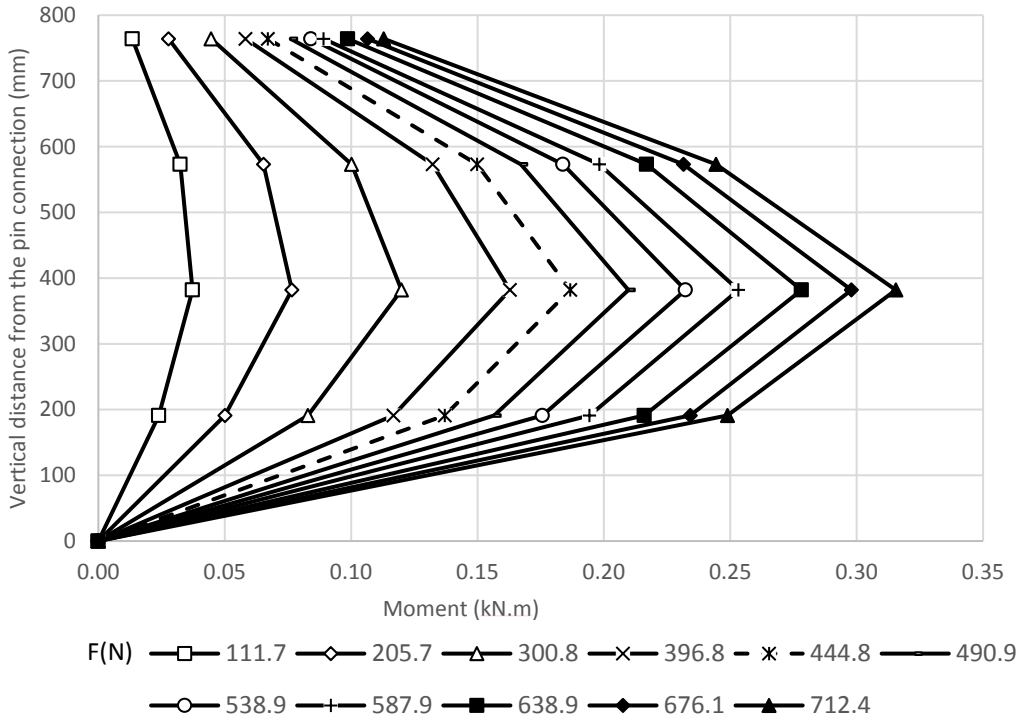

Figure A.80 Moments along the tensile side of the pile in Test H2 L2 S1 C1 D2.

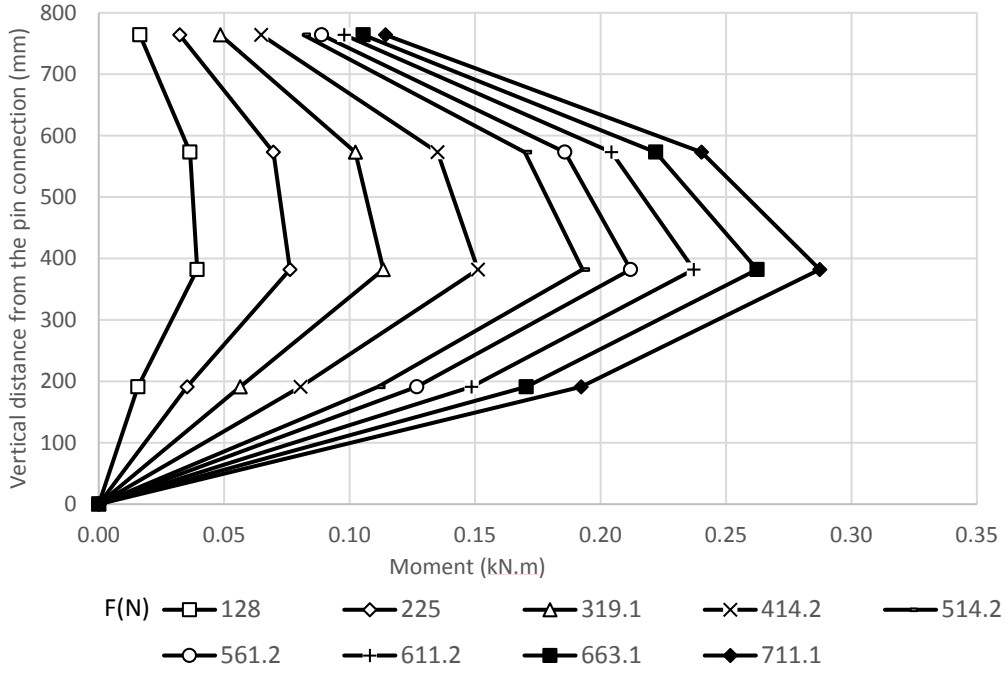

Figure A.81 Moments along the tensile side of the pile in Test H2 L2 S1 C1 D3.

Strain in the geogrid layers:

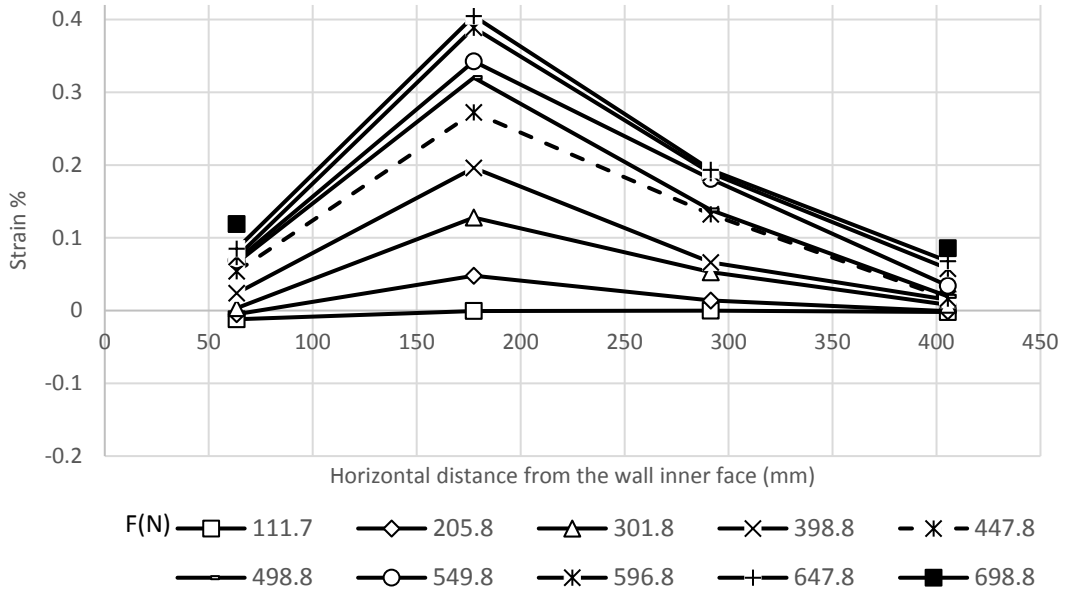

Figure A.82 Strains in the geogrid layer at 450 mm from the wall base (Test H2 L2 S1 C1 D1).

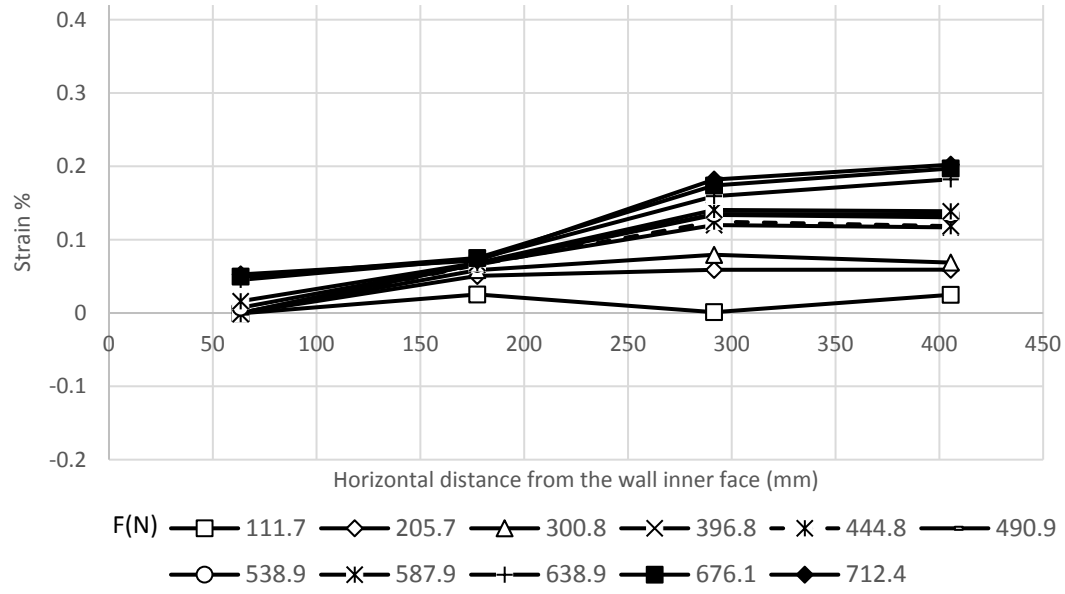

Figure A.83 Strains in the geogrid layer at 450 mm from the wall base (Test H2 L2 S1 C1 D2).

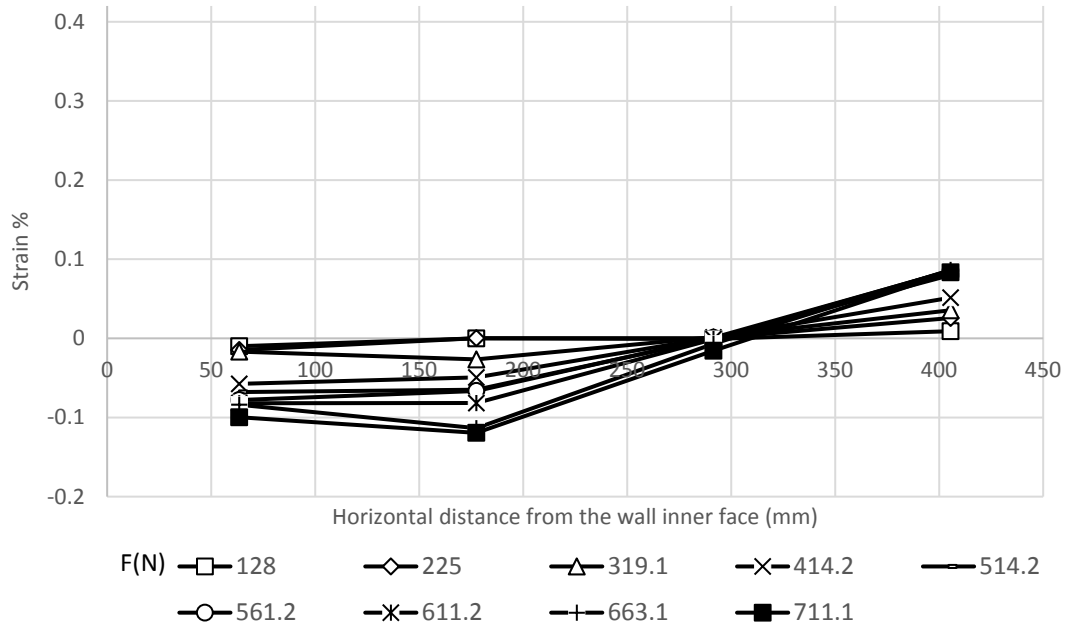

Figure A.84 Strains in the geogrid layer at 450 mm from the wall base (Test H2 L2 S1 C1 D3).

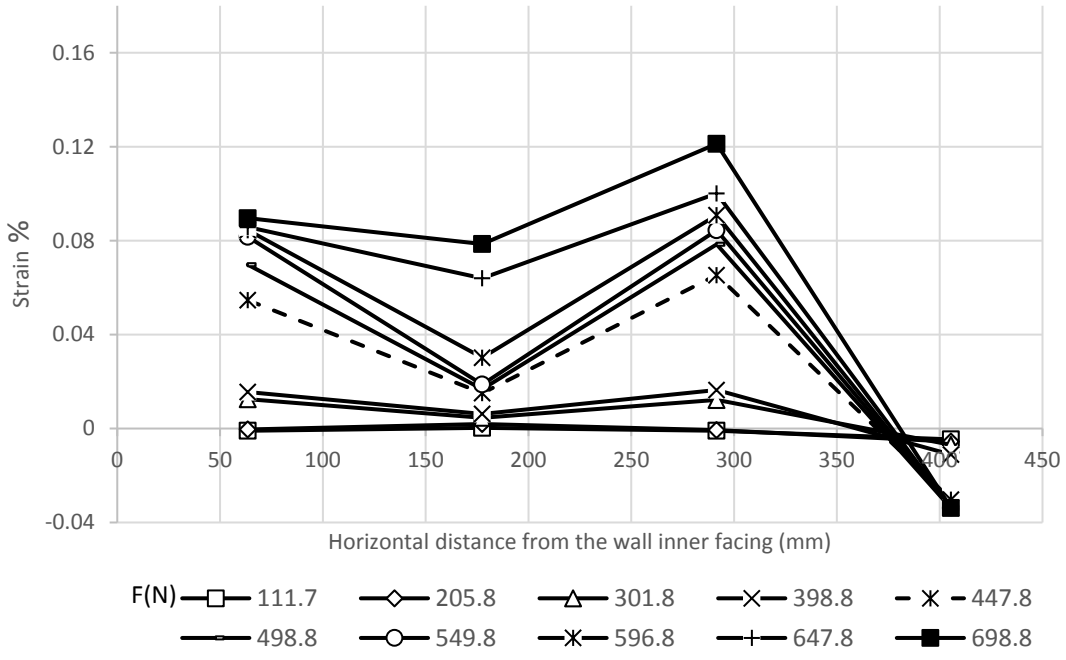

Figure A.85 Strains in the geogrid layer at 270 mm from the wall base (Test H2 L2 S1 C1 D1).

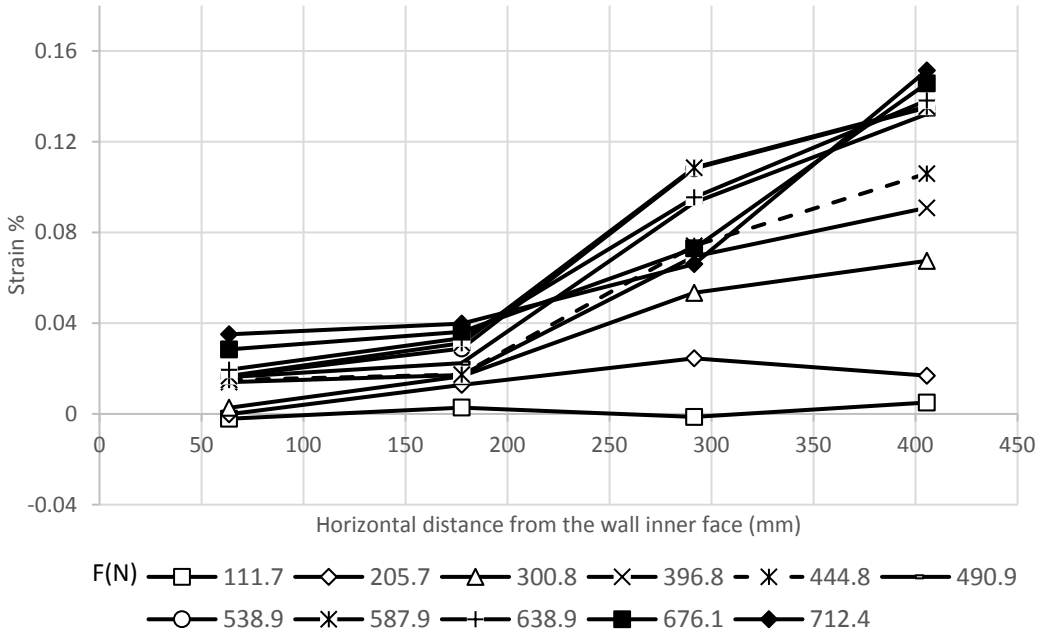

Figure A.86 Strains in the geogrid layer at 270 mm from the wall base (Test H2 L2 S1 C1 D2).

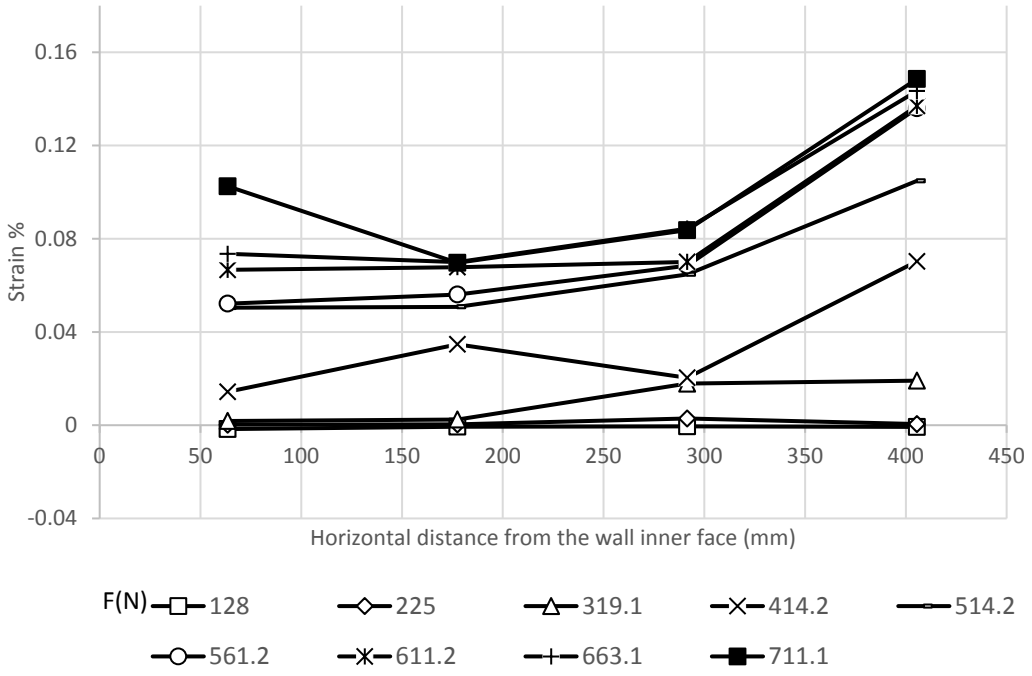

Figure A.87 Strains in the geogrid layer at 270 mm from the wall base (Test H2 L2 S1 C1 D3).

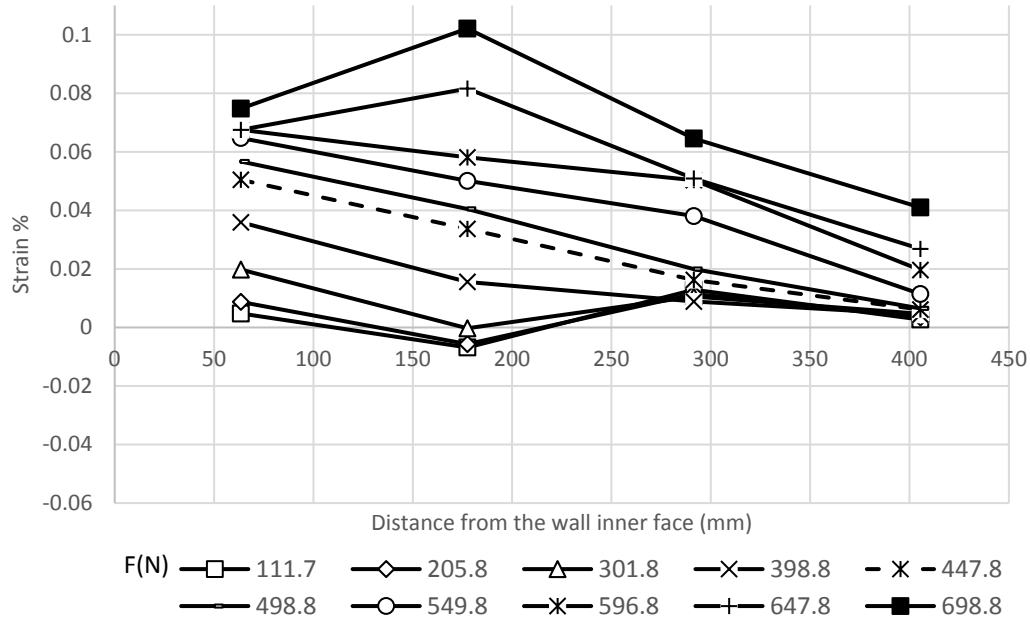

Figure A.88 Strains in the geogrid layer at 90 mm from the wall base (Test H2 L2 S1 C1 D1).

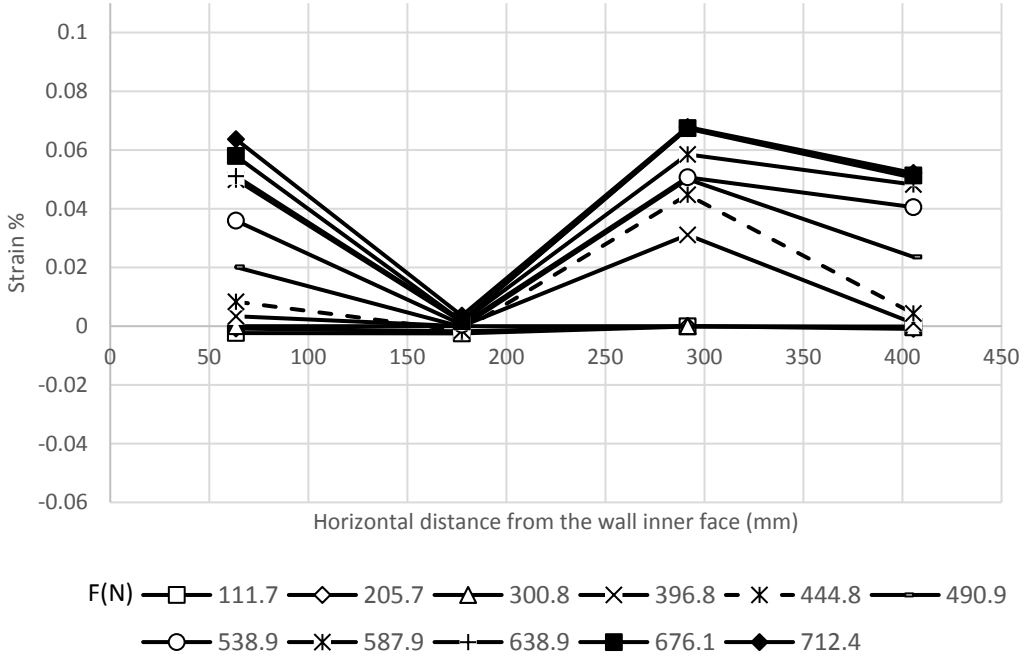

Figure A.89 Strains in the geogrid layer at 90 mm from the wall base (Test H2 L2 S1 C1 D2).

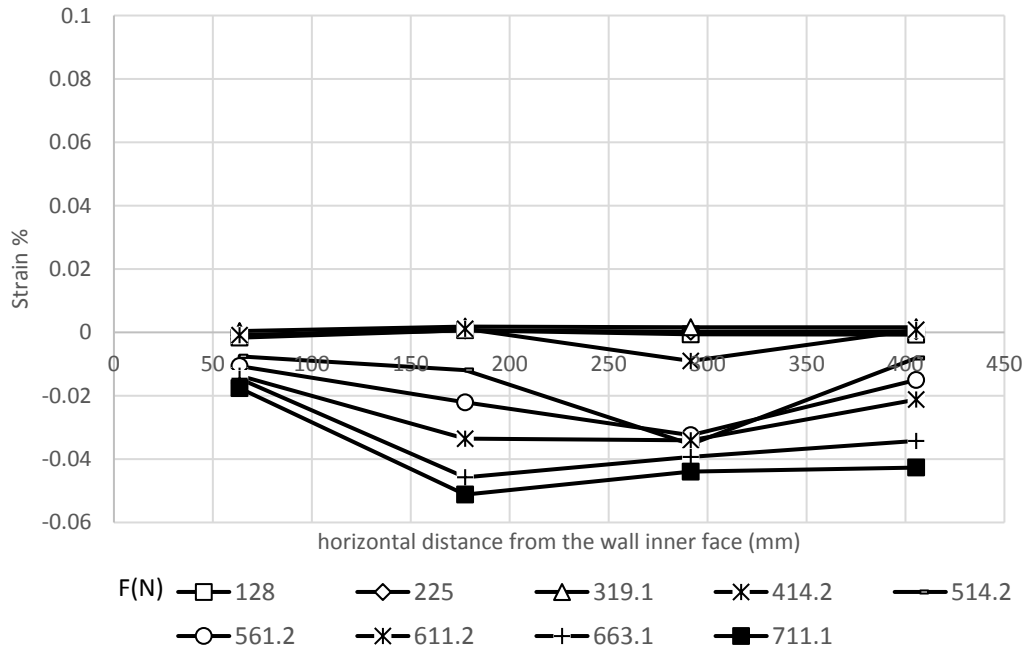

Figure A.90 Strains in the geogrid layer at 90 mm from the wall base (Test H2 L2 S1 C1 D3).

Pressure behind the wall facing:

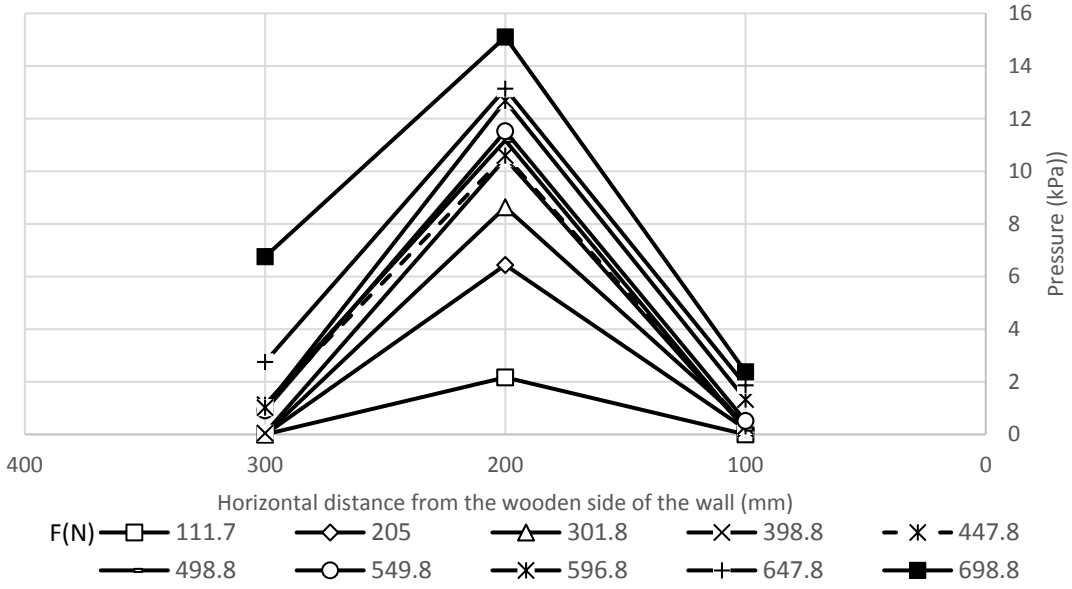

Figure A.91 Transverse pressure distributions at 607.5 mm from the wall base for Test H2 L2 S1 C1 D1.

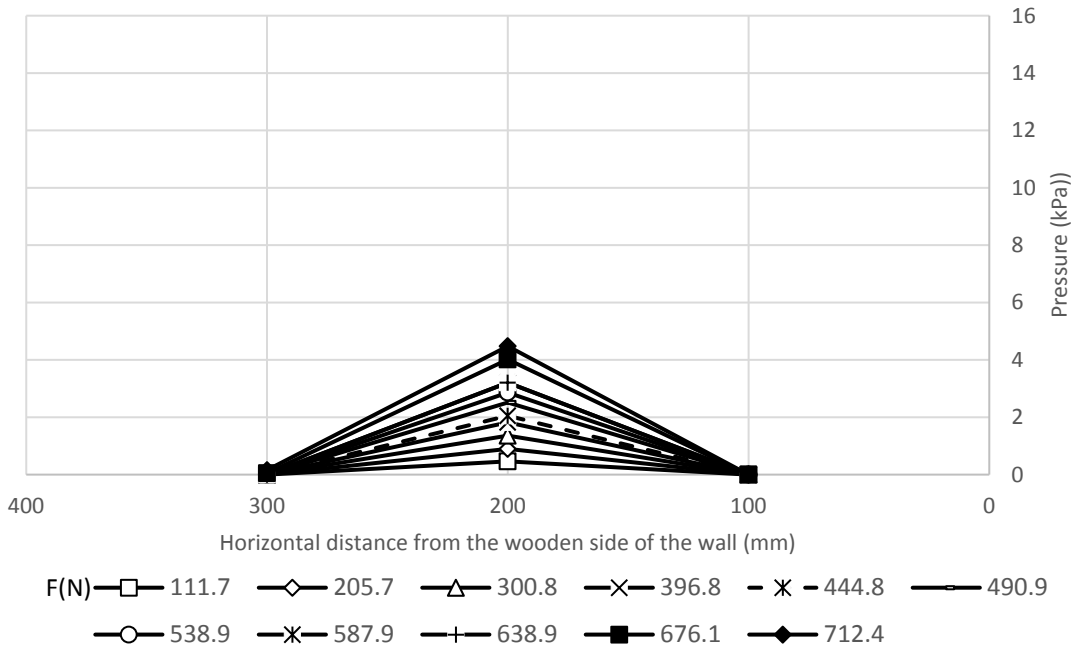

Figure A.92 Transverse pressure distributions at 607.5 mm from the wall base for Test H2 L2 S1 C1 D2.

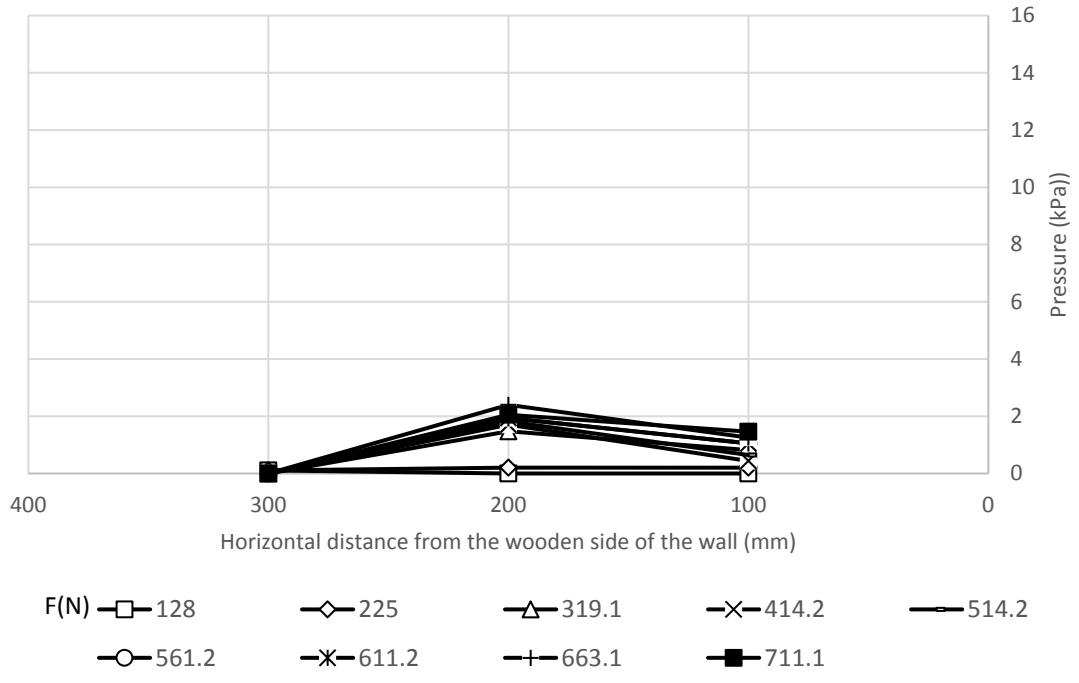

Figure A.93 Transverse pressure distributions at 607.5 mm from the wall base for Test H2 L2 S1 C1 D3.

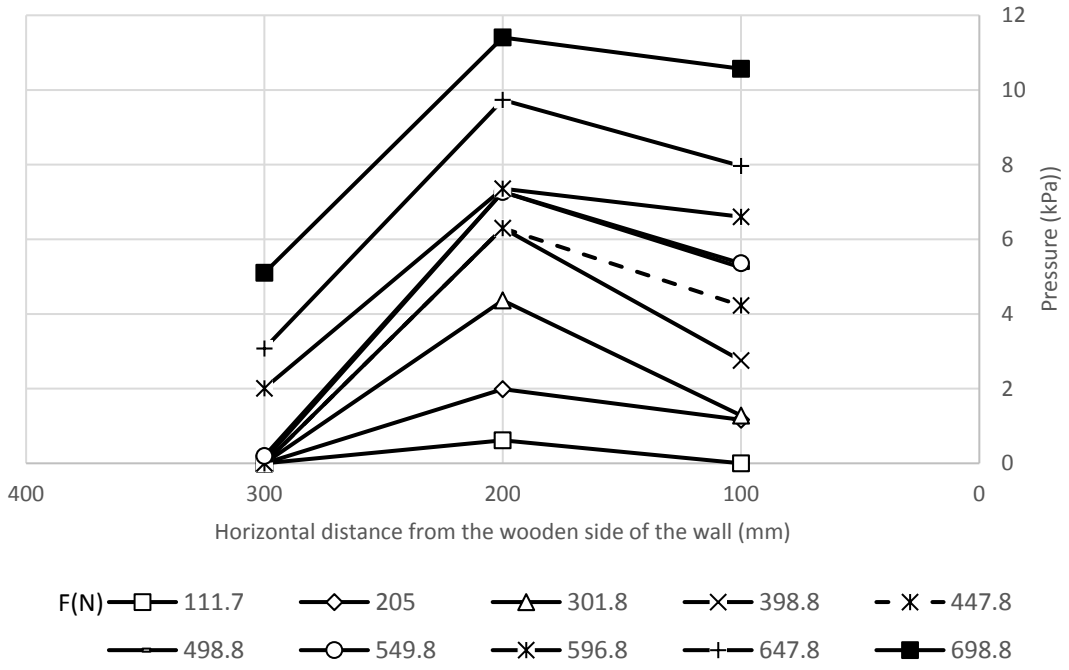

Figure A.94 Transverse pressure distributions at 337.5 mm from the wall base for Test H2 L2 S1 C1 D1.

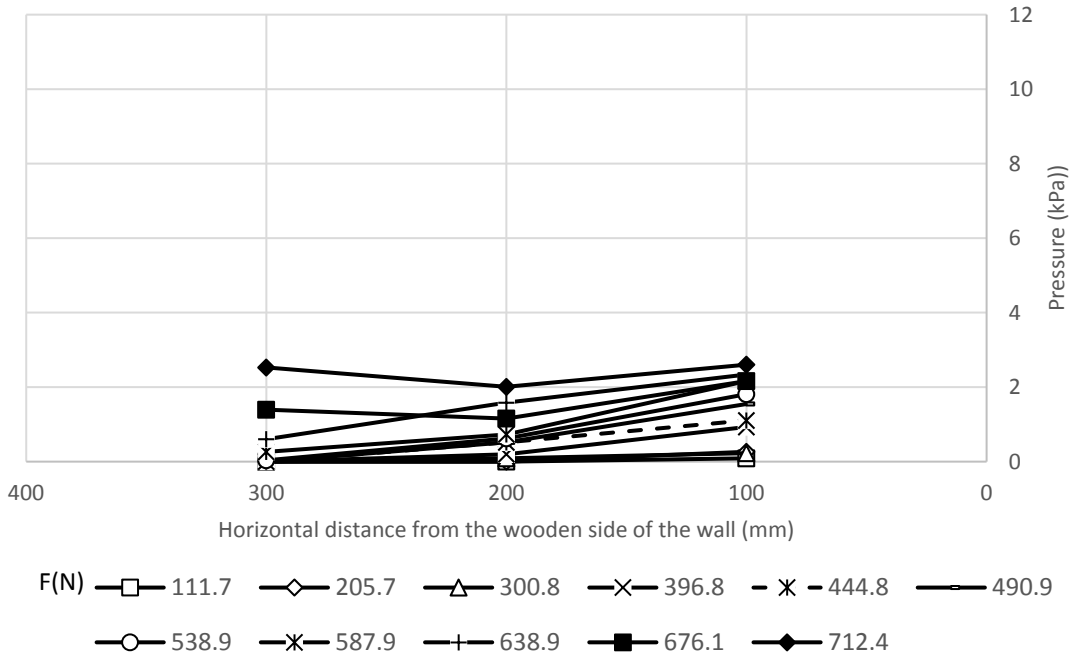

Figure A.95 Transverse pressure distributions at 337.5 mm from the wall base for Test H2 L2 S1 C1 D2.

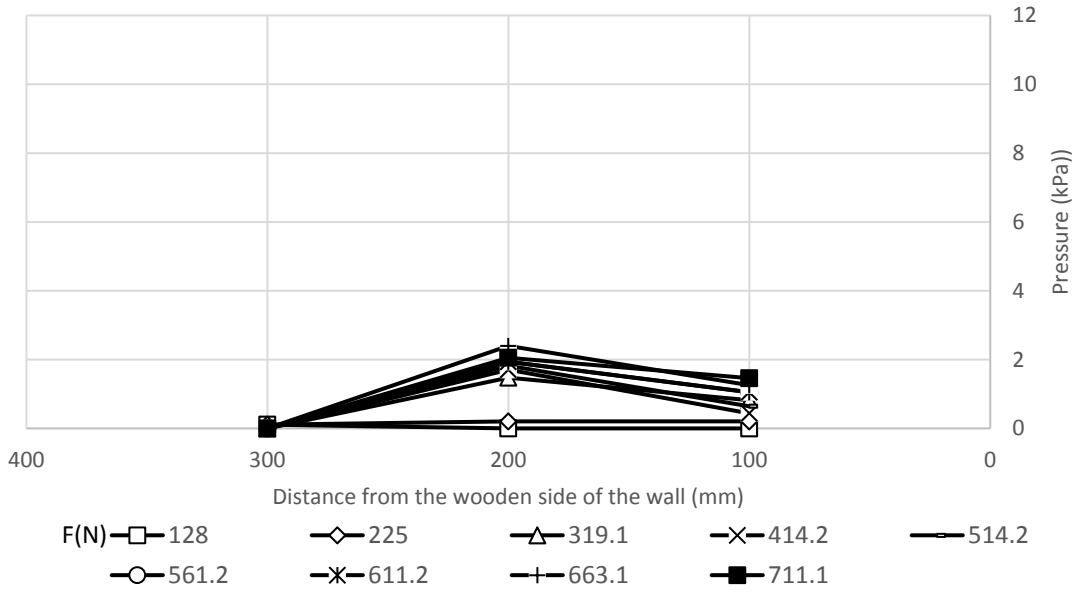

Figure A.96 Transverse pressure distributions at 337.5 mm from the wall base for Test H2 L2 S1 C1 D3.

A.3.3. Category (3)

Deflection of the wall facing:

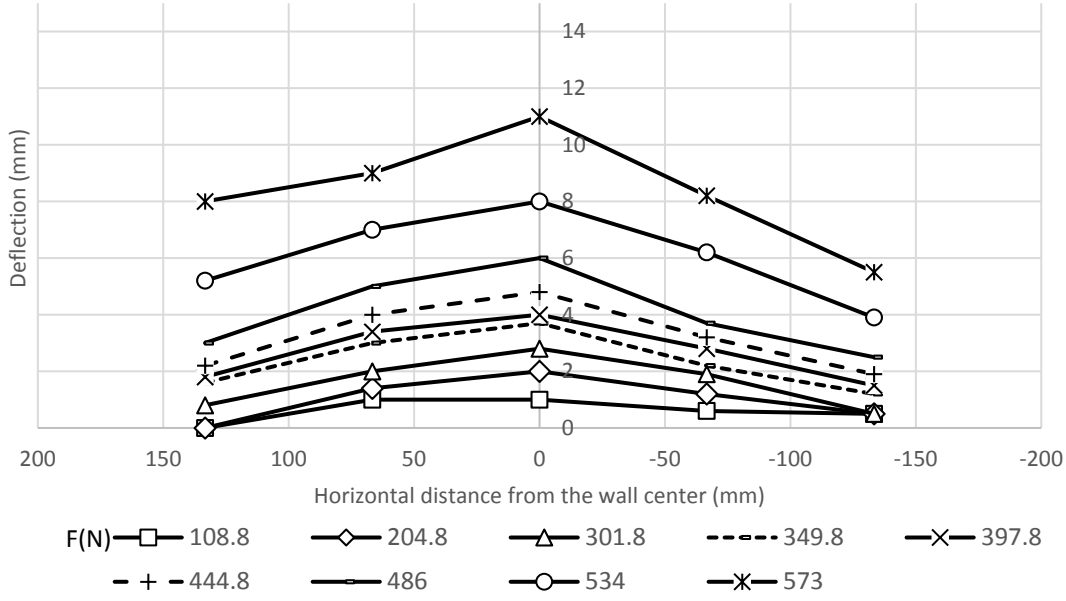

Figure A.97 Transverse deflection profiles at 472.5 mm from the wall base for Test H2 L2 S1 C2 D1.

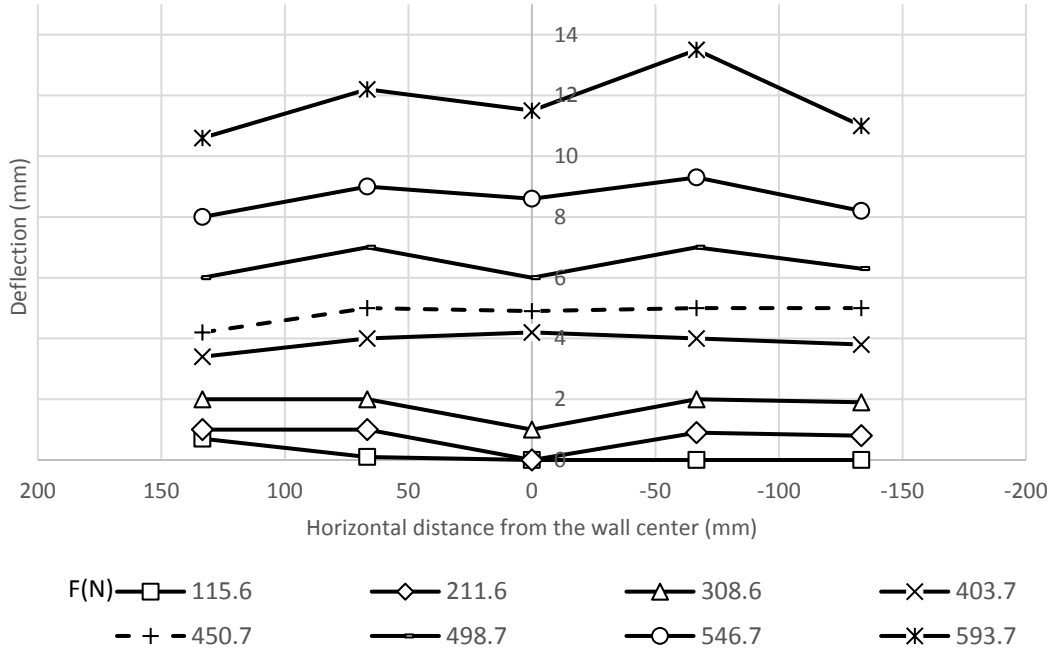

Figure A.98 Transverse deflection profiles at 472.5 mm from the wall base for Test H2 L2 S1 C2 D2.

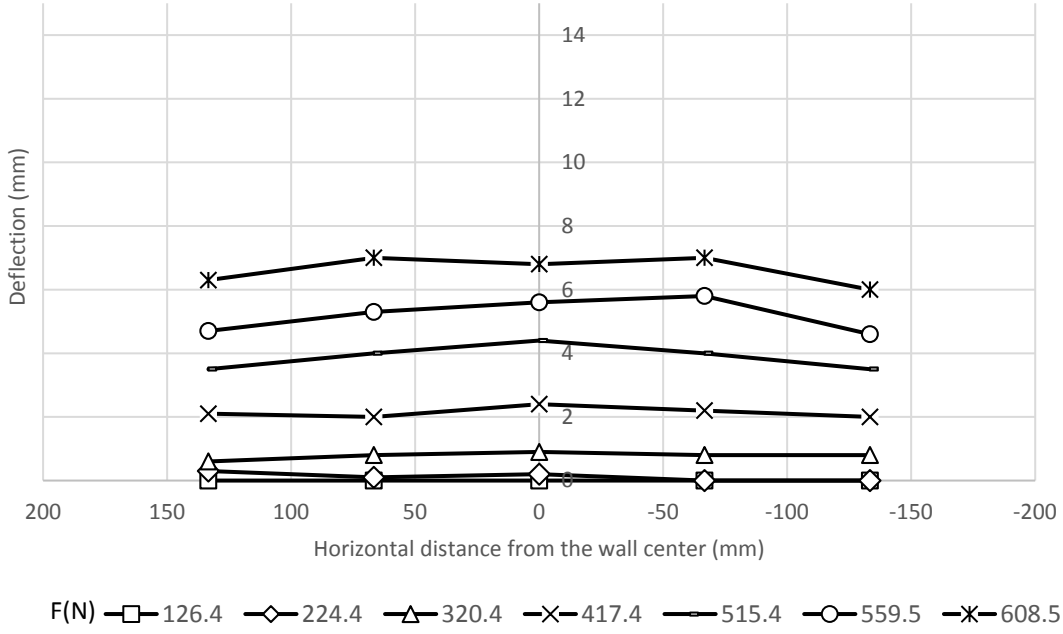

Figure A.99 Transverse deflection profiles at 472.5 mm from the wall base for Test H2 L2 S1 C2 D3.

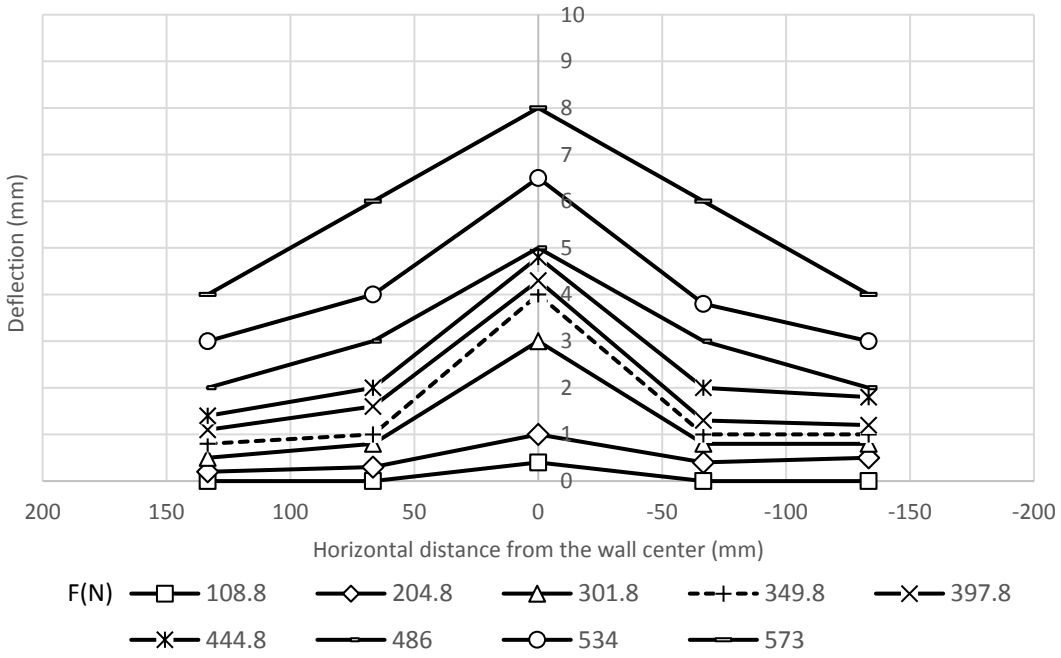

Figure A.100 Transverse deflection profiles at 337.5 mm from the wall base for Test H2 L2 S1 C2 D1.

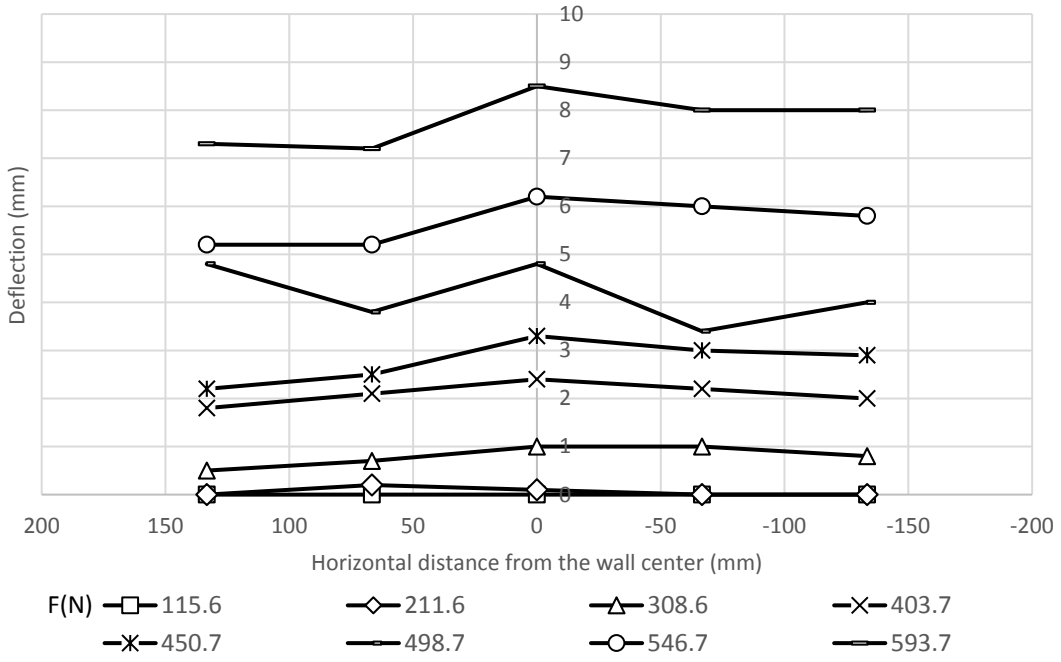

Figure A.101 Transverse deflection profiles at 337.5 mm from the wall base for Test H2 L2 S1 C2 D2.

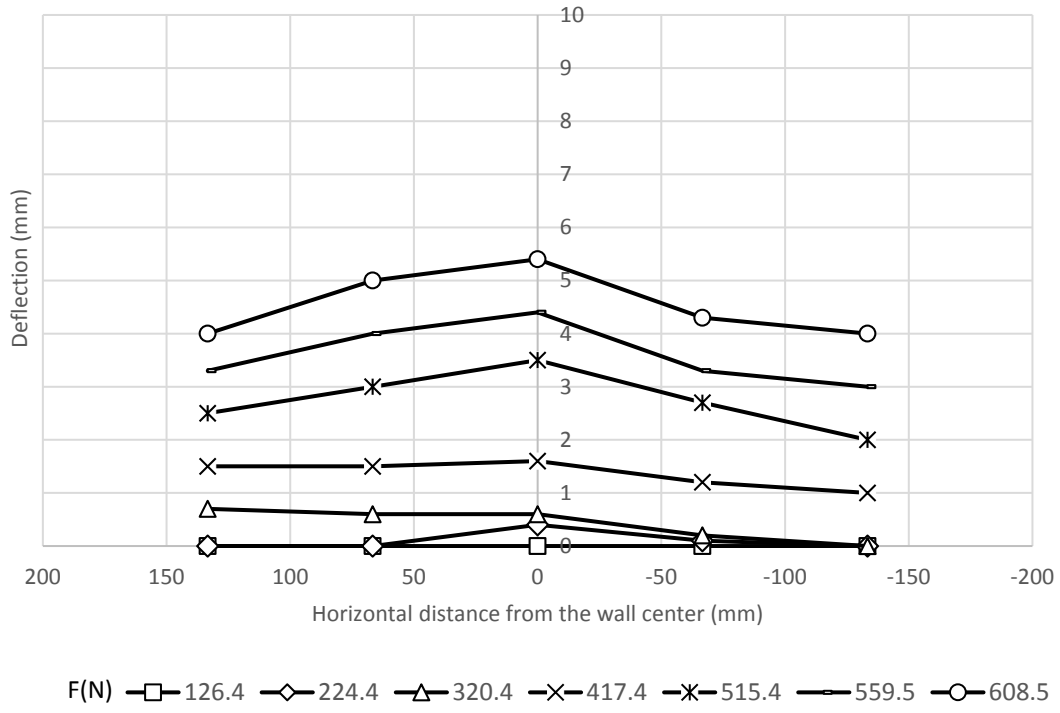

Figure A.102 Transverse deflection profiles at 337.5 mm from the wall base for Test H2 L2 S1 C2 D3.

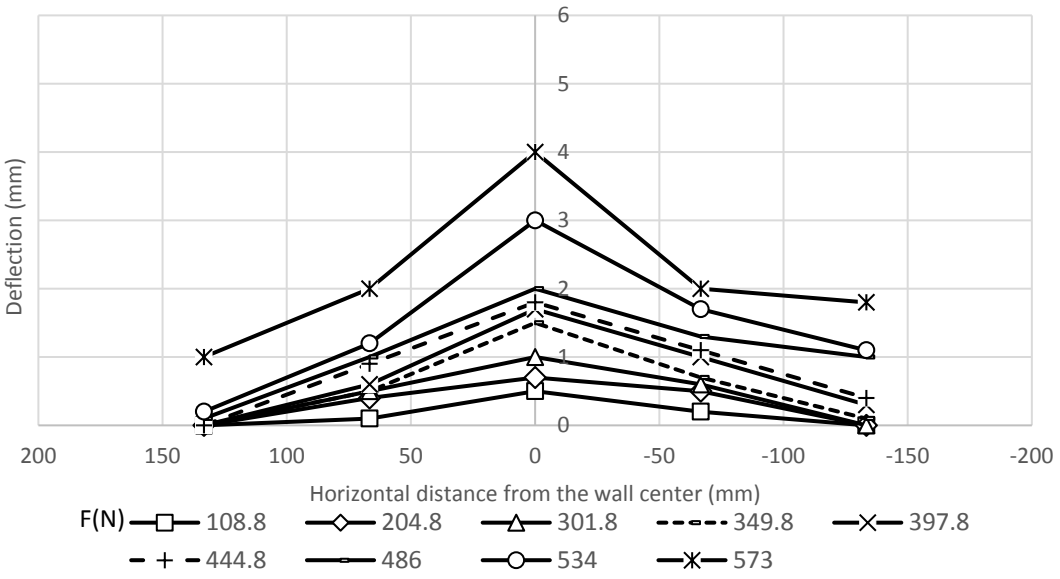

Figure A.103 Transverse deflection profiles deflection at 202.5 mm from the wall base for Test H2 L2 S1 C2 D1.

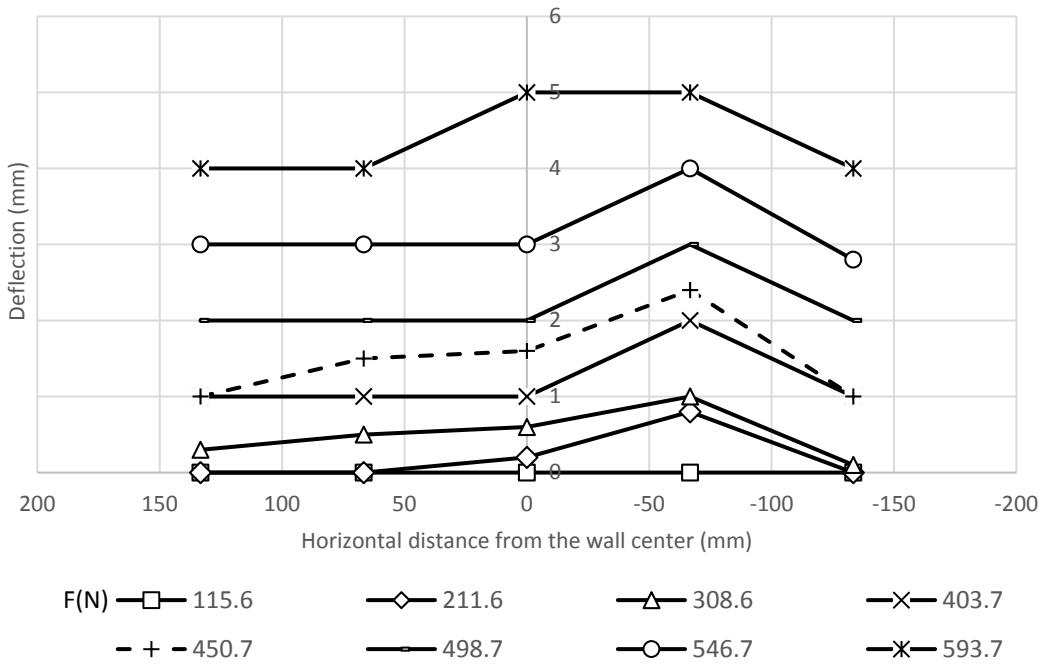

Figure A.104 Transverse deflection profiles at 202.5 mm from the wall base for Test H2 L2 S1 C2 D2.

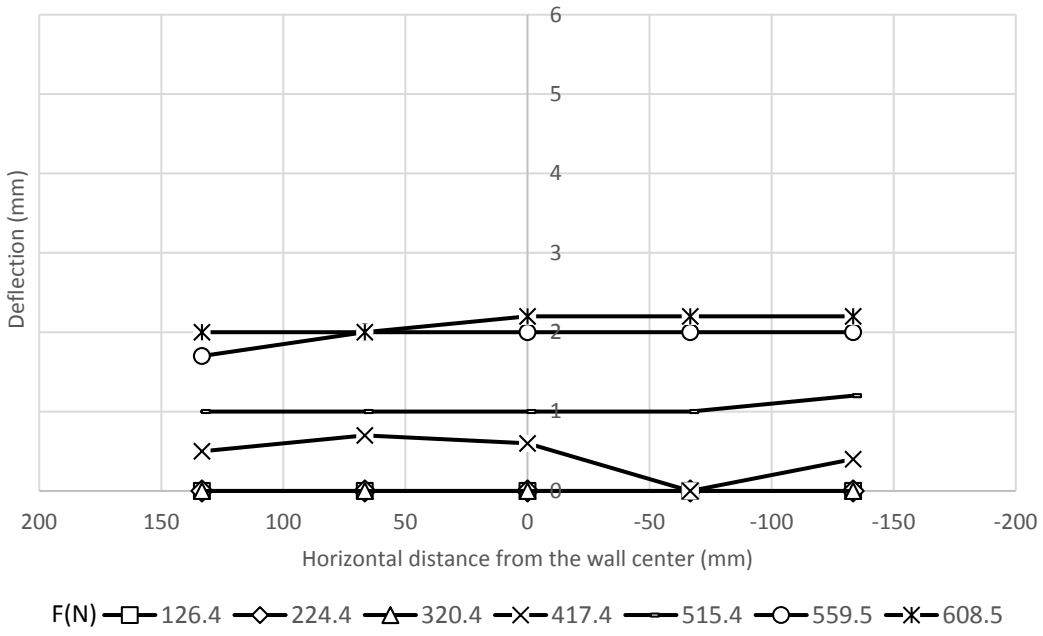

Figure A.105 Transverse deflection profiles at 202.5 mm from the wall base for Test H2 L2 S1 C2 D3.

Stress and moment of the pile:

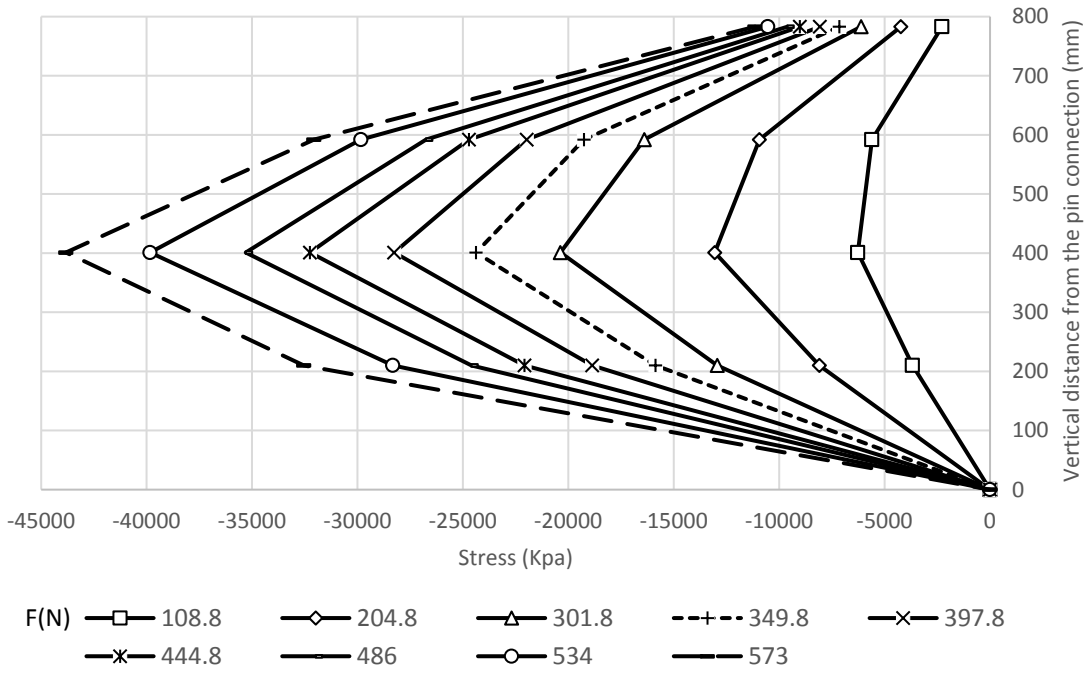

Figure A.106 Stresses along the compressive side of the pile in Test H2 L2 S1 C2 D1.

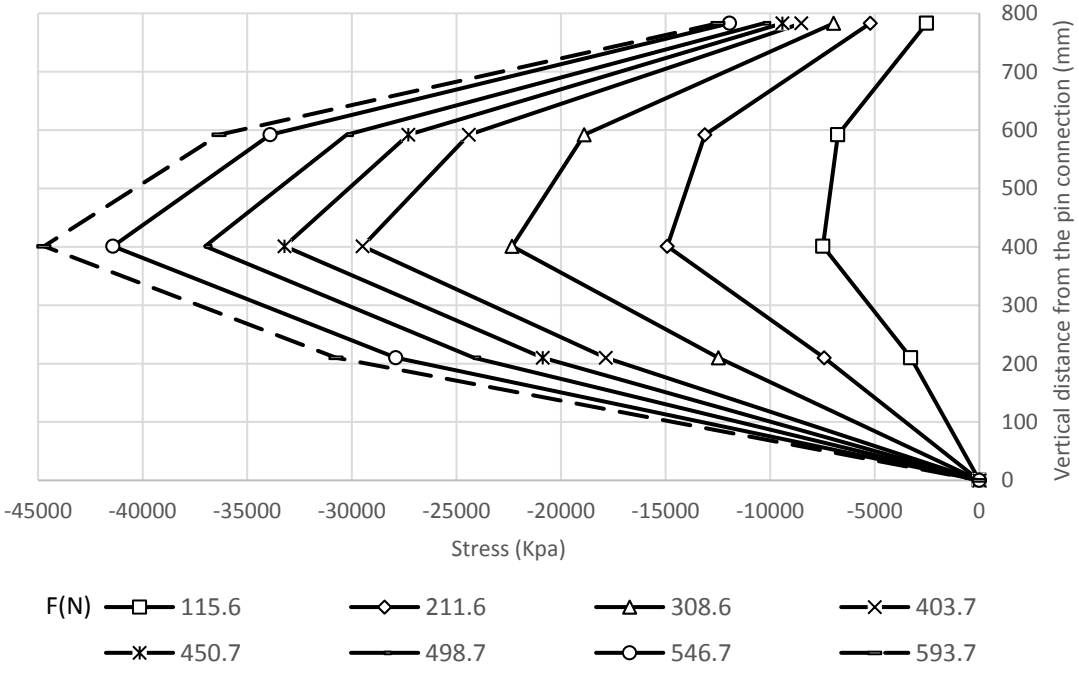

Figure A.107 Stresses along the compressive side of the pile in Test H2 L2 S1 C2 D2.

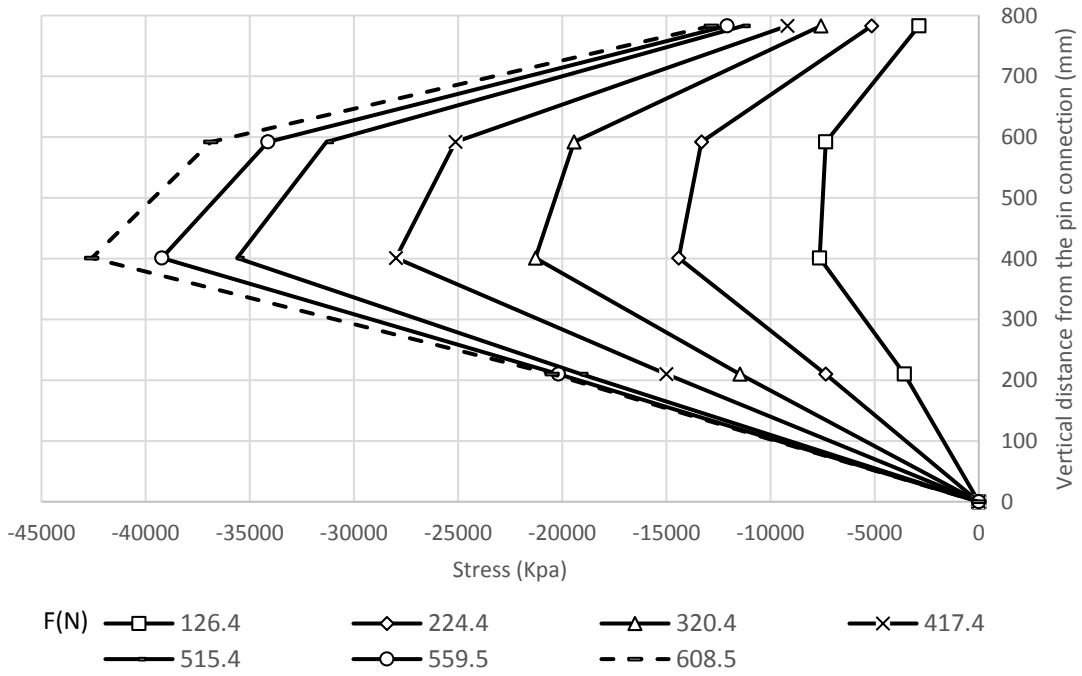

Figure A.108 Stresses along the compressive side of the pile in Test H2 L2 S1 C2 D3.

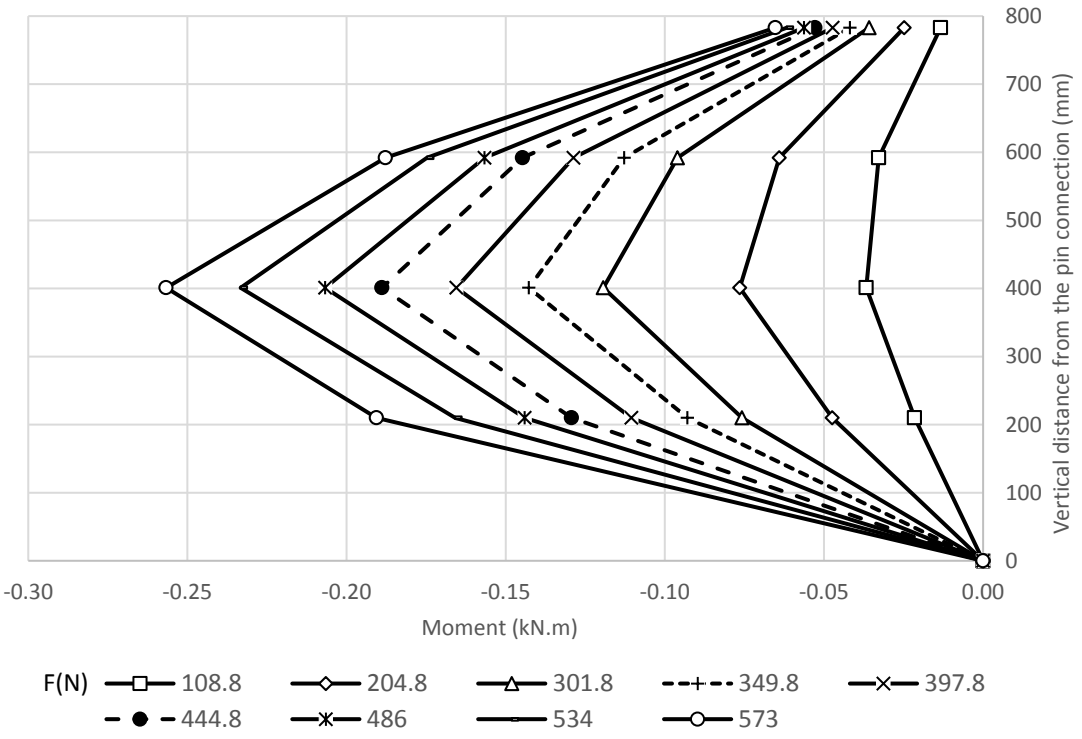

Figure A.109 Moments along the compressive side of the pile in Test H2 L2 S1 C2 D1.

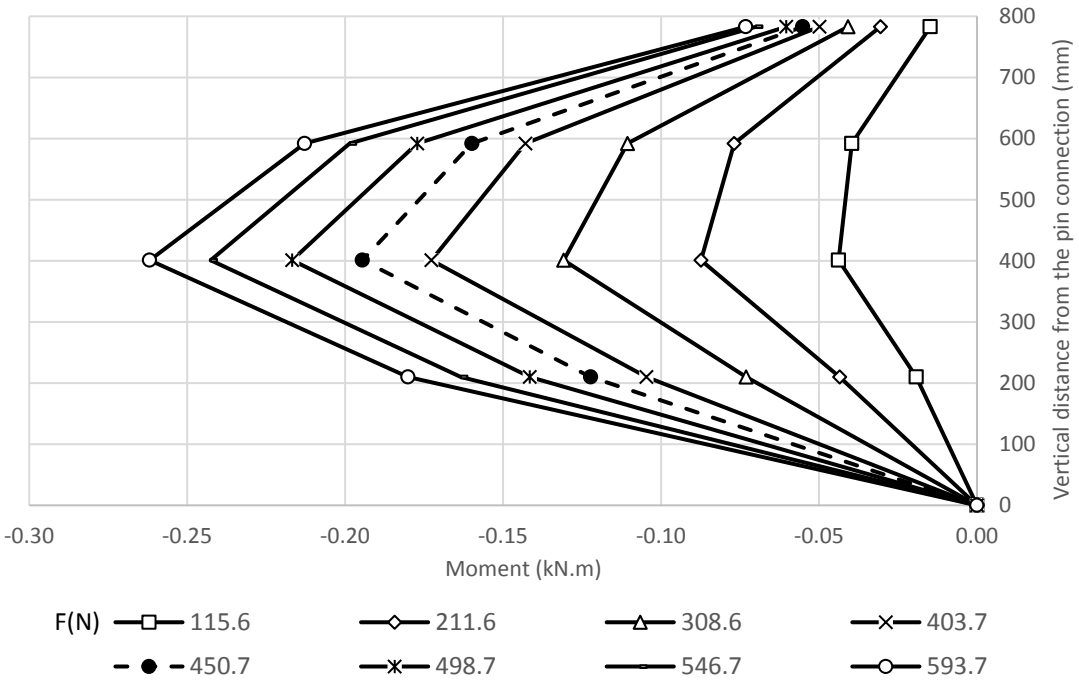

Figure A.110 Moments along the compressive side of the pile in Test H2 L2 S1 C2 D2.

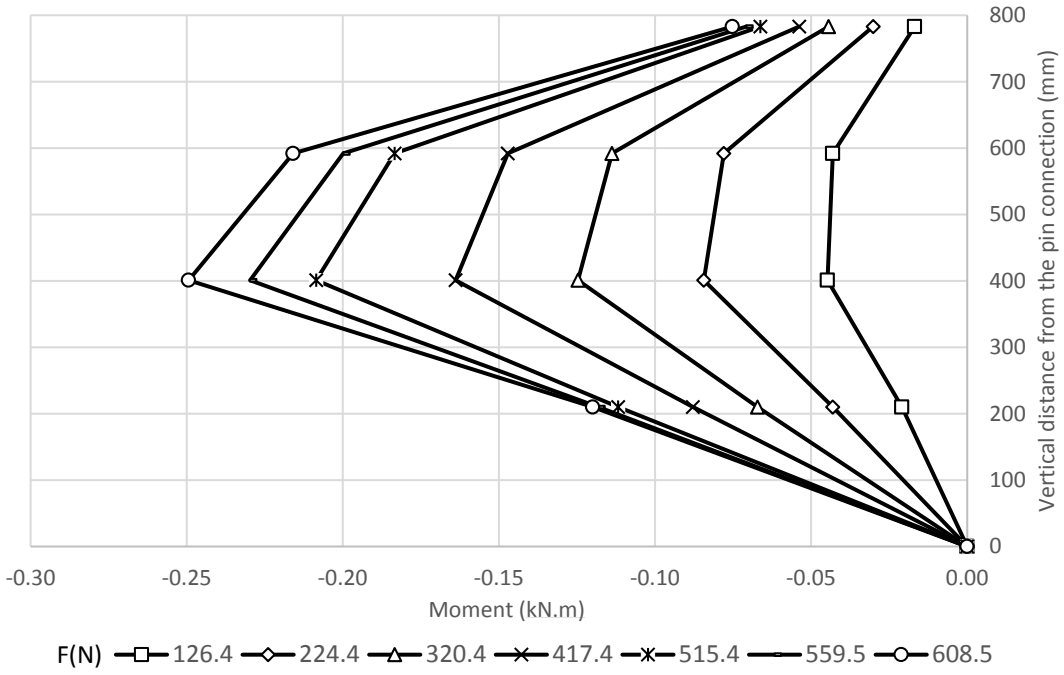

Figure A.111 Moment salong the compressive side of the pile in Test H2 L2 S1 C2 D3.

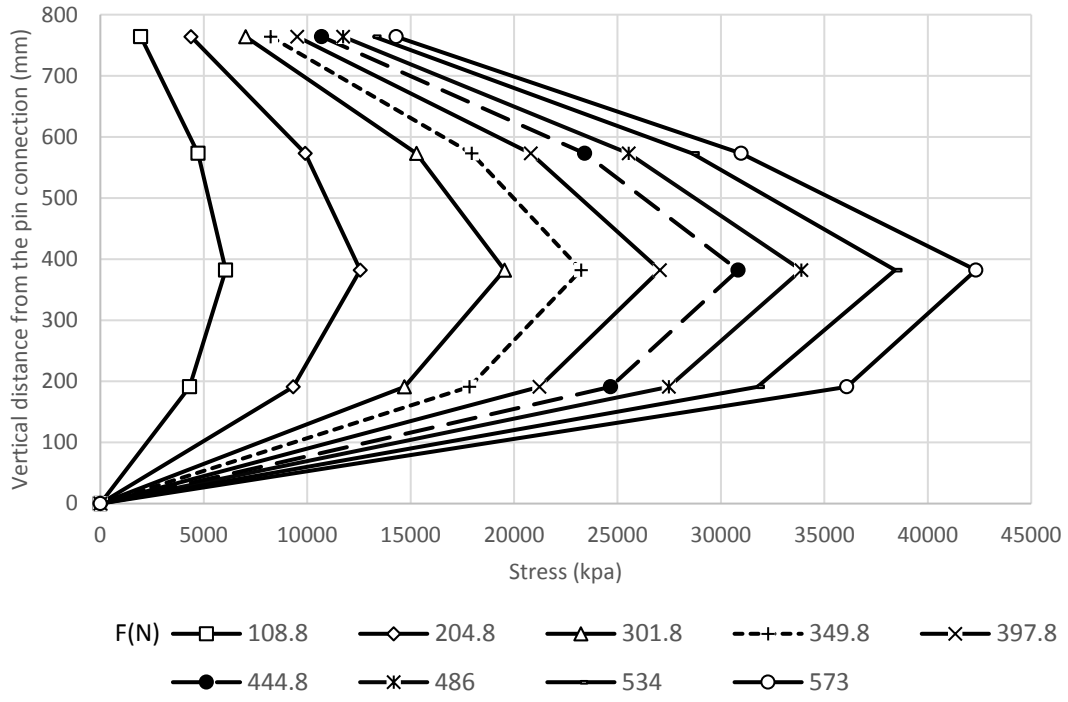

Figure A.112 Stresses along the compressive side of the pile in Test H2 L2 S1 C2 D1.

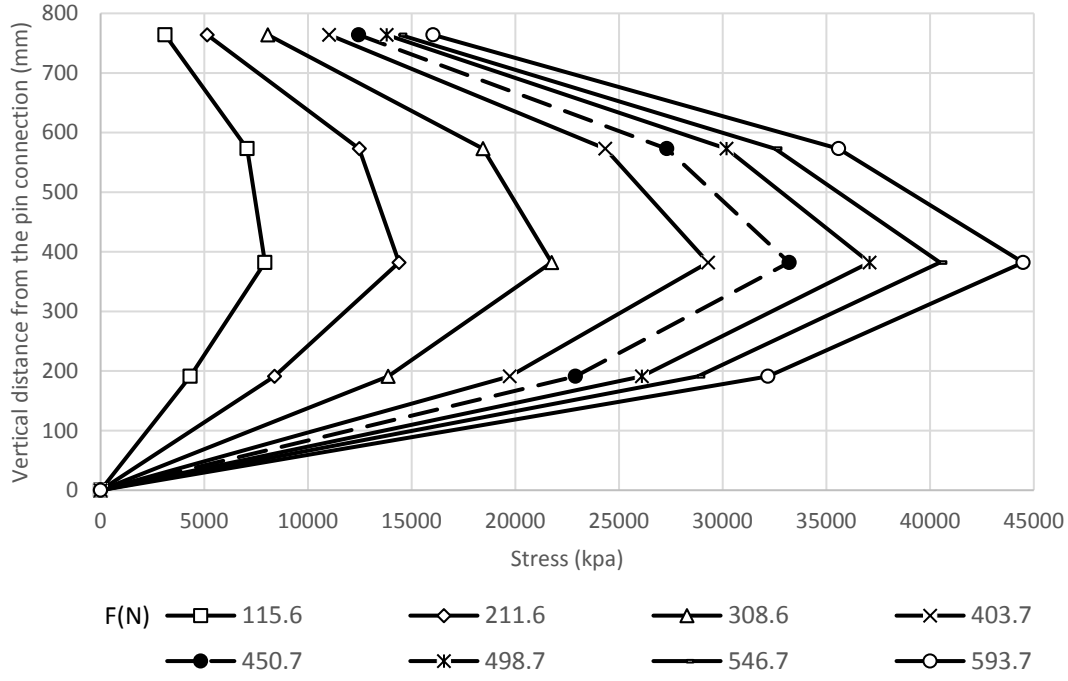

Figure A.113 Stresses along the compressive side of the pile in Test H2 L2 S1 C2 D2.

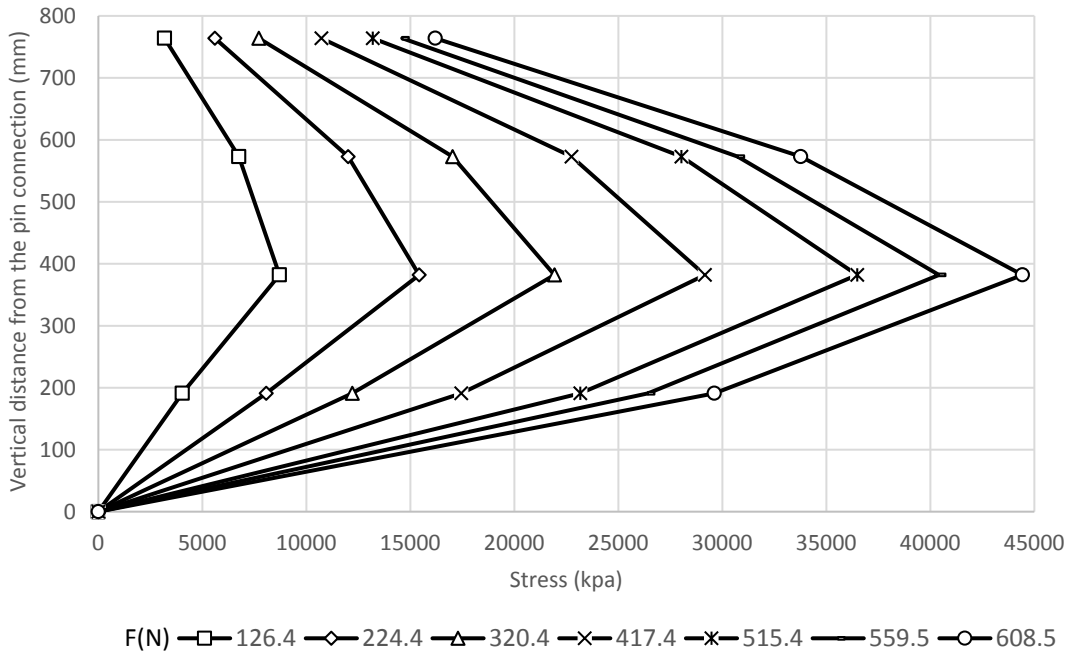

Figure A.114 Stresses along the compressive side of the pile in Test H2 L2 S1 C2 D3.

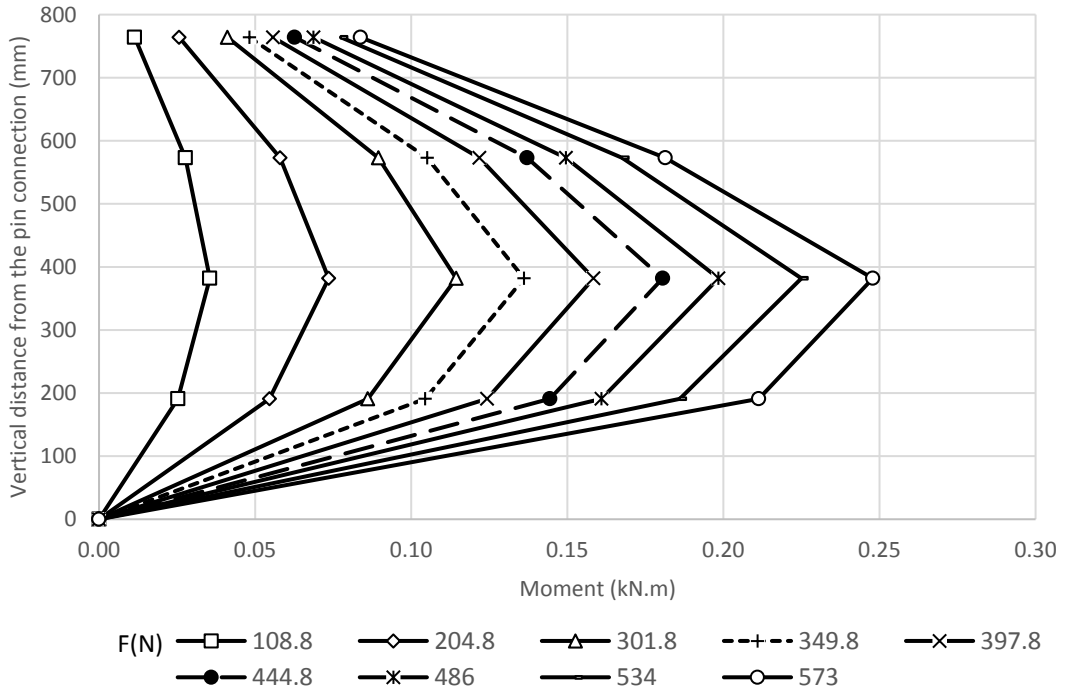

Figure 4.115 Moments along the tensile side of the pile in Test H2 L2 S1 C2 D1.

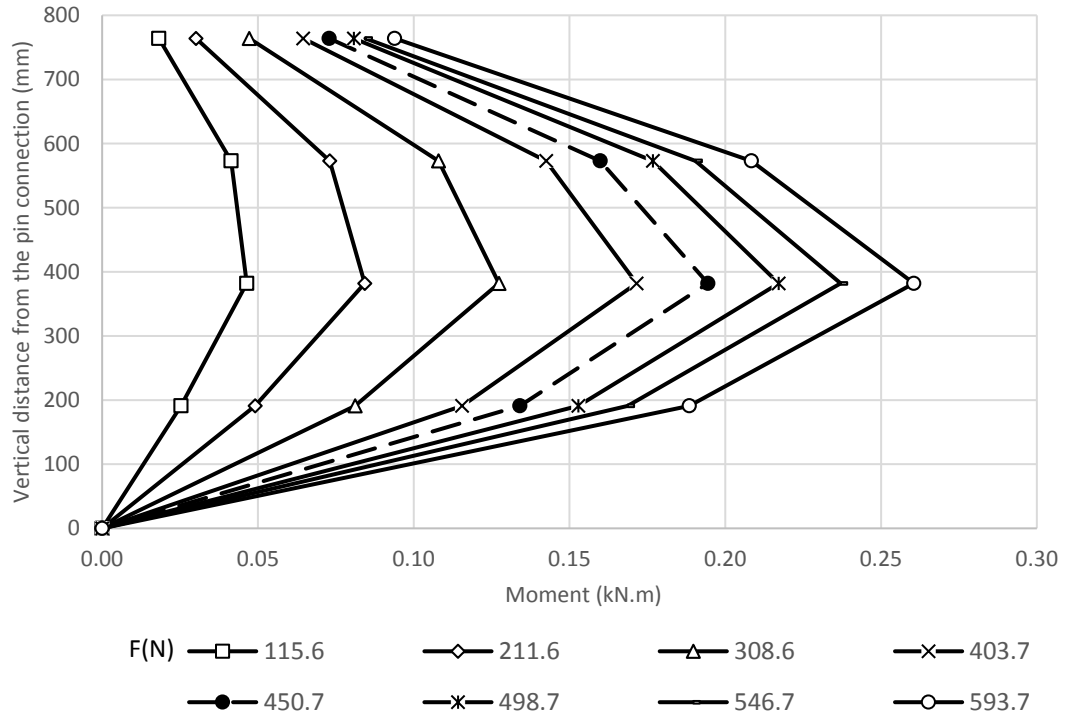

Figure 4.116 Moments along the tensile side of the pile in Test H2 L2 S1 C2 D2.

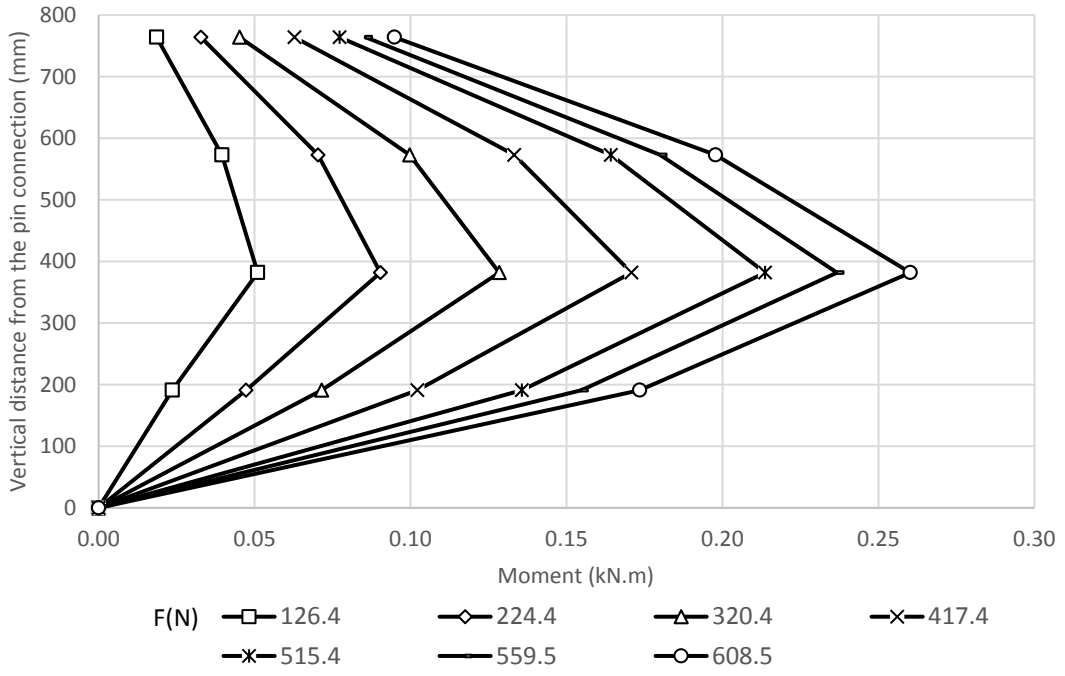

Figure 4.117 Moments along the tensile side of the pile in Test H2 L2 S1 C2 D3.

Strain in the geogrid layers:

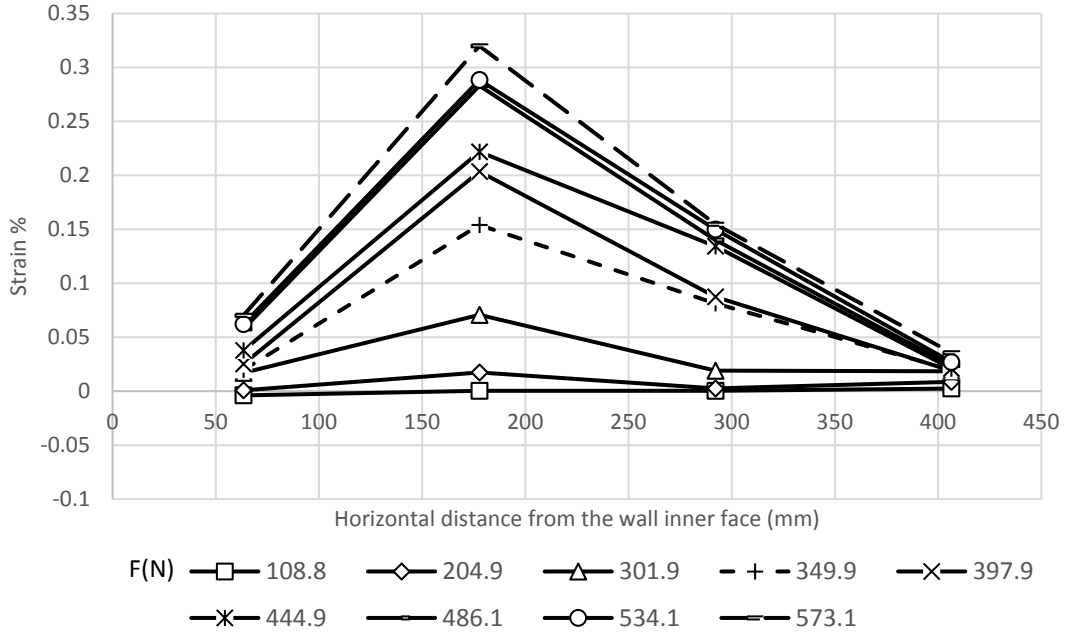

Figure A.118 Strains in the geogrid layer at 450 mm from the wall base (Test H2 L2 S1 C2 D1).

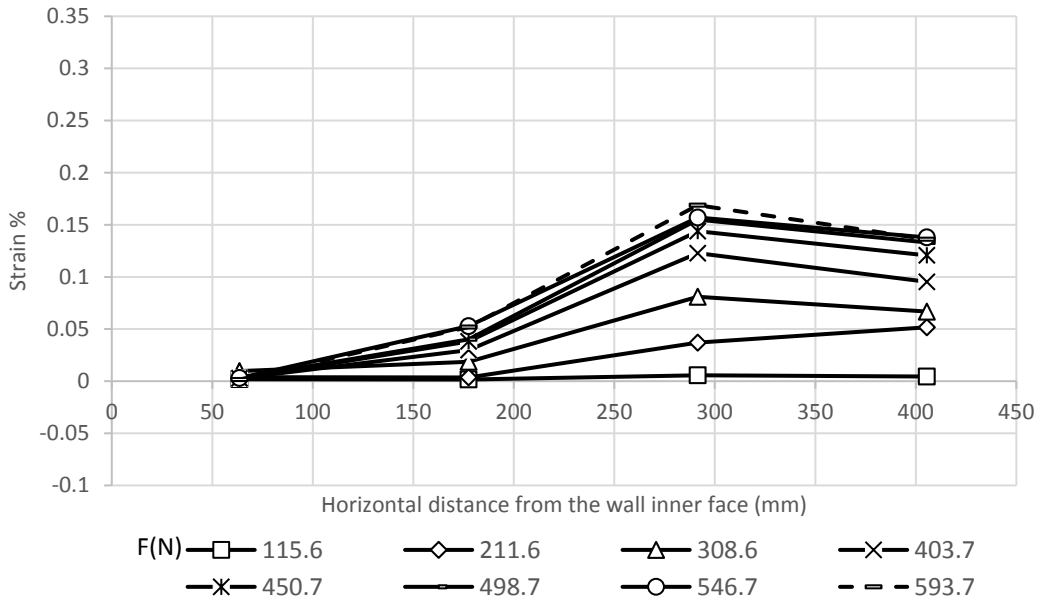

Figure A.119 Strains in the geogrid layer at 450 mm from the wall base (Test H2 L2 S1 C2 D2).

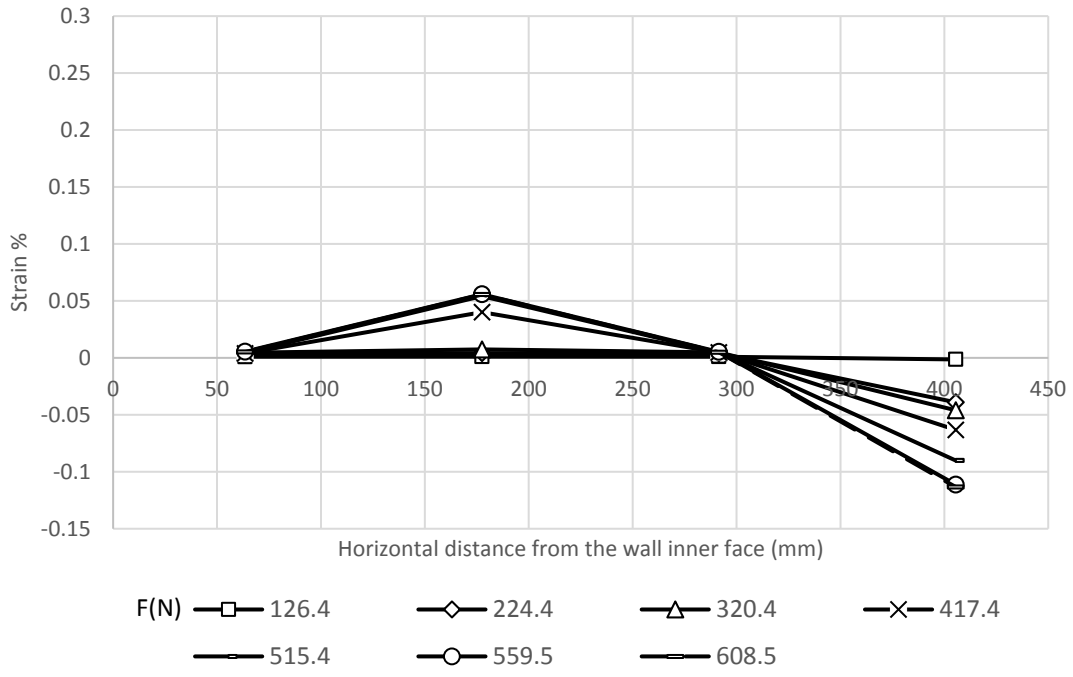

Figure A.120 Strains in the geogrid layer at 450 mm from the wall base (Test H2 L2 S1 C2 D3).

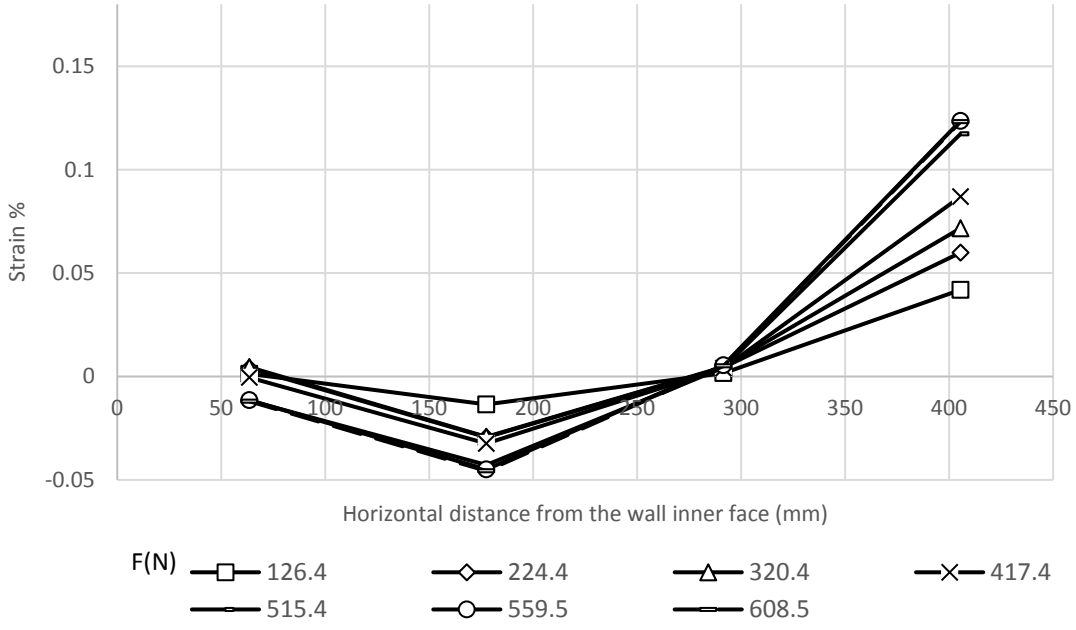

Figure A.121 Strains in the geogrid layer at 270 mm from the wall base (Test H2 L2 S1 C2 D1).

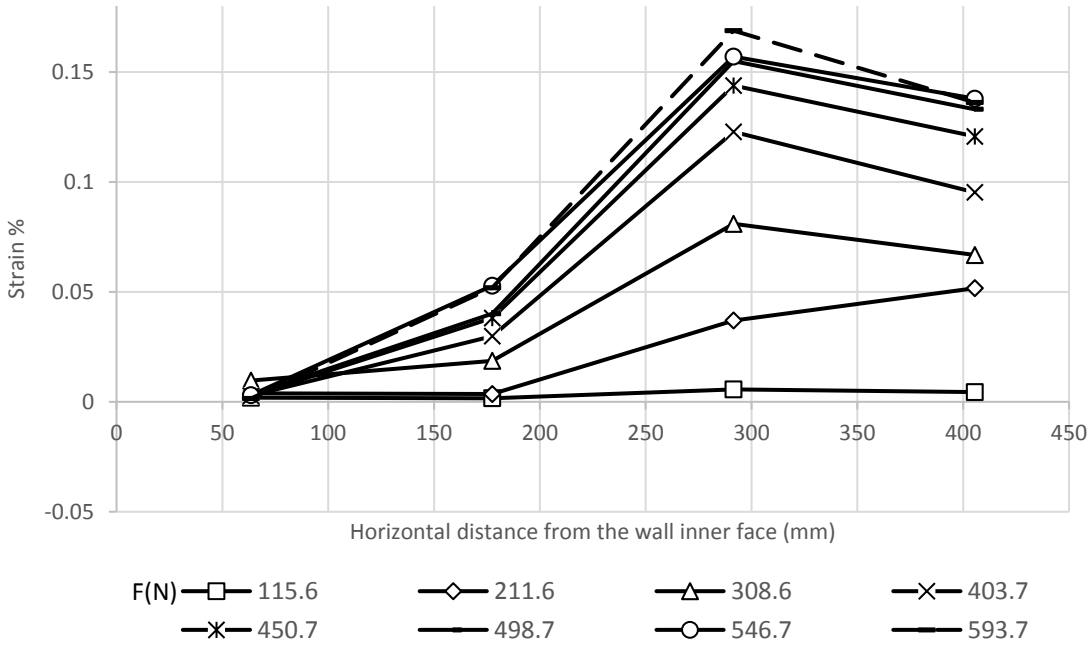

Figure A.122 Strains in the geogrid layer at 270 mm from the wall base (Test H2 L2 S1 C2 D2).

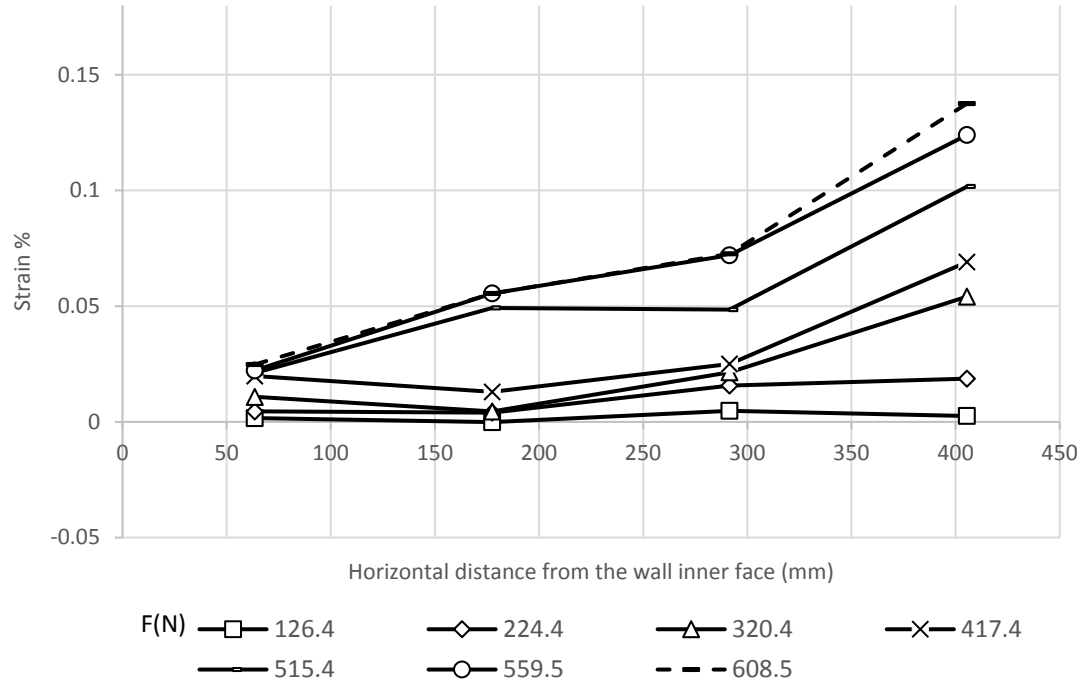

Figure A.123 Strains in the geogrid layer at 270 mm from the wall base (Test H2 L2 S1 C2 D3).

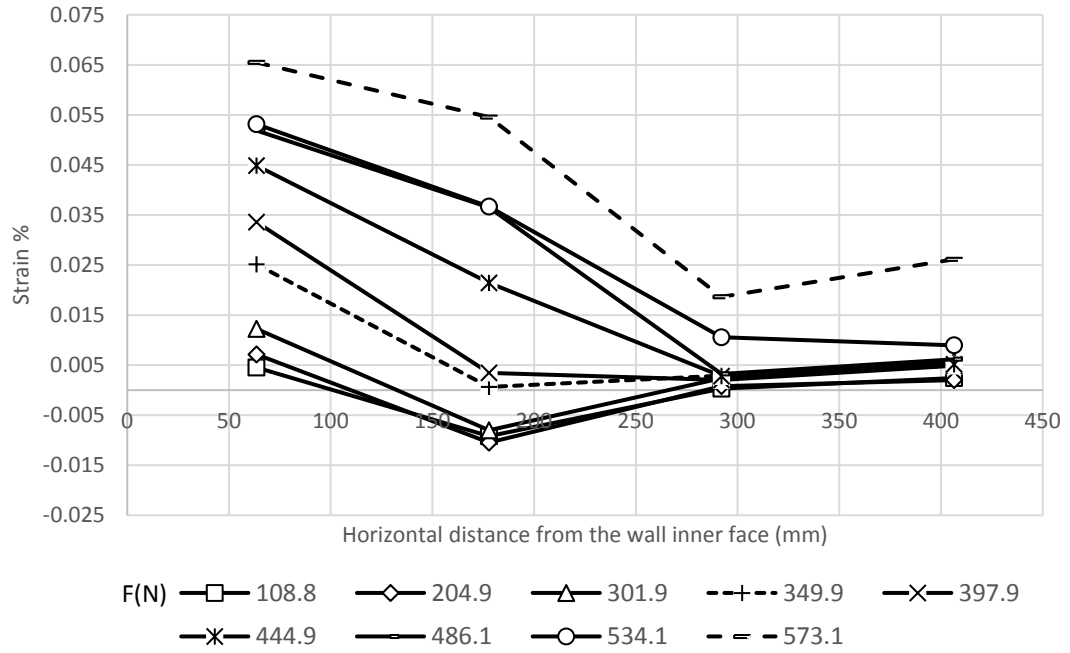

Figure A.124 Strains in the geogrid layer at 90 mm from the wall base (Test H2 L2 S1 C2 D1).

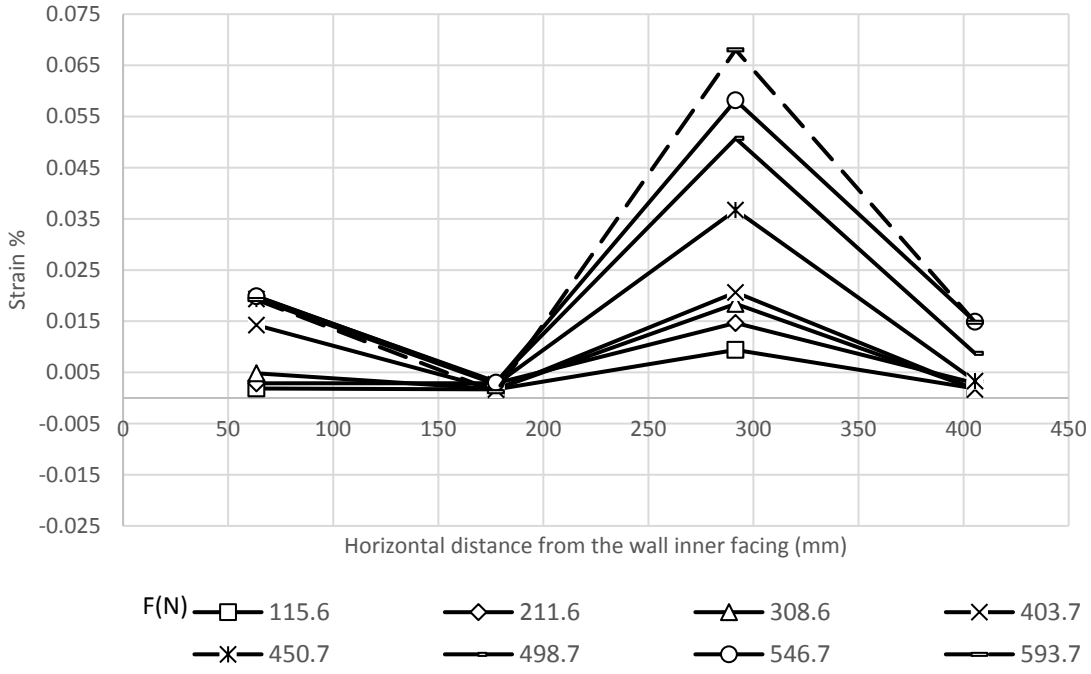

Figure A.125 Strains in the geogrid layer at 90 mm from the wall base (Test H2 L2 S1 C2 D2).

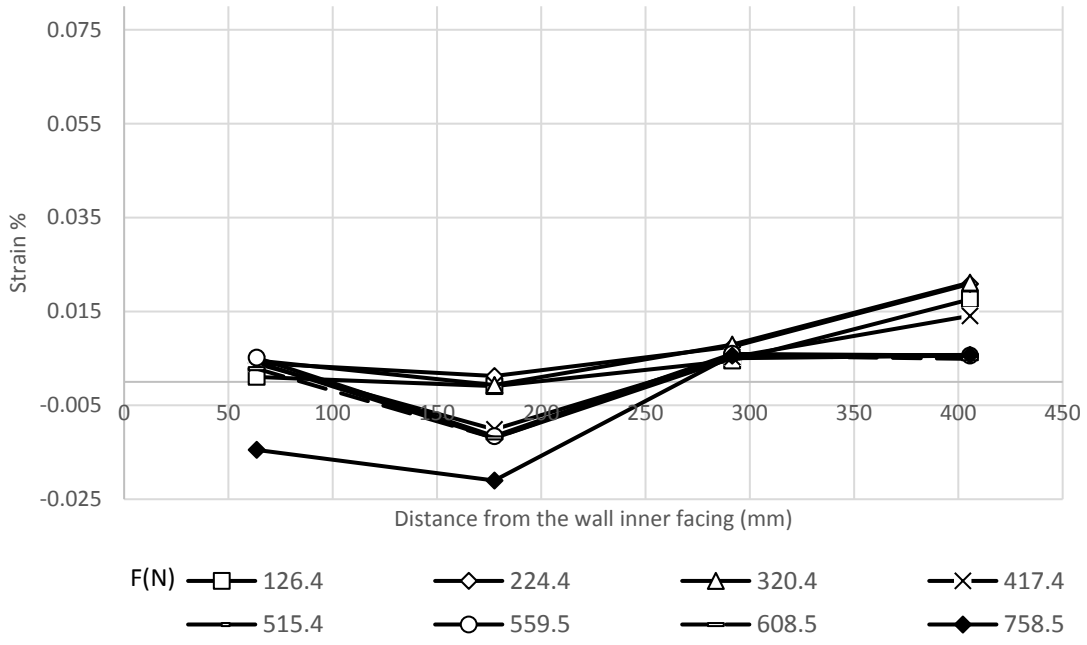

Figure A.126 Strains in the geogrid layer at 90 mm from the wall base (Test H2 L2 S1 C2 D3).

Pressure behind the wall facing:

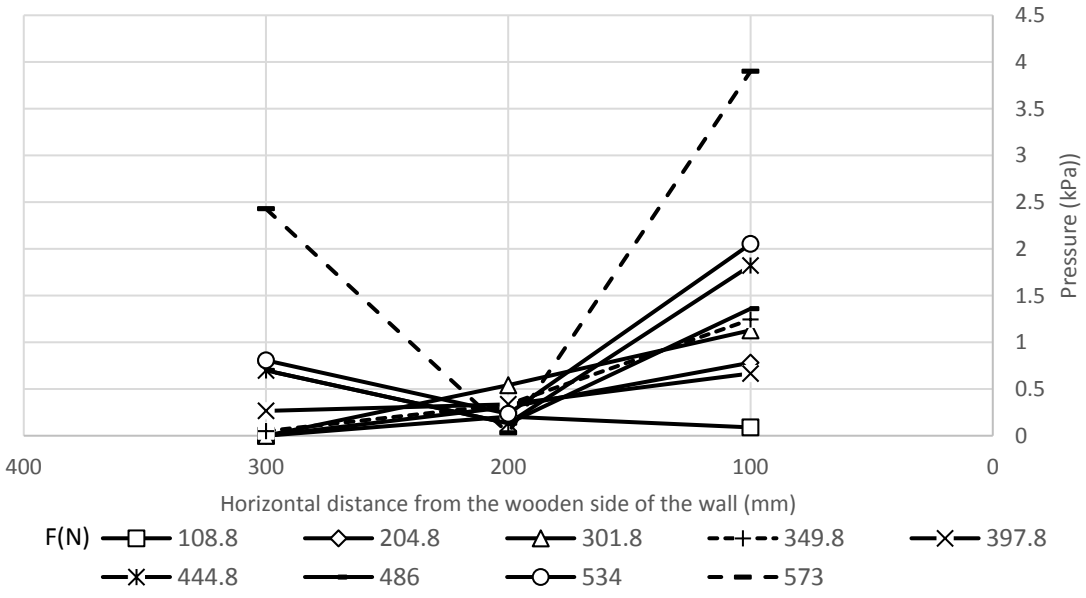

Figure A.127 Transverse pressure distributions at 607.5 mm from the wall base for Test H2 L2 S1 C2 D1.

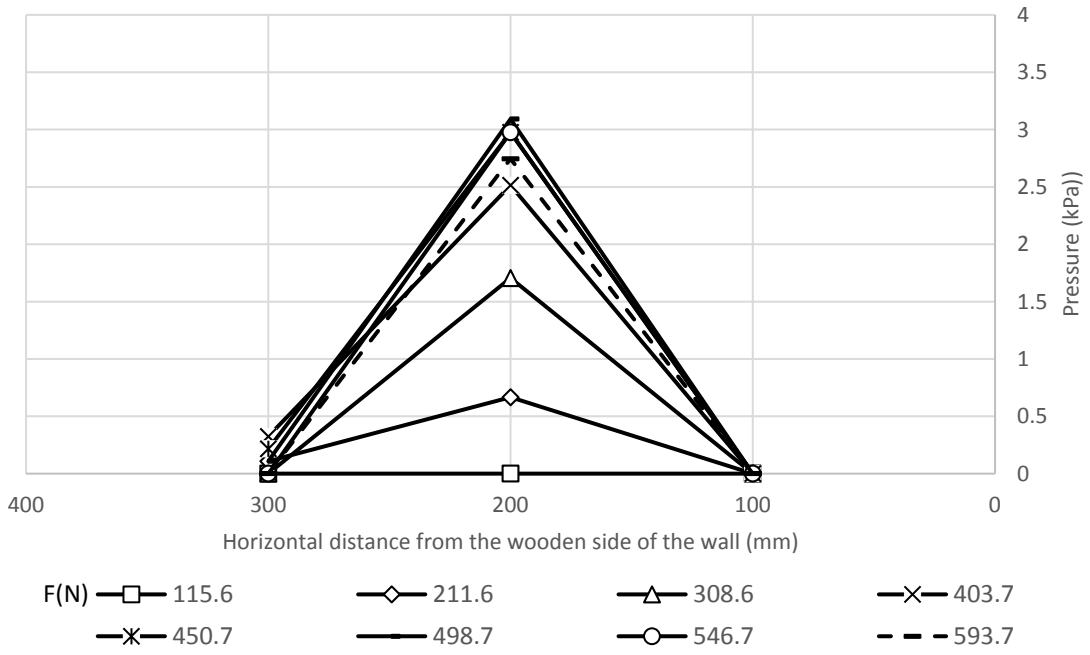

Figure A.128 Transverse pressure distributions at 607.5 mm from the wall base for Test H2 L2 S1 C2 D2.

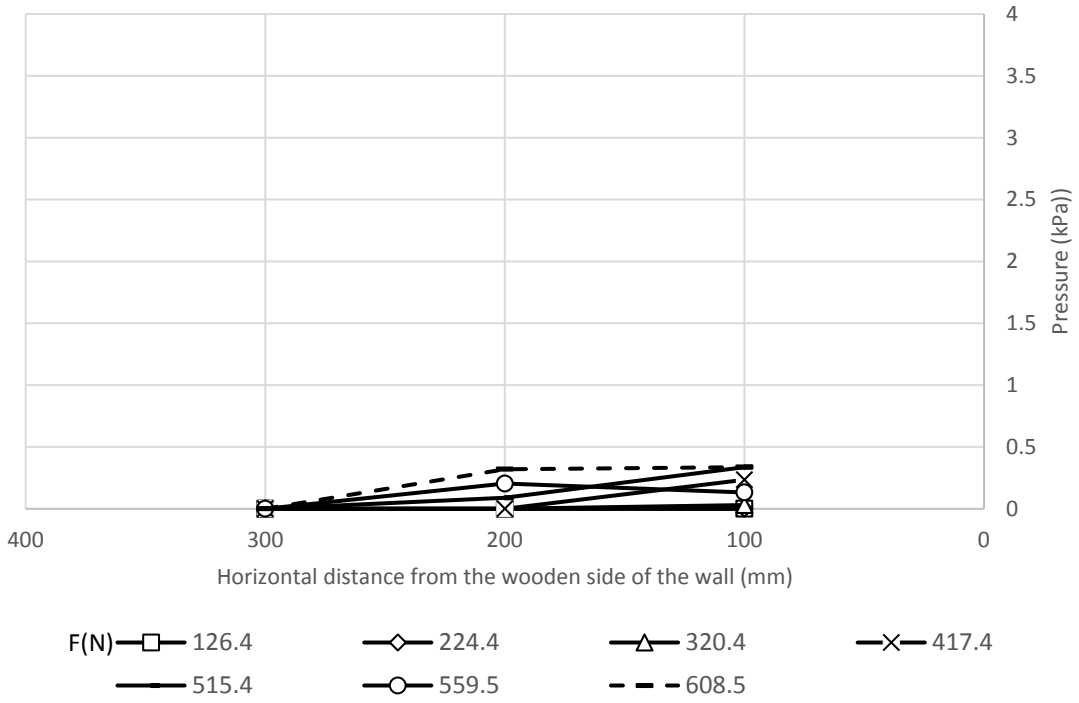

Figure A.129 Transverse pressure distributions at 607.5 mm from the wall base for Test H2 L2 S1 C2 D3.

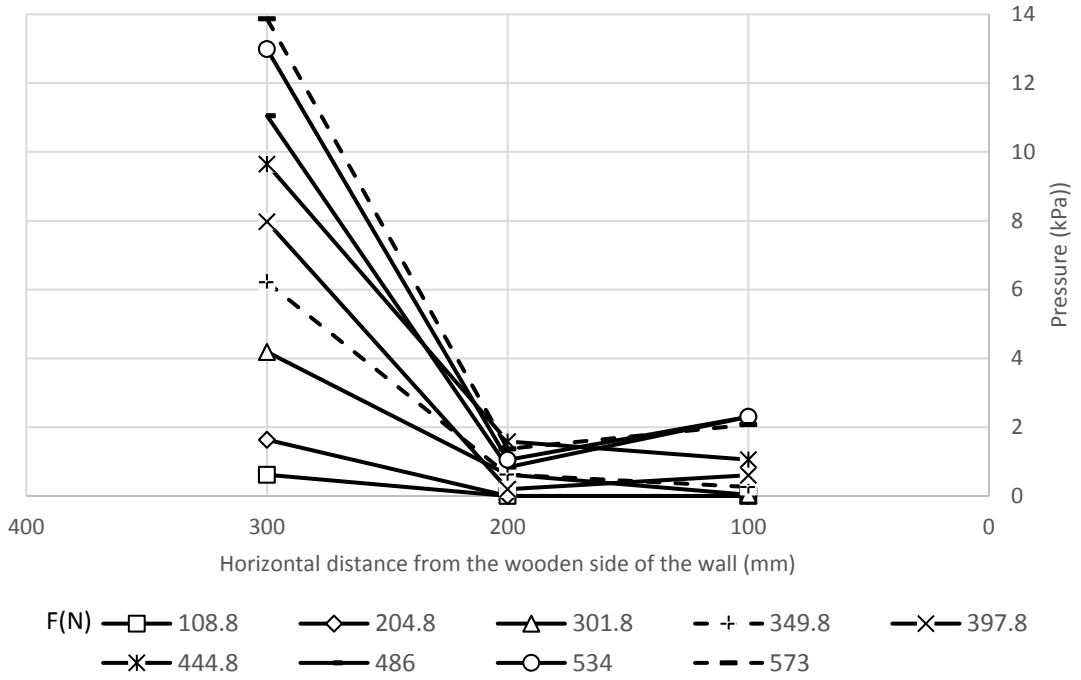

Figure A.130 Transverse pressure distributions at 337.5 mm from the wall base for Test H2 L2 S1 C2 D1.

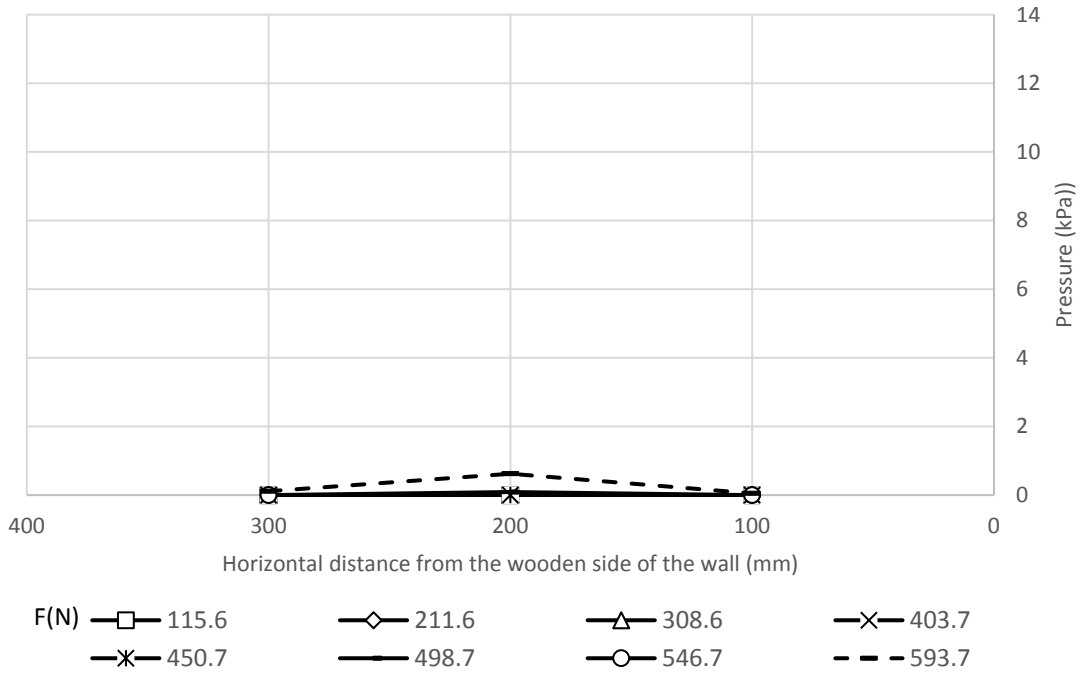

Figure A.131 Transverse pressure distributions at 337.5 mm from the wall base for Test H2 L2 S1 C2 D2.

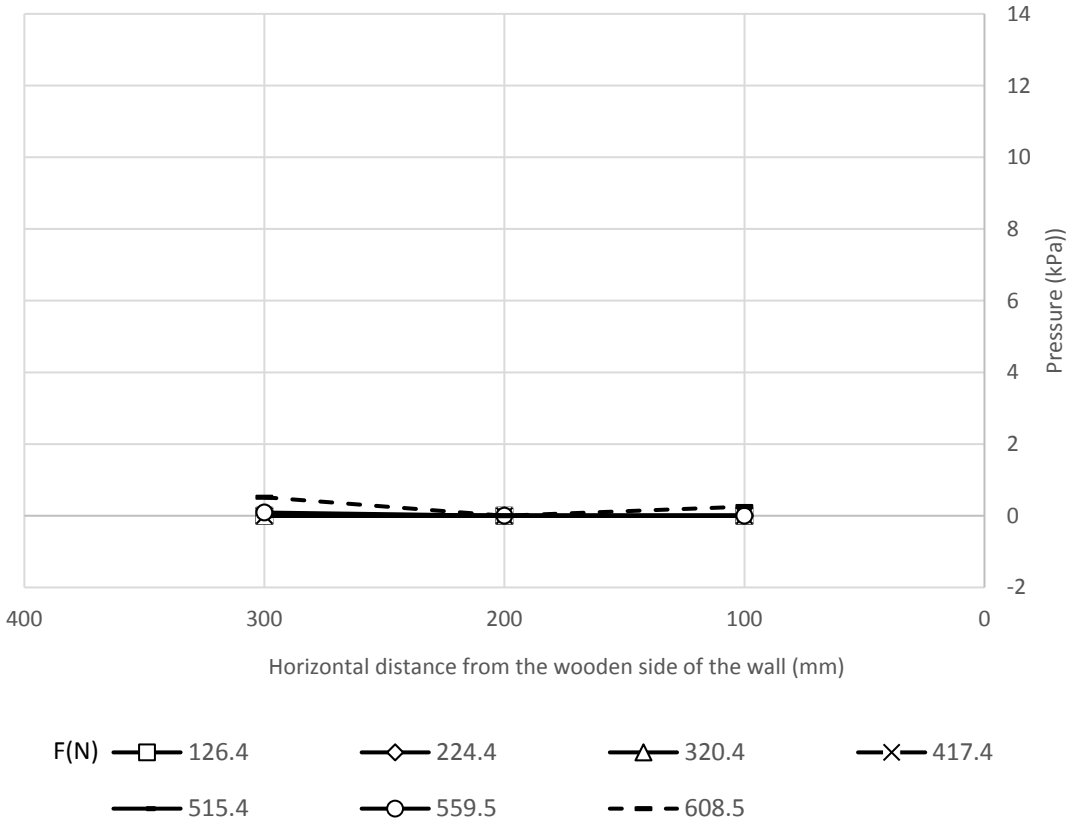

Figure A.132 Transverse pressure distributions at 337.5 mm from the wall base for Test H2 L2 S1 C2 D3.

A.4. Group 3

A.4.1. Category 1

Deflection of the wall facing:

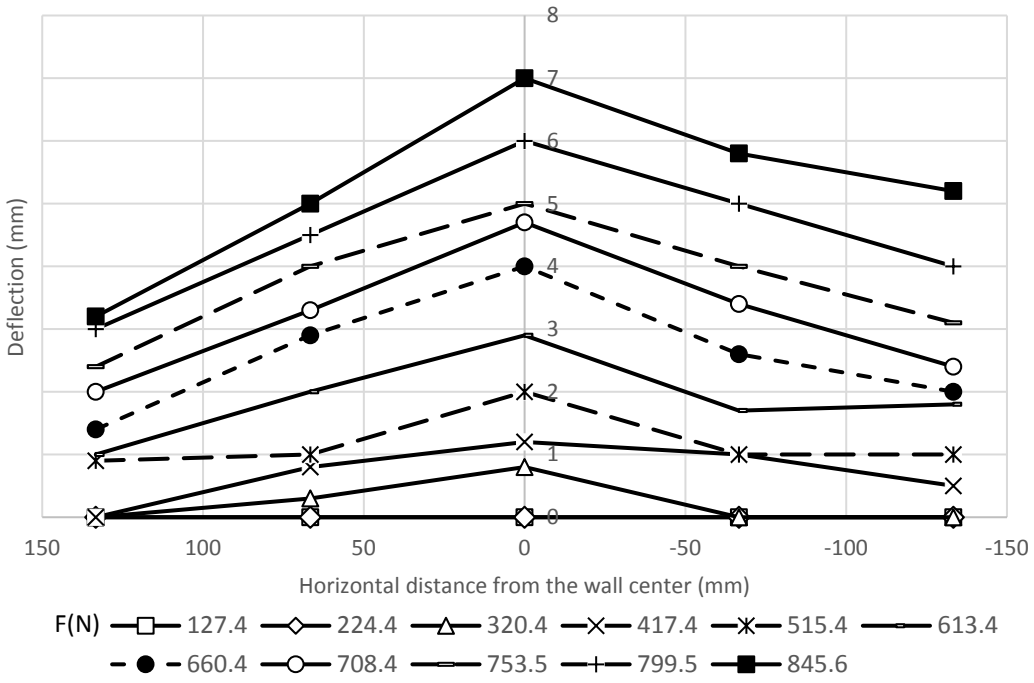

Figure A.133 Transverse deflection profiles at 472.5 mm from the wall base for Test H2 L3 S2 C1 D2.

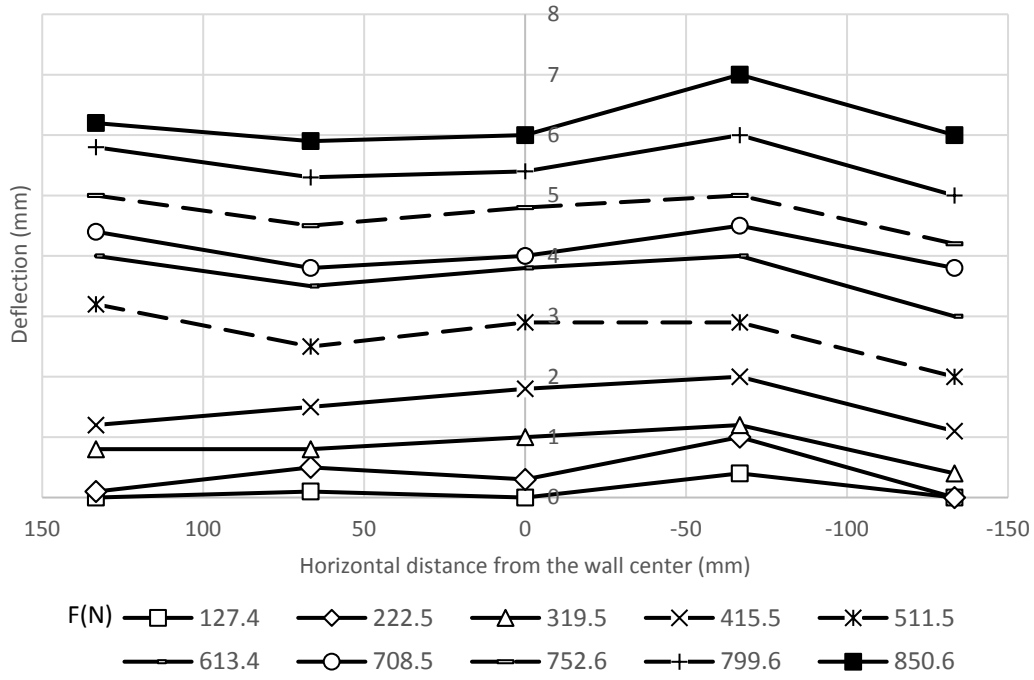

Figure A.134 Transverse deflection profiles at 472.5 mm from the wall base for Test H2 L3 S2 C1 D3.

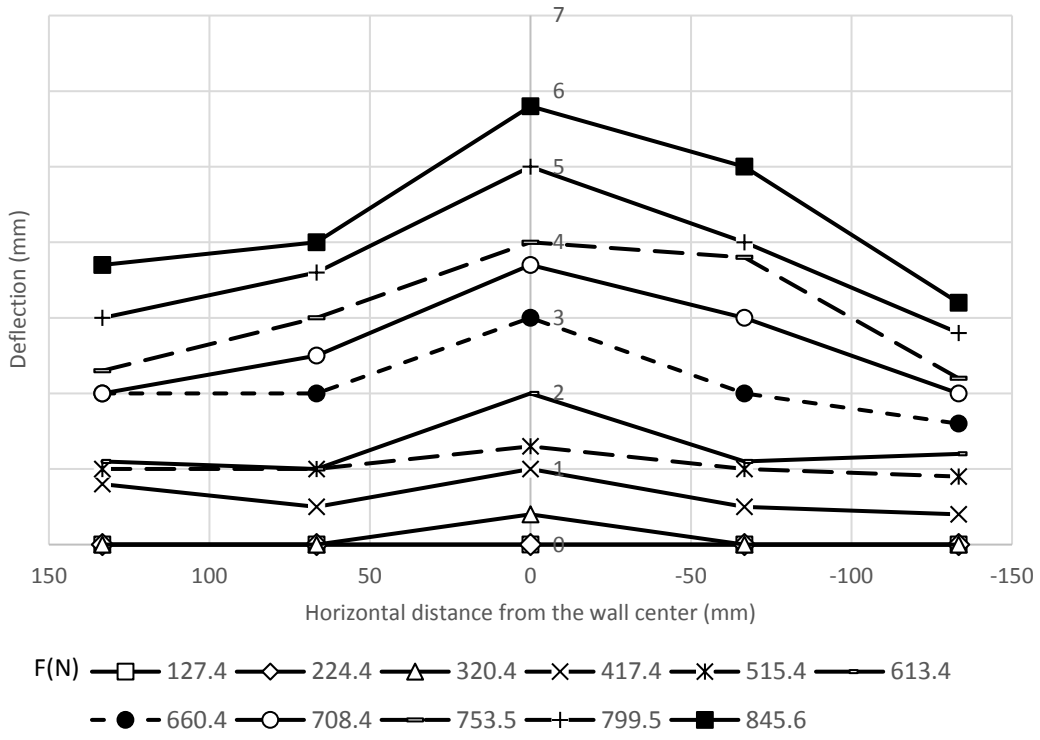

Figure A.135 Transverse deflection profiles at 337.5 mm from the wall base for Test H2 L3 S2 C1 D2.

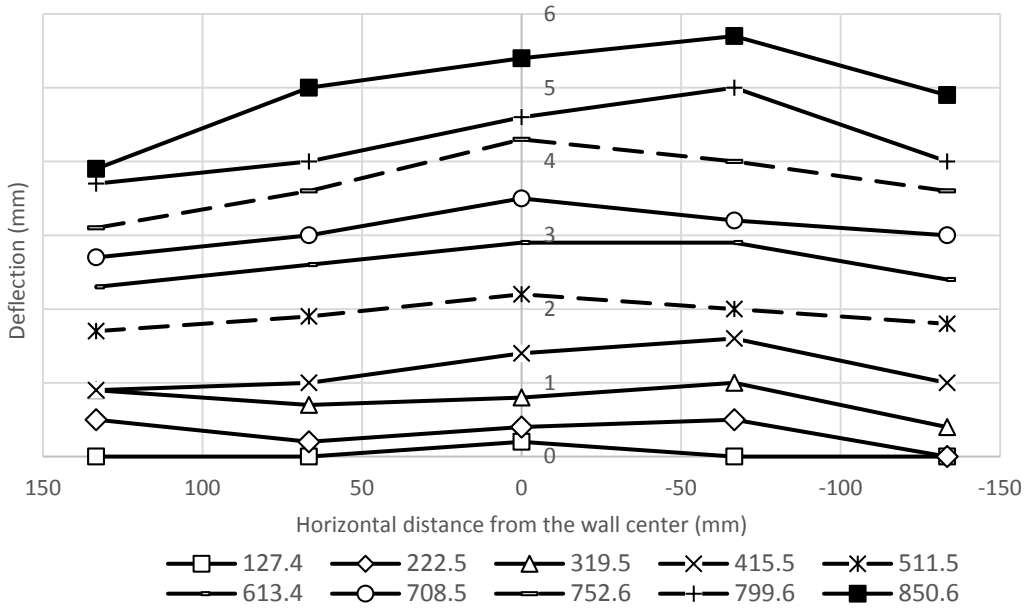

Figure A.136 Transverse deflection profiles at 337.5 mm from the wall base for Test H2 L3 S2 C1 D3.

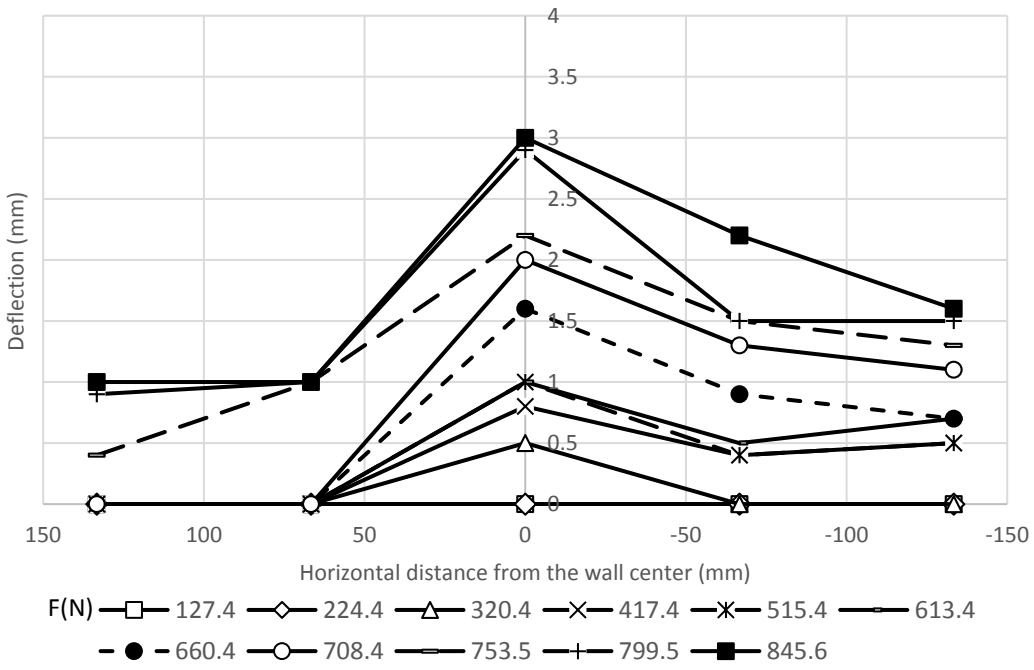

Figure A.137 Transverse deflection profiles at 202.5 mm from the wall base for Test H2 L3 S2 C1 D2.

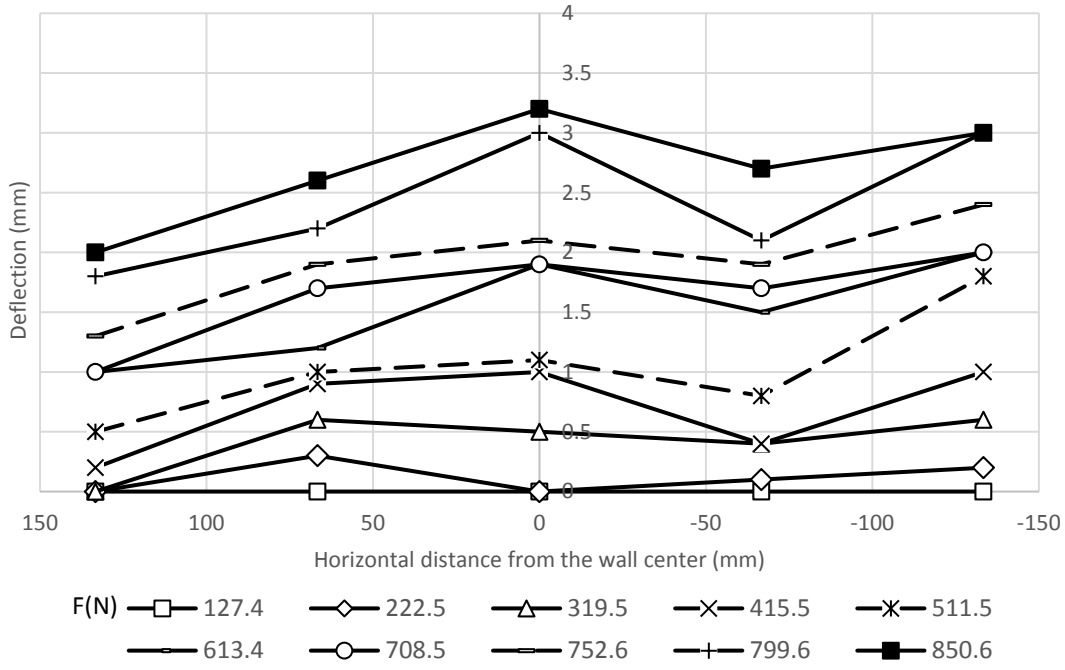

Figure A.138 Transverse deflection profiles at 202.5 mm the wall base for Test H2 L3 S2 C1 D3.

Stress and moment of the pile:

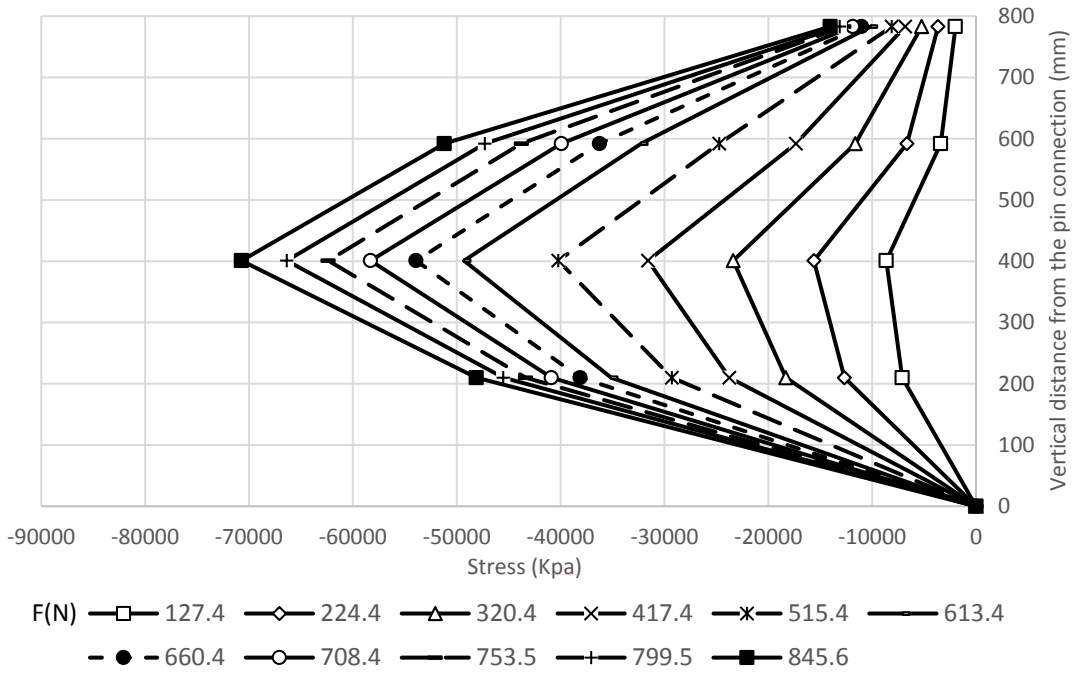

Figure A.139 Stresses along the compressive side of the pile in Test H2 L3 S2 C1 D2.

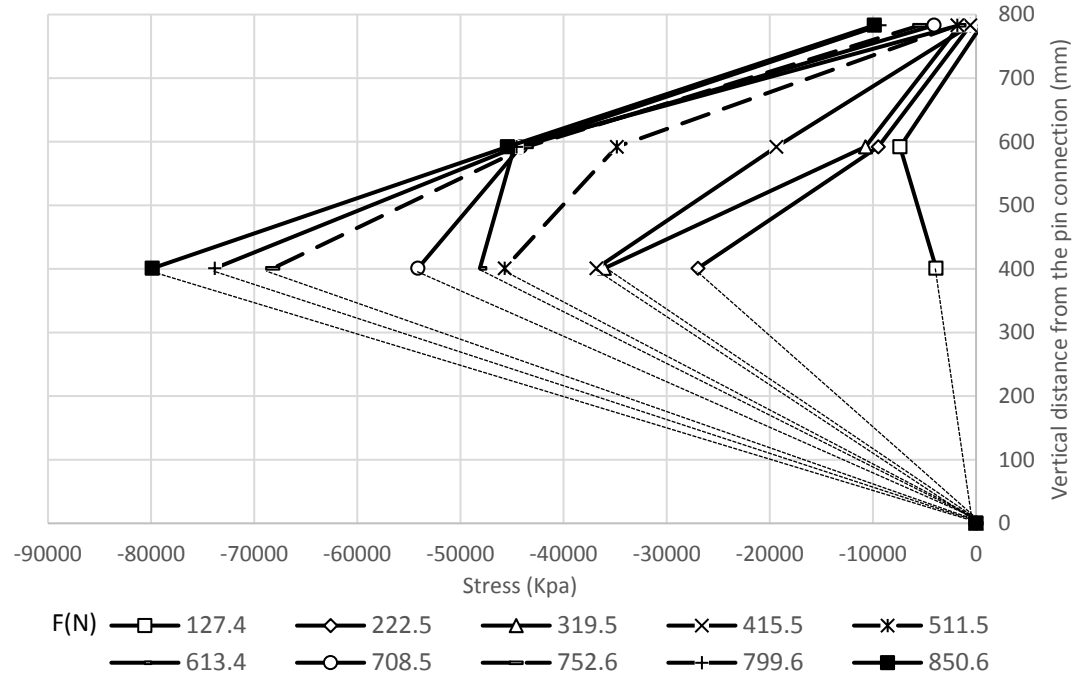

Figure A.140 Stresses along the compressive side of the pile in Test H2 L3 S2 C1 D3.

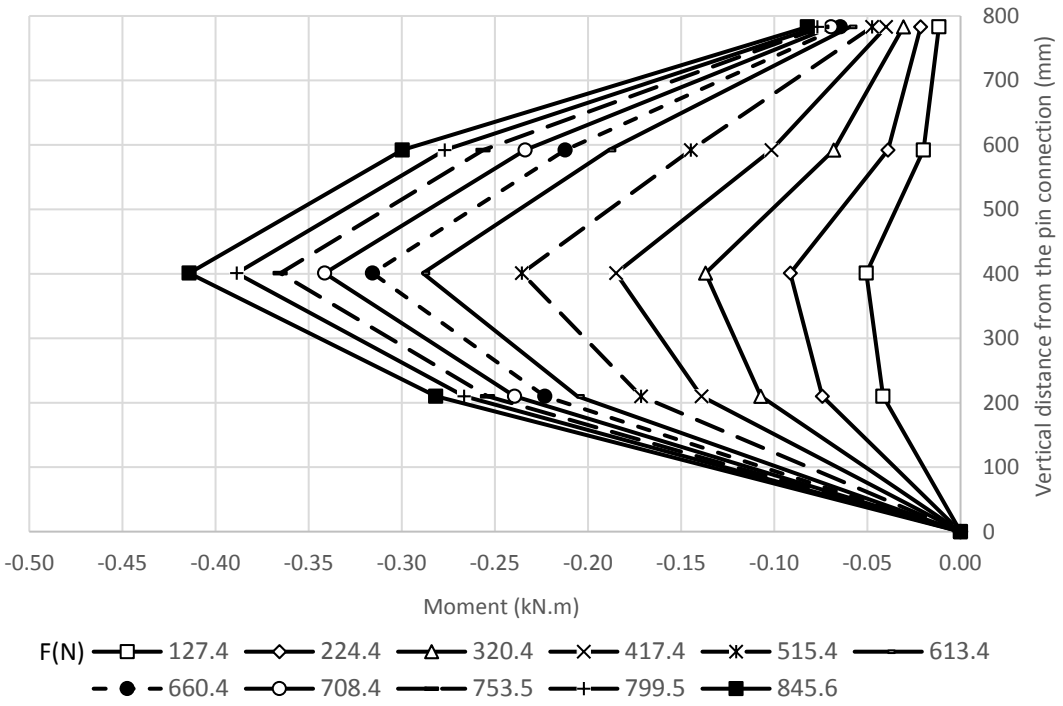

Figure A.141 Moments along the compressive side of the pile in Test H2 L3 S2 C1 D2.

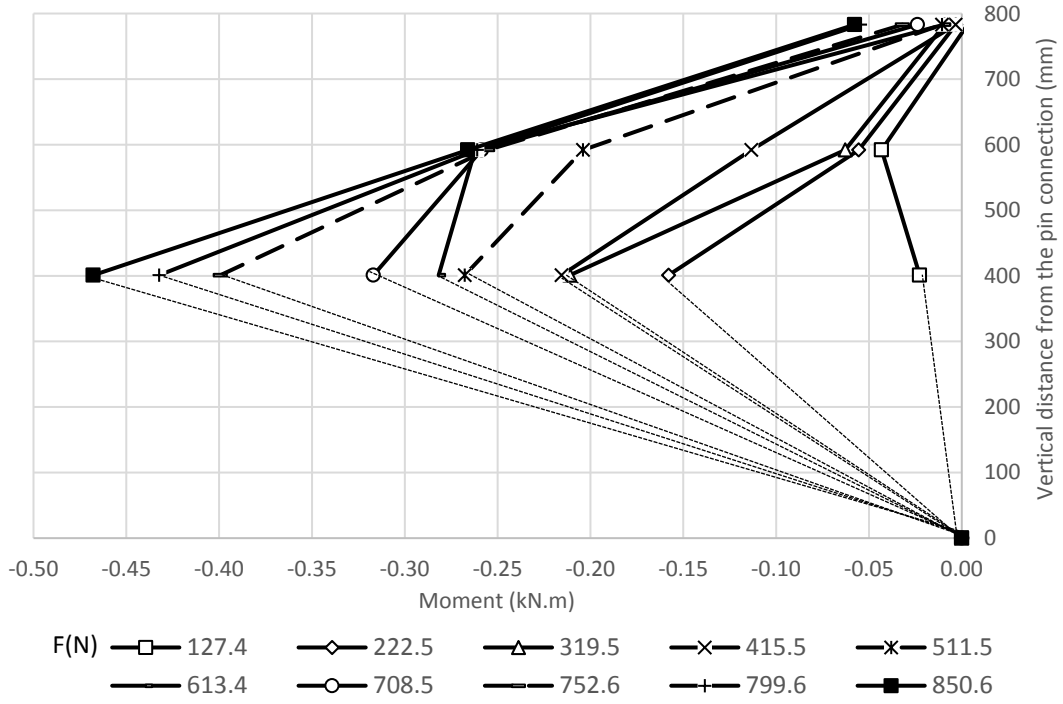

Figure A.142 Moments along the compressive side of the pile in Test H2 L3 S2 C1 D3.

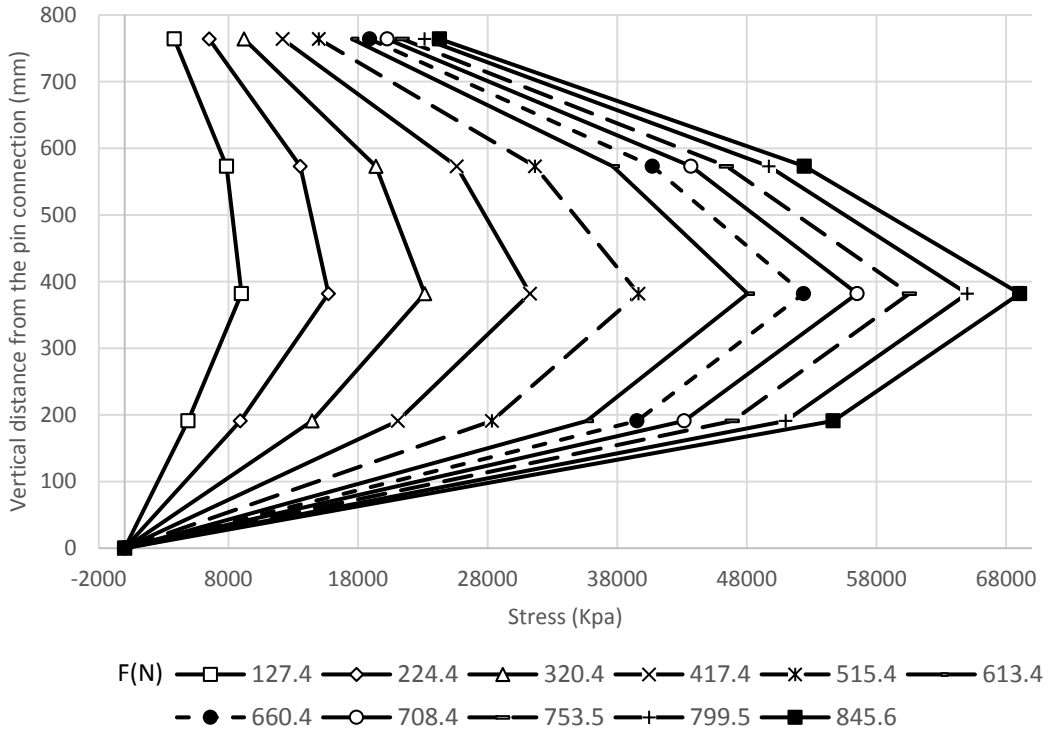

Figure A.143 Stresses along the compressive side of the pile in Test H2 L3 S2 C1 D2.

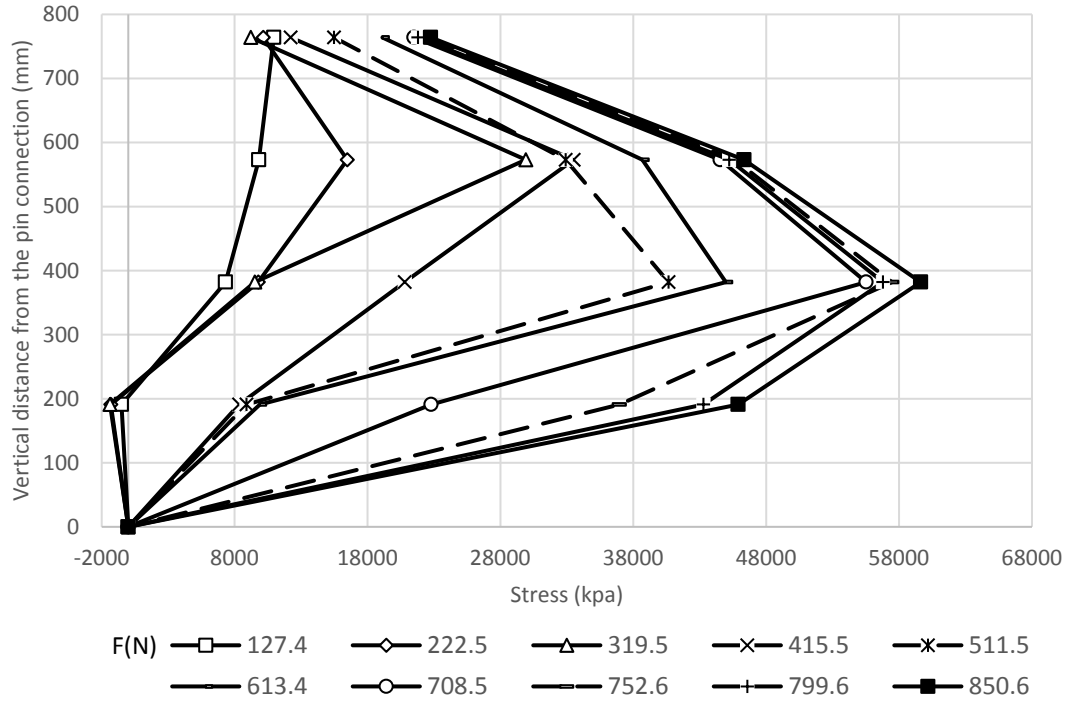

Figure A.144 Stresses along the compressive side of the pile in Test H2 L3 S2 C1 D3.

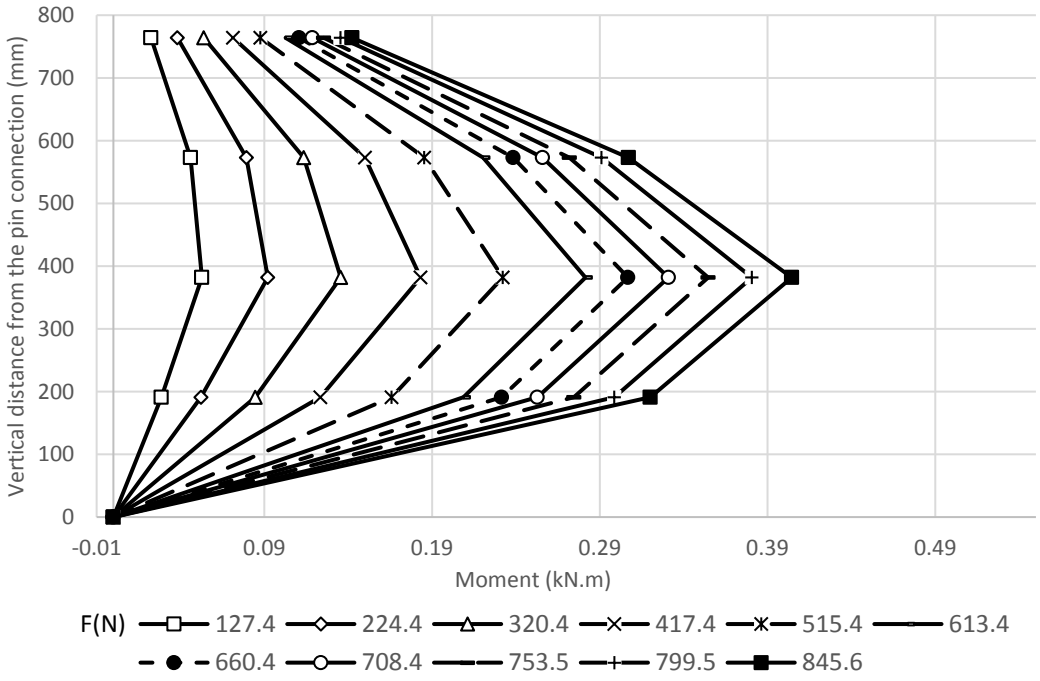

Figure A.145 Stresses along the compressive side of the pile in Test H2 L3 S2 C1 D2.

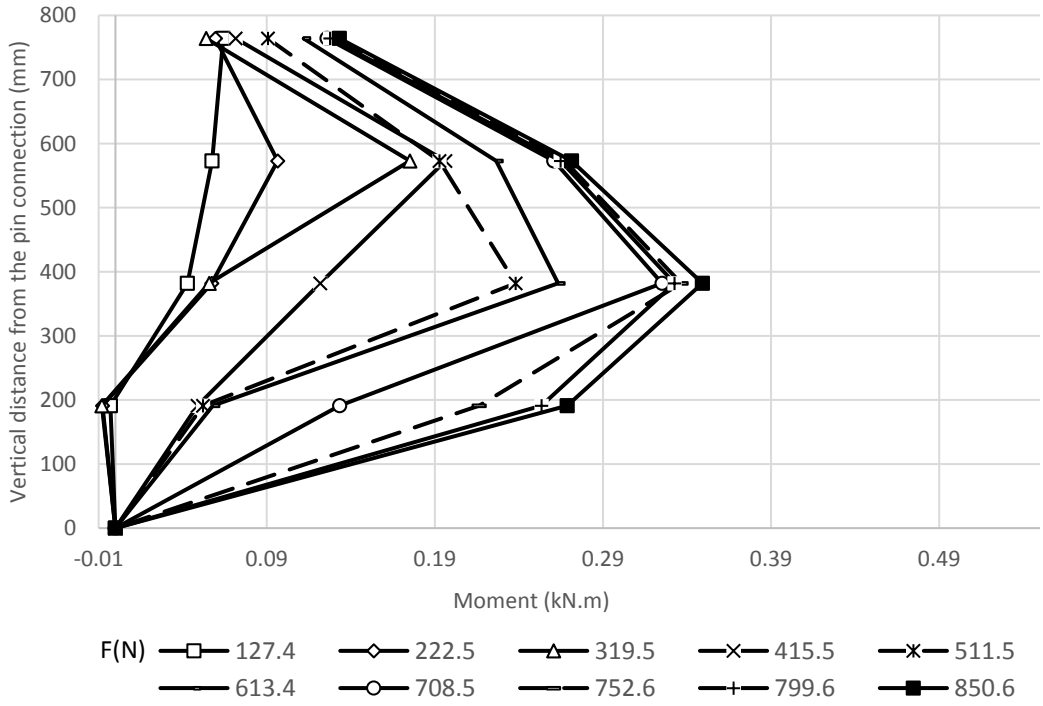

Figure 4.146 Moments along the tensile side of the pile in Test H2 L3 S2 C1 D3.

Strain in the geogrid layers:

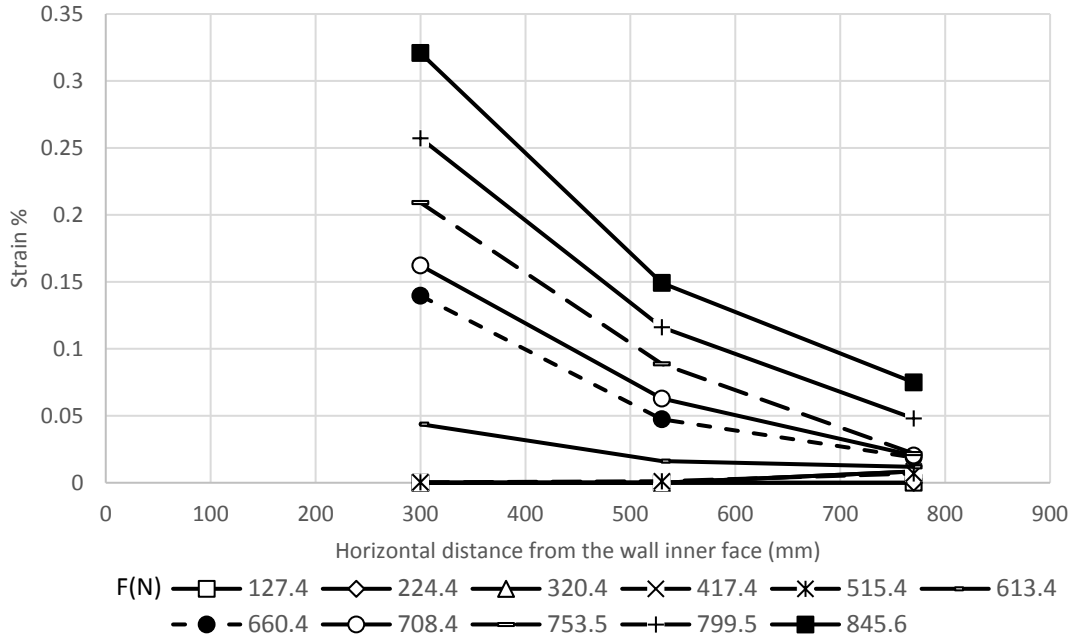

Figure A.147 Strains in the geogrid layer at 405 mm from the wall base (Test H2 L3 S2 C1 D2).

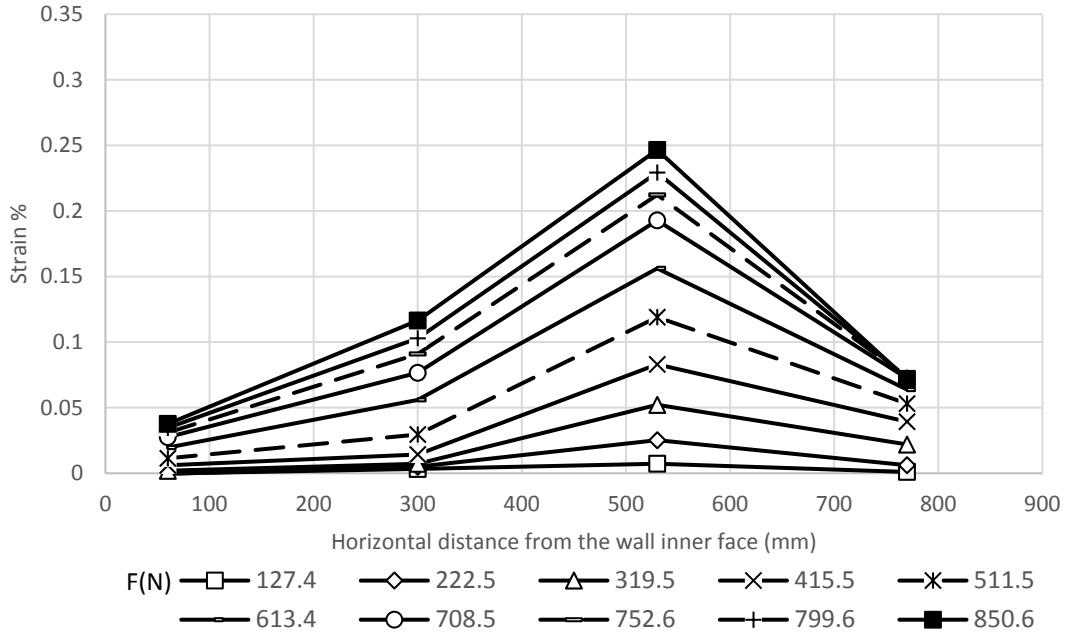

Figure A.148 Strains in the geogrid layer at 405 mm from the wall base (Test H2 L3 S2 C1 D3).

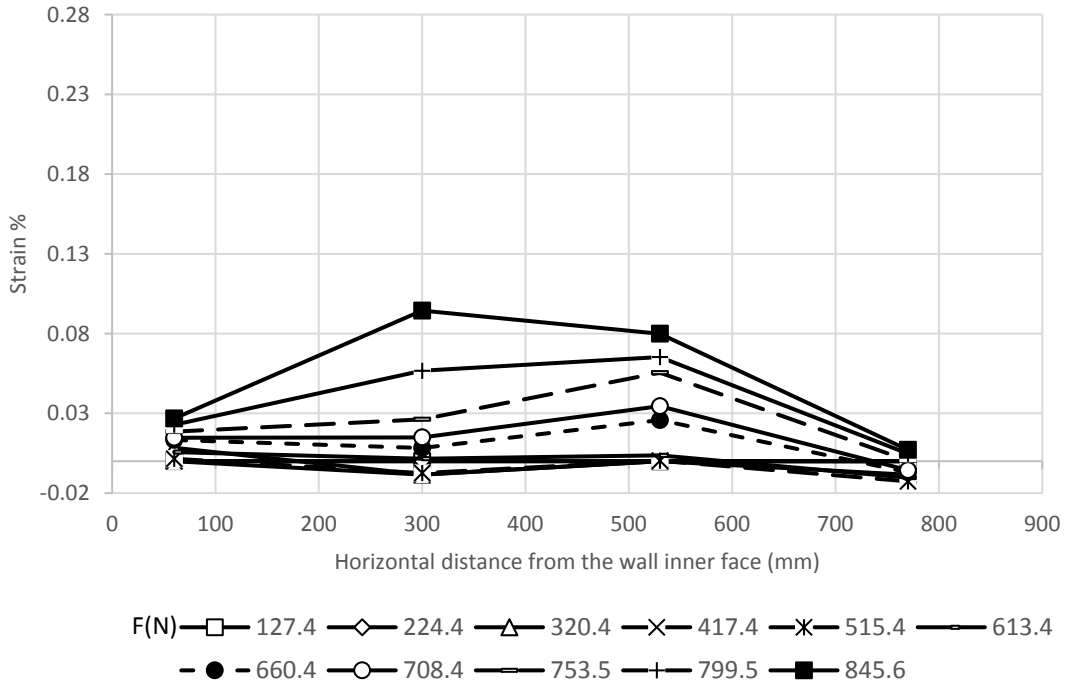

Figure A.149 Strains in the geogrid layer at 270 mm from the wall base (Test H2 L3 S2 C1 D2).

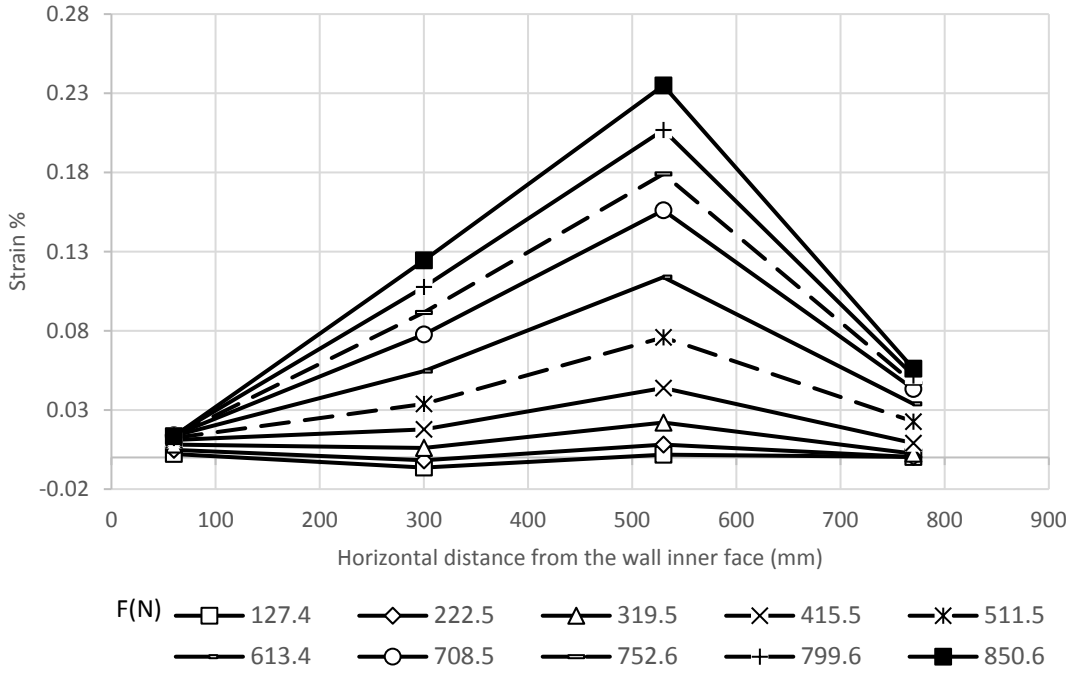

Figure A.150 Strains in the geogrid layer at 270 mm from the wall base (Test H2 L3 S2 C1 D3).

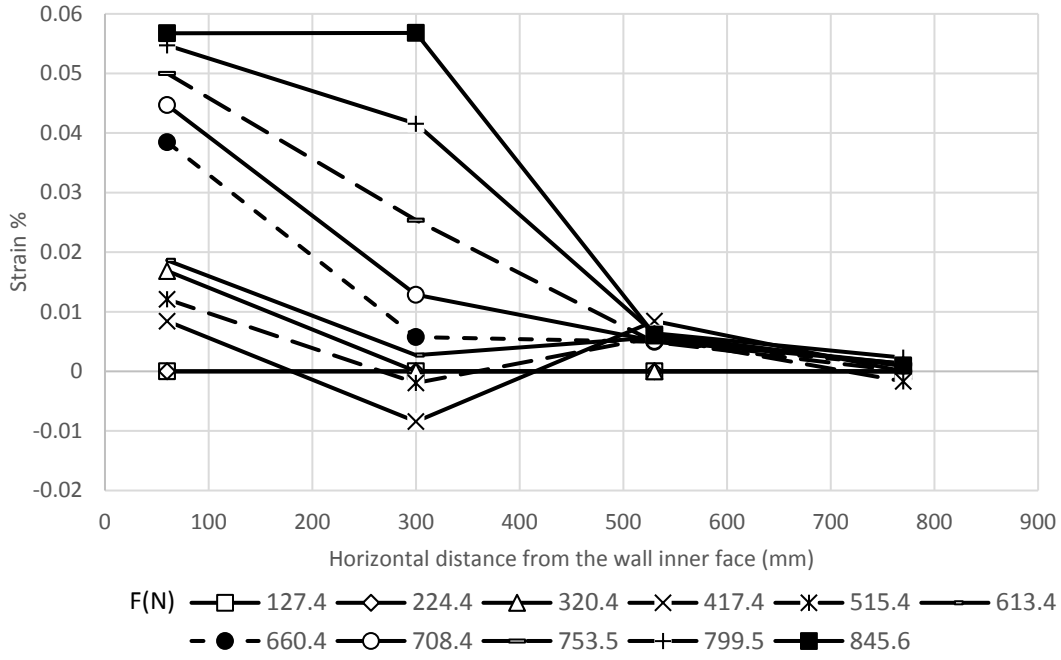

Figure A.151 Strains in the geogrid layer at 135 mm from the wall base (Test H2 L3 S2 C1 D2).

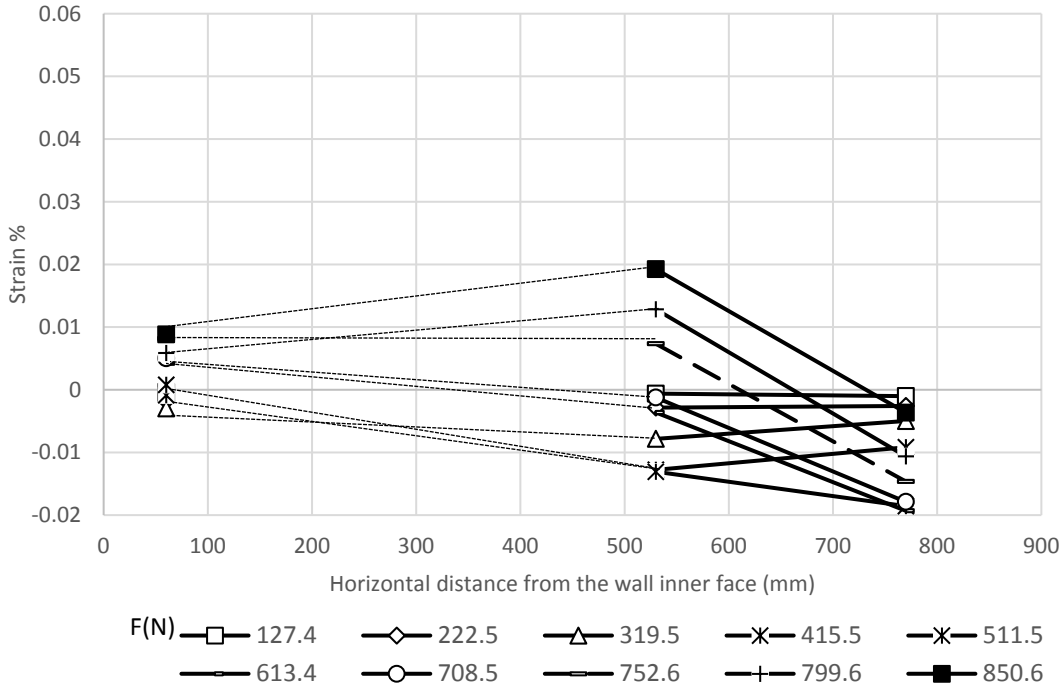

Figure A.152 Strains in the geogrid layer at 135 mm from the wall base (Test H2 L3 S2 C1 D3).

Pressure behind the wall facing

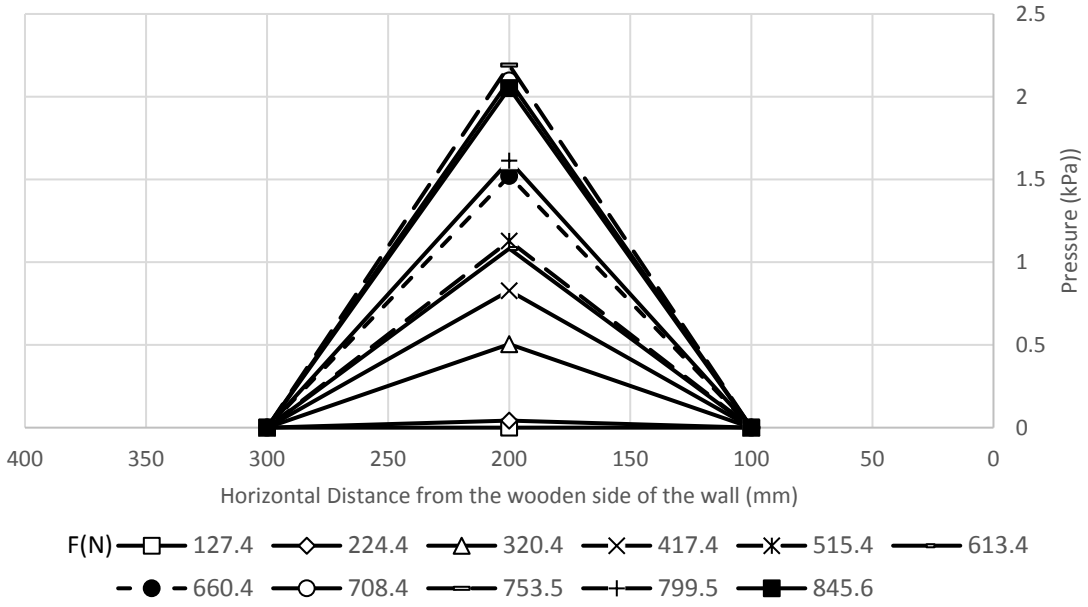

Figure A.153 Transverse pressure distributions at 607.5 mm from the wall base for Test H2 L3 S2 C1 D2.

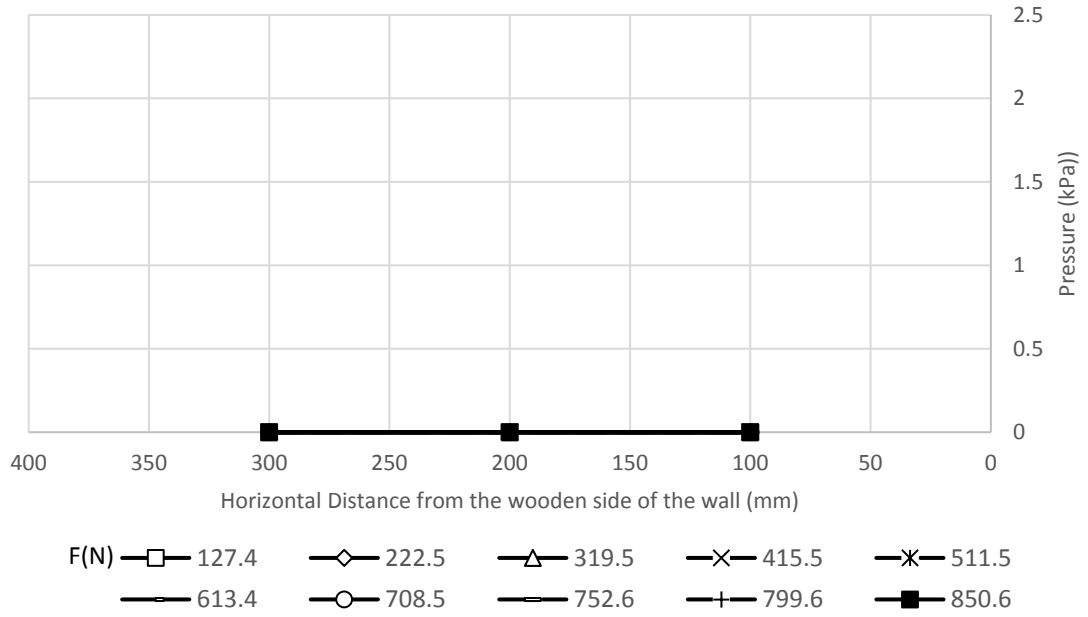

Figure A.154 Transverse pressure distributions at 607.5 mm from the wall base for Test H2 L3 S2 C1 D3.

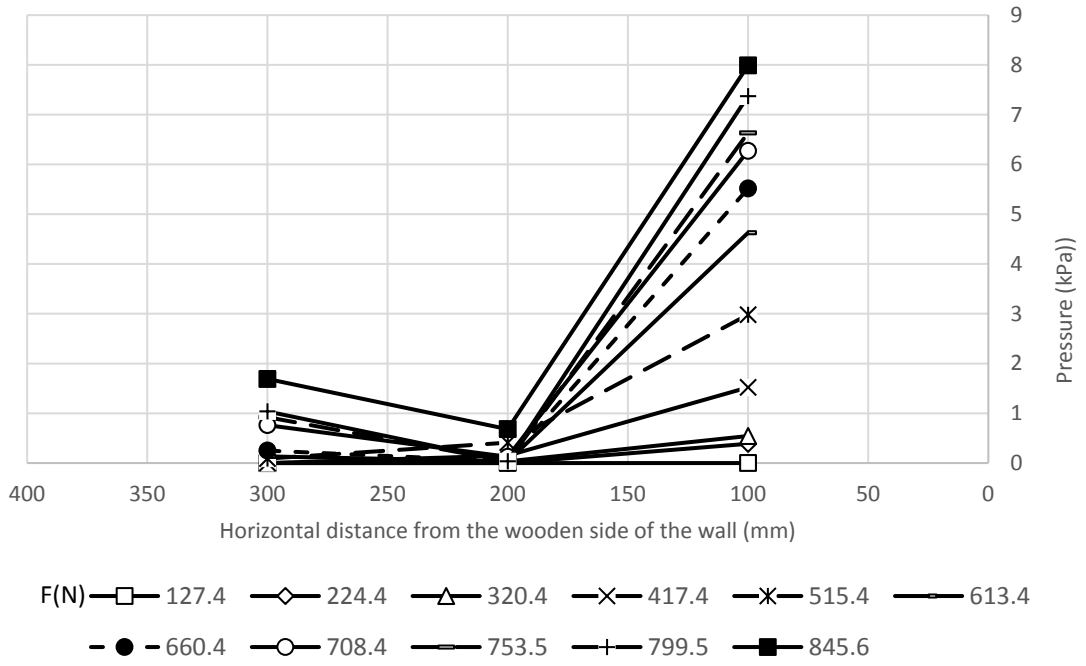

Figure A.155 Transverse pressure distributions at 337.5 mm from the wall base for Test H2 L3 S2 C1 D2.

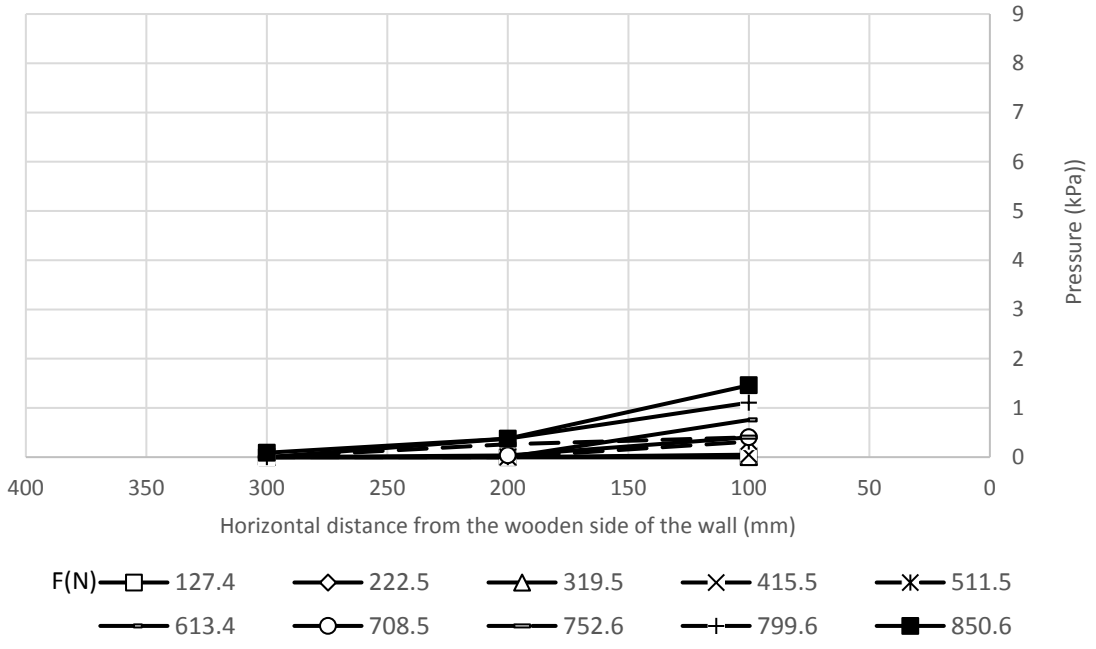

Figure A.156 Transverse pressure distributions at 337.5 mm from the wall base for Test H2 L3 S2 C1 D3.

A.4.2. Category 2

Deflection of the wall facing

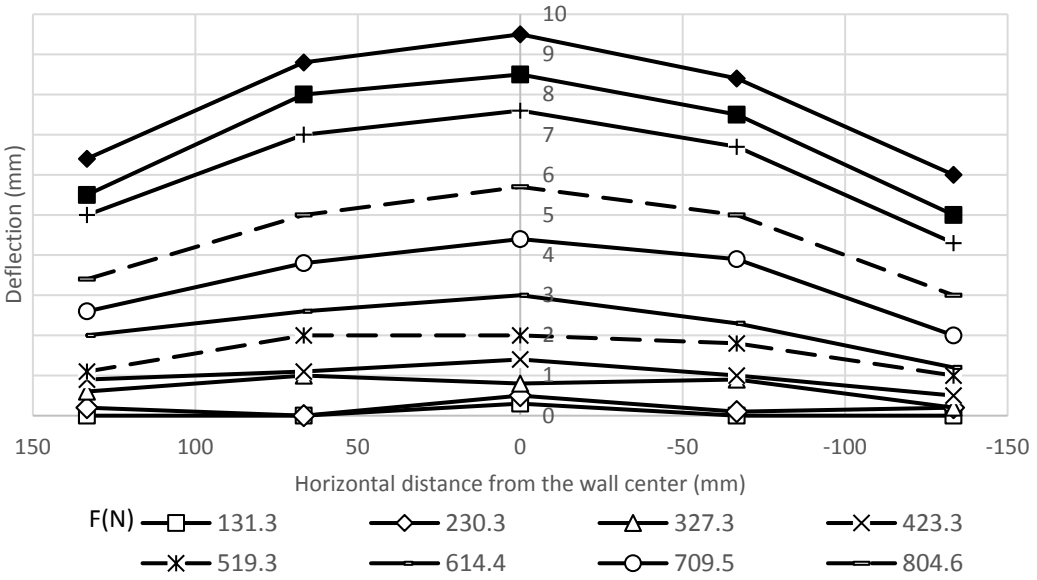

Figure A.157 Transverse deflection profiles at 472.5 mm from the wall base for Test H2 L3 S1 C1 D2.

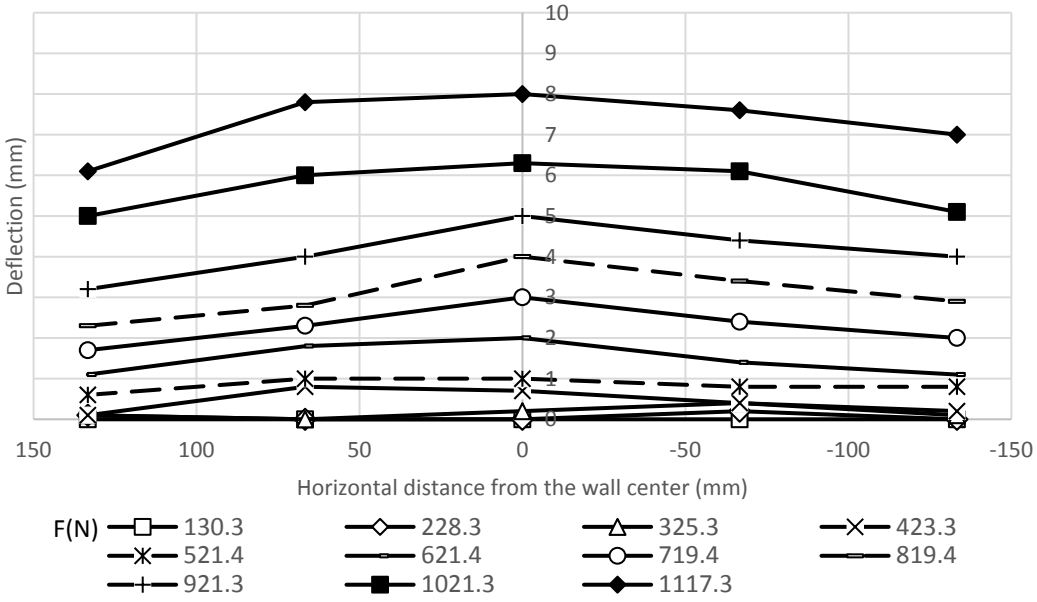

Figure A.158 Transverse deflection profiles at 472.5 mm from the wall base for Test H2 L3 S1 C1 D3.

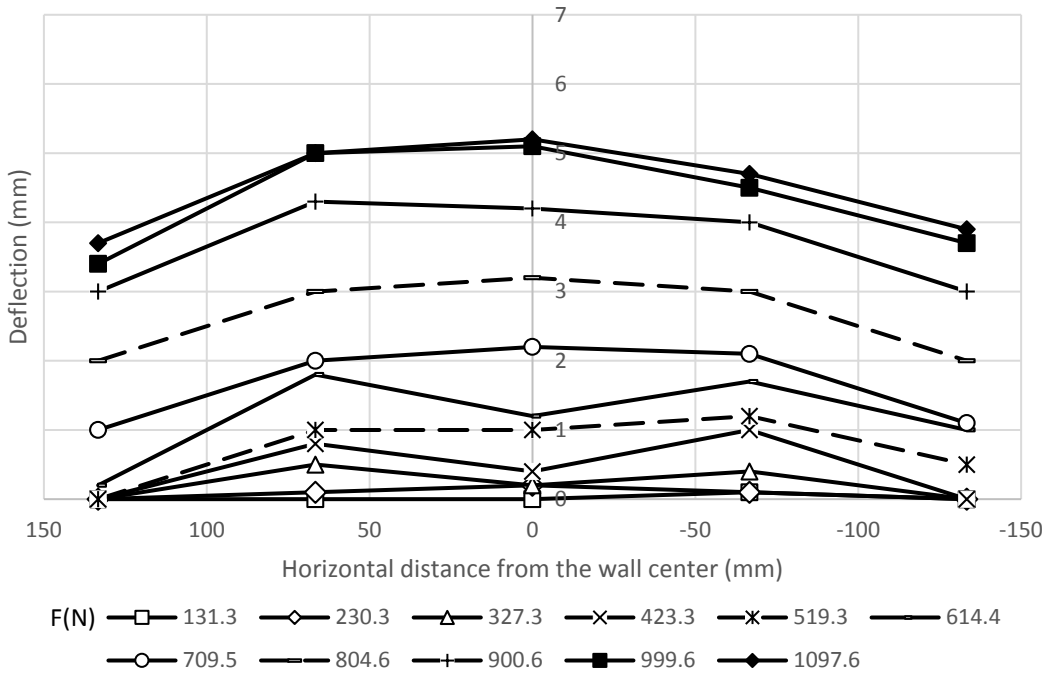

Figure A.159 Transverse deflection profiles at 337.5 mm from the wall base for Test H2 L3 S1 C1 D2.

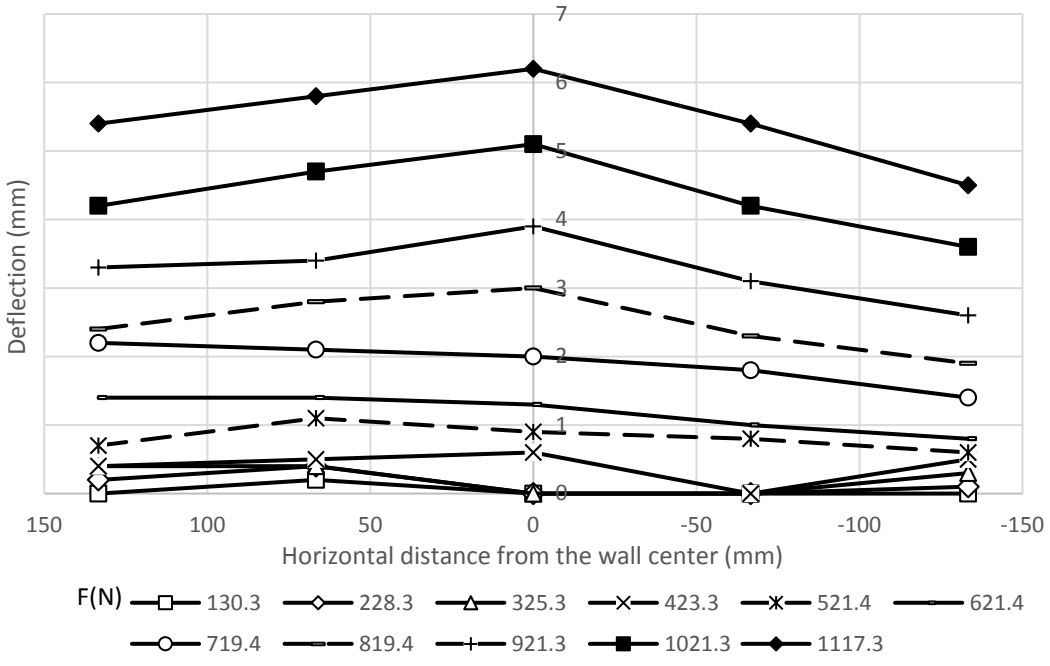

Figure A.160 Transverse deflection profiles at 337.5 mm from the wall base for Test H2 L3 S1 C1 D3.

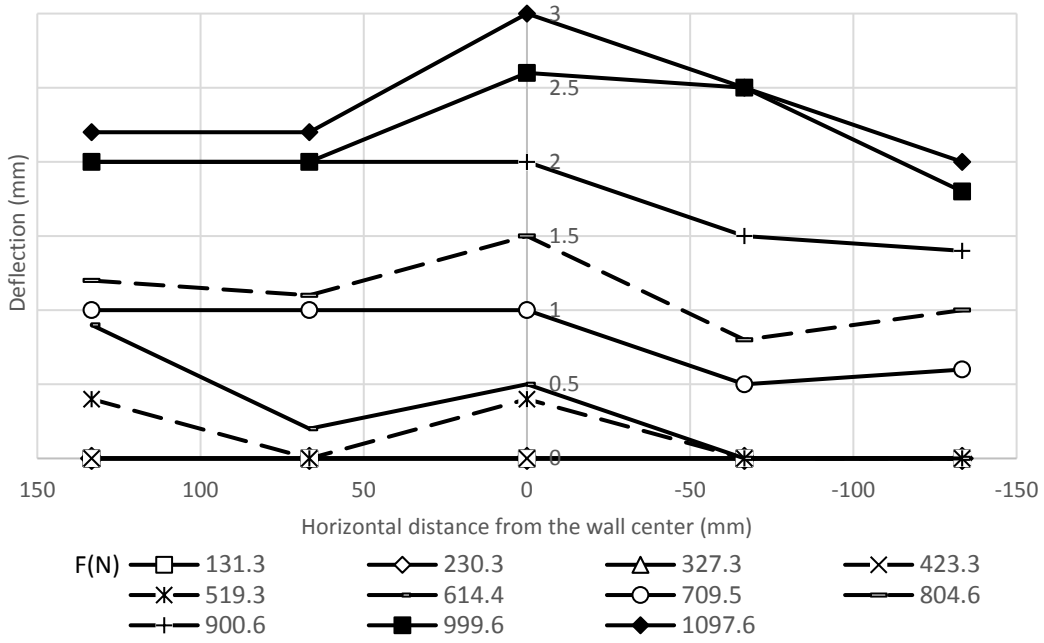

Figure A.161 Transverse deflection profiles at 202.5 mm from the wall base for Test H2 L3 S1 C1 D2.

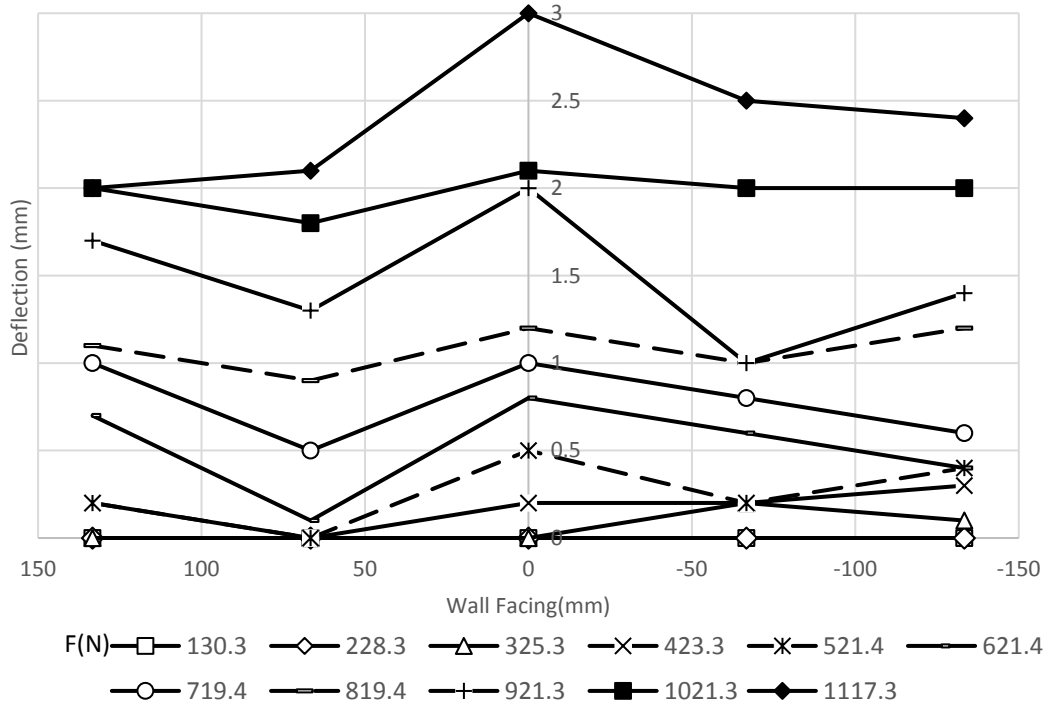

Figure A.162 Transverse deflection profiles at 202.5 mm from the wall base for Test H2 L3 S1 C1 D3.

Stress and moment of the pile:

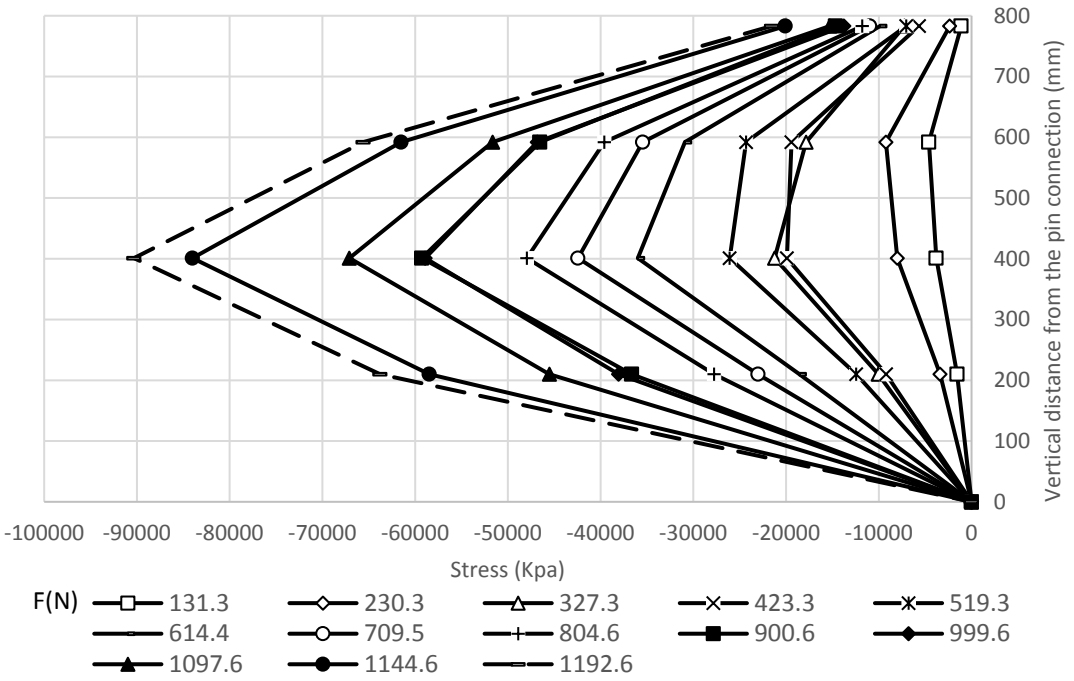

Figure A.163 Stresses along the compressive side of the pile in Test H2 L3 S1 C1 D2.

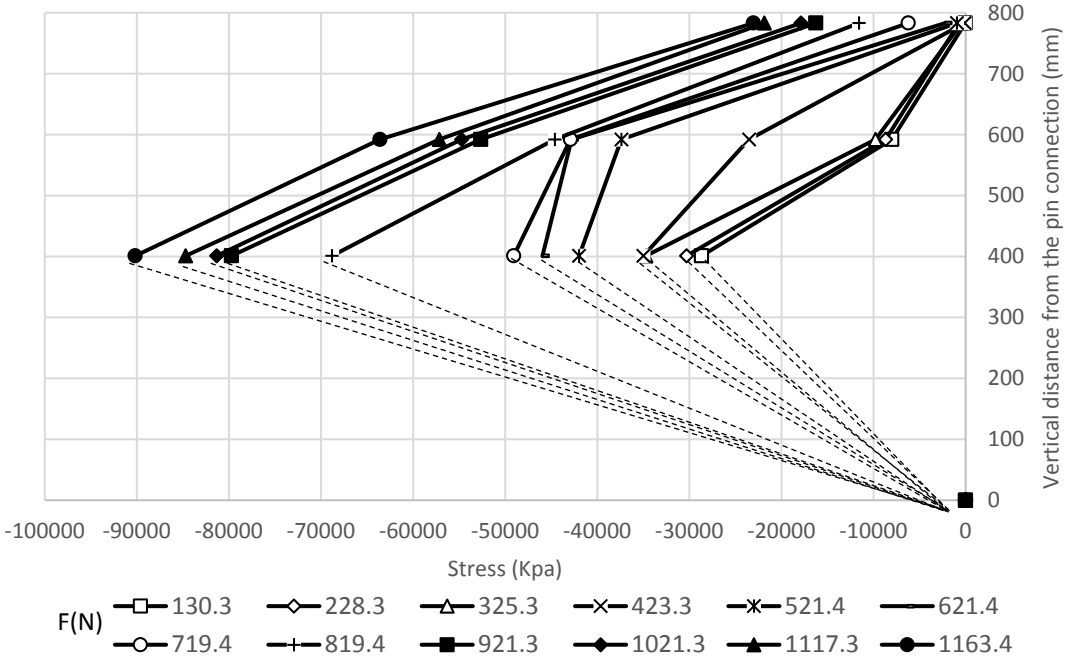

Figure A.164 Stresses along the compressive side of the pile in Test H2 L3 S1 C1 D3.

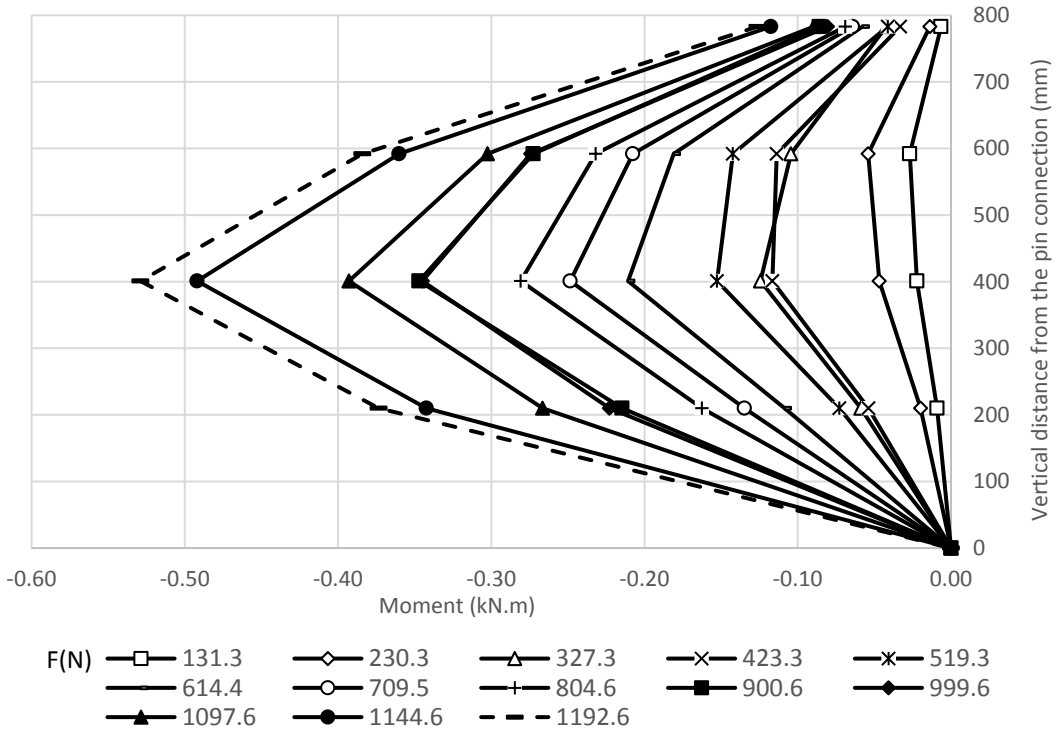

Figure A.165 Moments along the compressive side of the pile in Test H2 L3 S1 C1 D2.

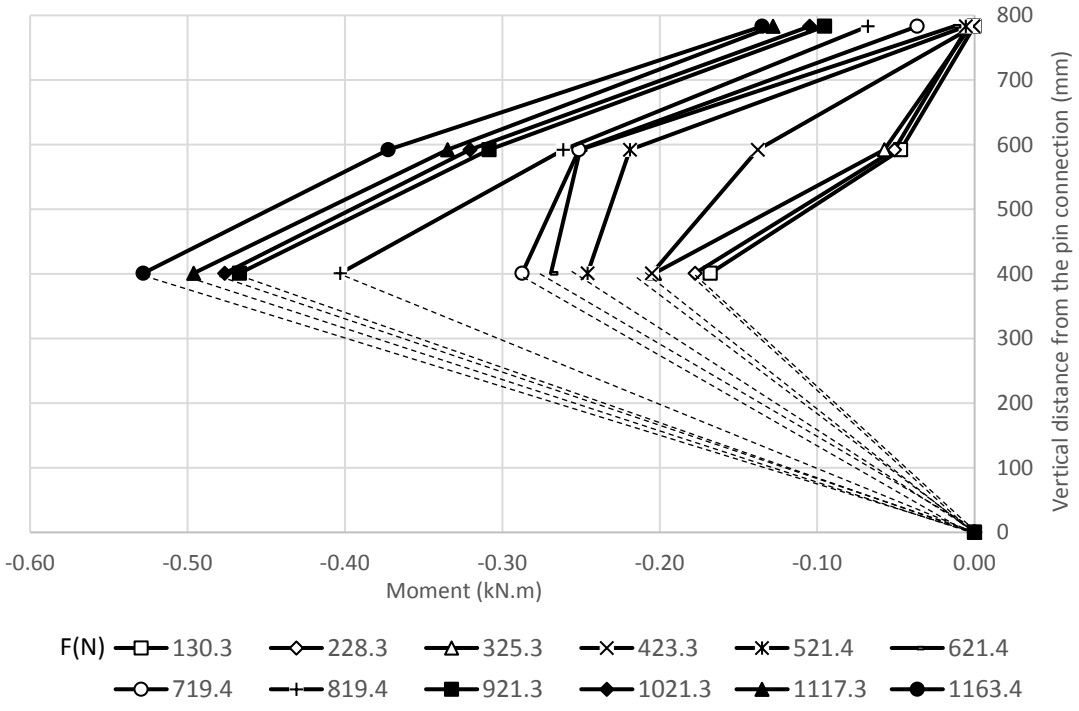

Figure A.167 Moments along the compressive side of the pile in Test H2 L3 S1 C1 D3.

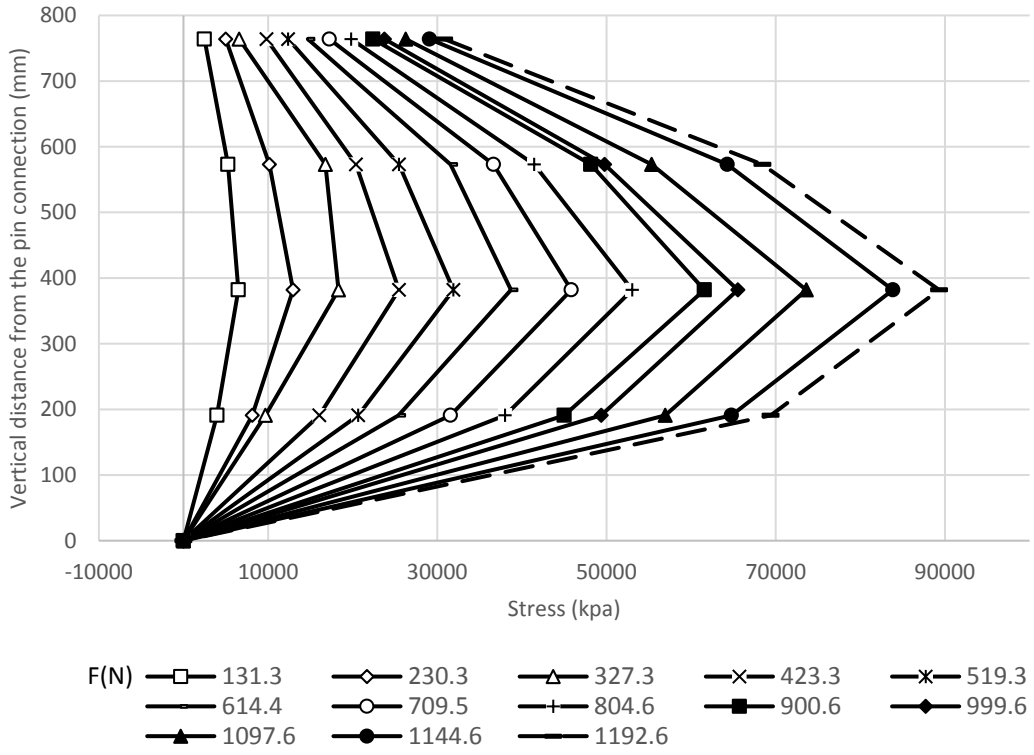

Figure A.168 Stresses along the compressive side of the pile in Test H2 L3 S1 C1 D2.

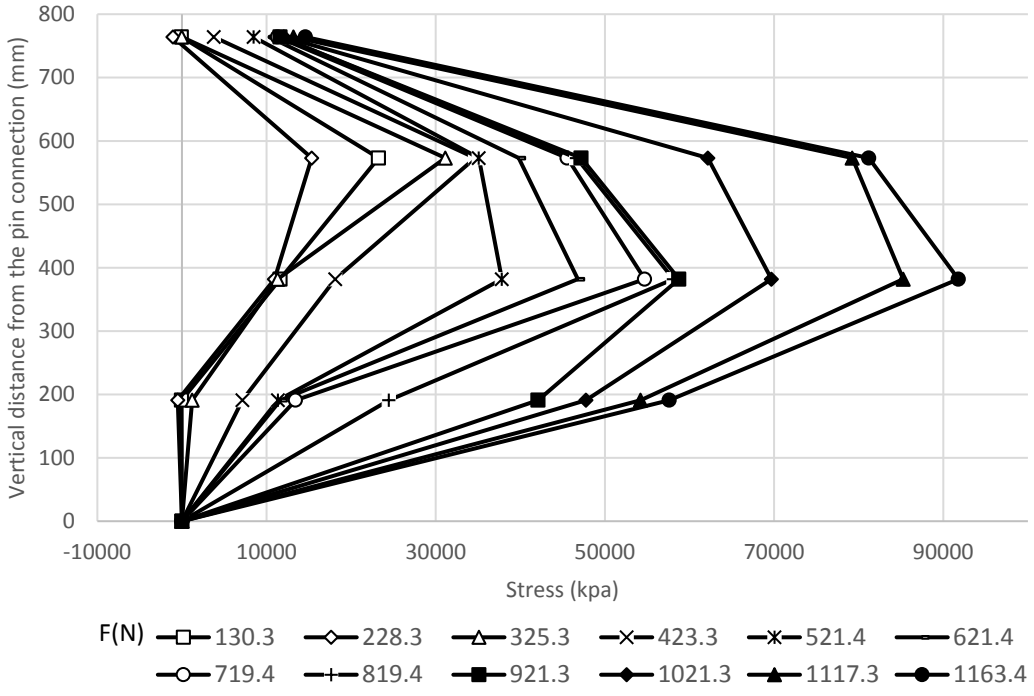

Figure A.169 Stresses along the compressive side of the pile in Test H2 L3 S1 C1 D3.

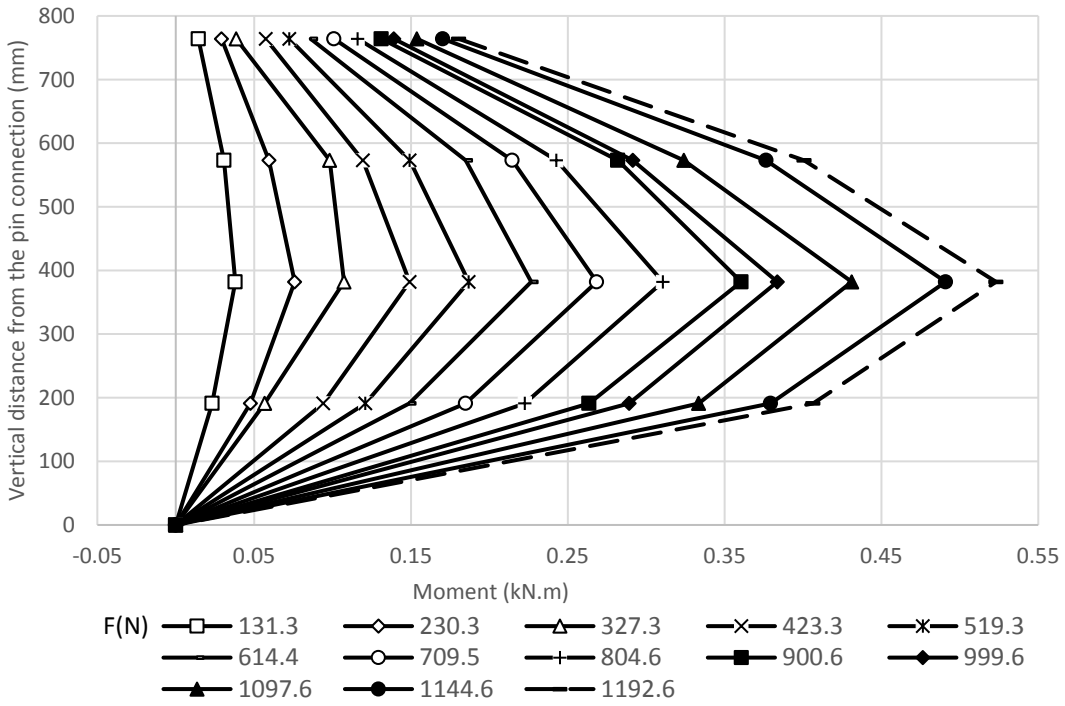

Figure A.170 Moments along the compressive side of the pile in Test H2 L3 S1 C1 D2.

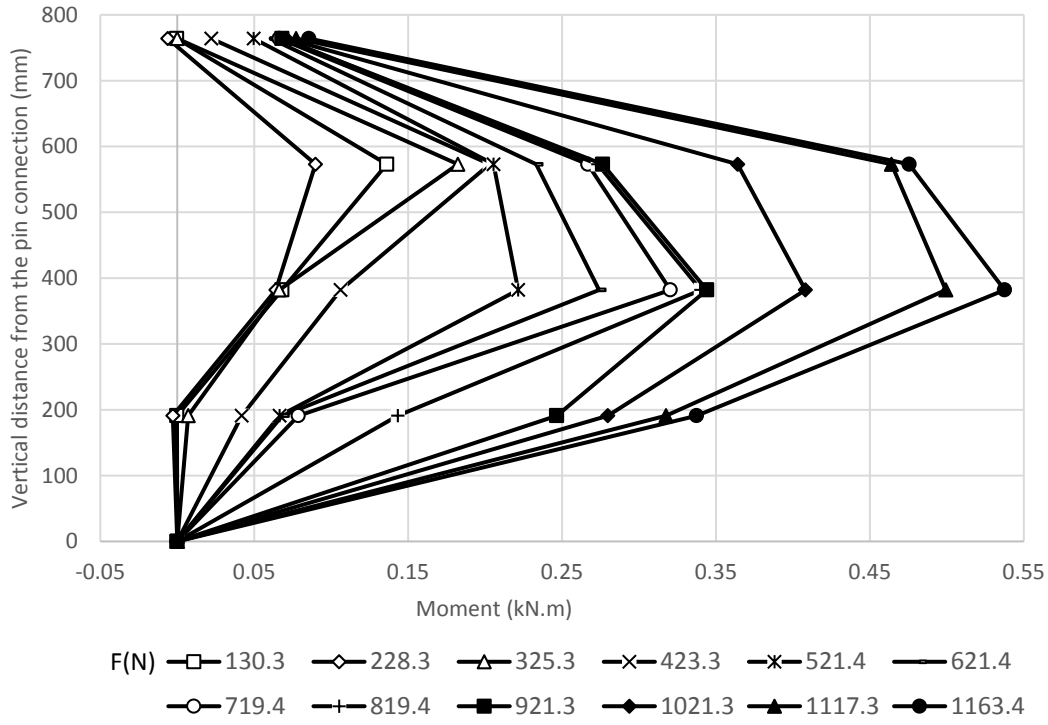

Figure 4.171 Moments along the tensile side of the pile in Test H2 L3 S1 C1 D3.

Strain in the geogrid layers

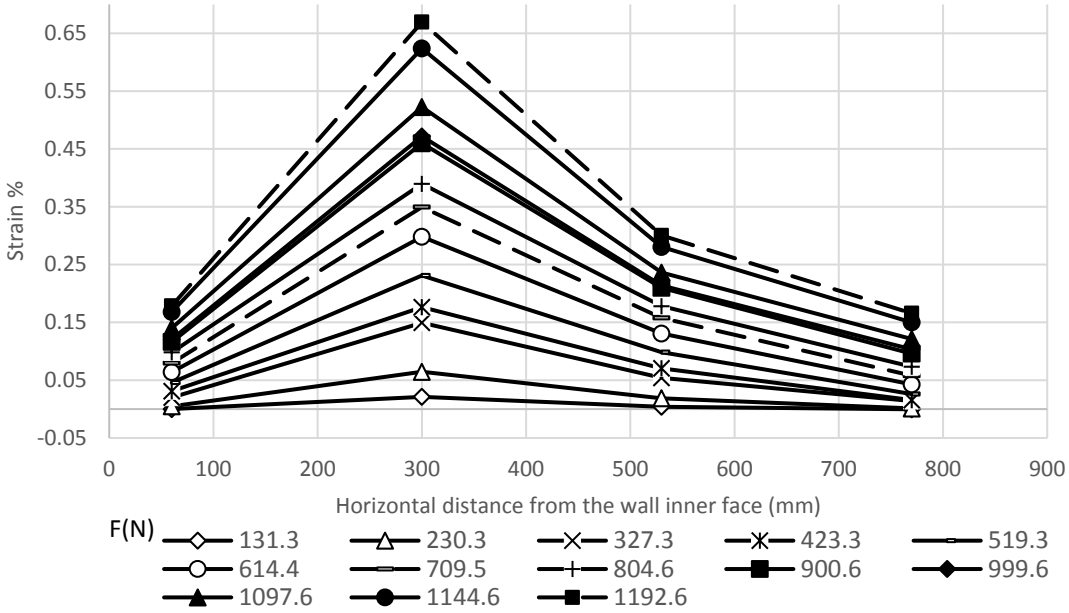

Figure A.172 Strains in the geogrid layer at 450 mm from the wall base (Test H2 L3 S1 C1 D2).

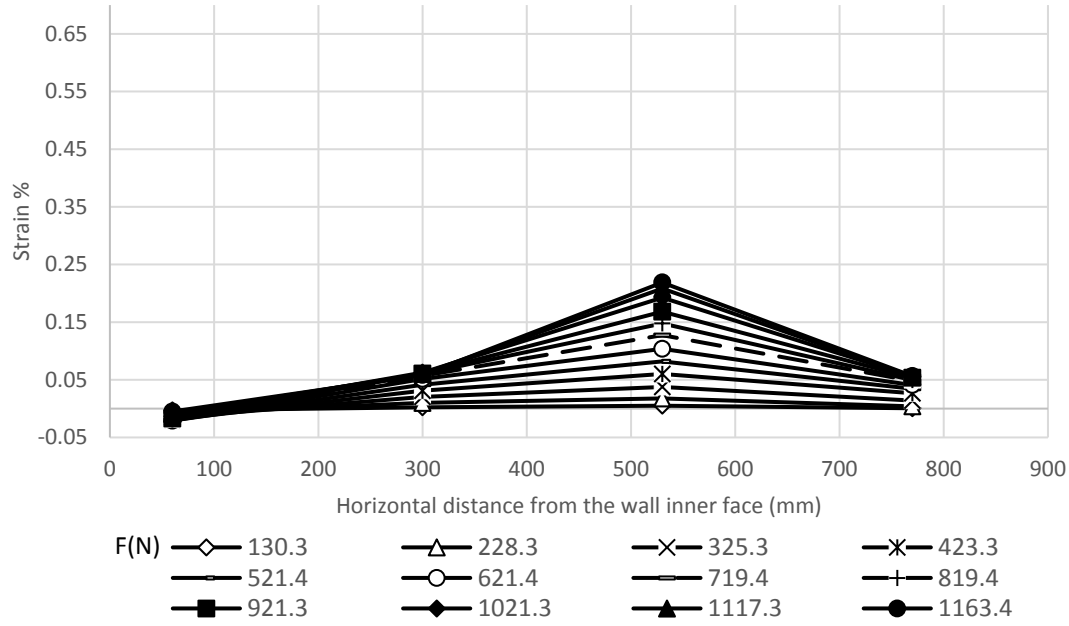

Figure A.173 Strains in the geogrid layer at 450 mm from the wall base (Test H2 L3 S1 C1 D3).

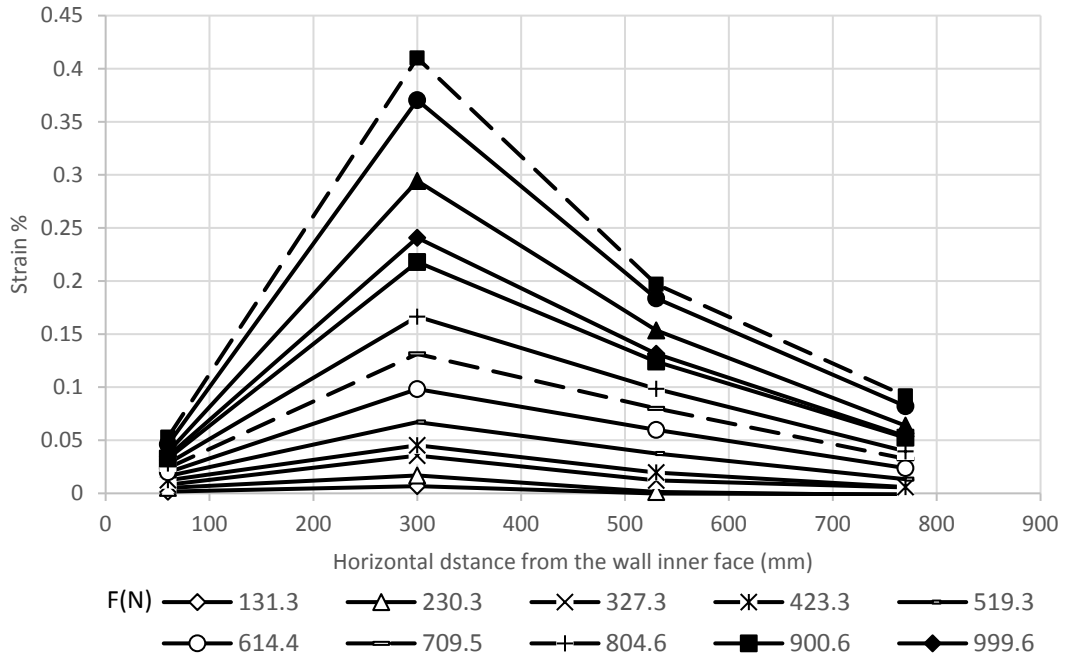

Figure A.175 Strains in the geogrid layer at 270 mm from the wall base (Test H2 L3 S1 C1 D2).

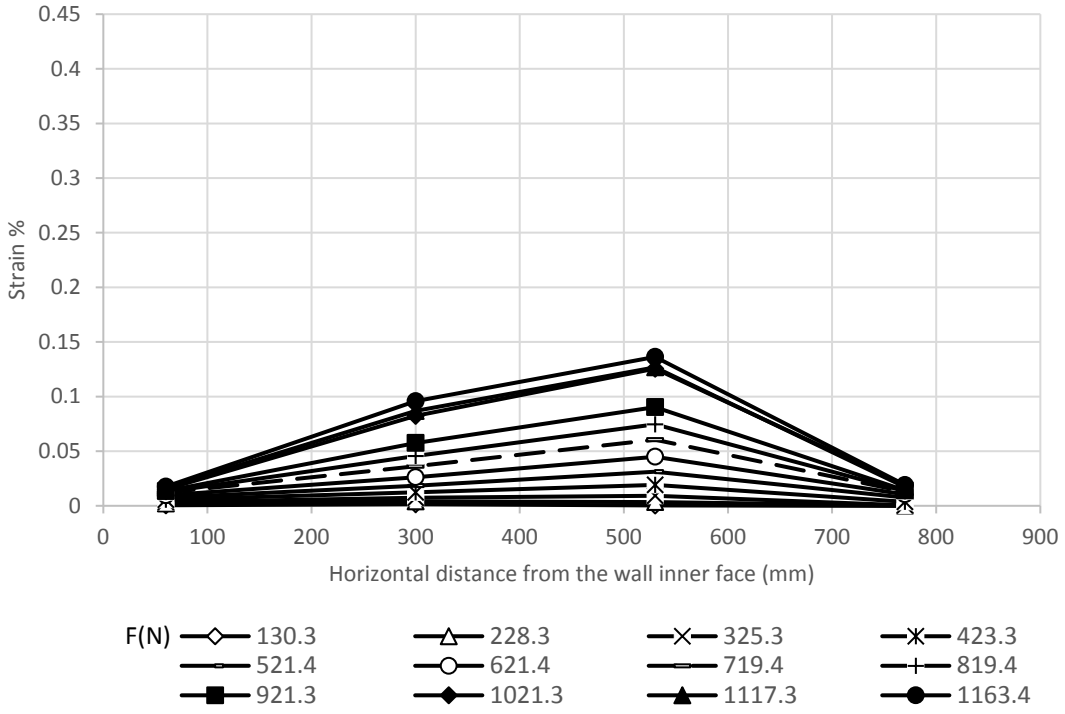

Figure A.176 Strains in the geogrid layer at 270 mm from the wall base (Test H2 L3 S1 C1 D3).

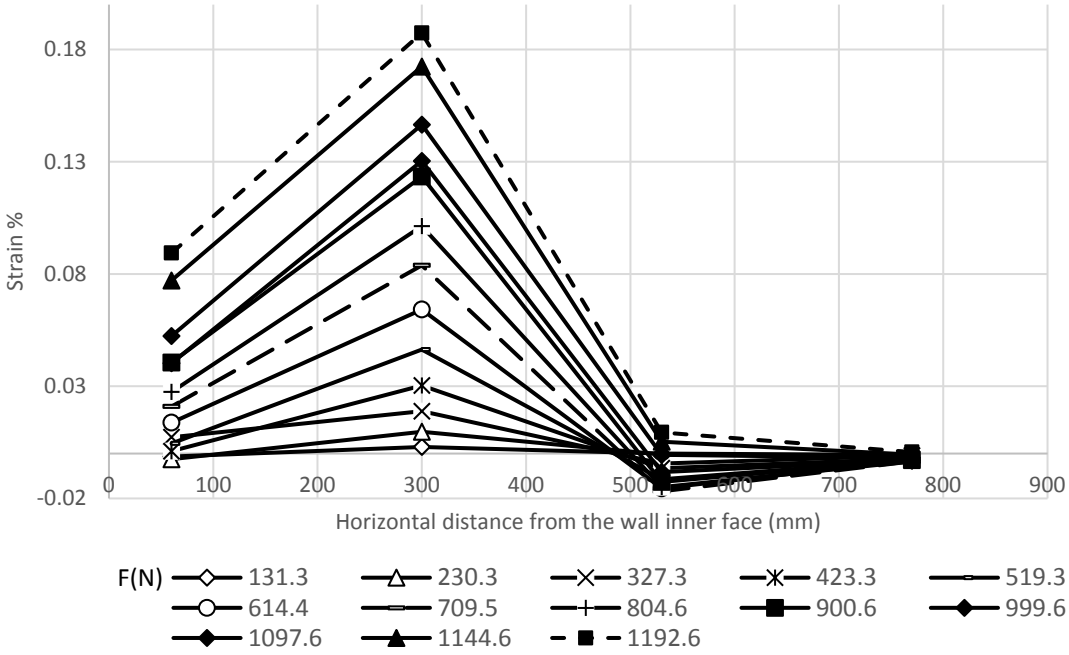

Figure A.177 Strains in the geogrid layer at 90 mm from the wall base (Test H2 L3 S1 C1 D2).

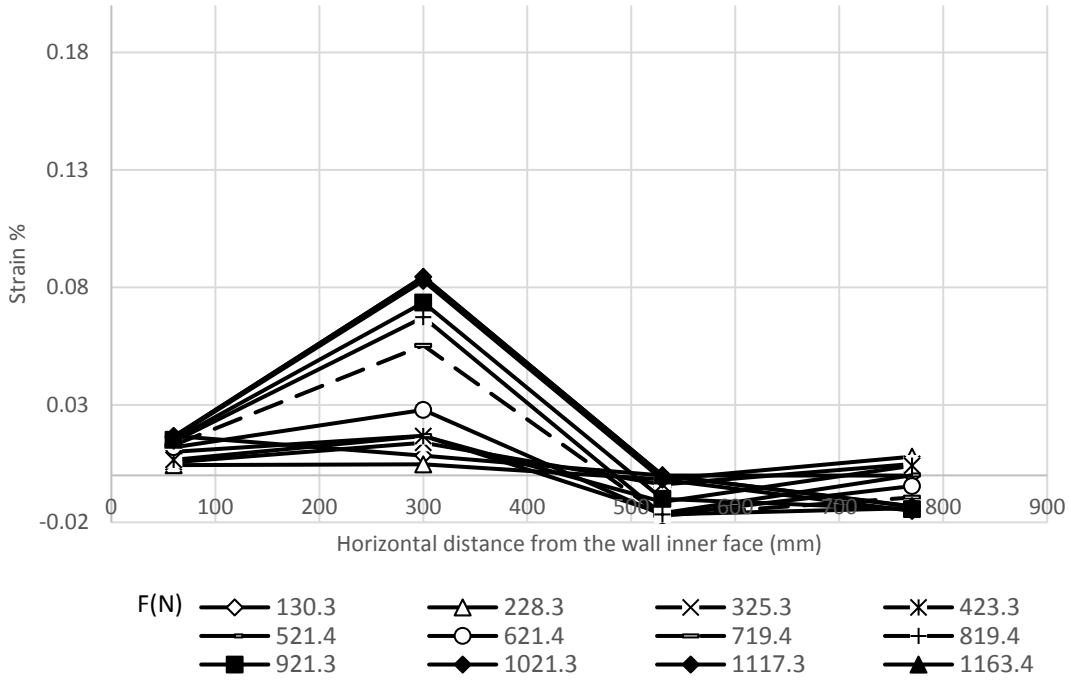

Figure A.178 Strains in the geogrid layer at 90 mm from the wall base (Test H2 L3 S1 C1 D3).

Pressure behind the wall facing:

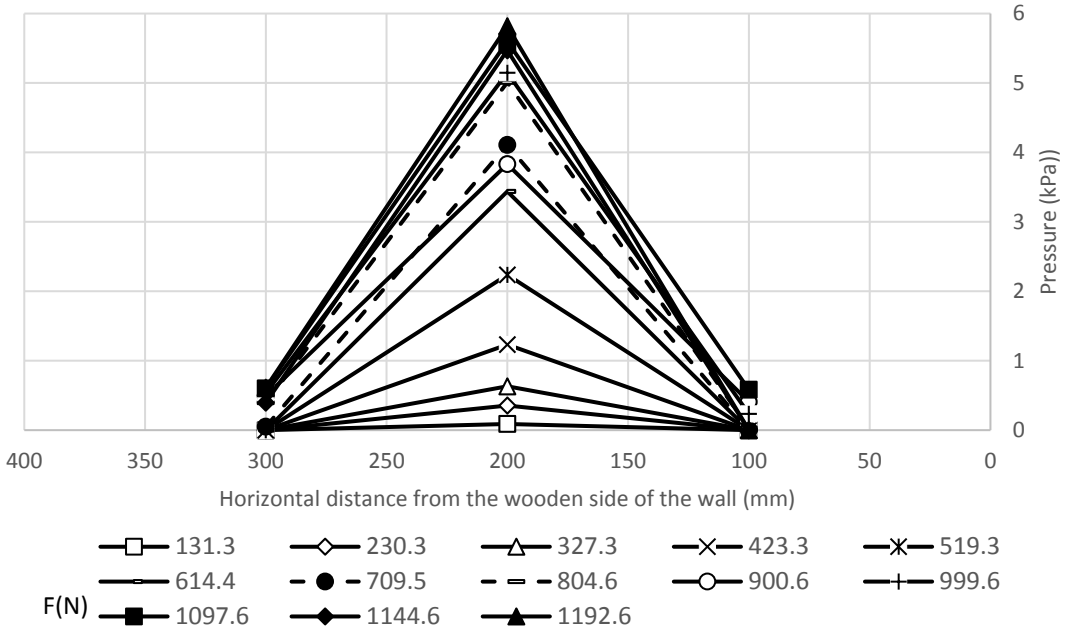

Figure A.179 Transverse pressure distributions at 607.5 mm from the wall base for Test H2 L3 S1 C1 D2.

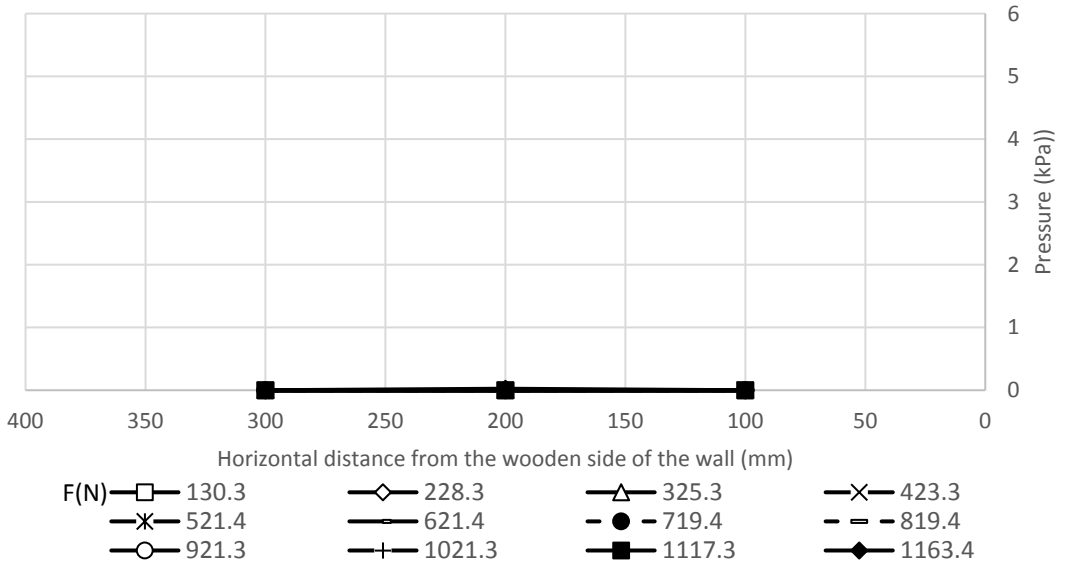

Figure A.180 Transverse pressure distributions at 607.5 mm from the wall base for Test H2 L3 S1 C1 D3.

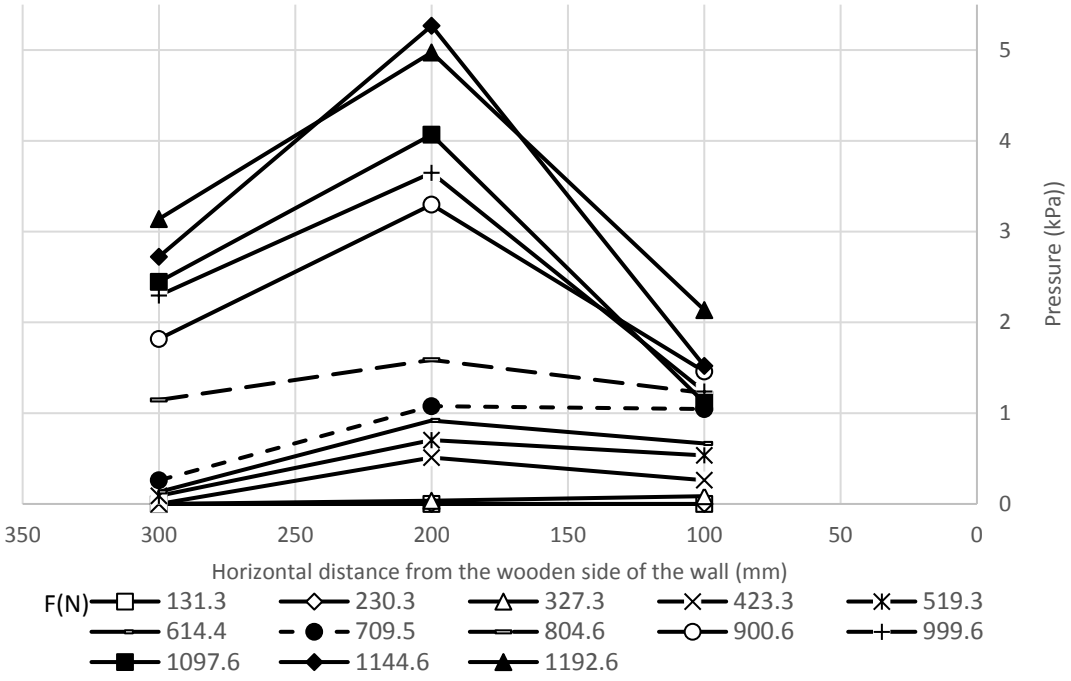

Figure A.181 Transverse pressure distributions at 337.5 mm from the wall base for Test H2 L3 S1 C1 D2.

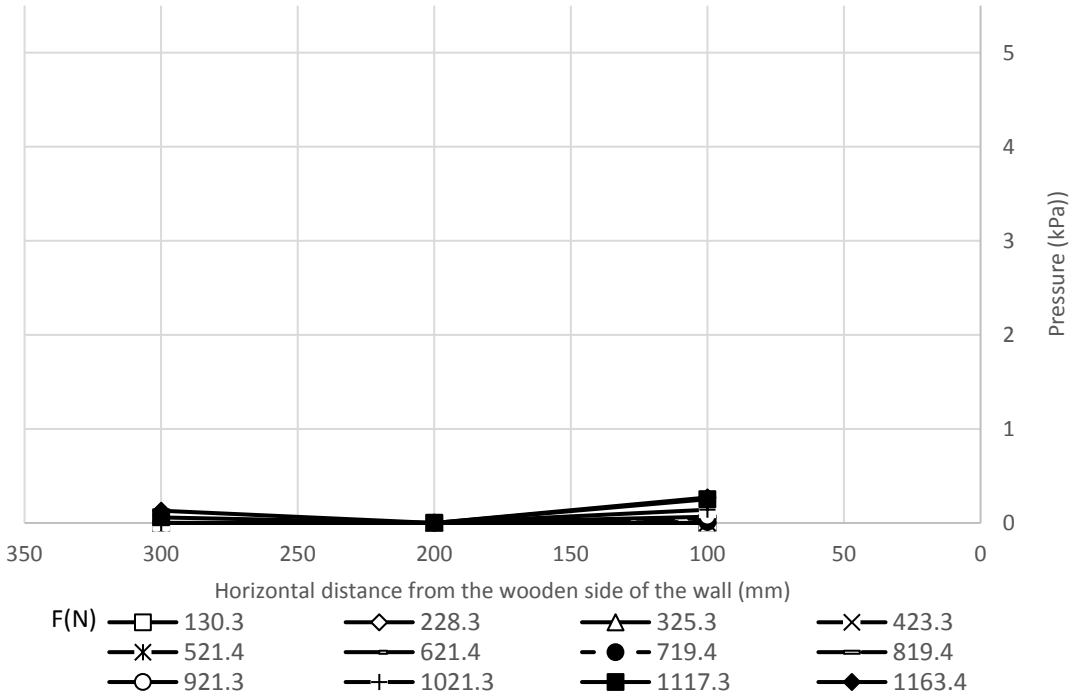

Figure A.182 Transverse pressure distributions at 337.5 mm from the wall base for Test H2 L3 S1 C1 D3.

A.4.3. Category 3

Deflection of the wall facing:

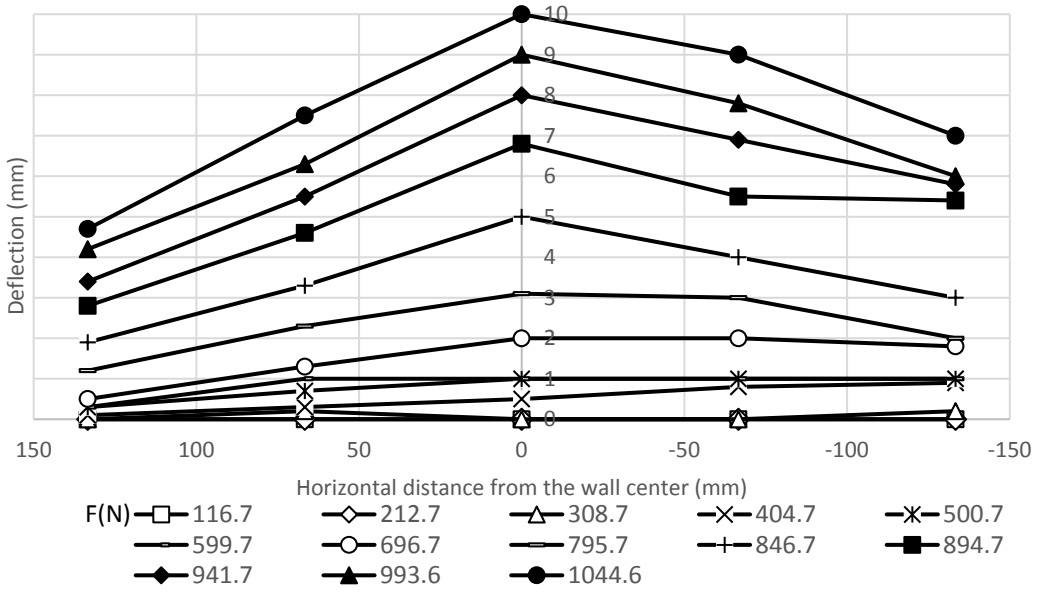

Figure A.183 Transverse deflection profiles at 472.5 mm from the wall base for Test H2 L3 S1 C2 D2.

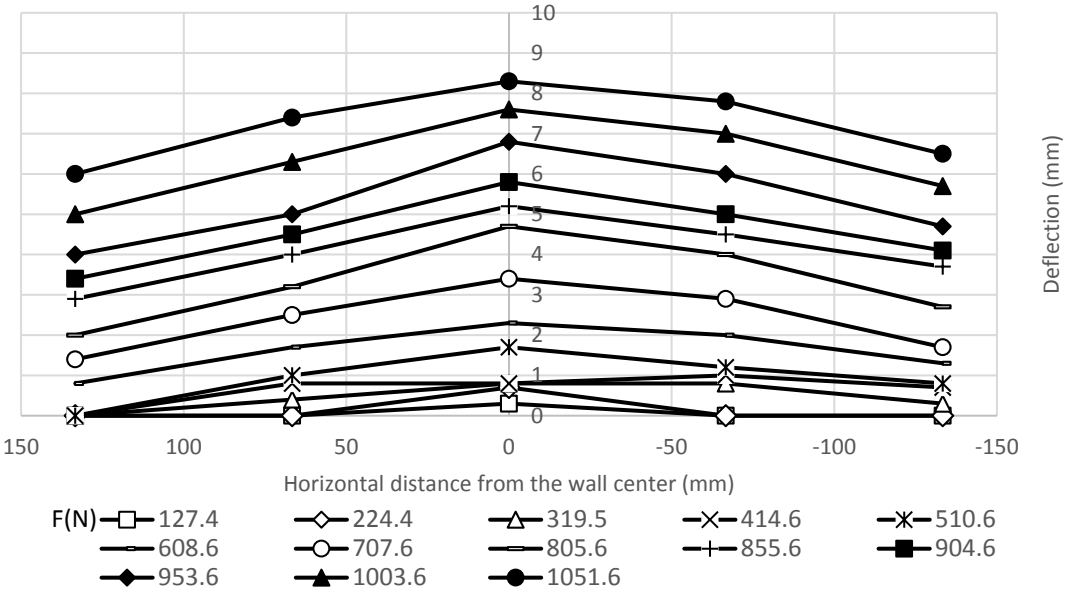

Figure A.184 Transverse deflection profiles deflection at 472.5 mm from the wall base for Test H2 L3 S1 C2 D3.

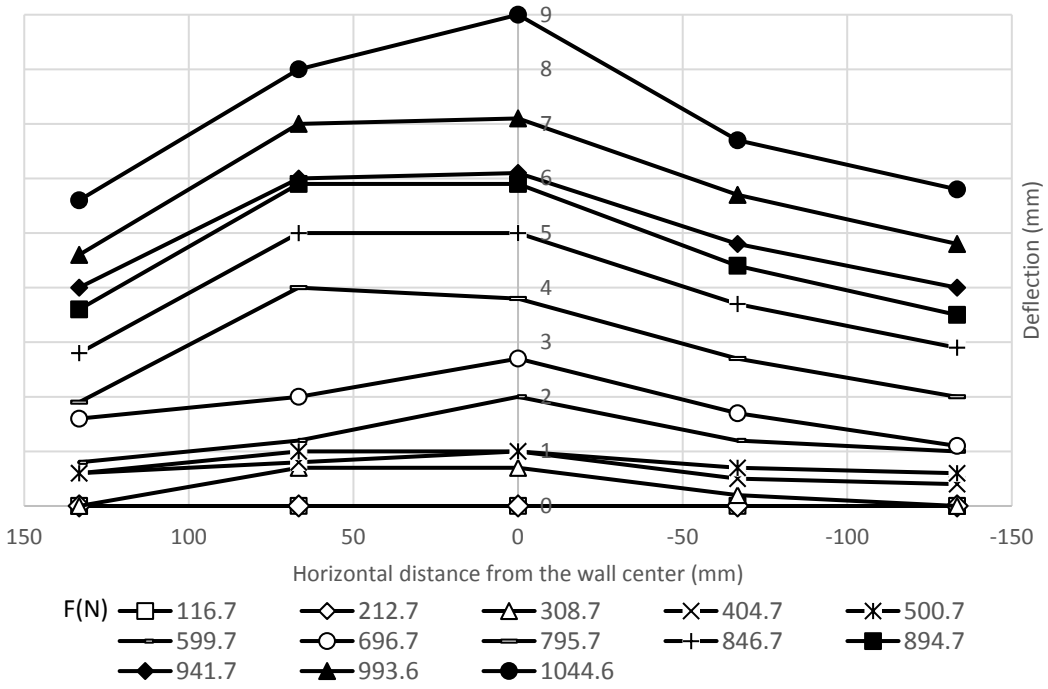

Figure A.186 Transverse deflection profiles at 337.5 mm from the wall base for Test H2 L3 S1 C2 D2.

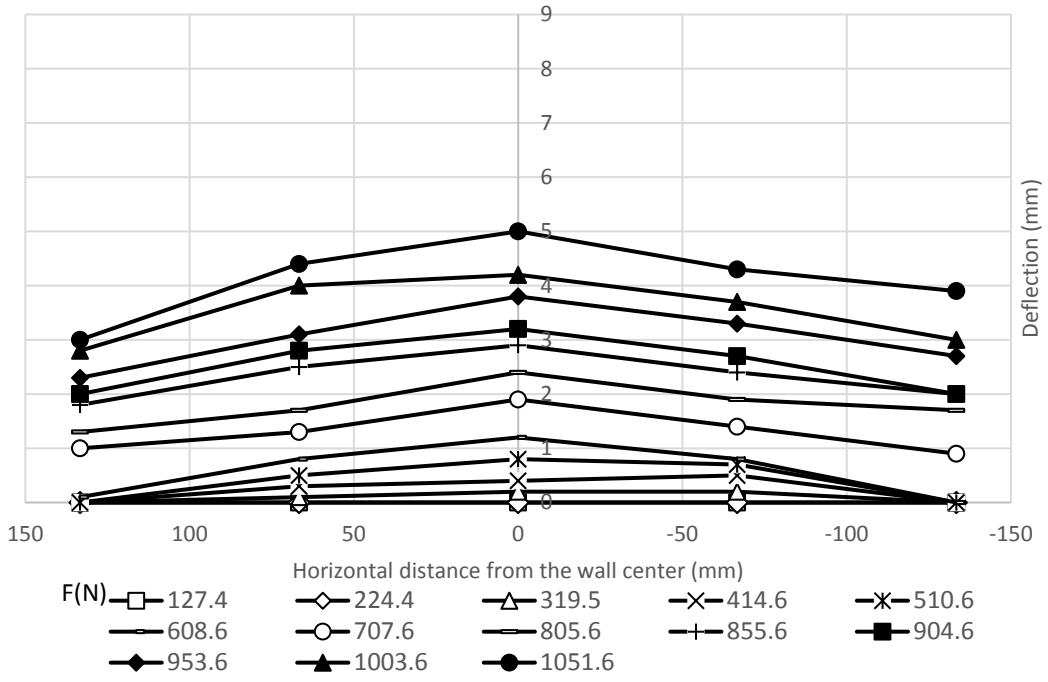

Figure A.187 Transverse deflection profiles at 337.5 mm from the wall base for Test H2 L3 S1 C2 D3.

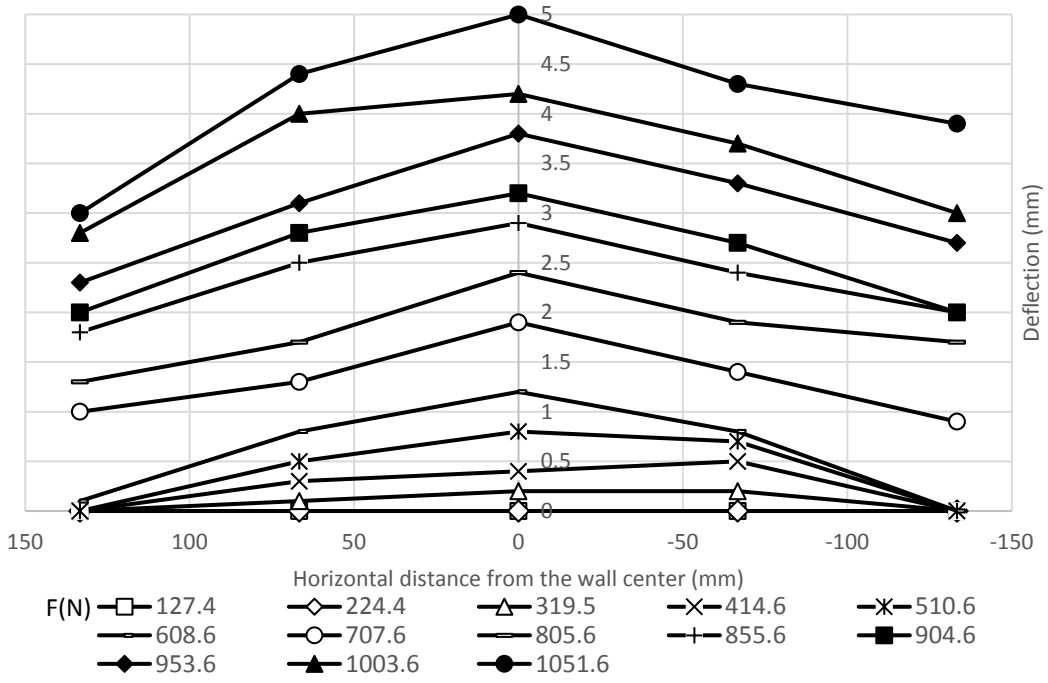

Figure A.188 Transverse deflection profiles at 202.5 mm from the wall base for Test H2 L3 S1 C2 D2.

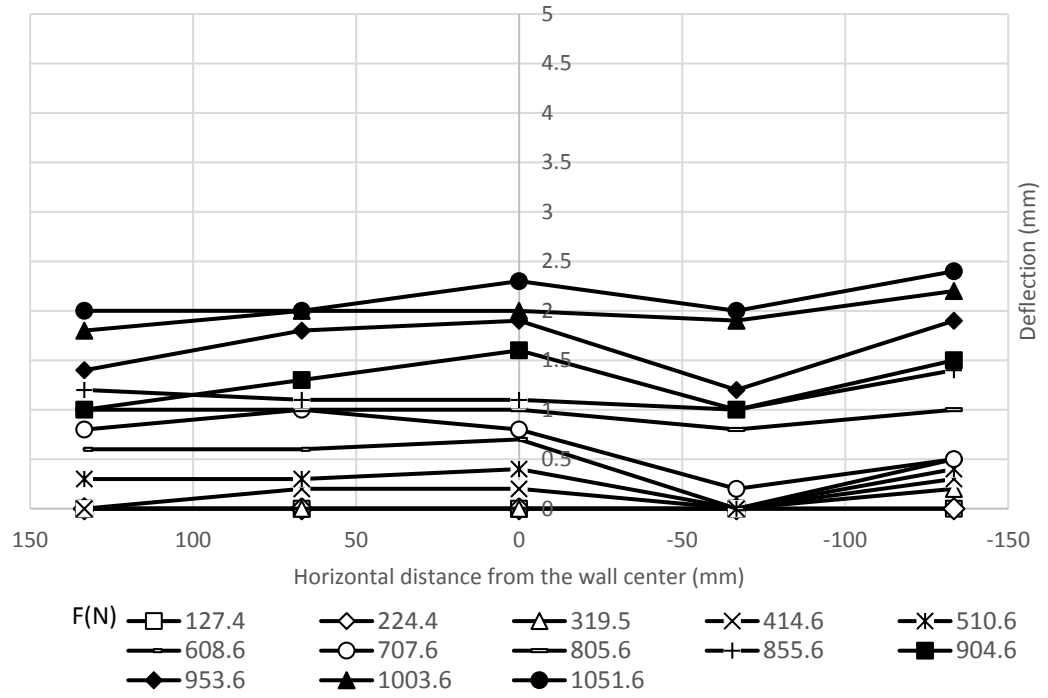

Figure A.189 Transverse deflection profiles at 202.5 mm from the wall base for Test H2 L3 S1 C2 D3.

Stress and moment of the pile:

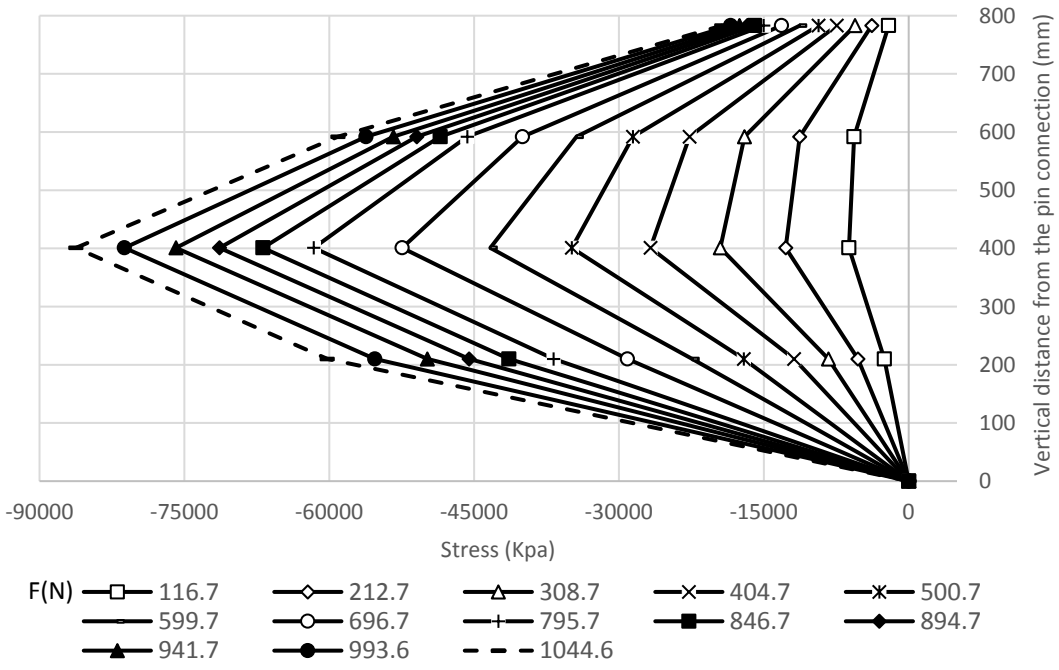

Figure A.190 Stresses along the compressive side of the pile in Test H2 L3 S1 C2 D2.

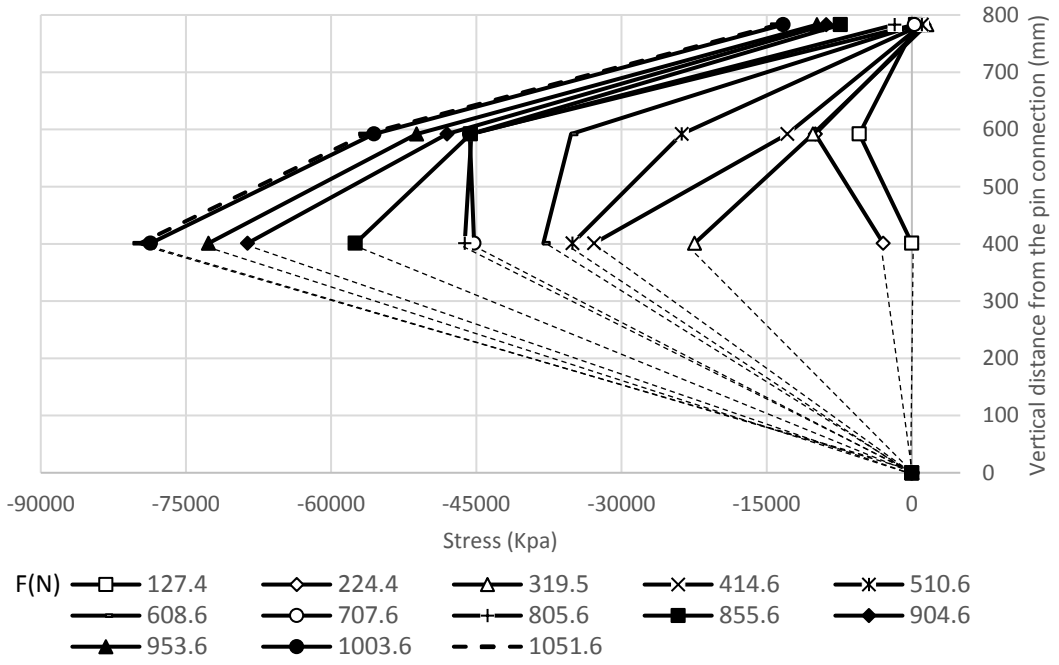

Figure A.191 Stresses along the compressive side of the pile in Test H2 L3 S1 C2 D3.

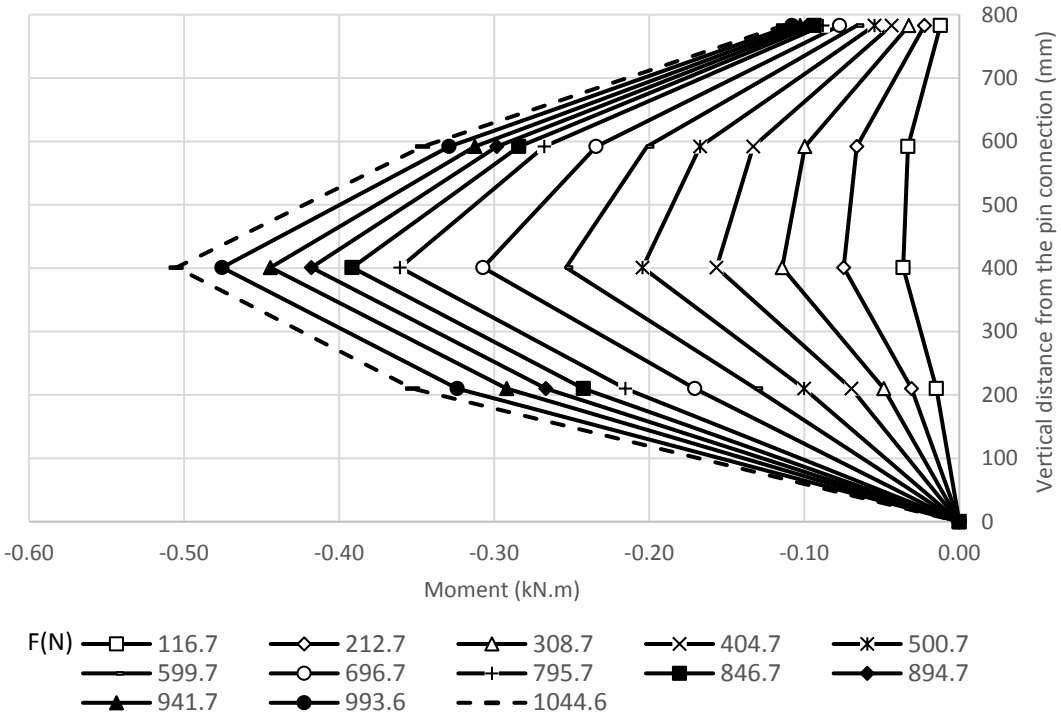

Figure A.192 Moments along the compressive side of the pile in Test H2 L3 S1 C2 D2.

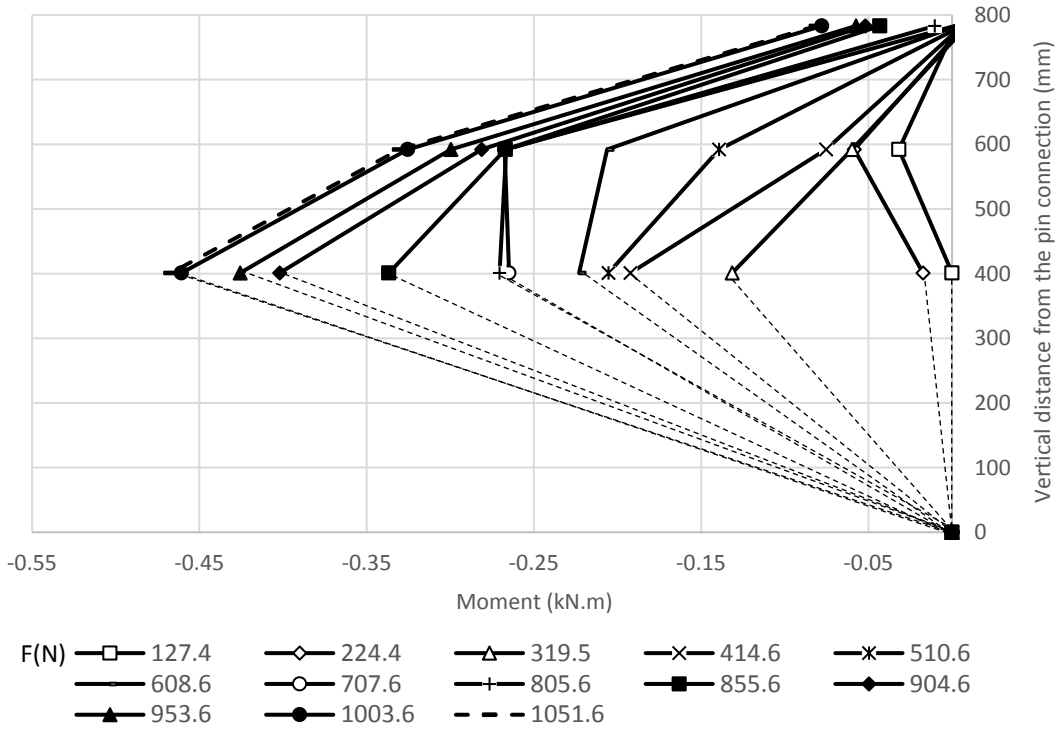

Figure A.193 Moments along the compressive side of the pile in Test H2 L3 S1 C2 D3.

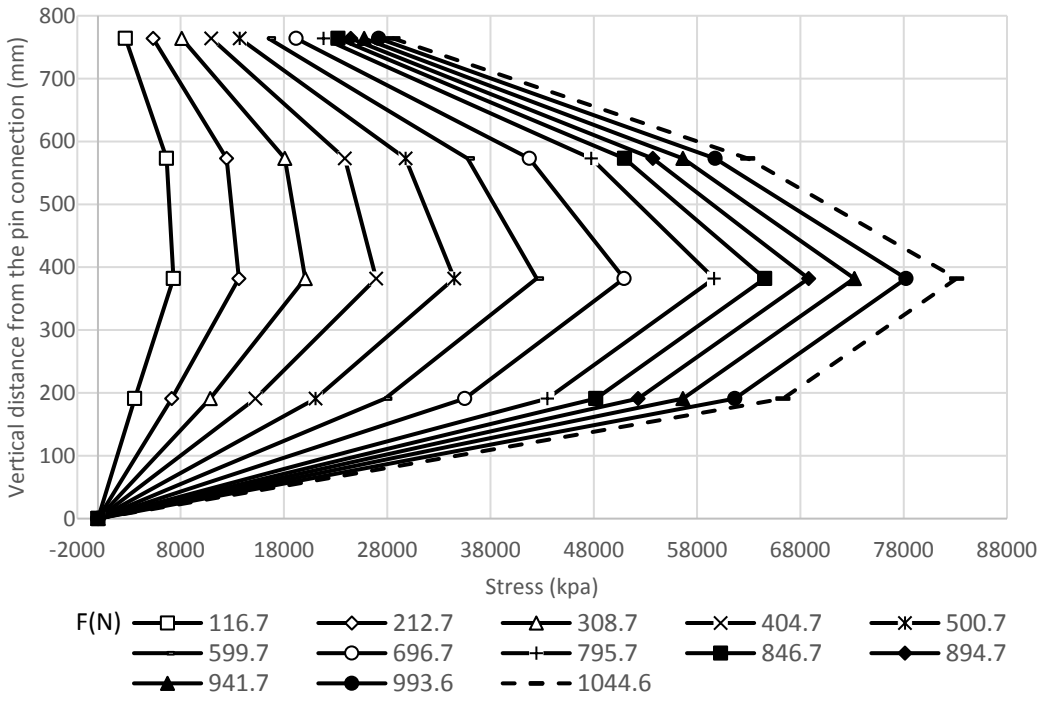

Figure A.193 Stresses along the tensile side of the pile in Test H2 L3 S1 C2 D2.

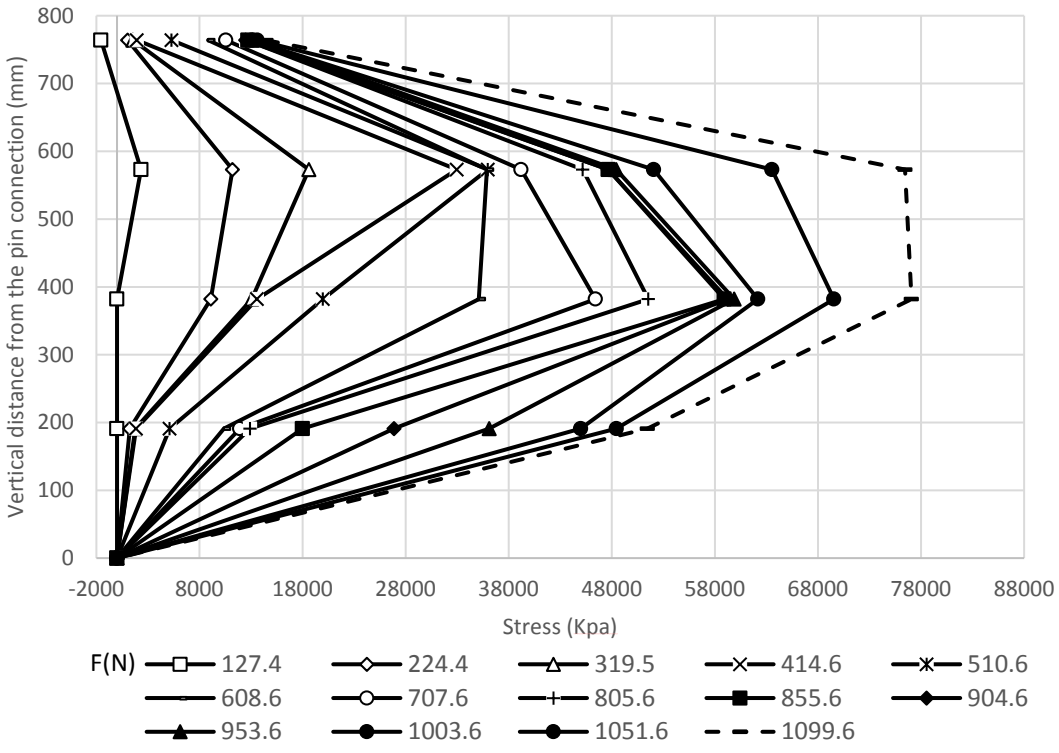

Figure A.194 Stresses along the tensile side of the pile in Test H2 L3 S1 C2 D3.

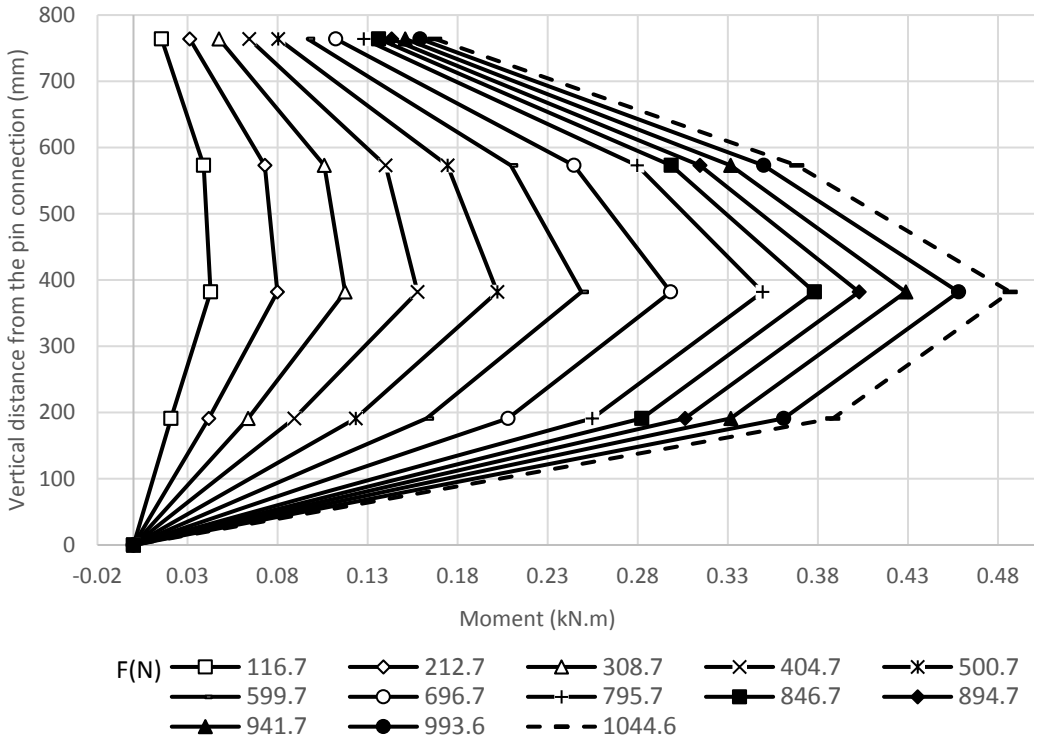

Figure A.195 Moments along the compressive side of the pile in Test H2 L3 S1 C2 D2.

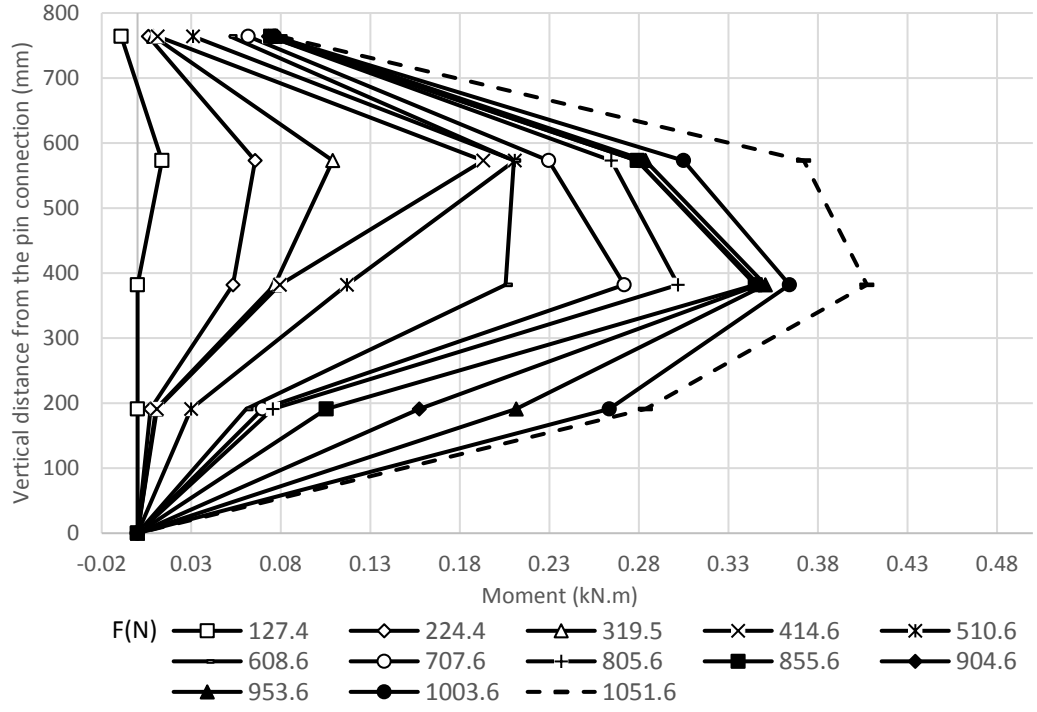

Figure 4.196 Moments along the tensile side of the pile in Test H2 L3 S1 C2 D3.

Strain in the geogrid layers:

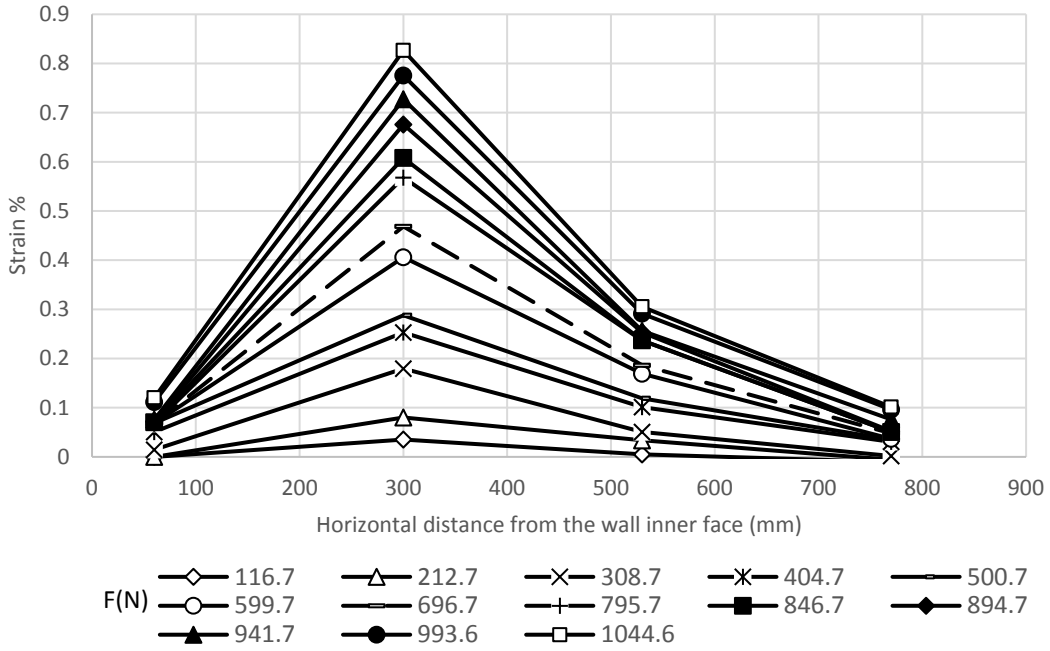

Figure A.197 Strains in the geogrid layer at 450 mm from the wall base (Test H2 L3 S1 C2 D2).

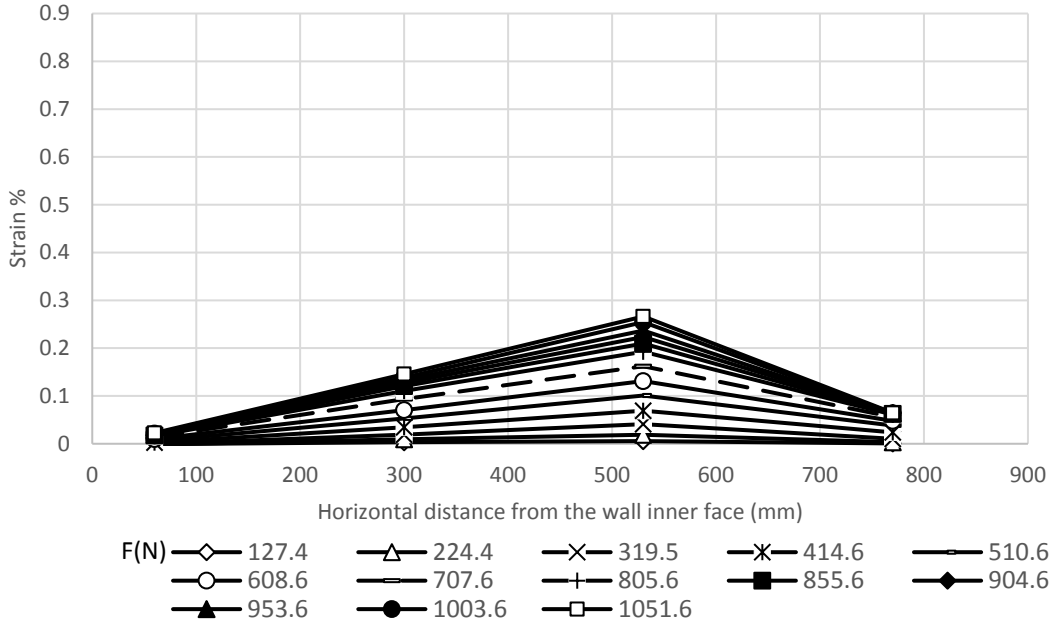

Figure A.198 Strains in the geogrid layer at 450 mm from the wall base (Test H2 L3 S1 C2 D3).

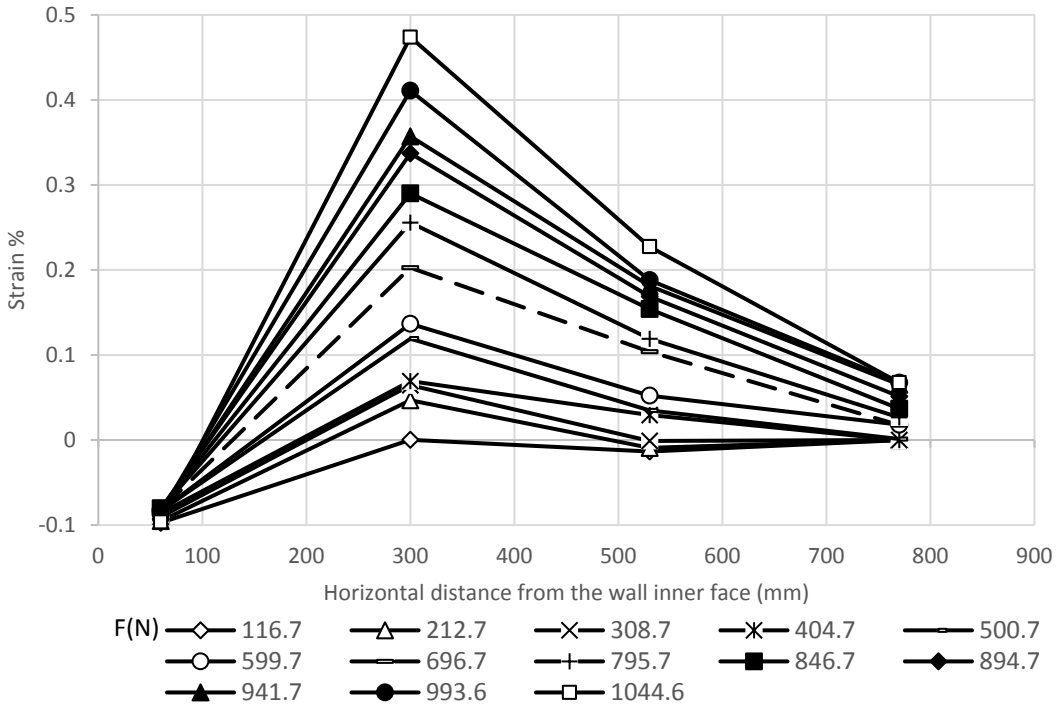

Figure A.199 Strains in the geogrid layer at 270 mm from the wall base (Test H2 L3 S1 C2 D2).

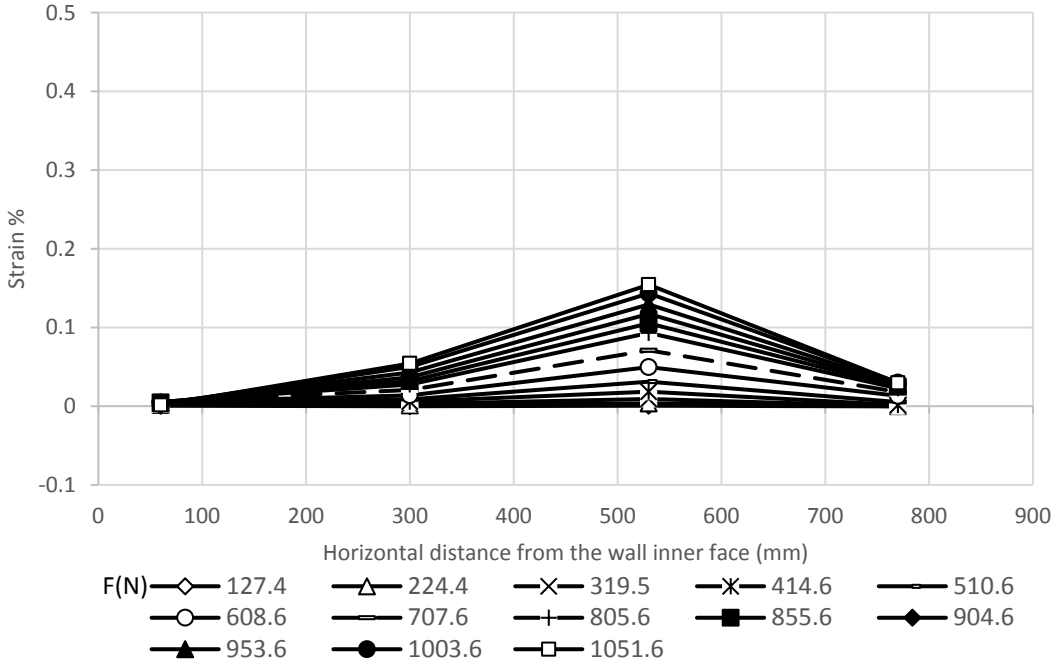

Figure A.200 Strains in the geogrid layer at 270 mm from the wall base (Test H2 L3 S1 C2 D3).

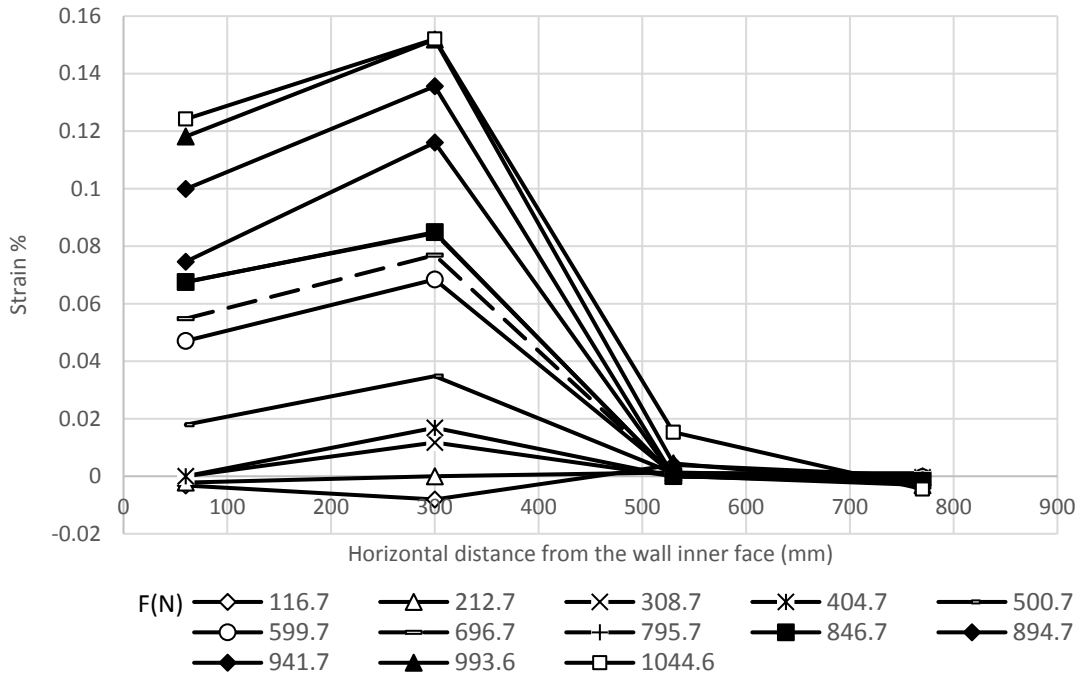

Figure A.201 Strains in the geogrid layer at 90 mm from the wall base (Test H2 L3 S1 C2 D2).

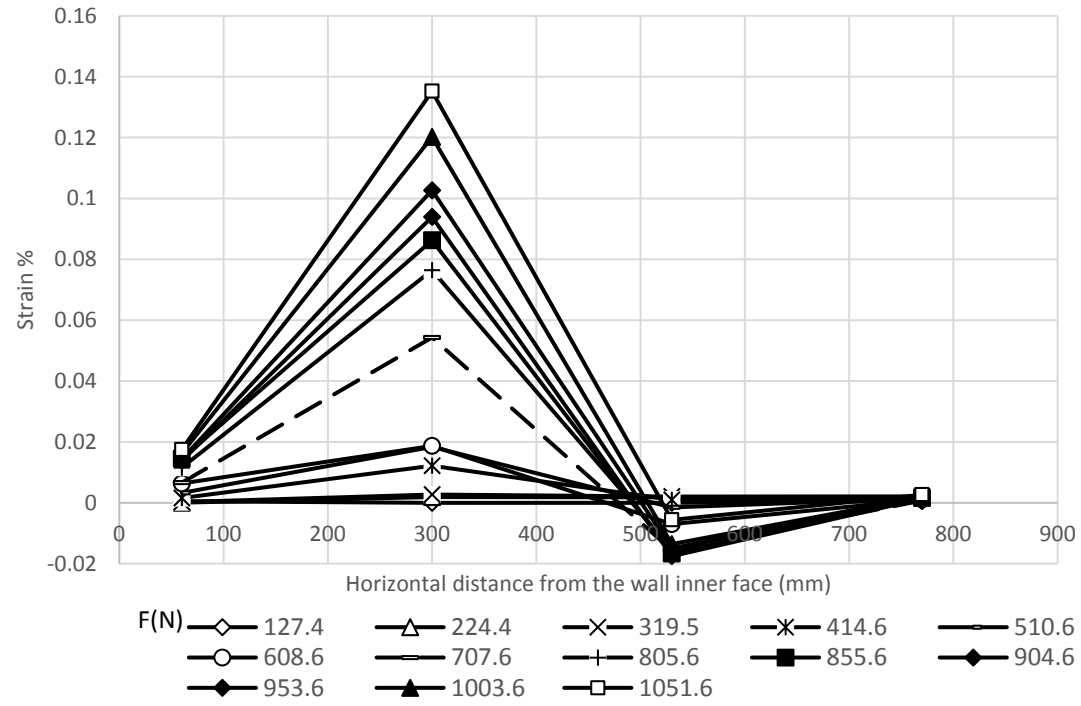

Figure A.203 Strains in the geogrid layer at 90 mm from the wall base (Test H2 L3 S1 C2 D3).

Pressure behind the wall facing

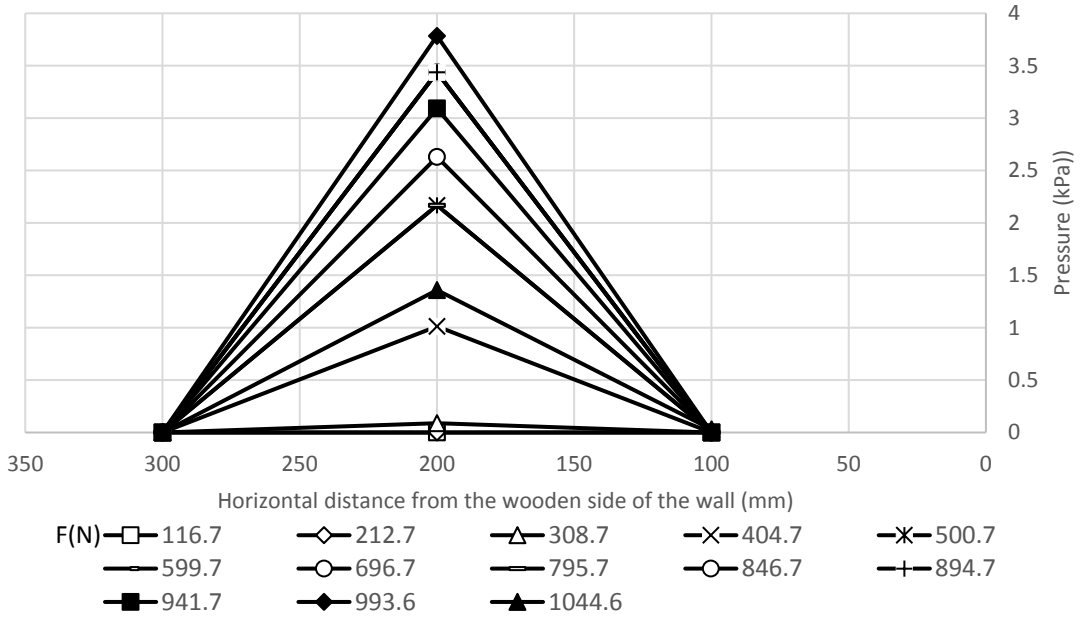

Figure A.204 Transverse pressure distributions at 607.5 mm from the wall base for Test H2 L3 S1 C2 D2.

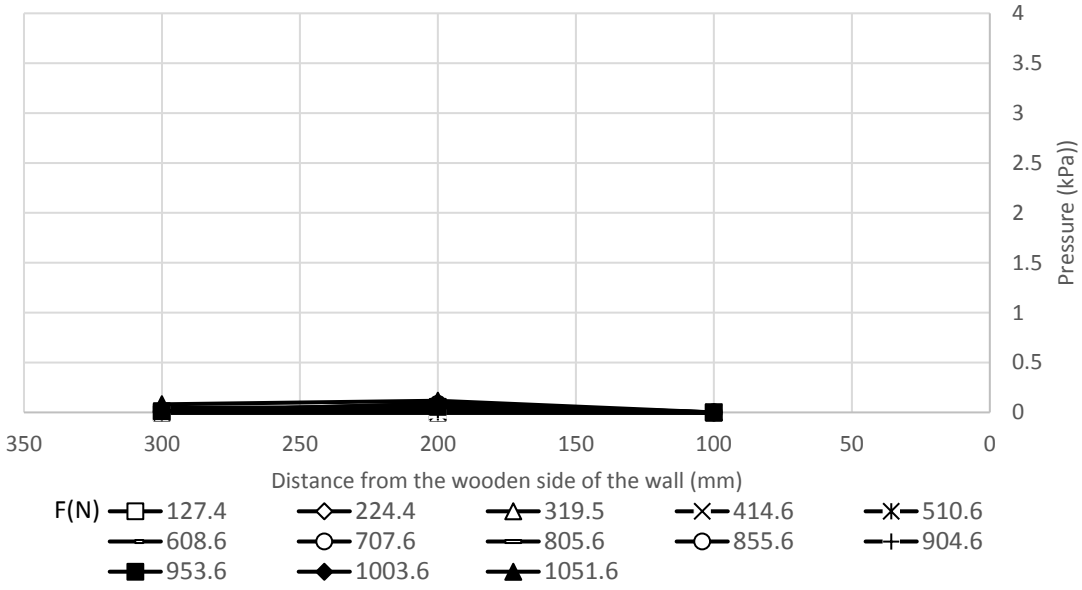

Figure A.205 Transverse pressure distributions at 607.5 mm from the wall base for Test H2 L3 S1 C2 D3.

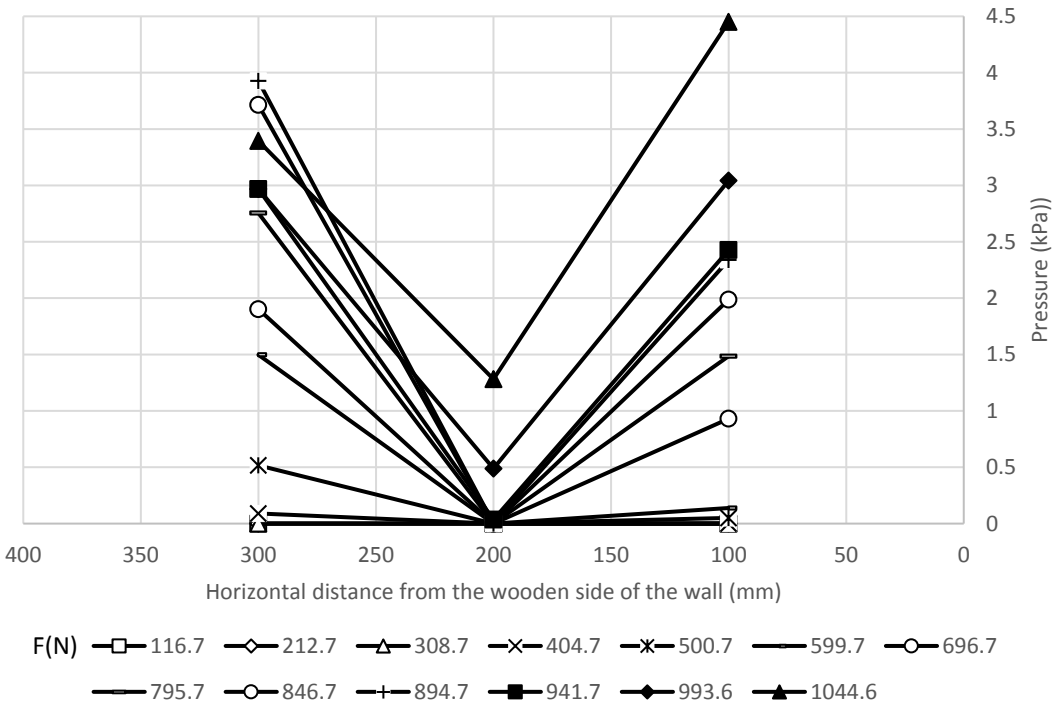

Figure A.206 Transverse pressure distributions at 337.5 mm from the wall base for Test H2 L3 S1 C2 D2.

Figure A.207 Transverse pressure distributions at 337.5 mm from the wall base for Test H2 L3 S1 C2 D3.